VOLUME SEVEN HUNDRED AND TWENTY EIGHT

METHODS IN
ENZYMOLOGY

Lipids and Membranes: Metabolism, Lipidation, and Lipid-Protein Interactions

METHODS IN ENZYMOLOGY

Editors-in-Chief

KAREN N. ALLEN, Ph.D.

Professor and Chair
Department of Chemistry
Professor of Material Science and Engineering
Boston University

DAVID CHRISTIANSON

Roy and Diana Vagelos Laboratories
Department of Chemistry
University of Pennsylvania
Philadelphia, PA

Founding Editors

SIDNEY P. COLOWICK and NATHAN O. KAPLAN

VOLUME SEVEN HUNDRED AND TWENTY EIGHT

METHODS IN ENZYMOLOGY

Lipids and Membranes: Metabolism, Lipidation, and Lipid-Protein Interactions

Edited by

JEREMY M. BASKIN
Associate Professor and Nancy and Peter Meinig Family Investigator in the Life Sciences
Department of Chemistry and Chemical Biology
Weill Institute for Cell and Molecular Biology
Cornell University, United States

ACADEMIC PRESS
An imprint of Elsevier

Academic Press is an imprint of Elsevier
50 Hampshire Street, 5th Floor, Cambridge, MA 02139, United States
125 London Wall, London, EC2Y 5AS, United Kingdom

First edition 2026

Copyright © 2026 Elsevier Inc. All rights are reserved, including those for text and data mining, AI training, and similar technologies.

For accessibility purposes, images in electronic versions of this book are accompanied by alt text descriptions provided by Elsevier. For more information, see https://www.elsevier.com/about/accessibility.

Books and Journals published by Elsevier comply with applicable product safety requirements. For any product safety concerns or queries, please contact our authorised representative, Elsevier B.V., at productsafety@elsevier.com.

Publisher's note: Elsevier takes a neutral position with respect to territorial disputes or jurisdictional claims in its published content, including in maps and institutional affiliations.

No part of this publication may be reproduced or transmitted in any form or by any means, electronic or mechanical, including photocopying, recording, or any information storage and retrieval system, without permission in writing from the publisher. Details on how to seek permission, further information about the Publisher's permissions policies and our arrangements with organizations such as the Copyright Clearance Center and the Copyright Licensing Agency, can be found at our website: www.elsevier.com/permissions.

This book and the individual contributions contained in it are protected under copyright by the Publisher (other than as may be noted herein).

Notices

Knowledge and best practice in this field are constantly changing. As new research and experience broaden our understanding, changes in research methods, professional practices, or medical treatment may become necessary.

Practitioners and researchers must always rely on their own experience and knowledge in evaluating and using any information, methods, compounds, or experiments described herein. In using such information or methods they should be mindful of their own safety and the safety of others, including parties for whom they have a professional responsibility.

To the fullest extent of the law, neither the Publisher nor the authors, contributors, or editors, assume any liability for any injury and/or damage to persons or property as a matter of products liability, negligence or otherwise, or from any use or operation of any methods, products, instructions, or ideas contained in the material herein.

ISBN: 978-0-443-43312-2
ISSN: 0076-6879

For information on all Academic Press publications
visit our website at https://www.elsevier.com/books-and-journals

Publisher: Zoe Kruze
Editorial Project Manager: Saloni Vohra
Production Project Manager: James Selvam
Cover Designer: Muthukumaran Thangaraj
Typeset by MPS Limited, India

Contents

Contributors *xvii*

1. De novo chemoenzymatic construction of lipid membranes **1**

Satyam Khanal, Alexander Harjung, and Alessandro Fracassi

1. Introduction 2
2. Chemical strategies for generating lipid membranes de novo 4
3. Chemoenzymatic phospholipid membrane synthesis 5
4. Methods 6
   - 4.1 Enzymatic phase: Generating fatty acids using bacterial type I FAS 6
   - 4.2 Chemical phase: Acylation of cysteine-modified lysophospholipids with acyl-CoAs 11
   - 4.3 Chemoenzymatic one-pot phospholipid formation mediated by cgFAS 12
   - 4.4 Vesicular phase: Characterization of de novo generated lipid membranes 13
   - 4.5 Safety considerations and standards 18
5. Conclusion and outlook 18

Declaration of generative AI and AI-assisted technologies in the writing process 19

References 19

2. Photoaffinity strategies to profile cholesterol metabolite interactomes and binding sites **23**

Yu-Shiuan Cheng and Alison E. Ondrus

1. Introduction 24
2. Before you begin 28
3. Live cell photoaffinity crosslinking and click chemistry tagging 30
   - 3.1 Vehicle, probe, and/or competitor treatment, and photocrosslinking 31
   - 3.2 Subcellular fractionation 34
   - 3.3 Copper-catalyzed click tagging 36
   - 3.4 In-gel fluorescence visualization of probe crosslinked, fluorophore-tagged proteins 38
   - 3.5 Streptavidin enrichment of probe-crosslinked, biotin-tagged proteins 41

3.6 Protein digestion and desalting 43
3.7 TMT labeling and label efficiency check 46
3.8 LC-MS^3 analysis 48
3.9 Data analysis notes 49
4. Binding site identification 50
4.1 Transfection, live cell compound treatment, and photoaffinity crosslinking 50
4.2 Cell lysis and target protein immunoprecipitation 52
4.3 S-Trap protein digestion and desalting 55
4.4 LC-MS analysis 57
4.5 Data analysis notes 58
5. Discussion 61
Acknowledgments 61
References 61

3. Expression and characterization of phospholipase Cβ and ε enzymes **65**

Hanna D. King, Ketaki A. Mahurkar, and Angeline M. Lyon

1. Introduction 66
2. Before you begin 68
2.1 PLCβ purification buffers 68
2.2 PLCε purification buffers 69
2.3 *In* vitro activity assay (IP1) buffers 70
2.4 ^{3}[H]-IPx accumulation assay buffers 71
3. Key resources table 72
4. Protein expression and purification 74
4.1 Materials and equipment for protein expression and purification 74
4.2 PLCβ expression 75
4.3 PLCβ purification 76
4.4 Expression of PLCε N-terminal truncations 79
4.5 PLCe purification 79
5. Activity Assays 82
5.1 Materials and equipment for activity assays 82
5.2 *In* vitro activity assay (IP1) 83
5.3 ^{3}[H]-IPx accumulation assay 86
6. Expected outcomes 88
7. Quantification and statistical analysis 92
8. Advantages 93

9. Limitations 94
10. Optimization and troubleshooting 95
10.1 Problem (low protein expression) 95
10.2 Problem (protein not binding to the Ni-NTA affinity column) 95
10.3 Problem (*In vitro* activity assay (IP1): Sample(s) have low signal) 95
10.4 Problem (^{3}[H]-IPx accumulation assay: Sample(s) have low signal) 96
11. Safety considerations and standards 96
12. Alternative methods/procedures 96
References 97

4. Assembling Retromer-coated membrane tubules for biochemical and structural studies 101

Kai-En Chen, Vikas A. Tillu, Nicholas Ariotti, and Brett M. Collins

1. Introduction 102
2. Experimental procedure 104
2.1 Expression and purification of ctRetromer pentameric complex 104
2.2 Liposome pelleting assay to assess membrane binding of the Retromer complex 107
2.3 Liposome tubulation 110
2.4 Additional notes 113
3. Concluding remarks 114
Acknowledgments 114
References 114

5. Quantitative analysis of S-acylation 117

Carla Busquets Hernández, Alexandra Tsiotsia, and Gemma Triola

1. Introduction 118
2. Sample preparation 121
2.1 Isolation of proteome from cell lysates 122
2.2 Treatment of the proteome with 2 M Hydroxylamine and isolation of the formed fatty acid hydroxamates 123
3. Preparation of the C19 FAH 124
4. Mass analysis 125
5. Data analysis 126
6. Notes 126
References 127

6. Detecting ZDHHC acyltransferase inhibition using acylation-coupled lipophilic induction of polarization (Acyl-cLIP) or LC-MS **129**

Wenzhe Chen, Jiaqi Zhao, Zhenquan Sun, Kewen Peng, Wendy K. Greentree, Maurine E. Linder, and Hening Lin

1. Introduction 130
   - 1.1 ZDHHCs 130
   - 1.2 Acyl-cLIP and LCMS-based method 131
2. Acyl-cLIP for ZDHHC enzymes 132
   - 2.1 Equipment 132
   - 2.2 Reagents 132
   - 2.3 Reagent setup 132
   - 2.4 Procedures 133
   - 2.5 Data processing 134
3. ZDHHC enzyme assay detected by LC-MS 135
   - 3.1 Equipment 135
   - 3.2 Reagents and buffers 135
   - 3.3 Reagents setup 136
   - 3.4 Procedures 136
4. Notes 139

References 140

7. One-pot biosynthesis of genetically encoded amphiphiles via protein prenylation **143**

Md Mahbubul Alam, Md Shahadat Hossain, James L. Hougland, and Davoud Mozhdehi

1. Introduction 144
2. Instruments and materials 148
   - 2.1 Instruments and equipment 148
   - 2.2 Reagents and consumables 148
3. Construction of orthogonal expression vectors 149
   - 3.1 Vector selection and design considerations 149
   - 3.2 Cloning the prenyltransferase machinery 150
   - 3.3 Assembly of the lipid biosynthesis and substrate co-expression system 151
4. One-pot biosynthesis and purification of prenylated ELPs 154
   - 4.1 Co-expression and culture conditions 154
   - 4.2 Purification of prenylated ELPs 156
   - 4.3 Assessment of protein modifications 157

5. Biophysical characterization of phase behavior and nano-assembly of prenylated ELPs 159
5.1 Variable-temperature turbidimetry 159
5.2 Dynamic light scattering 160
6. Geranylgeranylation of RhoA GTPase 161
6.1 Application of the co-expression system to RhoA 161
6.2 Isolation of RhoA isoforms 163
6.3 Validation of prenylation 163
7. Summary 165
Acknowledgments 165
References 165

8. Creation of an optogenetic membrane editor with ultralow background activity 169

Xiang-Ling Li and Jeremy M. Baskin

1. Introduction 170
2. Blue light irradiation setup 172
3. Rational design and cloning of engineered enzymes 172
3.1 Materials 174
3.2 Protocol 174
4. Quantification of enzyme activity by fluorescence labeling 175
4.1 Materials 176
4.2 Equipment 176
4.3 Protocol 176
5. Quantification of enzyme activity by LC-MS 177
5.1 Materials 178
5.2 Equipment 178
5.3 Protocol 178
5.4 LC-MS analysis 180
6. Summary and guidelines for further engineering 180
Acknowledgements 181
Competing interests 181
References 181

9. Inhibition of sterol transport protein function 183

Hogan P. Bryce-Rogers, Laura Depta, Thomas Whitmarsh-Everiss, and Luca Laraia

1. Introduction 184
2. Titration of fluorescent lipids against sterol transport proteins 187

2.1 Equipment and materials 189
2.2 Reagents 189
2.3 Procedure 190
2.4 Notes 192
3. Fluorescence polarization for competitive inhibitor discovery 193
3.1 Equipment and materials 193
3.2 Reagents 193
3.3 Procedure 193
3.4 Notes 195
4. Differential scanning fluorimetry to determine STP binding 195
4.1 Equipment and materials 196
4.2 Reagents 196
4.3 Procedure 197
4.4 Notes 199
5. FRET-based liposome assays for lipid transport inhibitor discovery 199
5.1 Equipment and materials 200
5.2 Reagents 200
5.3 Procedure 201
5.4 Notes 205
6. Conclusion 206
Acknowledgements 207
References 207

10. Preparation of K-Ras4B containing synthetic modifications via expressed protein ligation 211

Jiayue Hu, Yong-Xiang Chen, and Mark D. Distefano

1. Introduction 212
2. *Escherichia Coli* transformation 216
2.1 Reagents and materials 217
2.2 Equipment 217
2.3 Procedure 217
3. Expression and purification of K-Ras4BΔ15 (MESNA thioester) 218
3.1 Reagent and materials 218
3.2 Equipment 219
3.3 Procedure 219
4. Synthesis of the hypervariable region (HVR) peptide 221
4.1 Reagents and materials 222
4.2 Equipment 222
4.3 Procedure 222

5. Expressed protein ligation 225
5.1 Reagents and materials 225
5.2 Equipment 226
5.3 Procedure 226
6. Purification of the full-length ligated protein product 226
6.1 Reagents and materials 227
6.2 Equipment 227
6.3 Procedure 227
7. Enzymatic activity assay based on the fluorescence of K(Dns)K-Ras4B 228
7.1 Reagents and materials 229
7.2 Equipment 229
7.3 Procedure 229
8. Summary and conclusion 232
Acknowledgements 232
Funding 232
References 232

11. A fluorescence and HPLC-based activity assay system for lipid-modifying enzymes: Lipin/Pah phosphatidic acid phosphatase as an optimized example 235

Franceine S. Welcome, Lingshuang Wu, Tereza Vitkovska, Jiyao Chai, Shujuan Gao, and Michael V. Airola

1. Introduction 236
2. Purification 239
2.1 Equipment 239
2.2 Buffers and reagents 240
2.3 Transformation 240
2.4 Expression 241
2.5 Purification 241
3. Activity assay 243
3.1 Equipment 244
3.2 Buffers and reagents 244
3.3 Micelle preparation 245
3.4 Liposome preparation 245
3.5 Assay protocol 245
4. Quantification of DAG production 246
4.1 Diacylglycerol standard curve 246
4.2 Sample data and quantification 247
Acknowledgements 248
References 248

12. Use of novel synthetic analogs to decipher the interactome of phosphatidic acid species in neurosecretory cells **253**

Alexander Wolf, Emeline Tanguy, Charles Decraene, Steven Vertueux, Jean-Marc Strub, Stéphane Ory, Sébastien Balieu, Pierre-Yves Renard, Stéphane Gasman, and Nicolas Vitale

1. Introduction 254
2. Phosphatidic acid incorporation into cells 258
   - 2.1 PA preparation for cellular incorporation 258
   - 2.2 Validation of PA incorporation within cellular membranes 259
   - 2.3 Functional validation of synthetic PAs using ERK1/2 phosphorylation 260
3. Identification of PA interactors in live cells 263
   - 3.1 Photo-crosslinking of dedicated partners 263
   - 3.2 Click chemistry-based enrichment of PA-protein complexes 265
4. Conclusion 268
5. Reagents and materials 269

Acknowledgements 272
Author contribution 272
References 272

13. Expression and purification of Steroidogenic Factor-1 (NR5A1) nuclear receptor ligand binding domain complexed with the signaling phosphoinositide lipid PI(3,4,5)P_3 **277**

Alexis N. Campbell, Alexander J. Cutright, Jessica Martin, Arwa Kheda, Mong Na Claire Loi, and Raymond D. Blind

1. Introduction 278
2. Plasmid construction, transformation into escherichia coli, and glycerol stock preparation 279
3. *Escherichia coli* encoded His_6-SF-1-LBD expression and purification 281
   - 3.1 Equipment 281
   - 3.2 Materials 281
   - 3.3 Growth procedure 282
   - 3.4 SF-1 LBD purification protocol 282
   - 3.5 Expected outcomes 283
   - 3.6 Advantages 284
   - 3.7 Cautions and troubleshooting 284
4. Bacterial phospholipid exchange with PIP_3 of SF-1 LBD 284
   - 4.1 Equipment 284
   - 4.2 Materials 284

4.3 PIP_3 micelle preparation 285
4.4 SF-1/bPL exchange with PIP_3 285
4.5 Isolating SF-1/PIP3 by AIEX column 285
4.6 Expected outcomes 286
4.7 Advantages 286
4.8 Cautions and troubleshooting 286
5. Conclusions 287
References 287

14. Reconstitution strategies for exploring interactions of Ebola virus matrix protein with host membrane mimetics 289

Sreetama Pal, Shalini T. Low-Nam, and Robert V. Stahelin

1. Introduction 290
2. Materials and equipment 291
2.1 Materials 291
2.2 Equipment 293
3. Protocols for reagent generation 294
3.1 Endogenous EBOV VP40 294
3.2 Supported lipid bilayers (SLBs) 297
4. SLB-based assays for quantitative assessment of EBOV VP40 interaction with host membrane mimetics 299
4.1 Ensemble/single-molecule TIRF microscopy 299
4.2 Data analysis 301
5. Expected outcomes and conclusions 301
Acknowledgments 301
References 301

15. Palmitoylation-dependent probes for labeling the Golgi apparatus 305

Shunsuke Sawada, Keita Tsutsui, and Shinya Tsukiji

1. Introduction 306
2. Method 1: Chemical synthesis of myrGC^{3Me}-conjugated fluorescent probes 308
2.1 Before you begin 310
2.2 Synthesis of myr-^{Me}Gly-^{Me}Cys(Trt)-^{Me}Adox-Lys-NH_2 311
2.3 Synthesis of mgc^{3Me}FDA 315
2.4 Synthesis of mgc^{3Me}DEAC 315
2.5 Synthesis of mgc^{3Me}TMR 316

3. Method 2: Fluorescent staining of the Golgi apparatus in living cells 317
3.1 Before you begin 318
3.2 Staining and fluorescent imaging of live-cell Golgi 319
4. Method 3: Visualization of Golgi dynamics under drug treatment 320
4.1 Before you begin 320
4.2 Time-lapse fluorescence imaging of Golgi dynamics during BFA treatment 321
5. Method 4: Visualization of Golgi dynamics during cell division 322
5.1 Before you begin 322
5.2 Time-lapse fluorescence imaging of Golgi dynamics during cell division 323
Acknowledgments 323
References 324

16. Real-time measurement of the ATG8 lipidation reaction by fluorescence spectroscopy 327

Wenxin Zhang, Sharon A. Tooze, and Taki Nishimura

1. Before you begin 328
2. Key resources table 329
3. Materials and equipment 331
4. Step-by-step method details 332
4.1 Expression and purification of ATG7 from insect Sf9 cells 332
4.2 Expression and purification of ATG3 from bacteria BL21 (DE3) cells 334
4.3 Expression and purification of ATG8 (LC3B S3C) from bacteria BL21 (DE3) cells 336
4.4 NBD-labeling of LC3B S3C proteins with single cysteine mutation 337
4.5 Liposome preparation 338
4.6 Real-time ATG8 lipidation assay 340
5. Expected outcomes 341
6. Quantification and statistical analysis 342
7. Advantages 343
8. Limitations 343
9. Optimization and troubleshooting 343
Acknowledgments 344
References 344

17. Optogenetic phospholipase C for measuring phosphoinositide turnover and DAG generation **347**

Yeon-Jeong Kim, Ayako M. Watabe, and Toshihisa Ohtsuka

1. Introduction 348
2. Structure and operating mechanism of the opto-PLCβ system 349
3. Materials and methods 351
4. Before you begin 351
5. Key resources table 352
6. Materials and equipment 354
7. Step-by-step method details 354
   - 7.1 Cell preparation and transfection 354
   - 7.2 Live-cell imaging on confocal microscope 355
   - 7.3 Image analysis using FIJI 357
8. Expected outcomes 358
9. Quantification and statistical analysis 360
10. Advantages 360
11. Limitations 361
12. Optimization and troubleshooting 361
    - 12.1 Problem (low transfection efficiency) 361
    - 12.2 Potential solution to optimize the procedure (low transfection efficiency) 362
    - 12.3 Problem (Weak or inconsistent fluorescence signals). 362
    - 12.4 Potential solution to optimize the procedure (weak or inconsistent fluorescence signals) 362
    - 12.5 Problem (High background fluorescence). 362
    - 12.6 Potential solution to optimize the procedure (high background fluorescence) 362
13. Safety considerations and standards 363
14. Alternative methods/procedures 363
15. Discussion: Implications of lipid restoration kinetics 364
16. Conclusion 365
17. Future directions 365

Declaration of generative AI and AI-assisted technologies in the writing process 366

References 366

18. Pharmacological modulation of lipid signaling **369**

Ashutosh Sharma and Wonhwa Cho

1. Introduction 370
2. Development of lipid-protein interaction inhibitors 372
   - 2.1 A high-throughput inhibitor screening protocol 372
   - 2.2 Determination of inhibition constant 378
   - 2.3 Target validation 381
   - 2.4 Determination of in vivo inhibitory activity 384
3. Concluding Remarks 386

Acknowledgements 386

References 386

Contributors

Michael V. Airola
Department of Biochemistry and Cell Biology, Stony Brook University, Stony Brook, NY, United States

Md Mahbubul Alam
Department of Chemistry, Syracuse University, Syracuse, New York, United States

Nicholas Ariotti
Institute for Molecular Bioscience, The University of Queensland, St. Lucia, Brisbane, QLD, Australia

Sébastien Balieu
Université de Rouen Normandie, INSA Rouen Normandie, CNRS, Université de Caen Normandie, ENSICAEN, Normandie Université, CARMeN UMR 6064, INC3M FR, Rouen, France

Jeremy M. Baskin
Department of Chemistry and Chemical Biology; Weill Institute for Cell and Molecular Biology, Cornell University, Ithaca, NY, United States

Raymond D. Blind
Department of Biochemistry, Vanderbilt University School of Medicine; Division of Diabetes, Department of Medicine, Endocrinology & Metabolism, Vanderbilt University Medical Center, Nashville, TN, United States

Hogan P. Bryce-Rogers
Department of Chemistry, Technical University of Denmark, Kgs Lyngby, Denmark

Carla Busquets Hernández
Institute for Advanced Chemistry of Catalonia (IQAC-CSIC), Barcelona, Spain

Alexis N. Campbell
Department of Biochemistry, Vanderbilt University School of Medicine, Nashville, TN, United States

Jiyao Chai
Department of Biochemistry and Cell Biology, Stony Brook University, Stony Brook, NY, United States

Kai-En Chen
Institute for Molecular Bioscience, The University of Queensland, St. Lucia, Brisbane, QLD, Australia

Wenzhe Chen
Department of Medicine; Department of Chemistry, The University of Chicago, Chicago, IL; Department of Chemistry and Chemical Biology, Cornell University, Ithaca, NY, United States

Yong-Xiang Chen
Department of Chemistry, Tsinghua University, Beijing, China

Yu-Shiuan Cheng
Department of Chemistry, College of Liberal Arts and Sciences, University of Illinois Chicago, Chicago, IL, United States

Wonhwa Cho
Department of Chemistry, University of Illinois Chicago, Chicago, IL, United States

Brett M. Collins
Institute for Molecular Bioscience, The University of Queensland, St. Lucia, Brisbane, QLD, Australia

Alexander J. Cutright
Division of Diabetes, Department of Medicine, Endocrinology & Metabolism, Vanderbilt University Medical Center, Nashville, TN, United States

Charles Decraene
Institut des Neurosciences Cellulaires et Intégratives, Centre National de la Recherche Scientifique, Université de Strasbourg, Strasbourg, France

Laura Depta
Department of Chemistry, Technical University of Denmark, Kgs Lyngby, Denmark

Mark D. Distefano
University of Minnesota, Minneapolis, MN, United States

Alessandro Fracassi
Department of Chemistry and Biochemistry, University of California San Diego, La Jolla, CA, United States

Shujuan Gao
Department of Biochemistry and Cell Biology, Stony Brook University, Stony Brook, NY, United States

Stéphane Gasman
Institut des Neurosciences Cellulaires et Intégratives, Centre National de la Recherche Scientifique, Université de Strasbourg, Strasbourg, France

Wendy K. Greentree
Department of Molecular Medicine, Cornell University, Ithaca, NY, United States

Alexander Harjung
Department of Chemistry and Biochemistry, University of California San Diego, La Jolla, CA, United States

Md Shahadat Hossain
Department of Pharmaceutical Technology, Faculty of Pharmacy, University of Dhaka, Dhaka, Bangladesh

James L. Hougland
Department of Chemistry, Syracuse University, Syracuse, New York, United States

Jiayue Hu
University of Minnesota, Minneapolis, MN, United States

Satyam Khanal
Department of Chemistry, New York University, New York, NY, United States

Arwa Kheda
Division of Diabetes, Department of Medicine, Endocrinology & Metabolism, Vanderbilt University Medical Center, Nashville, TN, United States

Yeon-Jeong Kim
Department of Biochemistry, Faculty of Medicine, Graduate School of Medicine, University of Yamanashi, Yamanashi, Japan

Hanna D. King
James Tarpo Jr. and Margaret Tarpo Department of Chemistry, Purdue University, West Lafayette, IN, United States

Luca Laraia
Department of Chemistry, Technical University of Denmark, Kgs Lyngby, Denmark

Xiang-Ling Li
Department of Chemistry and Chemical Biology; Weill Institute for Cell and Molecular Biology, Cornell University, Ithaca, NY, United States

Hening Lin
Department of Medicine; Department of Chemistry, The University of Chicago, Chicago, IL; Department of Chemistry and Chemical Biology, Cornell University, Ithaca, NY; Howard Hughes Medical Institute, The University of Chicago, Chicago, IL, United States

Maurine E. Linder
Department of Molecular Medicine, Cornell University, Ithaca, NY, United States

Mong Na Claire Loi
Division of Diabetes, Department of Medicine, Endocrinology & Metabolism, Vanderbilt University Medical Center, Nashville, TN, United States

Shalini T. Low-Nam
Tarpo Department of Chemistry; Department of Physics; Purdue Institute of Inflammation, Immunology, and Infectious Disease, Purdue University, West Lafayette, IN, United States

Angeline M. Lyon
James Tarpo Jr. and Margaret Tarpo Department of Chemistry, Purdue University, West Lafayette, IN; Department of Biological Sciences, Purdue University, West Lafayette, Indiana, United States

Ketaki A. Mahurkar
James Tarpo Jr. and Margaret Tarpo Department of Chemistry, Purdue University, West Lafayette, IN, United States

Jessica Martin
Division of Diabetes, Department of Medicine, Endocrinology & Metabolism, Vanderbilt University Medical Center, Nashville, TN, United States

Davoud Mozhdehi
Department of Chemistry, Syracuse University, Syracuse, New York, United States

Taki Nishimura
Institute for Protein Research; Graduate School of Frontier Biosciences, The University of Osaka, Osaka, Japan

Toshihisa Ohtsuka
Department of Biochemistry, Faculty of Medicine, Graduate School of Medicine, University of Yamanashi, Yamanashi, Japan

Alison E. Ondrus
Department of Chemistry, College of Liberal Arts and Sciences; Department of Pharmaceutical Sciences, College of Pharmacy, University of Illinois Chicago, Chicago, IL, United States

Stéphane Ory
Institut des Neurosciences Cellulaires et Intégratives, Centre National de la Recherche Scientifique, Université de Strasbourg, Strasbourg, France

Sreetama Pal
Tarpo Department of Chemistry; Borch Department of Medicinal Chemistry and Molecular Pharmacology, Purdue University, West Lafayette, IN, United States

Kewen Peng
Department of Medicine; Department of Chemistry, The University of Chicago, Chicago, IL; Department of Chemistry and Chemical Biology, Cornell University, Ithaca, NY, United States

Pierre-Yves Renard
Université de Rouen Normandie, INSA Rouen Normandie, CNRS, Université de Caen Normandie, ENSICAEN, Normandie Université, CARMeN UMR 6064, INC3M FR, Rouen, France

Shunsuke Sawada
Department of Environment and Sustainability, Mukogawa Women's University, Nishinomiya, Japan

Ashutosh Sharma
Department of Chemistry, University of Illinois Chicago, Chicago, IL, United States

Robert V. Stahelin
Borch Department of Medicinal Chemistry and Molecular Pharmacology; Purdue Institute of Inflammation, Immunology, and Infectious Disease, Purdue University, West Lafayette, IN, United States

Jean-Marc Strub
Laboratoire de Spectrométrie de Masse BioOrganique, IPHC UMR 7178, CNRS, Université de Strasbourg; Infrastructure Nationale de Protéomique ProFI - UAR2048, Strasbourg, France

Zhenquan Sun
Department of Medicine; Department of Chemistry, The University of Chicago, Chicago, IL, United States

Emeline Tanguy
Institut des Neurosciences Cellulaires et Intégratives, Centre National de la Recherche Scientifique, Université de Strasbourg, Strasbourg, France

Vikas A. Tillu
Institute for Molecular Bioscience, The University of Queensland, St. Lucia, Brisbane, QLD, Australia

Sharon A. Tooze
Molecular Cell Biology of Autophagy Laboratory, The Francis Crick Institute, London, United Kingdom

Gemma Triola
Institute for Advanced Chemistry of Catalonia (IQAC-CSIC), Barcelona, Spain

Alexandra Tsiotsia
Institute for Advanced Chemistry of Catalonia (IQAC-CSIC), Barcelona, Spain

Shinya Tsukiji
Department of Nanopharmaceutical Sciences; Department of Life Science and Applied Chemistry; OptoBioTechnology Research Center, Nagoya Institute of Technology, Nagoya, Japan

Keita Tsutsui
Department of Nanopharmaceutical Sciences, Nagoya Institute of Technology, Nagoya, Japan

Steven Vertueux
Université de Rouen Normandie, INSA Rouen Normandie, CNRS, Université de Caen Normandie, ENSICAEN, Normandie Université, CARMeN UMR 6064, INC3M FR, Rouen, France

Nicolas Vitale
Institut des Neurosciences Cellulaires et Intégratives, Centre National de la Recherche Scientifique, Université de Strasbourg, Strasbourg, France

Tereza Vitkovska
Department of Biochemistry and Cell Biology, Stony Brook University, Stony Brook, NY, United States

Ayako M. Watabe
Institute of Clinical Medicine and Research, Research Center for Medical Sciences, The Jikei University School of Medicine, Chiba, Japan

Franceine S. Welcome
Department of Biochemistry and Cell Biology, Stony Brook University, Stony Brook, NY, United States

Thomas Whitmarsh-Everiss
Department of Chemistry, Technical University of Denmark, Kgs Lyngby, Denmark

Alexander Wolf
Institut des Neurosciences Cellulaires et Intégratives, Centre National de la Recherche Scientifique, Université de Strasbourg, Strasbourg, France

Lingshuang Wu
Department of Biochemistry and Cell Biology, Stony Brook University, Stony Brook, NY, United States

Wenxin Zhang
Mechanisms of Cellular Quality Control, Max Planck Institute of Biophysics, Frankfurt am Main, Hesse, Germany

Jiaqi Zhao
Department of Medicine; Department of Chemistry, The University of Chicago, Chicago, IL; Department of Chemistry and Chemical Biology, Cornell University, Ithaca, NY, United States

CHAPTER ONE

De novo chemoenzymatic construction of lipid membranes

Satyam Khanal[a], **Alexander Harjung**[b], **and Alessandro Fracassi**[b,*]
[a]Department of Chemistry, New York University, New York, NY, United States
[b]Department of Chemistry and Biochemistry, University of California San Diego, La Jolla, CA, United States
*Corresponding author. e-mail address: afracassi@ucsd.edu

Contents

1. Introduction 2
2. Chemical strategies for generating lipid membranes de novo 4
3. Chemoenzymatic phospholipid membrane synthesis 5
4. Methods 6
   4.1 Enzymatic phase: Generating fatty acids using bacterial type I FAS 6
   4.2 Chemical phase: Acylation of cysteine-modified lysophospholipids with acyl-CoAs 11
   4.3 Chemoenzymatic one-pot phospholipid formation mediated by cgFAS 12
   4.4 Vesicular phase: Characterization of de novo generated lipid membranes 13
   4.5 Safety considerations and standards 18
5. Conclusion and outlook 18
Declaration of generative AI and AI-assisted technologies in the writing process 19
References 19

Abstract

Phospholipid biogenesis couples fatty acid synthesis to glycerol acylation and headgroup installation, producing amphiphilic lipids that self-assemble into membranes. Reconstituting this process in the absence of pre-existing bilayers remains a central challenge for bottom-up synthetic biology and origins-of-life research. Here we describe a chemoenzymatic strategy that constructs phospholipids and membranes de novo in aqueous solution. A soluble type I fatty acid synthase generates palmitoyl-CoA from acetyl-CoA and malonyl-CoA, which is then coupled to cysteine-modified lysophospholipids through native chemical ligation to yield amidophospholipids that spontaneously assemble into bilayers. The approach is modular, permitting independent validation of enzymatic and chemical phases, yet also functions in one pot under uniform reaction conditions. This methodology provides a tractable platform for de novo membrane construction and offers a path toward fully synthetic lipid systems that link composition, growth, and function.

Methods in Enzymology, Volume 728
ISSN 0076-6879, https://doi.org/10.1016/bs.mie.2026.01.013
Copyright © 2026 Elsevier Inc. All rights are reserved, including those for text and data mining, AI training, and similar technologies.

1. Introduction

All living cells are enclosed by membrane compartments composed of self-assembled phospholipid bilayers. These membranes regulate the exchange of substances to and from the extracellular environment, compartmentalize and protect biochemical reactions, and contribute to the maintenance of cellular homeostasis (Holthuis & Menon, 2014; van Meer et al., 2008). At the molecular level, phospholipids are amphiphilic molecules featuring a hydrophilic headgroup attached to two hydrophobic fatty acyl chains.

Phospholipids are synthesized by all living organisms through conserved biosynthetic pathways that attach fatty acids to glycerol backbones (Fig. 1). This process starts with the acylation of glycerol-3-phosphate (G3P) by a glycerol-3-phosphate acyltransferase (GPAT), producing lysophosphatidic acid (LPA). A second acyl chain is then added at the *sn*-2 position by a lysophosphatidic acid acyltransferase (LPAAT), yielding phosphatidic acid (PA) (Li et al., 2017; Vance, 2015; Yao & Rock, 2013). PA serves as the

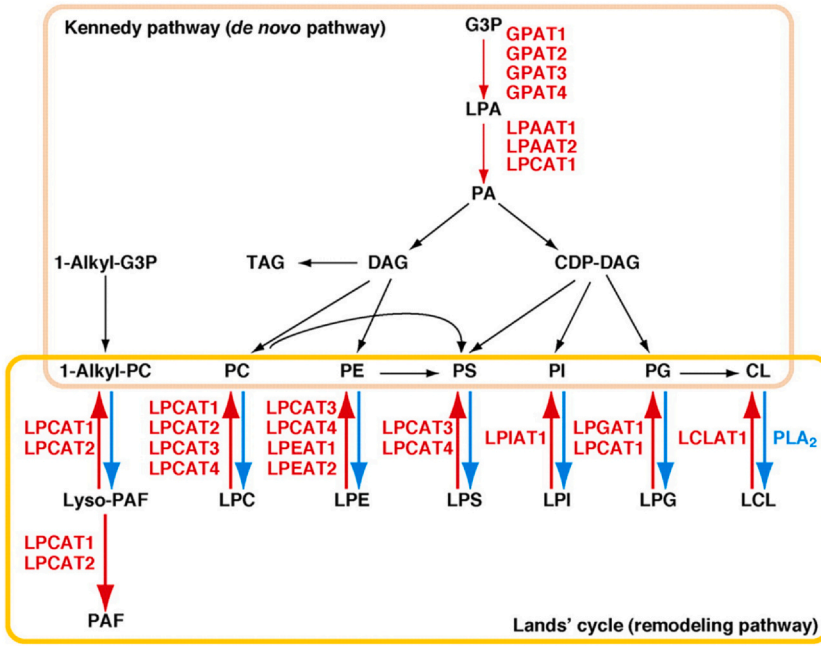

Fig. 1 Pathway of phospholipid biosynthesis. Phospholipids are first synthesized through the de novo pathway (Kennedy pathway) and then modified through the remodeling pathway (Lands cycle) (Shindou & Shimizu, 2009).

branching point for the synthesis of major phospholipids through the attachment of polar head groups (Athenstaedt & Daum, 1999). In many bacteria, PA is activated by condensation with cytidine triphosphate (CTP) to form cytidine diphosphate-diacylglycerol (CDP-DAG), which then reacts with head groups such as glycerol or inositol to generate phosphatidylglycerol, cardiolipin, or phosphatidylinositol (Kobayashi et al., 2024; Rock et al., 1996; Sohlenkamp & Geiger, 2016; Zhang & Rock, 2008). In contrast, most eukaryotic cells activate the head group itself by converting choline or ethanolamine to CDP-choline or CDP-ethanolamine, before transferring it to diacylglycerol (DAG) to produce phosphatidylcholine (PC) or phosphatidylethanolamine (PE) via the Kennedy pathway (Shindou & Shimizu, 2009; Yang et al., 2018). In addition, eukaryotic cells can also remodel phospholipid acyl chains through the Lands cycle, which involves phospholipase-mediated deacylation followed by reacylation through specific acyltransferases (Shindou & Shimizu, 2009; Wang & Tontonoz, 2019). This allows dynamic adjustment of lipid composition and membrane properties in response to physiological demands. Ultimately, phospholipid biosynthesis relies on de novo synthesized fatty acyl chains, which are generated by fatty acid synthases (FASs), multienzyme complexes that catalyze iterative condensation reactions of acetyl-CoA and malonyl-CoA (Maier et al., 2010; Schweizer & Hofmann, 2004).

Due to the universality of phospholipid biosynthesis in living cells, there is growing interest in reconstituting lipid biosynthetic pathways in artificial systems, as this enables autonomous membrane formation, self-maintenance, and dynamic remodeling, which are essential for constructing lifelike systems from the bottom-up (Exterkate & Driessen, 2019; Exterkate et al., 2018; Justice et al., 2024). However, despite detailed knowledge of individual biosynthetic steps, full pathway reconstitution remains challenging. Many of the required enzymes are integral membrane proteins that rely on a lipid bilayer for activity, and reconstitution is limited by challenges associated with their incorporation and functional assembly in synthetic membranes (Bailoni et al., 2023; Harjung et al., 2024; Matsubayashi et al., 2014; Schoenmakers et al., 2024). These challenges are further amplified in the context of de novo construction of lipid membranes, where no pre-existing bilayer is initially available to support membrane protein function. The dependence of membrane biosynthesis on integral membrane enzymes reveals a central paradox in both synthetic biology and origins of life research. Without a lipid bilayer, membrane proteins cannot function, yet these proteins are required for membrane biosynthesis. This raises the fundamental question of how the

first membranes could have formed and been maintained without the support of pre-existing lipid bilayers (Blobel, 1980). Understanding how membranes could have formed de novo, in absence of any lipid structures, is therefore essential for identifying the physical and chemical principles that enabled early cellular life.

To address the interdependence between lipid synthesis and membrane availability, researchers have developed bottom-up approaches to phospholipid production, ranging from purely chemical routes to enzyme-assisted strategies operating in defined synthetic environments (Chen et al., 2025; Flores et al., 2020). These efforts lay the foundation for building self-sustaining membrane systems across diverse applications, including synthetic biology, metabolic engineering, and origin of life research.

2. Chemical strategies for generating lipid membranes de novo

The de novo chemical generation of lipid membranes has emerged as a powerful strategy to bypass the complexities of enzymatic lipid biosynthesis and enable membrane formation in synthetic systems (Devaraj, 2017; Podolsky & Devaraj, 2021; Souto-Trinei et al., 2025). Several chemical reactions have been employed to couple single-chain amphiphiles into bilayer-forming lipids directly in aqueous environments, thereby facilitating spontaneous membrane assembly (Bhattacharya et al., 2023; Budin & Devaraj, 2012; Chen et al., 2024; Flores et al., 2022; Fracassi et al., 2025; Xiong et al., 2017; Zhou et al., 2021). While these approaches typically yield lipid analogues with non-natural linkages, a few acylation-based routes yield natural phospholipids, albeit with prolonged reaction times or non-physiological conditions (Liu et al., 2020; Rudd et al., 2020). Overcoming these constrains, a recently introduced photoredox lipid ligation reaction now enables the abiotic synthesis of natural phospholipids in a single step (Ji et al., 2025). Remarkably, this ligation reaction proceeds efficiently both in artificial membranes and living cells.

More biologically inspired strategies have explored the use of water-soluble thioester precursors, which mirror the central role of thioesters in cellular lipid metabolism. Native chemical ligation (NCL) has been leveraged for in situ phospholipid synthesis by coupling cysteine-functionalized lysolipids with fatty acid thioesters (Brea et al., 2014). This approach enables de novo vesicle formation, facilitates non-enzymatic membrane remodeling,

and permits the spontaneous reconstitution of functional transmembrane proteins into the chemically synthesized membranes (Brea et al., 2016; Cole et al., 2015). Furthermore, NCL has been reported to allow the spontaneous diacylation of cysteine with short-chain choline thioesters, broadening the range of possible pathways for protocell membrane formation (Cho et al., 2025). To further increase the biological relevance of these de novo membrane-forming systems, lipid precursors need to be formed from naturally occurring metabolites rather than synthetically tailored analogues. Moreover, current chemical methods depend on the external addition of preformed alkyl chains, whereas living cells generate fatty acid tails de novo from simple precursors via FASs. Bridging the gap between synthetic lipid assembly and natural lipid metabolism requires integrated biomimetic strategies that generate fatty acid chains in situ and couple them with headgroup precursors to form functional lipid membranes.

3. Chemoenzymatic phospholipid membrane synthesis

Combining chemical and enzymatic strategies enables a route to lipid membrane construction that more closely resembles natural biological processes. In a typical workflow, fatty acid tails are enzymatically activated (Fig. 2, *enzymatic phase*) and then coupled with lysophospholipids (Fig. 2, *chemical phase*), yielding phospholipids that spontaneously self-assemble into bilayers (Fig. 2, *vesicular phase*). One of the first demonstrations of a chemoenzymatic membrane

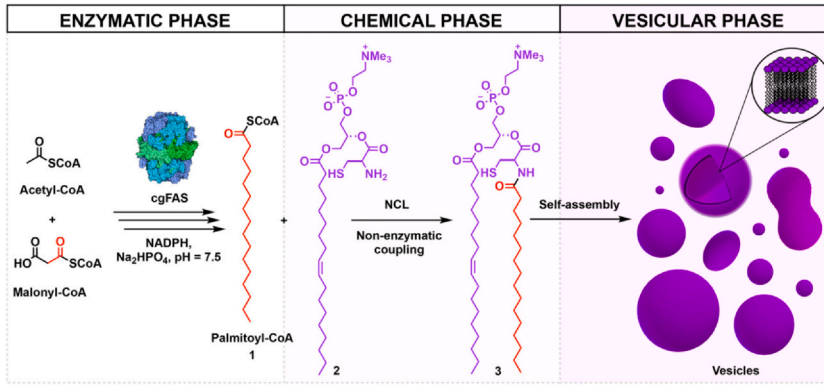

Fig. 2 Schematic representation chemoenzymatic phospholipid synthesis. A type I fatty acid synthase produces palmitoyl-CoA (*enzymatic phase*) that is coupled to cysteine-modified lysolipids by native chemical ligation (*chemical phase*) to yield bilayer-forming phospholipids (*vesicular phase*) (Khanal et al., 2021).

synthesis involved FadD10, a soluble adenylate-forming mycobacterial ligase (Bhattacharya et al., 2019). FadD10 catalyzes the activation of free fatty acids into fatty acyl adenylates (FAAs), which are natural high-energy intermediates capable of undergoing non-enzymatic coupling with amine-functionalized lysolipids to generate phospholipids. These phospholipids spontaneously self-assemble into vesicles, bypassing the need for pre-existing membranes. A key advantage of using enzymes-based systems is their compatibility with cell-free transcription-translation (TXTL) platforms, enabling lipid production under biologically relevant conditions. Several studies have demonstrated that lipid biosynthetic pathways can be expressed in cell-free systems, showing that membrane synthesis can be genetically encoded (Bhattacharya et al., 2021; Blanken et al., 2020; Eto et al., 2022; Scott et al., 2016).

A major advance in chemoenzymatic membrane synthesis is the integration of in situ fatty acid production from simple metabolic precursors. The first in vitro protocol to combine de novo fatty acid biosynthesis with a chemical ligation employed a soluble FAS to generate lipid tails (Khanal et al., 2021). In the enzymatic phase, the system relied on the soluble type I FAS from *Corynebacterium glutamicum* (cgFAS), selected for its ability to primarily produce palmitoyl-CoA rather than free fatty acids, thereby supplying an activated thioester that can be fed directly into the subsequent chemical ligation step (Fig. 2). Using only acetyl-CoA, malonyl-CoA and NADPH, cgFAS iteratively extends the two-carbon primer to generate palmitoyl-CoA. In the chemical phase, the enzymatically produced palmitoyl-CoA is subsequently ligated to a cysteine-functionalized lysolipid via NCL, yielding a non-canonical amidophospholipid that spontaneously assembles into membranes (Fig. 2). Such advances highlight the promise of chemoenzymatic membrane synthesis and demonstrate a progression that necessitates careful methodological consideration. Although developed in a specific enzymatic context, the methodological principles outlined here are broadly generalizable to the chemoenzymatic construction of lipid membranes.

4. Methods

4.1 Enzymatic phase: Generating fatty acids using bacterial type I FAS

4.1.1 Definition

Use of cgFAS to synthesize activated fatty acid tails in situ starting from simple metabolic precursors, such as acetyl-CoA and malonyl-CoA.

4.1.2 Rationale

In situ fatty acid synthesis provides a direct route to generate acyl chains within the reaction environment, ensuring a continuous and controlled supply of lipid tail precursors for subsequent synthetic steps. cgFAS catalyzes the iterative condensation of acetyl-CoA and malonyl-CoA into long-chain fatty acids without requiring pre-isolated acyl substrates, eliminating the need for external fatty acid preparation. By coupling cgFAS activity to subsequent biosynthetic or self-assembly steps, it is possible to better mimic native lipid biosynthesis pathways and improve integration into cell-free or synthetic systems.

4.1.3 Materials, equipment, and reagents

Expression and purification of cgFAS
Nanodrop spectrophotometer
Bacterial expression plasmid encoding His_6-tagged cgFAS (pBbE5c vector (a pET22b[+] derivative)) (Haushalter et al., 2014)
Competent *E. coli* expressing phosphopantetheine transferase (Sfp), prepared per New England Biolabs (NEB) protocol "Making your own electrocompetent cells" https://www.neb.com/protocols/2012/06/21/making-your-own-electrocompetent-cells
Chloramphenicol
Sterile Luria-Bertani (LB) growth medium
Ultra-pure water, nuclease free
Phenylmethylsulfonyl fluoride (PMSF)
Tris base (Tris(hydroxymethyl)aminomethane)
Tris hydrochloride
NaCl
HEPES sodium salt
HEPES
Dithiothreitol (DTT)
Isopropyl 1-thio-D-galactopyranoside (IPTG)
β-mercaptoethanol (BME)
Lysozyme
Protease inhibitor cocktail (SigmaFast®)
Amicon Ultra-4, 100 kDa molecular weight limit (Merck Millipore)
500 mM EDTA, pH 8.0, nuclease free (Invitrogen)
HisPur™ Ni-NTA Spin Purification Kit, 0.2 mL (Thermo Scientific)
Dialysis cassettes (Slide-A-Lyzer MINI, 20 kDa, Thermo Scientific)
Incubator-shaker
Refrigerated microcentrifuge

Superose 6 10/300 GL column, GE Healthcare,
Size exclusion chromatography buffer: 100 mM Na_2HPO_4/NaH_2PO_4 pH 7.4, 100 mM NaCl
Mini-PROTEAN TGX Stain-Free Precast Gel (Bio-Rad)

Measurement of cgFAS activity by NADPH consumption assay
Plate reader
Nicotinamide adenine dinucleotide phosphate (NADPH)
Ultra-pure water, nuclease free
NaH_2PO_4/Na_2HPO_4 buffer
Tris(2-carboxyethyl)phosphine (TCEP)
cgFAS protein
Acetyl-coenzyme A (Acetyl-CoA)
Malonyl-coenzyme A (Malonyl-CoA)

GC-MS analysis of fatty acid methyl esters (FAME) derived from cgFAS reactions
GC-MS system
Helium
Refrigerated microcentrifuge
1 M HCl in methanol
Hexanes

HPLC-MS quantification of palmitoyl-CoA produced by cgFAS
HPLC-MS system
trimethylamine
acetic acid
HPLC grade water
HPLC grade acetonitrile
Refrigerated microcentrifuge

4.1.4 Protocols

4.1.4.1 Expression and purification of cgFAS

This protocol outlines a brief procedure for expressing and purifying His_6-tagged cgFAS. Although this method has been reproduced several times, alternative lysis strategies and different lysis or purification buffers are expected to yield similar results. The purified cgFAS should be stored in aliquots at −80 °C, as storage at −20 °C, even in glycerol stocks, can compromise its activity. Corynebacteria encode two type I fatty acid synthases, FAS I-A and FAS I-B (Radmacher et al., 2005). FAS I-A supplies the majority of cellular fatty acids and is essential, whereas FAS I-B primarily produces palmitoyl-CoA. The protocol below was optimized for FAS I-B.

Type I bacterial FASs requires activation by an external Sfp that adds a phosphopantetheine arm onto a conserved serine residue of the enzyme. For this reason, an *E. Coli* strain expressing Sfp is necessary for the expression of active cgFAS (Haushalter et al., 2014).

1. Transform the cgFAS encoding plasmid into the competent, Sfp-expressing *E. coli* cells and grow them overnight at 37 °C in LB broth containing 0.1 mg/mL of chloramphenicol.
2. Inoculate 1 L of freshly autoclaved LB medium containing 0.1 mg/mL of chloramphenicol with 1 mL of the overnight culture. The rest of the overnight culture can be stored in 25 % glycerol at –80 °C.
3. Grow the culture at 37 °C in a shaker-incubator to an OD_{600} of 0.6.
4. Add 1 mL of a 1 M IPTG aqueous stock solution to induce the overexpression of cgFAS.
5. Grow the cells for 16 h at 18 °C, then harvest them by centrifuging at 6000 rcf for 20 min at 4 °C.
6. Resuspend the pellets by vortexing in 10 mL of lysis buffer containing 25 mM Tris buffer, pH 8.0, 0.5 M NaCl, 2 mM β-mercaptoethanol, 1 mg/mL lysozyme and protease inhibitors cocktail (SigmaFast®).
7. Following cell lysis by an ultrasonicator probe, remove cell debris by centrifuging (13,000 rcf, 20 min, 4 °C).
8. Incubate the supernatant in a gravity column with Ni^{2+}-nitrilo-triacetate (Ni-NTA) agarose resin pre-equilibrated with lysis buffer containing 10 mM imidazole on a shaker table for 3 h at 4 °C.
9. Discard the flow-through and wash the resin twice using 10 mL lysis buffer containing 20 mM imidazole for the first wash and 50 mM imidazole for the second.
10. Elute the His_6-tagged cgFAS with a 250 mM imidazole solution.
11. Concentrate the combined elutions using a centrifugal filter with a 100 kDa nominal molecular weight limit.
12. Further purify the sample by size exclusion chromatography.
13. Pool fractions containing cgFAS, concentrate, adjust to a final protein concentration of 1 μM in storage buffer with 10 % glycerol, aliquot, and store at –80 °C.

4.1.4.2 Measurement of cgFAS activity by NADPH consumption assay

This method provides a standardized NADPH consumption fluorescence assay to quantify the enzymatic activity of cgFAS. The assay monitors NADPH oxidation by measuring fluorescence emission at 470 nm, after

excitation at 340 nm. It was optimized for purified FAS I-B but may be adapted to related FAS enzymes.

1. Prepare a 45 µL pre-reaction mix per well by combining 30 µL of 100 mM NaH_2PO_4/Na_2HPO_4 buffer (pH 7.4, containing 10 mM TCEP), 5 µL acetyl-CoA (1 mM water stock), 5 µL NADPH (10 mM water stock) and 5 µL cgFAS (1 µM in elution buffer).
2. Record baseline fluorescence (ex 340 nm, em 470 nm) using a plate reader.
3. Start the reaction by adding 5 µL malonyl-CoA (7 mM water stock) and monitor fluorescence emission for 1 h.
4. As a control, set up the reaction as above but omit cgFAS and add elution buffer instead.
5. Subtract non-specific signal decay from each trace.
6. Generate an NADPH calibration curve to determine the amount of NADPH consumed.

4.1.4.3 GC-MS analysis of fatty acid methyl esters (FAME) derived from cgFAS reactions

To determine the chemical identity and relative abundance of fatty acids produced, the cgFAS reaction products are converted into fatty acid methyl ester (FAME) and subjected to GC-MS analysis. In the case of cgFAS I-B, the major peak is expected to be methyl palmitate (~93 %), alongside methyl stearate (~4 %) and other additional minor products.

1. Centrifuge the reaction mixture to remove protein debris.
2. Resuspend the sample in 300 µL of 1 M HCl in methanol and incubate at 65 °C for 30 min
3. Extract the FAMEs using 300 µL hexanes.
4. Analyze the extracted FAMEs by GC-MS.

Tip: The peak identity can be further confirmed by comparison to a FAME standard prepared from commercially available palmitoyl-CoA.

4.1.4.4 HPLC-MS quantification of palmitoyl-CoA product

Palmitoyl-CoA quantification is performed by HPLC-MS analysis with an Eclipse Plus C8 analytical column, using a 10 mM triethylamine/acetic acid aqueous solution adjusted at pH 9.0 (phase A) and acetonitrile (phase B) as the mobile phases. A multistep gradient is applied at a flow rate of 0.25 mL/min, starting with 7 % Phase B, increasing linearly to 60 % at 6 min, to 70 % at 9.5 min, and to 90 % at 10 min. Product quantification is performed by integrating peaks from the UV trace at 205 nm.

1. Withdraw a 10 μL aliquot of the reaction mixture.
2. Centrifuge to remove protein debris and transfer the clear supernatant to an HPLC vial.
3. Analyze the sample by HPLC-MS, monitoring elution with UV detection at 205 nm for product quantification.

4.2 Chemical phase: Acylation of cysteine-modified lysophospholipids with acyl-CoAs

4.2.1 Definition

Synthesizing phospholipids by chemical acylation of cysteine-modified lysophospholipids with long-chain thioesters.

4.2.2 Rationale

The chemical phase demonstrates that cysteine-modified lysophospholipids undergo acyl transfer under water-compatible conditions and provides a direct, chemistry-only readout of product formation independent of enzymatic steps, allowing the qualitative and quantitative evaluation of reaction kinetics and yield of the chemical step.

4.2.3 Materials, equipment, and reagents

4.2.3.1 Acylation of cysteine-modified lysophospholipids

Palmitoyl-CoA (Sigma Aldrich)
Cys-modified lysophospholipid
NaH_2PO_4/Na_2HPO_4 buffer
TCEP (Sigma Aldrich)
HPLC grade water
HPLC grade acetonitrile
HPLC grade methanol
Formic acid
Ultra-pure water, nuclease free
Trimethylamine
acetic acid
acetonitrile
HPLC-MS

4.2.4 Protocols

4.2.4.1 Acylation of cysteine-modified lysophospholipids

This method describes the phospholipid formation reaction performed by directly combining commercially available palmitoyl-CoA with cysteine-functionalized lysophospholipids in aqueous phosphate buffer

(pH 7.4, containing TCEP) at 37 °C, where the thioester functionality of palmitoyl-CoA reacts with the cysteine moiety under NCL conditions to yield the corresponding phospholipid. Although optimized using lysophospholipid **2** (Fig. 2), the method is expected to yield comparable results with other lysophopholipids used as starting materials. When adapting this aqueous acylation to other starting materials, potential shifts in the cysteine thiol pK_a should be considered. Substituents can shift the pK_a relative to free cysteine, substantially affecting reaction conversion. If low yield is observed with a new substrate, raising the pH may improve conversion. However, acyl-CoA thioester stability should be monitored to ensure that the increased pH does not promote acyl-CoA hydrolysis.

1. Prepare a 50 μL reaction by combining 5 μL palmitoyl-CoA (10 mM aqueous stock), 5 μL lysophospholipid **2** (10 mM aqueous stock) and 40 μL 100 mM NaH_2PO_4/Na_2HPO_4 pH 7.4 containing 10 mM TCEP.
2. Mix by gentle tapping and tumble the reaction mixture at 37 °C.
3. Analyze the sample by HPLC-MS, monitoring elution with UV detection at 205 nm.

Tip: Consider preparing the phospholipid product by chemical synthesis to serve as a standard (Khanal et al., 2021) The standard can be used to confirm product identity by comparing the HPLC-MS retention time and to generate a calibration curve for quantifying the NCL product.

4.3 Chemoenzymatic one-pot phospholipid formation mediated by cgFAS

4.3.1 Definition

Synthesizing phospholipids in one-pot by generating palmitoyl-CoA in situ with cgFAS and coupling it to cysteine-modified lysophospholipids.

4.3.2 Rationale

Combining the enzymatic generation of acyl-CoAs with the subsequent chemical acylation of cysteine-modified lysophospholipids in a single reaction vessel enables a direct test of reaction compatibility and efficiency. This approach allows kinetic and quantitative analysis of phospholipid formation, providing a clear measure of how well the enzymatic and chemical phases operate together under conditions relevant to the intended application.

4.3.3 Materials, equipment, and reagents

The materials, equipment, and reagents are the same as those listed in Sections 4.1 and 4.2, unless otherwise stated.

4.3.4 Protocols

One-pot chemoenzymatic synthesis of phospholipid.

This method outlines a one-pot chemoenzymatic route in which cgFAS synthesizes palmitoyl-CoA in situ, and the freshly produced acyl donor is directly captured by cysteine-functionalized lysophospholipids to produce the target phospholipids. The enzymatic and chemical steps proceed in the same reaction conditions (aqueous phosphate buffer at pH 7.4, 37 °C, in the presence of TCEP). The procedure was optimized using lysophospholipid **2**, and is expected to be transferable to other cysteine-modified lysophospholipids and to alternative acyl-CoA donors.

1. Add 2 μL lysophospholipid **2** (10 mM aqueous stock) to 33 μL 100 mM NaH_2PO_4/Na_2HPO_4 buffer pH 7.4 containing 10 mM TCEP, then add 5 μL acetyl-CoA (10 mM aqueous stock), 5 μL NADPH (100 mM aqueous stock), and 5 μL cgFAS (1 μM in elution buffer).
2. Add 5 μL of 70 mM malonyl-CoA (in sterile H_2O), and mix the solution by gentle tapping.
3. Tumble the reaction mixture at 37 °C.
4. Analyze the sample by HPLC-MS using an Eclipse Plus C8 analytical column, using water with 0.1 % formic acid (phase A) and methanol with 0.1 % formic acid (phase B) as the mobile phases. A multistep gradient is applied at a flow rate of 0.25 mL/min, starting with 5 % Phase B, increasing linearly to 50 % at 7 min, then to 70 % at 10 min, and to 95 % until 14 min runtime. Product quantification is performed by integrating peaks from the UV trace at 205 nm. For sample preparation:
   - Withdraw a small aliquot (10 μL) of the reaction mixture.
   - centrifuge to remove protein debris before injecting into the HPLC-MS.

Note: Validation in the presence of several additives such as cholesterol, guanidine hydrochloride (GuHCl) and 1-decanol showed that phospholipid formation proceeds reliably also in the presence of other amphiphilic molecules. However, different additives can alter the morphology, size and stability of the membranes formed, therefore the formulation should be optimized when translating the method to specific applications.

4.4 Vesicular phase: Characterization of de novo generated lipid membranes

4.4.1 Definition

Characterizing the membrane structure assembled from the synthesized phospholipids, including morphology and structural integrity analysis.

4.4.2 Rationale

Characterizing the assemblies formed from lipids generated de novo determines whether the synthetic products can self-assemble into stable bilayer membranes. These analyses are essential for evaluating the functional relevance of the synthetic pathway and for establishing suitability for biochemical or synthetic biology applications.

4.4.3 Materials, equipment, and reagents

Phospholipid hydration under standardized conditions
Purified phospholipid
$CHCl_3$
MeOH
Hydration buffer
Vial shaker
Light microscopy
Microscopy glass slides (Fisher brand)
Coverslips (Fisher brand)
Bright field light microscope
Nile Red (Sigma Aldrich)
Texas Red® 1,2-dihexadecanoyl-*sn*-glycero-3-phosphoethanolamine, triethylammonium salt (Texas Red® DHPE) (Life Technologies)
18:1 PE-TopFluor™ AF488 (Avanti Research)
18:1 PE-TopFluor™ AF594 (Avanti Research)
8-hydroxypyrene-1,3,6-trisulfonic acid (HPTS)
Confocal fluorescence microscope
Sephadex G-50 columns
Cryo-electron microscopy
Lacey Carbon grids
Glow-discharger
Vitrobot (Thermo Fisher Scientific)
Ethane
Liquid nitrogen
Cryo-electron microscope

4.4.4 Protocol

4.4.4.1 Phospholipid hydration under standardized conditions

This method provides a route to hydrate the final synthesized phospholipid and generate bilayer assemblies that function as reference samples for comparison with de novo formed membranes.

1. Pipette an appropriate volume of phospholipid stock dissolved in a volatile organic solvent such as chloroform or a chloroform/methanol mixture into a clean glass vial. The lipid amount should be chosen according to the intended final concentration.
2. Evaporate the solvent under a gentle stream of nitrogen or argon while rotating the vial to form a thin uniform lipid film on the glass wall.
3. Place the sample under high vacuum to remove the organic solvent completely.
4. Add buffer to reach the target lipid concentration.
5. Allow the film to swell without agitation for five minutes.
6. Gently tumble, rotate, or intermittently vortex until no visible dry film remains. The duration depends on lipid composition and temperature and typically ranges from 30 min to several hours.

4.4.4.2 Light microscopy

Light microscopy provides visualization of vesicle morphology and dynamics, enabling classification of micron-scale morphologies including vesicles, tubules, and sheets. It is well suited to time-lapse monitoring of de novo membrane formation, allowing correlation of reaction kinetics with membrane assembly kinetics. It also supports quantification of vesicle counts and size distributions and the observation of dynamic events such as coalescence, budding, tubulation, pearling, fusion, and vesicle rupture. Two complementary light-microscopy modalities, bright-field and confocal fluorescence imaging are commonly employed to visualize lipid assemblies.

Bright-field microscopy provides a label-free survey of lipid assembly populations and is ideal for tracking bulk morphological changes and dynamic events at the micron scale. Samples are prepared as follows:

1. Place the clean microscope glass slide (Fisher brand) on a flat surface.
2. Pipette 1–3 μL of the lipid dispersion onto the slide center.
3. Lower a coverslip (Fisherbrand) gently at 45° to the drop to displace air and avoid the presence of bubbles in the sample.
4. Do not press the coverslip down. Squeezing can disrupt the lipid assemblies and generate artifacts.
5. For long imaging sessions, seal the coverslip edges with a sealant to avoid solvent evaporation.

Tip: A spacer can be used to prevent mechanical compression of the lipid assemblies and to maintain a consistent liquid thickness.

Confocal fluorescence microscopy provides three-dimensional, molecule-specific imaging that resolves overlapping vesicles, maps internal

membrane topology, and supports quantitative fluorescence assays of membrane behavior. It enables dye influx assays to probe permeability and membrane integrity, and fluorescence recovery after photobleaching (FRAP) to quantify lateral mobility and membrane fluidity (Pincet et al., 2016). A fluorescent dye is required to visualize lipid assemblies. Hydrophobic probes partition into the bilayer, thereby providing clear contrast that delineates membranes. Commonly used hydrophobic probes include solvatochromic dyes such as Nile Red and membrane anchored fluorescent lipids such as Texas Red® DHPE, 18:1 PE-TopFluor™ AF488, and 18:1 PE-TopFluor™ AF594. A typical staining concentration is between 0.01 and 0.1 mol% relative to the total lipid. Different dyes exhibit distinct excitation and emission wavelengths, and when multiple dyes are used their spectral properties must be considered when selecting illumination sources, filter sets, and detectors to ensure adequate excitation and to minimize spectral overlap that would compromise image quality.

To stain membranes produced by the phospholipid hydration method described above, an appropriate amount of hydrophobic fluorescent probe is added from a stock solution in organic solvent together with the main lipid during film formation. During de novo membrane formation, addition of hydrophobic fluorescent probes prior to or during the reaction is not feasible because, in the absence of pre-existing lipid structures, the probe may self-aggregate or form non-membranous structures. Consequently, the hydrophobic fluorescent probe should be introduced only after the synthetic reaction has been completed. A concentrated stock of the probe should be prepared in an organic solvent fully miscible with the aqueous reaction buffer, for example methanol or ethanol, and a minimal volume of this stock should be added so that the final solvent concentration is kept as low as possible, typically below 0.5–1.0 % v/v, to avoid perturbation of assembled membranes or enzyme activity. The sample should be allowed to rest for at least 10 min to permit intercalation of the probe into the bilayer and to establish stable staining.

Hydrophilic dyes may be encapsulated to assess entrapment efficiency and to evaluate membrane permeability. The pH sensitive dye 8-hydroxypyrene-1,3,6-trisulfonic acid (HPTS) is commonly employed for this purpose. For HPTS the usable range is broad and may span from $<50\ \mu M$ to >5 mM, depending on the microscope sensitivity and detector saturation. A typical dye encapsulation protocol is as follows.

1. Prepare hydration or reaction buffer containing the hydrophilic dye at the target concentration.

2. For rehydrated phospholipid membranes, hydrate the lipid film as described in the phospholipid hydration protocol above, then proceed with the remaining steps. For de novo formed membranes, use the reaction buffer containing the dye during synthesis and allow assemblies to form.
3. Remove external non-encapsulated dye by size-exclusion chromatography, using Sephadex G-50 or G-25.
4. Samples can be prepared as described above for bright-field microscopy but using another coverslip instead of the microscope glass slide.

Note: Size exclusion chromatography is recommended as the fastest effective method to remove non-encapsulated dye. If vesicles are too fragile to tolerate centrifugation or other manipulations, dialysis against a large buffer volume with multiple exchanges is a gentle alternative. When vesicles cannot withstand any separation method, a tenfold dilution of the sample may create a concentration contrast that is visible by microscopy. Diluting the sample lowers the concentration of free dye in the external medium while dye entrapped within intact vesicles should remain at the intravesicular concentration.

4.4.4.3 Cryo-electron microscopy

Cryo-electron microscopy (cryo-EM) provides label-free, near-native imaging of membrane assemblies with nanometer scale resolution, enabling direct visualization of bilayer thickness, lamellarity, curvature, internal contents, and protein-membrane associations (Friedrich et al., 2010; Heberle et al., 2020; Kuntsche et al., 2011). Contrast in cryo-EM is generated by electron scattering, and therefore no fluorescent dye is required. Sample preparation for cryo-EM requires that vitrified, thin aqueous films be produced on appropriately prepared grids. Detailed cryo-EM imaging parameters and data processing are beyond the scope of this manuscript. We therefore limit the procedural notes to practical considerations for vitrification of lipid membranes, because specimen preparation critically determines particle retention, morphology, and size-dependent sampling bias during imaging.

Suggested step-by-step vitrification workflow.

1. Prepare grids (Lacey Carbon) by glow discharge prior to sample application. For optimal results, the sample should be loaded onto the grids within 45 min from completing glow discharge.
2. Apply 3-4 μL of sample to the grid in a 99 % humidity and 4 °C controlled plunge freezer. Sample concentration should be above 1 mM.

3. Blot the grid to achieve thin vitreous ice. Optimal blot force and the blotting time depends on the nature of the sample.
4. Plunge the grid into liquid ethane cooled by liquid nitrogen and transfer to liquid nitrogen for storage.
5. Analyze the sample by cryo-EM.

Note: The size of membrane assemblies produced de novo commonly spans from around 50 nm to several μm. Because cryo-EM requires vitrified ice not to exceed 400 nm in thickness, cryo-EM preferentially captures the nanometer scale fraction of a heterogeneous sample, with larger particles being underrepresented in cryo-EM images.

4.5 Safety considerations and standards

Follow the standard safety guidelines when dealing with biological samples including wearing appropriate PPE.

5. Conclusion and outlook

This work presents a procedure for the de novo chemoenzymatic construction of lipid membranes that combines enzymatic selectivity with chemical simplicity. It couples in situ generation of palmitoyl-CoA by cgFAS with NCL of cysteine-modified lysophospholipids to produce non-canonical amidophospholipids that spontaneously assemble into bilayers. The significance is both methodological and conceptual. The workflow recreates central steps of lipid biogenesis from simple metabolites, remains modular and quantitatively verifiable, and operates in a single aqueous buffer at physiological temperature. Compared with purely chemical routes, this methodology operates in buffered aqueous media at mild temperature, accepts simple metabolites and reduces side reactions. Compared with fully enzymatic reconstitution, it avoids complex membrane protein assemblies. Furthermore, it remains modular, with the enzymatic and chemical phases that can be validated and optimized independently. Importantly, the same framework can be extended to fully de novo synthesis of diacyl lipids in which both alkyl chains are produced in situ and installed under the same conditions, thereby broadening chemical scope and strengthening the connection between composition, mechanical properties, and function. This capability offers a tractable route to interrogate membrane growth and protein compatibility in cell-free settings, and it supplies a practical basis for studies that build cellular features from the bottom-up.

Declaration of generative AI and AI-assisted technologies in the writing process

During the preparation of this work the authors used ChatGPT 5.0 to edit and proofread the final draft. After using this service, the authors reviewed and edited the content as needed and take full responsibility for the content of the publication.

References

Athenstaedt, K., & Daum, G. (1999). Phosphatidic acid, a key intermediate in lipid metabolism. *European Journal of Biochemistry/FEBS, 266*(1), 1–16.

Bailoni, E., Partipilo, M., Coenradij, J., Grundel, D. A. J., Slotboom, D. J., & Poolman, B. (2023). Minimal out-of-equilibrium metabolism for synthetic cells: A membrane perspective. *ACS Synthetic Biology, 12*(4), 922–946.

Bhattacharya, A., Brea, R. J., Niederholtmeyer, H., & Devaraj, N. K. (2019). A minimal biochemical route towards de novo formation of synthetic phospholipid membranes. *Nature Communications, 10*(1) Article 1.

Bhattacharya, A., Cho, C. J., Brea, R. J., & Devaraj, N. K. (2021). Expression of fatty acyl-CoA ligase drives one-pot de novo synthesis of membrane-bound vesicles in a cell-free transcription-translation system. *Journal of the American Chemical Society, 143*(29), 11235–11242.

Bhattacharya, A., Tanwar, L., Fracassi, A., Brea, R. J., Salvador-Castell, M., Khanal, S., ... Devaraj, N. K. (2023). Chemoselective esterification of natural and prebiotic 1,2-amino alcohol amphiphiles in water. *Journal of the American Chemical Society, 145*(49), 27149–27159.

Blanken, D., Foschepoth, D., Serrão, A. C., & Danelon, C. (2020). Genetically controlled membrane synthesis in liposomes. *Nature Communications, 11*(1), 4317.

Blobel, G. (1980). Intracellular protein topogenesis. *Proceedings of the National Academy of Sciences, 77*(3), 1496–1500.

Brea, R. J., Cole, C. M., & Devaraj, N. K. (2014). In situ vesicle formation by native chemical ligation. *Angewandte Chemie International Edition, 53*(51), 14102–14105.

Brea, R. J., Rudd, A. K., & Devaraj, N. K. (2016). Nonenzymatic biomimetic remodeling of phospholipids in synthetic liposomes. *Proceedings of the National Academy of Sciences, 113*(31), 8589–8594.

Budin, I., & Devaraj, N. K. (2012). Membrane assembly driven by a biomimetic coupling reaction. *Journal of the American Chemical Society, 134*(2), 751–753.

Chen, J., Brea, R. J., Fracassi, A., Cho, C. J., Wong, A. M., Salvador-Castell, M., ... Devaraj, N. K. (2024). Rapid formation of non-canonical phospholipid membranes by chemoselective amide-forming ligations with hydroxylamines. *Angewandte Chemie International Edition, 63*(1), e202311635.

Chen, P.-H. B., Li, X.-L., & Baskin, J. M. (2025). Synthetic lipid biology. *Chemical Reviews, 125*(4), 2502–2560.

Cho, C. J., An, T., Lai, Y.-C., Vázquez-Salazar, A., Fracassi, A., Brea, R. J., ... Devaraj, N. K. (2025). Protocells by spontaneous reaction of cysteine with short-chain thioesters. *Nature Chemistry, 17*(1), 148–155.

Cole, C. M., Brea, R. J., Kim, Y. H., Hardy, M. D., Yang, J., & Devaraj, N. K. (2015). Spontaneous reconstitution of functional transmembrane proteins during bioorthogonal phospholipid membrane synthesis. *Angewandte Chemie International Edition, 54*(43), 12738–12742.

Devaraj, N. K. (2017). In situ synthesis of phospholipid membranes. *The Journal of Organic Chemistry, 82*(12), 5997–6005.

Eto, S., Matsumura, R., Shimane, Y., Fujimi, M., Berhanu, S., Kasama, T., & Kuruma, Y. (2022). Phospholipid synthesis inside phospholipid membrane vesicles. *Communications Biology, 5*(1), 1–11.

Exterkate, M., Caforio, A., Stuart, M. C. A., & Driessen, A. J. M. (2018). Growing membranes in vitro by continuous phospholipid biosynthesis from free fatty acids. *ACS Synthetic Biology, 7*(1), 153–165.

Exterkate, M., & Driessen, A. J. M. (2019). Continuous expansion of a synthetic minimal cellular membrane. *Emerging Topics in Life Sciences, 3*(5), 543–549.

Flores, J., Brea, R. J., Lamas, A., Fracassi, A., Salvador-Castell, M., Xu, C., ... Devaraj, N. K. (2022). Rapid and sequential dual oxime ligation enables de novo formation of functional synthetic membranes from water-soluble precursors. *Angewandte Chemie International Edition, 61*(29), e202200549.

Flores, J., White, B. M., Brea, R. J., Baskin, J. M., & Devaraj, N. K. (2020). Lipids: Chemical tools for their synthesis, modification, and analysis. *Chemical Society Reviews, 49*(14), 4602–4614.

Fracassi, A., Seoane, A., Brea, R. J., Lee, H.-G., Harjung, A., & Devaraj, N. K. (2025). Abiotic lipid metabolism enables membrane plasticity in artificial cells. *Nature Chemistry, 17*(6), 799–807.

Friedrich, H., Frederik, P. M., de With, G., & Sommerdijk, N. A. J. M. (2010). Imaging of self-assembled structures: Interpretation of TEM and Cryo-TEM Images. *Angewandte Chemie International Edition, 49*(43), 7850–7858.

Harjung, A., Fracassi, A., & Devaraj, N. K. (2024). Encoding extracellular modification of artificial cell membranes using engineered self-translocating proteins. *Nature Communications, 15*(1), 9363.

Haushalter, R. W., Kim, W., Chavkin, T. A., The, L., Garber, M. E., Nhan, M., ... Keasling, J. D. (2014). Production of anteiso-branched fatty acids in *Escherichia coli*; next generation biofuels with improved cold-flow properties. *Metabolic Engineering, 26*, 111–118.

Heberle, F. A., Doktorova, M., Scott, H. L., Skinkle, A. D., Waxham, M. N., & Levental, I. (2020). Direct label-free imaging of nanodomains in biomimetic and biological membranes by cryogenic electron microscopy. *Proceedings of the National Academy of Sciences, 117*(33), 19943–19952.

Holthuis, J. C. M., & Menon, A. K. (2014). Lipid landscapes and pipelines in membrane homeostasis. *Nature, 510*(7503), 7503 (Article).

Ji, P., Harjung, A., Knittel, C. H., Fracassi, A., Chen, J., Brea, R. J., & Devaraj, N. K. (2025). Photochemical synthesis of natural lipids in artificial and living cells. *Nature Communications, 16*(1), 5068.

Justice, I., Kiesel, P., Safronova, N., von Appen, A., & Saenz, J. P. (2024). A tuneable minimal cell membrane reveals that two lipid species suffice for life. *Nature Communications, 15*(1), 9679.

Khanal, S., Brea, R. J., Burkart, M. D., & Devaraj, N. K. (2021). Chemoenzymatic generation of phospholipid membranes mediated by type I fatty acid synthase. *Journal of the American Chemical Society, 143*(23), 8533–8537.

Kobayashi, K., Jimbo, H., Nakamura, Y., & Wada, H. (2024). Biosynthesis of phosphatidylglycerol in photosynthetic organisms. *Progress in Lipid Research, 93*, 101266.

Kuntsche, J., Horst, J. C., & Bunjes, H. (2011). Cryogenic transmission electron microscopy (cryo-TEM) for studying the morphology of colloidal drug delivery systems. *International Journal of Pharmaceutics, 417*(1), 120–137.

Li, Z., Tang, Y., Wu, Y., Zhao, S., Bao, J., Luo, Y., & Li, D. (2017). Structural insights into the committed step of bacterial phospholipid biosynthesis. *Nature Communications, 8*(1), 1691.

Liu, L., Zou, Y., Bhattacharya, A., Zhang, D., Lang, S. Q., Houk, K. N., & Devaraj, N. K. (2020). Enzyme-free synthesis of natural phospholipids in water. *Nature Communications, 12*(11) Article 11.

Maier, T., Leibundgut, M., Boehringer, D., & Ban, N. (2010). Structure and function of eukaryotic fatty acid synthases. *Quarterly Reviews of Biophysics, 43*(3), 373–422.

Matsubayashi, H., Kuruma, Y., & Ueda, T. (2014). In vitro synthesis of the E. coli sec translocon from DNA. *Angewandte Chemie International Edition, 126*(29), 7665–7668.
van Meer, G., Voelker, D. R., & Feigenson, G. W. (2008). Membrane lipids: Where they are and how they behave. *Nature Reviews. Molecular Cell Biology, 9*(2) Article 2.
Pincet, F., Adrien, V., Yang, R., Delacotte, J., Rothman, J. E., Urbach, W., & Tareste, D. (2016). FRAP to characterize molecular diffusion and interaction in various membrane environments. *PLoS One, 11*(7), e0158457.
Podolsky, K. A., & Devaraj, N. K. (2021). Synthesis of lipid membranes for artificial cells. *Nature Reviews Chemistry,* 1–19.
Radmacher, E., Alderwick, L. J., Besra, G. S., Brown, A. K., Gibson, K. J. C., Sahm, H., & Eggeling, L. (2005). Two functional FAS-I type fatty acid synthases in Corynebacterium glutamicum. *Microbiology (Reading, England), 151*(7), 2421–2427.
Rock, C. O., Jackowski, S., & Cronan, J. E. (1996). Lipid metabolism in prokaryotes. In In. D. E. Vance, & J. E. Vance (Vol. Eds.), *New comprehensive biochemistry: 31*, (pp. 35–74). Elsevier.
Rudd, A. K., Mittal, N., Lim, E. W., Metallo, C. M., & Devaraj, N. K. (2020). A small molecule fluorogenic probe for the detection of sphingosine in living cells. *Journal of the American Chemical Society, 142*(42), 17887–17891.
Schoenmakers, L. L. J., den Uijl, M. J., Postma, J. L., van den Akker, T. A. P., Huck, W. T. S., & Driessen, A. J. M. (2024). SecYEG-mediated translocation in a model synthetic cell. *Synthetic Biology, 9*(1), ysae007.
Schweizer, E., & Hofmann, J. (2004). Microbial type I fatty acid synthases (FAS): Major players in a network of cellular FAS systems. *Microbiology and Molecular Biology Reviews: MMBR, 68*(3), 501–517.
Scott, A., Noga, M. J., Graaf, P. de, Westerlaken, I., Yildirim, E., & Danelon, C. (2016). Cell-free phospholipid biosynthesis by gene-encoded enzymes reconstituted in liposomes. *PLoS One, 11*(10), e0163058.
Shindou, H., & Shimizu, T. (2009). Acyl-CoA: Lysophospholipid acyltransferases. *The Journal of Biological Chemistry, 284*(1), 1–5.
Sohlenkamp, C., & Geiger, O. (2016). Bacterial membrane lipids: Diversity in structures and pathways. *FEMS Microbiology Reviews, 40*(1), 133–159.
Souto-Trinei, F. A., Portasany, B., & Brea, R. J. (2025). Chemical tools for the synthesis and application of artificial lipids. In A. Nag (Ed.). *Synthesis and applications of carbohydrates, lipids, and steroids*. CRC Press.
Vance, J. E. (2015). Phospholipid synthesis and transport in mammalian cells. *Traffic (Copenhagen, Denmark), 16*(1), 1–18.
Wang, B., & Tontonoz, P. (2019). Phospholipid remodeling in physiology and disease. *Annual Review of Physiology, 81*(1), 165–188.
Xiong, F., Lu, L., Sun, T.-Y., Wu, Q., Yan, D., Chen, Y., ... Zhao, J. (2017). A bioinspired and biocompatible ortho-sulfiliminyl phenol synthesis. *Nature Communications, 8*(1), 15912.
Yang, Y., Lee, M., & Fairn, G. D. (2018). Phospholipid subcellular localization and dynamics. *The Journal of Biological Chemistry, 293*(17), 6230–6240.
Yao, J., & Rock, C. O. (2013). Phosphatidic acid synthesis in bacteria. *Biochim. Biophys. Acta (BBA) - Molecular and Cell Biology of Lipids, 1831*(3), 495–502.
Zhang, Y.-M., & Rock, C. O. (2008). Membrane lipid homeostasis in bacteria. *Nature Reviews. Microbiology, 6*(3), 222–233.
Zhou, Y., Yang, H., Wang, C., Xue, Y., Wang, X., Bao, C., & Zhu, L. (2021). In situ formation of a biomimetic lipid membrane triggered by an aggregation-enhanced photoligation chemistry. *Chemical Science, 12*(10), 3627–3632.

CHAPTER TWO

Photoaffinity strategies to profile cholesterol metabolite interactomes and binding sites

Yu-Shiuan Cheng[a] and **Alison E. Ondrus**[a,b,*]
[a]Department of Chemistry, College of Liberal Arts and Sciences, University of Illinois Chicago, Chicago, IL, United States
[b]Department of Pharmaceutical Sciences, College of Pharmacy, University of Illinois Chicago, Chicago, IL, United States
*Corresponding author: e-mail address: aondrus@uic.edu

Contents

1. Introduction 24
2. Before you begin 28
3. Live cell photoaffinity crosslinking and click chemistry tagging 30
   3.1 Vehicle, probe, and/or competitor treatment, and photocrosslinking 31
   3.2 Subcellular fractionation 34
   3.3 Copper-catalyzed click tagging 36
   3.4 In-gel fluorescence visualization of probe crosslinked, fluorophore-tagged proteins 38
   3.5 Streptavidin enrichment of probe-crosslinked, biotin-tagged proteins 41
   3.6 Protein digestion and desalting 43
   3.7 TMT labeling and label efficiency check 46
   3.8 LC-MS^3 analysis 48
   3.9 Data analysis notes 49
4. Binding site identification 50
   4.1 Transfection, live cell compound treatment, and photoaffinity crosslinking 50
   4.2 Cell lysis and target protein immunoprecipitation 52
   4.3 S-Trap protein digestion and desalting 55
   4.4 LC-MS analysis 57
   4.5 Data analysis notes 58
5. Discussion 61
Acknowledgments 61
References 61

Abstract

Cholesterol and its metabolites regulate diverse and essential roles in biological systems and feature prominently in human health and disease. Key to the activity of these molecules are the proteins that they interact with in a given cell type and

Methods in Enzymology, Volume 728
ISSN 0076-6879, https://doi.org/10.1016/bs.mie.2026.01.002
Copyright © 2026 Elsevier Inc. All rights are reserved, including those for text and data mining, AI training, and similar technologies.

condition. In this Chapter, we describe the use of chemical photoaffinity probes to map the interactome of cholesterol metabolites throughout the proteome and to pinpoint the site of binding within a protein of interest. We pay close attention to variables that influence the study of cholesterol-based molecules, describing experimental and data analysis parameters to optimize proteome/binding site coverage and robustness of results.

1. Introduction

Cholesterol is a major component of eukaryotic cell membranes and a diverse scaffold for molecular recognition. In mammalian cells, cholesterol is maintained at specific levels in different cell membranes to sustain essential processes in lipid homeostasis, shape organelle ultrastructure, and maintain cholesterol-responsive signaling pathways. Cholesterol distribution is also highly heterogenous within a given membrane, where regions of high local cholesterol organize nano-to-microscale domains that coordinate membrane protein interactions. At the same time, cholesterol is an exemplar of molecular complexity within the mammalian lipidome, enabling it to engage in nuanced cholesterol-protein interactions and providing a template for metabolites to convey important signaling information.

Studying the live cell interactions of a cholesterol metabolite is a formidable challenge. Photoaffinity labeling using functionalized analogs of the cholesterol metabolite of interest remains the only unbiased method to identify direct physical interactions throughout the proteome. This method is now well established, and several excellent reviews on its principles and applications are available (Burton, Kim, & Backus, 2021; Homan et al., 2024; West & Woo, 2022; Yu & Baskin, 2022). When performing photoaffinity labeling to identify the interactome of a small molecule, including a cholesterol metabolite, we consider two variables paramount: photoaffinity probe design and live cell crosslinking. The structure of the photoaffinity probe necessarily differs from the native metabolite, as it must incorporate functional groups for photocrosslinking and click-based tagging of protein interactors. We have typically selected diazirines for photoaffinity crosslinking and terminal alkynes for click chemistry-based tagging due to their small size and non-polar nature. The position at which these functionalities are added to the metabolite structure are also critical. To preserve native-like interactions, it is necessary for the probe to maintain key chemical elements that influence protein and/or membrane interactions. For cholesterol, the free C3-OH often engages in polar contacts with protein residues and/or

lipid headgroups, the C5-C6 double bond may participate in pi stacking interactions with aromatic residues in proteins, and the iso-octyl tail establishes hydrophobic interactions with binding site residues and fatty acid tails of membrane lipids. The molecular shape of the probe should also match the native cholesterol metabolite- namely the stereochemistry at ring junctions should be preserved to maintain the "flat" or "bent" tetracyclic structure of the native sterol (e.g., as in cholesterol or lithocholic acid, respectively) (Fig. 1). The length, steric bulk, and hydrophobicity of the iso-octyl tail should also be maintained to preserve native protein and membrane lipid interactions. At the same time, the diazirine and alkyne functional groups must be internally compatible (e.g., positioned to avoid intramolecular reactivity), positioned appropriately for protein contacts (e.g., with the diazirine placed as close as possible to potential residue interactions without sterically impeding binding), and accessible for click modification (e.g., terminal alkynes are more accessible for copper-catalyzed click reactions than internal alkynes). If available, the use of multiple probes for a given metabolite with alternatively positioned bioorthogonal groups can help to identify the broadest possible set of protein interactors. If multiple probes are unavailable, competition experiments with the native metabolite and specific constitutional, stereo-, or regio-isomers can be used to identify structure-selective, competable protein interactions.

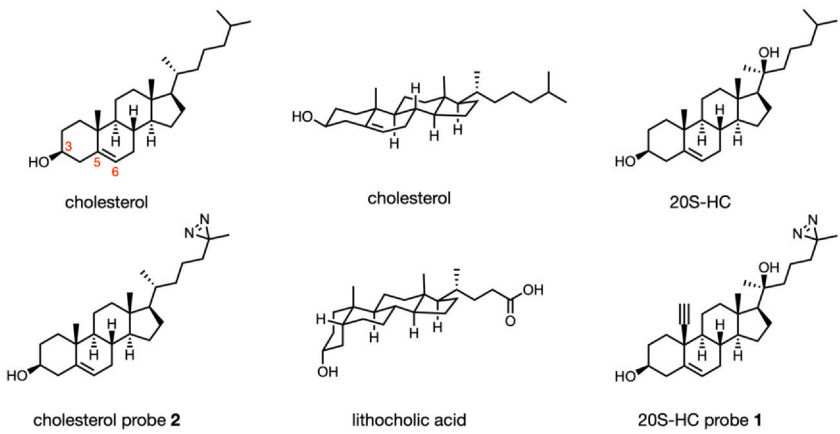

Fig. 1 Structures of cholesterol metabolites and probes used in this protocol. Left, from top to bottom: cholesterol and monofunctional cholesterol probe **2** (Mafi et al., 2021). Middle, from top to bottom: structures depicting differences in 3D architecture between cholesterol and the metabolite lithocholic acid. Right, from top to bottom: 20(*S*)-hydroxycholesterol (20S-HC) and 20S-HC probe **1** (Cheng et al., 2021).

Beyond careful selection/design of probe structure, the nature of cholesterol metabolite molecules brings additional challenges to target protein identification. Most cholesterol metabolites are hydrophobic and interact disproportionately with membrane proteins. The structural integrity of these proteins, their localization, local concentration, and participation in protein complexes heavily rely on a native membrane environment. As a result, live cell crosslinking is essential to preserving cholesterol metabolite-binding protein conformations and contexts that may be critical for native cellular functions.

Cholesterol metabolites differ from other small molecule ligands in several ways that also attenuate peptide yield in bottom-up proteomics; first, native metabolites engage in a broad range regulatory interactions, for example, with biosynthetic enzymes, proteins in organelles with a specific membrane cholesterol content, proteins that preferentially reside in high-cholesterol microdomains or interact with other proteins in such domains, and so forth. A consequence of this broad, multifaceted set of interactions is that cholesterol metabolites generally show a wide protein interactome that lacks the specificity of a synthetic ligand but nonetheless reflects a subset of functionally relevant contacts. This results in a distributed dataset with a lower proportion of clear "hits" in terms of affinity and a number of interactions whose functional significance is not directly proportional to fold change over vehicle. Robust statistical analysis therefore relies on sufficient peptides from multiple targets over multiple replicates to identify reproducible hits that may be worth pursuing. The hydrophobicity of most cholesterol metabolites and their protein targets also leads to challenges with wash and elution stringencies to balance non-specific adhesion of *bona fide* targets and contaminants to affinity resins, lower overall proportions of arginine and lysine residues for trypsin cleavage, altered chromatographic properties relative to soluble peptides, and potentially low ionization efficiency on the mass spectrometer, among other considerations, including the intrinsically low yield of diazirine crosslinking (estimated to be below 25 %, (MacKinnon, Garrison, Hegde, & Taunton, 2007)). Beyond experimental optimization, these considerations directly influence data analysis strategies, as discussed in Section 3.9 and Section 4.6.

Despite these challenges, live cell photoaffinity labeling with cholesterol metabolite probes remains a gold standard for direct, unbiased identification of protein interactions. Rationally designed probe structures, careful optimization of experimental conditions, and inclusion of multiple

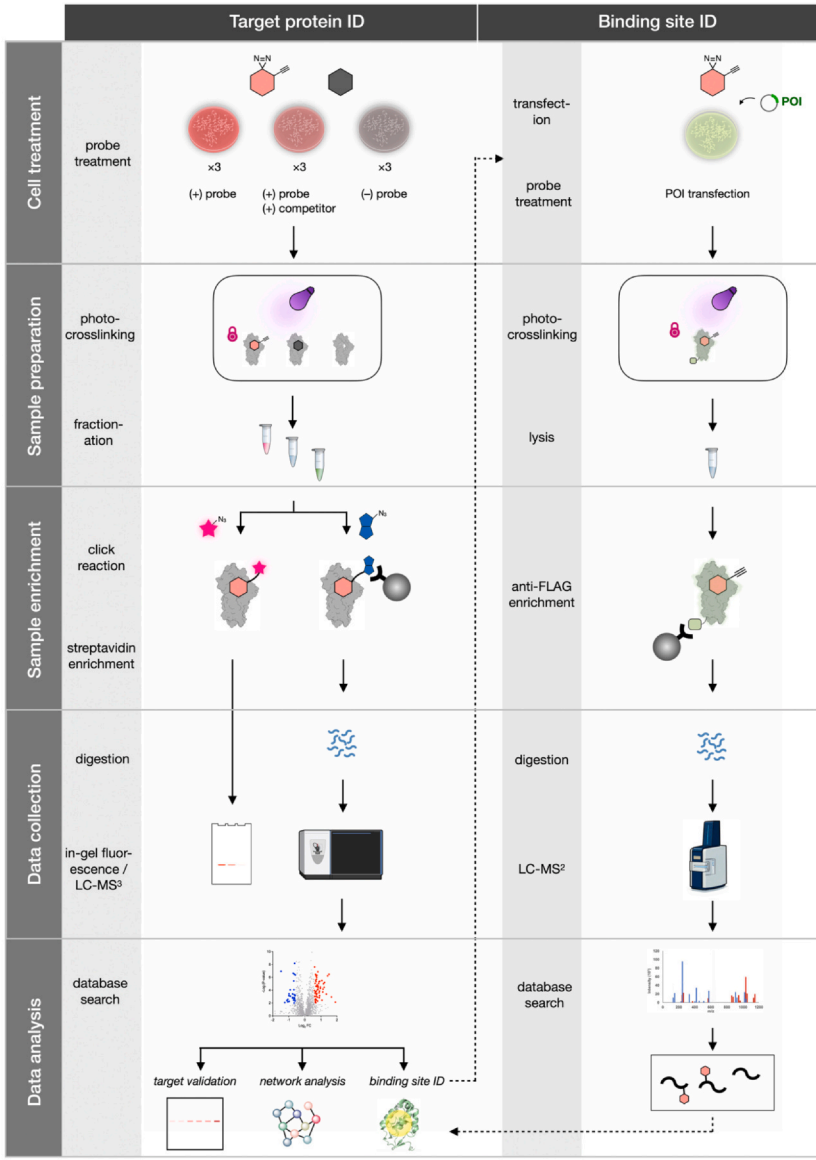

Fig. 2 Workflow summaries for chemoproteomics profiling of cholesterol metabolite targets and cholesterol metabolite binding site identification.

competition experiments and replicates provide an unparalleled toolkit for identifying and functionally interrogating the multifaceted roles of cholesterol metabolites in the fundamental operations of living cells.

The first protocols below describe unbiased identification of protein interactors in the membrane proteome of NIH-3T3 cells by a bifunctional photoaffinity probe for the cholesterol metabolite 20(*S*)-hydroxycholesterol (20S-HC), using either gel-based visualization of fluorescently labeled protein interactors or mass spectrometry-based identification of proteome-wide interactors (Fig. 2). Details regarding optimization and results are provided in (Cheng et al., 2021). The second protocol describes live cell identification of binding site residues in an epitope-tagged protein of interest in HEK293T cells by a monofunctional cholesterol photoaffinity probe. Details relevant to this protocol and obtained results can be found in (Mafi et al., 2021) and forthcoming reports from our lab.

2. Before you begin

- **Probe validation.** When using a probe for the first time, it is advisable to include control conditions in preliminary in-gel analysis experiments. These include assessment of the necessity of light for protein adduction (± UV) and of the click reaction for protein labeling (± copper catalyst). Dose-response measurements should be performed to determine the minimum concentration of probe required for reproducible labeling. Control experiments for probe validation in a given system are described in (Cheng et al., 2021; Flaxman, Miyamoto, & Woo, 2019; MacKinnon & Taunton, 2009).
- **Probe quantification.** An accurate method to quantify probe concentration is to use ^{1}H NMR integration of a known signal(s) in the probe relative to that of an added standard. Estimate the quantity of probe using an analytical balance or based on vendor specifications (0.05–25 mg) and dissolve it in 600 μL of a deuterated solvent in which the probe is soluble (e.g., $CDCl_3$, CD_3OD, DMSO–d_6, C_6D_6). Prepare a standard solution of an inert additive (e.g., DMF, *t*-BuOH) in the same (deuterated) solvent at a concentration such that 20 μL of the standard solution will contain approximately 0.1–1 equivalent of your probe material. Add 20 μL of the standard solution to the probe solution and collect a ^{1}H NMR spectrum for 16-128 scans (depending on quantity of probe) on a ≥ 400 MHz

instrument with a D_1 of 10 s or greater. Select an isolated ^{1}H NMR signal from the probe and a ^{1}H NMR signal from the standard, then use the relative signal integrations, proton stoichiometries, and quantities used to prepare the standard solution to calculate an accurate mass of the probe. For this analysis, the internal standard should contain one or more ^{1}H NMR signals that do not overlap with signals from the probe. Concentrate and/or lyophilize the solution to remove the standard and re-dissolve the probe in a known quantity of vehicle solvent (e.g., molecular biology-grade DMSO), aliquot, and store at –20 to –80 °C.

- **Cholesterol metabolite/probe storage and media preparation.** It is often convenient to prepare 5–100 × stock solutions of probes and competitors in molecular biology grade DMSO. Depending on chemical stability, these solutions can be aliquoted or frozen in bulk at –20 °C, then thawed and used as required. All sterol/lipid-based probes should be prepared in low serum media, and final media solutions of probe, competitor, and/or DMSO vehicle should be sterile filtered immediately before adding to cells. As noted above, highly hydrophobic probe/competitor molecules may be poorly soluble in DMSO. Some sterol derivatives (e.g., cyclopamine) may be more soluble in ethanol, particularly at lower concentrations. Ideally, final media solutions should have a concentration of less than 0.1 % DMSO or ethanol to avoid cell toxicity. In addition, some sterol molecules may precipitate immediately upon adding DMSO/ethanol stock to aqueous media solutions. Sometimes this is visibly obvious, whereas occasionally precipitate formation is not macroscopically perceptible and can only be detected with a light scattering device.
- **Cholesterol metabolite/probe complexation.** Certain probe and/or competitor sterol structures (e.g., cholesterol probes or cholesterol itself) are essentially insoluble in aqueous cell media. For efficient delivery of such molecules to cells, pre-complexation with a solubilizing agent (MβCD, HPCD, LDL, or other) may be advantageous. As with DMSO concentration, the overall MβCD concentration should be normalized among all conditions used for comparison (vehicle, probe ± inhibitor). However, "empty" cyclodextrins such as MβCD and HPCD can extract cholesterol from cell membranes and alter chemoproteomics results, so these agents should only be used if absolutely necessary. Procedures to prepare probe/inhibitor-cyclodextrin complexes are described in (Christian, Haynes, Phillips, & Rothblat, 1997; Luchetti et al., 2016; Zidovetzki & Levitan, 2007).

- **Affinity enrichment optimization.** Hydrophobic target and background proteins may stick to affinity purification beads (streptavidin agarose, anti-FLAG magnetic beads, etc.). In the protocols below, washing steps have been optimized to minimize background retention without losing *bona fide* target proteins. It is beneficial to perform initial optimization of washing and elution conditions for each probe and affinity resin by preparing wash/elution buffers of increasing stringency and assessing displacement of known target proteins. If no target proteins are known at the outset, in-gel analysis can be used to reveal the apparent molecular weight of competable proteins. Optimal wash/elution buffer stringency is attained when (1) minimal and maximal proportions of competable target(s) and non-specific resin binders, respectively, are removed during the wash, and (2) maximal and minimal proportions of competable targets and non-specific resin binders, respectively, are displaced during elution. Key parameters for optimization are the percentages of SDS and detergents (e.g., Igepal, Triton) in each buffer and number of washes/elutions.
- **Cell line selection.** Section 3 describes chemoproteomics analysis of bifunctional probe **1** (Fig. 1) in the membrane fraction of NIH-3T3 cells. We have successfully applied the same protocol to chemoproteomic profiling of probe **1** in HEK293T (adherent) and MV4-11 (suspension) cells, and the protocol should be general to most cell types. Section 4 describes binding site analysis of monofunctional probe **2** to an epitope-tagged target in HEK293T cells. We anticipate that this protocol will be applicable to all transfectable cell types. However, probe/competitor concentrations, incubation times, and culture conditions should be optimized for each cell line.

3. Live cell photoaffinity crosslinking and click chemistry tagging

Section 3 contains protocols for photocrosslinking 20S-HC probe **1** to live NIH-3T3 cells (Section 3.1) followed by membrane proteome fractionation (Section 3.2) and click reaction (Section 3.3) with either TAMRA-azide for in-gel fluorescence visualization (Section 3.4) or biotin-azide for chemoproteomics mass spectrometry analysis (Sections 3.5–3.9).

3.1 Vehicle, probe, and/or competitor treatment, and photocrosslinking

In Section 3.1, triplicate populations of live NIH-3T3 cells are treated with DMSO vehicle or 20S-HC probe **1**, with the latter in the presence or absence of a 20S-HC competitor (Fig. 3). Representative cell counts and reagent volumes for each application are provided in Table 1.

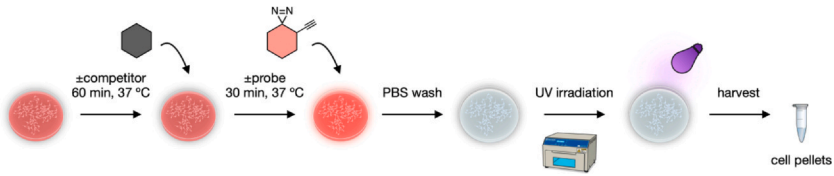

Fig. 3 Workflow summary for Section 3.1.

3.1.1 Materials and equipment

3.1.1.1 Equipment and instruments

- UV-crosslinker (Fisherbrand UV crosslinker with adjustable height, cat. no. 13-245-221)
- Five 368 nm bulbs for UV crosslinker (Fisher Scientific cat. no. 13-245-225)
- Class II A2 biosafety cabinet (REDISHIP Purifier Logic + Class II A2 Biosafety Cabinets, Labconco cat. no. 302419101)
- Incubator (CellXpert C170, Eppendorf cat. no. 6734010015)
- Refrigerated centrifuge (5430R refrigerated microcentrifuge, Eppendorf cat. no. 022620667)
- Vortex mixer (VWR mini vortex mixer, VWR cat. no. 76549-932)

3.1.1.2 Consumables and reagents

- Cell scrapers (cell scraper for dishes, VWR cat. no. 10062-906)
- 6-well cell culture plates for in-gel fluorescence visualization: Sterile TC-treated 6-well cell culture plates with lid (Corning cat. no. 353224)
- 15 cm cell culture plates for chemoproteomics analysis: Sterile TC-treated 150 mm cell culture dish with lid (Corning cat. no. 353025)
- Low-profile ice container (for UV crosslinker), e.g., the bottom tier of a stackable pipette tip box
- Sterile filters (Nalgene Rapid-Flow sterile filter units with PES membranes, Thermo Scientific cat. no. 5650020)
- 20S-HC photoaffinity probe **1** (Fig. 1, Cheng et al., 2021)
- 20S-HC competitor (CAS no. 516-72-3, 20α-hydroxycholesterol, Avanti Research cat. no. 700156P)

Table 1 Quantities of solutions and reagents for in-gel visualization and chemoproteomics analysis in Sections 3.1.1.2, 3.3.2, and 3.3.2.

Section 3.1.2.2		In-gel fluorescence visualization	Chemoproteomics analysis
Step	Plate format for seeding	6-well plate - 9 wells	15 cm plate - 9 plates
1	Seeding density (NIH/3T3)	1.5 × 10^5 cells/well	1 × 10^6 cells/plate
2	1x competitor/DMSO media	900 μL/well	9 mL/plate
3	10x probe/DMSO media	100 μL/well	1 mL/plate
4	PBS wash	1 mL/well	10 mL/plate
5	PBS for crosslinking	1 mL/well	10 mL/plate
6	PBS rinse of cells	300 μL/well	1 mL/plate
8	PBS rinses of cell pellet	300 μL/cell pellet	5 mL/cell pellet
Section 3.2.2			
Step		**In-gel fluorescence visualization**	**Chemoproteomics analysis**
1	Lysis Buffer A	70 μL	1 mL
2	Lysis Buffer B	70 μL	1 mL
3	Lysis Buffer C	70 μL	1 mL
Section 3.3.2			
Step		**In-gel fluorescence visualization**	**Chemoproteomics analysis**
1	1.2x total catalyst mixture	70 μL	1.2 mL
2	Cell lysate	56 μL	970 μL
2	Azide	1.3 μL 1.25 mM TAMRA azide	22 μL 5 mM picolyl biotin azide
3	Catalyst mixture per sample	6.4 μL	110 μL
5	4 volumes acetone	260 μL	4.5 mL

- Dimethyl sulfoxide (DMSO) (CAS No. 67-68-5, Sigma-Aldrich cat. no. D8418)
- Dulbecco's Modified Eagle's Medium (DMEM, Gibco cat. no. 11965118)
- Phenol red-free Dulbecco's Modified Eagle's Medium (DMEM, no phenol red, Gibco cat. no. 21063029)
- Bovine Calf Serum (BCS) (ATCC cat. no. 30-2030)
- Penicillin-Streptomycin (Pen-Strep) (Gibco, cat. no. 21063029)
- Sodium pyruvate (CAS no. 113-24-6, Sodium Pyruvate 100 mM, Gibco cat. no. 11360070)

3.1.1.3 Cell lines

- NIH-3T3 immortalized murine embryonic fibroblasts (ATCC, #CRL-1658)
  - Note: Cells should be subcultured according to manufacturer protocols and used between passages 4 and 15 for this protocol.

3.1.1.4 Buffers, solutions, and media

- NIH-3T3 cell culture media: 10 % BCS, 1 × Pen-Strep, and 1 mM sodium pyruvate in DMEM
- 1 × 20S-HC competitor media: 50 μM 20S-HC and 0.01 % total DMSO in phenol red-free DMEM
- 1 × DMSO media: 0.01 % DMSO in phenol red-free DMEM
- 10 × 20S-HC probe media: 10 μM 20S-HC probe and 0.1 % total DMSO in phenol red-free DMEM
- 10 × DMSO media: 0.1 % DMSO in phenol red-free DMEM

3.1.2 Protocol

- Note: Specific quantities (cell seeding numbers, reagent volumes, etc.) for in-gel fluorescence (Section 3.4) and proteomics mass spectrometry analysis (Sections 3.5–3.9) are listed in Table 1.

3.1.2.1 Prepare compound media solutions

1. Allow all DMSO stock solutions of probe and competitor(s) to warm to room temperature. Heat gently (to ≤40 °C), vortex, and agitate on a bath sonicator to ensure that solid is dissolved and the solution is homogenous.
2. Slowly add each stock solution to warm phenol red-free DMEM with constant mixing. Monitor for precipitate formation.

3. If necessary, add DMSO to each solution to equalize the percentage to 0.01 % in all conditions.
4. Filter each solution through a PES sterile filter before adding to cells.
   - *Note: Prepare media solutions on the day of use and avoid cooling, as this may result in compound precipitation.*

3.1.2.2 Culture cells and treat with compound media solutions

1. Seed NIH-3T3 cells at a density to achieve 70–80 % confluence after 24–72 h.
2. Gently replace culture media with 1 × 20S-HC competitor media or 1 × DMSO media and incubate cells at 37 °C and 5 % CO_2 for 1 h.
3. Carefully add 10 × 20S-HC probe media or 10 × DMSO media to the existing media, swirl the plate slowly to mix, and incubate the cells at 37 °C and 5 % CO_2 for another 30 min
4. Aspirate the media, wash the cells once with ice-cold PBS, and maintain on ice.
5. Place the plate(s) in a low-profile ice container, then remove the lid from each plate and irradiate for 5 min on ice at 368 nm using a UV crosslinker.
6. After crosslinking, detach the cells by scraping in cold PBS on ice. Transfer cells from each well to a pre-chilled 1.7 mL microcentrifuge tube or 15 mL falcon tube on ice. Immediately after transfer, rinse the well with additional ice-cold PBS and add this to the cell collection tube.
7. Centrifuge cell suspensions at 750 × *g* for 5 min at 4 °C.
8. Rinse the cell pellet by resuspending it in ice-cold PBS and centrifuging at 750 × *g* for 5 min at 4 °C. Repeat once for a total of two rinses.
9. After aspirating the PBS, proceed to Section 3.2 or snap freeze the cell pellet in liquid N_2 and store at −80 °C.

3.2 Subcellular fractionation

In Section 3.2, cell pellets from each sample are lysed and the membrane fraction is enriched through differential centrifugation (Fig. 4). Representative

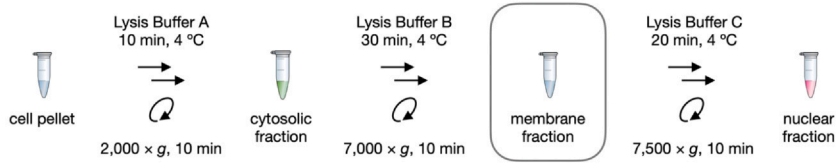

Fig. 4 Workflow summary for Section 3.2.

cell counts and reagent volumes for each downstream application (in-gel fluorescence visualization or chemoproteomics analysis) are provided in Table 1.

3.2.1 Materials and equipment

3.2.1.1 Equipment and instruments

- Mechanical tube rotator (Tube Revolver Rotator, Thermo Scientific cat. no. 88881001)
- Refrigerated centrifuge (5430R refrigerated microcentrifuge, Eppendorf cat. no. 022620667)
- Vortex mixer (VWR mini vortex mixer, VWR cat. no. 76549-932)

3.2.1.2 Consumables and reagents

- HEPES (CAS no. 7365-45-9, Sigma-Aldrich cat. no. H23830)
- Sodium chloride (CAS no. 7647-14-5, Sigma-Aldrich, cat. no. S9888)
- Hexylene glycol (CAS no. 107-41-5, Sigma-Aldrich cat. no. 68340)
- Digitonin (CAS no. 11024-24-1, Sigma-Aldrich cat. no. D141)
- cOmplete EDTA-free Protease Inhibitor Cocktail (Sigma-Aldrich, cat. no. 11836170001)
- IGEPAL-CA630 (CAS no. 9002-93-1, Sigma-Aldrich cat. no. I3021)
- Sodium deoxycholate (Sigma-Aldrich, cat. no. 30970)
- Sodium dodecyl sulfate (SDS) (Bio-Rad, cat. no.1610301)
- Benzonase (Sigma-Aldrich, cat. no. E1014)
- BCA protein assay kit (Pierce, Thermo Scientific cat. no. 23227)

3.2.1.3 Buffers, solutions, and media

- Lysis Buffer A: 50 mM HEPES pH 7.4, 150 mM NaCl, 1 M hexylene glycol, 25 μg/mL digitonin, and 1 × cOmplete EDTA-free Protease Inhibitor Cocktail
- Lysis Buffer B: 50 mM HEPES pH 7.4, 150 mM NaCl, 1 M hexylene glycol, 1 % IGEPAL-CA630, and 1 × cOmplete EDTA-free Protease Inhibitor Cocktail
- Lysis Buffer C: 50 mM HEPES pH 7.4, 150 mM NaCl, 1 M hexylene glycol, 0.5 % sodium deoxycholate, 0.1 % SDS, 25 U/mL benzonase, and 1 × cOmplete EDTA-free Protease Inhibitor Cocktail

3.2.2 Protocol

o *Note: Subcellular fractionation is conducted according to (Baghirova, Hughes, Hendzel, & Schulz, 2015).*

1. Resuspend cell pellets in ice cold Lysis Buffer A by gently vortexing and incubating on an end-over-end rotator for 10 min at 4 °C.
2. Centrifuge lysates at 2000 × *g* for 10 min at 4 °C.
3. Carefully collect the supernatants. This is the cytosolic fraction.
4. Resuspend the pellets in ice cold Lysis Buffer B by vortexing or pipetting up and down and incubate on an end-over-end rotator for 30 min at 4 °C.
5. Centrifuge at 7000 × *g* for 10 min at 4 °C.
6. Collect the supernatants. This is the membrane fraction.
7. Resuspend the pellets in ice cold Lysis Buffer C by vortexing or pipetting and incubate using an end-over-end rotator for 20 min at 4 °C.
8. Centrifuge at 7800 × *g* for 10 min at 4 °C.
9. Collect the supernatants. This is the nuclear fraction.
10. Determine the protein concentrations of each fraction using the BCA protein assay according to manufacturer protocols.
11. Normalize the protein concentration in all membrane fractions to the same value by dilution with Lysis Buffer B
    - *Note: We have used a normalized concentration of 40–60 μg protein for in-gel fluorescence analysis, 600–900 μg protein for mass spectrometry analysis, and ~100 μg protein for Western blot analysis of specific probe-labeled targets.*

3.3 Copper-catalyzed click tagging

In Section 3.3, the protein-normalized membrane fraction from each sample is subjected to copper-catalyzed click chemistry reaction with an azide linked to the appropriate tag (TAMRA for in-gel fluorescence visualization and biotin for chemoproteomics analysis) (Fig. 5). Representative cell counts and reagent volumes for each downstream application are provided in Table 1.

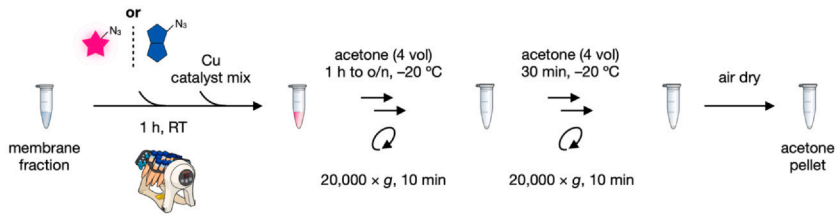

Fig. 5 Workflow summary for Section 3.3.

3.3.1 Materials and equipment

3.3.1.1 Equipment and instruments

- Mechanical tube rotator (Tube Revolver Rotator, Thermo Scientific cat. no. 88881001)
- Refrigerated centrifuge (5430R refrigerated microcentrifuge, Eppendorf cat. no. 022620667)
- Vortex mixer (VWR mini vortex mixer, VWR cat. no. 76549-932)
- –20 °C freezer

3.3.1.2 Consumables and reagents

- pH paper (mColorpHast pH 0–15 test strips, MilliporeSigma cat. no. 1.09535.0001)
- For in-gel fluorescence visualization: TAMRA azide (CAS no. 1228100-59-1, Vector Laboratories cat. no. CCT-AZ109)
- For chemoproteomics analysis: Picolyl biotin azide, (CAS no. 2222687-71-8, Vector Laboratories cat. no. CCT-1167)
- Tris[(1-benzyl-1H-1,2,3-triazol-4-yl)methyl]amine (TBTA) (CAS no. 510758-28-8, Vector Laboratories cat. no. CCT-106)
- *tert*-Butanol (*t*-BuOH) (CAS no. 75-65-0, Sigma-Aldrich cat. no. 308250)
- Dimethyl sulfoxide (DMSO) (CAS No. 67-68-5, Sigma-Aldrich cat. no. D8418)
- Copper(II) sulfate pentahydrate ($CuSO_4 \cdot 5H_2O$), (CAS no. 93-2959, Strem Chemicals cat. no. 93-2959)
- Tris(2-carboxyethyl)phosphine hydrochloride (TCEP) (CAS no. 51805-45-9, Sigma-Aldrich cat. no. C4706)
- Sodium hydroxide (NaOH) (CAS no. 1310-73-2, Sigma-Aldrich cat. no. 795429)
- Acetone (CAS no. 67-64-1, Fisher Chemical cat. no. A18-4)

3.3.1.3 Buffers, solutions, and media

- Catalyst mixture: TBTA (102 μM, from a 1.7 mM stock in 4:1 DMSO:*t*-BuOH), $CuSO_4$ (1 mM, from a 50 mM stock in H_2O), and TCEP (1 mM, from a 50 mM stock in H_2O, adjusted to pH 7–8 by 1 N NaOH immediately before adding to the catalyst mixture).
  - N*ote: The catalyst mixture is heterogeneous and should be vortexed periodically when aliquoting to samples.*
  - *Note: Prepare the catalyst mixture without TCEP on the day of the experiment; adjust the pH of TCEP and add to the catalyst mixture*

immediately before use. To adjust the pH of TCEP, add 1 N NaOH dropwise with vigorous mixing, monitoring with a pH strip periodically as the pH approaches 7–8.

3.3.2 Protocol

- *Note: Depending on available centrifuge/rotors, it may be necessary to split the volume of each sample into multiple 1.7 mL tubes for centrifugation.*

1. Prepare a ≥ 1.2 × volume of total catalyst mixture required for the click reactions. Do not adjust the pH of the TCEP solution or add it to the catalyst mixture until immediately before use.
2. Add 1.25 mM TAMRA azide in DMSO (for in-gel fluorescence visualization) or 5 mM picolyl biotin azide in DMSO (for streptavidin enrichment) to each sample and mix thoroughly by vortexing.
3. Add the catalyst mixture to each sample and mix thoroughly by vortexing.
4. Incubate on an end-over-end rotator for 1 h at room temperature.
5. Add 4 volumes of acetone, pre-cooled to –20 °C, and vortex briefly.
6. Maintain at –20 °C for 30 min to overnight.
7. Centrifuge at 20,000 × *g* for 10 min at 4 °C. Gently place the samples on ice, then efficiently and carefully discard the supernatant without touching the pellet.
8. Add the same volume of acetone as above and disrupt using a bath sonicator for 3 min to fully disperse the pellet.
   - *Note: Avoid vortexing, as this will spread the precipitate over the walls of the tube.*
9. Maintain at –20 °C for 30 min
10. Centrifuge at 20,000 × *g* for 10 min at 4 °C.
11. Gently place the samples on ice, then efficiently and carefully discard the supernatant without touching the pellet.
12. Optional: Repeat the acetone precipitation one more time.
13. Let the pellet air dry in each tube with the lid open at room temperature for 5–10 min
14. For in-gel fluorescence visualization, proceed to Section 3.4; for streptavidin enrichment, proceed to Section 3.5.

3.4 In-gel fluorescence visualization of probe crosslinked, fluorophore-tagged proteins

In Section 3.4, probe-crosslinked and TAMRA-conjugated proteins are resolved by SDS-PAGE and visualized using in-gel fluorescence (Figs. 6 and 15).

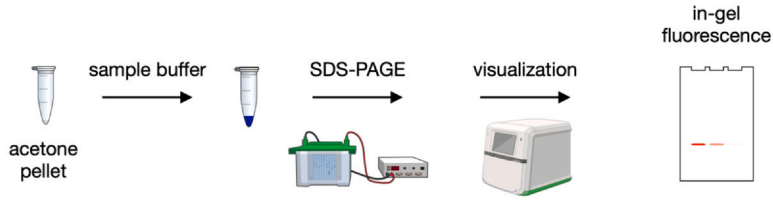

Fig. 6 Workflow summary for Section 3.4.

3.4.1 Materials and equipment

3.4.1.1 Equipment and instruments

- Thermomixer (Eppendorf ThermoMixer C, cat. no. 5382000023)
- SDS-PAGE equipment (Criterion Cell and PowerPac Basic Power Supply, Bio-Rad cat. no. 1656019)
- Fluorescent imager, (Bio-Rad ChemiDoc MP Imaging System, Bio-Rad cat. no. 12003154)
- Vortex mixer (VWR mini vortex mixer, VWR cat. no. 76549-932)
- Mini centrifuge (Corning LSE Mini Microcentrifuge, Corning cat. no. 6770)

3.4.1.2 Consumables and reagents

- Stain-free protein gels (4–15 % Criterion TGX Stain-Free Protein Gel, 18 well, 30 μL, Bio-Rad cat. no. 5678084)
- Protein ladder (Thermo Scientific Spectra Multicolor Broad Range Protein Ladder, Thermo Scientific cat. no. 26634)
- Tris/Glycine/SDS electrophoresis buffer (10 × Tris/Glycine/SDS, Bio-Rad cat. no. 1610772)
- cOmplete EDTA-free Protease Inhibitor Cocktail (Sigma-Aldrich cat. no. 11836170001)
- Sodium dodecyl sulfate (SDS) (CAS no. 151-21-3, Bio-Rad cat. no. 1610301)
- Tris(hydroxymethyl)aminomethane (Tris base) (CAS no. 77-86-1, Bio-Rad cat. no. 1610719)
- IGEPAL CA-630 (CAS no. 9002-93-1, Sigma-Aldrich cat. no. I3021)
- DL-Dithiothreitol (DTT) (CAS no. 3483-12-3, Fisher Scientific cat. no. BP172)
- Bromophenol blue (CAS no. 115-39-9, Sigma-Aldrich cat. no. 114391)
- Glycerol (CAS no. 56-81-5, Sigma-Aldrich cat. no. G7893)
- Hydrocholoric acid (HCl) (Hydrochloric acid, 37 %, Sigma-Aldrich cat. no. 258148)

- Acetic acid (Glacial acetic acid, CAS no. 64-19-7, Sigma-Aldrich cat. no. 695092)
- Methanol (CAS no. 67-56-1, Fisher Chemical cat. no. A412**)**

3.4.1.3 Buffers, solutions, and media

- 6 × SDS Sample Buffer: 300 mM Tris, adjusted to pH 6.8 with HCl, 50 % (v/v) glycerol, 12 % (w/v) SDS, 600 mM DTT, and 0.6 g/L bromophenol blue.
- Resuspension Buffer: 1 % IGEPEL CA-630 in PBS containing 1 × cOmplete EDTA-free Protease Inhibitor Cocktail.
- Fixation Solution: 50 % methanol and 10 % acetic acid in H_2O

3.4.2 Protocol

1. Add 30 μL of a 5:1 mixture of resuspension buffer and 6 × SDS sample buffer to the dried pellets from acetone precipitation.
2. Agitate using a bath sonicator for 3–5 min and vortex.
3. Incubate on a Thermomixer for 30 min at 950 rpm at 50 °C.
4. Spin the sample briefly on a mini centrifuge to collect condensation on the lid, then vortex thoroughly.
5. Subject the samples to SDS-PAGE; include a molecular weight ladder in one lane.
6. Visualize TAMRA fluorescence in the gel using a gel fluorescence imager with Alexa 546 settings (520–525 nm epi-green LED, 595/36 filter on the ChemiDoc MP).
7. Visualize the gel using stain-free in gel mode to assess equal protein loading in all sample (302 nm trans-UV activation, 590/110 nm filter on the ChemiDoc MP)
   - *Note: strong TAMRA signal may be visible in stain-free imaging mode*
8. Visualize the gel using the Coomassie Blue settings to visualize fluorescent bands in the protein ladder. (Trans-white illumination, 590/110 nm filter on the ChemiDoc MP)
9. (Optional): Fix the gel using Fixation Buffer 1 h to overnight to clear background TAMRA fluorescence.
10. Use Bio-Rad Image Lab or equivalent software to quantify the intensity of the band(s) of interest in the vehicle control, probe-only, and probe + competitor sample(s) to assess how intensely and how competably the probe labels protein(s) at a given apparent molecular weight.

3.5 Streptavidin enrichment of probe-crosslinked, biotin-tagged proteins

In Section 3.5, probe-crosslinked proteins clicked to biotin azide are enriched using streptavidin resin (Fig. 7).

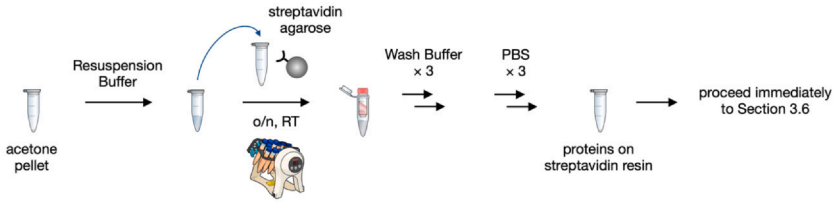

Fig. 7 Workflow summary for Section 3.5.

3.5.1 Materials and equipment

3.5.1.1 Equipment and instruments

- Vortex mixer (VWR mini vortex mixer, VWR cat. no. 76549-932)
- Thermomixer (Eppendorf ThermoMixer C, cat. no. 5382000023)
- Mechanical tube rotator (Tube Revolver Rotator, Thermo Scientific cat. no. 88881001)
- Centrifuge (5430R refrigerated microcentrifuge, Eppendorf cat. no. 022620667)

3.5.1.2 Consumables and reagents

- 0.8 mL Centrifuge columns (0.8 mL, Pierce Centrifuge Columns for Affinity Chromatography, Thermo Scientific cat. no. 89869)
- 1.5 mL Protein Lo-Bind tubes (Eppendorf, cat. no 022431081)
- Streptavidin agarose (Thermo Fisher, cat. no 20349)
- Biotin (Sigma-Aldrich, cat. no B4501)
- IGEPAL CA-630 (CAS no. 9002-93-1, Sigma-Aldrich cat. no. I3021)
- DL-Dithiothreitol (DTT) (CAS no. 3483-12-3, Fisher Chemical cat. no. BP172)
- Bromophenol blue (CAS no. 115-39-9, Sigma-Aldrich cat. no. 114391)
- Glycerol (CAS no. 56-81-5, Sigma-Aldrich cat. no. G7893)
- Hydrocholoric acid (HCl) (Hydrochloric acid, 37 %, Sigma-Aldrich cat. no. 258148)

3.5.1.3 Buffers, solutions, and media

- 6 × SDS Sample Buffer: 300 mM Tris adjusted to pH 6.8 with HCl, 50 % (v/v) glycerol, 12 % (w/v) SDS, 600 mM DTT, and 0.6 g/L bromophenol blue.

- Resuspension Buffer: 1 % IGEPEL CA-630 in PBS containing 1 × cOmplete EDTA-free Protease Inhibitor Cocktail
- Wash Buffer: 1 % IGEPEL CA630 and 0.1 % SDS in PBS
- Bead Rinse Buffer: 0.1 % IGELPAL CA630 in PBS

3.5.2 Protocol

- *Note 1: In this Protocol, a 1 % SDS in PBS is added to maximally solubilize the dried pellet. The re-solubilized pellet is then gradually diluted with resuspension buffer to reduce to final SDS percentage to a point compatible with the streptavidin agarose (0.1 % SDS).*
- *Note 2: To assess probe labeling/competition, ~5 % of each sample can be removed for far Western blot analysis (Fig. 16).*
- *Note 3: Depending on available centrifuge/rotors, it may be necessary to split the volume of each sample into multiple 1.7 mL tubes for centrifugation.*

1. Use a vortex to mix the streptavidin agarose resin thoroughly and dispense 100 μL to microcentrifuge tubes. Re-vortex periodically while dispensing to ensure that equivalent, homogenous aliquots are transferred to each tube.
2. Pre-wash the resin: Centrifuge at 2500 × *g* for 1 min at room temperature and discard the flow-through. Add 500 μL Bead Rinse Buffer, vortex thoroughly, centrifuge at 2500 × *g* for 1 min at room temperature, and discard the supernatant. Re-suspend with an additional 500 μL Bead Rinse Buffer, vortex, and store until use. Immediately before adding sample, centrifuge and discard the Bead Rinse Buffer.
3. Add 200 μL of a solution of 1 % SDS in PBS followed by 200 μL Resuspension Buffer to the dried pellet from acetone precipitation.
4. Agitate in a bath sonicator for 3–5 min and with intermittent vortexing.
5. Add an additional 800 μL Resuspension Buffer.
6. Agitate in a bath sonicator for 3–5 min and with intermittent vortexing.
7. Add an additional 800 μL of resuspension buffer, to a final concentration of 0.1 % SDS and 1 % IGEPAL CA-630 in PBS.
8. Agitate in a bath sonicator for 3–5 min and with intermittent vortexing.
9. Centrifuge at 7000 × *g* for 3 min at room temperature to pellet any insoluble proteins.
10. Transfer the supernatant to a microcentrifuge tube containing the pre-washed streptavidin agarose resin.

11. Incubate on an end-over-end rotator at room temperature overnight (12–16 h).
12. Place a Pierce centrifuge column in a 2 mL microcentrifuge tube.
13. Transfer the sample/agarose slurry to the column.
14. Centrifuge at 1000 × *g* for 1 min at room temperature and discard the flow-through.
15. Wash the resin with 500 µL of Wash Buffer, centrifuge at 1000 × *g* for 1 min at room temperature, and discard the wash. Repeat for a total of 3 washes.
16. Wash the resin with 500 µL PBS, centrifuge at 1000 × *g* for 1 min at room temperature, and discard the wash. Repeat for a total of 3 washes.
17. Use PBS to transfer the resin to a new 1.5 mL Protein Lo-Bind tube.
18. Centrifuge at 2500 × *g* for 1 min at room temperature and carefully discard the supernatant, taking care not to disturb the resin.
19. Proceed to Section 3.6 for on-bead trypsin digestion and desalting.

3.6 Protein digestion and desalting

In Section 3.6, enriched biotinylated proteins on streptavidin resin are digested with trypsin on the agarose resin, then eluted and de-salted to prepare for tandem mass tag labeling (Fig. 8).

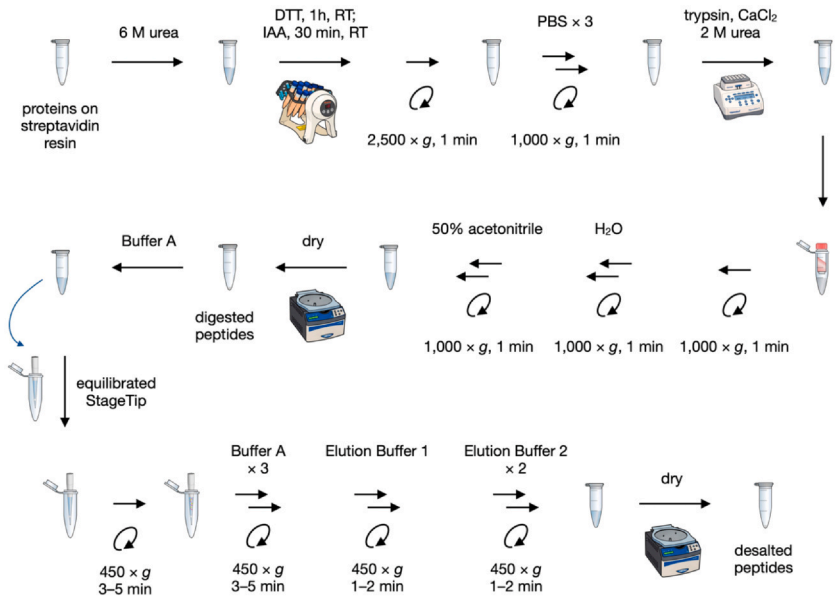

Fig. 8 Workflow summary for Section 3.6.

3.6.1 Materials and equipment

3.6.1.1 Equipment and instruments

- Mechanical tube rotator (Tube Revolver Rotator, Thermo Scientific cat. no. 88881001)
- Centrifuge (5430R refrigerated microcentrifuge, Eppendorf cat. no. 022620667)
- Thermomixer (Eppendorf ThermoMixer C, cat. no. 5382000023)
- Refrigerated centrifugal concentrator (Refrigerated CentriVac Centrifugal Vacuum Concentrator, Labconco cat. no. 7310022)

3.6.1.2 Consumables and reagents

- 0.8 mL Centrifuge columns (0.8 mL, Pierce Centrifuge Columns for Affinity Chromatography, Thermo Scientific cat. no. 89869)
- 1.5 mL Protein Lo-Bind tubes (Eppendorf cat. no. 022431081)
- Sequencing Grade Trypsin (0.5 μg/μL in 50 mM acetic acid, Promega cat. no. V5111)
- StageTips (CDS Analytical Empore C18 StageTips, CDS Analytical cat. no. 13-110-055)
- Urea (CAS no. 57-13-6, Bio-Rad cat. no. 1610731)
- DL-Dithiothreitol (DTT) (CAS no. 3483-12-3, Sigma-Aldrich cat. no. D0632)
- Iodoacetamide (IAA) (CAS no. 144-48-9, Sigma-Aldrich cat. no. 16125)
- Calcium chloride dihydrate ($CaCl_2 \cdot 2H_2O$) (CAS no. 10035-04-8, Sigma Aldrich cat. no. C3881)
- Formic acid (CAS no. 64-18-6, Fisher Chemical cat. no. A11710×1)

3.6.1.3 Buffers, solutions, and media

- Note: prepare the following solutions fresh immediately before use.
- 6 M urea in PBS
- 2 M urea in PBS
- 200 mM DTT in H_2O
- 500 mM IAA in H_2O
  - *Note: keep the solution covered with aluminum foil.*
- 100 mM $CaCl_2$ in H_2O
- Buffer A: 2 % acetonitrile and 0.2 % formic acid in H_2O
- Peptide Elution Buffer 1: 50 % acetonitrile, 50 % H_2O, 0.2 % formic acid
- Peptide Elution Buffer 2: 80 % acetonitrile, 50 % H_2O, 0.2 % formic acid

3.6.2 Protocol

1. Resuspend the streptavidin agarose resin sample in 400 μL of 6 M urea in PBS.
2. Add 24 μL of 200 mM DTT (to a final concentration of ~10 mM) and incubate on an end-over-end rotator for 1 h at room temperature.
3. Add 25 μL of 500 mM iodoacetamide (to a final concentration of ~25 mM) and incubate on an end-over-end rotator for 30 min at room temperature in the dark.
4. Centrifuge at 2500 × *g* for 1 min at room temperature and carefully discard the supernatant without disturbing the resin.
5. Add 500 μL PBS to the resin, centrifuge at 2500 × *g* for 1 min at room temperature, and carefully discard the supernatant without disturbing the resin. Repeat for a total of 2 rinses.
6. Resuspended the resin in 200 μL of 2 M urea in PBS.
7. Add 2.6 μL of 100 mM $CaCl_2$ (to a final concentration of ~1 mM) and 3 μL of 0.5 μg/μL trypsin.
8. Incubate the mixture on a Thermomixer for 12–16 h at 37 °C and 650 rpm.
9. Spin the tube briefly on a mini centrifuge, transfer the slurry to a 0.8 mL Pierce centrifuge column, and place the column in a 1.7 mL Protein Lo-Bind tube.
10. Add 200 μL water to wash the resin, centrifuge at 1000 × *g* for 1 min at room temperature, and transfer the wash to the above Lo-Bind tube.
11. Repeat the wash with 200 μL of 50 % acetonitrile and transfer the wash to the same Lo-Bind tube.
12. Concentrate the combined supernatant and washes to dryness using a CentriVac concentrator.
13. Resuspend the peptides in 50 μL of Buffer A, vortex, and agitate in a bath sonicator for 3 min
14. Test the pH of a 0.1 μL aliquot with a pH strip and adjust the pH to 2–3 with formic acid if necessary.
15. Activate the StageTip: Add 50 μL of 100 % acetonitrile to the StageTip, then centrifuge at 450 × *g* for 1 min at room temperature. Repeat for a total of 3 times.
16. Equilibrate the StageTip: Add 50 μL of Buffer A, then centrifuge at 450 × *g* for 2 min at room temperature. Repeat for a total of 3 times.
17. Load the resuspended peptides onto a StageTip, then centrifuge at 450 × *g* for 5 min at room temperature. Reload the flow through, centrifuge, and re-collect for a total of 3 times.

18. Wash the StageTip: Add 50 μL of Buffer A and centrifuge at 450 × *g* for 2 min at room temperature. Repeat for a total of 3 times.
19. Place the StageTip on a 1.7 mL Protein Lo-Bind tube for elution.
20. Elute peptides from the StageTip: Add 50 μL of Peptide Elution Buffer 1 and centrifuge at 450 × *g* for 1 min at room temperature.
21. Further elute peptides: Add 50 μL of Peptide Elution Buffer 2 and centrifuge at 450 × *g* for 1 min at room temperature. Repeat for a total of 2 times with Peptide Elution Buffer 2.
22. Combine the three elutions above and concentrate to dryness using a CentriVac concentrator and store at −80 °C or proceed to Section 3.7.

3.7 TMT labeling and label efficiency check

In Section 3.7, digested, de-salted peptides from each sample are labeled with a unique tandem mass tags (TMTs) and the efficiency of TMT labeling is assessed by mass spectrometry (Fig. 9).

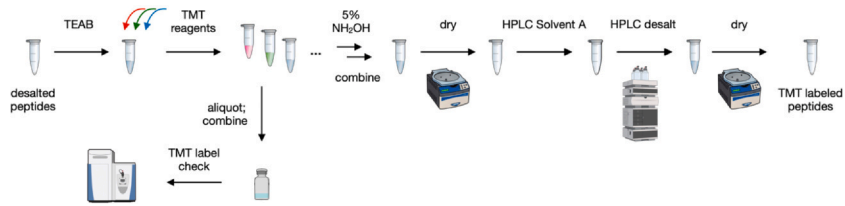

Fig. 9 Workflow summary for Section 3.7.

3.7.1 Materials and equipment

3.7.1.1 Equipment and instruments

- Thermomixer (Eppendorf ThermoMixer C, cat. no. 5382000023)
- Refrigerated centrifugal concentrator (Refrigerated CentriVac Centrifugal Vacuum Concentrator, Labconco cat. no. 7310022)

For TMT label check:

- EASY-nLC 1200 (Thermo Scientific)
- Orbitrap Q Exactive HF mass spectrometer (Thermo Scientific) equipped with a Nanospray Flex ion source (Thermo Scientific)
- C18 Aurora column (25 cm × 50 μm ID, 1.6 μm, Ion Opticks)

For HPLC desalting:

- Agilent 1100 HPLC System (Agilent Technologies)
- C4 peptide Macrotrap (3 × 8 mm; 200 μg maximum capacity, Optimize Technologies)

3.7.1.2 Consumables and reagents

- 1.5 mL Protein Lo-Bind tubes (Eppendorf cat. no. 022431081)
- TMT 10-plex isobaric label reagent (Thermo Scientific cat. no. 90110)
- Acetonitrile, anhydrous (CAS no. 75-05-8, Sigma-Aldrich cat. no. 900644)
- Acetonitrile, LC-MS grade (CAS no. 75-05-8, Sigma-Aldrich cat. no. 900667)
- Formic acid (CAS no. 64-18-6, Fisher Chemical cat. no. A11710×1)
- Hydroxylamine solution, 50 wt% in H_2O (CAS no. 7803-49-8, Sigma-Aldrich cat. no. 438227)

3.7.1.3 Buffers, solutions, and media

- 100 mM triethylammonium bicarbonate (TEAB), pH 8.5
- HPLC Solvent A: 2 % acetonitrile and 0.2 % formic acid in H_2O
- HPLC Solvent B: 95 % acetonitrile and 0.1 % formic acid in H_2O

3.7.2 Protocol

- *Note: When handling TMT reagents, use anhydrous acetonitrile and minimize exposure to water (*e.g.*, atmospheric moisture). If aliquoting TMT reagents, use a fresh ampule of anhydrous acetonitrile to dissolve to a known concentration (e.g., 20 μg/μL, as below) and work efficiently to mix, aliquot, and store sealed (e.g., with an aluminum foil plate sealer or a microcentrifuge tube) at −80 °C. Avoid further freeze-thaw cycles.*

1. Resuspend desalted peptides from the trypsin digest with 50 μL of 100 mM TEAB at pH 8.5 and 20 μL of a 20 μg/μL solution of TMT 10-plex isobaric label reagent in anhydrous acetonitrile.
2. Incubate labeling reactions at room temperature on a Thermomixer for 2 h at room temperature and 650 rpm.
3. Withdraw a 0.4 μL aliquot from each single-plex sample, combine, and concentrate to dryness using a CentriVac concentrator. This combined aliquot sample will be used for a preliminary check of TMT labeling efficiency (i.e., percent labeling of N-termini and lysine residues) prior to full HPLC-MS^3 analysis.
4. Freeze the remaining samples at −80 °C.
5. Check TMT labeling efficiency: resuspend the combined aliquots in 30 μL of HPLC Solvent A and analyze by LC-MS/MS analysis using a C18 Aurora column on an EASY-nLC 1200 fitted coupled to an Orbitrap Q Exactive HF mass spectrometer with a Nanospray Flex ion source. Proceed if all single-plex N-terminus and lysine labeling is $\geq$ 95 %.

6. After confirming labeling efficiency, thaw and quench each TMT labeling reaction with 4 μL 5 % hydroxylamine at room temperature for 15 min
7. Combine all TMT labeled samples and concentrate to dryness using a CentriVac concentrator.
8. Desalt the sample using HPLC: Resuspend the dried, combined, TMT-labeled peptides in 200 μL HPLC Solvent A and inject on an Agilent 1100 HPLC with an Optimized Technologies C4 peptide Macrotrap column.
9. Elute peptides with a mobile phase consisting of a gradient of HPLC Solvent A and HPLC Solvent B (0–100 % B) at a flow rate of 250 μL/min.
10. Collect the fractions containing the tryptic peptides and concentrate to dryness using a CentriVac concentrator, then store at –80 °C until LC-MS^3 analysis.

3.8 LC-MS^3 analysis

In Section 3.8, combined, desalted, TMT labeled peptide samples are analyzed by HPLC-MS^3 (Fig. 10).

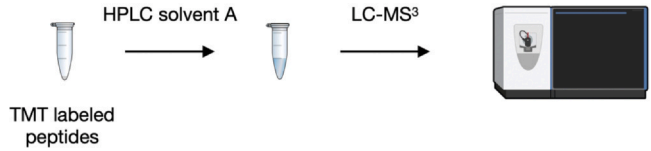

Fig. 10 Workflow summary for Section 3.8.

3.8.1 Materials and equipment

3.8.1.1 Equipment and instruments

- EASY-nLC 1200 (Thermo Scientific)
- UHPLC monolithic column (Capillary EX-Nano MonoCap C18 HighResolution 2000, 0.1 × 2000 mm, Merck)
- Orbitrap Eclipse Tribrid mass spectrometer (Thermo Fisher Scientific)
- PicoTip emitter (New Objective)

3.8.1.2 Consumables and reagents

- Acetonitrile, anhydrous (CAS no. 75-05-8, Sigma-Aldrich cat. no. 900644)
- Acetonitrile, LC-MS grade (CAS no. 75-05-8, Sigma-Aldrich cat. no. 900667)
- Formic acid (CAS no. 64-18-6, Fisher Chemical cat. no. A11710×1)
- Hydroxylamine solution, 50 wt% in H_2O (CAS no. 7803-49-8, Sigma-Aldrich cat. no. 438227)

3.8.1.3 Buffers, solutions, and media

- HPLC Solvent A: 2 % acetonitrile and 0.2 % formic acid in H_2O
- HPLC Solvent B: 80 % acetonitrile and 0.2 % formic acid in H_2O

3.8.2 Protocol

1. Resuspend the dried desalted peptides in an appropriate volume of HPLC Solvent A (98 % H_2O, 2 % acetonitrile, 0.2 % formic acid).
2. Perform MS^3 analysis: Subject ~2 μL of the resuspended sample to HPLC-MS^3 analysis on an EASY-nLC 1000 with a UHPLC monolithic column, coupled to an Orbitrap Eclipse Tribrid mass spectrometer fitted with a silica coated PicoTip emitter. Elute peptides using a HPLC Solvent B:HPLC Solvent A gradient of 2:98–98:2 at a flow rate of 0.4 μL/min.
3. Analyze the raw data using Proteome Discoverer (PD) or other appropriate software (Section 3.9).

3.9 Data analysis notes

There are ever-expanding software options for raw mass spectrometer data preprocessing and subsequent analysis. For contemporary reviews, see (Palmblad, Hoopmann, & Dorfer, 2025; Schneider et al., 2025). In the data shown in Fig. 16, we used a modified PD prebuilt process workflow "PWF_Tribrid_TMT(pro)_Quan_SPS_MS3_SequestHT_Percolator" in the PD software with the TMT reagent batch numbers from the experiment, and we employed the SEQUEST HT search algorithm against reviewed proteins in the UniProt mouse proteome (UP000000589, downloaded July 2020) and common contaminant proteins (MaxQuant contaminants database, downloaded July 2020). We followed a modified prebuilt PD consensus workflow "CWF_Comprehensive_Enhanced Annotation_Reporter_Quan_MS3". Additional details about PD parameters are available in the Supplementary Information from (Cheng et al., 2021). Notably, the data in Fig. 16 were generated using the RTS–SPS-MS^3 modification, as described in (McAlister et al., 2014; Schweppe et al., 2020).

Regardless of the software used, several factors must be considered when evaluating data from chemoproteomics analysis of cholesterol metabolite and other photoaffinity probes. Because the mass spectrometer analyzes only the probe-enriched population, the peptide yield per cell input is inherently modest and, importantly, is expected to vary between treatment conditions. For the data in Fig. 16, we chose to normalize protein input at the point of streptavidin enrichment; thus, we anticipated a higher number of identified proteins in samples treated with the probe, which enables crosslinking and biotinylation,

than in vehicle control or probe + competitor samples. Consequently, we elected to compare non-normalized protein-level abundance values after raw data preprocessing. To avoid missing low-abundance proteins or peptides, we surveyed a variety of imputation methods by comparing peptide counts/missing values from the PD output with the fold changes produced by each method (Shi, Zhong, Rogalski, & Foster, 2025). We found that imputation of missing values within each treatment group using probabilistic minimum imputation (MinProb) provided the best balance of preserving a diverse dataset while minimizing false positives. After imputation, we used the mean of the $\log_2$ fold changes of replicates within each condition to calculate the differences in protein abundance between conditions, and we tested the statistical significance of differences between conditions using a two-tailed unpaired *t*-test.

Ultimately, careful inspection of peptide counts is required to identify the optimal raw data analysis program, imputation method, sample comparison/normalization, and significance assessment.

4. Binding site identification

Section 4 describes identification of the peptide- or residue-level binding site(s) of a cholesterol metabolite within a protein of interest. The FLAG-tagged protein is expressed in HEK293T cells, then cells are treated with a monofunctional, diazirine-containing cholesterol metabolite probe (e.g., probe **2**, Fig. 1). After live cell crosslinking, cells are lysed and the protein of interest is enriched on anti-FLAG resin and digested with trypsin in solution. The tryptic peptides are subjected to MS/MS analysis, and the data is analyzed to identify the probe-crosslinked peptide(s) and residue(s).

4.1 Transfection, live cell compound treatment, and photoaffinity crosslinking

In Section 4.1, cells are transfected with a FLAG-tagged protein of interest, treated with the monofunctional cholesterol metabolite photoaffinity probe **2** (Fig. 1), and subject to live-cell photoaffinity crosslinking (Fig. 11).

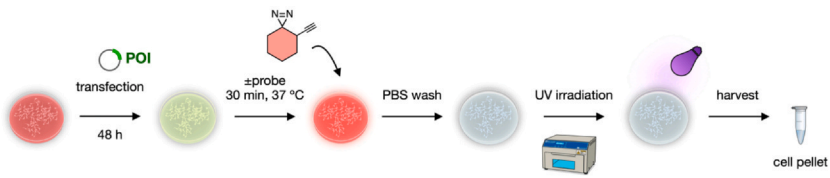

Fig. 11 Workflow summary for Section 4.1.

4.1.1 Materials and equipment

4.1.1.1 Equipment and instruments

- UV-crosslinker (Fisherbrand UV crosslinker with adjustable height, cat. no. 13-245-221)
- Five 368 nm bulbs for UV crosslinker (Fisher Scientific cat. no. 13-245-225)
- Class II A2 biosafety cabinet (REDISHIP Purifier Logic + Class II A2 Biosafety Cabinets, Labconco, VWR cat. no. 76317-622)
- Incubator (CellXpert C170, Eppendorf cat. no. 6734010015)
- Vortex mixer (VWR mini vortex mixer, VWR cat. no. 76549-932)
- Mini centrifuge (Corning LSE Mini Microcentrifuge, Corning cat. no. 6770)

4.1.1.2 Consumables and reagents

- Mammalian expression plasmid for the FLAG-tagged protein of interest.
  - o *Note: literature precedent and/or knowledge of protein structure and function should be used to select the N- or C-terminal location of the tag and inclusion of flexible linkers.*
- DNA transfection reagent (Lipofectamine 3000, Invitrogen cat. no. L3000008)
- Reduced serum medium for transfection (Opti-MEM, Gibco cat. no. 11058021)
- Monofunctional cholesterol photoaffinity probe **2** (Fig. 1) (Mafi et al., 2021)
- Cell scrapers (cell scraper for dishes, VWR cat. no. 10062-906)
- Sterile TC-treated 100 mm cell culture dish with lid (Corning cat. no. 353003)
- Low-profile ice container (for UV crosslinker), e.g., the bottom tier of a stackable pipette tip box
- Dulbecco's Modified Eagle's Medium (DMEM, Gibco cat. no. 11965118)
- Phenol red-free Dulbecco's Modified Eagle's Medium (DMEM, no phenol red, Gibco cat. no. 21063029)
- Fetal Bovine Serum (FBS) (Life Technologies cat. no. 26140079)
- L-glutamine (CAS no. 56-85-9, Oakwood Chemical cat. no. M02960)
- Penicillin-Streptomycin (Pen-Strep) (Gibco, cat. no. 21063029)
- Sodium pyruvate (CAS no. 113-24-6, Sodium Pyruvate 100 mM, Gibco cat. no. 11360070)

4.1.1.3 Cell lines

- HEK293T immortalized human embryonic kidney cells (ATCC cat. no. CRL-3216)
  - o *Note: Cells should be subcultured according to manufacturer protocols and used between passages 4 and 15 for this protocol.*

4.1.1.4 Buffers, solutions, and media

- HEK293T cell culture media: 10 % FBS, 4 mM L-glutamine, 1 × Pen-Strep, and 1 mM sodium pyruvate in DMEM
- HEK293T low-serum media (phenol red-free): 0.5 % FBS, 4 mM L-glutamine, 1 × Pen-Strep, and 1 mM sodium pyruvate in phenol red-free DMEM
- 1 × cholesterol probe media: 10 μM cholesterol probe **2** in low-serum media

4.1.2 Protocol

1. Seed 2×10^6 cells HEK293T cells in a 10 cm dish one day before transfection.
2. Transfect the cells with 10–15 μg of DNA using Lipofectamine 3000 according to manufacturer instructions. Culture for an additional 2 days.
3. Replace culture media from the cells with 5 mL 1 × cholesterol probe media and incubate the cells at 37 °C for 30 min
4. Wash the cells once with 5 mL ice-cold PBS and maintain the cells in PBS on ice.
5. Remove the lid from plate and irradiate for 5 min on ice with 368 nm light using a UV crosslinker.
6. After crosslinking, detach the cells by scraping in cold PBS on ice.
7. Centrifuge the collected cells at 750 × *g* for 5 min at 4 °C.
8. Aspirate the supernatant, then resuspend the cell pellet in 3 mL ice-cold PBS and centrifuge the collected cells at 750 × *g* for 5 min at 4 °C. Repeat for a total of 2 washes.
9. Snap-freeze the cell pellet in liquid N_2 and store at −80 °C or proceed to Section 4.2.

4.2 Cell lysis and target protein immunoprecipitation

In Section 4.2, pellets from transfected HEK293T cells that have been photocrosslinked to cholesterol probe **2** are lysed and FLAG-tagged proteins are enriched on anti-FLAG resin (Fig. 12).

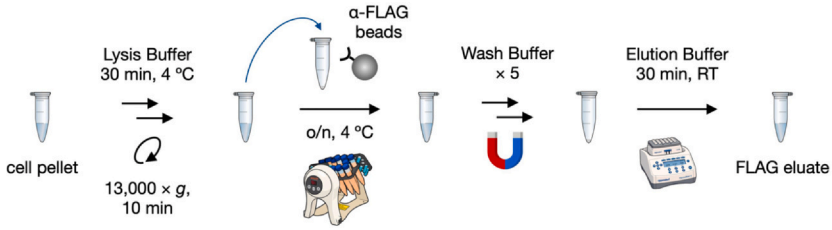

Fig. 12 Workflow summary for Section 4.2.

4.2.1 Materials and equipment

4.2.1.1 Equipment and instruments

- Mechanical tube rotator (Tube Revolver Rotator, Thermo Scientific cat. no. 88881001)
- Magnetic stand (Invitrogen DynaMag-2 Magnet, Thermo Scientific cat. no. 12321D)
- Thermomixer (Eppendorf ThermoMixer C, cat. no. 5382000023)

4.2.1.2 Consumables and reagents

- Anti-DYKDDDDK Magnetic Agarose (Thermo Scientific, A36797, pre-washed twice with 0.1 % IGEPAL-CA630 in PBS)
- FLAG peptide (DYKDDDK (FLAG) peptide, GenScript, RP10586-1)
- 1.5 mL Protein Lo-Bind tubes (Eppendorf cat. no. 022431081)
- BCA protein assay kit (Pierce, Thermo Scientific cat. no. 23227)
- cOmplete EDTA-free Protease Inhibitor Cocktail (Sigma-Aldrich, cat. no. 11836170001)
- Phosphatase inhibitor cocktail (Roche PhosSTOP, Sigma-Aldrich cat. no. 4906845001)
- IGEPAL-CA630 (CAS no. 9002-93-1, Sigma-Aldrich cat. no. I3021)
- Triton X-100 (CAS no. 9002-93-1, Bio-Rad cat. no. 1610407)
- DL-Dithiothreitol (DTT) (CAS no. 3483-12-3, Fisher cat. no. BP172)
- Bromophenol blue (CAS no. 115-39-9, Sigma-Aldrich cat. no. 114391)
- Glycerol (CAS no. 56-81-5, Sigma-Aldrich cat. no. G7893)

4.2.1.3 Buffers, solutions, and media

- Bead Rinse Buffer 1: 0.1 % Igepal CA-630, 1 × cOmplete EDTA-free Protease Inhibitor Cocktail, 1 × PhosSTOP phosphatase inhibitor cocktail in PBS

- IP lysis buffer: 1 % Triton X-100, 2 % IGEPAL-CA630, 1 × cOmplete EDTA-free Protease Inhibitor Cocktail, 1 × PhosSTOP phosphatase inhibitor cocktail in PBS
- Dilution Buffer: 1 × cOmplete EDTA-free Protease Inhibitor Cocktail, 1 × PhosSTOP phosphatase inhibitor cocktail in PBS
- Wash Buffer: 1 % Igepal, 0.5 % Triton, 1 × cOmplete EDTA-free Protease Inhibitor Cocktail, 1 × PhosSTOP phosphatase inhibitor cocktail in PBS
- Elution Buffer: 1.5 mg/mL FLAG peptide in PBS containing 0.5 % IGEPAL-CA630
- 6 × SDS Sample Buffer: 300 mM Tris, adjusted to pH 6.8 with HCl, 50 % (v/v) glycerol, 12 % (w/v) SDS, 600 mM DTT, and 0.6 g/L bromophenol blue.

4.2.2 Protocol

1. Mix the anti-FLAG magnetic beads thoroughly by vortexing and dispense 25 μL to microcentrifuge tubes. Re-vortex periodically to ensure that equivalent, homogenous aliquots are transferred to each tube.
2. Pre-wash the resin: Resuspend the beads with 200 μL Bead Rinse Buffer, invert the tube several times, spin the sample briefly on a mini centrifuge, and place the tube on the magnet to collect the magnetic beads. Discard the supernatant. Resuspend with an additional 200 μL Bead Rinse Buffer, and store until use. Immediately before adding sample, place the tube on the magnet and discard the Bead Rinse Buffer.
3. Resuspend the cell pellets in 500 μL ice-cold IP Lysis Buffer by gentle vortexing and incubate using an end-over-end rotator for 30 min at 4 °C.
4. Centrifuge the lysate at 13,000 × *g* for 10 min at 4 °C.
5. Collect the supernatant in a 1.5 mL microcentrifuge tube.
6. Determine the protein concentration of the supernatant using the BCA protein assay according to manufacturer protocols.
7. Normalize all samples to the same protein concentration by dilution with IP Lysis Buffer.
   - *Note: one 10 cm dish of HEK-293T cells generally yields 2–3 mg total protein.*
8. Dilute the normalized cell lysate 1:1 with Dilution Buffer.
9. Transfer the cell lysate to a microcentrifuge tube containing 50 μL prewashed FLAG magnetic agarose resins.

10. Incubate on an end-over-end rotator overnight (12–16 h) at 4 °C.
11. Place the tube on the magnet and aspirate the supernatant.
12. Wash the resin by removing the tube from the magnet and resuspending the beads with 200 µL Wash Buffer. Gently invert the tube several times, place the tube on the magnet to collect the magnetic beads, and remove the supernatant.
13. Repeat for a total of 5 washes with Wash Buffer, then transfer a suspension of the beads in the last wash to a new 1.5 mL tube.
14. Place the tube on the magnet and aspirate the last wash.
15. Elute the proteins by incubating the resin in 54 µL Elution Buffer on a Thermomixer for 30 min at 25 °C and 950 rpm.
16. Place the tube on the magnet and transfer the eluent to a new 1.5 mL microcentrifuge tube.
17. Store the eluate at –20 °C or proceed to Section 4.4.

4.3 S-Trap protein digestion and desalting

In Section 4.3, proteins eluted from the anti-FLAG resin are digested with trypsin and desalted using an S-Trap (Fig. 13).

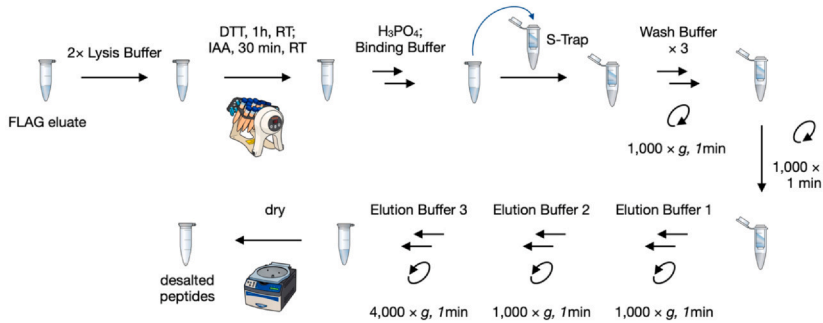

Fig. 13 Workflow summary for Section 4.3.

4.3.1 Materials and equipment

4.3.1.1 Equipment and instruments

- Thermomixer (Eppendorf ThermoMixer C, cat. no. 5382000023)
- Centrifuge (5430 R refrigerated microcentrifuge, Eppendorf cat. no. 022620667)
- Refrigerated centrifugal concentrator (Refrigerated CentriVac Centrifugal Vacuum Concentrator, Labconco cat. no. 7310022)

4.3.1.2 Consumables and reagents

- S-Trap micro columns (PortiFi cat. no. C02-micro-40)
- 1.5 mL Protein Lo-Bind tubes (Eppendorf cat. no. 022431081)
- Sequencing Grade Trypsin (0.5 μg/μL in 50 mM acetic acid, Promega cat. no. V5111)
- DL-Dithiothreitol (DTT) (CAS no. 3483-12-3, Sigma-Aldrich cat. no. D0632)
- Iodoacetamide (CAS no. 144-48-9, Sigma-Aldrich cat. no. 16125)
- Formic acid (CAS no. 64-18-6, Fisher Chemical cat. no. A11710×1)
- Triethylammonium bicarbonate buffer (TEAB) (1 M, CAS no. 15715-58-9, Sigma-Aldrich cat. no. T7408)
- Phosphoric acid (o-Phosphoric Acid, 85 % (Certified ACS), CAS no. 7664-38-2, Fisher Chemical cat. no. A242**)**

4.3.1.3 Buffers, solutions, and media

- 2 × Lysis Buffer: 10 % SDS in 100 mM TEAB at pH 8.5
- 500 mM DTT in H_2O. *Note: prepare fresh immediately before use.*
- 500 mM Iodoacetamide in H_2O. *Note: prepare fresh immediately before use and shield from light.*
- 2 % phosphoric acid in H_2O
- Binding/Wash Buffer: 100 mM TEAB at pH 7.55 in 90 % methanol
- Digestion Buffer: 0.08 μg/μL trypsin in 50 mM TEAB at pH 8.5
- Elution buffer 1: 50 mM TEAB at pH 8.5
- Elution buffer 2: 0.2 % formic acid in H_2O
- Elution buffer 3: 50 % acetonitrile and 0.2 % formic acid in H_2O

4.3.2 Protocol

1. Add 54 μL 2 × Lysis Buffer to the sample in 54 μL Elution Buffer to yield a final volume of 110 μL and vortex to mix.
2. Add 4.5 μL 500 mM DTT (to a final concentration of 20 mM DTT), mix and incubate at 50 °C for 30 min on a Thermomixer at 950 rpm.
3. Allow the sample to cool to room temperature and add 9.8 μL 500 mM iodoacetamide in water (to a final concentration of 40 mM iodoacetamide), mix and incubate at room temperature for 30 min
4. Add 13.6 μL of 2 % phosphoric acid in water and vortex.
5. Add 815.4 μL of Binding/Wash Buffer to the sample and mix.
6. Place an S-Trap micro column in a 2 mL receiving tube and apply the sample to the column.

7. Centrifuge the S-Trap column at 1000 × *g* for 30 s at room temperature. Discard the flow through.
8. Add 150 μL of Binding/Wash Buffer, then centrifuge at 1000 × *g* for 30 s at room temperature. Repeat for a total of 3 washes, discarding the flow through as necessary.
9. Centrifuge the S-Trap column at 1000 × *g* for 1 min at room temperature to fully remove residual Binding/Wash Buffer.
10. Transfer the S-Trap column to a clean 1.7 mL sample tube.
11. Add 25 μL Digestion Buffer to the center of the S-trap column and cap the S-Trap loosely.
12. Incubate for 1–2 h at 47 °C or overnight at 37 °C.
13. Allow the sample to cool to room temperature and add 40 μL Elution Buffer 1 to the center of the S-Trap, then centrifuge at 1000 × *g* for 1 min at room temperature.
14. Transfer the eluted peptides to a new 1.5 mL Lo-bind tube.
15. Add 40 μL Elution Buffer 2 to the S-Trap and centrifuge at 1000 × *g* for 1 min at room temperature.
16. Transfer the eluted peptides to the Lo-bind tube containing the first elution sample.
17. Add 40 μL of Elution Buffer 3 to the center of the S-Trap and centrifuge at 1000 × *g* for 1 min at room temperature, followed by 4000 × *g* for 1 min at room temperature.
18. Transfer the eluted peptides to the Lo-bind tube containing the first and second elution samples.
19. Concentrated the eluted peptides to dryness using a Centrivap concentrator at room temperature.
20. Stored the dried peptides at −80 °C.

4.4 LC-MS analysis

In Section 4.4, the desalted peptides are analyzed using an LC-MS^2 spectrometer (Fig. 14).

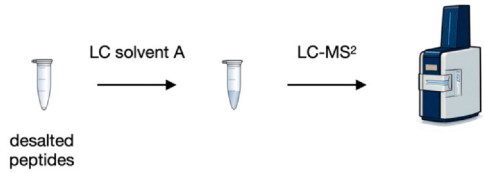

Fig. 14 Workflow summary for Section 4.4.

4.4.1 Materials and equipment

4.4.1.1 Equipment and instruments

- NanoElute 2 coupled to a TimsTOF HT mass spectrometer (Bruker Daltonics)
- C18 column (1.5 μm C18 particles packed in a 25 cm long, 150 μm i.d., Bruker Daltonics/Pepsep)

4.4.1.2 Consumables and reagents

- Formic acid (CAS no. 64-18-6, Fisher Chemical cat. no. A11710×1)
- Acetonitrile, LC-MS grade (CAS no. 75-05-8, Sigma-Aldrich cat. no. 900667)

4.4.1.3 Buffers, solutions, and media

- LC Solvent A: 0.1 % formic acid in H_2O
- LC Solvent B: 0.1 % formic acid in acetonitrile

4.4.2 Protocol

1. Resuspend the dried desalted peptides in appropriate volume of LC Solvent A
2. Subject the samples to mass spectrometry analysis. Inject the sample into a nanoElute 2 fitted with a 25 cm long, 150 μm i.d. microcapillary packed with 1.5 μm C18 particles coupled to a TimsTOF HT mass spectrometer. Elute the peptides at a flow rate of 500 nL/min over a 30-minute linear gradient (5–95 % Buffer B) at 50 °C.
3. Analyze the data using Proteome Discoverer or FragPipe (Figs. 15 and 16)

4.5 Data analysis notes

The main challenge to binding site identification is detecting the modified peptide. As noted above, this is due to both intrinsic diazirine crosslinking efficiency and sample handling with hydrophobic/transmembrane proteins. In our experience, >90 % coverage of the target protein is required to confidently identify the modified peptide and/or residue. We have used Proteome Discoverer (PD) for raw data analysis from an Orbitrap Q Exactive HF mass spectrometer according to the parameters in (Mafi et al., 2021) and FragPipe Version 20 for data analysis from a TimsTOF HT mass spectrometer (Khalil & Plisnier, 2025). To identify modified peptides on a specific protein target, spectra can be searched against a custom FASTA file containing the recombinant protein sequence and a database of common

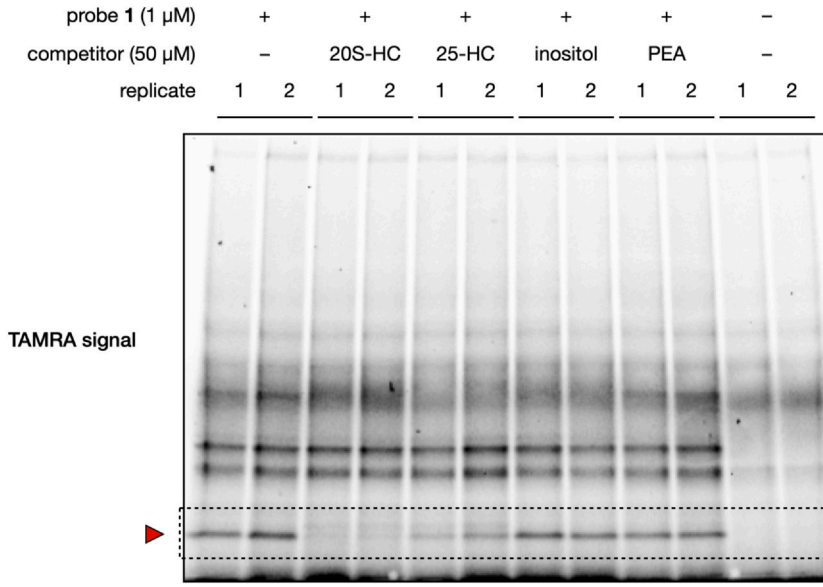

Fig. 15 In gel visualization of TAMRA labeled proteins using probe 1. TAMRA-labeled proteins from NIH-3T3 cells after photocrosslinking to photoaffinity probe **1** and click chemistry tagging with TAMRA azide. The red arrowhead highlights TAMRA-labeled band that is attenuated to various extents in the presence of different competitors. 20S-HC: 20(S)-hydroxycholesterol; 25-HC: 25-hydroxycholesterol; PEA: palmitoylethanolamine. *Data from Cheng et al. (2021).*

contaminant proteins using SEQUEST or an equivalent program. The SEQUEST HT search is conducted with the standard parameters described in (Mafi et al., 2021). It is advisable to manually validate both MS^1 and MS^2 spectra for modified peptide to assess the robustness of the assignments (Fig. 17) (Frédérique, Simon, Manor, & Dirk, 2025).

To perform a closed search for the mass of a diazirine photoaffinity probe, it is necessary to calculate the mass of the original probe minus N_2. In addition, we have found that functional groups in the probe may be sensitive to sample processing or mass spectrometry analysis; thus, the mass of the searched-for modification must be adjusted accordingly. For example, the tertiary alcohol in probes derived from 20S-HC (Fig. 1) are susceptible to dehydration; thus, both modification by the original probe and modification by altered probe structure(s) should be calculated and included in the search.

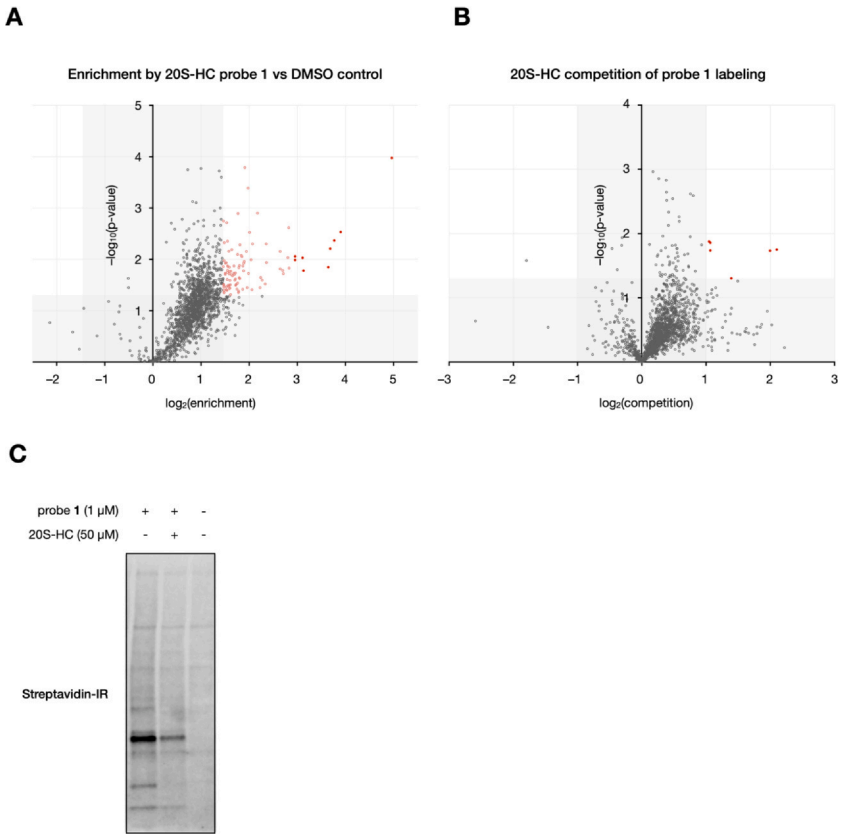

Fig. 16 Chemoproteomics results for 20S-HC probe 1 in live NIH-3T3 cells. (A) Enrichment of biotinylated proteins in cells photocrosslinked to probe **1** (1 μM) vs control. The horizontal grey area represents proteins with a p-value of < 0.05; the vertical grey area represents proteins with fold change for probe **1** vs vehicle control of > 2.75. (B) Competition of protein biotinylation by probe **1** (1 μM) in the presence of the competitor 20S-HC (50 μM). The horizontal grey area represents proteins with a p-value of < 0.05; the vertical grey area represents proteins with fold change for probe **1** vs probe **1** + 20S-HC of > 2.00. (C) Visualization of biotinylated proteins from NIH-3T3 cells after photocrosslinking to photoaffinity probe **1** and click chemistry tagging with biotin picolyl azide. Lanes 1, 2, and 3 represent combined aliquots taken from the streptavidin beads after washing (2 % of total agarose volume per sample). Aliquots from triplicate samples from the same condition (probe, probe + competition, or vehicle) were combined and subjected to far Western blot analysis with visualization using Streptavidin IRDye 800CW (LICORbio cat. no. 926–32230). This analysis serves as a quality control check before proceeding to LC-MS^3 analysis. *Data from Cheng et al. (2021).*

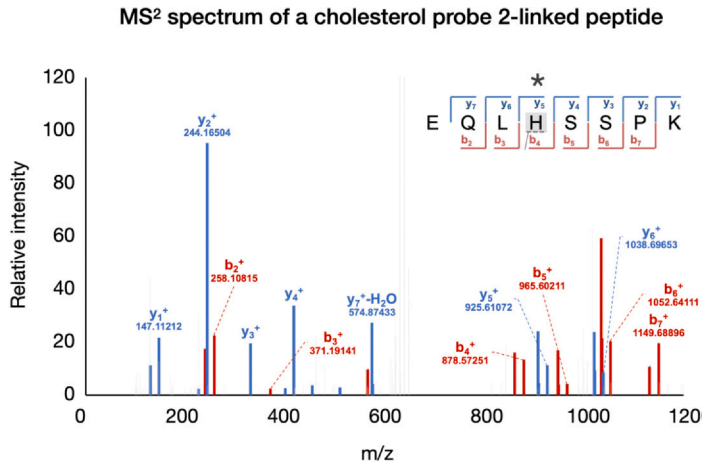

Fig. 17 Binding site identification of cholesterol probe 2. MS^2 spectrum of a probe **2**-modified peptide showing crosslinking at the histidine residue marked by an asterisk. *Data from Mafi et al. (2021).*

5. Discussion

Extending the breadth of interactome analysis to include metabolite-protein networks requires a set of distinct tools, strategies, and considerations. This is particularly true for cholesterol metabolites; their hydrophobicity and the nature of their protein targets present unique analytical challenges. Nonetheless, cholesterol metabolite probes provide a transformative approach to link precise, quantitative network- and residue-level protein interactions with the multifaceted roles of cholesterol metabolism in physiology and disease.

Acknowledgments

We acknowledge Prof. Alexander Adibekian and Dr. Daniel Abegg for collaboration on Section 4. This work was supported the National Institute of General Medical Sciences under award number R35GM152119. Select figure icons were created using BioRender (biorender.com).

References

Baghirova, S., Hughes, B. G., Hendzel, M. J., & Schulz, R. (2015). Sequential fractionation and isolation of subcellular proteins from tissue or cultured cells. *MethodsX, 2*, 440–445. https://doi.org/10.1016/j.mex.2015.11.001.

Burton, N. R., Kim, P., & Backus, K. M. (2021). Photoaffinity labelling strategies for mapping the small molecule-protein interactome. *Organic & Biomolecular Chemistry, 19*(36), 7792–7809. https://doi.org/10.1039/d1ob01353j.

Cheng, Y. S., Zhang, T., Ma, X., Pratuangtham, S., Zhang, G. C., Ondrus, A. A., ... Ondrus, A. E. (2021). A proteome-wide map of 20(S)-hydroxycholesterol interactors in cell membranes. *Nature Chemical Biology, 17*(12), 1271–1280. https://doi.org/10.1038/s41589-021-00907-2.

Christian, A. E., Haynes, M. P., Phillips, M. C., & Rothblat, G. H. (1997). Use of cyclodextrins for manipulating cellular cholesterol content. *Journal of Lipid Research, 38*(11), 2264–2272. https://doi.org/10.1016/s0022-2275(20)34940-3.

Flaxman, H. A., Miyamoto, D. K., & Woo, C. M. (2019). Small molecule interactome mapping by photo-affinity labeling (SIM-PAL) to identify binding sites of small molecules on a proteome-wide scale. *Current Protocols in Chemical Biology, 11*(4), e75. https://doi.org/10.1002/cpch.75.

Frédérique, V., Simon, A., Manor, A., & Dirk, V. (2025). Defining spectral quality in mass spectrometry-based proteomics: A retrospective review. *Mass Spectrometry Reviews*, 10.1002/mas.21933. https://doi.org/10.1002/mas.21933. Advance online publication.

Homan, R. A., Lapek, J. D., Woo, C. M., Niessen, S., Jones, L. H., & Parker, C. G. (2024). Photoaffinity labelling with small molecules. *Nature Reviews Methods Primers, 4*(1), https://doi.org/10.1038/s43586-024-00308-4.

Khalil, S., & Plisnier, M. (2025). Comparative analysis of MS/MS search algorithms in label-free shotgun proteomics for monitoring host-cell proteins using trapped ion mobility and ddaPASEF. *Journal of Pharmaceutical and Biomedical Analysis Open, 6*, 100082. https://doi.org/10.1016/j.jpbao.2025.100082.

Luchetti, G., Sircar, R., Kong, J. H., Nachtergaele, S., Sagner, A., Byrne, E. F., et al. (2016). Cholesterol activates the G-protein coupled receptor Smoothened to promote Hedgehog signaling. *eLife, 5*. https://doi.org/10.7554/elife.20304.

MacKinnon, A. L., Garrison, J. L., Hegde, R. S., & Taunton, J. (2007). Photo-leucine incorporation reveals the target of a cyclodepsipeptide inhibitor of cotranslational translocation. *Journal of the American Chemical Society, 129*(47), 14560–14561. https://doi.org/10.1021/ja076250y.

MacKinnon, A. L., & Taunton, J. (2009). Target identification by diazirine photo--cross-linking and click chemistry. *Current Protocols in Chemical Biology, 1*(1), 55–73. https://doi.org/10.1002/9780470559277.ch090167.

Mafi, A., Purohit, R., Vielmas, E., Lauinger, A. R., Lam, B., Cheng, Y. S., et al. (2021). Hedgehog proteins create a dynamic cholesterol interface. *PLoS One, 16*(2), e0246814. https://doi.org/10.1371/journal.pone.0246814.

McAlister, G. C., Nusinow, D. P., Jedrychowski, M. P., Wühr, M., Huttlin, E. L., Erickson, B. K., et al. (2014). MultiNotch MS3 enables accurate, sensitive, and multiplexed detection of differential expression across cancer cell line proteomes. *Analytical Chemistry, 86*(14), 7150–7158. https://doi.org/10.1021/ac502040v.

Palmblad, M., Hoopmann, M. R., & Dorfer, V. (2025). A special software issue in celebration of Margaret Dayhoff's 100th birthday. *Journal of Proteome Research, 24*(3), 977–978. https://doi.org/10.1021/acs.jproteome.5c00147.

Schneider, M., Zolg, D. P., Samaras, P., Ben Fredj, S., Bold, D., Guevende, A., et al. (2025). A scalable, web-based platform for proteomics data processing, result storage and analysis. *Journal of Proteome Research, 24*(3), 1241–1249. https://doi.org/10.1021/acs.jproteome.4c00871.

Schweppe, D. K., Eng, J. K., Yu, Q., Bailey, D., Rad, R., Navarrete-Perea, J., ... Gygi, S. P. (2020). Full-featured, real-time database searching platform enables fast and accurate multiplexed quantitative proteomics. *Journal of Proteome Research, 19*(5), 2026–2034. https://doi.org/10.1021/acs.jproteome.9b00860.

Shi, Y., Zhong, H., Rogalski, J. C., & Foster, L. J. (2025). Optimizing imputation strategies for mass spectrometry-based proteomics considering intensity and missing value rates. *Computational and Structural Biotechnology Journal, 27*, 1818–1826. https://doi.org/10.1016/j.csbj.2025.04.041.

West, A. V., & Woo, C. M. (2022). Photoaffinity labeling chemistries used to map biomolecular interactions. *Israel Journal of Chemistry, 63*(1–2), https://doi.org/10.1002/ijch.202200081.

Yu, W., & Baskin, J. M. (2022). Photoaffinity labeling approaches to elucidate lipid-protein interactions. *Current Opinion in Chemical Biology, 69*, 102173. https://doi.org/10.1016/j.cbpa.2022.102173.

Zidovetzki, R., & Levitan, I. (2007). Use of cyclodextrins to manipulate plasma membrane cholesterol content: Evidence, misconceptions and control strategies. *Biochimica Et Biophysica Acta (BBA) - Biomembranes, 1768*(6), 1311–1324. https://doi.org/10.1016/j.bbamem.2007.03.026.

CHAPTER THREE

Expression and characterization of phospholipase Cβ and ε enzymes

Hanna D. King[a,1], **Ketaki A. Mahurkar**[a,1], **and Angeline M. Lyon**[a,b,*]
[a]James Tarpo Jr. and Margaret Tarpo Department of Chemistry, Purdue University, West Lafayette, IN, United States
[b]Department of Biological Sciences, Purdue University, West Lafayette, Indiana, United States
*Corresponding author. e-mail address: lyonam@purdue.edu

Contents

1. Introduction 66
2. Before you begin 68
   2.1 PLCβ purification buffers 68
   2.2 PLCε purification buffers 69
   2.3 *In vitro* activity assay (IP1) buffers 70
   2.4 ^{3}[H]-IPx accumulation assay buffers 71
3. Key resources table 72
4. Protein expression and purification 74
   4.1 Materials and equipment for protein expression and purification 74
   4.2 PLCβ expression 75
   4.3 PLCβ purification 76
   4.4 Expression of PLCε N-terminal truncations 79
   4.5 PLCε purification 79
5. Activity Assays 82
   5.1 Materials and equipment for activity assays 82
   5.2 *In vitro* activity assay (IP1) 83
   5.3 ^{3}[H]-IPx accumulation assay 86
6. Expected outcomes 88
7. Quantification and statistical analysis 92
8. Advantages 93
9. Limitations 94
10. Optimization and troubleshooting 95
   10.1 Problem (low protein expression) 95
   10.2 Problem (protein not binding to the Ni-NTA affinity column) 95
   10.3 Problem (*In vitro* activity assay (IP1): Sample(s) have low signal) 95
   10.4 Problem (^{3}[H]-IPx accumulation assay: Sample(s) have low signal) 96
11. Safety considerations and standards 96
12. Alternative methods/procedures 96
References 97

[1] These authors contributed equally to this work.

Methods in Enzymology, Volume 728
ISSN 0076-6879, https://doi.org/10.1016/bs.mie.2026.01.004
Copyright © 2026 Elsevier Inc. All rights are reserved, including those for text and data mining, AI training, and similar technologies.

Abstract

Phospholipase C enzymes play a key role in regulating intracellular calcium release downstream of G protein-coupled receptors and receptor tyrosine kinases. PLCβ and PLCε play key roles in maximal cardiac contractility, cardiac hypertrophy, opioid analgesia, and oncogenesis. Structural and biochemical studies of PLCs have been essential in furthering our understanding of their basal regulation and activation by small G proteins and heterotrimeric G protein subunits. Here, we detail purification protocols for PLCβ and PLCε variants. The resulting proteins have been successfully used for high-resolution structural studies as well as detailed functional studies *in vitro*. We also describe a receptor-independent *in vitro* assay, allowing studies of PLC regulation and activation to be carried out using purified proteins. Finally, we describe also detail the methodology for a radioactivity-based assay that can be used to characterize these lipases *in cellulo*.

1. Introduction

Phospholipase C enzymes (PLC) hydrolyze phosphatidylinositol phosphates, at the cytoplasmic leaflets, of membranes, generating inositol polyphosphates (IPs) and diacylglycerol (DAG). Phosphatidylinositol-4,5-bisphosphate (PIP_2) is the canonical substrate of these enzymes, and its cleavage produces the second messengers inositol-1,4,5-triphosphate (IP_3) and diacylglycerol (DAG). These molecules trigger the release of intracellular Ca^{2+} and activate protein kinase C (PKC)-mediated signaling cascades, respectively (Gresset, Sondek, & Harden, 2012; Kadamur & Ross, 2013; Katan & Cockcroft, 2020). There are six families of PLCs, all of which have four tandem EF hands, a catalytic triose phosphate isomerase (TIM) barrel, and a C2 domain (Gresset et al., 2012; Kadamur & Ross, 2013; Katan & Cockcroft, 2020; Shu, Ryu, Moon, Suh, & Rhee, 1988). Most also contain an N-terminal Pleckstrin Homology (PH) domain (Gresset et al., 2012; Kadamur & Ross, 2013; Katan & Cockcroft, 2020). Additional domains in each subfamily contribute to membrane association and regulation. Here, we focus on the PLCβ and PLCε subfamilies, which are activated downstream of G protein-coupled receptors (GPCRs) and receptor tyrosine kinases (RTKs).

The distinctive feature of PLCβ family members is an extended C terminal region that is approximately 400 amino acids in length. The first ~25 residues are designated as the proximal C-terminal domain (CTD), a highly conserved region involved in autoinhibition and activation by the heterotrimeric G protein subunit Gαq. The proximal CTD is followed by a variable length linker (~20–60 residues) connecting it to the distal CTD.

This coiled-coiled domain contains approximately 300 amino acids, and is essential for membrane association, Gαq binding, and maximum activity (Lyon et al., 2011; Lyon, Dutta, Boguth, Skiniotis, & Tesmer, 2013; Waldo et al., 2010). The activity of PLCβ2 and PLCβ3 can also be increased by the Gβγ heterodimer (Smrcka & Sternweis, 1993). The PLCβ family are important as they play a prominent role in cardiovascular (Descorbeth & Anand-Srivastava, 2008, 2010; Ushio-Fukai, Griendling, Akers, Lyons, & Alexander, 1998), neuronal (Kim et al., 1997) and immunological signaling (Sasai et al., 2021).

PLCε has ~350 residues at its extreme N-terminus that are contribute to its activity but have not been biochemically or structurally characterized, followed by a CDC25 domain and the catalytic core, defined as the PH-C2 domains (Jin et al., 2001; Kelley, Reks, Ondrako, & Smrcka, 2001; Sieng et al., 2021). Following the catalytic core, there are two C-terminal Ras association (RA) Domains, RA1 and RA2 (Bunney et al., 2006; Kelley et al., 2001). The CDC25 domain is guanine nucleotide exchange factor (GEF) for the Rap1A GTPase (Jin et al., 2001; Satoh, Edamatsu, & Kataoka, 2006). Rap1A also activates PLCε by binding to the RA2 domain (Sieng et al., 2021), as do Ras GTPases (Bunney et al., 2006; Seifert, Zhou, Hicks, Sondek, & Harden, 2008). Recent studies have revealed structural insights into the lipase, including the structure of the largest PLCε variant to date, PLCε PH-C (Ohri et al., 2025; Samassekou et al., 2025). Here, we describe a method that has been successfully used to purify variants of PLCε (Ohri et al., 2025; Rugema et al., 2020; Samassekou et al., 2025; Sieng et al., 2021).

In the cardiovascular system, PLCε is required for maximal cardiac contractility. However, persistent activation of PLCε can result in cardiovascular disease; (Wang et al., 2005; Zhang et al., 2013). PLCε is activated through the direct binding of Rap1A (Jin et al., 2001; Zhang et al., 2013), Ras GTPases (Bunney et al., 2006; Kelley et al., 2001), RhoA (Seifert et al., 2008; Ohri et al., 2025), and the Gβγ heterodimer (Madukwe, Garland-Kuntz, Lyon, & Smrcka, 2018).

Two methods for measuring basal and G protein-dependent activation of PLCβ and PLCε are also described here. An *in vitro* IP1 homogeneous time-resolved FRET (HTRF) activity assay is used to measure the activity of purified PLC proteins, whereas the ^{3}[H]-IP$_{x}$ accumulation assay is used to measure activity in mammalian cells (Ohri et al., 2025; Phan et al., 2021, 2022; Samassekou et al., 2025). The cell-based assay is useful for screening a mutants and/or variants that are difficult to purify.

2. Before you begin

Timing: 1–4 hours.

2.1 PLCβ purification buffers

1. Lysis Buffer
   a. 20 mM HEPES, pH 8.0
   b. 200 mM NaCl
   c. 10 mM 2-Mercaptoethanol (β-ME)
   d. 0.1 mM EDTA
   e. 0.1 mM EGTA
   f. 1x PTT (133 μM phenylmethylsulfonyl fluoride (PMSF), 21 μg/mL tosyllysine Chloromethyl Ketone (TLCK), and 0.5 μg/mL tosyl phenylalanyl chloromethyl ketone (TPCK))
   g. 1 ng/mL aprotinin
   h. 1 ng/mL pepstatin
2. Dilution Buffer (Optional)
   a. 10 mM HEPES, pH 8.0
   b. 10 mM β-ME
   c. 0.1 mM EDTA
   d. 0.1 mM EGTA
   e. 1x PTT (133 μM PMSF, 21 μg/mL TLCK, and 0.5 μg/mL TPCK)
   f. 1 ng/mL aprotinin
   g. 1 ng/mL pepstatin
3. Wash Buffer 1
   a. 10 mM HEPES, pH 8.0
   b. 100 mM NaCl
   c. 10 mM β-ME
   d. 0.1 mM EDTA
   e. 0.1 mM EGTA
   f. 1x PTT (133 μM PMSF, 21 μg/mL TLCK, and 0.5 μg/mL TPCK)
   g. 1 ng/mL aprotinin
   h. 1 ng/mL pepstatin
4. Wash Buffer 2
   a. 10 mM HEPES, pH 8.0
   b. 100 mM NaCl
   c. 10 mM β-ME
   d. 0.1 mM EDTA

e. 0.1 mM EGTA
f. 10 mM imidazole
g. 1x PTT (133 μM PMSF, 21 μg/mL TLCK, and 0.5 μg/mL TPCK)
h. 1 ng/mL aprotinin
i. 1 ng/mL pepstatin

5. Elution Buffer
a. 10 mM HEPES, pH 8.0
b. 100 mM NaCl
c. 10 mM β-ME
d. 0.1 mM EDTA
e. 0.1 mM EGTA
f. 200 mM imidazole
g. 1x PTT (133 μM PMSF, 21 μg/mL TLCK, and 0.5 μg/mL TPCK)
h. 1 ng/mL aprotinin
i. 1 ng/mL pepstatin

6. Size Exclusion Chromatography Buffer
a. 20 mM HEPES, pH 8.0
b. 150 mM NaCl
c. 2 mM Dithiothreitol (DTT)
d. 0.1 mM EDTA
e. 0.1 mM EGTA

2.2 PLCε purification buffers

1. Hypotonic Lysis Buffer
a. 20 mM HEPES, pH 8.0
b. 50 mM NaCl
c. 10 mM β-Me
d. 0.1 mM EDTA
e. 0.1 mM EGTA
f. cOmplete™ ULTRA Tablets, Mini, EDTA-free, *EASYpack* Protease Inhibitor Cocktail, 2 per 300 mL

2. HisTrap Binding Buffer
a. 20 mM HEPES, pH 8.0
b. 300 mM NaCl
c. 20 mM imidazole
d. 10 mM β-Me
e. 0.1 mM EDTA
f. 0.1 mM EGTA

3. HisTrap Elution Buffer
   a. 20 mM HEPES, pH 8.0
   b. 100 mM NaCl
   c. 500 mM imidazole
   d. 10 mM β-Me
   e. 0.1 mM EDTA
   f. 0.1 mM EGTA
4. Ion Exchange Start Buffer
   a. 20 mM HEPES, pH 8.0
   b. 100 mM NaCl
   c. 2 mM DTT
   d. 0.1 mM EDTA
   e. 0.1 mM EGTA
5. Ion Exchange High Salt Buffer
   a. 20 mM HEPES, pH 8.0
   b. 500 mM NaCl
   c. 2 mM DTT
   d. 0.1 mM EDTA
   e. 0.1 mM EGTA
6. Size Exclusion Chromatography Buffer
   a. 20 mM HEPES, pH 8.0
   b. 150 mM NaCl
   c. 2 mM DTT
   d. 0.1 mM EDTA
   e. 0.1 mM EGTA

2.3 *In vitro* activity assay (IP1) buffers

1. 2X Assay Buffer
   a. 100 mM HEPES, pH 7.4
   b. 160 mM KCl
   c. 6 mM EGTA
2. 6X Incubation Buffer
   a. 100 mM HEPES, pH 7.4
   b. 100 mM NaCl
   c. 10 mM $MgCl_2$
   d. 6 mM EGTA
   e. 6 mM EDTA

3. Sonication Buffer
   a. 1X Assay Buffer
   b. 1 mM DTT
4. Calcium Buffer
   a. 1X Assay Buffer
   b. 1 mM DTT
   c. 180 mM $CaCl_2$
5. Quench Buffer
   a. 1X Assay Buffer
   b. 1 mM DTT
   c. 210 mM EGTA
6. PLC BSA Buffer
   a. 1X Assay buffer
   b. 3 mM DTT
   c. 3 mg/mL Bovine Serum Albumin (BSA)
   d. PLC
7. G Protein Buffer
   a. 1X Incubation Buffer
   b. 0.1 M DTT
   c. 1 % CHAPS
   d. G protein
   e. G Protein Purification Buffer

2.4 ^{3}[H]-IPx accumulation assay buffers

1. Complete Dulbecco's Modified Eagle Medium (DMEM): DMEM, supplemented with
   a. 1x Penicillin-Streptomycin
   b. 10 % FBS
   c. 5 % Glutamax
2. 1x Phosphate-buffered saline (PBS)
3. 1 M LiCl
4. 50 mM formic acid
5. 100 mM formic acid
6. 1.2 M ammonium formate, 0.1 M formic acid
7. 2 M ammonium format, 0.1 M formic acid
8. Uniscint BD for high salt

3. Key resources table

Note that not all areas will be used in every protocol.

Reagent or resource	Source	Identifier
Bacterial and Virus Strains		
MAX Efficiency™ DH10Bac Competent Cells	ThermoFisher	10361012
Chemicals, Peptides, and Recombinant Proteins		
HEPES (Fine White Crystals/Molecular Biology)	ThermoFisher	BP310-1
Trypan Blue	ThermoFisher	MT25900CI
NaCl	Fisher	S271-10
2-Mercaptoethanol (β-Me)	Acros Organics	60-24-2
EDTA	BDH	BDH4528-1KGP
EGTA	Acros Organics	67-42-5
Dithiothreitol (DTT)	Fisher	BP172-5
phenylmethylsulfonyl fluoride (PMSF)	Fisher	AC215740100
Tosyllysine Chloromethyl Ketone (TLCK)	Cayman Chemical	13074
Tosyl phenylalanyl chloromethyl ketone (TPCK)	Cayman Chemical	20166
aprotinin	Sigma	A1153-25MG
pepstatin	Sigma	P5318-25MG
imidazole	Fisher	O3196-500
complete™ ULTRA Tablets, Mini, EDTA-free, *EASYpack* Protease Inhibitor Cocktail	Sigma	5892791001
Coomassie stain	BioRad	1610787
KCl	Fisher	BP366-500
$MgCl_2$	Fisher	M33-500
$CaCl_2$	Fisher	AC349610250
Bovine Serum Albumin	Fisher	BP9703100
CHAPS	Sigma	220201-10GM

Egg L-α-phosphatidylethanolamine	Avanti	840021P-25MG
Soy L-α-phosphatidylinositol	Avanti	840044C-25mg
Phosphate Buffered Saline	Fisher	MT21040CV
Fugene	Promega	E2692
LiCl	Acros Organics	7447-41-8
Formic Acid	Fisher	A119-P-1
ammonium formate	Fisher	AC401150050
Inositol, Myo, -[2-3H(N)]-, Ethanol Solution	Perkin Elmer	NET114005MC
Unscint BD for high salt	National Diagnostics	LS-276
chloroform	Fisher	C298-4
methanol	Fisher	A452-4
Penicillin-Streptomycin Solution, 100x	Fisher	30-002-CI
Glutamax	Fisher	35050-061
BLUEstain™ Protein ladder, 11-245 kDa	GoldBio	P007-500
Dulbecco's Modified Eagle Medium (DMEM)	Corning	15-013-CV
Fetal Bovine Serum (FBS)	Bio-Techne	S11150
F-10	Fisher	11-550-043
ESF 921 Media	Expression Systems	96-001-01
Critical Commercial Assays		
HTRF IP-One Gq Detection Kit	Revvity	62IPAPEB
Experimental Models: Cell Lines		
Sf9	Expression Systems	94-001S
High Five™ Cells (BTI-TN-5B1-4)	ThermoFisher	B85502
COS-7 (CRL-1651™)	ATCC	CRL-1651™
Recombinant DNA		
pFastBac™ HT vector	ThermoFisher	10584027

Software and Algorithms		
GraphPad Prism	Dotmatics	
Other		
Scintillation Vials	RPI	121043BP
AG 1-X8 Resin	BioRad	1401444
Poly-Prep® Chromatography Columns	BioRad	#7311550
Thermo Scientific™ Nalgene™ Polycarbonate Baffled Culture Flasks	ThermoFisher	10-042-5M
BioLite 12 Well Multidish	ThermoFisher	130185

4. Protein expression and purification

4.1 Materials and equipment for protein expression and purification

4.1.1 Virus production

- pFastBac HT vector encoding protein of interest
- DH10Bac cells
- Bacmid with protein insert
- Transfection reagent (Fugene, or similar)
- Transfection media (serum free)
- ESF 921 media
- Sf9 cells
- Polycarbonate baffled culture flasks
- Room temperature shaker (e.g. Thermo Scientific MaxQ 8000)
- Tabletop centrifuge (e.g. Thermo Scientific Sorvall ST 8 R)

Alternatives: (Alternative materials or equipment can be called out in this format).

- Any baculovirus expression vector can be used, such as BacMam and dual-expression vectors.

4.1.2 Protein expression/purification

- High Five or Sf9 cells (PLCβ and PLCε respectively)
- High Five media or ESF 921 media
- Penicillin-Streptomycin Solution
- Nickel resin or FPLC nickel columns

- Anion exchange resin (or anion exchange column for FPLC)
- gravity columns
- column stand
- Ultracentrifuge (e.g. Beckman Coulter Avanti J-30I)
- 50 mL Polycarbonate bottle with cap assembly, or other polycarbonate bottles compatible with ultracentrifuge
- Dounce homogenizer
- Protein concentrators (of appropriate molecular weight (MW) cutoffs)
- FPLC (e.g. Äkta pure)
- Size exclusion chromatography columns (i.e. Superdex S200)
- Coomassie
- SDS-PAGE Gels (5 % stacking, 10 % resolving)
- Protein Ladder (BLUEstain™, 11-245 kDa), or similar

Alternatives: (Alternative materials or equipment can be called out in this format).

- Any insect cell media for High Five or Sf9 cells can be used, provided the cells are adapted to it.

4.2 PLCβ expression

Timing: 48 h.

1. Protein is expressed using a baculovirus system. For protein expression, infect 1 L of High Five cells at a density of 1.8–2.2 × 106 cells/mL with 10–20 mL of a P2 virus (assume an MOI of 1).
2. Maximum protein expression is observed when the infection is allowed to proceed for 48 h. Maintain the cells at 27 °C and continuous shaking at 120 rpm.
3. Visually confirm the High Five cells are infected using a brightfield microscope. Infected cells appear swollen, are granular, and larger than uninfected cells, Fig. 1.
4. Harvest infected cells at 48 h by centrifugation at 5000 *x g* for 10 min at 4 °C.
5. Discard the supernatant, resuspend the pellet with 20 mL of 1x PBS and transfer to 50 mL conical. Centrifuge the sample again 5000 *x g* for 10 min at 4 °C.
   a. Alternative: After the first centrifugation, step 4, pour off supernatant. Fill 50 mL conical roughly 1/3 full of liquid nitrogen. Using a spatula, scrape pieces of the cell pellet into liquid nitrogen and snap freeze.
6. Discard the supernatant, and snap freeze the pellet in liquid nitrogen. Store at −80 °C until needed.

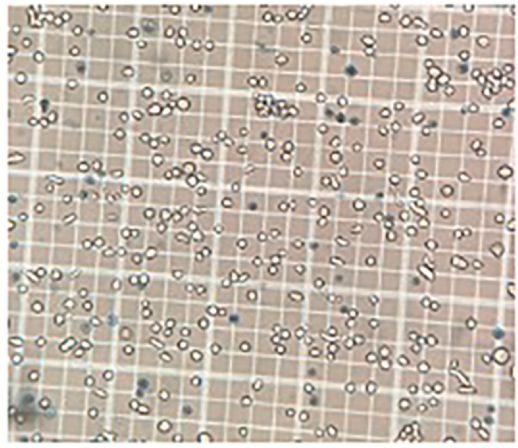

Fig. 1 Insect cell protein expression. HighFive cells infected with P2 virus, after 48 h incubation. Cells stained with trypan blue to assess cell death.

Critical: If cells do not appear infected it is strongly recommended that expression be confirmed by SDS-PAGE before proceeding with the purification. Protein expression can also be assessed using the P1 virus and western blot.

Critical: Viruses have a limited shelf life, and expression is best when viruses are newly made.

4.3 PLCβ purification

Timing: For best results, protein purification should be completed in one day. Purifications taking longer than 24 h will result in protein deg.

4.3.1 Lysis

1. Add 20 mL of chilled lysis buffer to a 1 L cell pellet and thaw on ice.
2. Resuspend pellet until the mixture is homogenous, then add lysis buffer to increase the volume to 40 mL total.
3. Add 20 mL of resuspended cells and 20 mL of lysis buffer to a 50 mL Dounce homogenizer on ice. Dounce the mixture 10 times with the loose pestle, followed by 10 times with the tight-fitting pestle. Keep homogenizer on ice as much as possible.
4. Using the remaining 20 mL of resuspended cells from Step 3, repeat steps 4-5. Cell lysis can be confirmed using brightfield microscopy.
5. Collect a 10 μL sample of the lysed cells for analysis by SDS-PAGE.

6. Ultracentrifuge lysed cells at 100,000 *x g* for 1 h at 4 °C. Collect the supernatant which contains PLCβ.
   a. OPTIONAL: PLCβ can also be partially purified by salting out. To do so, add 10 mL of lysis buffer to 20 mL of lysate, followed by 10 mL of 4 M NaCl. The NaCl must be added last.
   b. If the protein is salted out, the NaCl concentration must be decreased prior to purification by Ni-NTA affinity chromatography. Use the dilution buffer to lower NaCl overall concentration. The final NaCl concentration is dependent upon the resin used in this step.
7. Filter the supernatant through a glass fiber filter into an autoclaved bottle (~160 mL total volume)
8. Collect a 10 μL sample of the lysed cells for analysis by SDS-PAGE.

4.3.2 Ni-NTA affinity chromatography

For a 1 L prep, a bed volume of 2 mL of most Ni-NTA resins is sufficient. The binding capacity will vary depending on the manufacturer.

1. Wash the column 10 column volumes (CVs) with lysis buffer.
2. Load filtered supernatant onto HisTrap and collect the flow-through.
   a. Pause Point: Protein can be loaded overnight in a 4 °C cold room or deli case, but care must be taken to ensure the column does not run dry.
3. Collect a 10 μL sample of the flow-through for SDS-PAGE.
4. Wash the HisTrap column with 10 CVs of wash buffer 1 and collect the flow through in a separate container. Collect a 10 μL sample of the flow-through for SDS-PAGE.
5. Wash HisTrap column with 10 CVs of wash buffer 2. Collect what flows through in a clean beaker and collect a 10 μL for SDS-PAGE.
6. Elute the protein from the HisTrap column using 10 mL of elution buffer and collect eluent in a separate container. Collect a 10 μL sample of the elution for SDS-PAGE.
7. To ensure all bound protein was eluted from the HisTrap column, wash with 5 CVs of elution buffer collected in a separate container. Collect a 10 μL sample for SDS-PAGE.
8. Add SDS loading dye to each sample (cell lysate, cell pellet, supernatant, load, flow through, wash 1, wash 2, elution, and bump) and run SDS PAGE. Stain with Coomassie to confirm protein expression and elution from the Ni-NTA affinity column.
9. The majority of partially purified PLCβ protein should be in the elution, with smaller amounts potentially observed in wash 1, wash 2, and/or the

bump. Depending on the relative purity of these samples they can be pooled and concentrated for further purification.

Note: This protocol is written for purification using a HisTrap column but can be adapted to any Ni-NTA affinity column, including gravity columns and FPLCs.

4.3.3 Size exclusion chromatography

1. Wash 1 mL injection loop and equilibrate tandem Superdex S200 columns with SEC buffer.
2. Wash protein concentrator with a 100 kDa molecular weight cut-off with SEC buffer.
3. Concentrate the Ni-NTA elution (and other fractions, if desired) to a final volume of ~1 mL. If protein expression is very high, it may not be possible to concentrate to this volume. In this case, multiple column runs are likely necessary.
4. Transfer concentrated sample to a sterile 1.5 mL Eppendorf tube and centrifuge at 12,000 × *g* for 5 mins at 4 °C to remove any aggregates prior to loading onto the S200 columns.
   a. Alternative: Sample can be run through a 0.2 μm sterile filter before loading on the FPLC.
5. Inject sample into FPLC for purification by SEC using 1 CV of SEC buffer (here, 1 CV corresponds to the total column volumes of both S200 columns).
6. Based on UV absorbance, identify fractions most likely corresponding to purified protein. Collect 8 μL of each fraction for analysis by SDS-PAGE.
7. Prepare a new protein concentration (100 kDa molecular weight cut-off) with SEC buffer, and pool and concentration fractions containing purified PLCβ. Protein should be concentrated to 3–4 mg/mL before aliquoting in 10–50 μL volumes for flash freezing in liquid nitrogen. Store samples at −80 °C.

Note: PLCβ enzymes typically have a smaller elution volume than expected based on their molecular weights. This is because they can adopt extended conformations in solution due to the flexibly connected distal C-terminal domain.

Critical: While concentrating your sample for SEC, stop concentrating immediately if the sample becomes viscous, begins to turn yellow, and/or you observe any precipitant.

Pause Point: FPLC can be run overnight. Fractions should not be pooled and concentrated until after SDS-page analysis.

4.4 Expression of PLCε N-terminal truncations

Timing: 48 h.

1. Infect 1 L of SF9 cells at a density of 1.8–2.2 × 106 million cells/mL with 10 mL of P2 virus (MOI of 1). Allow infection to proceed for 48 h at 27 °C with continuous shaking at 120 rpm.
2. Harvest cells by centrifugation at 5000 × *g* for 10 min at 4 °C.
3. Discard the supernatant and resuspend the pellet with 20 mL of 1x PBS and transfer to 50 mL conical and centrifuged again at 5000 × *g* for 10 min at 4 °C.
   a. Alternative: After first centrifugation, step 4, pour off supernatant. Fill 50 mL conical roughly 1/3 full of liquid nitrogen. Use a spatula to scrape chunks of pellet into liquid nitrogen to snap freeze them.
4. Discard the supernatant, and snap freeze the pellet in liquid nitrogen. Store at −80 °C until needed.

Critical: Viruses have a limited shelf life and protein expression is best when viruses are fresh.

4.5 PLCε purification

Timing: 2–3 days. Longer times compromises protein integrity.

4.5.1 Lysis

1. Add 40 mL of chilled hypotonic lysis buffer to 1 L of cell pellets and thaw on ice. Resuspend the pellet using a sterile pipette.
2. Transfer resuspended cells to a 50 mL Dounce homogenizer. Lyse cells by homogenizing 10 times with the loose-fitting pestle and 10 times with the tight-fitting pestle. If the cell pellet is highly viscous, dilute the 50 mL of resuspended cells to 100 mL total volume with hypotonic lysis buffer and lyse by Dounce homogenizer. Lysis can be visually confirmed by brightfield microscopy.
3. Collect a 10 μL sample of the lysate for SDS-PAGE.
4. Dilute lysate to ~300 mL with hypotonic lysis buffer. Clarify the lysate by ultracentrifugation at 100,000 × *g* for 45 mins at 4 °C.
5. The recombinant PLCε is in the supernatant. Collect samples of both the supernatant and pellet for SDS-PAGE.

4.5.2 Ni-NTA affinity chromatography with nickel resin or HisTag affinity columns

Note: The yield of purified PLCε is increased using HisTrap Columns on an FPLC system. We have also successfully used Ni-NTA resin in a gravity column to purify the lipase.

1. Equilibrate the HisTrap with 5 CVs of affinity binding buffer.
2. Pass the supernatant through a glass fiber filter and measure the volume. Supplement with imidazole to a final concentration of 20 mM, NaCl to a final concentration of 300 mM, and β-mercaptoethanol to a final concentration of 10 mM.
3. Add affinity binding buffer to the protein solution to a final volume of ~800 mL. Filter the protein solution through a 0.45 μm filter into an autoclaved bottle. Collect a 10 μL sample for SDS-PAGE.
4. Load the protein sample onto the HisTrap column. Collect the flow-through in a separate, clean container.
5. Wash the column with 5 CVs with affinity binding buffer.
6. If using an FPLC, elute the protein using a gradient starting with 100 % affinity binding buffer and 0 % elution buffer, and ending with 0 % affinity binding buffer and 100 % elution buffer over 20 CVs**.** Collect 1 mL fractions.
   a. If using a gravity Ni-NTA column, wash with 10 CVs of binding buffer. Elute with 10 CVs of elution buffer, collecting the elution in 1 mL fractions.
7. Identify fractions containing PLCε by UV absorbance and collect 10 μL samples for SDS-PAGE. If the fractions have many other contaminants, or the sample needs to be extremely high purity, proceed to ion exchange chromatography. If the fractions are sufficiently pure, then proceed to size exclusion chromatography.

Note: If using Ni-NTA resin and a gravity column, collect a sample of all washes and elution fractions for SDS PAGE gel analysis. If running an FPLC column, collect fractions that correspond to UV peaks for SDS PAGE gel analysis. Collect 10 μL samples of all washes and elution for SDS-PAGE.

4.5.3 Ion exchange chromatography

Note: We have found it most convenient to use an ion exchange column on an FPLC, but ion exchange resin in a gravity column is an appropriate alternative. One caveat with the latter approach is that eluting the protein via a salt gradient may be more challenging. Based on the isoelectric point of PLCεPH-C, it will be positively charged at pH 8 and should bind to an anion column. However, we have observed that PLCε PH-C will also bind to cation exchange columns. One round of either ion exchange chromatography should be sufficient to remove most contaminants. If necessary, anion and cation chromatography can be done sequentially.

1. Equilibrate the anion exchange column with 10 CVs of High Salt buffer, and then with 10 CVs of start buffer. If using an FPLC, use separate pumps for each equilibration and prime the injection loop with start buffer.
2. Pool the HisTrap fractions containing partially purified PLCε PH-C (or other PLCε variant).
3. Wash a protein concentration with 100 kDa molecular weight cutoff with ion exchange start buffer.
4. Buffer exchange the protein into ion exchange start buffer using the concentrator. Concentrate the protein to ~ 1 mL, add 5X excess of start buffer, and concentrate to 1 m again. Repeat this step 2 times to ensure the protein is fully buffer exchanged. For ion exchange chromatography using an FPLC, concentrate the protein to ~1 mL. If the protein begins to show signs of aggregation or precipitation, or cannot be further concentrated, do not force it. Instead, load the protein via the pump or repeat this protocol with multiple 1 mL injections. Prior to applying the sample to the column, collect a 10 μL sample for SDS-PAGE.
5. Inject the protein and collect the flow-through in a clean bottle. Collect a 10 μL sample for SDS-PAGE.
6. Wash the column with 5 CVs start buffer and collect flowthrough in a clean bottle. Collect a 10 μL sample for SDS-PAGE.
7. Elute the protein using a gradient elution. Start with 100 % start buffer and 0 % high salt buffer and end with 0 % start buffer and 100 % high salt buffer, over 60 CVs. Collect 1 mL fractions using fraction collector. Collect 5 μL sample of each fraction for SDS-PAGE.
8. Wash column with 5 CVs of high salt buffer, collect flow-through in a clean bottle. Collect a 10 μL sample for SDS-PAGE.
9. Identify samples containing PLCε by SDS-PAGE. Wash a concentrator with a 100 kDa molecular weight cut-off with SEC buffer and concentrate the fractions containing the lipase to ~1 mL.

4.5.4 Size exclusion chromatography

1. Prime 1 mL injection loop and equilibrate tandem Superdex S200 columns with SEC buffer.
2. Wash a concentrator with a 100 kDa molecular weight cut-off with SEC buffer and concentrate the fractions containing the lipase to ~1 mL.
3. Inject concentrated protein sample onto the tandem S200 columns and elute with 1 CV of SEC buffer.

4. Identify fractions containing PLCε by UV absorbance and collect a 5 μL sample of each for SDS-PAGE.
5. Pool fractions corresponding to PLCε PH-C. In a new concentrator with 100 kDa molecular weight cut-off and prewashed with SEC buffer, concentration fractions to at least ~2 mg/mL. Aliquot into 10-50 μL fractions, flash freeze in liquid nitrogen, and store at −80 °C.

4.5.5 Pause point

FPLC runs can be set up and completed overnight, and so serve as a good stopping point. The next morning, run an SDS-PAGE gel prior to pooling and concentrating fractions. Typically, we have found it possible to complete the lysis and affinity chromatography steps on the first day and set up to run the ion exchange column elution on the FPLC overnight. The remaining steps can be completed on the second day. On occasion, it may be necessary to load the HisTrap or SEC columns overnight, but every effort should be made to purify the protein as quickly as possible.

5. Activity Assays

5.1 Materials and equipment for activity assays

5.1.1 In vitro activity assay (IP1)

- Purified protein(s)
- Heat block
- HTRF IP-One Gq Detection Kit (e.g. Revvity)
- Low-volume 384 well plates
- Plate seal or parafilm
- Plate reader (e.g.BioTek Synergy Neo2) with the following filter sets: Filter Set 1 (Dual PMT): Excitation: 330/80, Emission: 620/10, Filter Set 2 (Dual PMT): Excitation: 330/80, Emission: 665/8
- Centrifuge with plate rotor (e.g.Thermo Scientific Sorvall ST 8 R)
- Phosphatidylinositol
- Phosphatidylethanolamine
- Chloroform
- Methanol

5.1.2 ^{3}[H]-IPx (activity assay)

- COS-7 cells
- CO_2 Incubator (e.g.Thermo Scientific Forma Steri-Cycle)

- 12 well cell culture plate
- Dulbecco's Modified Eagle Medium (DMEM)
- Fetal Bovine Serum (FBS)
- Penicillin-Streptomycin Solution
- Glutamax
- F10 media
- Transfection reagent (e.g. Fugene)
- DNA
  1. PLC variant
  2. G protein
  3. empty vector
- Inositol, Myo, -[2-3H(N)]-, Ethanol Solution (^{3}[H]-myo-inositol)
- Ammonium formate
- Formic acid
- Poly-Prep® Chromatography Columns, or similar
- AG 1-X8 Resin
- Scintillation counter (e.g.PerkinElmer Tri-Carb 2910 TR)
- Scintillation fluid
- Scintillation vials

Alternatives: (Alternative materials or equipment can be called out in this format).

- Other mammalian cells can be used but would likely have higher background due to endogenous PLCs.

5.2 *In vitro* activity assay (IP1)

Timing: 4–8 h.

5.2.1 Assay set up

1. Reaction volume: 30 μL
   a. 10 μL liposomes
   b. 5 μL G protein stock or G protein blank buffer
   c. 10 μL PLC

5.2.2 Preparing lipid stocks

Note: Liposomes are prepared using a 1:2.5 molar ratio of Egg PE:Soy PI.

1. Aliquot stock lipids (in 66.7 % chloroform, 30 % methanol, and 3.3 % water) into glass vials such that each tube has a final concentration of 300 mM PE and 750 mM PI when resuspended in 310 μL buffer.

2. Dry the lipids under nitrogen, seal with two layers of parafilm and tape securely.
3. Store dried lipids at −20 °C.

5.2.3 Preparing lipids for assay

1. Add 312 μL sonication buffer to lipid tube and seal with parafilm.
2. Vortex tubes to rehydrate the dried lipids. The solution should be cloudy. Incubate the tubes at room temperature for 5 min to ensure the dried lipid cake is fully rehydrated.
3. Generate liposomes using a bath sonicator. Sonicate for two 30 s bursts, incubating the lipids on ice for 10 s in between to minimize heat damage. The solution should be clear at this point, but an additional round of sonication may be required in some cases.
4. Keep sonicated lipids on ice until ready to use.

5.2.4 PLC stock

1. Thaw protein on ice and either centrifuge it for 5 min at 17,900 × *g* at 4 °C or filter through a 0.2 μm filter unit (Amicon Ultrafree) pre-washed with S200 buffer at 12,000 × *g* for 2 min at 4 °C. Measure protein concentration.
2. Make the PLC BSA Buffer. For each assay point, 10 μL of PLC stock will be added to a final volume of 30 μL in the reaction. Thus, the PLC BSA Solution must be 3X its final concentration in the assay.
   a. Typically, for a single point assay, a final concentration of PLCβ at 15 ng/uL is used. Therefore, the PLCβ is at 45 ng/μL in the PLCβ BSA Solution. PLCε is typically at 0.067 ng/uL in the assay, therefore the PLCε is at 0.2 ng/μL in the PLCε BSA solution.
   b. **Note:** To minimize pipetting errors associated with transferring very small volumes, we recommend making intermediate dilutions using S200 buffer for PLCβ or PLCε, as appropriate.

5.2.5 G Protein buffers

Notes: The exact composition of the G protein buffer will vary depending on the G protein used.

A. For basal lipase activity measurements, prepare a G protein blank buffer consisting of 1x incubation buffer, 1 mM DTT, and 3.5 mM CHAPS.
B. For measuring G protein-dependent activation, prepare solutions as in Table 1:

Table 1 G protein buffer preparation.

Reagent	G protein blank buffer	G protein buffer
2X Incubation Buffer	1X	1X
CHAPS[a]	3.5 mM	3.5 mM[a]
DTT	1 mM	1 mM
G protein or G protein purification buffer	G protein purification buffer	G protein[a]

[a]**Note:** 5 μL of the G protein buffer will be added to each assay tube. Ensure that the G protein in the G protein buffer is in 6-fold molar excess relative to the desired final concentration. High concentrations of detergent in the G protein buffers may disrupt the liposomes. The assay has been successful with the use of a final concentration of 4 mM CHAPS or lower in the G protein blank buffer/G protein buffer. If the addition of the G protein/G protein purification buffer results in higher than 4 mM CHAPS, adjust the supplemented CHAPS such that the final concentration of it is 4 mM or lower.

5.2.6 Assay reactions

1. Ensure a heat block is to 30 °C.
2. Add reagents the reagents to the bottom of a 1.5 mL Eppendorf tube in the following order:
   a. 10 μL Lipids
   b. 5 μL G protein blank buffer (for basal activity) or G protein stock (for G protein-dependent activation)
   c. 10 μL PLC in PLC BSA buffer
3. Transfer tubes to heat block and allow to equilibrate to 30 °C for 2 min. Extended periods of time on the heat block will result in protein degradation. Do not allow for incubation to proceed beyond 2 min.
4. The reaction is initiated by the addition of the calcium buffer. Add 5 μL calcium buffer to the reaction tubes or 5 μL sonication buffer to the no calcium control tubes. Allow the reaction to proceed for 15 min. This period is typically sufficient to quantify activity, but timings can be adjusted for time courses and/or variants with higher or lower basal activity.
5. Quench reaction exactly 15 min after the addition of the calcium buffer or sonication buffer by adding 5 μL quench buffer to each tube.
6. Transfer samples from heat block to room temperature.

5.2.7 Quantification of the assay

1. Make the following IP1 standards in 1x assay buffer (adapted from HTRF IP-One Gq Detection Kit Revvity protocol): 11,000 nM, 2750 nM, 688 nM, 172 nM, 43 nM, 11 nM, 2.7 nM, and 0 nM.

2. In a low-volume 384 plate, add 14 μL of each standard for the curve in triplicate.
3. Plate 14 μL of each assay reaction.
4. Add 3 μL d2-IP reagent, reconstituted in lysis and detection buffer, to every well containing the IP1 standard or the assay reaction.
5. Add 3 μL anti-IP cryptate reagent, reconstituted in lysis and detection buffer and filtered, to every well containing the IP1 standard or the assay reaction.
6. Seal plate with Parafilm or a plate seal
7. Centrifuge the plate at 1000 x *g* for 2 min at room temperature.
8. Incubate for 1 h at room temp in the dark.
9. Read the assay in a plate reader with the following parameters.
   a. Filter Set 1 (Dual PMT): Excitation: 330/80, Emission: 620/10
   b. Filter Set 2 (Dual PMT): Excitation: 330/80, Emission: 665/8
   c. Optics: Top
   d. Gain: Autoscale
      - Note: Use autoscale to set gain for all plates being read. Gain must be the same to compare across plates, if using multiple 384 well plates in one assay day.
   e. Time resolved: Delta 100 μsec, Collection time 300 μsec
   f. Light source: Xenon Flash, Lamp energy: Low, Standard dynamic range
   g. Read Speed: Normal, Delay: 0 msec, Measurements/Data Point: 10
   h. Read Height: 5 mm

Critical: This assay is adapted from the HTRF IP-One Gq Detection Kit (Revvity), which measures lipase activity in cells.

5.3 ^{3}[H]-IPx accumulation assay

Timing: 4 days.

5.3.1 Day 1

1. Plate 100,000 COS-7 cells per well in a 12 well cell culture plate in 1 mL of complete DMEM media.

5.3.2 Day 2

1. Transfect cells with the construct(s) of interest.
   a. Typically, 400 ng of PLC DNA and 200 ng of G protein DNA are sufficient for robust activity measurements.
   b. Constitutively active mutants of small GTPases can be used to ensure the G proteins remain in their fully active state throughout the experiment.

5.3.3 Day 3

1. Aspirate media and wash cells with 1 mL F-10 media.
2. Prepare a master mix of serum-free F-10 media and [^{3}H]-myo-inositol such that each well receives 500 μL of media containing 1.5 μL [^{3}H]-myo-inositol (stock concentration 1 mCi/mL).
3. Incubate cells for 24 h to allow [^{3}H]-myo-inositol to be incorporated into the lipid head groups.

5.3.4 Day 4

1. Add 5 μL of 1 M LiCl to each well, such that the final concentration per well is 10 mM LiCl. Incubate for 1 h at 37 °C.

   Optional: If testing small molecule compounds, add the molecule and incubate at 37 °C for 30 min or time point of interest.
2. While cells are incubating, prepare one 1 mL DOWEX AX1-X8 200-400 mesh ion exchange column for each well. Wash each column with the following:
   a. 10 mL H_2O
   b. 10 mL 2 M ammonium formate, 0.1 M formic acid mixture.
   c. Wash twice with 10 mL H_2O
   d. 10 mL 50 mM formic acid
3. After the 1 h incubation, remove the media from the cells and wash twice with 1 mL of chilled 1X PBS.
4. Add 1 mL of 50 mM formic acid to each well and incubate for a minimum of 30 min on ice to lyse the cells.
   a. Remove lysate from well and apply directly to the ion exchange column. Each sample from an individual well should be run on its own column.
   b. If needed, the samples can be stored in an Eppendorf tube at −20 °C for up to 72 h. Longer storage may be possible but has not been tested. Upon thawing, centrifuge the lysates for 10 min at 14,000 *x g*. Apply the supernatant to freshly equilibrated columns.
5. Wash each column twice with 10 mL 50 mM formic acid.
6. Wash each column twice with 10 mL 100 mM formic acid.
7. Elute bound [3H]-IPx species from the column with 3 mL of 1.2 M ammonium formate, 0.1 M formic acid solution into a pre-labeled scintillation vial. Elute each sample into its own vial.
8. Add 10 mL Uniscint BD Scintisafe to each eluted sample into the vial and quantify by scintillation counting.
   a. Set count per minute (CPM) channel cutoffs at a lower limit of 2.0 and an upper limit of 18.6.

9. Regenerate columns for the next use.
   a. 10 mL of H_2O
   b. 10 mL 2 M ammonium formate, 0.1 M formic acid mixture.
   c. Wash 2X with 10 mL of H_2O
   d. 10 mL of 50 mM formic acid

Note: The Dowex columns can be regenerated by washing with:

a. 10 mL H_2O
b. 10 mL 2 M ammonium formate, 0.1 M formic acid mixture.
c. Wash twice with 10 mL of H_2O
d. 10 mL of 50 mM formic acid

6. Expected outcomes

PLC expression is typically robust enough it can be readily detected at every purification step by SDS-PAGE, Fig. 2. If gravity columns are used for Ni-NTA affinity purification and/or ion exchange chromatography (if needed), it is not uncommon to observe some PLC in the washes, especially wash 2. SEC is a critical step in ensuring full-length lipase is purified, as PLCβ in particular is well-known to undergo proteolysis that results in loss of the distal CTD. Note that the elution volume of PLCs can differ from molecular weight standards due to their ability to adopt extended conformations in solution, Fig. 3. Typical yields of PLCβ and

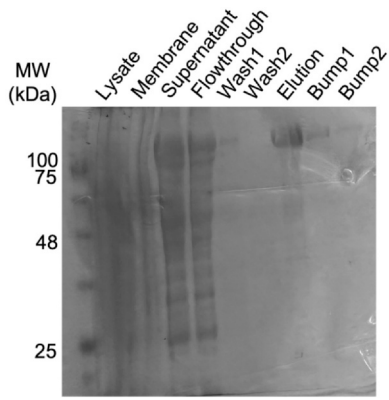

Fig. 2 Ni-NTA gravity column of PLC β3 Δ892. Samples from a Ni-NTA gravity column for PLC β3 Δ892 on a SDS-PAGE gel stained with Coomassie brilliant blue. Ladder with molecular weight in kDa depicted on the left. Sample corresponds to appropriate lane labeled above. PLC β3 Δ892 approximate weight 100 kDa.

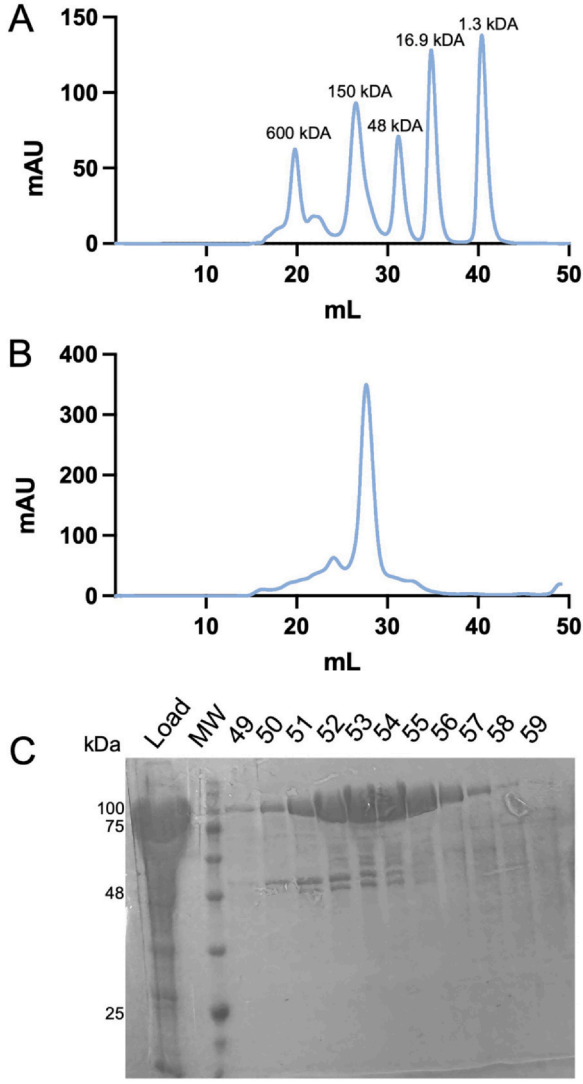

Fig. 3 Size exclusion chromatography of PLC β3 Δ892. (A) Chromatograph of BioRad Gel Filtration standards (#1511901) on tandem Superdex S200 columns. Molecular weight in kDa depicted above corresponding peak. UV readout on Y-axis and volume on X-axis. (B) SEC chromatograph of PLC β3 Δ892 UV readout on Y-axis and volume on X-axis. (C) Samples of SEC fractions for PLC β3 Δ892 purification on an SDS-PAGE gel stained with Coomassie Brilliant Blue. Molecular weight in kDa depicted on the left corresponding to ladder in lane 2. Samples labeled with corresponding lane. Numbers are SEC fractions, collected every 0.5 mL. Molecular weight of PLC β3 Δ892 is approximately 100 kDa.

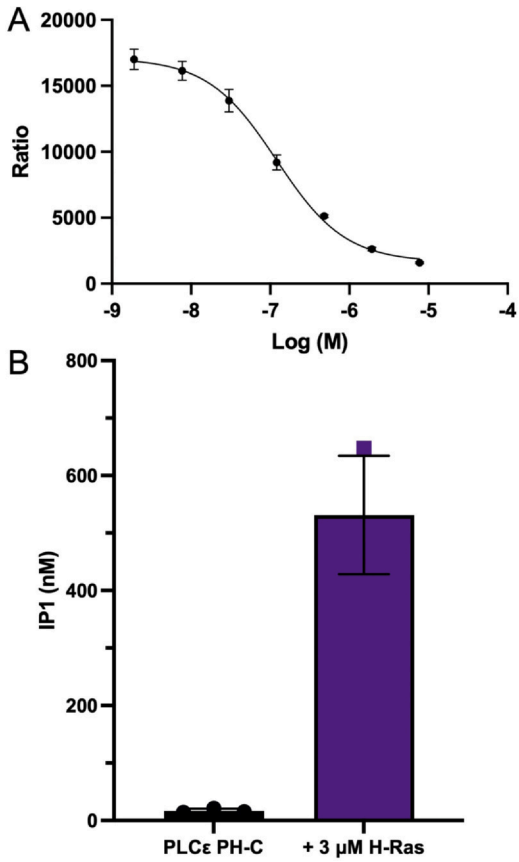

Fig. 4 *In vitro* activity assay (IP1). (A) HTRF IP-One Gq Detection Kit (Revvity) Standard Curve. X-axis depicts concentration, M, in log scale. Y-axis depicts ratio of standard concentration. Ratio is equivalent to $\frac{signal\ 665\ nm}{signal\ 620\ nm} \times 10^4$. (B) Basal and G-protein activated activity of PLCε PH-C. Liposome based activity assay of *R. norvegicus* PLCε PH-C (837–2282) at 0.07 ng/mL with and without 3 mM of H-Ras·GTP. Each data point represents one technical replicate.

PLCε variants are ~100–150 μL of protein at final concentrations of 1–5 mg/mL from 1 L of cell pellet. Yields are highly dependent on the strength of the baculovirus and speed of purification.

After completing the in vitro IP1 assay, it is expected to have robust measurements of basal PLCβ and PLCε activity. Comparisons of activity to previously published studies(Ghosh & Smrcka, 2004; Rugema et al., 2020) will vary, as this assay uses PI as the lipase substrate rather than PIP_2.

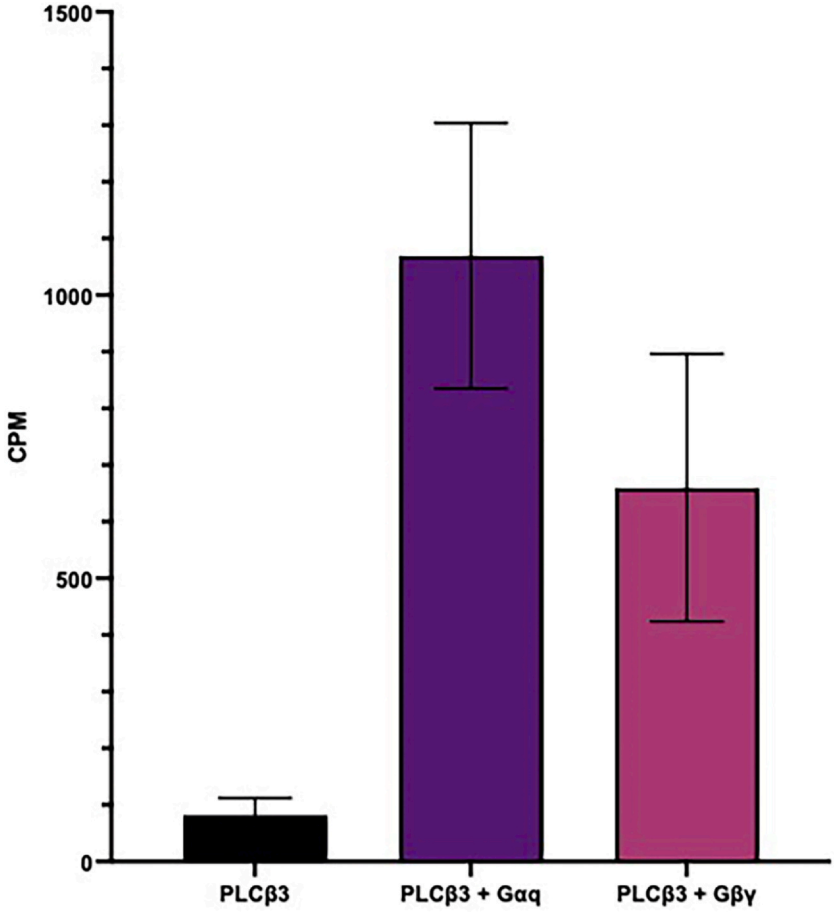

Fig. 5 ^{3}[H]-IPx accumulation assay. Cell-based activity assay with PLCβ3 and G protein activators Gαq and Gβγ. COS-7 cells were transfected with 400 ng of PLCβ3 and with 200 ng of empty vector DNA in the basal condition, or 200 ng of Gαq, or 200 ng of Gβ and 200 ng of Gγ plasmid. Y-axis is counts per minute (CPM), with the lower limit of 2.0 and an upper limit of 18.7 on the scintillation machine. Data shown as the mean of 2 biological replicates, each with a technical triplicate.

Activation assays with small GTPases or heterotrimeric G proteins will result in activities several folds higher than basal levels, at minimum, Fig. 4.

In the [^{3}H]-IPx, increased CPM correlates with increased PLC activity. Typically, background activity for empty vector controls is ~100–300 CPMs. COS-7 cells are highly recommended for these assays, as they have minimal background due to low endogenous PLC activity.

Empty vector + G protein activity will be higher than empty vector alone, as the transfected G protein can activate endogenous PLC pathways. Under the conditions described here, PLCβ is typically activated ~10-fold over basal when co-transfected with heterotrimeric G protein subunits, Fig. 5. G protein activation of PLCε or PLCε domain deletion variants is more modest, typically 3–5-fold over basal.

7. Quantification and statistical analysis

Protein quantification can be done by quantifying the absorbance at 280 nm, Bradford assay, or other standard methods.

To process and quantify data from the IP1 assay, GraphPad Prism is recommended.

1. Calculate the ratio of the acceptor and donor emission signals for each well.

$$Ratio = \left(\frac{Signal\ 665\ nm}{Signal\ 620\ nm}\right) * 10^4$$

2. Input the data into prism using the X-Y table format. Input the concentrations of the standard curve as the X values and the ratio as the Y values. The experimental conditions can be added as the row title, corresponding to the Y value ratios.
3. Calculate the concentrations of the IP1 standard curve such that they are in log units:

$$X = \log[IP1\,(M)]$$

4. Plot the standard curve with the concentration in log scale on the X axis, and the ratio on the Y axis (Fig. 4).
5. Interpolate the Y values of your experimental conditions using the best fit line of log(inhibitor) vs. response (three parameters). Note that other fitting parameters may be more appropriate depending on the experimental question.
6. Transform the interpolated data into nM

$$nM\ IP1 = 10^{\ interpolated\ data)} * 10^9$$

7. Each condition tested in the IP1 assay should be carried out in technical triplicates. At least two independent protein purifications should be tested for biological replicates.

To process and quantify data from the [^{3}H]-IPx assay, GraphPad Prism is recommended.

1. Each ^{3}[H]-IPx assay should be performed in technical replicates. Average the technical replicates to get the daily assay average. Assays should be carried out at least three times, on different days, from independent transfections to ensure robust biological replicates.
2. The data can be displayed in various ways depending on the question of interest.
   a. Raw data: Plot the CPM from each condition in one graph without further analysis.
   b. Background subtraction: subtract the average of the corresponding empty vector condition from the experimental data. For example, G proteins can activate endogenous PLCs and thus this activity needs to be subtracted out from the sample. To do so subtract the empty vector plus G protein sample from the PLC plus G protein condition. This will remove background PLC activity from all conditions.
   c. Fold Change: Divide a G protein activated condition or PLC variant/mutant by the WT/basal PLC condition. This will show how much more or less active the PLC is when impacted by an activator, or a variant/mutant.
   d. Maximal activity: Subtract the basal activity from the G protein stimulated activity to determine maximal activity of the PLC variant.

8. Advantages

Large-scale PLC expression is best accomplished using a baculovirus system. PLCs are complex, multidomain proteins and therefore need to be expressed in eukaryotic systems rather than bacterial systems to ensure proper folding. Although it is possible to express some truncations of PLCs in bacteria, it is extremely difficult to generate sufficient quantities of folded, functional protein for biochemical assays. In contrast, insect and mammalian cells synthesize functional PLCs in large amounts. However, the use of a baculovirus system over a BacMam system is more cost effective and thus preferred.

Full-length PLCε is challenging to purify in sufficient quantities for biochemical and structural studies (Ghosh, Wang, Kelley, & Smrcka, 2004). This protocol has been used to purify truncations of PLCε in sufficient quantities for biochemical assays, and structure determination using X-ray

crystallography and cryo-electron microscopy (cryo-EM) (Ohri et al., 2025; Rugema et al., 2020; Samassekou et al., 2025; Sieng et al., 2021).

The in vitro activity assay (IP1) is advantageous as the activity of purified proteins can be directly compared. Most commercially available lipase activity assays detect the amount of diacylglycerol (DAG) produced, which is a less specific readout. By determining PLC activity using the amount of inositol phosphate (IP1) generated, it provides a more direct measurement of activity. Additionally, the IP1 assay is receptor independent, and any IP1 detected is produced only by the lipase of interest.

The [^{3}H]-IPx assay allows more rapid quantification of PLC activity in cells, without the need to generate purified reagents or prepare liposomes. It also provides a more physiologically relevant output than the in vitro assay given that the preferred PIP_2 substrate is present in the cells.

9. Limitations

Protein expression for a baculovirus system is time consuming, taking ~1 month to prepare each baculovirus. Furthermore, baculovirus titers diminish over time, reducing the infection efficiency. This method of protein production also has batch variability in which the same construct that has produced two different viruses may not yield the same amount of purified protein.

Purifying PLCs by gravity columns followed by FPLC takes at minimum two days, which leads to overall protein degradation, especially within the PLCβ family as the distal CTD is proteolyzed in solution.

The in vitro activity assay (IP1) is limited in that PI is not the preferred substrate. In addition to lower activity, it also limits comparisons to PLC activity reported in the literature. We have also found that the assay is noisy, in part due to the substrate used and the limited range of the standard curve in vitro. This also leads to challenges in optimizing PLC and G protein concentrations in the assay. Finally, differences in biological triplicate activity can vary due to prep-to-prep variation.

Limitations of the [^{3}H]-IPx assay include the use of COS-7 cells, which have undetectable expression of endogenous PLCs. However, these cells also express heterotrimeric G protein subunits and G proteins that can be detected at baseline. Additionally, we consistently see increased expression of PLCε and PLCε variants upon co-transfection with small GTPases. These differences in expression must be considered when analyzing the data.

10. Optimization and troubleshooting

10.1 Problem (low protein expression)

Virus effectiveness diminishes over time. If expression was previously high and decreased over time, new viruses will need to be made. If expression is low and the virus is new, test expressions (50–100 mL of cells 1.8–2.2 × 10^6 cells/mL) with an increasing amount of P2 virus are a useful diagnostic. Additionally, expression can be low if the virus is too strong as it kills cells before allowing them to synthesize the protein. Check for cell death after infection every 24 h. Similarly, if cell death is high, test expressions with lower volumes of P2 virus are recommended.

10.2 Problem (protein not binding to the Ni-NTA affinity column)

Protein not binding to the nickel column could be due to the histidine tag being partially or wholly occluded by the lipase. N-terminal histidine tags have been successfully used to purify PLCβ isoforms and PLCε variants, but depending on the construct, C-terminal tags may be superior. Alternatively, if tag placement is not an issue, impaired binding may be due to buffer incompatibility with the Ni-NTA resin. Ensure that the buffers are compatible with the specific Ni-NTA resin, particularly components that can impact binding such as salt and reducing agents. Buffer composition may also need to be adjusted if the protein initially binds the column but elutes in the washes.

10.3 Problem (*In vitro* activity assay (IP1): Sample(s) have low signal)

If no signal is detected for controls, it is possible that the sonicated lipids are not forming liposomes. This could be due to several factors. First, the lipids can oxidize over time, in which case new stocks should be made. Secondly, the liposomes may not be properly formed. If the lipids are still cloudy after the first two rounds of bath sonication, additional rounds may be necessary. It is important to be familiar with the bath sonicator being used to most efficiently generate liposomes. In our experience, this is often the most challenging step. A third consideration is that low signal may be due to old detection agents. This can often be diagnosed by generating a standard curve. Lastly, if none of these solve your issue it could be that your protein is not functional, or the protein concentration is inaccurate. Different protein concentrations can be tested to address the latter issue. If protein quality is a concern, SDS-PAGE can be used to test whether the protein is

intact, and differential scanning fluorimetry or other methods of measuring thermal stability can inform on whether the protein is stable. It is also possible for the activity to be higher and off the standard curve. If so, repeat the assay with lower concentrations of PLC.

10.4 Problem (^{3}[H]-IPx accumulation assay: Sample(s) have low signal)

If control sample(s) have low radioactive signal this could be due to low PLC expression. To test this, complete a western blot or HiBiT assay if proteins are tagged to determine protein expression. If expression is low, try a fresh bottle of transfection reagent. If the control has normal expression but a mutant does not it could be that the mutation destabilizes the protein and thus expression is affected. If signal remains low, ensure that the cells are serum starved as this is pertinent for [^{3}H]-myo-inositol uptake. Additionally, overall cell viability will determine protein expression and [^{3}H]-myo-inositol uptake. If higher amounts of DNA are being used during transfection, ensure cells are viable as this can cause cellular toxicity. Preparing fresh reagents, especially fresh DNA and LiCl, can help in getting better signal as well.

11. Safety considerations and standards

The techniques described within this paper yield biological specimens such as DNA, viruses, cellular components etc. which require proper treatment and disposal of waste. Guidelines on how to deal with biological specimens will differ per college, industry, or governmental lab and should be crosschecked with your institution.

The ^{3}[H]-IPx assay requires radioactive material, [^{3}H]-myo-inositol. Tritium ([^{3}H]) emits weak beta particles and does not require any additional personal protective equipment (PPE) beyond standard PPE for BSL1/BSL2-level experiments, i.e., lab coats, disposable gloves, and safety glasses. Use of this material requires training per the guidelines of your institution and local regulations.

12. Alternative methods/procedures

An alternative to the insect baculovirus system is the BacMam System (ViraPowerTM BacMam Expression System & BacMam pCMV - DEST Vector Kit User Guide, n.d.). To utilize the BacMam system, you will

need to clone the protein of interest into a BacMam compatible vector such as BacMam pCMV-DEST vector. After confirmation that you have the construct desired, you will transform the plasmid into BH10Bac cells and isolate the recombinant Bacmid DNA. Mammalian cells will be transfected with the recombinant Bacmid DNA. Subsequent viral amplification can take place if needed, dependent upon titer. Mammalian cells can then be infected with the virus for protein production.

As an alternative to the ^{3}[H]-IPx Accumulation Assay, the HTRF IP-One Gq Detection Kit by Revvity (Cat# 62IPAPEB) can be used as designed. Similar to the ^{3}[H]-IPx Accumulation Assay, cells are transfected to produce the desired proteins and lysed for data collection. The experiments differ as the IP1 is a competitive HTRF based activity assay, in which d2-IP1 is added to the lysates followed by the addition of cryptate-labeled IP1 antibody. The antibody binds to either endogenous unlabeled IP1, or the added d2 labeled IP1. When the cryptate antibody is bound to d2-IP1, there is an energy transfer from the d2 to the cryptate, leading to a fluorescent signal. Exact IP1 levels of each sample are determined by using a standard curve.

References

Bunney, T. D., Harris, R., Gandarillas, N. L., Josephs, M. B., Roe, S. M., Sorli, S. C., ... Katan, M. (2006). Structural and mechanistic insights into ras association domains of phospholipase C epsilon. *Molecular Cell, 21*(4), 495–507. https://doi.org/10.1016/j.molcel.2006.01.008.

Descorbeth, M., & Anand-Srivastava, M. B. (2008). High glucose increases the expression of Gq/11alpha and PLC-beta proteins and associated signaling in vascular smooth muscle cells. *American Journal of, 295*(5), H2135–H2142. https://doi.org/10.1152/ajpheart.00704.2008.

Descorbeth, M., & Anand-Srivastava, M. B. (2010). Role of growth factor receptor transactivation in high glucose-induced increased levels of Gq/11α and signaling in vascular smooth muscle cells. *Journal of Molecular and Cellular Cardiology, 49*(2), 221–233. https://doi.org/10.1016/j.yjmcc.2009.12.010.

Ghosh, M., & Smrcka, A. V. (2004). Assay for G protein-dependent activation of phospholipase C beta using purified protein components. *Methods in Molecular Biology (Clifton, N. J.), 237*, 67–75. https://doi.org/10.1385/1-59259-430-1:67.

Ghosh, M., Wang, H., Kelley, G. G., & Smrcka, A. V. (2004). Purification of phospholipase C beta and phospholipase C epsilon from Sf9 cells. *Methods in Molecular Biology (Clifton, N. J.), 237*, 55–64. https://doi.org/10.1385/1-59259-430-1:55.

Gresset, A., Sondek, J., & Harden, T. K. (2012). The phospholipase C isozymes and their regulation. In T. Balla, M. Wymann, & J. D. York (Eds.). *Phosphoinositides I: Enzymes of synthesis and degradation* (pp. 61–94) Springer Netherlands. https://doi.org/10.1007/978-94-007-3012-0_3.

Jin, T.-G., Satoh, T., Liao, Y., Song, C., Gao, X., Kariya, K., ... Kataoka, T. (2001). Role of the CDC25 homology domain of phospholipase Cε in amplification of Rap1-dependent signaling. *Journal of Biological Chemistry, 276*(32), 30301–30307. https://doi.org/10.1074/jbc.M103530200.

Kadamur, G., & Ross, E. M. (2013). Mammalian phospholipase C. *Annual Review of Physiology, 75*(75, 2013), 127–154. https://doi.org/10.1146/annurev-physiol-030212-183750.

Katan, M., & Cockcroft, S. (2020). Phospholipase C families: Common themes and versatility in physiology and pathology. *Progress in Lipid Research, 80*, 101065. https://doi.org/10.1016/j.plipres.2020.101065.

Kelley, G. G., Reks, S. E., Ondrako, J. M., & Smrcka, A. V. (2001). Phospholipase C(epsilon): A novel Ras effector. *The EMBO Journal, 20*(4), 743–754. https://doi.org/10.1093/emboj/20.4.743.

Kim, D., Jun, K. S., Lee, S. B., Kang, N.-G., Min, D. S., Kim, Y.-H., ... Shin, H.-S. (1997). Phospholipase C isozymes selectively couple to specific neurotransmitter receptors. *Nature, 389*(6648), 290–293. https://doi.org/10.1038/38508.

Lyon, A. M., Dutta, S., Boguth, C. A., Skiniotis, G., & Tesmer, J. J. G. (2013). Full-length Gαq–Phospholipase C-β3 structure reveals interfaces of the C-terminal Coiled-Coil domain. *Nature Structural & Molecular Biology, 20*(3), 355–362. https://doi.org/10.1038/nsmb.2497.

Lyon, A. M., Tesmer, V. M., Dhamsania, V. D., Thal, D. M., Gutierrez, J., Chowdhury, S., ... Tesmer, J. J. G. (2011). An autoinhibitory helix in the C-terminal region of phospholipase C-β mediates Gαq activation. *Nature Structural & Molecular Biology, 18*(9), 999–1005. https://doi.org/10.1038/nsmb.2095.

Madukwe, J. C., Garland-Kuntz, E. E., Lyon, A. M., & Smrcka, A. V. (2018). G protein βγ subunits directly interact with and activate phospholipase Cε. *The Journal of Biological Chemistry, 293*(17), 6387–6397. https://doi.org/10.1074/jbc.RA118.002354.

Ohri, V., Samassekou, K., Muralidharan, K., Garland-Kuntz, E. E., Fisher, I. J., Hogan, W. C., ... Lyon, A. M. (2025). RhoA allosterically activates phospholipase Cε via its EF hands. *Communications Biology, 8*(1), 1368. https://doi.org/10.1038/s42003-025-08742-0.

Phan, H. T. N., Kim, N. H., Wei, W., Tall, G. G., & Smrcka, A. V. (2021). Uveal melanoma-associated mutations in PLCβ4 are constitutively activating and promote melanocyte proliferation and tumorigenesis. *Science Signaling, 14*(713), eabj4243. https://doi.org/10.1126/scisignal.abj4243.

Phan, H. T. N., Loomis, J., Abraham, S., He, Q., Bastepe, M., & Smrcka, A. V. (2022). A naturally occurring membrane-anchored Gαs variant, XLαs, activates phospholipase Cβ4. *The Journal of Biological Chemistry, 298*(8), 102134. https://doi.org/10.1016/j.jbc.2022.102134.

Rugema, N. Y., Garland-Kuntz, E. E., Sieng, M., Muralidharan, K., Van Camp, M. M., O'Neill, H., ... Lyon, A. M. (2020). Structure of phospholipase Cε reveals an integrated RA1 domain and previously unidentified regulatory elements. *Communications Biology, 3*(1), https://doi.org/10.1038/s42003-020-01178-8 Article 1.

Samassekou, K., Garland-Kuntz, E. E., Ohri, V., Fisher, I. J., Erramilli, S. K., Muralidharan, K., ... Lyon, A. M. (2025). Cryo-EM structure of phospholipase Cε defines N-terminal domains and their roles in activity. *Commun Biol, 8*, 1429.

Sasai, M., Ma, J. S., Okamoto, M., Nishino, K., Nagaoka, H., Takashima, E., ... Yamamoto, M. (2021). Uncovering a novel role of PLCβ4 in selectively mediating TCR signaling in CD8+ but not CD4+ T cells. *The Journal of Experimental Medicine, 218*(7), e20201763. https://doi.org/10.1084/jem.20201763.

Satoh, T., Edamatsu, H., & Kataoka, T. (2006). Phospholipase Cε guanine nucleotide exchange factor activity and activation of Rap1. *Methods in enzymology*, *407*, Academic Press 281–290. https://doi.org/10.1016/S0076-6879(05)07024-2.

Seifert, J. P., Zhou, Y., Hicks, S. N., Sondek, J., & Harden, T. K. (2008). Dual activation of phospholipase C-ϵ by Rho and Ras GTPases*. *Journal of Biological Chemistry, 283*(44), 29690–29698. https://doi.org/10.1074/jbc.M805038200.

Sieng, M., Selvia, A. F., Garland-Kuntz, E. E., Hopkins, J. B., Fisher, I. J., Marti, A. T., & Lyon, A. M. (2021). Functional and structural characterization of allosteric activation of phospholipase Cε by Rap1A. *The Journal of Biological Chemistry, 295*(49), 16562–16571. https://doi.org/10.1074/jbc.RA120.015685.

Smrcka, A. V., & Sternweis, P. C. (1993). Regulation of purified subtypes of phosphatidylinositol-specific phospholipase C beta by G protein alpha and beta gamma subunits. *Journal of Biological Chemistry, 268*(13), 9667–9674. https://doi.org/10.1016/S0021-9258(18)98401-2.

Shu, P.-G., Ryu, S. H., Moon, K. H., Suh, H. W., & Rhee, S. G. (1988). Cloning and sequence of multiple forms of phospholipase C. *Cell, 54*(2), 161–169. https://doi.org/10.1016/0092-8674(88)90548-X.

Ushio-Fukai, M., Griendling, K. K., Akers, M., Lyons, P. R., & Alexander, R. W. (1998). Temporal dispersion of activation of phospholipase C-β1 and -γ isoforms by angiotensin ii in vascular smooth muscle cells: Role of αq/11, α12, and βγ G protein subunits*. *Journal of Biological Chemistry, 273*(31), 19772–19777. https://doi.org/10.1074/jbc.273.31.19772.

ViraPower™ BacMam Expression System and BacMam pCMV - DEST Vector Kit User Guide. (n.d.). Life Technologies Corporation. https://documents.thermofisher.com/TFS-Assets/LSG/manuals/virapower_BacMam_express_SystDEST_Kit_man.pdf.

Waldo, G. L., Ricks, T. K., Hicks, S. N., Cheever, M. L., Kawano, T., Tsuboi, K., ... Harden, T. K. (2010). Kinetic scaffolding mediated by a phospholipase C-beta and Gq signaling complex. *Science (New York, N. Y.), 330*(6006), 974–980. https://doi.org/10.1126/science.1193438.

Wang, H., Oestreich, E. A., Maekawa, N., Bullard, T. A., Vikstrom, K. L., Dirksen, R. T., ... Smrcka, A. V. (2005). Phospholipase Cε modulates β-adrenergic receptor– dependent cardiac contraction and inhibits cardiac hypertrophy. *Circulation Research*. https://doi.org/10.1161/01.RES.0000196578.15385.bb.

Zhang, L., Malik, S., Pang, J., Wang, H., Park, K. M., Yule, D. I., ... mrcka, A. V. (2013). Phospholipase Cε hydrolyzes perinuclear phosphatidylinositol 4-phosphate to regulate cardiac hypertrophy. *Cell, 153*(1), 216–227. https://doi.org/10.1016/j.cell.2013.02.047.

CHAPTER FOUR

Assembling Retromer-coated membrane tubules for biochemical and structural studies

Kai-En Chen, Vikas A. Tillu, Nicholas Ariotti, and Brett M. Collins*
Institute for Molecular Bioscience, The University of Queensland, St. Lucia, Brisbane, QLD, Australia
*Corresponding author. e-mail address: b.collins@imb.uq.edu.au

Contents

1. Introduction 102
2. Experimental procedure 104
   2.1 Expression and purification of ctRetromer pentameric complex 104
   2.2 Liposome pelleting assay to assess membrane binding of the Retromer complex 107
   2.3 Liposome tubulation 110
   2.4 Additional notes 113
3. Concluding remarks 114
Acknowledgments 114
References 114

Abstract

The evolutionarily conserved Retromer complex, composed of Vps29, Vps26 and Vps35, is an essential regulator of endosomal retrieval of transmembrane cargo proteins. For cargo sorting and trafficking to take place, Retromer assembles into coated tubulovesicular carriers together with various sorting nexin (SNX) adaptor proteins including SNX3 and SNX27 in metazoans, and Snx3 or the dimeric Vps5-Vps17 SNX-BAR proteins in yeast. Although Retromer-coated tubulovesicular carriers are vital for its function, the *in vitro* reconstitution of these membrane assemblies for structural and functional studies can be technically challenging. Approaches include the use of giant unilamellar vesicles and supported membrane tubules for fluorescence imaging, or smaller multilamellar vesicles (MLVs) to generate uniform tubules for imaging by cryoelectron tomography (CryoET). This chapter describes protocols for producing MLVs for membrane binding studies of Retromer and assembling the yeast Retromer–Vps5–Vps17 heteropentameric complex for reconstituting membrane tubulation for CryoET studies. We also discuss our observations of both poorly ordered and well-ordered Retromer coats observed in this experimental setup.

Methods in Enzymology, Volume 728
ISSN 0076-6879, https://doi.org/10.1016/bs.mie.2026.01.012
Copyright © 2026 Elsevier Inc. All rights are reserved, including those for text and data mining, AI training, and similar technologies.

1. Introduction

Endosomes are sorting organelles found in all eukaryotic cells that are essential for directing transmembrane protein and lipid cargoes to specific cellular compartments. Once a cargo reaches the endosome, it undergoes either lysosomal degradation or is recycled to other organelles including the trans-Golgi network (TGN) and the plasma membrane by a complex and dynamic network of protein trafficking machineries (Cullen & Steinberg, 2018). Sequence-dependent recycling of transmembrane proteins is primarily driven by protein complexes that generate tubulovesicular carriers (Chen et al., 2019; Gopaldass et al., 2024; Hierro et al., 2015). Among the protein machineries involved in cargoes recycling, the Retromer complex (composed of Vps35, Vps26 and Vps29) is conserved in eukaryotic species and mediates trafficking of a large array of different proteins (Burd & Cullen, 2014; Chen et al., 2019; Gopaldass et al., 2024; Seaman, 2012). Retromer-depended endosomal transport of cargoes requires cooperation with different adaptors from the sorting nexin (SNX) protein family. SNX proteins all possess a phox homology (PX) domain that typically binds to phosphatidylinositol 3-phosphate (PtdIns3*P*) (Chandra et al., 2019), a landmark lipid enriched in endo-lysosomal compartments. The known adaptors in yeast include the Vps5–Vps17 heterodimer (Kovtun et al., 2018; Seaman et al., 1998) and Snx3 (Harrison et al., 2014; Leneva et al., 2021). Vps5 and Vps17 are SNX proteins that also possess bin-amphiphysin-rvs (BAR) domains with inherent membrane curvature properties. In humans and other metazoans SNX3 is conserved, while the homologues of the Vps5-Vps17 have evolved into a distinct complex known as ESCPE-1 (Collins & Cullen, 2025; Lopez-Robles et al., 2023; Simonetti et al., 2019). In contrast, SNX27 is responsible for recycling of cargoes with specific PDZ-binding motifs from endosomes to plasma membrane and exists only in metazoan species (Clairfeuille et al., 2016; Steinberg et al., 2013).

When originally discovered in budding yeast, *Saccharomyces cerevisiae*, Retromer was shown to form a heteropentameric complex with Vps5 and Vps17, responsible for the transport of cargoes such as the carboxy peptide Y (CPY) receptor Vps10 from endosomes to the Golgi (Marcusson et al., 1994; Seaman et al., 1997; Seaman et al., 1998). In the heteropentameric complex assembly, it is commonly accepted that the core Retromer trimer acts as a scaffold for cargo sorting (Kendall et al., 2020; Kovtun et al., 2018), while Vps5 and Vps17 mediate membrane association (Seaman & Williams, 2002; van Weering et al., 2012). Our recent study showed that Retromer

and the Vps5-Vps17 heterodimer associates primarily through PL and [K/R] Φ motifs located in the N-terminal disordered domain of Vps5 (Chen et al., 2025). These motifs are unique to Vps5 in yeast, and are not present in the human homologues SNX1/2. Using Cryo-electron tomography (CryoET), we found that Retromer forms conserved asymmetrical arches where Vps29 is located at membrane-distal apex, Vps35 forms the "legs" of these arches and Vps26 lies on top of the SNX-BAR array at the membrane surface (Chen et al., 2025; Kovtun et al., 2018).

A key finding from the CryoET structures of Retromer assembled with either Vps5 homodimers (Kovtun et al., 2018; Leneva et al., 2021) or with Vps5-Vps17 heterodimers (Chen et al., 2025) is that Vps26 does not directly contact the membrane (Chen et al., 2025; Kovtun et al., 2018) (Fig. 1). This observation is consistent with biochemistry studies showing that Retromer alone does not interact with membranes (Chandra et al., 2025; Chen et al., 2025; Kovtun et al., 2018). Interestingly, the later CryoET study of the Retromer–SNX3 coat suggests that whereas Vps29 and Vps35 forms a similar asymmetric dimer arrangement, the Vps26 subunit in this context directly interacts with lipids together with SNX3, creating a membrane-bound array distinct from the Retromer and SNX-BAR complexes (Fig. 1) (Leneva et al., 2021). These CryoET structures provide fundamental insights into how Retromer acts as a key scaffold for generating tubulovesicular cargo carriers, although many questions remain. For example, how does Retromer assemble coats with SNX27 and associated cargoes, what is the potential role of the actin-nucleating WASH complex in Retromer-SNX27 coat assembly, and can hybrid coats contain more than one type of SNX adaptor as suggested by recent fluorescent microscopy of supported membrane tubules (SMTs) showing co-integration yeast Retromer, Vps5-Vps17 and Snx3 (Gopaldass et al., 2025).

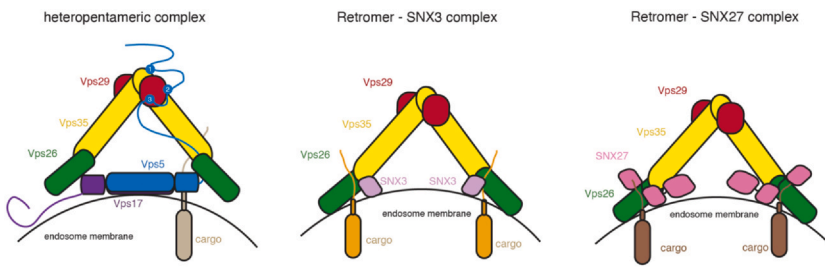

Fig. 1 Schematic diagram showing the proposed models for the assembly of the heteropentameric yeast Retromer–Vps5–Vps17 complex, the Retromer–SNX3 complex and the Retromer–SNX27 complex required for endosomal cargo recycling.

Advances in CryoET have provided opportunities to explore how Retromer forms membrane-associated coats with different binding partners, as well as a variety of other membrane coats such as ESCPE-1 (Lopez-Robles et al., 2023), COPI (Dodonova et al., 2017; Faini et al., 2012), COPII (Pyle et al., 2025) and the Vps34 kinase (Tremel et al., 2021). A prerequisite for Retromer membrane-binding and structural studies is a robust, systematic method to generate coated membranes with different SNX adaptors. In this Chapter we provide detailed protocols for purification of Retromer and Vps5-Vps17 complexes from the thermophilic yeast *Chaetomium thermophilum,* producing MLVs, performing membrane pelleting experiments, and assembling Retromer-coated tubules for structural studies.

2. Experimental procedure

2.1 Expression and purification of ctRetromer pentameric complex

An important prerequisite for generating Retromer-coated membrane tubules for *in vitro* structural studies is the expression and purification of Retromer and its sorting nexin binding partners (in this case Vps5 and Vps17) in sufficient quantities, which allows the formation of heteropentameric complex assembly. Here, we describe detailed procedures for expressing both complexes from a standard BL21(DE3) *Escherichia coli* strain, followed by purification and heteropentameric complex formation as described previously (Chen et al., 2021; Chen et al., 2025). Note that the $Vps17_{PX\text{-}BAR}$ construct used here lacks the N-terminal disordered region which can be highly sensitive to degradation.

2.1.1 Material and reagents

- Expression plasmids.
  - pRSF-His_6-ctVps5
  - pMCSG10-His_6-GST-TEV-ctVps17$_{PX\text{-}BAR}$
  - pGEX4T2-GST- PreScission-ctVps29
  - pET28a-His_6-ctVps26
  - pET28a-ctVps35
- Autoinduction media.
  (LB, 1 mM $MgSO_4$, 1 ×5052, 1 x NPS)

- Lysis buffer.
  (50 mM Tris-HCl (pH 7.5), 200 mM NaCl, 2 mM β-ME, 50 μg/mL Benzamidine, 20 μg/mL DNase).
- Protein buffer
  (50 mM Tris-HCl pH 8.0, 200 mM NaCl, 1 mM TCEP)
- Glutathione Sepharose
- Talon® affinity agarose
- Antibiotics
  - Kanamycin
  - Ampicillin

2.1.2 Protocol

1. Co-transform pRSF-His_6-ctVps5 and pMCSG10-His_6-GST-TEV-ctVps17$_{PX\text{-}BAR}$ into BL21 (DE3) competent cells using the standard heat shock method. Similarly, co-transform pGEX4T2-GST-PreScission-ctVps29 with pET28a-ctVps35, while pET28a-ctVps26 is transformed individually. Colonies from co-transformed plasmids are selected on agar plates containing both ampicillin and kanamycin.
2. The following day, colonies are used directly to inoculate overnight 10 mL LB cultures of ctVps5-ctVps17$_{PX\text{-}BAR}$, ctVps35-ctVps29 and ctVps26, supplemented with appropriate antibiotics as listed in Table 1.
3. For protein expression, inoculate 10 mL of each overnight cultures into autoinduction medium as described in detail previously (Studier, 2005). Cultures are grown at 37 °C for 4 h, followed by overnight incubation at 20 °C with shaking at 200 rpm. A culture volume of 6 L would typically be sufficient to obtain ~5 mg purified protein(s).

Table 1 Plasmids and constructs used in the heteropentameric complex formation.

Plasmids	Protein residues	Antibiotic
pRSF-His_6-ctVps5	1–1589	Kanamycin
pMCSG10-His_6-GST-TEV-ctVps17$_{PX\text{-}BAR}$	157–544	Ampicillin
pGEX4T2-GST- PreScission -ctVps29	1–201	Ampicillin
pET28a-His_6-ctVps26	1–316	Kanamycin
pET28a-ctVps35	1–869	Kanamycin

4. Harvest the expressed cells by centrifugation at 6000 rpm for 10 min. The cell pellets are then resuspended in lysis buffer, placed in Falcon tubes, and stored at −80 °C until required.
5. To obtain the ctRetromer complex, mix the cell pellet containing ctVps35-ctVps29 with an equal volume of the ctVps26 cell pellet. The ctRetromer-containing and Vps5-Vps17-containing cell pellets can be lysed using a Constant System TS-series high pressure cell disruptor in the lysis buffer.
6. Clarify the lysates by centrifugation (Beckman JA25.5 rotor at 20,000 rpm for 30 min). The supernatant is incubated with Glutathione Sepharose 4B resin (Cytiva) for 1 h at 4 °C and then loaded onto a gravity flow column (*e.g.* glass Econo-columns, Bio-Rad, cat no. 7372522). For a typical purification we recommend using 1 mL of Glutathione Sepharose resin per 4 L of culture.
7. Allow the soluble homogenate to pass through the column, then wash the Glutathione Sepharose resin with 100 mL protein buffer.
8. Perform on-column protease cleavage overnight at 4 °C. For ctVps5-ctVps17$_{PX\text{-}BAR}$, add purified TEV protease directly to the protein–Sepharose mixture. For ctRetromer, add purified PreScission Protease. In both cases, use a 1:20 (protease:protein) ratio.
9. The next day, collect the flow-through containing GST-cleaved ctVps5-ctVps17$_{PX\text{-}BAR}$ and ctRetromer. Further purify ctVps5-ctVps17$_{PX\text{-}BAR}$ by concentrating the sample and perform size-exclusion chromatography (SEC) using either a Superdex™ 200 increase 15/300 column (Cytiva) or a Superose™ 6 increase column (Cytiva).
10. Measure the protein concentration using absorbance at 280 nm.
11. To achieve the correct 1:1:1 stoichiometry of ctRetromer, the GST-cleaved and eluted complex can be further purified using Talon® affinity purification to remove excess ctVps29. Elute the ctRetromer from Talon® resin with elution buffer (50 mM Tris-HCl pH 7.5, 200 mM NaCl, 350 mM imidazole, 1 mM TCEP).
12. Concentrate the eluted ctRetromer and perform a final purification using the same size exclusion chromatography column as ctVps5-ctVps17$_{PX\text{-}BAR}$.
13. Measure the protein concentration of ctRetromer using NanoDrop measuring absorbance at 280 nm.
14. To assemble the heteropentameric complex, mix freshly purified ctRetromer with ctVps5-ctVps17$_{PX\text{-}BAR}$ in a 1:1 ratio and incubate overnight at 4 °C.

Points to consider: Add 1x EDTA-free Protease inhibitor cocktail tablet into the protein complex mixture to reduce non-specific proteolysis. Because ctVps5-ctVps17$_{PX\text{-}BAR}$ can degrade rapidly, use freshly purified protein to ensure successful complex formation.

15. The next day, concentrate the mixture to 100 μL with a final protein concentration of ≥3 mg/mL before injecting onto a Superdex™ 200 increase 15/300 column or Superose™ 6 increase column for SEC purification in protein buffer.
16. Analyze fractions by SDS-PAGE to confirm the purify and integrity of the heteropentameric complex. Representative SEC chromatogram and SDS-PAGE gels are shown in Fig. 2A.

    Points to consider: Add 1 x EDTA-free Protease inhibitor cocktail tablet into the protein complex mixture to reduce non-specific proteolysis. Because ctVps5-ctVps17$_{PX\text{-}BAR}$ can degrade rapidly, use freshly purified protein to ensure successful complex formation.
17. Optional: Determine the molecular mass of the purified heteropentameric complex using mass photometry. To do this, load 100 nM of complex onto a Refeyn OneMP mass photometer following the protocol described previously (Wu & Piszczek, 2021) (Fig. 2B).

2.2 Liposome pelleting assay to assess membrane binding of the Retromer complex

Generally liposomes can be defined as either multilamellar vesicles (MLVs) or single unilamellar vesicles that are further categorised based on size as

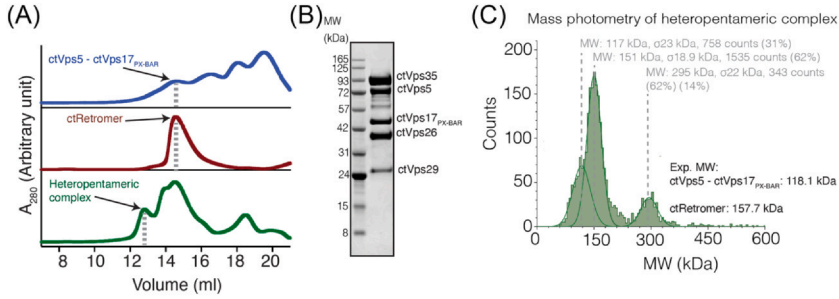

Fig. 2 Purification of the heteropentameric Retromer–Vps5–Vps17 complex from *C. thermophilum*. (A) The typical size-exclusion chromatogram of ctVps5–ctVps17$_{PX\text{-}BAR}$ heterodimer (blue), ctRetromer (brown) and heteropentameric complex (green). (B) The SDS-PAGE of heteropentameric complex showing the five distinguishable bands represent ctVps35, ctVps5, ctVps17PX-BAR, ctVps26, and ctVps29. (C) Mass photometry of the heteropentameric complex.

small unilamellar vesicles (SUVs; 20–100 nm), large unilamellar vesicles (LUVs; 100–1000 nm) or giant unilamellar vesicles (GUVs; >1000 nm) (Rideau et al., 2018). A typical protocol for the formation of MLVs for the liposome pelleting assay is presented here. The procedure is optimized for Retromer and Vps5–Vps17, but the conditions including lipid composition, and protein incubation time can be further adjusted for other SNX proteins or different membrane binding proteins.

2.2.1 Material and reagents

- Brain extract from bovine brain, Type I, Folch I (Sigma-Aldrich).
- palmitoyl-2-oleoyl-sn-glycero-3-phosphocholine (16:0-18:1 POPC) (Sigma-Aldrich).
- palmitoyl-2-oleoyl-sn-glycero-3-phosphoethanolamine (16:0-18:1 POPE), (Sigma-Aldrich).
- Phosphatidylinositol-3-phosphate (PI(3)P) diC16 (Echelon Bioscience).

2.2.2 Protocol

1. Preparation of multilamellar vesicles (MLV) for the liposome pelleting assay is carried out using the freeze-thaw method, as described on the Avanti Research webpage (https://avantiresearch.com/tech-support/liposome-preparation/lmv) with slight modification.
2. Prior to liposome preparation, note that commercially available phosphatidylinositol-3-phosphate (PtdIns(3)P) diC16 powder does not efficiently incorporate into liposomes. It is important to first protonate the phosphoinositide (convert to the uncharged, acid form) before use. We applied the HCl method following the protocol from Olga Perisic, Roger L Williams lab (https://www2.mrc-lmb.cam.ac.uk/groups/hmm/techniqs/PIPprot.html) with slight modification.
3. To protonate phosphoinositides, 1 mg of PtdIins(3)P diC16 powder is resuspended in 1 mL of chloroform solution, dry under a N_2 stream to yield a lipid film, and leave under vacuum for 1 h.
4. Next, resuspend the lipid film with 1 mL of chloroform – 100 % methanol - 1 M HCl solution in molar ratio of 2:1:0.01. Let the mixture stand for 15 min at room temperature, then again dry under a N_2 stream, and leave under vacuum for 1 h.
5. Repeat the above step by resuspend the lipid film with 1 mL of chloroform – 100 % methanol solution in molar ratio of 3:1. Dry under a N_2 stream to lipid film.

6. Again, resuspend the lipid film with 1 mL of chloroform and dry under a N_2 stream.
7. Finally, resuspend the lipid film with 1 mL of chloroform to make 1 mg/mL stock solution. Store at −20 °C until use.
8. To prepare control PC/PE liposomes, mix 34.2 μL of POPC at 13.2 mM and 3.6 μL of POPE at 13.9 mM in a 90:10 molar ratio, to a final volume of 500 μL chloroform (see Table 2), in a mini round bottom glass flask.
9. For the Folch I supplemented with 10 % PtdIns(3)*P* liposomes, 50 μL of 10 mg/mL Folch I and 47.8 μL of di-C16 PtdIns(3)*P* at 1.045 mM are added to a final volume of 500 μL chloroform.
10. Carefully evaporate the chloroform under a dry N_2 stream to yield a lipid film at the bottom of the glass flask. Leave under vacuum overnight to dry completely.

    Point to consider: 3–4 h of drying is typically sufficient.
11. The next day, hydrate the lipid film with 500 μL protein buffer and incubate for 30 min at 20 °C with shaking at 180 rpm. The shaking step ensures complete resuspension of the lipid film.
12. To generate MLVs, the lipid film resuspended in protein buffer then undergoes 10 rapid freeze-thaw cycles using hot water and dry ice.
13. Assess liposome integrity by negative-stain electron microscopy as described in the next section (Fig. 3A).
14. A typical liposome pelleting assay is performed in a total volume of 60 μL, comprising equal volume of 10 μM ctRetromer, ctVps5-

Table 2 Lipids premixture for liposome pelleting and tubulation study.

Preparation ratio	Volume (to make 500 μL solution)
90 % POPC: 10 % POPE	34.2 μL
- POPC stock solution = 13.16 mM (10 mg/mL)	3.6 μL
- POPE stock solution = 13.93 mM (10 mg/mL)	
90 % POPC: 10 % POPE: 10 % PtdIns(3)*P*	34.2 μL
- POPC stock solution = 13.16 mM (10 mg/mL)	3.6 μL
- POPE stock solution = 13.93 mM (10 mg/mL)	47.8 μL
- PtdIns(3)*P* diC16 = 1.045 mM (1 mg/mL)	
1 mg/mL Folch I supplement with 10 % PtdIns(3)*P*	50 μL
- 10 mg/mL Folch I	47.8 μL
- PtdIns(3)*P* diC16 = 1.045 mM (1 mg/mL)	

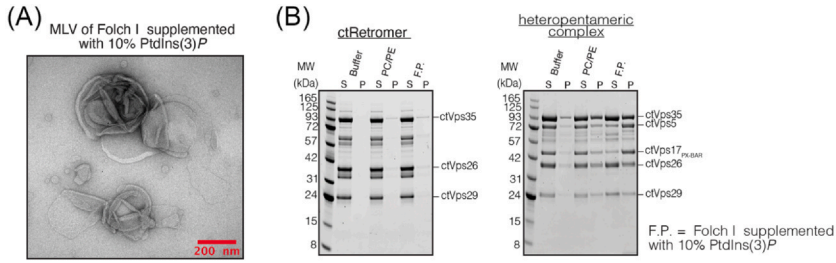

Fig. 3 Liposome-pelleting of the heteropentameric Retromer–Vps5–Vps17 complex. (A) Negative-stained image of typical MLV liposome. (B) The SDS-PAGE of ctRetromer (left) and heteropentameric complex (right) with liposome composed of PC/PE and Folch I supplemented with 10 % PtdIns(3)*P*.

ctVps17$_{PX\text{-}BAR}$ or heteropentameric complex mixed with liposomes. Incubate the protein – liposome reaction at room temperature for 30 min, followed by ultracentrifugation at 60,000 rpm (rotor TLA100) for 35 min.

Point to consider: The incubation time, protein concentration and buffer composition have been optimised for these proteins but can be adjusted for different proteins and lipid interactions.

15. After ultracentrifugation, carefully separate the supernatant from the pellet. Note, the pellet is generally small and translucent (in particular, PC/PE liposome), making it difficult to handle.
16. Resuspend the pellet in an equal volume of protein buffer containing 1 % SDS.
17. Analyze both supernatant and resuspended pellet fractions by SDS-PAGE gel (Fig. 3B).

2.3 Liposome tubulation

A key aspect of the procedures presented here is to obtain well-populated and homogenous protein-coated tubules for CryoET studies. While MLVs are suitable for pelleting assays, unilamellar vesicles (typically LUVs) are required for membrane tubulation and structural studies. The method can be further optimized for different Retromer-binding partners.

2.3.1 Material and reagents

- Brain extract from bovine brain, Type I, Folch I (Sigma-Aldrich).
- 1,2-Dioleoyl-sn-glycero-3-phosphocholine, DOPC (Sigma-Aldrich).
- 1,2-Dioleoyl-sn-glycero-3-phosphoethanolamine, DOPE (Sigma- Aldrich).
- 1,2-Dioleoyl-sn-glycero-3-phospho-L-serine, DOPS (Sigma-Aldrich).

- Phosphatidylinositol 3-phosphate (PtdIns(3)*P*) diC16 (Echelon Bioscience).
- Mini-Extruder set (Avanti Polar lipids).
- Formvar on carbon film coated grids (ProSciTech).
- C-flat copper TEM grid, CF-2/1-3C (Electron Microscopy Science).
- Protein-A Gold

2.3.2 Protocol

1. To prepare liposomes for the tubulation assays, Folch I supplement with PtdIns(3)*P* liposomes are made at the same concentration and under the same conditions as for the pelleting assay.
2. After freeze-thaw cycles, the MLVs are then extruded 21 times through a 400 nm pore-size membrane using a mini-Extruder set (Avanti) to produce large unilamellar vesicles (LUVs).
3. Keep the freshly prepared LUVs at room temperature and use them immediately for the tubulation assay.
4. For the assay, mix freshly purified heteropentameric complex with Folch I supplemented with 10 % PtdIns(3)*P* liposomes at a final concentration of 5 μM protein and 0.5 mg/mL of liposome in protein buffer.
5. For study by negative stain EM incubate the mixture at room temperature for 30 min before applying 4 μL onto a glow discharged carbon/formvar coated copper mesh grids.
6. Wash the grid once with protein buffer (10 μL), followed by three washes with MilliQ water (10 μL each) prior to negative staining with 2 % uranyl acetate (10 μL) for 30 s
7. Examine the grids using a transmission electron microscope (in our case, JEOL JEM1011 or JEOL JEM-1400Flash). Typical heteropentameric complex-coated tubules are shown in Fig. 4A.
8. To examine protein-coated tubules under cryogenic conditions for CryoET, incubate the complex at a final concentration of 6–7 μM protein with 0.6 mg/mL of freshly prepared Folch I supplemented with PtdIns(3)*P* liposomes in protein buffer for 30 min at room temperature. Prior to blotting, add 10 nm Protein A-gold (PAG) fiducials (Cell Microscopy Core, UMC Utrecht) to the protein-liposome mixture at a 1:5 ratio.

   Point to consider: The incubation time and protein concentration has been optimized for these proteins but can be adjusted for different proteins and lipid interactions.

   Point to consider: The choice of gold fiducial markers for CryoET data collection depends on the sample. In our case, better results were

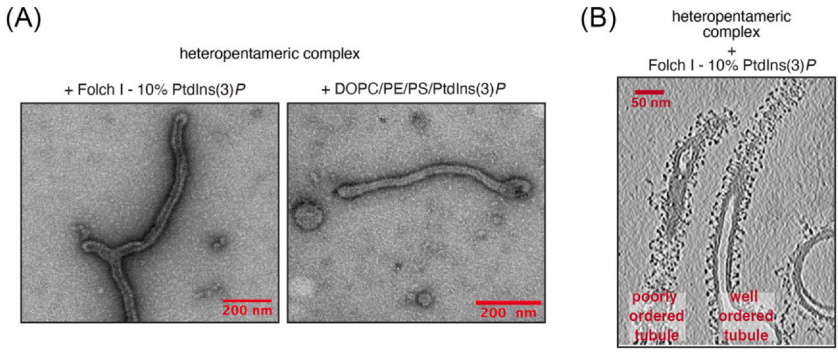

Fig. 4 Membrane tubulation and coat formation by the heteropentameric Retromer–Vps5–Vps17 complex. (A) Negative-stained image of heteropentameric complex incubated with Folch I liposomes supplemented with 10 % PtdIns(3)*P* (right) and DOPC/PE/PS/10 % PtdIns(3)*P* liposomes (left). (B) A single slice from a 3D tomographic reconstruction showing examples of well-ordered and poorly ordered Retromer-coated tubules (Chen et al., 2025). In this case images were acquired on a 200 kV Talos Arctica (Thermo Fisher Scientific) transmission electron microscope fitted with a Falcon 3EC direct electron detector.

obtained by adding PAG. It is essential, however, to choose fiducial markers that are evenly distributed around the region of interest without forming aggregates or clumps.

9. Blotting is carried out by loading 2.2–3.2 μL of the mixture onto a glow-discharged holey carbon C-flat-2/1-3 C grid (Protochips).

   Point to consider: C-flat grids have a relatively thin carbon film and easy to break, therefore, we typically glow-discharge only one side at low power to avoid damage.

10. Plunge-freezing is performed using a Vitrobot IV (Thermo Fisher Scientific) for 4.5–5.0 s with 100 % humidity, a blot force of −2 at room temperature for optimal result.

    Point to consider: Plunge-freezing can alternatively be performed by applying 2.5 μL of sample to the back side of glow-discharged C-flat grids using a Leica EM GP automatic plunger.

    Point to consider: The plunge-freezing condition mentioned in step 10 has been optimised to get the robust heteropentameric complex coated lipid tubules. The freezing condition including blotting time, force and temperature can be adjusted for different proteins and lipids used in the study.

11. The plunge-frozen grid is stored immersed in liquid nitrogen until data acquisition using a cryo-electron microscope.

12. Tilt series are typically collected using a parallelised acquisition with dose-symmetric scheme with a tilt range of ±60°, 3° angular increment, and at 45,000 x magnification.
13. Tomogram assembly from the acquired movies is processed using the IMOD package following established protocols (Chen et al., 2025; Kovtun et al., 2018; Leneva et al., 2021). A representative tomogram of Retromer-coated tubules is shown in Fig. 4B.

2.4 Additional notes

- It is strongly recommended to assemble the pentameric complex using freshly purified proteins. In particular, the N-terminal disordered loop of Vps5 degrades rapidly, which may compromise pentameric complex assembly.
- For the liposome pelleting assay, it is also possible to prepare heavy MLVs by resuspending the lipid film in sucrose solution (50 mM Tris-HCl pH 8.0, 200 mM NaCl, 330 mM sucrose) instead of the protein buffer prior to the freeze-and-thaw step. Heavy MLVs facilitate the pelleting without the need of using ultra-high-speed centrifugation, which is critical for proteins that tend to aggregate or sediment on their own during high-speed centrifugation.
- The incubation time required for protein–liposome mixtures to form tubules can be varied depending on the specific cargo adaptors and the protein concentration used.
- Based on our anecdotal experience, liposomes composed of DOPC/DOPE/DOPS/PtdIns(3)*P* produce more homogenous Retromer-coated tubules than Folch I liposomes. However, the exact liposome composition can be adjusted depending on the specific SNX adaptors under investigation.
- In our sample preparations, we often observed a substantial proportion of poorly ordered tubules compared to well-ordered ones (Chen et al., 2025). We speculate that incorporating membrane bound cargo proteins to the heteropentameric complex assembly could enhance the overall stability and homogeneity of the coated tubules. A similar observation was reported in the CryoET study of the human ESCPE-1 (SNX1–SNX5) membrane coat (Lopez-Robles et al., 2023).
- We also observed a small portion of free, unbound Vps5–Vps17 following the heteropentameric complex assembly. We believe that the presence of unbound SNX proteins during the liposome reconstitution may also lead to the formation of some poorly-ordered and heterogenous tubules.

3. Concluding remarks

This chapter describes a step-by-step protocol beginning with the production of the heteropentameric complex and continuing through liposome reconstitution to generate coated tubules for structural studies such as CryoET. A critical factor to consider is the importance of forming tubules that are highly populated with well-ordered Retromer coats with relatively few regions of poorly ordered coat formation. The well-ordered Retromer coated tubules are much more suitable for the downstream CryoET data processing. The quality of coat formation can be optimized through adjustments in sample preparation and lipid composition. The protein concentration, lipid composition and incubation time for tubulation presented in the chapter serve as guidelines and can be further optimized depending on the specific type of SNX proteins used. Moreover, the protocol described here should be readily applicable not only to Retromer and its SNX binding partners but also to other proteins capable of associating with Retromer, or distinct membrane-binding assemblies.

Acknowledgments

We acknowledge the use of the Australian Microscopy and Microanalysis Research Facility at the Center for Microscopy and Microanalysis at The University of Queensland. We also would like to thank Dr. Juanfang Ruan at the Electron Microscope Unit, Mark Wainwright Analytical Centre at University of New South Wales for the help with CryoET data collection. This work is supported by funds to BMC from the Australian Research Council (ARC) (DP160101743), National Health and Medical Research Council (NHMRC) (APP1156493), and Bright Focus Foundation (A2018627S). BMC was supported by an NHMRC Senior Research Fellowship and NHMRC Investigator Grant (APP1136021; APP2016410). NA is supported by a Human Frontiers Science Program Grant (RGP2023/011).

References

Burd, C., & Cullen, P. J. (2014). Retromer: A master conductor of endosome sorting. *Cold Spring Harbor Perspectives in Biology, 6*.

Chandra, M., Chin, Y. K., Mas, C., Feathers, J. R., Paul, B., Datta, S., et al. (2019). Classification of the human phox homology (PX) domains based on their phosphoinositide binding specificities. *Nature Communications, 10*, 1528.

Chandra, M., Kendall, A. K., Ford, M. G. J., & Jackson, L. P. (2025). VARP binds SNX27 to promote endosomal supercomplex formation on membranes. *Science Advances, 11*, eadr9340.

Chen, K. E., Guo, Q., Hill, T. A., Cui, Y., Kendall, A. K., Yang, Z., et al. (2021). De novo macrocyclic peptides for inhibiting, stabilizing, and probing the function of the retromer endosomal trafficking complex. *Science Advances, 7*, eabg4007.

Chen, K. E., Healy, M. D., & Collins, B. M. (2019). Towards a molecular understanding of endosomal trafficking by Retromer and Retriever. *Traffic, 20*, 465–478.

Chen, K. E., Tillu, V. A., Gopaldass, N., Chowdhury, S. R., Leneva, N., Kovtun, O., et al. (2025). Molecular basis for the assembly of the Vps5-Vps17 SNX-BAR proteins with Retromer. *Nature Communications, 16*, 3568.

Clairfeuille, T., Mas, C., Chan, A. S., Yang, Z., Tello-Lafoz, M., Chandra, M., et al. (2016). A molecular code for endosomal recycling of phosphorylated cargos by the SNX27-retromer complex. *Nature Structural & Molecular Biology, 23*, 921–932.

Collins, B. M., & Cullen, P. J. (2025). Separation of powers: A key feature underlying the neuroprotective role of Retromer in age-related neurodegenerative disease? *Current Opinion in Cell Biology, 94*, 102516.

Cullen, P. J., & Steinberg, F. (2018). To degrade or not to degrade: Mechanisms and significance of endocytic recycling. *Nature Reviews Molecular Cell Biology, 19*, 679–696.

Dodonova, S. O., Aderhold, P., Kopp, J., Ganeva, I., Röhling, S., Hagen, W. J. H., ... Briggs, J. A. G. (2017). 9Å structure of the COPI coat reveals that the Arf1 GTPase occupies two contrasting molecular environments. *eLife, 6*, e26691.

Faini, M., Prinz, S., Beck, R., Schorb, M., Riches, J. D., Bacia, K., ... Briggs, J. A. (2012). The structures of COPI-coated vesicles reveal alternate coatomer conformations and interactions. *Science, 336*, 1451–1454.

Gopaldass, N., Chen, K. E., Collins, B., & Mayer, A. (2024). Assembly and fission of tubular carriers mediating protein sorting in endosomes. *Nature Reviews Molecular Cell Biology*.

Gopaldass, N., Chowdhury, S. R., Alves, A. C., Mayer, L. M., Comte-Miserez, V., & Mayerv, A. (2025). Hybrid endosomal coats containing different classes of sorting nexins. *bioRxiv* 2025.2007.2029.667382.

Harrison, M. S., Hung, C. S., Liu, T. T., Christiano, R., Walther, T. C., & Burd, C. G. (2014). A mechanism for retromer endosomal coat complex assembly with cargo. *Proceedings of the National Academy of Sciences of the United States of America, 111*, 267–272.

Hierro, A., Gershlick, D. C., Rojas, A. L., & Bonifacino, J. S. (2015). Formation of tubulovesicular carriers from endosomes and their fusion to the trans-Golgi network. *International Review of Cell and Molecular Biology, 318*, 159–202.

Kendall, A. K., Xie, B., Xu, P., Wang, J., Burcham, R., Frazier, M. N., ... Nakagawa, T., et al. (2020). Mammalian Retromer is an adaptable scaffold for cargo sorting from endosomes. *Structure, 28*, 393–405 e394.

Kovtun, O., Leneva, N., Bykov, Y. S., Ariotti, N., Teasdale, R. D., Schaffer, M., ... Collins, B. M. (2018). Structure of the membrane-assembled retromer coat determined by cryo-electron tomography. *Nature, 561*, 561–564.

Leneva, N., Kovtun, O., Morado, D. R., Briggs, J. A. G., & Owen, D. J. (2021). Architecture and mechanism of metazoan retromer:SNX3 tubular coat assembly. *Science Advances, 7*.

Lopez-Robles, C., Scaramuzza, S., Astorga-Simon, E. N., Ishida, M., Williamson, C. D., Banos-Mateos, S., et al. (2023). Architecture of the ESCPE-1 membrane coat. *Nature Structural & Molecular Biology, 30*, 958–969.

Marcusson, E. G., Horazdovsky, B. F., Cereghino, J. L., Gharakhanian, E., & Emr, S. D. (1994). The sorting receptor for yeast vacuolar carboxypeptidase-Y Is encoded by the Vps10 gene. *Cell, 77*, 579–586.

Pyle, E., Miller, E. A., & Zanetti, G. (2025). Cryo-electron tomography reveals how COPII assembles on cargo-containing membranes. *Nature Structural & Molecular Biology, 32*, 513–519.

Rideau, E., Dimova, R., Schwille, P., Wurm, F. R., & Landfester, K. (2018). Liposomes and polymersomes: A comparative review towards cell mimicking. *Chemical Society Reviews, 47*, 8572–8610.

Seaman, M. N. (2012). The retromer complex - endosomal protein recycling and beyond. *Journal of Cell Science, 125*, 4693–4702.

Seaman, M. N., Marcusson, E. G., Cereghino, J. L., & Emr, S. D. (1997). Endosome to Golgi retrieval of the vacuolar protein sorting receptor, Vps10p, requires the function of the VPS29, VPS30, and VPS35 gene products. *Journal of Cell Biology, 137*, 79–92.

Seaman, M. N., McCaffery, J. M., & Emr, S. D. (1998). A membrane coat complex essential for endosome-to-Golgi retrograde transport in yeast. *Journal of Cell Biology, 142*, 665–681.

Seaman, M. N., & Williams, H. P. (2002). Identification of the functional domains of yeast sorting nexins Vps5p and Vps17p. *Molecular Biology of the Cell, 13*, 2826–2840.

Simonetti, B., Paul, B., Chaudhari, K., Weeratunga, S., Steinberg, F., Gorla, M., ... Cullen, P. J. (2019). Molecular identification of a BAR domain-containing coat complex for endosomal recycling of transmembrane proteins. *Nature Cell Biology, 21*, 1219–1233.

Steinberg, F., Gallon, M., Winfield, M., Thomas, E. C., Bell, A. J., Heesom, K. J., ... Cullen, P. J. (2013). A global analysis of SNX27-retromer assembly and cargo specificity reveals a function in glucose and metal ion transport. *Nature Cell Biology, 15*, 461–471.

Studier, F. W. (2005). Protein production by auto-induction in high density shaking cultures. *Protein Expression and Purification, 41*, 207–234.

Tremel, S., Ohashi, Y., Morado, D. R., Bertram, J., Perisic, O., Brandt, L. T. L., et al. (2021). Structural basis for VPS34 kinase activation by Rab1 and Rab5 on membranes. *Nature Communications, 12*, 1564.

van Weering, J. R., Verkade, P., & Cullen, P. J. (2012). SNX-BAR-mediated endosome tubulation is co-ordinated with endosome maturation. *Traffic, 13*, 94–107.

Wu, D., & Piszczek, G. (2021). Standard protocol for mass photometry experiments. *European Biophysics Journal, 50*, 403–409.

CHAPTER FIVE

Quantitative analysis of S-acylation

Carla Busquets Hernández, Alexandra Tsiotsia, and Gemma Triola*
Institute for Advanced Chemistry of Catalonia (IQAC-CSIC), Barcelona, Spain
*Corresponding author. e-mail address: gemma.triola@iqac.csic.es

Contents

1. Introduction 118
2. Sample preparation 121
   2.1 Isolation of proteome from cell lysates 122
   2.2 Treatment of the proteome with 2 M Hydroxylamine and isolation of the formed fatty acid hydroxamates 123
3. Preparation of the C19 FAH 124
4. Mass analysis 125
5. Data analysis 126
6. Notes 126
References 127

Abstract

S-acylation is a protein post-translational modification that relies on the attachment of a hydrophobic fatty acid chain to a cysteine residue through the formation of a thioester bond. This reversible modification is controlled by the counteraction of protein acyltransferases and acyl protein thioesterases. The bonded lipid moiety can modulate the physicochemical properties of the substrate proteins, their membrane-binding affinity, subcellular localization, protein stability, or interactions with other proteins or cell components, thereby playing a key role in several cell processes such as protein trafficking, signal transduction, or cell proliferation. Moreover, increasing evidence has associated S-acylation malfunction with several pathological processes, including various types of cancers or neurodegenerative disorders, making S-acylation and its controlling enzymes an ideal target for therapeutic strategies. S-acylation has been commonly known as S-palmitoylation because palmitic acid was considered the predominant fatty acid attached to proteins. However, recent advances, especially in the mass spectrometry field, have suggested a diversity in the identity of the attached lipids greater than that previously considered. Moreover, since variations in the length and saturation degree of the fatty acyl chains may alter the intracellular localization and biological function of proteins, its potential role in the regulation of protein function is just being explored. However, this heterogeneous lipid composition could not be systematically studied, mainly due to the lack of suitable methods. In order to address these challenges, this protocol reports a method to identify and quantify the fatty acids attached to S-acylated proteins.

Methods in Enzymology, Volume 728
ISSN 0076-6879, https://doi.org/10.1016/bs.mie.2025.12.001
Copyright © 2026 Elsevier Inc. All rights are reserved, including those for text and data mining, AI training, and similar technologies.

1. Introduction

The attachment of a fatty acid residue to a cysteine amino acid of a protein through the formation of a thioester bond is known as S-acylation, and it is reported to be extremely common in organisms —about 10–20 % of the human proteome is potentially S-acylated (Blanc et al., 2019). There is accumulating evidence that this lipid post-translational modification (PTM) is heterogeneous, inferring that not only palmitate, but also other fatty acids with different chain lengths and unsaturation degrees can also S-acylate proteins. However, due to the high abundance of palmitate (C16:0), S-acylation has been traditionally referred to as palmitoylation.

S-acylation is a reversible modification, regulated by a family of protein acyltransferases known as DHHC-PAT and a set of thioesterases (Chamberlain & Shipston, 2015). A particular feature of this modification is that the acylation/deacylation cycle that a protein undergoes can be shorter than its lifetime, providing dynamic control of the protein's subcellular localization and function. Notably, palmitoylation turnover varies among different proteins. For example, PSD95 has an S-acylation half-life of approximately 2 h, (El-Husseini et al., 2002) whereas the half-life of the S-acyl moiety on H-Ras is 2.4 h and of N-Ras is less than 20 min (Roy et al., 2005; Rocks et al., 2010). In contrast, palmitoylation turnover is much slower in other proteins. In synaptotagmin-2, palmitoylation turnover remains undetectable even after 6 h, suggesting it serves as a structural signal for proper targeting (Kang et al., 2004). Similarly, in the TEAD transcription factors, palmitoylation decreases by only 40 % after 48 h, and the modification is linked to maintaining protein stability (Noland et al., 2016).

The attachment of a hydrophobic fatty acid chain can affect the physicochemical features of proteins. Thus, it can mediate the temporary association with membranes, affect protein-protein interactions, or facilitate conformational changes, ultimately leading to different subcellular localizations or biological functions (Fig. 1) (Mesquita et al., 2024). As a result, the dysregulation of this lipid modification — caused for example by mutations, upregulated protein expression, or malfunction of the enzymes involved in their regulation — is closely related to a plethora of human diseases such as cancer, metabolic and neurodegenerative disorders, amongst others (Tate et al., 2024; Wlodarczyk et al., 2024).

From the initial studies using isotopically labeled fatty acids to the most recent mass spectrometry (MS) advances, there has been increasing evidence that S-acylation may not be restricted to palmitate and may include a

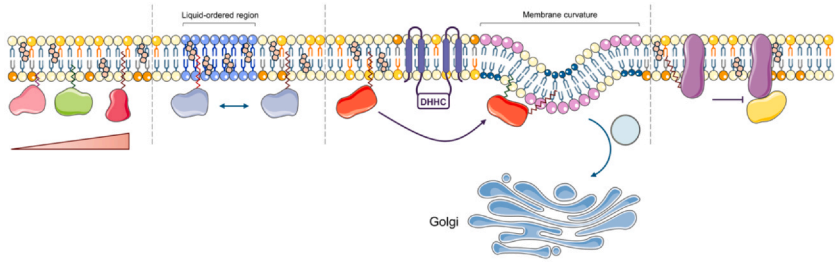

Fig. 1 Heterogeneous lipidation and protein function. Different acyl chains might affect the strength of association of proteins with membranes (left), impact the lateral distribution of proteins between ordered and disordered membrane domains, or favor their interaction with membranes that have a distinct curvature, which could have an impact on internalization processes. These effects can also change the localization of the protein and modulate its interaction with other proteins (right).

vast range of different fatty acids. Moreover, the potential consequences in protein function of having a single cysteine residue acylated with different fatty acids have just started to be elucidated. Thus, biophysical studies showed that an N-Ras protein modified with C16:0 clustered at the boundaries of liquid-ordered domains or rafts, whereas the presence of a palmitoleate (C16:1) resulted in higher membrane insertion rates and in the localization of the protein in liquid domains (Schulte-Zweckel et al., 2019). Another example of heterogeneous acylation with consequences on protein function is the guanine nucleotide-binding protein G (GNAI) protein, which is involved in the activation of the PI3K-AKT-mTORC1 pathway, promoting cell survival. Nůsková and coworkers showed that GNAI proteins could be acylated either by palmitate or oleate (C18:1) at Cys3. Whereas palmitoylated GNAI resulted in increased proliferation, oleoylation caused GNAI proteins to shift out of cell membrane detergent-resistant fractions, where they potentiated EGFR signaling, thereby reducing AKT activation and potentially decreasing oncogenic signaling (Nůsková et al., 2021).

Lipidomics — a field of study focused on the identification and quantification of lipid species, usually employing MS-based techniques — has enabled important advances in the study of lipid-modified proteins. Our group has been intensively working in recent years on the development of MS-based techniques aimed at profiling and quantifying the S-bound fatty acids present in S-acylated proteins. Our approach exploited the known capability of hydroxylamine (NH_2OH) to selectively cleave thioester bonds and generate the corresponding fatty acid hydroxamates

(FAHs) that could later be analyzed by MS. An initial method was reported in 2019 based on a hydroxylamine derivative (Schulte-Zweckel et al., 2019). However, it required large amounts of this synthetic compound, which made its wider application and further optimization difficult. More recently, we have described a protocol for the quantitative analysis of the S-linked fatty acids (S-acylome) of protein derived from cultured cells based on the use of hydroxylamine (Busquets-Hernandez et al., 2024). Optimized LC-MS conditions were employed to improve the detection of the FAHs. This robust and simple methodology, together with the reagent employed, which is commercially available and inexpensive, has enabled an unprecedented and extensive characterization of the S-acylome in different cell lines.

The developed procedure consists of the precipitation of the proteome of lysed cells through centrifugation with organic solvents (Fig. 2) (Wessel & Flügge, 1984). This proteome is then treated with hydroxylamine to release the corresponding S-linked fatty acids as FAHs that are extracted from the crude using a mixture of methanol-chloroform-water (Bligh & Dyer, 1959). Finally, the FAH mixture is evaporated to dryness, diluted in methanol, and injected into the LC-HRMS instrument for its analysis.

In the following sections, we describe the protocols for the identification and quantification of the fatty acids bound to S-acylated proteins. The sections include information about sample preparation and data analysis of the formed FAHs. We also provide a protocol for the synthesis of the internal standard required for proper quantification.

The following sections describe the protocols for the preparation of the samples for the analysis of S-linked fatty acids (Section 2). More specifically, Section 2.1 provides a method for the preparation of protein samples from cultured cells, and Section 2.2 includes the treatment of the proteome with hydroxylamine and the subsequent isolation of FAHs. Section 3 describes the synthesis of the internal standard employed for quantification. Descriptions of the mass spectrometric and follow-up analysis are provided in Sections 4 (Mass spectrometry) and 5 (Data analysis), respectively.

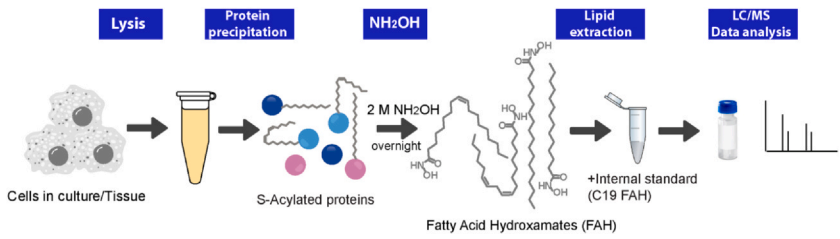

Fig. 2 The workflow for the identification and quantification of S-linked fatty acids.

2. Sample preparation

Materials, reagents, and equipment.

- Plate reader (BioTek Synergy H1)
- 96 well-plates (Thermo Scientific, catalog # 137101)
- Centrifuge (Eppendorf, 5810 R)
- Ultrasonics Sonifier™ SFX150 Cell Disruptor (Branson)
- SAVANT SPD131DDA SpeedVac Concentrator (Thermo Scientific) coupled to a Thermo Scientific OFP400 Vacuum Pump and a SAVANT RVT5105 Refrigerated Vapor Trap
- Thermoshaker PHMT (Fisher Scientific)
- Rotator (Thermo Scientific, catalog # 88881002)
- Semi-Micro Balance (Sartorius, CP225D)
- pH-meter (GLP SENSION+ PH31)
- ACQUITY Premier BEH C18 Column, 1.7 μm, 2.1 × 50 mm UPLC column (Waters, catalog # 186009452)
- High-resolution mass spectrometer (LC-HRMS), Acquity Ultra High-Performance Liquid Chromatography (UHPLC) System (Waters, USA) connected to a time-of-flight (TOF; LCT Premier XE) using electrospray ionization (ESI)
- Cell Scraper (Corning, catalog # 3010)
- Water was purified with a AriumPro UV (Sartorius)
- T75 cm^2 cell culture flasks with vented cap (Corning, catalog # 430641U)
- Dulbecco's Modified Eagle Medium (DMEM) (Merck, catalog # D5796)
- Fetal Bovine Serum (FBS) (Gibo, catalog # A5256801)
- Penicillin-Streptomycin (PIS) (Sigma catalog # P4333)
- Trypsin – EDTA 10X in PBS (Biowest, catalog # X0930)
- Methanol (MeOH) (Sigma, catalog # 1.06018.2500)
- Chloroform ($CHCl_3$) (Carlo Erba, catalog # 438601)
- Water (H2O) (Sigma, catalog # 1.15333.2500)
- Formic acid (Sigma, catalog # 1.00264.1000)
- Ammonium Formate (Sigma, catalog # 70221-25G-F)
- Bicinchonic acid (BCA) kit (Thermo Scientific, catalog # 23227)
- Tergitol solution (NP-40) (Sigma, catalog #NP40S-mL)
- Hydroxylamine Hydrochloride ($NH_2OH{\cdot}HCl$; TCI, catalog # H1581)
- Palmostatin B (PalmB) (MilliporeSigma™ catalog # 5.08738.0001)
- Protease Inhibitors Pi: complete (Pi25x) (Roche, catalog # 11697498001)
- Phosphate-Buffered saline (PBS) (Sigma, catalog # P4417-100TAB)

- Tris(hydroxymethyl)-aminomethane (Merck, catalog # 108382)
- Hydrochloric acid fuming 37 % (Sigma, catalog # 1.00317.1000)
- Conic UPLC glass vial (Waters, catalog # 186000327 C)
- Ethyl Acetate (PanReac AppliChem, ITW Reagents, catalog # 131318)
- Propylphosphonic anhydride solution ≥50 % wt. in ethyl acetate (Sigma, catalog # 431303-10 ML)
- Acetonitrile (Fisher Scientific, catalog # A/0627/17)
- Triethylamine (Sigma, catalog # 90340–250 ML)
- Nonadecanoic acid (TCI, catalog # N0283)
- Sodium chloride (Carlo Erba, catalog # 479687)
- Rotary evaporator (Buchi R-210, B-491)
- Silica gel for chromatography 60A 45-70μ (Carlo Erba, catalog # P2000027)
- Dichloromethane (Carlo Erba, catalog # 463314)

2.1 Isolation of proteome from cell lysates

In this section, we provide a protocol for the preparation of protein samples derived from cells in culture.

2.1.1 Cell culture

1. Seed cultured cells in T75 flasks until 90 % confluence.
2. Remove media and wash the cells carefully with 4 mL of phosphate-buffered saline (PBS).
3. Collect cells using a scraper and put them in 15 mL plastic Falcon tubes.
4. Quantify the number of cells
5. Centrifuge the cell suspension (400 g, 3 min)
6. Remove supernatant with aspiration.
7. Add 2 mL of PBS
8. Centrifuge cell suspension (400 g, 3 min)
9. Aspirate excess PBS
10. Repeat cell wash
11. Store the cell pellet in the fridge until sample preparation

Timing: 20–30 min.

2.1.2 Preparation of solutions and buffers

Prepare adequate volumes of the following solutions:

- Reaction buffer (RB): 50 mM Tris·HCl, 150 mM NaCl, pH 7.2. To prepare 100 mL of RB, add 2.5 mL Tris·HCl 1 M, 3.75 mL of NaCl 4 M, 95 mL purified water, and adjust pH to 7.2 using a 6 M HCl solution.

- Lysis buffer (LB): 50 mM Tris·HCl, 150 mM NaCl, 1 % NP-40, Protease inhibitors (Pi), 10 μM PalmB, pH 7.2, To prepare ~2 mL of LB, add 1.9 mL of RB, 80 μL Pi 25x, 20 μL NP-40, and 4 μL of a 5 mM solution of Palmostatin B.
- Hydroxylamine solution (HA): 4 M NH_2OH·HCl, pH 7.4. To prepare 5 mL of HA 4 M solution, weigh 1.4 g of NH_2OH·HCl and dissolve it in 3 mL of RB. Adjust pH to 7.4 using a 6 M solution of HCl and adjust to a final volume of 5 mL with RB.

2.1.3 Preparation of cell lysates

1. Resuspend the cell pellet in an approximately 10×10^6 cells/mL ratio with 1.0 mL of LB.
2. Transfer the solution into a 1.5 mL Eppendorf tube.
3. Lyse the cell pellet by sonication at 0 °C (10 cycles, 5 s sonication followed by 5 s resting period, intensity at 50 %).
4. Clarify the lysate (3000 g, 5 min, room temperature (r. t.)).
5. Transfer the cell lysate (supernatant) into 15 mL plastic Falcon tubes
   Timing: 10–15 min.

2.1.4 Protein precipitation

1. Add 4 volumes of methanol (with respect to the LB added previously) and homogenize the solution in a vortex mixer
2. Add 1.5 volumes of chloroform and mix the solution, and homogenize the solution in a vortex mixer
3. Add 3 volumes of purified water and homogenize the solution in a vortex mixer
4. Centrifuge the solution at 6000 g for 20 min at room temperature (r. t.)
5. Remove the upper aqueous layer with a pipette
6. Add 3 volumes of methanol on top of the protein pellet
7. Centrifuge at 6000 g for 10 min at room temperature (r. t.).
8. Remove the remaining organic layer with aspiration
9. Carefully dry the protein pellet under a stream of nitrogen.
   Timing: 40–50 min

2.2 Treatment of the proteome with 2 M Hydroxylamine and isolation of the formed fatty acid hydroxamates

In this section, we provide a protocol for the cleavage of thioesters using a 2 M Hydroxylamine solution and the extraction of the formed FAHs for their analysis.

2.2.1 Hydroxyaminolysis of thioesters

1. Resuspend the protein pellet in reaction buffer (RB) using the same volume of LB that was previously added to the cell pellet in Step 1 of Section "Preparation of cell lysates".
2. Perform a BCA assay (refer to the manufacturer's protocol) to determine the protein concentration of the pellet.
3. Transfer the pellet into 1.5 mL Eppendorf tubes in aliquots that correspond to 600 μg of protein.
4. Add the same volume of RB (for the blanks) or hydroxylamine solution (HA) for the samples to achieve a final HA concentration of 2 M.
5. Incubate overnight at room temperature with end-over-end rotation.
   Timing: 14–16 h.

2.2.2 Lipid extraction

1. Add 100 pmol of the nonadecanoic hydroxamic acid internal standard (C19 FAH) from a stock solution of 10 μM in MeOH.
2. Transfer the solution to glass vials of ~6 mL capacity.
3. Add 3.75 volumes of a 1:2 (v/v) solution of chloroform and methanol, and homogenize the solution in a vortex mixer
4. Add 1.25 volumes of chloroform, and homogenize the solution in a vortex mixer
5. Add 1.25 volumes of purified water, and homogenize the solution in a vortex mixer
6. Wait for 1–2 min to facilitate the separation into two phases
7. Remove the top aqueous phase
8. Transfer the organic phase (bottom) into a conic UPLC glass vial using a micropipette.
9. Evaporate the samples to dryness using a SpeedVac concentrator or under a gentle stream of nitrogen to obtain the lipid extracts.
   Timing: 2–3 h.

3. Preparation of the C19 FAH

For the synthesis of the C19 FAH employed as an internal standard:

1. Add 246 μL of a 50 % T3P® solution in ethyl acetate (414 μmol, 1.2 eq) in a 10 mL round-bottom flask equipped with a magnetic bar and a stopper covering the top of the flask

2. Add 2 mL of acetonitrile, 192 μL of triethylamine (1.38 mmol, 4.1 eq) and 100 mg of nonadecanoic acid (336 μmol, 1.0 eq) into the reaction mixture.
3. Stir the solution for 30 min at room temperature using a magnetic stirrer
4. Add 49 mg of $NH_2OH{\cdot}HCl$ (711 μmol, 2.1 eq) and stir the solution overnight at room temperature
5. Add 30 mL of ethyl acetate to the crude mixture and extract the organic phase using a separatory funnel
6. Wash the organic phase twice with a NaCl-saturated aqueous solution and evaporate the solvent to dryness using a rotary evaporator.
7. Purify the crude by column chromatography on silica gel using a gradient of 1–10 % methanol in dichloromethane.
8. Confirm identity and purity by ^{1}H, ^{13}C NMR and HPLC-MS. This protocol and the analysis of this product have been reported (Busquets-Hernandez et al., 2024).
9. Store the evaporated product in the freezer at −20 °C
10. Prepare a 10 μM stock dilution in MeOH.

4. Mass analysis

1. Resuspend the lipid extract in 300 μL of HPLC-grade methanol and sonicate until completely dissolved
2. Prepare fresh eluents for the LC-HRMS analysis of the lipid extracts: Solvent A is 2 mM ammonium formate, containing 0.2 % formic acid in purified water; solvent B is 1 mM ammonium formate, 0.2 % formic acid in methanol.
3. Install an Acquity Premier C18 column (1.7 μm, 2.1 × 50 mm) in the LC–HRMS system and bring the column temperature to 30 °C.
4. Samples are introduced via a cooled autosampler with a temperature set to 10 °C and a volume of 8 μL is injected.
5. The gradient begins at 65 % of B and holds for 2 min, then increases to 90 % of B in 8 min, and to 99 % of B in 5 min. It holds for 2 min at 99 %, then returns to the initial conditions in 3 min and re-equilibrates for 2 additional minutes. The total run time is 22 min at a flow of 0.3 μL/min
6. The acquisition range of the TOF detector should be set at m/z 50–1.800, the capillary voltage to 3.0 kV, the desolvation temperature to 350 °C, and the desolvation gas flow rate to 600 liters/h.

5. Data analysis

Once data are acquired from the LC–HRMS instrument, proceed as follows:

1. Calculate the exact masses of the expected FAHs using the MassLynx V4.2 software (Molecular Weight Calculator)
2. Examine each chromatogram using MassLynx, setting the Mass Chromatogram Window to 0.01.
3. Search for the FAHs of interest and the spiked internal standard (C_{19} FAH) in the injected samples. Confirm their presence if the observed m/z deviates by no more than ± 0.005. For each confirmed peak, record the detected mass, retention time, and integrated peak area.
4. Convert the peak areas of all detected FAH to picomoles (pmol). Quantification is performed in relation to the C19 FAH internal standard spiked into the sample (100 pmol)

$$pmols\ of\ FAH = \frac{Area\ FAH \times 100}{Area\ C19\ FAH}$$

5. Data displayed as pmol/mg of protein can be obtained by dividing the number of pmol by 0.6 mg of total protein.
6. Data can also be displayed as a percentage of total FAHs by dividing the pmol of a FAH by the whole (sum of all detected FAHs)

6. Notes

- Commercially available Palmostatin B is dissolved in purified water and is frozen in small aliquots to avoid degradation of the inhibitor by continuous thaw cycles.
- A tablet of commercially available cOmplete™ Protease Inhibitor Cocktail (Pi) is dissolved in 2 mL of purified water to obtain a Pi25x stock dilution, then it is frozen in small aliquots to avoid degradation of the protein by continuous thaw cycles.
- Hydroxylamine solution (HA) needs to be freshly prepared each day and its pH adjusted carefully using HCl 6 M. Keep refrigerated until use.
- Dried lipid extracts can be temporarily kept in the freezer at −20 °C prior to their injection in the mass detector.

- Stock solutions of the internal standard (C19 FAH) should be prepared frequently to avoid solvent evaporation and changes in the final concentration.
- Correct performance of the method and the column in the LC-HRMS analysis can be verified by injecting blank samples (methanol) and a vial containing a mix of standard reference compounds palmitic acid hydroxamate (C16-FAH), myristic acid hydroxamate (C14-FAH), and erucic acid hydroxamate (C22:1-FAH) at a 10 μM concentration in methanol.
- To avoid incorrect interpretation of peaks, it is recommended to validate the correct retention times upon injection of pure samples of the corresponding FAHs that can be analogously prepared and purified as described for C19 FAH.
- Using the reported conditions, a two-carbon increase in the FAH increased the retention time by ~1 min, whereas introduction of a double bond decreased the retention time by ~0.7 min
- Typically, 3–4 mg of protein is obtained from 8–10·10^6 cells.

References

Blanc, M., David, F. P. A., & van der Goot, F. G. (2019). *SwissPalm 2: Protein S-palmitoylation database. Methods in Molecular Biology*. Humana Press Inc. 203–214. https://doi.org/10.1007/978-1-4939-9532-5_16.

Bligh, E. G., & Dyer, W. J. (1959). A rapid method of total lipid extraction and purification. *Canadian Journal of Biochemistry and Physiology, 37*, 911–917. https://doi.org/10.1139/o59-099.

Busquets-Hernandez, C., Ribo, S., Gratacos-Batlle, E., Carbajo, D., Tsiotsia, A., Blanco-Canosa, J. B., et al. (2024). Quantitative analysis of protein lipidation and acyl-CoAs reveals substrate preferences of the S-acylation machinery. *Chemical Science, 15*, 12845–12855. https://doi.org/10.1039/D4SC02235A.

Chamberlain, L. H., & Shipston, M. J. (2015). The physiology of protein S-acylation. *Physiological Reviews, 95*, 341–376. https://doi.org/10.1152/physrev.00032.2014.

El-Husseini, A. E. D., Schnell, E., Dakoji, S., Sweeney, N., Zhou, Q., Prange, O., et al. (2002). Synaptic strength regulated by palmitate cycling on PSD-95. *Cell, 108*, 849–863. https://doi.org/10.1016/S0092-8674(02)00683-9.

Kang, R., Swayze, R., Lise, M. F., Gerrow, K., Mullard, A., Honer, W. G., et al. (2004). Presynaptic trafficking of synaptotagmin I is regulated by protein palmitoylation. *The Journal of Biological Chemistry, 279*, 50524–50536. https://doi.org/10.1074/jbc.M404981200.

Noland, C. L., Gierke, S., Schnier, P. D., Murray, J., Sandoval, W. N., Sagolla, M., et al. (2016). Palmitoylation of TEAD transcription factors is required for their stability and function in hippo pathway signaling. *Structure (London, England: 1993), 24*, 179–186. https://doi.org/10.1016/J.STR.2015.11.005.

Nůsková, H., Serebryakova, M. V., Ferrer-Caelles, A., Sachsenheimer, T., Lüchtenborg, C., Miller, A. K., et al. (2021). Stearic acid blunts growth-factor signaling via oleoylation of GNAI proteins. *Nature Communications, 12*, 1–15. https://doi.org/10.1038/s41467-021-24844-9.

Rocks, O., Gerauer, M., Vartak, N., Koch, S., Huang, Z. P., Pechlivanis, M., et al. (2010). The palmitoylation machinery is a spatially organizing system for peripheral membrane proteins. *Cell, 141*, 458–471.

Roy, S., Plowman, S., Rotblat, B., Prior, I. A., Muncke, C., Grainger, S., et al. (2005). Individual palmitoyl residues serve distinct roles in H-ras trafficking, microlocalization, and signaling. *Molecular and Cellular Biology, 25*, 6722–6733. https://doi.org/10.1128/mcb.25.15.6722-6733.2005.

Mesquita, F. S., Abrami, L., Linder, M. E., Bamji, S. X., Dickinson, B. C., & van der Goot, F. G. (2024). Mechanisms and functions of protein S-acylation. *Nature Reviews. Molecular Cell Biology, 2024*, 1–22. https://doi.org/10.1038/s41580-024-00700-8.

Schulte-Zweckel, J., Dwivedi, M., Brockmeyer, A., Janning, P., Winter, R., & Triola, G. (2019). A hydroxylamine probe for profiling S-acylated fatty acids on proteins †. *Chemical Communications, 55*, 11183. https://doi.org/10.1039/c9cc05989j.

Tate, E. W., Soday, L., de la Lastra, A. L., Wang, M., & Lin, H. (2024). Protein lipidation in cancer: Mechanisms, dysregulation and emerging drug targets. *Nature Reviews. Cancer, 24*(4), 240–260. https://doi.org/10.1038/s41568-024-00666-x.

Wessel, D., & Flügge, U. I. (1984). A method for the quantitative recovery of protein in dilute solution in the presence of detergents and lipids. *Analytical Biochemistry, 138*, 141–143. https://doi.org/10.1016/0003-2697(84)90782-6.

Wlodarczyk, J., Bhattacharyya, R., Dore, K., Ho, G. P. H., Martin, D. D. O., Mejias, R., et al. (2024). Altered protein palmitoylation as disease mechanism in neurodegenerative disorders. *The Journal of Neuroscience, 44*. https://doi.org/10.1523/JNEUROSCI.1225-24.2024.

CHAPTER SIX

Detecting ZDHHC acyltransferase inhibition using acylation-coupled lipophilic induction of polarization (Acyl-cLIP) or LC-MS

Wenzhe Chen[a,b,c], Jiaqi Zhao[a,b,c], Zhenquan Sun[a,b], Kewen Peng[a,b,c], Wendy K. Greentree[d], Maurine E. Linder[d], and Hening Lin[a,b,c,e,*]

[a]Department of Medicine, The University of Chicago, Chicago, IL, United States
[b]Department of Chemistry, The University of Chicago, Chicago, IL, United States
[c]Department of Chemistry and Chemical Biology, Cornell University, Ithaca, NY, United States
[d]Department of Molecular Medicine, Cornell University, Ithaca, NY, United States
[e]Howard Hughes Medical Institute, The University of Chicago, Chicago, IL, United States
*Corresponding author. e-mail address: linh1@uchicago.edu

Contents

1. Introduction 130
   1.1 ZDHHCs 130
   1.2 Acyl-cLIP and LCMS-based method 131
2. Acyl-cLIP for ZDHHC enzymes 132
   2.1 Equipment 132
   2.2 Reagents 132
   2.3 Reagent setup 132
   2.4 Procedures 133
   2.5 Data processing 134
3. ZDHHC enzyme assay detected by LC-MS 135
   3.1 Equipment 135
   3.2 Reagents and buffers 135
   3.3 Reagents setup 136
   3.4 Procedures 136
4. Notes 139
References 140

Abstract

Acylation of protein substrates by ZDHHC (zinc finger Asp–His–His–Cys) acyltransferases is a key regulator of cell signaling. Potent and selective small molecule inhibitors for ZDHHCs have been long desired for the field but so far still do not exist. Robust activity assay methods are needed to discover selective ZDHHC inhibitors. Here we present two complementary assays for in vitro ZDHHC activity assay and inhibitor profiling. The Acylation-Coupled Lipophilic Induction of

Methods in Enzymology, Volume 728
ISSN 0076-6879, https://doi.org/10.1016/bs.mie.2026.01.015
Copyright © 2026 Elsevier Inc. All rights are reserved, including those for text and data mining, AI training, and similar technologies.

Polarization (Acyl-cLIP) assay is a homogeneous fluorescence polarization (FP) assay that uses a fluorophore-tagged peptide substrate; upon palmitoylation by ZDHHC enzymes, the substrate partitions into detergent micelles, increasing FP signal. This assay enables real-time kinetic measurements in 384-well plates suitable for high-throughput screening. As an orthogonal validation method, we use liquid chromatography–mass spectrometry (LC–MS) to directly detect palmitoylation through a +238 Da mass shift on model peptide substrates, allowing more reliable quantification and confirmation. Together, these methods offer a platform for identifying and validating ZDHHC inhibitors.

1. Introduction

1.1 ZDHHCs

ZDHHC (Asp-His-His-Cys) enzymes are membrane-bound protein acyltransferases that catalyze *S*-acylation (also called *S*-palmitoylation) of cysteine residues on target proteins. In a two-step "ping-pong" mechanism, the enzyme first autoacylates on its conserved cysteine within the ZDHHC motif using palmitoyl-CoA or other similar acyl-CoAs and then transfers that acyl group to a substrate cysteine (Linder & Jennings, 2013). *S*-acylation is a reversible lipid modification affecting thousands of human proteins. By attaching hydrophobic fatty acids to proteins, ZDHHC enzymes regulate the membrane association, stability, localization, and function of many signaling and membrane trafficking proteins (Mesquita et al., 2024).

ZDHHC-mediated palmitoylation influences diverse cellular processes and is implicated in human disease. For example, ZDHHC7 has been shown to be important for the immune response through S-acylation of substrates including STAT3, NLRP3, MAVS, and SMAD2 (Zhang et al., 2025; Liu et al., 2024; Yu et al., 2024; Zhang et al., 2020). Various ZDHHCs, including ZDHHC3, 9 and 20, have been shown to promote tumor proliferation of different cancers (Yeste-Velasco et al., 2015; Young et al., 2014). Thus, ZDHHC enzymes are considered attractive drug targets (Das et al., 2021; Lin, 2021; Yeste-Velasco et al., 2015).

The most common ZDHHC probe, 2-bromopalmitate (2BP), is an irreversible, broad-spectrum inhibitor that affects many lipid-modifying enzymes. Due to 2BP's promiscuity, other ZDHHC inhibitors have also been developed but still have limitations such as potency, selectivity, cell permeability, and bioavailability (Azizi et al., 2021; Hong et al., 2021;

Salaun et al., 2022). There is therefore a clear need for better ZDHHC inhibitors. To achieve that goal, high-throughput assays for ZDHHC enzymes are needed.

1.2 Acyl-cLIP and LCMS-based method

In Acyl-cLIP, a fluorophore-tagged peptide or protein is mixed with a ZDHHC enzyme and acyl-CoA. When the substrate is acylated, the increased hydrophobicity causes the product to partition into detergent micelles or hydrophobic carriers, slowing its rotation and raising the fluorescence polarization (Fig. 1) (Lanyon-Hogg et al., 2019). Because Acyl-cLIP is a homogeneous, mix-and-read assay, it provides a real-time readout of protein lipidation that can be adapted to high-throughput screening (Hong et al., 2021).

As an orthogonal method, we use liquid chromatography–mass spectrometry (LC-MS) to confirm the S-acylation of the substrate. In this approach, a peptide is used as the substrate and the enzymatic reaction mixtures are analyzed by LC-MS. LC-MS equipped with a reversed-phase C18 column can separate acylated and non-acylated forms by the elution time and molecular weight. Thus, LC-MS provides an independent biochemical validation that can accurately quantify the extent of the *S*-acylation reaction. Together, the Acyl-cLIP assay provides a high-throughput screen of ZDHHC activity, whereas LC-MS offers a more accurate confirmation of the enzyme's activity, enabling small-molecule inhibitor development (Lan et al., 2021).

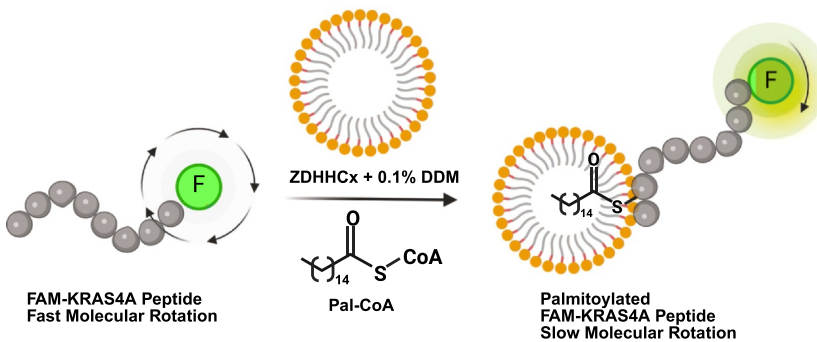

Fig. 1 Principle of the Acyl-cLIP assay for ZDHHC inhibitor screen. A fluorescently labeled substrate peptide (blue) is acylated by a ZDHHC enzyme with a palmitoyl-CoA. The acylated peptide product binds to detergent micelles (gray), slowing its tumbling and increasing fluorescence polarization.

2. Acyl-cLIP for ZDHHC enzymes

2.1 Equipment

- Cytation 5 (BioTek, or similar plate readers)
- Optical filter cube with EX 485/20, EM 528/20, dichroic mirror 510 nm (BioTek part# 8040561)
- LC-MS (Shimadzu, ThermoFisher, or similar)
- Benchtop centrifuge

2.2 Reagents

- Black 384-well plates suitable for fluorescence polarization (flat bottom, non-binding). Cover to prevent evaporation.
- Purified ZDHHC proteins (following a published protocol (Malgapo & Linder, 2019))
- N-terminally labeled substrate peptide with fluorescein (FAM): e.g. FAM-KRAS4A-WW (FAM-ISKEEKTPGCVKIKKCIIMWW, synthesized by Biomatik)
- Palmitoyl-CoA (Sigma cat#P9716)
- TCEP (Sigma cat#75259)
- n-Dodecyl-β-D-maltoside (DDM) (Sigma cat# 850520P)
- 2-Morpholinoethanesulfonic acid monohydrate (MES) (Sigma cat# 1061260025)
- DMSO (Thermo cat#J66650. AK)
- Any potential ZDHHC inhibitor to be tested (e.g. 2-BP, Sigma cat# 238422).

2.3 Reagent setup

- **FAM-labeled peptide stock**

  Dissolve N-terminally FAM labeled peptide in DMSO to a final concentration of 5 mM. This solution can be stored at −20 °C for several months.
- **TCEP stock**

  Dissolve TCEP in ddH_2O to a final concentration of 40 mM. This solution should be made fresh before use.
- **MES (50 mM, pH 6.4)**

  Dissolve 50 mM MES in ddH_2O and adjust the pH to 6.4. This solution can be stored at room temperature for several months.
- **MES reaction buffer**

  Combine the MES (50 mM, pH 6.4) buffer with 0.1 % wt/vol DDM. This solution should be made fresh before use.

- **Palmitoyl-CoA stock**

  Dissolve palmitoyl-CoA in DMSO to a final concentration of 2.5 mM. This solution should be made fresh before use.
- **ZDHHC inhibitor stock**

  Any potential ZDHHC inhibitor to be tested will be dissolved in DMSO at proper concentration so only1 μL of inhibitor needs to be added. For example, for the 20 μL reaction system to test 10 μMinhibitor, a solution of 200 μM inhibitor should be prepared.

2.4 Procedures

The reactions are carried out in the flat-bottom, non-binding black 384-well plates at a total volume of 20 μL. The following procedure is designed for 10 reactions. The volume of reagents can be scaled up accordingly for more reactions.

1. Prepare the master mix by combining 197.5 μL of MES reaction buffer with 2.5 μL of TCEP stock to a final concentration of 0.5 mM. Place the master mix on ice (Note 1).
2. Prepare the Solution A by taking 95.8 μL of the master mix and combining with 1 μL FAM-KRAS4A-WW peptide stock and 3.2 μL palmitoyl-CoA stock. Vortex briefly to mix well and place on ice. The concentrations of the FMA-KRAS4A-WW peptide and palmitoyl-CoA in Solution A are 50 μM and 80 μM, respectively.
3. Thaw ZDHHC7 protein stock on ice. Prepare the Solution B by diluting ZDHHC7 protein stock in the master mix to a final concentration of 0.67 μM in a total of 100 μL volume. Place on ice.
4. Prepare the tracer-only sample by combining 99.5 μL 50 mM MES (pH 6.4) with 0.5 μL of FAM-KRAS4A-WW peptide stock. Vortex to mix well. Load 20 μL of the tracer-only sample to one well of the 384-well plate with triplicates. These serve as the reference wells (Note 2 and 3).
5. Add 1 μL of DMSO or inhibitor stock to each well of the 384-well plate. Then add 9 μL of Solution B to each sample well (Note 4). Pipette up and down a few times to mix.
6. Centrifuge the 384-well plate at 500 g for 3 min at room temperature. Incubate the plate at 37 °C for 30 min (Note 5 and 6).
7. After incubation, add 10 μL of Solution A to each sample well, pipette up and down to mix and initiate the enzymatic reaction. Briefly centrifuge the 384-well plate at 500 g for 30 s

8. To measure the kinetics of the inhibition, program the plate reader to measure parallel and perpendicular intensities at 1-2 min intervals for 30–60 min at 37 °C. After centrifugation, immediately place the plate in Cytation5 and monitor using optical filter cube with EX 485/20, EM 528/20, dichroic mirror 510 nm (Note 7).
9. To measure the end-point fluorescence polarization, the 384-well plate can be incubated at 37 °C for one hour and then quench the reaction by adding 4 μL of 6 mM non-labeled KRAS4A-WW peptide. Measure the fluorescence polarization using Cytation5 with the same filter cube as in step 8. Example results are shown in Figs. 2 and 3.

2.5 Data processing

- Calculate Grating factor G by $G = \frac{I_{parallel}}{I_{perpendicular}}$ of the reference sample (default G = 1).
- Calculate the fluorescence polarization based on the following equations (Note 8)

i) $FP\,(mP) = \frac{I_{parallel} - G * I_{perpendicular}}{I_{parallel} + G * I_{perpendicular}}$

ii) $\Delta FP\,(mP) = FP_{sample} - FP_{reference}$

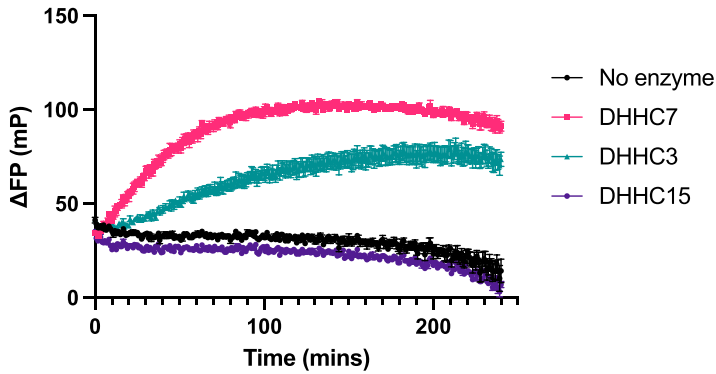

Fig. 2 Fluorescence polarization kinetics over time for different ZDHHCs. FAM-KRAS4A-WW peptide was tested against different purified ZDHHC enzymes, and the fluorescence polarization changes were monitored over 4 h. ZDHHC3 and 7, but not ZDHHC15, showed clear fluorescence polarization increase over time.

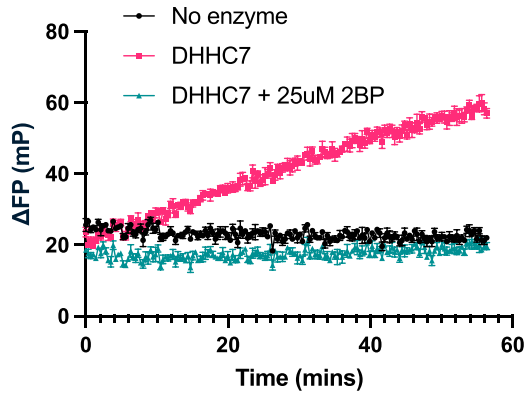

Fig. 3 Fluorescence polarization kinetics for the commonly used ZDHHC inhibitor 2-BP. Purified ZDHHC7 protein was pre-incubated with or without 2BP at 37 °C for 30 min. FAM-KRAS4A-WW peptide was then added, and the fluorescence polarization kinetics were monitored over 1 h. Pre-incubation with 2BP reduced the fluorescence polarization to the level of the control group without enzyme.

3. ZDHHC enzyme assay detected by LC-MS

3.1 Equipment

- LC-MS (Shimazdu, ThermoFisher, or similar)
- Kinetex 5 μm EVO C18 100 A column 150 × 4.6 mm (Phenomenex part#00F-4633-E0)
- SecurityGuard ULTRA cartridge/holder (Phenomenex part#AJ0-9296, AJ0-9000)
- Benchtop centrifuge

3.2 Reagents and buffers

- LC/MS-grade Acetonitrile (Sigma cat#1000291000)
- LC/MS-grade Water (Sigma cat#1153331000)
- LC/MS-grade Formic acid (Sigma cat#5330020050)
- Purified ZDHHC proteins (following protocol in (Malgapo & Linder, 2019))
- Peptide substrate e.g. KRAS4A-WW (ISKEEKTPGCVKIKKCIIMWW, synthesized by Biomatik)
- Palmitoyl-CoA (Sigma cat#P9716)
- TCEP (Sigma cat#75259)
- n-Dodecyl-β-D-maltoside (DDM) (Sigma cat# 850520P)
- 2-Morpholinoethanesulfonic acid monohydrate (MES) (Sigma cat# 1061260025)

- DMSO (Thermo cat#J66650.AK)
- Any potential ZDHHC inhibitor to be tested (e.g. 2-BP, Sigma cat# 238422).

3.3 Reagents setup

- **Peptide stock**

  Dissolve the peptide substrate (e.g. KRAS4A-WW) in DMSO to a final concentration of 5 mM. This solution can be stored at –20 °C for several months.
- **TCEP stock**

  Dissolve TCEP in ddH_2O to final concentration of 40 mM. This solution should be made fresh before use.
- **MES (50 mM, pH 6.4)**

  Dissolve MES in ddH_2O and adjust the pH to 6.4. This solution can be stored at room temperature for several months.
- **MES reaction buffer**

  Combine the MES (50 mM, pH 6.4) buffer with 0.1 % wt/vol DDM. This solution should be made fresh before use.
- **Palmitoyl-CoA stock**

  Dissolve palmitoyl-CoA in DMSO to a final concentration of 2.5 mM. This solution should be made fresh before use.
- **HPLC mobile phase A**

  Combine LC/MS grade water with 1 % vol/vol formic acid.
- **HPLC mobile phase B**

  Combine LC/MS grade acetonitrile with 1 % vol/vol formic acid.
- **ZDHHC inhibitor stock**

  Any potential ZDHHC inhibitor to be tested will be dissolved in DMSO at proper concentration so only 1 μL of inhibitor needs to be added. For example, for the 25 μL reaction system to test 10 μM inhibitor, a solution of 250 μM inhibitor should be prepared.

3.4 Procedures

Reactions are carried out in a 1.5 mL Eppendorf tube at a total volume of 25 μL. The following procedure is designed for 10 reactions. The amount of reagents can be scaled up accordingly for more reactions.

1. Prepare the master mix by combining 247 μL of MES reaction buffer with 3.1 μL of TCEP stock to a final concentration of 0.5 mM. Vortex briefly to mix well and place on ice (Note 1).

2. Prepare the Solution A by taking 116.5 μL of the master mix and combining with 2.5 μL KRAS4A-WW peptide stock and 6 μL palmitoyl-CoA stock. Vortex briefly to mix well and place on ice. The concentrations of the KRAS4A-WW peptide and palmitoyl-CoA in Solution A are 100 μM and 120 μM, respectively.
3. Thaw ZDHHC7 protein stock on ice. Prepare the reaction solution B by diluting ZDHHC7 protein stock in the master mix to a final concentration of 0.67 μM in a total of 125 μL volume. Place on ice.
4. Add 1 μL of DMSO or inhibitor stock to each 1.5 mL Eppendorf tube. Then add 11.5 μL of reaction solution B to each tube. Incubate the tubes at 37 °C for 30 min (Note 5).
5. After incubation, add 12.5 μL of solution A to each tube to initiate the enzymatic reaction. Briefly and gently vortex tubes 2–3 times to mix well. Incubate the reaction mixture at 37 °C for 90 min.
6. Quench the reaction by adding the same volume (25 μL) of acetonitrile/1 % formic acid.
7. Centrifuge the tubes at 17,000 g at 4 °C for 10 min to remove precipitated protein (Note 9).
8. Inject 20 μL of the supernatant into the LC/MS (Note 10, 11, and 12).
9. Run on Kinetex 5 μm EVO C18 100 A column 150 × 4.6 mm column using the following gradient program with flow rate at 0.3 min/mL.

Time (min)	Gradient (%B)
0.00	0
2.00	0
6.00	50
16.00	70
16.01	100
21.00	100
21.01	0
25.00	0

10. HPLC chromatograms were collected at 280 nm and mass spectra were collected in ESI positive mode for the corresponding m/z range based on the peptide size. Example results are shown in Fig. 4.

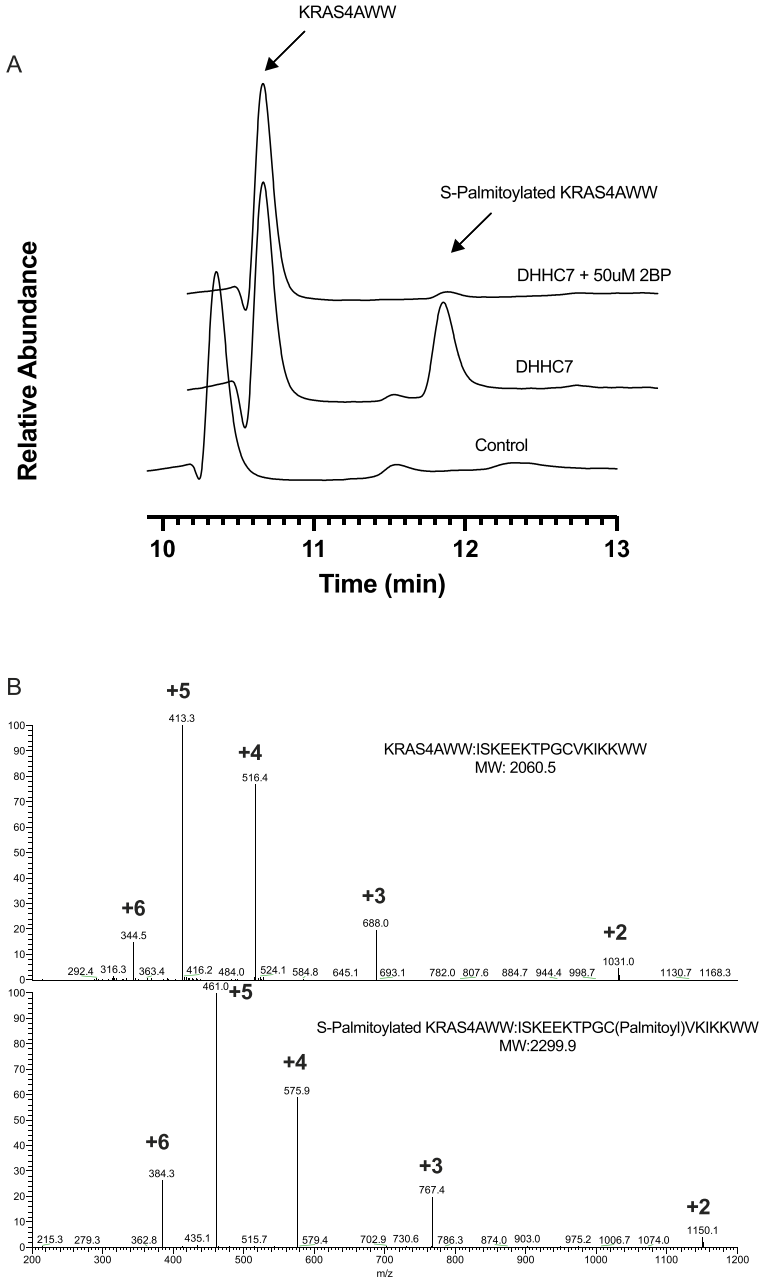

Fig. 4 Sample data from the LC-MS assay. (A) Representative HPLC chromatograms of ZDHHC7 in-vitro enzyme reactions with KRAS4A-WW peptide. The S-palmitoylated

4. Notes

1. TCEP is easily oxidized, so it is highly recommended to prepare a fresh stock right before use for each experiment.
2. Another useful control sample would be adding every reaction component but not the FAM-labeled probe. In this way, the autofluorescence coming from the buffer itself can be eliminated. Note that most commonly used buffers have very low autofluorescence.
3. The KRAS4A peptide has a polybasic region (KIKK), so it has some affinity towards negatively charged lipid membranes even without *S*-palmitoylation. Thus, it is important to avoid detergent in the reference wells to allow free rotation of the tracer.
4. Palmitoyl-CoA can compete with some covalent inhibitors, such as 2BP. Thus, it is important to avoid palmitoyl-CoA during preincubation of ZDHHC with the inhibitors.
5. This 30 min incubation is optional if testing non-covalent inhibitors. In that case, skip the incubation and proceed to add solution B.
6. Due to the small volume, it is crucial that the 384-well plate is properly covered with a lid. The incubation is preferably performed in a water bath.
7. The plate reader temperature should be pre-equilibrated to 37 °C to maximize accuracy and reproducibility.
8. To calculate percent conversion, synthetic *S*-palmitoylated peptide can be used as a positive control with 100 % conversion while no enzyme sample serves as 0 % conversion. Percent conversion can be calculated based on the peak area in the HPLC chromatogram.
9. This step is crucial to exclude the insoluble parts from the system. It would be detrimental to the instrument if insoluble parts such as enzyme aggregates are injected.

KRAS4A-WW peptide was separated from the KRAS4A-WW substrate peptide. (B) Representative ESI+ mass spectra of KRAS4A-WW (ESI-MS calcd. for $C_{96}H_{156}N_{24}O_{24}S$ $[M+2H^+]^{2+}$ $m/z = 1031.1$, found 1031.0, $C_{96}H_{157}N_{24}O_{24}S$ $[M+3H]^{3+}$ $m/z = 687.7$, found 688.0, $C_{96}H_{158}N_{24}O_{24}S$ $[M+4H]^{4+}$ $m/z = 516.0$, found 516.4, $C_{96}H_{159}N_{24}O_{24}S$ $[M+5H]^{5+}$ $m/z = 413.0$, found 413.3, $C_{96}H_{160}N_{24}O_{24}S$ $[M+6H]^{6+}$ $m/z = 344.4$, found 344.5) and S-palmitoylated KRAS4A-WW peptide (ESI-MS calcd. for $C_{112}H_{186}N_{24}O_{25}S$ $[M+2H]^{2+}$ $m/z = 1150.2$, found 1150.1, $C_{112}H_{187}N_{24}O_{25}S$ $[M+3H]^{3+}$ $m/z = 767.1$, found 767.4, $C_{112}H_{188}N_{24}O_{25}S$ $[M+4H]^{4+}$ $m/z = 575.6$, found 575.9, $C_{112}H_{189}N_{24}O_{25}S$ $[M+5H]^{5+}$ $m/z = 460.7$, found 461.0, $C_{112}H_{190}N_{24}O_{25}S$ $[M+6H]^{6+}$ $m/z = 384.1$, found 384.3).

10. Make sure to avoid possible insoluble particles at the bottom of the tubes.
11. *S*-Palmitoylated peptides could be very hydrophobic and tend to stick to the plastic tube/plate. Use low binding tubes and inject samples as soon as possible.
12. It is recommended to pre-equilibrate the column with 100 % mobile phase A to prevent substrate/product being flushed out at the very beginning.

References

Azizi, S.-A., Lan, T., Delalande, C., Kathayat, R. S., Banales Mejia, F., Qin, A., ... Dickinson, B. C. (2021). Development of an acrylamide-based inhibitor of protein S-acylation. *ACS Chemical Biology, 16*(8), 1546–1556. https://doi.org/10.1021/acschembio.1c00405.

Das, T., Yount, J. S., & Hang, H. C. (2021). Protein S-palmitoylation in immunity. *Open Biology, 11*(3), 200411. https://doi.org/10.1098/rsob.200411.

Hong, J. Y., Malgapo, M. I. P., Liu, Y., Yang, M., Zhu, C., Zhang, X., ... Lin, H. (2021). High-throughput enzyme assay for screening inhibitors of the ZDHHC3/7/20 acyltransferases. *ACS Chemical Biology, 16*(8), 1318–1324. https://doi.org/10.1021/acschembio.1c00258.

Lan, T., Delalande, C., & Dickinson, B. C. (2021). Inhibitors of ZDHHC family proteins. *Current Opinion in Chemical Biology, 65*, 118–125. https://doi.org/10.1016/j.cbpa.2021.07.002.

Lanyon-Hogg, T., Ritzefeld, M., Sefer, L., Bickel, J. K., Rudolf, A. F., Panyain, N., ... Tate, E. W. (2019). Acylation-coupled lipophilic induction of polarisation (Acyl-cLIP): A universal assay for lipid transferase and hydrolase enzymes. *Chemical Science (Royal Society of Chemistry: 2010), 10*(39), 8995–9000. https://doi.org/10.1039/c9sc01785b.

Lin, H. (2021). Protein cysteine palmitoylation in immunity and inflammation. *The FEBS Journal, 288*(24), 7043–7059. https://doi.org/10.1111/febs.15728.

Linder, M. E., & Jennings, B. C. (2013). Mechanism and function of ZDHHC S-acyltransferases. *Biochemical Society Transactions, 41*(1), 29–34. https://doi.org/10.1042/BST20120328.

Liu, Y., Hou, D., Chen, W., Lu, X., Komaniecki, G. P., Xu, Y., ... Lin, H. (2024). MAVS Cys508 palmitoylation promotes its aggregation on the mitochondrial outer membrane and antiviral innate immunity. *Proceedings of the National Academy of Sciences of the United States of America, 121*(34), e2403392121. https://doi.org/10.1073/pnas.2403392121.

Malgapo, M. I. P., & Linder, M. E. (2019). Purification of recombinant ZDHHC proteins using an insect cell expression system. *Methods in Molecular Biology, 2009*, 179–189. https://doi.org/10.1007/978-1-4939-9532-5_14.

Mesquita, S., Abrami, F., Linder, L., Bamji, M. E., Dickinson, S. X., B. C, & van der Goot, F. G. (2024). Mechanisms and functions of protein S-acylation. *Nature Reviews. Molecular Cell Biology, 25*(6), 488–509. https://doi.org/10.1038/s41580-024-00700-8.

Salaun, C., Takizawa, H., Galindo, A., Munro, K. R., McLellan, J., Sugimoto, I., ... Chamberlain, L. H. (2022). Development of a novel high-throughput screen for the identification of new inhibitors of protein S-acylation. *The Journal of Biological Chemistry, 298*(10), 102469. https://doi.org/10.1016/j.jbc.2022.102469.

Yeste-Velasco, M., Linder, M. E., & Lu, Y.-J. (2015). Protein S-palmitoylation and cancer. *Biochimica et Biophysica Acta, 1856*(1), 107–120. https://doi.org/10.1016/j.bbcan.2015.06.004.

Young, E., Zheng, Z.-Y., Wilkins, A. D., Jeong, H.-T., Li, M., Lichtarge, O., & Chang, E. C. (2014). Regulation of Ras localization and cell transformation by evolutionarily conserved palmitoyltransferases. *Molecular and Cellular Biology, 34*(3), 374–385. https://doi.org/10.1128/MCB.01248-13.

Yu, T., Hou, D., Zhao, J., Lu, X., Greentree, W. K., Zhao, Q., ... Lin, H. (2024). NLRP3 Cys126 palmitoylation by ZDHHC7 promotes inflammasome activation. *Cell Reports, 43*(4), 114070. https://doi.org/10.1016/j.celrep.2024.114070.

Zhang, M., et al. (2025). SMAD2 S-palmitoylation promotes its linker region phosphorylation and TH17 cell differentiation in a mouse model of multiple sclerosis. *Science Signaling, 18*, eadr2008. https://doi.org/10.1126/scisignal.adr2008.

Zhang, M., Zhou, L., Xu, Y., Yang, M., Xu, Y., Komaniecki, G. P., ... Lin, H. (2020). A STAT3 palmitoylation cycle promotes TH17 differentiation and colitis. *Nature, 586*(7829), 434–439. https://doi.org/10.1038/s41586-020-2799-2.

CHAPTER SEVEN

One-pot biosynthesis of genetically encoded amphiphiles via protein prenylation

Md Mahbubul Alam[a], Md Shahadat Hossain[b], James L. Hougland[a], and Davoud Mozhdehi[a,*]

[a]Department of Chemistry, Syracuse University, Syracuse, New York, United States
[b]Department of Pharmaceutical Technology, Faculty of Pharmacy, University of Dhaka, Dhaka, Bangladesh
*Corresponding author. e-mail address: dmozhdeh@syr.edu

Contents

1. Introduction 144
2. Instruments and materials 148
   2.1 Instruments and equipment 148
   2.2 Reagents and consumables 148
3. Construction of orthogonal expression vectors 149
   3.1 Vector selection and design considerations 149
   3.2 Cloning the prenyltransferase machinery 150
   3.3 Assembly of the lipid biosynthesis and substrate co-expression system 151
4. One-pot biosynthesis and purification of prenylated ELPs 154
   4.1 Co-expression and culture conditions 154
   4.2 Purification of prenylated ELPs 156
   4.3 Assessment of protein modifications 157
5. Biophysical characterization of phase behavior and nano-assembly of prenylated ELPs 159
   5.1 Variable-temperature turbidimetry 159
   5.2 Dynamic light scattering 160
6. Geranylgeranylation of RhoA GTPase 161
   6.1 Application of the co-expression system to RhoA 161
   6.2 Isolation of RhoA isoforms 163
   6.3 Validation of prenylation 163
7. Summary 165
Acknowledgments 165
References 165

Abstract

Despite the well-established role of post-translational lipidation in regulating diverse facets of cellular biology, scalable access to lipidated proteins remains limited by reliance on complex eukaryotic expression systems or labor-intensive semisynthetic

Methods in Enzymology, Volume 728
ISSN 0076-6879, https://doi.org/10.1016/bs.mie.2026.01.038
Copyright © 2026 Elsevier Inc. All rights are reserved, including those for text and data mining, AI training, and similar technologies.

approaches. To address these limitations, we describe a robust, genetically encoded platform for production of prenylated proteins in prokaryotes through metabolic and genetic engineering. We apply this system to synthesize prenylated intrinsically disordered protein polymers derived from the elastin consensus sequence as genetically encodable amphiphiles as a model system to investigate how prenylation syntax controls self-assembly and phase behavior. We further demonstrate the platform's versatility by extending it to natively geranylgeranylated globular proteins, such as RhoA, establishing a scalable, protein-agnostic toolkit for biomaterials and biochemical research.

1. Introduction

Post-translational lipidation enables cells to regulate the spatiotemporal flow of life-sustaining matter, energy, and information by controlling protein localization, interactions, and function (Hang & Linder, 2011; Jiang, et al., 2018; Matsumoto et al., 2025; Nadolski & Linder, 2007; Přáda Brichtová et al., 2025). Notwithstanding this biological significance, access to lipidated proteins for biochemical studies and biomaterials applications has historically been limited because common prokaryotic expression hosts lack eukaryotic lipidation machinery (Sahdev et al., 2008). As a result, lipidated proteins are primarily obtained through two strategies: expression in eukaryotic systems or convergent semisynthesis (Bader et al., 2000; Brunsveld et al., 2006; Hanna et al., 2022; Khow & Suntrarachun, 2012). The former is often limited by high production costs and heterogeneous modification profiles, (Joosten et al., 2003; Sahdev et al., 2008; Xie et al., 2023) whereas the latter necessitates technically challenging and labor-intensive workflows (Hanna et al., 2022). Furthermore, a fundamental and underappreciated limitation of chemical approaches is the intrinsic mismatch in solubility of hydrophobic lipid donors and folded proteins in aqueous buffers. Therefore, these methods demand extensive case-by-case optimization of organic cosolvents, detergents, and denaturants to maintain solubility and reactivity of reagents (Mejuch & Waldmann, 2016; Mozhdehi et al., 2019). Together, these constraints have restricted systematic interrogation of lipidation syntax and delayed the development of predictive design rules, slowing the adoption of lipidation as a programmable handle in biomaterials and biotherapeutic development.

These bottlenecks have spurred efforts to engineer prokaryotic hosts that can recapitulate eukaryotic lipidation. An instructive example is N-myristoylation—the modification of an N-terminal glycine with tetradecanoic acid

(myristate, C14:0). Pioneering work by Gordon and coworkers showed that this pathway can be reconstituted in E. coli by coexpressing a target protein with a Saccharomyces cerevisiae N-myristoyltransferase (NMT) and supplementing the culture with myristic acid (Duronio et al., 1990; Gordon et al., 1991). In this minimal system, E. coli imports fatty acids (via FadL) and converts them to the corresponding acyl-CoA donors (via FadD), enabling NMT to co-translationally transfer myristate to the nascent protein substrate (Bhatnagar et al., 1999; Nunn & Simons, 1978). The elegant simplicity of this system has provided broad access to myristoylated proteins for biochemical and biological characterization and, importantly, has enabled production of engineered lipidated proteins—with non-native lipid chemistries, substrates, or site contexts—at quantities sufficient for materials and biomedical applications (Hossain et al., 2024; Hossain et al., 2020a, 2022a; Ji et al., 2023; Luginbuhl et al., 2017; Mozhdehi et al., 2018; Zhang et al., 2024). This capability arises from the orthogonality of the reconstituted myristoylation pathway to E. coli biology, which provides a blank canvas (chassis) in which lipid identity, site context, and scaffold architecture can be varied with minimal interference from endogenous processes (Duronio et al., 1990; Hossain et al., 2020a, 2020b; Mozhdehi et al., 2018).

This chapter summarizes our efforts to extend this paradigm to prenylation by establishing prokaryotic platforms for the scalable production of chemically defined prenylated proteins and engineered variants via metabolic and genetic engineering. Before discussing the details of this system, a brief review of prenylation is provided. Protein prenylation is the covalent attachment of an isoprenoid lipid to a protein side chain, most commonly via formation of a thioether linkage to a cysteine residue near the C-terminus (Kamiya et al., 1978; Palsuledesai & Distefano, 2015; Wang & Casey, 2016). In eukaryotes, the predominant forms are farnesylation (C15) and geranylgeranylation (C20), although emerging examples of non-canonical prenylation chemistry (e.g., Tyr O-geranylation in cyanobacteria) suggest that the chemical scope and biological roles of this post-translational modification (PTM) may be broader than currently appreciated (Morita et al., 2018; Zhang & Casey, 1996). Protein prenylation draws on activated prenyl donors generated by central isoprenoid biosynthesis. Condensation of isopentenyl diphosphate (IPP) and dimethylallyl diphosphate (DMAPP) yields geranyl diphosphate (GPP, C10), and sequential IPP additions produce farnesyl diphosphate (FPP, C15) and geranylgeranyl diphosphate (GGPP, C20), which serve as lipid donors for specialized protein prenyltransferases (Tetali, 2019). Three major prenyltransferases operate in

eukaryotes: protein farnesyltransferase (FTase), geranylgeranyltransferase type I (GGTase-I), and geranylgeranyltransferase type II (GGTase-II, also known as Rab GGTase). FTase and GGTase-I typically recognize C-terminal CaaX motifs (C, cysteine; a, aliphatic residue; X residue determines FTase/GGTase specificity), whereas GGTase-II recognizes and modifies Rab GTPases bearing non-CaaX motifs via a Rab escort protein–dependent mechanism (Casey & Seabra, 1996; Palsuledesai & Distefano, 2015).

We developed an operationally simple biosynthetic route for producing prenylated proteins in prokaryotes by coexpressing the target protein with the minimal enzymatic machinery (Fig. 1). Because charged prenyl pyrophosphates exhibit poor membrane permeability and E. coli lacks transporters for these metabolites, we generated the requisite lipid donors in situ. For FPP, we relied on E. coli endogenous 2-methyl-D-erythritol-4-phosphate (MEP) pathway to convert carbon metabolites into the isoprenoid precursors IPP and DMAPP, which are further condensed to FPP via an endogenous farnesyl diphosphate synthase (Hossain et al., 2022). To produce

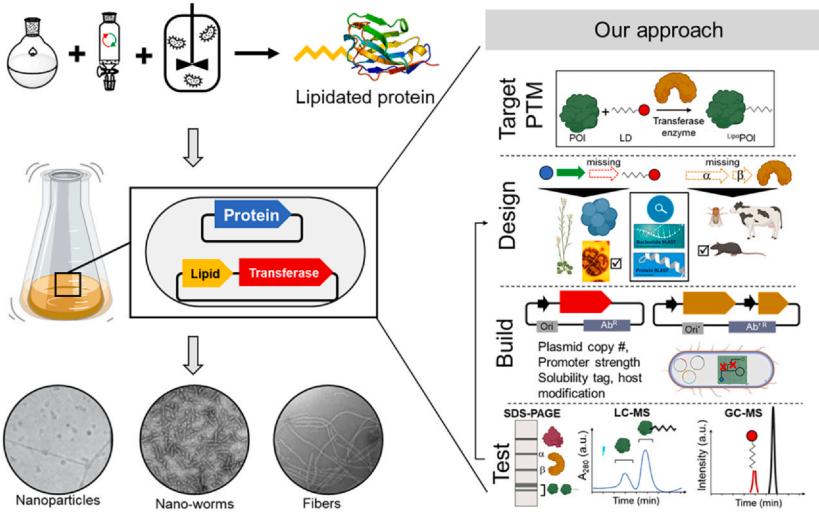

Fig. 1 Strategy for engineering recombinant prenylation platforms for nanobiomaterials. The approach follows a Design-Build-Test cycle: (1) selection of enzymes for lipid synthesis and transfer; (2) cloning of genes into orthogonal plasmids for co-expression; and (3) Screening and optimization to identify conditions for high-yield production of prenylated proteins as genetically encodable amphiphiles. *Created with BioRender.com. Adapted with permission from Hossain et al. (2022). Temperature-responsive nano-biomaterials from genetically encoded farnesylated disordered proteins. ACS Applied Bio Materials, 5 (5), 1846–1856. https://doi.org/10.1021/acsabm.1c01162. Copyright 2022 American Chemical Society.*

GGPP, we augmented this pathway via expression of an additional enzyme, a geranylgeranyl diphosphate synthase (GGS) from *Deinococcus radiodurans*, an extremophilic bacterium with high isoprenoid flux, anticipating that its prokaryotic origin would promote stability and solubility in E. coli (Liu et al., 2014). Finally, to complete the minimal prenylation pathway, we opted to use two mammalian protein prenyltransferases, Rattus norvegicus FTase and GGTase-I, which have been shown to express in functional form in bacterial hosts and exhibit broad substrate tolerance (Hossain et al., 2025).

As detailed in the methods section, this minimal prenylation pathway can be easily deployed in standard E. coli strains using two compatible plasmids in a protein agnostic manner. Moreover, the modularity of this platform facilitates the systematic exploration of "prenylation syntax" by accelerating the design–build–test cycle. Creating new variants is accomplished simply at the genetic level—by swapping the gene for the protein of interest, the CaaX motif, or the coexpressed prenylation machinery. For instance, we have used this platform to biosynthesize prenylated isoforms (farnesylated and geranylgeranylated) of various proteins, including model intrinsically disordered protein polymers such as elastin-like polypeptides (ELPs), globular model proteins such as mCherry, and naturally geranylgeranylated GTPases such as Rap1B and RhoA in parallel. This library enabled us to examine how physicochemistry of the farnesyl or geranylgeranyl lipid and the interplay between the sequence of CaaX-box motif and the prenyl group influences the phase behavior, nano-assembly, and membrane interactions of these proteins.

Importantly, scalable access to prenylated proteins has enabled the use of this post-translational modification as a design handle for functional nanobiomaterials based on protein polymers such as ELPs. In these systems, the hydrophobic prenyl group drives self-assembly into well-defined nanoparticles, while the disordered protein corona remains available for environmental sensing. This sequence-defined architecture allows the creation of tunable nanomaterials that undergo programmable transitions in response to cues such as temperature. By varying either the lipid identity (farnesyl vs. geranylgeranyl) or the protein sequence, we were able to control key parameters—including particle stability, size, and thermal behavior—with a level of precision that is difficult to achieve using heterogeneous conjugates. We anticipate that this approach can be extended to other engineered protein polymers (e.g., resilin, silk, abductin) to generate nanoparticles with orthogonal sensing mechanisms, broadening the utility of prenylation as a modular tool in biomaterials development.

Here, we describe a robust framework for the one-pot biosynthesis of prenylated proteins. We validate the system through the expression and biophysical analysis of lipidated elastin-like polypeptides. Subsequently, we expand the methodology to natively geranylgeranylated globular proteins, highlighting the platform's simplicity and broad scope.

2. Instruments and materials

2.1 Instruments and equipment

- PCR thermal cycler (BioRad T100)
- Refrigerated bench-top centrifuges (e.g., Sorvall Legend Micro 21 R, Sorvall Legend XTR) and high-capacity centrifuges (Sorvall RC 3 C plus).
- Refrigerated orbital incubator shaker (e.g., Amerex Instruments Gyromax 747 R)
- Shimadzu HPLC system series 2030 (Analytical and Semi-Prep) equipped with UV-Vis/PDA detectors. Columns: Phenomenex Jupiter C18 (5 μm, 300 Å) in analytical (250 × 4.6 mm) and semi-prep (250 × 10 mm) dimensions.
- Bio-Rad Mini-PROTEAN Tetra Cell, Trans-Blot Turbo Blotting System, and Gel-DOC EZ / ChemiDoc MP imaging systems
- Lyophilizer (Labconco FreeZone 4.5, −84 °C)
- MALDI-TOF MS (Bruker Autoflex III with MSP 96 polished steel target)
- LC-MS (Thermo Scientific UltiMate 3000 HPLC coupled to Orbitrap Fusion™ Lumos™ Tribrid™ MS).
- Agilent Cary 100 equipped with a Peltier temperature controller
- Malvern Panalytical Zetasizer NanoZS

2.2 Reagents and consumables

- **Bacterial Strains:** Chemically competent *E. coli* NEB5α, BL21(DE3), and T7 Express (New England Biolabs).
- **Enzymes and Kits:** Q5 High-Fidelity DNA Polymerase, NEBuilder HiFi DNA Assembly Master Mix, T4 DNA Ligase, Restriction Enzymes (*Nde*I, *Bam*HI-HF, *Bse*RI, *Acu*I, *Bgl*I, *Asc*I, *Nco*I-HF, *Xho*I, *Xba*I, *Not*I-HF), and kits for plasmid miniprep, gel extraction, and PCR cleanup (New England Biolabs); Trypsin Platinum (Promega); Lysozyme and DNase I (ThermoFisher Scientific).
- **Chemicals:** Isopropyl β-D-1-thiogalactopyranoside (IPTG), sinapinic acid, zinc sulfate ($ZnSO_4$), trifluoroacetic acid (TFA), magnesium

chloride ($MgCl_2$), β-mercaptoethanol (BME), glycerol, phenylmethylsulfonyl fluoride (PMSF), dithiothreitol (DTT), Tris base, sodium phosphate, sodium chloride (NaCl), imidazole, HEPES, tris(2-carboxyethyl) phosphine (TCEP), chloroacetamide, ammonium bicarbonate, Bacterial Protein Extraction Reagent (B-PER) (Sigma Aldrich/ThermoFisher Scientific).

- **Media and Antibiotics:** Tryptone, yeast extract, ampicillin, kanamycin, chloramphenicol (BIOBASIC).
- **Solvents:** HPLC and LC-MS grade acetonitrile, formic acid, ethanol, and isopropanol.
- **Protein Standards and Antibodies:** Apomyoglobin, Cytochrome C, Aldolase (Sigma Aldrich); Bovine Serum Albumin (BSA), 6 × His Tag Monoclonal Antibody (HIS.H8), Alexa Fluor™ 488 (ThermoFisher Scientific).
- **Electrophoresis and Blotting:** Mini-PROTEAN TGX stain-free precast gels, Precision Plus Protein Standards (Unstained & Stained), 10X Tris-Glycine-SDS (TGS) Running Buffer, Trans-Blot Turbo Transfer pack, Tween 20, EveryBlot Blocking Buffer (Bio-Rad); SimplyBlue™ Safe Stain (Novex).
- **Consumables:** 0.2 μm PVDF and CA syringe filters, nitrocellulose membranes, C18 ZipTips, Eppendorf and culture tubes, Luer lock syringes.

3. Construction of orthogonal expression vectors

3.1 Vector selection and design considerations

Because prenyltransferases are heterodimeric enzymes, a minimalist prokaryotic expression system requires the co-expression of three genes (for farnesylation) or four genes (for geranylgeranylation): the target protein fused to a CaaX motif, α and β subunits of the prenyltransferase, and the optional GGS (for geranylgeranylation) (Liu et al., 2014; London et al., 2011; Zhang et al., 2015). To accomplish this, we adopted a modular strategy in which prenyltransferase subunits were encoded on one vector, and the protein substrate and lipid biosynthesis machinery (if applicable) were encoded on a second compatible vector.

While in principle, two compatible bicistronic vectors (e.g., pETDuet and pACYCDuet) are sufficient for implementing this design, we selected a translationally coupled, single-operon architecture for co-expression of the α/β subunits (based on a pET23 backbone) to link the production of α and

β subunits and heterodimer assembly (Mayer et al., 1993). In parallel, an orthogonal bicistronic pACYCDuet vector placed the protein substrate and (when needed) GGS under independent T7lac promoters. These plasmids, characterized by compatible origins of replication (pBR322 and p15A) and antibiotic resistance markers (Amp^R and Cm^R), allow for recombinant prenylation of the desired proteins in commonly used strains such as *E. coli* BL21(DE3) (Hartman et al., 2004; Zimmerman et al., 1998).

3.2 Cloning the prenyltransferase machinery

In this design, the cDNA for β-subunit is positioned immediately upstream of the α-subunit, placing the synthetic operon under the control of a single T7 promoter, Fig. 2 (Mayer et al., 1993; Zimmerman et al., 1998). To enforce translational coupling, the 3′-end of the β-subunit cDNA was mutated to

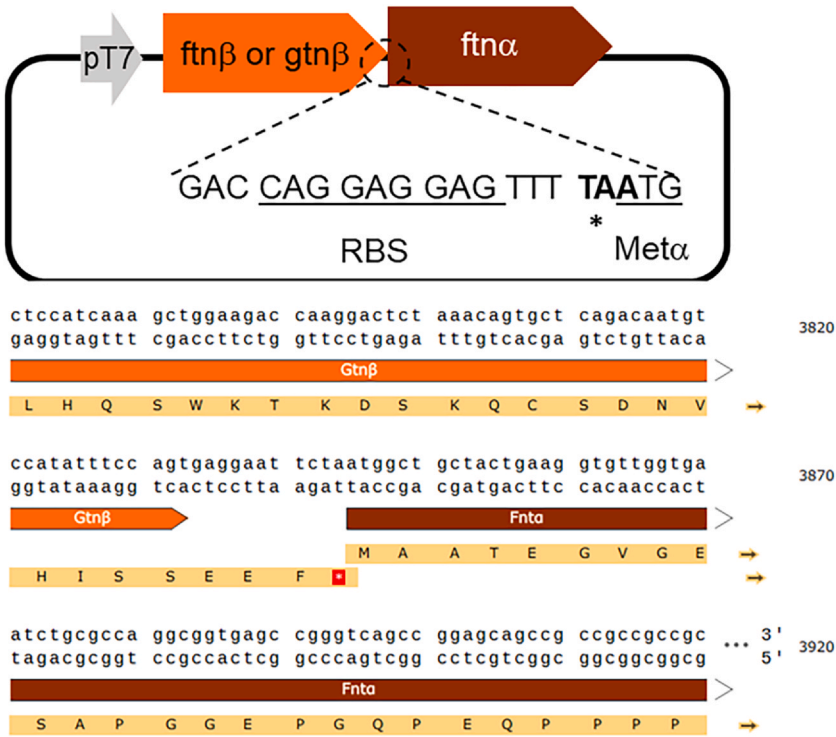
pT7
ftnβ or gtnβ
ftnα
GAC CAG GAG GAG TTT TAATG
RBS
*
Metα
ctccatcaaa gctggaagac caaggactct aaacagtgct cagacaatgt
gaggtagttt cgaccttctg gttcctgaga tttgtcacga gtctgttaca
3820
Gtnβ
L H Q S W K T K D S K Q C S D N V
ccatatttcc agtgaggaat tctaatggct gctactgaag gtgttggtga
ggtataaagg tcactcctta agattaccga cgatgacttc cacaaccact
3870
Gtnβ
Fnta
M A A T E G V G E
H I S S E E F
atctgcgcca ggcggtgagc cgggtcagcc ggagcagccg ccgccgccgc
tagacgcggt ccgccactcg gcccagtcgg cctcgtcggc ggcggcggcg
3920
Fnta
S A P G G E P G Q P E Q P P P P

Fig. 2 Schematic showing the translational coupling architecture of prenyltransferases subunits. *Modified with permission from Hossain et al. (2022). Temperature-responsive nano-biomaterials from genetically encoded farnesylated disordered proteins. ACS Applied Bio Materials, 5 (5), 1846–1856. https://doi.org/10.1021/acsabm.1c01162. Copyright 2022 American Chemical Society.*

encode an epitope tag (EEF) with the codons for glutamic acids functioning as a de novo ribosome binding site (RBS) for the downstream gene. Furthermore, the stop codon of the β-subunit (bold TAA) overlaps with the start codon of the α-subunit (underlined ATG). This fully assembled cassette can be cloned into the pET23 vector (or user-defined backbones) using Gibson Assembly.

1. Obtain codon-optimized cDNA for *R. norvegicus* FTase and GGTase-I as synthetic gene fragments (e.g., from Integrated DNA Technologies). Because FTase and GGTase-I share an identical α-subunit but have distinct β-subunits, a cost-effective solution is to design one shared fragment encoding the α-subunit and two β-subunits (FTase β and GGTase-I β) such that the α fragment can be assembled with either fragment. Design 20-bp overlaps at each junction, targeting an overlap T_m of ~50 °C to match the recipient vector.
2. Linearize the recipient vector (e.g., pET23) by digestion with *XbaI* and *NotI*, and gel-purify the linearized backbone by 1 % agarose gel electrophoresis (130 V, 40 min) followed by extraction with the Monarch Gel Extraction Kit (NEB).
3. Assemble the linearized vector (50 ng) with the synthetic insert(s) at an approximately 1:2 vector-to-insert molar ratio using NEBuilder HiFi DNA Assembly Master Mix (50 °C, 1 h).
4. Transform 2 μL of the assembly reaction into chemically competent *E. coli* NEB5α cells by heat shock (42 °C, 30 s) and plate on LB agar containing 100 μg/mL ampicillin.

Screen colonies by colony PCR using T7 and T7-term primers and confirm positive constructs by DNA sequencing.

3.3 Assembly of the lipid biosynthesis and substrate co-expression system

The optimal workflow to construct the vectors described here depends on the availability of in-house backbones, template genes, and local cloning capabilities. Consequently, we outline the rationale behind our approach and provide a model workflow that users can follow directly or adapt to alternative vector systems. Given advances in high-throughput DNA synthesis and the commercial availability of high-efficiency assembly methods (e.g., Gibson assembly), vector construction is best approached using a modular parallel strategy. However, the repetitive cDNA of protein polymers such as ELPs often hinders commercial gene synthesis and PCR amplification. Accordingly, we describe a model protocol for constructing

a bicistronic pACYCDuet-1 expression vector that encodes the lipid donor biosynthesis enzyme GGS in multiple cloning site 1 (MCS1) and the target ELP, fused to a C-terminal CaaX motif, in MCS2. In this workflow, GGS is first cloned into MCS1 using NEBuilder® HiFi DNA Assembly, the ELP gene is then modified to introduce the desired lipidation site sequence (i.e., a CaaX box motif) using PRe-RDL, (McDaniel et al., 2010) and the resulting ELP insert is finally cloned into MCS2 of the same vector.

3.3.1 Cloning of the lipid synthase (GGS)

1. Amplify the GGS gene from donor plasmid using GGS-F (GTT TAA CTT TAA TAA GGA GAT ATA CAT GCA TCA TCA TCA CCA CCA CCG CCC G) and GGS-R primers (AGC TTG TCG ACC TGC AGG TCA TTA TCA TTT TTC GCG GGT GGC) in a PCR reaction containing 3 ng template DNA, 500 nM of each primer, and Q5 High-Fidelity Hot Start master mix (NEB). Use the following cycling conditions: 98 °C for 30 s; 30 cycles of 98 °C for 10 s, 70 °C for 30 s, and 72 °C for 30 s; final extension at 72 °C for 2 min. Purify the PCR product using the Monarch PCR & DNA Cleanup Kit (NEB).
2. Linearize pACYCDuet-1 by double digestion with *AscI* and *NcoI*, resolve the digest on a 1 % agarose gel, and gel-purify the linearized backbone.
3. Assemble the purified PCR product with the linearized pACYCDuet-1 backbone at a 1:2 molar ratio (insert:vector) using NEBuilder HiFi Master Mix (50 °C, 30 min).
4. Transform 2 μL of the assembly reaction into 25 μL chemically competent NEB5α cells by heat shock and plate on LB agar containing 25 μg/mL chloramphenicol.

Screen colonies by colony PCR using pACYCDuetUP-1 and DuetDown-1 primers and confirm positive clones by DNA sequencing.

3.3.2 Genetic fusion of the C-terminal CaaX motif to ELPs

1. Anneal phosphorylated sense (CTGTGTTTTATTATAATGATAATG ATCTTCAG) and antisense (GATCCTGAAGATCATTATCATTAT AATAAAACACAGCC) oligonucleotides encoding the CVLL sequence by heating to 95 °C for 5 min and then cooling to room temperature in annealing buffer (50 mM Tris-HCl, 10 mM $MgCl_2$, 1 mM ATP, 10 mM DTT, pH 7.5).
2. Linearize pET24 vector by double digestion with *BseRI* and *BamHI*, resolve the digest on an agarose gel, and gel-purify the linearized backbone.

3. Ligate the annealed duplex into the linearized vector using a quick ligation kit at a 1:3 vector-to-insert molar ratio. Incubate at room temperature for 15 min
4. Transform the ligation reaction into chemically competent E. coli NEB5α cells by heat shock (42 °C, 30 s) and plate on LB agar containing 45 μg/mL kanamycin.
5. Identify positive constructs by Sanger sequencing using the T7-term primer.
6. To append the CVLL sequence to the C-termini of ELP variants, use recursive directional ligation by plasmid reconstruction (PRe-RDL) as described previously (McDaniel et al., 2010). Digest 1 μg of the ELP plasmid with *AcuI* and *BglI* and, in parallel, digest 1 μg of the *CVLL* plasmid with *BseRI* and *BglI* for 3 h at 37 °C.
7. Separate digestion products on a 1 % agarose gel (130 V, 40 min), excise the desired ELP and CVLL fragments, and purify the DNA using the Monarch Gel Extraction Kit (NEB).
8. Ligate the purified ELP and CVLL fragments using quick ligation kit by mixing the fragments as an equimolar ratio. Transform the ligation reaction into chemically competent E. coli NEB5α cells by heat shock and plate on LB agar containing 45 μg/mL kanamycin, as described above.
9. Verify the constructs (pET24_ELP-CVLL) by Sanger sequencing across the ELP–CaaX junction using T7-term primer.

3.3.3 Assembly of the dual-expression vector (pACYCDuet_GGS_ELP-CaaX)

1. Linearize 1 μg of pACYCDuet_GGS (prepared in Section 3.3.1) by double digestion with *NdeI* and *XhoI*. In parallel, digest 1 μg of pET24_ELP-CVLL (prepared in Section 3.3.2) with same enzymes to excise the ELP-CVLL insert. Resolve both digests on an agarose gel and gel-purify the linearized pACYCDuet_GGS backbone and the ELP-CVLL fragment.
2. Ligate the purified ELP-CVLL insert into the linearized pACYCDuet_GGS backbone using a quick ligation kit at 1:3 vector-to-insert molar ratio (15 min, room temperature).
3. Transform the ligation reaction into chemically competent E. coli NEB5α cells by heat shock (42 °C, 30 s) and plate on LB agar containing 25 μg/mL chloramphenicol.
4. Verify the sequence by Sanger sequencing across the MCS2 junction. Because repetitive ELP inserts may be prone to rearrangement during

propagation, verify the final expression plasmid by whole-plasmid long-read sequencing (e.g., Oxford Nanopore-based services such as Plasmidsaurus) to confirm integrity of the repetitive region and the absence of recombination events.

Notes.

1. The CaaX-box specificities of FTase and GGTase-I partially overlap, and donor availability can further bias these selectivities. For example, CVLL can be farnesylated by either enzyme when FPP is the predominant donor, whereas CVLS is exclusively farnesylated by FTase. To produce farnesylated ELPs bearing a CVLS motif, the workflow in Sections 3.3.2 and 3.3.3 can be followed with minor modifications: encode and append the CVLS motif to the ELP and clone the resulting ELP-CVLS substrate into an empty pACYCDuet-1 backbone to generate pACYCDuet_()_ELP-CVLS.
2. The upstream enzymes for the MEP pathway (*dxs* and *idi*), as well as the GGS gene, can be sourced from Addgene Kit #1000000152 and subcloned into the desired expression vectors. Additionally, a PCR-amplifiable short ELP gene, encoding thirty repeats of the GVGVP pentapeptide, is available on Addgene (Plasmid #67014). The specific pACYCDuet_GGS vector constructed for this work is available from the corresponding author's laboratory upon request.

4. One-pot biosynthesis and purification of prenylated ELPs

This section describes a model protocol for the co-expression of ELPs with the enzymatic machinery required for geranylgeranylation. To facilitate the evaluation of the lipidation outcome, we recommend that protein expression is performed in parallel under four conditions (Fig. 3A) corresponding to the presence or absence of geranylgeranyl diphosphate synthase (GGS) and geranylgeranyl transferase (GGT): -GGS/-GGT and +GGS/-GGT produce unmodified protein; -GGS/+GGT produces farnesylated protein (utilizing endogenous E. coli FPP); and +GGS/+GGT produces geranylgeranylated protein.

4.1 Co-expression and culture conditions

1. Co-transform chemically competent E. coli BL21(DE3) cells with the designated plasmid pair (Fig. 3A) using standard heat shock procedures (42 °C, 30 s).

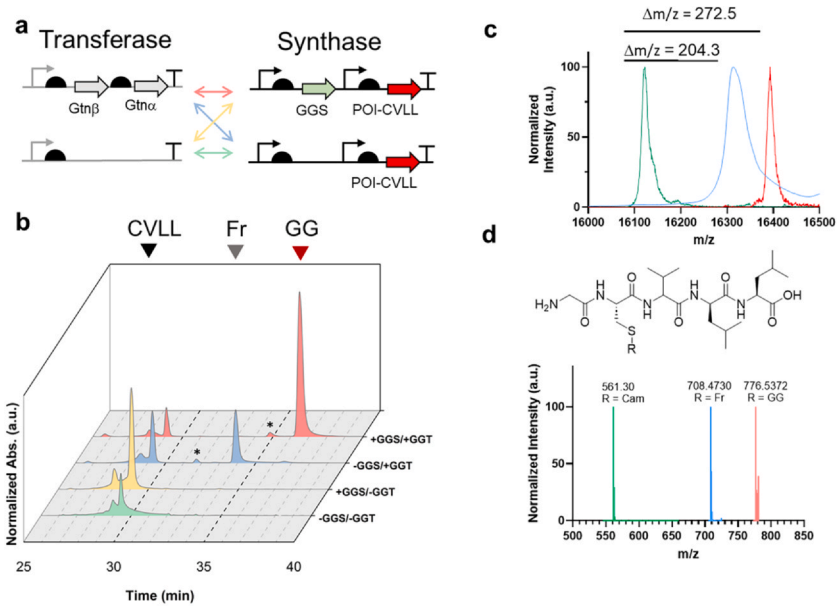

Fig. 3 Co-expression and analysis of prenylated proteins. (A) Schematic of the orthogonal plasmid system for co-expressing the target protein, Geranylgeranyl Synthase (GGS), and Geranylgeranyl Transferase (GGT). (B) RP-HPLC chromatograms of a model ELP expressed under four conditions (± GGS / ± GGT). Unmodified monomer and dimer are observed in the absence of GGT. Expression with GGT alone yields farnesylated protein, while co-expression with GGS and GGT yields geranylgeranylated protein. Asterisks (*) denote oxidized (sulfoxide) forms. (C) MALDI-TOF spectra showing molecular weight shifts corresponding to farnesyl and geranylgeranyl modifications. (D) Mass spectra of trypsin-digested peptides identifying the site of lipidation at the CaaX box. Carboxymethylacetamide (Cam) is used for alkylating free thiols of the unmodified constructs to prevent dimerization. *Reprinted with permission from Hossain et al. (2025). Scalable one-pot production of geranylgeranylated proteins in engineered prokaryotes. Bioconjugate Chemistry, 36 (3), 415–423. https://doi.org/10.1021/acs.bioconjchem.4c00493. Copyright 2025 American Chemical Society.*

2. Plate the transformation mixture onto LB agar plates supplemented with ampicillin (150 μg/mL) and chloramphenicol (25 μg/mL). Incubate overnight at 37 °C.
3. Inoculate a single colony from the transformation plate into a culture tube containing 50 mL of 2xYT medium supplemented with ampicillin (150 μg/mL) and chloramphenicol (25 μg/mL). Incubate at 37 °C with orbital shaking (250 rpm) until the optical density at 600 nm (OD_{600}) reaches approximately 0.7.

4. Harvest the starter culture by centrifugation (5000 g, 10 min, 4 °C). Aseptically decant the supernatant and resuspend the cell pellet in 5 mL of chilled, sterile PBS. This wash step is critical to remove secreted β-lactamase, which can degrade ampicillin in the larger expression culture, leading to plasmid loss.
5. Inoculate 1 L of 2xYT expression medium (containing 150 μg/mL ampicillin and 25 μg/mL chloramphenicol) with 1 mL of resuspended starter culture. Incubate at 37 °C with shaking (250 rpm) until the OD_{600} reaches 0.7.
6. Supplement the culture with $ZnSO_4$ to a final concentration of 1 mM.
7. After 10 min, induce protein expression by the addition of IPTG to a final concentration of 0.5 mM.
8. Incubate the culture at 28 °C for 16 h with shaking (250 rpm).
9. Harvest the cells by centrifugation (5000 g, 35 min, 4 °C). Discard the supernatant and store the cell pellet at −80 °C.

Notes

1. Co-expression vectors can exhibit variable translational efficiency. Verify expression of the target protein and all transferase components by Western blot before scale-up. If imbalanced expression is observed, modify the coding sequence of the target gene or swap the order of GGS and the protein of interest to improve expression yield (Bonde et al., 2016; Kudla et al., 2009; Tolia & Joshua-Tor, 2006).
2. Typical expressions yield for ELPs under these conditions are 5 mg/L. However, growth conditions (induction temperature, time, and IPTG concentration) should be optimized empirically for each new construct. For instance, expression of hydrophilic ELPs is best performed in T7 Express cells using a higher concentration of IPTG (1 mM).
3. To produce farnesylated proteins, flux through the endogenous MEP pathway can be upregulated either by supplementing the media with glycerol (1 % v/v) or by co-expressing the upstream enzyme 1-deoxy-D-xylulose-5-phosphate synthase (Dxs).

4.2 Purification of prenylated ELPs

This protocol utilizes a rapid organic extraction method that exploits the differential solubility of ELPs in alcohols to isolate the target protein from the E. coli proteome in approximately 40 min (Sweet et al., 2021).

1. Resuspend the harvested cell pellets in 4 volumes (v/w) of isopropanol (e.g., 4 mL isopropanol per 1 g wet pellet) by vigorous vortexing for 10 min

2. Sonicate the suspension in a bath sonicator for 15 min to ensure complete cell lysis and the release of ELPs into the solvent phase.
3. Centrifuge the lysate (15,000 g, 10 min, 25 °C) to pellet cellular debris and insoluble contaminants. Carefully transfer the supernatant, which contains the solubilized ELPs, to a fresh centrifuge tube.
4. Precipitate the ELPs from the supernatant by adding acetonitrile to a final concentration of 70 % (v/v). Invert the tube several times to mix.
5. Centrifuge (15,000 g, 10 min, 4 °C) to recover the ELP precipitate. Discard the supernatant.
6. Resuspend the protein pellet in a 50 % (v/v) ethanol:water mixture (4 mL per 1 g of original pellet weight).
7. Centrifuge (15,000 g, 5 min, 25 °C) to remove any remaining insoluble impurities. Collect the supernatant containing the purified ELP.
8. Filter the supernatant through a 0.22 μm PVDF syringe filter.
9. Analyze a small aliquot via analytical RP-HPLC to assess purity and lipidation status (Section 4.3.1). After confirmation of lipidation status, perform polishing steps using preparative HPLC or inverse transition cycling (ITC) (Meyer & Chilkoti, 1999) to achieve >95 % purity prior to biophysical characterization.

4.3 Assessment of protein modifications

Purified ELPs are characterized to verify molecular mass and selective prenylation at the C-terminal CaaX motif.

4.3.1 RP-HPLC profiling

1. Equip the HPLC system with a Phenomenex Jupiter C18 column (5 μm, 300 Å, 250 × 4.6 mm).
2. Prepare mobile phases consisting of Solvent A (water with 0.1 % TFA) and Solvent B (acetonitrile with 0.1 % TFA).
3. Inject 50 μL of the filtered ELP sample following organic extraction.
4. Elute proteins using a linear gradient from 0 % to 90 % Solvent B over 40 min at a flow rate of 1.0 mL/min.
5. Determine lipidation status by comparing retention times across the four expression conditions (Fig. 3B). Unmodified ELPs (–GGS/–GGT and +GGS/–GGT) elute earliest, typically as monomers or disulfide-bonded dimers. Farnesylated proteins (–GGS/+GGT) elute later (∼+4 min), whereas geranylgeranylated proteins (+GGS/+GGT) are the most hydrophobic and elute last (∼+6 min).

4.3.2 Intact mass determination (MALDI-TOF-MS)

Molecular weight confirmation is performed using Matrix-Assisted Laser Desorption/Ionization Time-of-Flight Mass Spectrometry (MALDI-TOF-MS).

1. Mix the protein sample 1:1 (v/v) with a saturated matrix solution consisting of sinapinic acid in 70 % acetonitrile with 0.1 % trifluoroacetic acid (TFA). Prepare serial dilutions of the protein sample to obtain a range of protein-to-matrix ratios.
2. Deposit 3 μL of the mixture onto a polished steel MALDI target plate and allow it to dry at room temperature to form crystals.
3. Acquire mass spectra in linear positive mode. Calibrate the instrument externally using a protein standard mix (e.g., Protein Standard I, Bruker) containing standards that flank the expected molecular weight of the target protein. Average at least 500 laser shots to improve the signal-to-noise ratio. Confirm lipidation by mass shifts of +204.36 Da for farnesylated proteins (–GGS/+GGT) and +272.47 Da for geranylgeranylated proteins (+GGS/+GGT) compared to unlipidated isoform (Fig. 3C).

4.3.3 Peptide mapping

Evaluate site-selective prenylation by tryptic digestion followed by MALDI-TOF or LC–MS analysis (Section 6.3.2).

1. Add sequencing-grade trypsin to the protein sample at an enzyme-to-protein ratio of 1:50 (w/w) in a digestion buffer supplemented with 20 % (v/v) acetonitrile. Incubate overnight at 37 °C. The addition of acetonitrile is required to maintain the solubility of hydrophobic, lipidated fragments.
2. Acidify the digest with TFA (pH < 3) to quench the reaction.
3. Desalt and fractionate the peptides using a C18 ZipTip. Equilibrate the tip with 0.1 % TFA, bind the peptides, and wash with 0.1 % TFA in water.
4. Elute the peptides using a step-gradient of increasing acetonitrile concentrations (e.g., separate 10 μL fractions of 40 %, 60 %, and 80 % acetonitrile containing 0.1 % TFA) to ensure the recovery of the hydrophobic, lipidated C-terminal fragment.
5. Mix 1 μL of the elution fractions 1:1 (v/v) with a saturated solution of α-cyano-4-hydroxycinnamic acid (CHCA) matrix in 50 % acetonitrile/0.1 % TFA. Spot onto the MALDI target plate and allow it to dry.

6. Acquire spectra in reflector positive mode to maximize isotopic resolution. Calibrate the instrument externally using two standards that flank the expected molecular weight of the target fragment. Average at least 200 laser shots with lower laser intensity (15 %) to improve the signal-to-noise ratio. Confirm lipidation by mass shifts of +204.1878 Da for farnesylated proteins and +272.2504 Da for geranylgeranylated proteins relative to unlipidated isoform (Fig. 3D).

5. Biophysical characterization of phase behavior and nano-assembly of prenylated ELPs

To assess the impact of prenylation on ELP liquid–liquid phase separation, construct temperature–composition phase diagrams for each isoform using a UV–Vis spectrophotometer equipped with temperature control. Determine the transition temperature (T_t) across a range of protein concentrations as described below.

5.1 Variable-temperature turbidimetry

1. Prepare a dilution series of the purified protein in cold PBS to define the concentration dependence of the transition temperature (e.g., 1–200 μM, prepared as a twofold serial dilution). Maintain all samples on ice (4 °C) prior to analysis to ensure they remain in the soluble phase.
2. Transfer the samples into quartz cuvettes (1 cm pathlength) and load them into a UV-Vis spectrophotometer equipped with a Peltier-controlled sample holder, chilled to 15 °C. Equilibrate the samples for minimum of 5 min at this temperature.
3. Apply a linear thermal ramp of 1 °C/min to 65 °C while continuously recording the absorbance at 350 nm (OD_{350}). Higher endpoint temperatures may be required for more hydrophilic variants at lower concentrations.
4. Define the transition temperature (T_t) for each concentration as the inflection point of the turbidimetry plot (the maximum of the first derivative of absorbance with respect to temperature), Fig. 4A.
5. Construct a phase diagram by plotting the measured T_t values against the logarithm of the protein concentration (Fig. 4B). Unmodified and geranylgeranylated ELPs typically exhibit phase boundaries well described by linear regression, with geranylgeranylated ELPs showing a pronounced decrease in both slope and intercept. In contrast, farnesylated ELPs display a sigmoidal relationship intermediate between these two extremes.

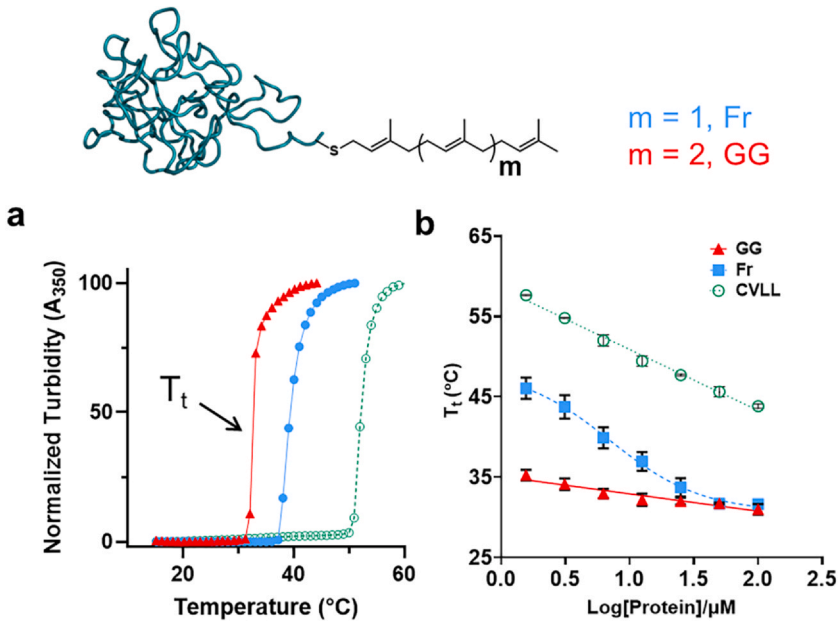

Fig. 4 Biophysical impact of prenylation on the phase behavior of model disordered proteins. (A) Representative turbidimetry plots for prenylated and unmodified ELPs, 6 μM in PBS. Prenylation increases the propensity of ELPs to phase separate by lowering their transition temperature (T_t). (B) Representative temperature-composition phase diagrams for unmodified, Fr-, and GG-modified ELPs. Prenylation alters the phase boundaries, with the extent of this alteration dependent on the nature of the attached lipid. Data represent mean ± s.d. (n = 3). *Adapted with permission from Hossain et al. (2025). Scalable one-pot production of geranylgeranylated proteins in engineered prokaryotes. Bioconjugate Chemistry, 36 (3), 415–423. https://doi.org/10.1021/acs.bioconjchem.4c00493. Copyright 2025 American Chemical Society.*

5.2 Dynamic light scattering

Characterize nano-assembly of lipidated isoforms by dynamic light scattering (DLS) by monitoring hydrodynamic diameter as a function of temperature as described below.

1. Filter the protein sample (50 μM in PBS) through a 0.22 μm syringe filter directly into a dust-free cuvette. Keep the sample on ice to prevent temperature-induced aggregation.
2. Place the cuvette in a DLS instrument prechilled to 15 °C. Program a stepwise temperature ramp from 15 °C to 60 °C (or higher, as required by the construct) in 1 °C increments.

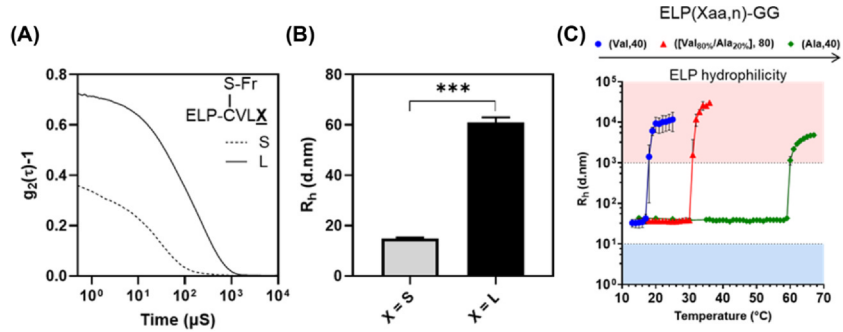

Fig. 5 Lipid length influences the nano-assembly of prenylated proteins in a lipidation-site-dependent manner. (A) DLS correlograms and (B) hydrodynamic radii (R_h) of Farnesylated ELPs with different lipidation sites (CaaX motif where X = Ser or Leu) at 15 °C. Farnesylated ELPs self-assemble only when fused to a hydrophobic CaaX box sequence**.** (C) Variable-temperature DLS of GG-modified ELPs confirms the formation of stable nanoparticles with a sharp micelle-to-coacervate transition, regardless of ELP guest residue hydrophobicity. Background colors represent phase states: blue (unimers), white (micelles), and red (coacervates). Data in b and c represent mean ± s.d. (n = 3). Statistical significance in b was determined by a *t*-test (***$p < 0.001$). *Adapted with permission from Hossain et al. (2022) [a, b] and reprinted with permission from Hossain et al. (2025) [c]. doi.org/10.1021/acsabm.1c01162 and doi.org/10.1021/acs.bioconjchem.4c00493. Copyright 2022 and 2025 American Chemical Society.*

3. Equilibrate the sample for 2 min at each temperature prior to data acquisition. Measure scattering data in triplicate at each temperature and confirm that the extracted hydrodynamic radius (R_h) is invariant across technical replicates.
4. Analyze the autocorrelation functions using the Cumulants method to determine the Z-average hydrodynamic diameter (R_h) and Polydispersity Index (PDI) as a function of temperature (Fig. 5).

6. Geranylgeranylation of RhoA GTPase

To demonstrate the versatility of the co-expression system beyond ELP model proteins, we applied the method to RhoA, a small GTPase that is natively geranylgeranylated.

6.1 Application of the co-expression system to RhoA

1. Co-transform E. coli *BL21(DE3)* cells with the plasmid pair pET23a_GGTβ_GGTα and pACYCDuet_GGS_6xHis-RhoA using heat shock method (Fig. 6A).

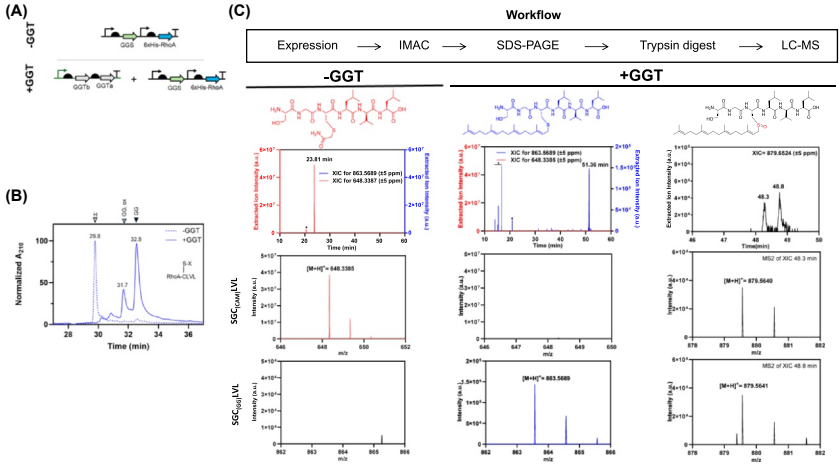

Fig. 6 Experimental workflow and analysis of recombinant production of GG-modified RhoA. (A) Schematic representation of the plasmids used for geranylgeranylation of RhoA. As a negative control, RhoA is co-expressed with GGS alone (-GGT condition). After expression, the soluble fraction was purified using immobilized metal affinity chromatography and analyzed by RP-HPLC. (B) RP-HPLC chromatograms of RhoA isoforms expressed under each condition. Co-expression yields 96 % geranylgeranylation (73.5 % reduced, 22.5 % sulfoxide), whereas only unmodified RhoA is detected in the absence of GGT. (C) LC-MS analysis of tryptic C-terminal peptide fragments. Extracted Ion Chromatograms and mass spectra for each condition. The unmodified fragment elutes at 23.8 min (red trace) and is the sole species in the -GGT sample. In the +GGT sample, the GG-modified fragment is dominant (51.4 min, blue trace). Oxidation of the thioether bond results in sulfoxide formation (+16 Da), creating a new chiral center that resolves as two diastereomeric peaks (48.3 and 48.8 min). *Modified with permission from Hossain et al. (2025). Scalable one-pot production of geranylgeranylated proteins in engineered prokaryotes. Bioconjugate Chemistry, 36 (3), 415–423. https://doi.org/10.1021/acs.bioconjchem.4c00493. Copyright 2025 American Chemical Society.*

2. Plate the transformation mixture on LB agar supplemented with 150 μg/mL ampicillin and 25 μg/mL chloramphenicol. Incubate overnight at 37 °C.
3. Perform the expression as described in Section 4.1
4. To confirm expression, pellet 1 mL of culture, resuspend in 50 μL PBS followed by 50 μL 2 × Laemmli buffer, boil for 10 min to reduce viscosity, and load onto a 4–20 % gradient Mini-PROTEAN TGX Stain-Free gel.
5. Visualize the protein bands using a Gel Doc EZ imager with a stain-free activation.
6. For immunodetection, transfer the proteins to nitrocellulose membrane using a Trans-Blot Turbo system (25 V, 7 min).

7. Wash the membrane three times with 1 × TBS.
8. Block non-specific binding sites by incubating the membrane in EveryBlot Blocking Buffer for 1 h at room temperature with gentle agitation.
9. Incubate the membrane overnight at 4 °C in 10 mL of blocking buffer containing a mixture of fluorescently labelled 6x His Tag Monoclonal Antibody (HIS.H8) (1:2000 dilution).
10. Wash the membrane three times for 10 min each with TBS-T to remove unbound antibodies.
11. Image the membrane using a ChemiDoc MP imager to confirm the expression of his tagged RhoA.

6.2 Isolation of RhoA isoforms

1. Resuspend the harvested cell pellet in 4 volumes of B-PER Bacterial Protein Extraction Reagent supplemented with lysozyme (50 mg/mL), DNase I (2500 U/mL), $MgCl_2$ (5 mM), glycerol (10 % v/v), β-mercaptoethanol (5 mM), and PMSF (1 mM).
2. Incubate the mixture at room temperature for 15 min to ensure complete lysis.
3. Centrifuge the lysate at 21,000 g for 10 min at 4 °C to remove insoluble debris.
4. Collect the supernatant and add wash buffer (25 mM Tris, 300 mM NaCl, 5 mM $MgCl_2$, 10 % glycerol, 5 mM β-mercaptoethanol, 1 mM PMSF, and 25 mM imidazole, pH 7.4).
5. Incubate the supernatant with HisPur™ Ni-NTA Resin on an end-over-end rotator for 30 min at 4 °C.
6. Collect the flow-through and wash the resin three times with 2 resin bed volumes of Wash Buffer.
7. Elute the His-tagged proteins by incubating the resin with 1 vol of elution buffer (Same composition as wash buffer, except for imidazole adjusted to 300 mM). Perform three consecutive elutions and pool the fractions. Confirm their purity by SDS-PAGE, followed by staining with Coomassie blue.

6.3 Validation of prenylation

6.3.1 Chromatographic profiling

Analyze purified RhoA fractions by RP-HPLC as described in Section 4.3.1, injecting 100 μL of pooled elution fractions (Fig. 6B).

6.3.2 Identification of isoforms via LC-MS

1. Excise the purified RhoA protein band from the SDS-PAGE gel using a clean scalpel. Cut the slice into 2 × 2 mm cubes and transfer to a 1.5 mL low-protein-binding tube.
2. Add 100 μL of water, incubate for 10 min, and discard the supernatant.
3. Add 100 μL of destaining solution (50 mM ammonium bicarbonate in 50 % acetonitrile) and incubate for 30 min at 37 °C to remove Coomassie dye. Discard the supernatant.
4. Dehydrate the gel pieces by adding 100 μL of 100 % acetonitrile. Incubate for 10 min until opaque, then remove the liquid.
5. Add 50 μL of reduction buffer (10 mM DTT in 100 mM ammonium bicarbonate) and incubate at 56 °C for 45 min. Discard the buffer.
6. Add 50 μL of alkylation buffer (55 mM iodoacetamide in 100 mM ammonium bicarbonate) and incubate for 30 min at room temperature in the dark.
7. Wash the gel pieces with 100 μL of 100 mM ammonium bicarbonate for 10 min, then dehydrate with 100 μL of 100 % acetonitrile. Remove all liquid.
8. Add 20 μL of trypsin solution (0.01 μg/μL) and incubate on ice for 30 min. Add 10 μL of 50 mM ammonium bicarbonate and incubate overnight at 37 °C.
9. Add 50 μL of extraction buffer (75 % acetonitrile, 5 % formic acid) and sonicate for 10 min. Collect the supernatant. Repeat extraction one more time. Combine extracts, lyophilize, and resuspend in 85 % acetonitrile with 5 % NH_4OH.

Table 1 LC gradient parameters.

Time (min)	Flow (μL/min)	%B
0.00	0.500	3.0
0.01	0.500	3.0
5.00	0.350	5.0
60.00	0.350	85.0
70.00	0.500	85.0
71.00	0.500	3.0
75.00	0.500	3.0

10. Inject 2 μL of digested sample onto a nano-LC column (75 μm inner diameter packed to 25 cm with 3 μm, 120 Å, C18AQ particles (Dr. Maisch)) and separate the peptides using a 60 min gradient (Mobile Phase A: Water + 0.1 % formic acid; Mobile Phase B: Acetonitrile + 0.1 % formic acid) according to the parameters in Table 1.
11. Operate the Orbitrap Lumos mass spectrometer with a nanoelectrospray source at 2.5 kV.
12. Collect MS1 scans at 120,000 resolution with a maximum injection time of 50 ms. Analyze the Extracted Ion Chromatograms (XIC) for the targeted peptide masses using a tolerance window of ±5 ppm (Fig. 6C).

7. Summary

The technical challenges associated with synthesizing lipidated proteins have limited the exploration of lipidation as a tool for engineering protein behavior and designing functional materials. Here, we present a robust, genetically encoded system for the one-pot production of prenylated proteins in *E. coli*. By reconstituting the eukaryotic prenylation pathway, this method provides a scalable alternative to chemical synthesis, eliminating the need for harsh reagents and complex refolding steps. The recombinant and modular nature of our platform enables future extensions, including the evolution of strains capable of incorporating non-natural isoprenoid analogues and the installation of downstream prenylation processing steps, such as CaaX proteolysis and carboxyl methylation. By overcoming longstanding production bottlenecks, this system paves the way for advances in lipoengineering, synthetic biology, and next generation protein therapeutics.

Acknowledgments

This work was supported by the National Science Foundation (NSF) (BMAT-2105193 and CAREER-2146168) and the National Institutes of Health (NIH) (R35GM142899 and R01GM132606).

References

Bader, B., Kuhn, K., Owen, D. J., Waldmann, H., Wittinghofer, A., & Kuhlmann, J. (2000). Bioorganic synthesis of lipid-modified proteins for the study of signal transduction. *Nature, 403*(6766), 223–226. https://doi.org/10.1038/35003249.

Bhatnagar, R. S., Fütterer, K., Waksman, G., & Gordon, J. I. (1999). The structure of myristoyl-CoA: Protein *N*-myristoyltransferase. *Biochimica et Biophysica Acta (BBA) - Molecular and Cell Biology of Lipids, 1441*(2), 162–172. https://doi.org/10.1016/S1388-1981(99)00155-9.

Bonde, M. T., Pedersen, M., Klausen, M. S., Jensen, S. I., Wulff, T., Harrison, S., ... Sommer, M. O. A. (2016). Predictable tuning of protein expression in bacteria. *Nature Methods, 13*(3), 233–236. https://doi.org/10.1038/nmeth.3727.

Brunsveld, L., Kuhlmann, J., Alexandrov, K., Wittinghofer, A., Goody, R. S., & Waldmann, H. (2006). Lipidated Ras and Rab peptides and proteins—Synthesis, structure, and function. *Angewandte Chemie International Edition, 45*(40), 6622–6646. https://doi.org/10.1002/anie.200600855.

Casey, P. J., & Seabra, M. C. (1996). Protein prenyltransferases (∗). *Journal of Biological Chemistry, 271*(10), 5289–5292. https://doi.org/10.1074/jbc.271.10.5289.

Duronio, R. J., Jackson-Machelski, E., Heuckeroth, R. O., Olins, P. O., Devine, C. S., Yonemoto, W., ... Gordon, J. I. (1990a). Protein N-myristoylation in Escherichia coli: Reconstitution of a eukaryotic protein modification in bacteria. *Proceedings of the National Academy of Sciences, 87*(4), 1506–1510. https://doi.org/10.1073/pnas.87.4.1506.

Gordon, J. I., Duronio, R. J., Rudnick, D. A., Adams, S. P., & Gokel, G. W. (1991). Protein N-myristoylation. *Journal of Biological Chemistry, 266*(14), 8647–8650. https://doi.org/10.1016/S0021-9258(18)31490-X.

Hang, H. C., & Linder, M. E. (2011). Exploring protein lipidation with chemical biology. *Chemical Reviews, 111*(10), 6341–6358. https://doi.org/10.1021/cr2001977.

Hanna, C. C., Kriegesmann, J., Dowman, L. J., Becker, C. F. W., & Payne, R. J. (2022a). Chemical synthesis and semisynthesis of lipidated proteins. *Angewandte Chemie International Edition, 61*(15), e202111266. https://doi.org/10.1002/anie.202111266.

Hartman, H. L., Bowers, K. E., & Fierke, C. A. (2004). Lysine Beta311 of protein geranylgeranyltransferase type I partially replaces magnesium. *Journal of Biological Chemistry, 279*(29), 30546–30553. https://doi.org/10.1074/jbc.M403469200.

Hossain, M. S., Alam, M. M., Huang, Z., Mousazadeh, F., Sarangi, R., de Jong, E., ... Mozhdehi, D. (2025). Scalable one-pot production of geranylgeranylated proteins in engineered prokaryotes. *Bioconjugate Chem, 36*(3), 415–423. https://doi.org/10.1021/acs.bioconjchem.4c00493.

Hossain, M. S., Ji, J., Lynch, C. J., Guzman, M., Nangia, S., & Mozhdehi, D. (2022a). Adaptive recombinant nanoworms from genetically encodable star amphiphiles. *Biomacromolecules, 23*(3), 863–876. https://doi.org/10.1021/acs.biomac.1c01314.

Hossain, M. S., Liu, X., Maynard, T. I., & Mozhdehi, D. (2020b). Genetically encoded inverse bolaamphiphiles. *Biomacromolecules, 21*(2), 660–669. https://doi.org/10.1021/acs.biomac.9b01380.

Hossain, M. S., Maller, C., Dai, Y., Nangia, S., & Mozhdehi, D. (2020a). Non-canonical lipoproteins with programmable assembly and architecture. *Chemical Communications, 56*(71), 10281–10284. https://doi.org/10.1039/D0CC03271A.

Hossain, M. S., Wang, A., Anika, S., Zhang, Z., & Mozhdehi, D. (2024). Genetically engineered liposwitch-based nanomaterials. *Biomacromolecules, 25*(12), 8058–8068. https://doi.org/10.1021/acs.biomac.4c01388.

Hossain, Md. S., Zhang, Z., Ashok, S., Jenks, A. R., Lynch, C. J., Hougland, J. L., & Mozhdehi, D. (2022b). Temperature-responsive nano-biomaterials from genetically encoded farnesylated disordered proteins. *ACS Applied Bio Materials, 5*(5), 1846–1856. https://doi.org/10.1021/acsabm.1c01162.

Ji, J., Hossain, M. S., Krueger, E. N., Zhang, Z., Nangia, S., Carpentier, B., ... Mozhdehi, D. (2023). Lipidation alters the structure and hydration of myristoylated intrinsically disordered proteins. *Biomacromolecules, 24*(3), 1244–1257. https://doi.org/10.1021/acs.biomac.2c01309.

Jiang, H., Zhang, X., Chen, X., Aramsangtienchai, P., Tong, Z., & Lin, H. (2018). Protein lipidation: Occurrence, mechanisms, biological functions, and enabling technologies. *Chemical Reviews, 118*(3), 919–988. https://doi.org/10.1021/acs.chemrev.6b00750.

Joosten, V., Lokman, C., van den Hondel, C. A., & Punt, P. J. (2003). The production of antibody fragments and antibody fusion proteins by yeasts and filamentous fungi. *Microbial Cell Factories, 2*(1), 1. https://doi.org/10.1186/1475-2859-2-1.

Kamiya, Y., Sakurai, A., Tamura, S., Takahashi, N., Abe, K., Tsuchiya, E., ... Fujino, M. (1978). Structure of Rhodotorucine-A, a novel lipopeptide, inducing mating tube formation in rhodosporidium-toruloides. *Biochemical and Biophysical Research Communications, 83*(3), 1077–1083. https://doi.org/10.1016/0006-291X(78)91505-X.

Khow, O., & Suntrarachun, S. (2012). Strategies for production of active eukaryotic proteins in bacterial expression system. *Asian Pacific Journal of Tropical Biomedicine, 2*(2), 159–162. https://doi.org/10.1016/S2221-1691(11)60213-X.

Kudla, G., Murray, A. W., Tollervey, D., & Plotkin, J. B. (2009). Coding-sequence determinants of gene expression in Escherichia coli. *Science, 324*(5924), 255–258. https://doi.org/10.1126/science.1170160.

Liu, C., Sun, Z., Shen, S., Lin, L., Li, T., Tian, B., & Hua, Y. (2014a). Identification and characterization of the geranylgeranyl diphosphate synthase in deinococcus radiodurans. *Letters in Applied Microbiology, 58*(3), 219–224. https://doi.org/10.1111/lam.12181.

London, N., Lamphear, C. L., Hougland, J. L., Fierke, C. A., & Schueler-Furman, O. (2011). Identification of a novel class of farnesylation targets by structure-based modeling of binding specificity. *PLOS Computational Biology,* 7(10), e1002170. https://doi.org/10.1371/journal.pcbi.1002170.

Luginbuhl, K. M., Mozhdehi, D., Dzuricky, M., Yousefpour, P., Huang, F. C., Mayne, N. R., ... Chilkoti, A. (2017). Recombinant synthesis of hybrid lipid–peptide polymer fusions that self-assemble and encapsulate hydrophobic drugs. *Angewandte Chemie International Edition, 56*(45), 13979–13984. https://doi.org/10.1002/anie.201704625.

Matsumoto, R., Niwa, T., Kuno, K., Shimane, Y., Kuruma, Y., & Kanamori, T. (2025). Lipid modification and membrane localization of proteins in cell-free system. *ACS Synthetic Biology, 14*(7), 2729–2738. https://doi.org/10.1021/acssynbio.5c00155.

Mayer, M. P., Prestwich, G. D., Dolence, J. M., Bond, P. D., Hong-yu, W., & Dale Poulter, C. (1993). Protein farnesyltransferase: Production in *Escherichia coli* and imrmmoaffinity purification of the heterodimer from *Saccharomyces cerevisiae*. *Gene, 132*(1), 41–47. https://doi.org/10.1016/0378-1119(93)90512-2.

McDaniel, J. R., MacKay, J. A., Quiroz, F. G., & Chilkoti, A. (2010). Recursive directional ligation by plasmid reconstruction allows rapid and seamless cloning of oligomeric genes. *Biomacromolecules, 11*(4), 944–952. https://doi.org/10.1021/bm901387t.

Mejuch, T., & Waldmann, H. (2016). Synthesis of lipidated proteins. *Bioconjugate Chemistry, 27*(8), 1771–1783. https://doi.org/10.1021/acs.bioconjchem.6b00261.

Meyer, D. E., & Chilkoti, A. (1999). Purification of recombinant proteins by fusion with thermally-responsive polypeptides. *Nature Biotechnology, 17*(11), 1112–1115. https://doi.org/10.1038/15100.

Morita, M., Hao, Y., Jokela, J. K., Sardar, D., Lin, Z., Sivonen, K., ... Schmidt, E. W. (2018). Post-translational tyrosine geranylation in cyanobactin biosynthesis. *Journal of the American Chemical Society, 140*(19), 6044–6048. https://doi.org/10.1021/jacs.8b03137.

Mozhdehi, D., Luginbuhl, K. M., Dzuricky, M., Costa, S. A., Xiong, S., Huang, F. C., ... Chilkoti, A. (2019). Genetically encoded cholesterol-modified polypeptides. *Journal of the American Chemical Society, 141*(2), 945–951. https://doi.org/10.1021/jacs.8b10687.

Mozhdehi, D., Luginbuhl, K. M., Simon, J. R., Dzuricky, M., Berger, R., Varol, H. S., ... Chilkoti, A. (2018). Genetically encoded lipid–polypeptide hybrid biomaterials that exhibit temperature-triggered hierarchical self-assembly. *Nature Chemistry, 10*(5), 496–505. https://doi.org/10.1038/s41557-018-0005-z.

Nadolski, M. J., & Linder, M. E. (2007). Protein lipidation. *FEBS Journal, 274*(20), 5202–5210. https://doi.org/10.1111/j.1742-4658.2007.06056.x.

Nunn, W. D., & Simons, R. W. (1978). Transport of long-chain fatty acids by Escherichia coli: Mapping and characterization of mutants in the fadL gene. *Proceedings of the National Academy of Sciences, 75*(7), 3377–3381. https://doi.org/10.1073/pnas.75.7.3377.

Palsuledesai, C. C., & Distefano, M. D. (2015). Protein prenylation: Enzymes, therapeutics, and biotechnology applications. *ACS Chemical Biology, 10*(1), 51–62. https://doi.org/10.1021/cb500791f.

Přáda Brichtová, E., Edu, I. A., Li, X., Becher, F., Gomes Dos Santos, A. L., & Jackson, S. E. (2025). Effect of lipidation on the structure, oligomerization, and aggregation of glucagon-like peptide 1. *Bioconjugate Chemistry, 36*(3), 401–414. https://doi.org/10.1021/acs.bioconjchem.4c00484.

Sahdev, S., Khattar, S. K., & Saini, K. S. (2008). Production of active eukaryotic proteins through bacterial expression systems: A review of the existing biotechnology strategies. *Molecular and Cellular Biochemistry, 307*(1–2), 249–264. https://doi.org/10.1007/s11010-007-9603-6.

Sweet, C., Aayush, A., Readnour, L., Solomon, K. V., & Thompson, D. H. (2021). Development of a fast organic extraction–Precipitation method for improved purification of elastin-like polypeptides that is independent of sequence and molecular weight. *Biomacromolecules, 22*(5), 1990–1998. https://doi.org/10.1021/acs.biomac.1c00096.

Tetali, S. D. (2019). Terpenes and isoprenoids: A wealth of compounds for global use. *Planta, 249*(1), 1–8. https://doi.org/10.1007/s00425-018-3056-x.

Tolia, N. H., & Joshua-Tor, L. (2006). Strategies for protein coexpression in Escherichia coli. *Nature Methods, 3*(1), 55–64. https://doi.org/10.1038/nmeth0106-55.

Wang, M., & Casey, P. J. (2016). Protein prenylation: Unique fats make their mark on biology. *Nature Reviews Molecular Cell Biology, 17*(2), 110–122. https://doi.org/10.1038/nrm.2015.11.

Xie, Z., He, J., Peng, S., Zhang, X., & Kong, W. (2023). Biosynthesis of protein-based drugs using eukaryotic microalgae. *Algal Research, 74*, 103219. https://doi.org/10.1016/j.algal.2023.103219.

Zhang, F. L., & Casey, P. J. (1996). Protein prenylation: Molecular mechanisms and functional consequences. *Annual Review of Biochemistry, 65*(65, 1996), 241–269. https://doi.org/10.1146/annurev.bi.65.070196.001325.

Zhang, Y., Blanden, M. J., Sudheer, Ch, Gangopadhyay, S. A., Rashidian, M., Hougland, J. L., & Distefano, M. D. (2015). Simultaneous site-specific dual protein labeling using protein prenyltransferases. *Bioconjugate Chemistry, 26*(12), 2542–2553. https://doi.org/10.1021/acs.bioconjchem.5b00553.

Zhang, Z., Ji, J., Shahadat Hossain, M., Bailey, B., Nangia, S., & Mozhdehi, D. (2024). Lipidation alters the phase-separation of resilin-like polypeptides. *Soft Matter*. https://doi.org/10.1039/D4SM00358F.

Zimmerman, K. K., Scholten, J. D., Huang, C., Fierke, C. A., & Hupe, D. J. (1998). High-level expression of rat farnesyl: Protein transferase in*Escherichia coli*as a translationally coupled heterodimer. *Protein Expression and Purification, 14*(3), 395–402. https://doi.org/10.1006/prep.1998.0979.

CHAPTER EIGHT

Creation of an optogenetic membrane editor with ultralow background activity

Xiang-Ling Li[a,b] **and Jeremy M. Baskin**[a,b,*]
[a]Department of Chemistry and Chemical Biology, Cornell University, Ithaca, NY, United States
[b]Weill Institute for Cell and Molecular Biology, Cornell University, Ithaca, NY, United States
*Corresponding author. e-mail address: jeremy.baskin@cornell.edu

Contents

1. Introduction 170
2. Blue light irradiation setup 172
3. Rational design and cloning of engineered enzymes 172
   3.1 Materials 174
   3.2 Protocol 174
4. Quantification of enzyme activity by fluorescence labeling 175
   4.1 Materials 176
   4.2 Equipment 176
   4.3 Protocol 176
5. Quantification of enzyme activity by LC-MS 177
   5.1 Materials 178
   5.2 Equipment 178
   5.3 Protocol 178
   5.4 LC-MS analysis 180
6. Summary and guidelines for further engineering 180
Acknowledgements 181
Competing interests 181
References 181

Abstract

Membranes play important biological roles in compartmentalization, transport, and signaling, but the study of their lipid constituents is challenging due to constant flux through their complex metabolic and interorganelle transport pathways. To overcome these challenges, we developed optogenetic membrane editors for spatiotemporally precise manipulation of the lipid composition of organelle membranes. In this chapter, we describe the design and validation of LOVPLD, an ultralow background optogenetic membrane editor that enables acute production of phosphatidic acid (PA) on organelle membranes of interest. LOVPLD comprises the insertion of a blue light-sensitive conformational switch, a LOV domain, into the sequence of

Methods in Enzymology, Volume 728
ISSN 0076-6879, https://doi.org/10.1016/bs.mie.2025.12.002
Copyright © 2026 Elsevier Inc. All rights are reserved, including those for text and data mining, AI training, and similar technologies.

phospholipase D (PLD), a phosphatidic acid-synthesizing enzyme, rendering PLD activity dependent upon blue light stimulation. We envision that the "LOVification" strategy described herein may be applicable to other lipid-modifying enzymes to create membrane editors for targeting different lipid classes.

1. Introduction

Lipids are crucial to life in their role as the main components of membranes, and defects in lipid homeostasis have been linked to numerous diseases (Dias & Nylandsted, 2021; Harayama & Riezman, 2018). Unfortunately, lipids are notoriously difficult to study. Due to their small size and hydrophobicity, lipids have high freedom of movement throughout the membrane, making them difficult to capture using imaging techniques (Bumpus, Liang, & Baskin, 2020; Fujiwara, Ritchie, Murakoshi, Jacobson, & Kusumi, 2002; Van Meer, Voelker, & Feigenson, 2008). Furthermore, lipids are not genetically encoded, making it challenging to directly manipulate lipid levels in cells (Bumpus et al., 2020; Chen, Li, & Baskin, 2025). Because of these challenges, studies of lipids in biological membranes are often performed using in vitro or *in silico* approaches (Chen et al., 2025; Mayor, Bhat, & Kusumi, 2023). Yet many properties of membranes in live cells, such as the formation of lipid microdomains and interactions of lipids with membrane-associated proteins, are difficult to replicate outside of cells. Moreover, a central function of cellular membranes lies in their role in compartmentalizing the cell into distinct yet interconnected organelles, so maintaining the separation of organelle compartments is critical to studying the biological activity of membranes (Jackson, Walch, & Verbavatz, 2016; Uematsu & Baskin, 2023). Current experimental approaches in membrane biology include the use of small-molecule activators and inhibitors of lipid-synthesizing enzymes, and genetic tools to manipulate expression levels of those enzymes (Chen et al., 2025; Kim et al., 2022; Nagarajan, Butler, & Hoy, 2021). These strategies are effective but often lead to global changes in lipid levels throughout the cell, without organelle-level details. Additionally, effects of chemical or genetic perturbations often require hours to days to fully manifest, but lipid metabolism and transport can occur on the timescale of seconds (Derose, Miyamoto, & Inoue, 2013; Tei & Baskin, 2021).

To address these challenges, we have developed optogenetic membrane editors for improved spatial and temporal resolution in perturbating the lipid composition of cellular membranes. Simply put, an optogenetic

membrane editor is a light-controlled enzyme capable of addition or removal of a particular lipid to/from a single organelle membrane in live cells. Our first class of membrane editor, termed optogenetic phospholipase D (optoPLD), harnesses the blue-light activated CRY2–CIBN heterodimerization system to enable rapid membrane recruitment of a PLD, which converts phosphatidylcholine (PC), the most abundant phospholipid in mammalian cell membranes, to phosphatidic acid (PA), a much lower-abundance lipid with potent signaling activity and important biosynthetic roles (Tei & Baskin, 2020). This localized membrane editing approach enables acute production of PA on a specific organelle membrane upon blue light stimulation, and it allows the study of PA signaling with spatiotemporal resolution. However, a liability of optoPLD, and its second-generation optogenetic super-active PLDs (superPLDs (Tei, Bagde, Fromme, & Baskin, 2023)), was the background activity of the PLD enzyme in the cytosol, as it was still stochastically encountering membrane PCs even in the supposedly "off" state in the dark, resulting in a chronic background production of PA and cytotoxicity.

To eliminate this background activity, we developed a second class of optogenetic membrane editor for PA, named LOVPLD (Li, Tei, Uematsu, & Baskin, 2024). Instead of optogenetically controlling the recruitment of a constitutively active PLD to the substrate, we devised a strategy to directly control the enzymatic activity of PLD by insertion of a photoswitching domain into the enzyme such that the enzyme is forced into an inactive conformation in the dark and recovers the active conformation as the photoswitch relaxes upon blue light stimulation. For this purpose, we used a light-oxygen-voltage (AsLOV2) domain derived from *A. sativa*, which has become popular in recent years as an optogenetic switch for exerting spatiotemporal control over cellular machinery and proximity labeling (Halavaty & Moffat, 2007; Hoffmann, Bubeck, Eils, & Niopek, 2018; Lee et al., 2023). Compared to optoPLD, LOVPLD displays near-zero background activity when kept in the dark, no discernible cytotoxicity, and improved compatibility with multiple organelles and cell lines. Using LOVPLD, we discovered striking differences of PA signaling and rates of PA metabolism between different organelles membranes, confirming that localized membrane editing is essential for elucidating the biological activity of lipids in full biological context (Li et al., 2024).

In this chapter, we first describe building an optogenetics experiment setup from scratch, followed by detailed design principles and cloning strategies that are used to create a panel of potential LOVPLD variants. We also

include two methods for screening LOVPLD activity. The first method involves fluorescent quantification of PLD activity using a chemoenzymatic labeling method developed in our lab termed Imaging Phospholipase D Activity with Clickable Alcohols via Transphosphatidylation (IMPACT), which enables high throughput, single-cell level activity quantification via flow cytometry (Bumpus & Baskin, 2016, 2017; Bumpus et al., 2020). The second method involves LC-MS quantification of whole-cell lipidomes, which is lower throughput but has wide applicability to all lipid types. Last, we also provide guidance on further engineering and optimization of the optogenetic membrane editors to maximize compatibility with biological systems and experiments. Though this chapter focuses on how to "LOVify" PLD to enable editing of PC to PA on target membranes, we envision that this "LOVification" strategy could serve as a template for creating additional membrane editors, starting from lipid-modifying enzymes other than PLD, to target other classes of lipids beyond PA.

2. Blue light irradiation setup

To perform optogenetic experiments, we built a custom light box by attaching six strips of dimmable, 12 V blue-LED tape light (1000Bulbs.com) on the inside of a plastic tray. The light box was placed inside the CO_2 incubator and power was supplied using an AC outlet power bank (Omars; 24,000 mAh, 80 W). Because cell culture dishes exhibited a tendency to heat up under long periods of blue light, we used an outlet timer (BN-LINK) to switch the light on and off automatically to enable 3-s intervals of blue light every 1 min. Alternatively, a dimmer can be used to lower the intensity of blue light and thus reduce the temperature. However, the duration and/or intensity of light required may vary with different photoswitch domains used.

3. Rational design and cloning of engineered enzymes

There are several points to be considered when selecting a suitable enzyme to use as the basis for a membrane editor. First, the enzyme should ideally be of non-mammalian origin, to avoid crosstalk with native cellular enzymes when expressed in mammalian cells. Additionally, to facilitate targeting to different cellular membranes using membrane-associating peptide tags, a soluble enzyme is preferable over membrane-associated or

membrane-embedded enzymes. We chose superPLD, which is an engineered version of a soluble PLD originating from *Streptomyces* sp. strain PMF. Compared to the wild type PLD^{PMF}, superPLD is more stable in mammalian cells and has more than 100-fold higher activity (Tei et al., 2023). When it comes to the choice of a photoswitch domain, there are multiple published photoswitches engineered to enhance turn on/turn off kinetics and reduce background (Geng, Shen, & Wang, 2021; Kawano, Aono, Suzuki, & Sato, 2013; Kawano, Suzuki, Furuya, & Sato, 2015). We used a further engineered version of the blue-light activated AsLOV2 domain with faster on/off kinetics and tighter dark state binding (Kim et al., 2017). Other versions of LOV domains and/or other photoswitches can also be used with the same principles.

Once the photoswitch was selected, we then conducted evolutionary conservation analysis on the PLD enzyme using Consurf (https://consurfdb.tau.ac.il/index.php) by uploading a crystal structure of the enzyme (PDB ID: 1V0W). We then mapped the Consurf conservation scores onto each residue in the crystal structure and examined it using ChimeraX (Fig. 1). We identified prospective positions of LOV domain insertion according to three criteria:

1) Conservation score value lower than 5
2) Located near or within a flexible loop
3) For long flexible loops, pick 2-3 positions distributed along the length of the loop

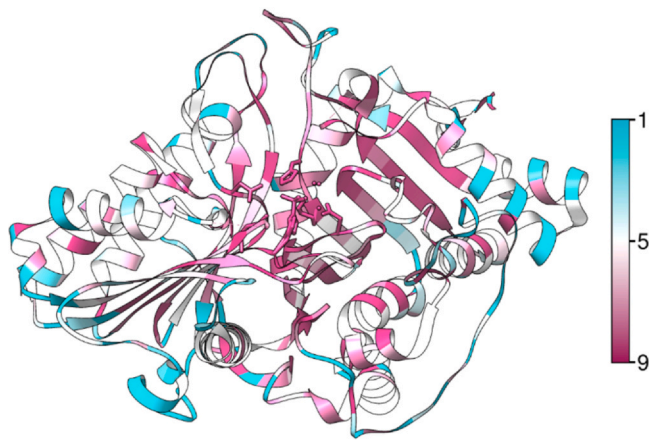

Fig. 1 Structure of PLD (PDB ID: 1V0W), color coded by conservation scores (9 = most conserved).

The exact number of candidate sites to select is up to discretion; we chose 19 insertion sites to allow for a large but manageable library for one-by-one testing as described below. We used molecular cloning to insert the LOV domain sequence after the chosen residue, so that the enzyme is split into two portions: the N terminal fragment (PLD(N)) and the C terminal fragment (PLD(C)). The materials and protocol are as follows:

3.1 Materials

3.1.1. DNA template for PLD (or other enzyme)
3.1.2. DNA template for LOV domain (or other photoswitch)
3.1.3. DNA template for mCherry (or other fluorescent protein)
3.1.4. pcDNA3 vector backbone or other mammalian expression vector
3.1.5. Restriction enzymes

3.2 Protocol

3.2.1. Choose restriction sites on the plasmid that do not appear in the DNA templates to serve as the insertion points for each DNA fragment (Fig. 2). We chose the sites *Kpn*I, *Bam*HI, *Eco*RI, *Not*I, and *Apa*I.
3.2.2. Design primers and amplify mCherry using PCR with the *Kpn*I and *Bam*HI restriction sites at each end.
3.2.3. Digest both the PCR product and the vector backbone with the same restriction enzymes and ligate the two fragments. Amplify the plasmid in *E. coli*.

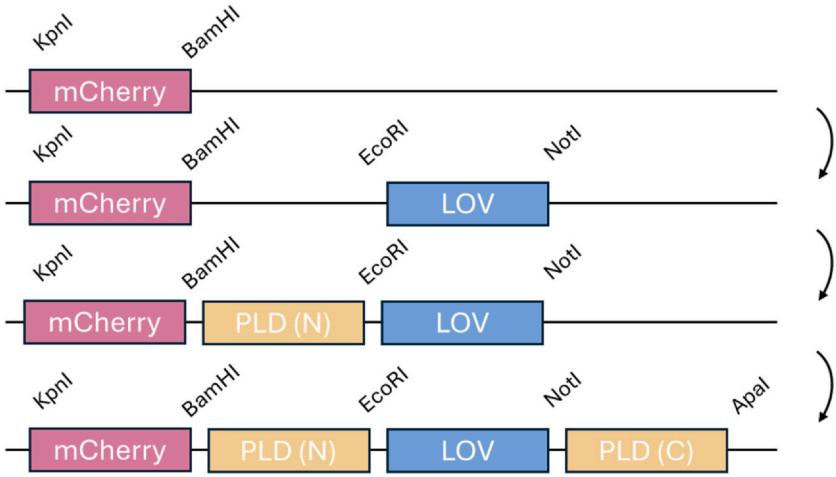

Fig. 2 Sequence of cloning events and restriction sites for the generation of mCherry-tagged LOVPLD constructs.

3.2.4. Amplify the LOV domain using PCR with *Eco*RI and *Not*I restriction sites at each end and repeat step 3.

3.2.5. Optional step: if targeting to a particular membrane is desired, a membrane targeting tag may be cloned in at this point. For LOVPLD, we cloned in a plasma membrane targeting tag (Lyn_{10}) at the N terminus of mCherry. We observed that the membrane editor often functions better when the membrane targeting tag is separated from the enzyme itself, either by a flexible linker or by the fluorescent protein, possibly due to the separation allowing more freedom of movement for the enzyme.

3.2.6. For each LOV domain insertion site, design primers to amplify each PLD(N) with the *Bam*HI and *Eco*RI sites on each side, and amplify the corresponding PLD(C) with the *Not*I and *Apa*I sites on each side. Using the plasmid from step 4 as the vector, repeat step 3 for each of the PLD(N) sequences, then repeat the cloning with each of the resulting vectors and corresponding PLD(C) sequences to generate the 19 different LOVPLD constructs.

4. Quantification of enzyme activity by fluorescence labeling

After obtaining the constructs for a panel of LOVPLD variants, we expressed them in mammalian cells to screen their activities in the dark and under blue light using IMPACT, a PLD activity assay previously developed in our lab, (Bumpus & Baskin, 2016, 2017; Bumpus et al., 2020) Briefly, we harness the ability of PLDs to accept azide-functionalized primary alcohols in a transphosphatidylation reaction, wherein a phosphatidylalcohol is produced instead of phosphatidic acid. By treating cells with a low concentration of an azide-functionalized primary alcohol and, after a rinse, subsequently treating cells with a cyclooctyne-functionalized fluorophore (BCN-BODIPY), we can quantify the transphosphatidylation product by fluorescence. Similar principles can be in principle used to quantify the activity of certain other enzymes by treating with a clickable mimic of the enzyme's substrate, then labeling with BCN-BODIPY. The ideal optogenetic membrane editor should have near-zero activity in the dark and high activity under blue light. The steps for IMPACT labeling and subsequent analysis by flow cytometry are described below:

4.1 Materials

- DMEM (Corning)
- FBS (Corning)
- Penicillin/streptomycin (Corning)
- poly-L-lysine (Sigma Aldrich)
- PBS (Corning)
- HEK 293 T cells
- pcDNA3 or other mammalian expression vector carrying the LOVPLD construct
- PEI MAX (Polysciences)
- 4 % paraformaldehyde (Electron Microscopy Sciences)
- 48-well plate (Corning)
- 96-well V-bottom plate (Greiner)
- 5 mL Snap Cap Polystyrene Tubes (Corning)
- bicyclononyne-BODIPY (BCN-BODIPY (Alamudi et al., 2016), synthesized in house)
- 3-azido-1-propanol (AzPrOH, AFG Bioscience)

4.2 Equipment

4.2.1. Attune NxT cytometer (Thermo Fisher)

4.3 Protocol

4.3.1. In 48 well plates, add enough 0.1 mg/mL poly-L-lysine to cover the bottom of each well and incubate for 20 min at 37 °C.

4.3.1.1. Note: at least two plates should be used, as cells intended for blue light treatment are seeded in a separate plate from cells that will not receive light treatment.

4.3.2. Aspirate the poly-L-lysine solution and rinse three times with PBS. Seed HEK 293 T cells in each well at 20 % confluency and culture for 24 h at 37 °C in a 5 % CO_2 atmosphere in DMEM supplemented with 10 % FBS and 1 % penicillin/streptomycin.

4.3.3. After 24 h, replace the media in each well with fresh DMEM (supplemented with FBS).

4.3.4. In polystyrene tubes, add each plasmid to DMEM (without FBS) at a ratio of 1 μg LOVPLD plasmid per 200 μL DMEM. In a separate polystyrene tube, make a master mix of PEI MAX in DMEM at a ratio of 5 μg PEI MAX per 200 μL DMEM. Incubate separately for 5 min, then mix the mix the PEI MAX and plasmid solutions in equal volumes and incubate for another 20 min at room temperature.

4.3.5. Add 70 μL plasmid mix to each well and swirl to mix. Cover the plates with aluminum foil to keep cells in the dark and incubated for another 16–24 h.

4.3.6. For IMPACT labeling, treat cells with 3 mM azidopropanol (AzPrOH) for 30 min at 37 °C under blue light irradiation. Control cells are labeled with AzPrOH for the same duration but kept under foil during the blue light illumination.

4.3.6.1. Note: to avoid activation of LOVPLD under ambient light, steps 6–8 should be performed in a dark room with red light for illumination when needed.

4.3.7. After AzPrOH labeling, rinse the cells 3 times with PBS, then 1 μM BCN-BODIPY for 15 min at 37 °C.

4.3.8. Rinse cells three times with PBS, and then add 100 μL 0.5 % trypsin solution to each well and incubate at 37 °C for 15 min or until cells are detached.

4.3.9. Quench the trypsin by adding 100 μL DMEM with 10 % FBS, and transfer cells to a V-bottom 96 well plate. Centrifuge the plate for 5 min at 3000 × g at 4 °C to pellet cells to the bottom.

4.3.10. Aspirate the supernatant in each well and resuspend cells in 4 % paraformaldehyde. Incubate on ice for 10 min to fix cells and then centrifuge the plate again for 5 min at 3000 × g. Aspirate the supernatant and resuspend cells in PBS for flow cytometry analysis.

4.3.11. For comparisons of labeling efficiency, mean BCN-BODIPY fluorescence (detected in the GFP channel) is obtained for the mCherry-positive populations of at least 5000 live cells, as determined by forward/side scattering.

5. Quantification of enzyme activity by LC-MS

If the proxy activity assay by IMPACT is insufficient, or if validation of biological activity is desired, the production of PA can be directly quantified by LC-MS. Compared to flow cytometry, which relies on a fluorescence labeling technique such as IMPACT, the LC-MS method can be more versatile for expanding the technique to enzymes that may not have fully developed fluorescence activity assays, as it directly measures the levels of cellular lipids based on mass spectrometry. However, LC-MS quantifies activity on the bulk cell population instead of each single cell and thus requires the majority of the cells to be expressing LOVPLD. For this

reason, this method is most effective when cells are transduced by lentivirus instead of transiently transfected to express LOVPLD. We cloned the entire LOVPLD construct into the pCDH1 lentivirus vector and used it to generate lentivirus carrying the LOVPLD sequence.

5.1 Materials

- HEK 293 TN cells
- HEK 293 T cells
- Transfectagro (Corning) or Opti-MEM (Thermo Fisher)
- Lipofectamine 2000 (Thermo Fisher)
- pCDH1 or other lentivirus vector carrying the LOVPLD construct
- Envelope plasmid (Addgene #1733)
- Packaging plasmid (Addgene #12260)
- DMEM (Corning)
- FBS (Corning)
- Penicillin/streptomycin (Corning)
- PBS (Corning)
- 5 mL Snap Cap Polystyrene Tubes (Corning)
- 0.45 μm syringe filter (Millipore Sigma)
- Methanol, LC-MS grade (Fisher)
- Chloroform, HPLC grade (Fisher)
- Ammonium hydroxide for HPLC, 35 % in water (Thermo Fisher)

5.2 Equipment

5.2.1. Agilent 6230 electrospray ionization–time-of-flight MS

5.2.2. Agilent 1260 HPLC

5.2.3. Luna 3 μm Silica LC Column (Phenomenex; 50 × 2 mm).

5.3 Protocol

5.3.1. Seed HEK 293TN cells in 6-well plates at 20 % confluency. culture for 24 h at 37 °C in a 5 % CO_2 atmosphere in DMEM supplemented with 10 % FBS and 1 % penicillin/streptomycin.

5.3.2. After 24 h, replace the media in each well with Transfectagro (or Opti-MEM) supplemented with 10 % FBS.

5.3.3. In polystyrene tubes, mix 0.5 μg envelope plasmid, 1.5 μg packaging plasmid, and 1.5 μg LOVPLD lentivirus plasmid in 200 μL Transfectagro. In a separate polystyrene tube, make a master mix of 6 μL Lipofectamine 2000 per 200 μL Transfectagro. Incubate separately for 5 min, then mix the Lipofectamine and plasmid solutions in equal volumes and incubate for another 20 min at room temperature.

5.3.4. Add the plasmid mix to each well and swirl to mix. Return to the incubator for 8–16 h and then replace the media with fresh DMEM supplemented with 10 % FBS and 1 % penicillin/streptomycin.

5.3.5. To harvest lentivirus, collect the cell culture media from each well after at least 8 h of incubation, and filter using 0.45 μm syringe filters. The virus-containing media can be stored at 4 °C for up to a week or flash frozen and stored at −80 °C for long-term storage.

5.3.5.1. Optional step: lentivirus can be repeatedly harvested from the same cells for 2-3 days by replacing the culture media immediately after each collection.

5.3.6. For LC-MS analysis, seed HEK 293 T cells at 50 % confluency in 12-well plates in 0.5 mL virus-containing media, 0.5 mL fresh DMEM, and 0.8 μg/mL polybrene. Cover plates with foil and incubate overnight at 37 °C, then replace the media with fresh culture media. Culture for an additional 24−48 h at 37 °C.

5.3.6.1. Optional step: 24 h after transduction, add 1 μg/mL puromycin to the cell culture media to select for transduced cells. This step can be omitted if the transduction efficiency is sufficiently high.

5.3.7. To activate LOVPLD, subject the cells to blue light irradiation for 30 min. Immediately after the blue light irradiation period, aspirate the culture media and lyse cells by adding 250 μL methanol to each well.

5.3.8. Using a cell scraper or pipette tip, scrape cells from the bottom of each well and pipette up and down to ensure complete lysis. Transfer the methanol/cell mixture to 1.5 mL Eppendorf tubes.

5.3.9. Add 125 μL acetic acid (20 mM in water) and 100 μL PBS to each tube, then add 500 μL chloroform to each tube. Cap the tubes and mix thoroughly by shaking vigorously for 5 min, then let rest for 5 min so that the organic phase separates from aqueous phase.

5.3.9.1. Optional step: centrifuge the tubes briefly to facilitate phase separation.

5.3.10. Collect the bottom organic layer from each tube and filter using 0.45 μm syringe filters. Inject 5 μL for each LC-MS analysis.

5.3.11. Optional step: The lipid extracts are stable at room temperature for up to 1 week. For longer term storage, transfer the organic layer into new tube and dry under a steady stream of nitrogen gas. The dried lipid film can be stored at −80 °C for up to 2 months. To use, resuspend the lipid film in 150 μL chloroform/methanol/water mix (73:23:3) and filter through a 0.45 μm syringe filter.

5.4 LC-MS analysis

For LC-MS separation, we used a linear gradient from 100 % solvent A to 100 % solvent B over 10 min, followed by 4 min at 0 % solvent A to allow the column to re-equilibrate. Solvent A was chloroform/methanol/ammonium hydroxide (85:15:0.5) and solvent B was chloroform/methanol/water/ammonium hydroxide (60:34:5:0.5). Phospholipid species were detected in negative mode. For LOVPLD, we observed significant increases in PA species in the blue light treated group compared to the dark control.

6. Summary and guidelines for further engineering

Optogenetic membrane editors have the potential to reveal the dynamics and functions of lipids in cellular membranes. In this chapter, we describe our protocols for designing and validating an optogenetic membrane editor, LOVPLD. Out of 19 variants, we identified one with very low dark activity and substantial activity under blue light. However, for long-term expression in cells and some sensitive experiments, a complete silencing of enzymatic activity is required in the dark. For this purpose, we also had success with combining the LOVPLD with a second, translocation-based optogenetic system, such as iLID or CRY2-CIBN. Another consideration is the speed of turn-on and turn-off. Although the LOV domain itself is capable of repeated switching between on and off states, we found that LOVPLD does not turn off completely once turned on, possibly due to the steric bulk of the PLD interfering with the conformation recovery of the LOV domain. However, after combining the "LOVification" of PLD with the iLID system so that the return to dark after blue light stimulation initiated both conformational change to the inactive state and dissociation from the target membrane, we observed that LOVPLD activity dropped completely and immediately after the light is turned off (Li et al., 2024).

In this membrane editor design, the choice of fluorescent protein can also be quite influential on enzyme activity. After testing several options, we chose mCherry to minimize fluorescence excitation and emission overlap with BCN-BODIPY. We found that mScarlet, super-TagRFP, TagBFP, and EGFP also produced similar results. However, we found that fluorescent proteins whose N- and C-termini are close together, such as miRFP670, interfered with the activity of the enzyme. We have also had

success with using HaloTag in place of a fluorescent protein, adding a HaloTag fluorescent probe in the same step as BCN-BODIPY and keeping all other experimental conditions the same. We envision that the principles described herein should be useful in enabling the development of other LOV-based membrane editors based on different lipid-modifying enzymes.

Acknowledgements

This work is supported by an award to J.M.B. from the National Institutes of Health (R01GM151682). X.L. was supported by a Natural Sciences and Engineering Research Council of Canada Postgraduate Scholarship.

Competing interests

The authors declare no competing interests.

References

Alamudi, S. H., Satapathy, R., Kim, J., Su, D., Ren, H., Das, R., ... Chang, Y. T. (2016). Development of background-free tame fluorescent probes for intracellular live cell imaging. *Nature Communications, 7*(1), 1–9. https://doi.org/10.1038/ncomms11964.

Bumpus, T. W., & Baskin, J. M. (2016). A chemoenzymatic strategy for imaging cellular phosphatidic acid synthesis. *Angewandte Chemie International Edition, 55*(42), 13155–13158. https://doi.org/10.1002/ANIE.201607443.

Bumpus, T. W., & Baskin, J. M. (2017). Clickable substrate mimics enable imaging of phospholipase D activity. *ACS Central Science, 3*(10), 1070–1077. https://doi.org/10.1021/ACSCENTSCI.7B00222/SUPPL_FILE/OC7B00222_SI_010.AVI.

Bumpus, T. W., Liang, D., & Baskin, J. M. (2020). IMPACT: Imaging phospholipase D activity with clickable alcohols via transphosphatidylation. In D. M. Chenoweth (Vol. Ed.), *Chemical Tools for Imaging, Manipulating, and Tracking Biological Systems: Diverse Chemical, Optical and Bioorthogonal Methods: Vol. 641. Methods in enzymology* (pp. 75–94). Academic Press. https://doi.org/10.1016/bs.mie.2020.04.037.

Chen, P.-H. B., Li, X.-L., & Baskin, J. M. (2025). Synthetic lipid biology. *Chemical Reviews, 125*(4), 2502–2560. https://doi.org/10.1021/acs.chemrev.4c00761.

Derose, R., Miyamoto, T., & Inoue, T. (2013). Manipulating signaling at will: Chemically-inducible dimerization (CID) techniques resolve problems in cell biology. *Pflugers Archiv European Journal of Physiology, 465*(3), 409–417. https://doi.org/10.1007/S00424-012-1208-6/FIGURES/3.

Dias, C., & Nylandsted, J. (2021). Plasma membrane integrity in health and disease: Significance and therapeutic potential. *Cell Discovery, 7*(1), 4. https://doi.org/10.1038/s41421-020-00233-2.

Fujiwara, T., Ritchie, K., Murakoshi, H., Jacobson, K., & Kusumi, A. (2002). Phospholipids undergo hop diffusion in compartmentalized cell membrane. *The Journal of Cell Biology, 157*(6), 1071–1082. https://doi.org/10.1083/jcb.200202050.

Geng, L., Shen, J., & Wang, W. (2021). Circularly permuted AsLOV2 as an optogenetic module for engineering photoswitchable peptides. *Chemical Communications, 57*(65), 8051–8054. https://doi.org/10.1039/d1cc02643g.

Halavaty, A. S., & Moffat, K. (2007). N- and C-terminal flanking regions modulate light-induced signal transduction in the LOV2 domain of the blue light sensor phototropin 1 from avena sativa. *Biochemistry, 46*(49), 14001–14009. https://doi.org/10.1021/bi701543e.

Harayama, T., & Riezman, H. (2018). Understanding the diversity of membrane lipid composition. *Nature Reviews. Molecular Cell Biology, 19*(5), 281–296. https://doi.org/10.1038/nrm.2017.138.

Hoffmann, M. D., Bubeck, F., Eils, R., & Niopek, D. (2018). Controlling cells with light and LOV. *Advanced Biology, 2*(9), https://doi.org/10.1002/adbi.201800098.

Jackson, C. L., Walch, L., & Verbavatz, J. M. (2016). Lipids and their trafficking: An integral part of cellular organization. *Developmental Cell, 39*(2), 139–153. https://doi.org/10.1016/j.devcel.2016.09.030.

Kawano, F., Aono, Y., Suzuki, H., & Sato, M. (2013). Fluorescence imaging-based high-throughput screening of fast- and slow-cycling LOV proteins. *PLoS ONE, 8*(12), https://doi.org/10.1371/journal.pone.0082693.

Kawano, F., Suzuki, H., Furuya, A., & Sato, M. (2015). Engineered pairs of distinct photoswitches for optogenetic control of cellular proteins. *Nature Communications, 6*. https://doi.org/10.1038/ncomms7256.

Kim, M. W., Wang, W., Sanchez, M. I., Coukos, R., von Zastrow, M., & Ting, A. Y. (2017). Time-gated detection of protein-protein interactions with transcriptional readout. *eLife, 6*. https://doi.org/10.7554/ELIFE.30233.

Kim, Y. J., Sengupta, N., Sohn, M., Mandal, A., Pemberton, J. G., Choi, U., & Balla, T. (2022). Metabolic routing maintains the unique fatty acid composition of phosphoinositides. *EMBO Reports, 23*(7), e54532. https://doi.org/10.15252/embr.202154532.

Lee, S.-Y., Cheah, J. S., Zhao, B., Xu, C., Roh, H., Kim, C. K., ... Francisco, S. (2023). Engineered allostery in light-regulated LOV-turbo enables precise spatiotemporal control of proximity labeling in living cells. *bioRxiv*. https://doi.org/10.1101/2023.03.09.531939.

Li, X.-L., Tei, R., Uematsu, M., & Baskin, J. M. (2024). Ultralow background membrane editors for spatiotemporal control of phosphatidic acid metabolism and signaling. *ACS Central Science, 10*(3), 543–554. https://doi.org/10.1021/acscentsci.3c01105.

Mayor, S., Bhat, A., & Kusumi, A. (2023). A survey of models of cell membranes: Toward a new understanding of membrane organization. *Cold Spring Harbor Perspectives in Biology, 15*(10), a041394. https://doi.org/10.1101/cshperspect.a041394.

Nagarajan, S. R., Butler, L. M., & Hoy, A. J. (2021). The diversity and breadth of cancer cell fatty acid metabolism. *Cancer & Metabolism, 9*(1), 2. https://doi.org/10.1186/s40170-020-00237-2.

Tei, R., Bagde, S. R., Fromme, J. C., & Baskin, J. M. (2023). Activity-based directed evolution of a membrane editor in mammalian cells. *Nature Chemistry, 15*, 1030–1039. https://doi.org/10.1038/s41557-023-01214-0.

Tei, R., & Baskin, J. M. (2021). Induced proximity tools for precise manipulation of lipid signaling. *Current Opinion in Chemical Biology, 65*, 93–100. https://doi.org/10.1016/J.CBPA.2021.06.005.

Tei, R., & Baskin, J. M. (2020). Spatiotemporal control of phosphatidic acid signaling with optogenetic, engineered phospholipase Ds. *The Journal of Cell Biology, 219*(3), https://doi.org/10.1083/JCB.201907013/133675.

Uematsu, M., & Baskin, J. M. (2023). Chemical approaches for measuring and manipulating lipids at the organelle level. *Cold Spring Harbor Perspectives in Biology, 15*(12), a041407. https://doi.org/10.1101/cshperspect.a041407.

Van Meer, G., Voelker, D. R., & Feigenson, G. W. (2008). Membrane lipids: Where they are and how they behave. *Nature Reviews. Molecular Cell Biology, 9*(2), 112–124. https://doi.org/10.1038/nrm2330.

CHAPTER NINE

Inhibition of sterol transport protein function

Hogan P. Bryce-Rogers, Laura Depta, Thomas Whitmarsh-Everiss, and Luca Laraia*
Department of Chemistry, Technical University of Denmark, Kgs Lyngby, Denmark
*Corresponding author. e-mail address: luclar@kemi.dtu.dk

Contents

1. Introduction 184
2. Titration of fluorescent lipids against sterol transport proteins 187
   2.1 Equipment and materials 189
   2.2 Reagents 189
   2.3 Procedure 190
   2.4 Notes 192
3. Fluorescence polarization for competitive inhibitor discovery 193
   3.1 Equipment and materials 193
   3.2 Reagents 193
   3.3 Procedure 193
   3.4 Notes 195
4. Differential scanning fluorimetry to determine STP binding 195
   4.1 Equipment and materials 196
   4.2 Reagents 196
   4.3 Procedure 197
   4.4 Notes 199
5. FRET-based liposome assays for lipid transport inhibitor discovery 199
   5.1 Equipment and materials 200
   5.2 Reagents 200
   5.3 Procedure 201
   5.4 Notes 205
6. Conclusion 206
Acknowledgements 207
References 207

Abstract

Intracellular sterol transport proteins (STPs) are key regulators of cholesterol homeostasis and potential drug targets in a broad range of diseases including atherosclerosis, infectious diseases and cancer. Therefore, the ability to rapidly identify and validate small molecule inhibitors of these transporters is of great significance. In this chapter, we outline a series of biophysical and biochemical assays of increasing

Methods in Enzymology, Volume 728
ISSN 0076-6879, https://doi.org/10.1016/bs.mie.2026.01.009
Copyright © 2026 Elsevier Inc. All rights are reserved, including those for text and data mining, AI training, and similar technologies.

complexity to screen small molecules for inhibition of STPs in medium-to-high throughput. These include differential scanning fluorimetry to determine compound binding, competitive fluorescence polarization assays employing fluorescent sterols as tracers, and FRET-based lipid transport assays in synthetic liposomes. As these assays are now established for the majority of human STPs, compounds can also directly be profiled for selectivity across structurally and functionally related targets.

1. Introduction

Maintaining cholesterol homeostasis is critical for healthy human physiology, because cholesterol performs a wealth of functions including being a key membrane component, a precursor to steroid hormones, oxysterols and bile acids, as well as a signaling molecule in its own right (Luo et al., 2020). Impairment of its homeostasis can lead to a wide variety of diseases including neurodegenerative diseases, atherosclerosis and cancer. Unsurprisingly, cholesterol levels and localization within a cell are tightly regulated processes with extensive feedback loops and redundancies. Cholesterol can be taken up through the diet or biosynthesized in the body, with the latter being under stringent transcriptional control. Cholesterol levels can also be regulated by its metabolism, where the production of the more soluble and easily excreted oxysterols keeps cholesterol levels constant through different mechanisms.

An often overlooked aspect of cholesterol homeostasis is its intracellular transport (Luo et al., 2019). Cholesterol is not distributed evenly between cellular membranes, with it making up approximately 40% of plasma membrane (PM) lipids but only 5% of the endoplasmic reticulum (ER) lipids. The transport of cholesterol between intracellular membranes is carried out by at least four different classes of proteins. The Niemann Pick disease type C class of proteins include NPC1 and NPC2, which are responsible for low-density lipoprotein (LDL)-derived cholesterol uptake in lysosomes. Mutations in these proteins leads to lysosomal cholesterol accumulation and serious genetic diseases (Yanjanin et al., 2010). As such, inhibition of NPC proteins by small molecules should be avoided. The focus of this chapter will be on the identification of inhibitors of the other three classes of STPs (Fig. 1): the steroidogenic acute regulatory protein (StAR) related lipid transfer domain containing (STARD) proteins, the oxysterol binding protein (OSBP) related proteins (ORPs) and the Asters (Depta et al., 2022).

The STARD family of transporters consists of 15 members with a wide variety of non-overlapping biological functions and lipid specificities, with only five members being confirmed sterol transporters. STARD1 functions

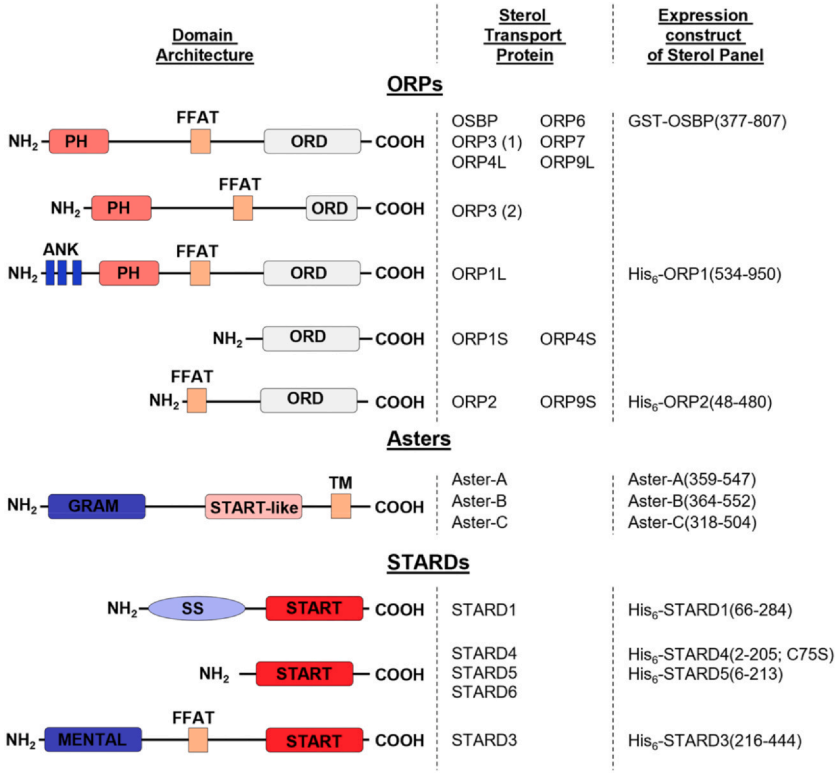

Fig. 1 Domain architecture and expression constructs of confirmed sterol transport proteins.

exclusively in the mitochondria, transporting cholesterol from the outer (OMM) to the inner mitochondrial matrix (IMM), fueling steroidogenesis, the production of steroid hormones (Miller, 2025). The inhibition of steroidogenesis has been proposed as a therapeutic strategy in Cushing's disease, adrenocortical carcinoma, breast cancer and prostate cancer. In contrast, STARD3 is reported to transfer cholesterol from the ER to the endosome (Wilhelm et al., 2017). It is overexpressed in *HER2*-positive breast cancers, and has been touted as an interesting new therapeutic target to pursue (Vassilev et al., 2015). STARD-4, -5 and -6 consist only of a StART sterol-binding domain and are cytoplasmic, but have vastly different lipid specificities, tissue distributions and physiological roles. STARD4 is widely distributed and is reported to transport cholesterol from the PM to the endocytic recycling compartment (ERC) (Iaea et al., 2020). STARD5 has been suggested to transport either cholesterol or bile acids, with its specific

function not fully resolved (Létourneau et al., 2012; Rodriguez-Agudo et al., 2005). STARD6 is expressed exclusively in the testis (Gomes et al., 2005), and has been suggested to transport testosterone, rather than cholesterol (Létourneau et al., 2016). The uncertainty in function has been the main driver to study this subfamily of lipid transporters in more detail.

The ORP family of lipid transporters contains 15 members, of which four are short splicing isoforms. While all family members appear to transport phosphoinositides (PI4P in particular) through their ORD domain, only some transport sterols. OSBP, the prototypical and first-described protein in the family, transports cholesterol from the ER to the Golgi, with PI4P being transported in the opposite direction (Mesmin et al., 2013). Inhibition of OSBP is suggested to be a promising anti-cancer and anti-infective strategy (Cigler et al., 2025; He et al., 2025; Roberts et al., 2019), via a mechanism that involves Golgi fragmentation and degradation, as well as inhibition of retrograde trafficking. Notably, some of the first well-validated inhibitors of STPs were natural products from diverse classes, shown to inhibit, and in some cases degrade, OSBP (Burgett et al., 2011). ORP4L and ORP4S are highly similar to OSBP, making selective inhibition challenging, but not impossible (He et al., 2025; Zhong et al., 2019). Other sterol-binding ORPs are also putative drug targets, with ORP1L playing a role in autophagy (Wijdeven et al., 2016), while ORP9 deletion, similarly to OSBP, also leads to Golgi fragmentation (Ngo and Ridgway, 2009).

The Aster family of proteins (also previously known as the GRAMD1 family) consists of three members (Aster-A, -B, and -C) which have all been shown to transport cholesterol from the PM to the ER, through their ASTER or StART-like domain (Sandhu et al., 2018). However, additional, diverging functions have also been ascribed to the individual family members. For example, Aster-A has been reported to regulate autophagy, with inhibitors shown to inhibit the process (Laraia et al., 2019). While Aster-A is ubiquitously expressed, Aster-B is primarily expressed in steroidogenic tissue and is linked to supplying cholesterol to mitochondria to enable steroidogenesis (Andersen et al., 2020). Finally, Aster-C has a more enigmatic role in human physiology, but its removal has been reported to affect mitochondrial respiration, mTOR signaling and autophagy (Ng et al., 2022; Zhang et al., 2020).

Despite their differences in biological functions and disease implications, very similar principles can be distilled from our efforts in designing and developing biophysical and biochemical assays to identify inhibitors of the STARDs, ORPs and Asters. We also believe that the protocols outlined below should be generally applicable to any lipid transfer protein, irrespective

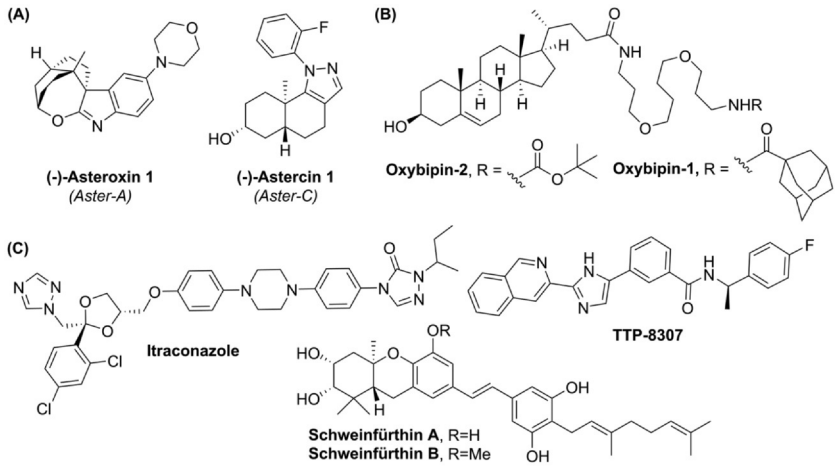

Fig. 2 Structures of STP inhibitors discovered and profiled using the assays reported herein. (A) Aster inhibitors; (B) recently discovered OSBP inhibitors; (C) previously reported OSBP inhibitors, characterized using our screening platform.

of its cargo. The protocols outlined in this chapter reflect our general strategies when working with lipid transporters: (a) titrate fluorescent lipids against the recombinantly-produced, purported lipid-binding domain, to determine lipid binding selectivity and establish conditions for competitive assays; (b) establish thermal shift assays for direct, non-competitive binding; (c) build competitive fluorescence polarization or intensity assays for compound ranking and potency optimization; and finally d) Förster Resonance Energy Transfer (FRET) assays using synthetic liposomes to measure more physiologically relevant inhibition of transport between membranes. This approach has led to the identification of inhibitors of Aster-A (Bro et al., 2025) and Aster-C (Whitmarsh-Everiss et al., 2021) (Fig. 2A), as well as the discovery and profiling of new OSBP inhibitors (He et al., 2025) (Fig. 2B). The collection of assays has also been used for the general selectivity profiling of previously reported OSBP inhibitors and naturally occurring oxysterols and synthetic derivatives (Fig. 2C) (Depta et al., 2025a, 2025b).

2. Titration of fluorescent lipids against sterol transport proteins

When working with STPs, and lipid transport proteins more generally, it is recommended to determine the lipid specificity, to more clearly understand

the STP substrates and facilitate future inhibitor screens. A large number of fluorescent lipids are commercially available or readily synthesized and can be titrated against recombinantly produced lipid-binding domains (Fig. 3).

Importantly, two different fluorescence-based measurements can be carried out in the same experiment. Fluorescence Intensity (FI) measurements can be used to determine whether the overall fluorescence emission changes upon lipid binding to its transport protein. Here, environment-sensitive fluorophores such as nitrobenzodiazole (NBD) are commonly employed, as they typically show increased fluorescence in hydrophobic environments. In parallel, changes in fluorescence polarization upon binding can also be measured. Fluorescence Polarization (FP) monitors the change in emission of plane-polarized light depending on the environment of the excited fluorophore. For example, a fluorescent lipid will emit a larger proportion of light in the same plane when it is bound to its target than when it is free in solution and is able to rotate more rapidly (Fig. 4).

For these assays, typically the lipid-binding domain, rather than the full-length protein, is employed. This choice also facilitates protein expression, which can be carried out in *E. coli*. The ORD of OSBP (377-807) was expressed with a glutathione-*S*-transferase (GST)-tag to maintain sufficient stability and solubility of the protein (He et al., 2025). Importantly, GST

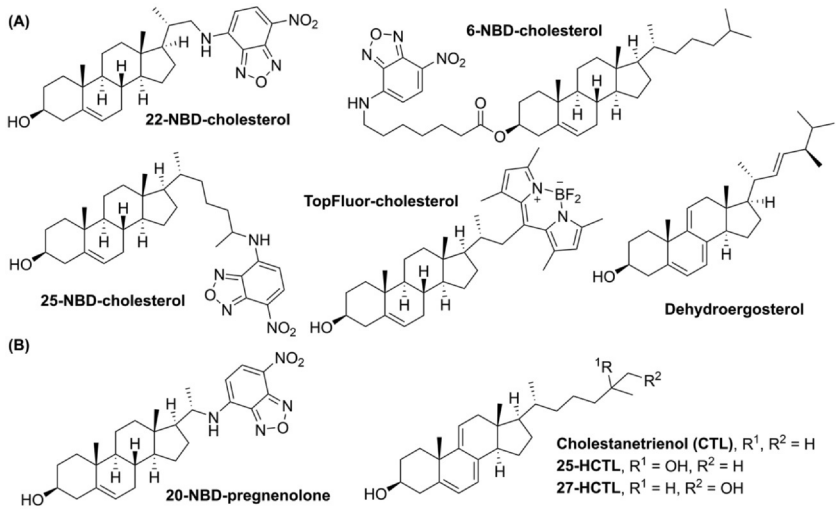

Fig. 3 Structures of fluorescently labeled or inherently fluorescent sterol probes. (A) commercially available fluorescent sterols; (B) readily synthesizable fluorescent sterols.

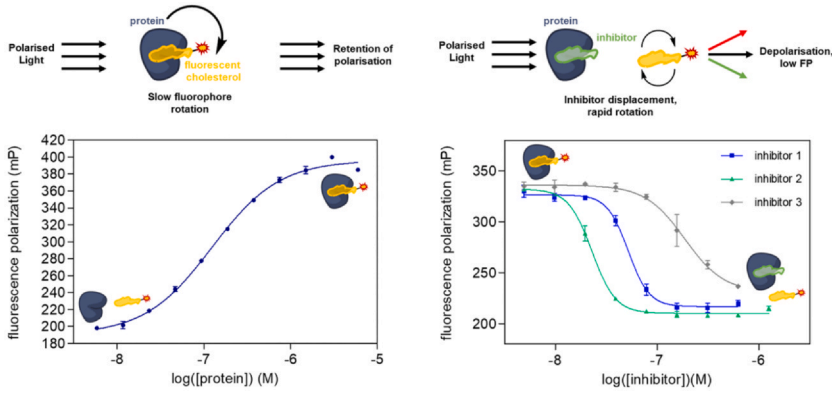

Fig. 4 Principles of the FP assay. *Left*: titration of sterol transport protein against a fixed concentration of fluorescent lipid. This setup enables the determination of dissociation constants; *Right*: competitive FP assays with fixed concentrations of fluorescent lipids and proteins, and variable inhibitor concentrations enable IC_{50} determination.

alone was shown not to interfere with 22-NBD-cholesterol binding. The sterol binding ORDs of ORP1 and ORP2, and the StART domain of STARD1 were expressed with an N-terminal His6 tag, whereas the ASTER domains of the Aster proteins were also expressed with a GST tag to improve their solubility (Whitmarsh-Everiss et al., 2021). In this case the GST tag was removed from the Aster proteins via protease cleavage.

2.1 Equipment and materials

384-well black flat-bottomed plates (both types can be used):

- Corning 384-Well Solid Black Polystyrene Microplates (Item No. 3573)
- Greiner MICROPLATE, 384-well, PP, F-BOTTOM (Item No. 781209)
- Tecan Spark Cyto plate reader

2.2 Reagents

- HEPES Buffer (pH 7.5, 300 mM NaCl)
- Buffer without glycerol (**Buffer A**): HEPES Buffer, 0.01% (vol/vol) tween-20, 2 mM DTT
- Buffer with glycerol (**Buffer B**): "buffer without glycerol" including 0.5% glycerol
- 22-NBD-Chol (2 μM in ethanol, intermediate solution)
- 22-NBD-Chol (60 nM): 1:1000 dilution of 22-NBD-Chol (2 mM) stock in buffer with glycerol

- Appropriate amount of 2 μM solution diluted in buffer with glycerol
- Adjust DMSO content to assay DMSO content (approximately 0.4% in the final assay)

2.3 Procedure

2.3.1 Preparation of fluorophore and protein

1. Prepare plate maps and calculate dilutions beforehand.
2. Prepare fluorophore solutions from 2 mM stocks:
   - Predilute the 2 mM stock of labelled sterol fluorophore in ethanol, in a 1:999 ratio with **Buffer B**.
   - Perform a second dilution of the 2 μM fluorophore solution to 2x the final assay concentration (Table 1) in **Buffer B**
     - Prepare protein dilution solutions at 2x the highest assay concentration in **Buffer A**.
     - Perform a 3-fold dilution series of the protein in a 96-well plate.

2.3.2 Plating the titration

1. Using a multichannel pipette transfer 15 μL of the protein solution (in duplicate) into each assay well.
2. Next, transfer 15 μL of the 2x fluorophore solution into each well on the 384-well plate except the buffer control wells.
3. Finally, add 15 μL of **Buffer B** to each of the buffer control wells.
4. Spin down the plate in a centrifuge at 100 rpm for 10 seconds and begin incubation time (Table 1).

Table 1 Summary of the FP titration conditions for each protein.

Protein	Fluorophore	Fluorophore concentration	Incubation time (Protein/NBD cholesterol)	Expected K_D
Aster-A	22-NBD-cholesterol	20 nM	20 min	300-400 nM
Aster-B	22-NBD-cholesterol	20 nM	20 min	300-400 nM
Aster-C	22-NBD-cholesterol	20 nM	20 min	60-80 nM
STARD1	22-NBD-cholesterol	20 nM	20 min	500-600 nM
OSBP	22-NBD-cholesterol	20 nM	20 min	100-200 nM
ORP1	25-NBD-cholesterol	80 nM	20 min	100-200 nM
ORP2	25-NBD-cholesterol	80 nM	20 min	500-700 nM

2.3.3 Instrument settings

FP measurements are performed using the Tecan Spark Cyto plate reader. The polarization module consists of a flash lamp as light source, monochromators and/or filters for wavelength selection, a measurement head, and a photomultiplier tube detector. Polarizers are installed on the measurement head and switched in automatically when performing polarization measurements.

1. Select the wells to be measured in the experiment from the top panel of the user interface (Fig. 5).
2. **Fluorophore:** Select other if working with a fluorophore that is not included in the list of fluorophores.
3. **Excitation wavelength:** For the NBD-labeled sterols, the excitation is: Filter, 485 (20).
4. **Emission wavelength:** For the NBD-labeled sterols, the emission is: Filter, 535 (25).
5. **Choose Z-position calculated from well:** Select a fluorophore or buffer blank well as well to be used to determine the Z-position.
6. **G-factor calculated from reference well (BF, fluorophore only) and blank (BL, Buffer only).**
7. **Select gain:** optimal
8. **Settle Time:** 0–5 ms is appropriate as a 384-well plate observes minimal surface fluctuations due to the low surface area and high surface tension of aqueous solutions.

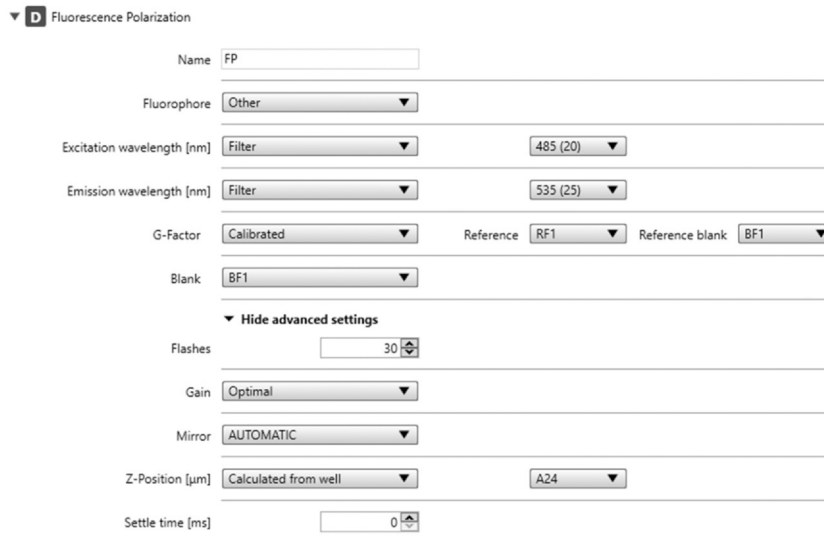

Fig. 5 Fluorescence Polarisation module of the Tecan Spark Cyto.

2.3.4 Measurement and analysis

1. Insert the plate into the plate reader and start the measurement.
2. Transpose data and copy the raw FP data into GraphPad Prism.
3. Plot the data on an XY scatter graph of Fluorescence polarization on the y-axis and log([protein]) on the x-axis (as in Fig. 4)
4. Fit the graph using Non-linear fit "log(inhibitor) vs. response – Variable slope (four parameters)"

   $Y = \text{Bottom} + (\text{Top} - \text{Bottom})/(1 + 10\hat{}((\text{LogIC}_{50} - X) * \text{HillSlope}))$

5. The K_d will be provided and can be compared with Table 1.

2.4 Notes

- Troubleshooting common issues: G-factor calibration can at times fail. For the NBD labelled fluorophores, if everything has been carried out correctly, the G-factor of a previous measurement (provided the fluorophore concentrations are the same) can be manually entered into the instrument settings. If there is high variation randomly distributed throughout the plate, centrifuging and checking for bubbles that have disrupted the surface can often reduce the outlier occurrence. However, if outliers persist then they can be flagged during analysis, and an additional replication of the experiment is recommended.
- The excitation and emission of the commercially available and newly synthesized sterol probes that have been used in investigations into STPs are outlined below (Table 2). However, 25- and 27-HCTL (Fig. 3B) cannot be used in FP assays. The inherent fluorescence of these two tracers is not intense enough to allow for the stable measurement of changes in polarization, and they are quenched in aqueous environments. Therefore, 25- and 27-HCTL are investigated in fluorescence intensity titrations. Furthermore, the fluorescent properties of the HCTLs allow them to be measured by tryptophan-tracer FRET and thus the

Table 2 Excitation and emission settings for different fluorescent sterols.

Ligand	Ex/Em	
NBD-cholesterol analogs	485(20) nm/535(25) nm	Filter
TopFluor cholesterol	485(20) nm/535(25) nm	Filter
TopFluor-TMR-cholesterol	535(25) nm/590(20) nm	Filter
25-/27-HCTL	325(10) nm/400(10)	Monochromator

fluorescence increase upon binding the two tracers gain a significant window in fluorescence that allows for their titration. However, it is important that the fluorescence of each protein against HCTL titration is normalized against protein only titration. By doing this the changes in fluorescence are those only derived from that of the complexation of a HCTL and the protein.

3. Fluorescence polarization for competitive inhibitor discovery

In a competitive FP assay, a predetermined concentration of fluorescent ligand/lipid and protein are used, based on titration experiments described in section 2. The interaction between fluorescent lipid and STP can be competed out by non-fluorescent inhibitors (Fig. 4). This enables the calculation of IC_{50} and K_i data, which enable the rapid comparison of compound activity and potency. The assays are performed with an Echo acoustic dispenser for maximum speed and reproducibility but can also be performed with other liquid handlers or manually; however, these changes will require adjustment of volumes and final DMSO concentrations.

3.1 Equipment and materials

- The equipment and materials required are the same as in Section 2.1.
- Labcyte Echo 550 acoustic dispenser.

3.2 Reagents

- The same reagents are required as in Section 2.2.

3.3 Procedure

3.3.1 Assay execution

1. Prepare echo source plate: Prepare compound stock solutions and load adequate volume (including dead volume) into the source plate (384 well, LDV plate, volume range 3–12 μL).
2. Centrifuge the plate for 30 seconds to remove trapped air bubbles.
3. Clean the bottom of the plate with paper towel.
4. Transfer compound dilution series and DMSO from source plate on destination plate via echo acoustic dispenser; centrifuge destination plate after transfer.
5. Source plate: Echo Qualified 384-well Cyclic Olefin Copolymer (COC) Source Microplate, Low Dead Volume.

6. Destination plate:
   a. Corning 384-Well Solid Black or White Polystyrene Microplates (Item No. 3573) or
   b. Greiner MICROPLATE, 384 WELL, PP, F-BOTTOM (Item No. 781209)
7. Combine an equal volume of protein and fluorophore solutions (1:1) at the desired concentrations (Table 3) and incubate on ice for 20 min.
8. Transfer 30 μL of pre-mixed fluorophore:protein solution into each compound containing well for a final assay volume of 30 μL via multichannel pipette.
9. Add control wells to the plate 30 μL of buffer for the blank:
   a. 15 μL of fluorophore and 15 μL buffer for the low mP control (100% inhibition).
   b. 30 μL of fluorophore:protein mixture for the high mP control (0% inhibition).
10. Wrap plate in foil and incubate for 20 min at room temperature before reading.

3.3.2 Measurement

The measurement and instrument settings were performed as in **2.3.3**–**2.3.4**.

3.3.3 Data analysis

1. Input data into GraphPad Prism.
2. Transform the X axis to log[compound] (M)

Table 3 Summary of the competitive FP assay conditions for each protein.

Protein	Protein conc. for selectivity measurements	Protein conc. for dose response measurements
Aster-A	1 μM	0.5 μM
Aster-B	1 μM	0.5 μM
Aster-C	1 μM	0.5 μM
STARD1	1 μM	1 μM
OSBP	1 μM	0.2 μM
ORP1	1 μM	0.2 μM
ORP2	1 μM	0.7 μM

3. Normalize data:
   a. 0% set as mean of protein + fluorophore wells
   b. 100% set as mean of fluorophore well (same control for both wells)
4. Fit curve using the Log(inhibitor) vs. normalized response - variable slope analysis.

$$Y = /(1 + 10\hat{}((\text{LogIC}_{50} - X) * \text{HillSlope}))$$

5. The IC_{50} can then be extrapolated from the curve.

3.4 Notes

- Avoid using DTT that has been thawed more than 3 times; use fresh DMSO.
- Centrifuge protein after thawing, never vortex proteins, check protein concentration with a NanoDrop and calculate protein concentration in μM before starting the assay.
- Keep proteins on ice, avoid freeze-thawing protein aliquots more than 3 times; freeze proteins in liquid nitrogen and store in a -80 °C freezer.
- Prepare fresh compound dilutions for Echo source plate for each replicate (avoids precipitation issues, problems with Echo transfer and improves data quality); if there is a critical amount for certain stock solutions remove stock solutions from Echo source plates after each use.
- Avoid exposing the fluorophore to ambient light for extended periods.

4. Differential scanning fluorimetry to determine STP binding

Differential scanning fluorimetry (DSF) involves the measurement of protein unfolding in response to increasing temperature. The unfolding process can be measured using an environment-sensitive dye such as SYPRO Orange, whose fluorescence is quenched in aqueous environments, but is restored upon binding to hydrophobic portions of proteins, typically exposed upon unfolding (Fig. 6a). Typically, a ligand that interacts with a protein target can lead to its stabilization towards heat-induced unfolding, which can be easily measured using a simple set-up (Fig. 6b). When experiments are run with a range of compound concentrations, two parameters can be extracted: 1) the apparent K_d, which is a reasonable approximation of the real K_d when operating

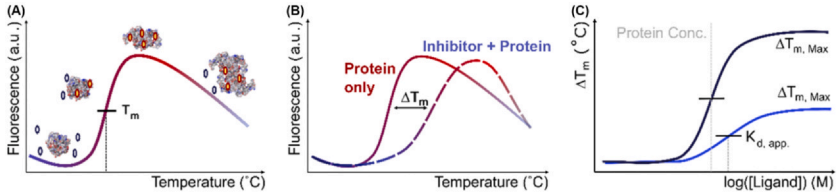

Fig. 6 Principles of DSF assays. (a) illustration of protein unfolding and resultant hydrophobic dye complexation providing a fluorescence against temperature melting curve yielding a melting temperature (T_m); (b) representative melting curves of an apo-protein and a stabilized protein yielding the change in melting temperature (ΔT_m); (c) exemplified dose response curves of a potent high stabilizing ligand at the limit of detection of the assay (navy blue) and a less potent ligand (light blue) with lower maximal stabilization ($\Delta T_{m,\ Max}$).

outside the titration range; and 2) the maximal thermal stabilization ($\Delta T_{m,\ Max}$), which is particularly useful when comparing ligands at the limit of detection of the assay, where apparent K_d are not useful. The disadvantages of DSF screens include the need for higher protein concentrations (usually >1 μM), ambiguity between change in melting temperature and potency of protein-ligand binding, the requirement of an indirect measure of readout in the use of a third-party dye in the assay, and the destructive nature of the assay which results in single measurement runs with no possibility of kinetic investigations. DSF can be performed using a range of thermal cyclers that are able to measure fluorescence, however this protocol has been optimized for the Roche LightCycler 480 in a 384-well format, to reduce protein consumption. The assay works equally well in 96-well plates.

4.1 Equipment and materials

- LabCyte Echo 550 acoustic dispenser
- Roche LightCycler 480 II
- LightCycler® 480 Multiwell Plate 384, white
- Roche TSA analysis program
- GraphPad Prism

4.2 Reagents

- DSF Buffer: 20 mM HEPES pH 7.5, 300 mM NaCl (Assay Stock Buffer), and 2 mM DTT in Milli-Q water
- 5000x SYPRO Orange (Sigma-Aldrich, S5692)

4.3 Procedure

4.3.1 Preparation of ligands and protein

1. Prepare plate maps and calculate dilutions beforehand.
2. Prepare ligand solutions from 10 mM stocks:
   - Predilute the 10 mM stock of ligands in DMSO, in a 1.5:8.5 ratio with DMSO 1.5 mM predilution for a final assay conc. of 50 μM highest concentration.
   - Predilute the 10 mM stock of ligands in DMSO, in a 3:7 ratio with DMSO 3 mM predilution for a final assay conc. of 100 μM highest concentration.
3. Transfer 10 μL of the 1.5/3 mM predilutions of each test ligand into the Echo source plate and then transfer 10 μL of DMSO and 5000x SYPRO Orange (SO) into 4 wells each.
4. Prepare protein solutions at 2.5 μM (STARD3 and STARD4) and 5 μM (STARD5) by diluting in **DSF Buffer.**

4.3.2 Plating the protein

1. Using a multichannel pipette transfer 10 μL of the protein solution (in triplicate) into each well of the LightCycler® 480 Multiwell Plate 384 (Fig. 7).
2. Spin down both the Echo source plate and the assay plate for 10 s at 1000 rpm.

4.3.3 Transferring compounds, DMSO and Sypro Orange

1. Using the Echo liquid handler, transfer compounds dose dependently from the Echo source plate to the destination plate (LightCycler® 480 Multiwell Plate 384) as illustrated in Fig. 7.

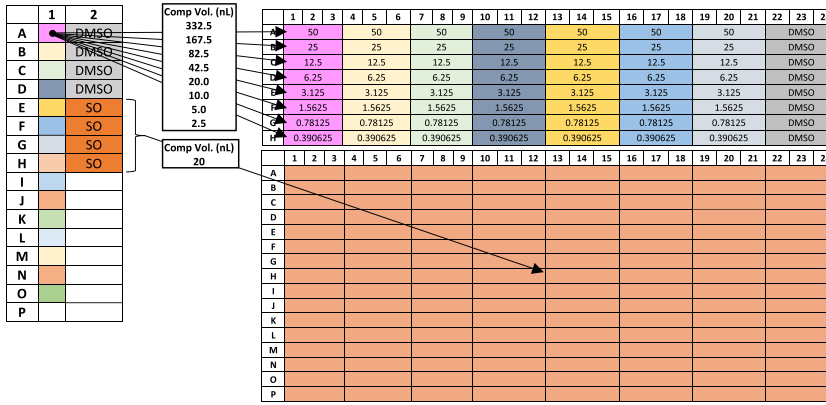

Fig. 7 Labcyte Echo source plate layout and dispensing pattern into assay plates.

2. Transfer 332.5 nL of DMSO to the DMSO control wells (grey, A 22;H24).
3. Lastly, transfer 20 nL of 5000× SYPRO Orange to every well on the plate (final concentration of 10×).
4. Centrifuge the plate at 1000 rpm for 10 seconds.
5. Seal the plate with a clear hydrophobic sealing foil provided with the LightCycler® 480 Multiwell Plates.
6. Begin incubation time.

4.3.4 Instrument settings and measurement

1. Incubate the plate at room temperature for 10 minutes. Ramp the temperature from 30 °C, by steps of 0.2 °C, up to 90 °C with incubation for 5 seconds at each step.
2. Measure the fluorescence intensity (Excitation 465 nm/Emission 580 nm) in a Roche LightCycler 480 II, ramping the temperature from 35 °C, at a rate of 4.8 °C/s, up to 95 °C. The protocol measures 5 acquisitions per second.

4.3.5 Analysis

1. Import the .ixo raw data file into the Roche analysis software.
2. Create a new analysis and select all data sets.
3. The first derivative of the raw data curves (fluorescence against temperature) will be automatically calculated and plotted (dF/dT against temperature) by the Roche analysis software (illustrated in Fig. 8 for the 25-HCTL stabilization of STARD4). The peak of the dF/dT returns the T_m of the data set and is reported.
4. Export the resulting data file as a.csv
5. In Microsoft Excel, take the average melting temperature (T_m) of the DMSO controls and subtract it from all other data points to provide the ΔT_m of each well.
6. Transpose the ΔT_m data series from A1-A24 horizontally, repeat this for B1-B24 in the next row below the A data series. Continue with C-P data series in the same manner.
7. Copy the transposed ΔT_m data into GraphPad Prism and plot the data on an XY scatter plot of ΔT_m (°C) against log([ligand]) (M).
8. Extrapolate the nonlinear regression by "log(inhibitor) vs. response – Variable slope (four parameters)"
9. The $K_{d,\ app.}$ and $\Delta T_{m,\ Max}$ for each ligand can then be extrapolated as in Fig. 6.

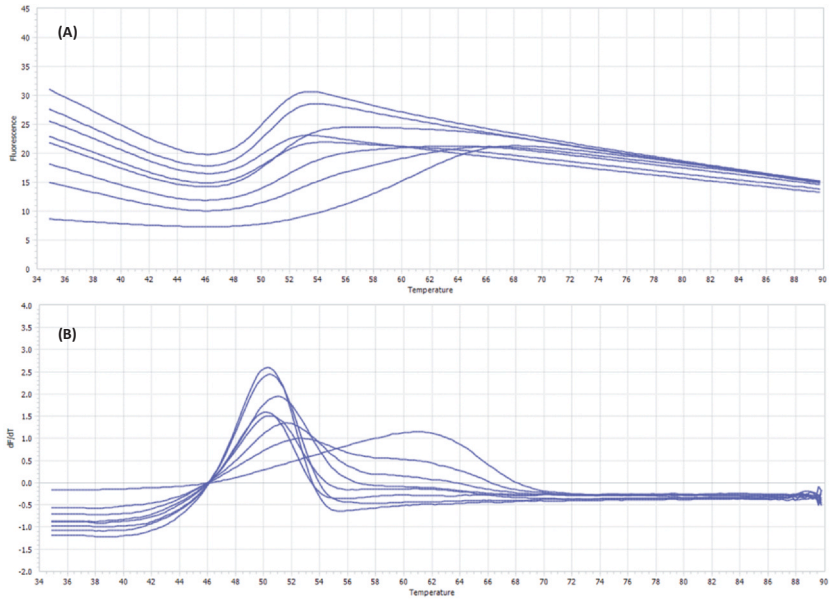

Fig. 8 Raw and processed DSF data as obtained using the Roche analysis software. A) Changes in SYPRO Orange fluorescence upon binding of 25-HCTL to STARD4; each blue curve represents a different concentration of 25-HCTL. B) The first derivative (dF/dT) of the data in (A) plotted against increasing temperature. The peak maxima correspond to the melting temperature.

4.4 Notes

- SYPRO Orange can, in some cases, interact with the lipid-binding site in the folded state. In those cases, it can be used as a fluorescent tracer in FI or FP assays (sections 2 and 3) but will most likely not be usable for the establishment of a DSF assay.
- Either stabilization or destabilization effects can be the result of a ligand binding to the active site of the protein or binding allosterically, however, no information on which type of binding occurs is obtained.

5. FRET-based liposome assays for lipid transport inhibitor discovery

To determine whether a compound can inhibit the *transport* of an STP, a variety of FRET-based assays have been established. These assays require the preparation of synthetic liposomes which contain a pair of fluorescent lipids with suitable excitation and emission spectra to undergo

FRET. The assay can be carried out in two different formats: A) the fluorescent lipids can be placed in the same "donor" liposomes, where transport to a non-fluorescent "acceptor" liposome leads to a reduction in FRET signal (Fig. 9A and B); the fluorescent lipids can be placed in two different liposomes, where transport from one to the other leads to an increase in FRET signal (Fig. 9B). Here we describe both strategies, including two different FRET pairs commonly used in the field.

5.1 Equipment and materials

- Avanti Mini Extruder (Avanti Research).
- Tecan Spark Cyto plate reader.

5.2 Reagents

- **STA Buffer**: 20 mM HEPES pH 7.5, 300 mM NaCl and 2 mM DTT.
- 1,2-dioleoyl-sn-glycero-3-phosphocholine (DOPC, Avanti Polar Lipids, 850375 C) was prepared in chloroform (10 mg/mL).
- 23-(dipyrromethene boron difluoride)-24-norcholesterol (TopFluor® Cholesterol, Avanti Polar Lipids, 810255).
- N-(lissamine rhodamine B sulfonyl)-1,2-dihexadecanoyl-sn-glycero-3-phosphoethanolamine (triethylammonium salt) (Rh-DHPE, Invitrogen, L1392) were prepared in methanol (100 μM).
- A 2 mM stock solution of DHE in absolute ethanol was prepared from 1 mg solid (Avanti Polar Lipids, #810253).
- Dansyl-PE (1 mL, 1 mg/mL) in chloroform was obtained from Avanti Polar Lipids (#810333 A).

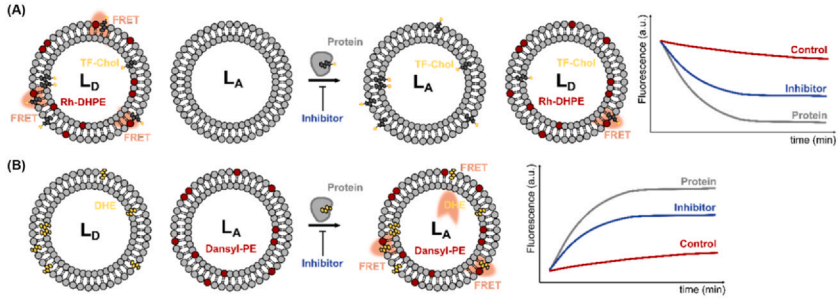

Fig. 9 Two different set-ups for liposome-based lipid transfer assays. (A) TopFluor-Cholesterol (TF-Chol) setup of the sterol transfer assay resulting in a decrease in fluorescence on addition of protein. (B) Dehydroergosterol (DHE) setup of the sterol transfer assay resulting in a fluorescence increase as DHE is transported to an acceptor liposome. L_D – donor liposome. L_A – acceptor liposome. Control – without protein.

- A stock solution of DOPC in chloroform (10 mg/mL) had previously been prepared from a 25 mg/mL solution (Avanti Polar Lipids #850375 C).

5.3 Procedure

5.3.1 General comments

– Only handle lipids with glass, as lipids will stick to any type of plastic
– It is good to prepare two sets of each donor and acceptor liposomes as backups
– Lipid stocks should be stored under an atmosphere of nitrogen/argon to slow oxidation and decomposition

5.3.2 Lipid film preparation, TopFluor Setup

The following steps all take place in glass-vials covered in aluminum foil, to keep the light sensitive lipids in the dark as much as possible:

1. For "donor" lipid films consisting of a mixture of DOPC:TF-Chol:Rh-DHPE (99:0.5:0.5):
   a. Into a glass vial with a lid containing a rubber septum, add the following via glass Hamilton syringe: 6 μL of TopFluor cholesterol (100 μM stock), 6 μL of Rh-DHPE (100 μM stock), 8.7 μL of DOPC (10 mg/mL stock), and 0.979 mL chloroform
   b. Wrap this vial in aluminum foil to protect from light
2. For "acceptor" lipid films consisting of DOPC only:
   a. Into a glass vial with a lid containing a rubber septum, add the following via glass Hamilton syringe: 8.7 μL of DOPC (10 mg/mL stock) and 0.991 mL chloroform
3. Evaporate the solvent in the vials under a stream of nitrogen.
4. After 1–2 hours, the solvent should be fully evaporated.
5. Place lids onto vials and connect to vacuum and leave overnight (this removes residual organic solvent which can inhibit formation of liposomes).

5.3.3 Lipid film preparation, DHE Setup

The following steps all took place in glass-vials covered in aluminum foil, to keep the light sensitive lipids in the dark as much as possible:

1. For "donor" lipid films consisting of a mixture of 90/10 DOPC/DHE:
   a. Into a glass vial with a lid containing a rubber septum, add the following via glass Hamilton syringe: 57 μL of DHE (2 mM stock), 40 μL of DOPC (10 mg/mL stock), and 0.9 mL chloroform.

2. For "acceptor" lipid films consisting of 97.5/2.5 DOPC/Dansyl-PE:
   a. Into a glass vial with a lid containing a rubber septum, add the following via glass Hamilton syringe: 61 μL of DOPC (10 mg/mL stock), 20 μL of Dansyl-PE (1 mg/mL stock) and 0.9 mL chloroform.
3. Evaporate the solvent in the vials under a stream of nitrogen.
4. After 1–2 hours, the solvent should be fully evaporated.
5. Place lids onto vials and connect to vacuum and leave overnight (this removes residual organic solvent which can inhibit formation of liposomes).

5.3.4 Multilamellar vesicle preparation

1. Remove vials from vacuum source (*lipid films can be stored at − 20 °C at this stage, store under nitrogen/argon in the same vial with parafilm, good for at least 1 month).*
2. Hydrate lipid films with 800 μL of **STA Buffer** (Aster-related lipid transfer uses 20 mM HEPES pH 7.5, 300 mM NaCl, 2 mM DTT).
   a. Final liposome Conc.: TopFluor setup – 60 μM; DHE Setup – 260 μM.
3. Vortex the vial until the film has been fully suspended in the buffer (*typically between 1–2 minutes, lipid films will appear cloudy at this stage).*
4. Sonicate both vials at 40 °C for 1 minute.
5. Generate large multilamellar vesicles via 5 freeze-thaw cycles; freeze in liquid nitrogen, and thaw in a 40 °C water bath.
6. Sonicate both vials at 40 °C for 5 minutes.

5.3.5 Liposome extrusion

1. Heat the Avanti extruder heating block on a hotplate to 40 °C.
2. Wash the extruder components with ethanol followed by MilliQ water, then thoroughly dry all components.
3. Assemble extruder components as shown in Fig. 10, wetting the filter support discs and 0.1 μM polycarbonate membrane with buffer (when taking filter support discs, double check you are only taking one, when held up to light you should be able to see through them easily).
4. Test the system for leaks by filling the syringe on the right hand side of the extruder with 800 μL buffer, and pass it through the extruder ~6 times (when inserting syringes, do not twist them as this can result in leaking) – ideally there should be minimal (100 μL) loss of buffer (if you feel no resistance at all, then the membrane has been placed incorrectly).

Fig. 10 Assembly of the extruder components.

5. Fill the syringe in the right-hand side with the lipid vesicle solution and place the extruder assembly on the heating block, allowing to equilibrate for ~5 minutes.
6. Pass the lipid solution through the extruder >13 times, with the final extrusion into the "destination" syringe on the left-hand side.
7. Remove this syringe and immediately transfer the liposomes into a clean glass vial (do not lift the syringes up when removing as this can cause fractures in the syringe)
8. Store liposomes on ice and in darkness.
9. Disassemble and clean the extruder and syringes before extruding the other set of liposomes (filter support discs and membranes are one-time use only).

5.3.6 Microplate-based cholesterol transfer assay

In a non-binding clear-bottom 96-well plate (Greiner Bio-One, cat# 655906) wells are prepared as detailed in the following sections.

5.3.7 Topfluor Setup

Preparation for run:

1. A master mix of donor and acceptor liposomes is prepared in buffer (20 mM HEPES pH 7.5, 300 mM NaCl, 2 mM DTT) affording a final assay concentration for both donor and acceptor as 8 μM (total liposome concentration 16 μM) and a final assay volume of 100 μL.
2. For compound containing runs, protein and compound are incubated at a concentration 20 times the desired assay concentration for 15 min.

The run:

1. 95 μL of liposome mixture are added to each well (maximally 6 wells per run).
2. Fluorescence intensity measurements are performed in a Tecan Spark Cyto plate reader at 25 °C, measuring from the bottom at 10 sec intervals.
3. The excitation filter is set at 485 ± 25 nm and the emission filter to 590 ± 20 nm.
4. After approximately 2 minutes, the measurement is paused, the plate is ejected, and 5 μL protein (or protein + compound pre-mix) is added as quickly as possible and mixed with a pipette to a desired final concentration.
5. The measurement is continued, for a total measuring time of 12 min.
6. Data is normalized to I_0 of the donor + acceptor (before adding protein) and plotted in GraphPad Prism, an example of which is shown below where 10 μM 25-hydroxycholesterol (25-HC) inhibits the OSBP dependent trafficking of TopFluor cholesterol between liposomes (Fig. 11).

5.3.8 DHE Setup

Preparation for run:

1. A master mix of donor and acceptor liposomes is prepared in buffer (20 mM HEPES pH 7.5, 300 mM NaCl, 2 mM DTT) affording a final assay concentration for both donor and acceptor as 12.5 μM (total liposome concentration 25 μM) and a final assay volume of 100 μL.
2. For compound containing runs, protein and compound are incubated at a concentration 20 times the desired assay concentration for 15 min.

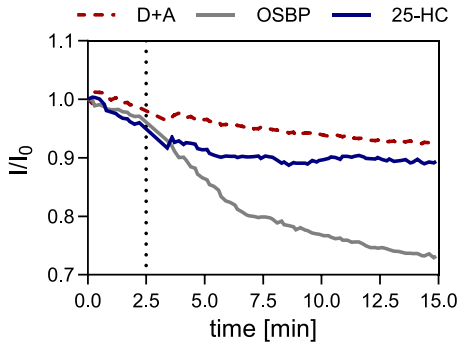

Fig. 11 Inhibition of GST-OSBP(ORD) mediated sterol transport by 25-HC. D = donor liposome, A = acceptor liposome.

The run:

1. 95 μL of liposome mixture is added to each well (maximally 6 wells per run).
2. Fluorescence intensity measurements are performed in a Tecan Spark Cyto plate reader at 25 °C, measuring from the bottom at 10 sec intervals.
3. The excitation filter is set to 340 ± 20 nm and the emission filter to 535 ± 20 nm.
4. After approximately 2 minutes, the measurement is paused, the plate is ejected, and 5 μL protein (or protein + compound pre-mix) is added as quickly as possible and mixed with a pipette to a desired final concentration.
5. The measurement is continued, for a total measuring time of 12 min.
7. Data is normalized to I_0 of the donor + acceptor (before adding protein) and plotted in GraphPad Prism. An example of which is shown below where 5 μM 25-HCTL inhibits the STARD4 dependent trafficking of DHE between liposomes (Fig. 12).

5.4 Notes

- When cleaning the syringes, do not remove the barrel. This is important as doing so can cause degradation of the plunger gasket, breaking the airtight seal. This results in leaking and loss of liposomes.
- The maximum working temperature of the syringes is 40 °C, above this, the adhesives used in the assembly can start to degrade.
- Do not use these 1 mL Hamilton syringes with organic solvents other than ethanol/isopropanol.

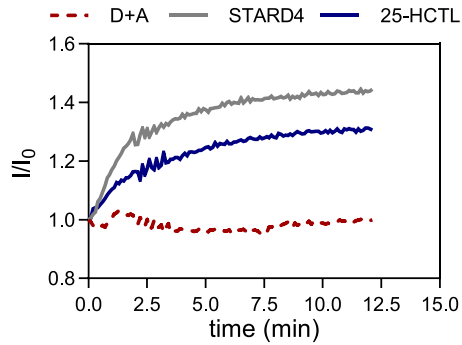

Fig. 12 Inhibition of STARD4 mediated transport of DHE by 25-HCTL. D = donor liposome, A = acceptor liposome.

- The limitations for the sterol transfer assays include the fluorescence interference, photobleaching, kinetic resolution, sample volume, liposome uniformity and composition, and lifetime of liposomes. Fluorescence interference can be mediated by selecting ensuring that inherently fluorescent ligands that may interfere with the readout are used at lower concentrations or observed strictly in a qualitative manner. Photobleaching of FRET partners can be corrected by switching to more robust fluorescent moieties, reducing the intensity of excitation or elongating the kinetic interval. However, these corrections themselves bring about their own complications.
- If a quantitative study is being conducted, then kinetic resolution, especially at the early timepoints, must be high. Optimizing protein concentration, window and liposome composition to ensure that the initial rate of transfer is neither too fast that resolution is not possible or too slow where equilibrium and window suffer the most. Sample volume is a challenging parameter to optimize for these complex systems. With generally less soluble ingredients available making highly concentrated low volume additions can endanger the stability and reproducibility of these assays and so they are preferentially carried out in a 96-well, 100 μL format.

6. Conclusion

This chapter provides protocols for developing and applying assays to identify small molecule inhibitors of STPs. Importantly, the assays serve different purposes depending on the stage of inhibitor discovery. The DSF and FP assays are particularly suitable to HTS, requiring low volumes and protein amounts. In contrast, the FRET-based lipid transfer assay measures a more physiologically relevant transport event but should be reserved for more advanced hits and leads, as it can only be carried out for a handful of compounds at a time. In addition to the proteins mentioned explicitly, we envisage that similar assays could be developed for other lipid transport proteins in a more general manner. We note for example that similar lipid transport assays have also been developed for the ceramide transport protein (CERT) (Samaha et al., 2020). Given the increased importance of LTPs as drug targets, we envisage that similar assay cascades will be increasingly valuable to academic and industrial pharmaceutical labs.

Acknowledgements

The Laraia Laboratory was supported by funding from the Novo Nordisk Foundation (NNF19OC0055818, NNF19OC0058183, NNF21OC0067188), the Carlsberg Foundation (CF19-0072), and the European Union (ERC, ChemBioChol, 101041783). We thank all the people who have contributed to the expression and purification of the proteins and assay development, including Asger Hegelund Olsen, Anna Wiehl Bønke, Mjaftime Ismaili and David Frej Nielsen.

References

Andersen, J.-P., Zhang, J., Sun, H., Liu, X., Liu, J., Nie, J., & Shi, Y. (2020). Aster-B coordinates with Arf1 to regulate mitochondrial cholesterol transport. *Molecular Metabolism, 42*, 101055. https://doi.org/10.1016/j.molmet.2020.101055.

Bro, F. S., Depta, L., Dekker, N. J., Bryce-Rogers, H. P., Madsen, M. L., Præstegaard, K. F., ... Laraia, L. (2025). Identification of a Privileged Scaffold for Inhibition of Sterol Transport Proteins through the Synthesis and Ring Distortion of Diverse, Pseudo-Natural Products. *ACS Cent. Sci. 11*, 136–146. https://doi.org/10.1021/acscentsci.4c01657.

Burgett, A. W. G., Poulsen, T. B., Wangkanont, K., Anderson, D. R., Kikuchi, C., Shimada, K., ... Shair, M. D. (2011). Natural products reveal cancer cell dependence on oxysterol-binding proteins. *Nature Chemical Biology, 7*, 639–647. https://doi.org/10.1038/nchembio.625.

Cigler, M., Imrichova, H., Frommelt, F., Caramelle, L., Depta, L., Rukavina, A., ... Winter, G. E. (2025). Orpinolide disrupts a leukemic dependency on cholesterol transport by inhibiting OSBP. *Nature Chemical Biology, 21*, 193–202. https://doi.org/10.1038/s41589-024-01614-4.

Depta, L., Bryce-Rogers, H. P., Dekker, N. J., Bønke, A. W., Camporese, N., Qian, M., ... Laraia, L. (2025a). Endogenous and fluorescent sterols reveal the molecular basis for ligand selectivity of human sterol transporters. *Journal of Lipid Research, 66*, 100738. https://doi.org/10.1016/j.jlr.2024.100738.

Depta, L., He, N., Madsen, M. L., Nielsen, M. L. H., Bryce-Rogers, H. P., Waterworth, S. C., ... Laraia, L. (2025b). Schweinfurthins and their analogues are highly selective cellular probes for oxysterol-binding protein. *RSC Med. Chem*. https://doi.org/10.1039/D5MD00625B.

Depta, L., Whitmarsh-Everiss, T., & Laraia, L. (2022). Structure, function and small molecule modulation of intracellular sterol transport proteins. *Bioorganic & Medicinal Chemistry, 68*, 116856. https://doi.org/10.1016/j.bmc.2022.116856.

Gomes, C., Oh, S.-D., Kim, J.-W., Chun, S.-Y., Lee, K., Kwon, H.-B., & Soh, J. (2005). Expression of the Putative Sterol Binding Protein Stard6 Gene Is Male Germ Cell Specific1. *Biology of Reproduction, 72*, 651–658. https://doi.org/10.1095/biolreprod.104.032672.

He, N., Depta, L., Rossetti, C., Caramelle, L., Cigler, M., Bryce-Rogers, H. P., ... Laraia, L. (2025). Inhibition of OSBP blocks retrograde trafficking by inducing partial Golgi degradation. *Nature Chemical Biology, 21*, 203–214. https://doi.org/10.1038/s41589-024-01653-x.

Iaea, D. B., Spahr, Z. R., Singh, R. K., Chan, R. B., Zhou, B., Bareja, R., ... Maxfield, F. R. (2020). Stable reduction of STARD4 alters cholesterol regulation and lipid homeostasis. *Biochimica et Biophysica Acta (BBA) - Molecular and Cell Biology of Lipids, 1865*, 158609. https://doi.org/10.1016/j.bbalip.2020.158609.

Laraia, L., Friese, A., Corkery, D. P., Konstantinidis, G., Erwin, N., Hofer, W., ... Waldmann, H. (2019). The cholesterol transfer protein GRAMD1A regulates autophagosome biogenesis. *Nature Chemical Biology, 15*, 710–720. https://doi.org/10.1038/s41589-019-0307-5.

Létourneau, D., Bédard, M., Cabana, J., Lefebvre, A., LeHoux, J.-G., & Lavigne, P. (2016). STARD6 on steroids: solution structure, multiple timescale backbone dynamics and ligand binding mechanism. *Scientific Reports, 6*, 28486. https://doi.org/10.1038/srep28486.

Létourneau, D., Lorin, A., Lefebvre, A., Frappier, V., Gaudreault, F., Najmanovich, R., ... LeHoux, J.-G. (2012). StAR-related lipid transfer domain protein 5 binds primary bile acids[S]. *Journal of Lipid Research, 53*, 2677–2689. https://doi.org/10.1194/jlr.M031245.

Luo, J., Jiang, L.-Y., Yang, H., & Song, B.-L. (2019). Intracellular Cholesterol Transport by Sterol Transfer Proteins at Membrane Contact Sites. *Trends in Biochemical Sciences, 44*, 273–292. https://doi.org/10.1016/j.tibs.2018.10.001.

Luo, J., Yang, H., & Song, B.-L. (2020). Mechanisms and regulation of cholesterol homeostasis. *Nature Reviews. Molecular Cell Biology, 21*, 225–245. https://doi.org/10.1038/s41580-019-0190-7.

Mesmin, B., Bigay, J., Moser von Filseck, J., Lacas-Gervais, S., Drin, G., & Antonny, B. (2013). A Four-Step Cycle Driven by PI(4)P Hydrolysis Directs Sterol/PI(4)P Exchange by the ER-Golgi Tether OSBP. *Cell, 155*, 830–843. https://doi.org/10.1016/j.cell.2013.09.056.

Miller, W. L. (2025). Thirty years of StAR gazing. Expanding the universe of the steroidogenic acute regulatory protein. *Journal of Endocrinology, 264*, e240310. https://doi.org/10.1530/JOE-24-0310.

Ng, M. Y. W., Charsou, C., Lapao, A., Singh, S., Trachsel-Moncho, L., Schultz, S. W., ... Simonsen, A. (2022). The cholesterol transport protein GRAMD1C regulates autophagy initiation and mitochondrial bioenergetics. *Nature Communications, 13*, 6283. https://doi.org/10.1038/s41467-022-33933-2.

Ngo, M., & Ridgway, N. D. (2009). Oxysterol Binding Protein–related Protein 9 (ORP9) Is a Cholesterol Transfer Protein That Regulates Golgi Structure and Function. *MBoC, 20*, 1388–1399. https://doi.org/10.1091/mbc.e08-09-0905.

Roberts, B. L., Severance, Z. C., Bensen, R. C., Le-McClain, A. T., Malinky, C. A., Mettenbrink, E. M., ... Burgett, A. W. G. (2019). Differing activities of oxysterol-binding protein (OSBP) targeting anti-viral compounds. *Antiviral Research, 170*, 104548. https://doi.org/10.1016/j.antiviral.2019.104548.

Rodriguez-Agudo, D., Ren, S., Hylemon, P. B., Redford, K., Natarajan, R., Del Castillo, A., ... Pandak, W. M. (2005). Human StarD5, a cytosolic StAR-related lipid binding protein. *Journal of Lipid Research, 46*, 1615–1623. https://doi.org/10.1194/jlr.M400501-JLR200.

Samaha, D., Hamdo, H. H., Cong, X., Schumacher, F., Banhart, S., Aglar, Ö., ... Arenz, C. (2020). Liposomal FRET Assay Identifies Potent Drug-Like Inhibitors of the Ceramide Transport Protein (CERT). *Chemistry – A European Journal, 26*, 16616–16621. https://doi.org/10.1002/chem.202003283.

Sandhu, J., Li, S., Fairall, L., Pfisterer, S. G., Gurnett, J. E., Xiao, X., ... Tontonoz, P. (2018). Aster Proteins Facilitate Nonvesicular Plasma Membrane to ER Cholesterol Transport in Mammalian Cells. *Cell, 175*, 514–529.e20. https://doi.org/10.1016/j.cell.2018.08.033.

Vassilev, B., Sihto, H., Li, S., Hölttä-Vuori, M., Ilola, J., Lundin, J., ... Ikonen, E. (2015). Elevated Levels of StAR-Related Lipid Transfer Protein 3 Alter Cholesterol Balance and Adhesiveness of Breast Cancer Cells: Potential Mechanisms Contributing to Progression of HER2-Positive Breast Cancers. *The American Journal of Pathology, 185*, 987–1000. https://doi.org/10.1016/j.ajpath.2014.12.018.

Whitmarsh-Everiss, T., Olsen, A. H., & Laraia, L. (2021). Identification of Inhibitors of Cholesterol Transport Proteins Through the Synthesis of a Diverse, Sterol-Inspired Compound Collection. *Angewandte Chemie International Edition, 60*, 26755–26761. https://doi.org/10.1002/anie.202111639.

Wijdeven, R. H., Janssen, H., Nahidiazar, L., Janssen, L., Jalink, K., Berlin, I., & Neefjes, J. (2016). Cholesterol and ORP1L-mediated ER contact sites control autophagosome transport and fusion with the endocytic pathway. *Nature Communications, 7*, 11808. https://doi.org/10.1038/ncomms11808.

Wilhelm, L. P., Wendling, C., Védie, B., Kobayashi, T., Chenard, M., Tomasetto, C., ... Alpy, F. (2017). STARD3 mediates endoplasmic reticulum-to-endosome cholesterol transport at membrane contact sites. *The EMBO Journal, 36*, 1412–1433. https://doi.org/10.15252/embj.201695917.

Yanjanin, N. M., Vélez, J. I., Gropman, A., King, K., Bianconi, S. E., Conley, S. K., ... Porter, F. D. (2010). Linear clinical progression, independent of age of onset, in Niemann–Pick disease, type C. *American Journal of Medical Genetics Part B: Neuropsychiatric Genetics, 153B*, 132–140. https://doi.org/10.1002/ajmg.b.30969.

Zhang, J., Andersen, J.-P., Sun, H., Liu, X., Sonenberg, N., Nie, J., & Shi, Y. (2020). Aster-C coordinates with COP I vesicles to regulate lysosomal trafficking and activation of mTORC1. *EMBO Reports, 21*, e49898. https://doi.org/10.15252/embr.201949898.

Zhong, W., Xu, M., Li, C., Zhu, B., Cao, X., Li, D., ... Yan, D. (2019). ORP4L Extracts and Presents PIP2 from Plasma Membrane for PLCβ3 Catalysis: Targeting It Eradicates Leukemia Stem Cells. *Cell Reports, 26*, 2166–2177.e9. https://doi.org/10.1016/j.celrep.2019.01.082.

CHAPTER TEN

Preparation of K-Ras4B containing synthetic modifications via expressed protein ligation

Jiayue Hu[a], Yong-Xiang Chen[b], and Mark D. Distefano[a,*]
[a]University of Minnesota, Minneapolis, MN, United States
[b]Department of Chemistry, Tsinghua University, Beijing, China
*Corresponding author. e-mail address: diste001@umn.edu

Contents

1. Introduction 212
2. *Escherichia Coli* transformation 216
   2.1 Reagents and materials 217
   2.2 Equipment 217
   2.3 Procedure 217
3. Expression and purification of K-Ras4BΔ15 (MESNA thioester) 218
   3.1 Reagent and materials 218
   3.2 Equipment 219
   3.3 Procedure 219
4. Synthesis of the hypervariable region (HVR) peptide 221
   4.1 Reagents and materials 222
   4.2 Equipment 222
   4.3 Procedure 222
5. Expressed protein ligation 225
   5.1 Reagents and materials 225
   5.2 Equipment 226
   5.3 Procedure 226
6. Purification of the full-length ligated protein product 226
   6.1 Reagents and materials 227
   6.2 Equipment 227
   6.3 Procedure 227
7. Enzymatic activity assay based on the fluorescence of K(Dns)K-Ras4B 228
   7.1 Reagents and materials 229
   7.2 Equipment 229
   7.3 Procedure 229
8. Summary and conclusion 232

Methods in Enzymology, Volume 728
ISSN 0076-6879, https://doi.org/10.1016/bs.mie.2026.01.007
Copyright © 2026 Elsevier Inc. All rights are reserved, including those for text and data mining, AI training, and similar technologies.

Acknowledgements 232
Funding 232
References 232

Abstract

Prenylation is a lipid post-translational modification (PTM) on proteins that plays a critical role in regulating the interaction of proteins with the membrane. Approximately 2 % of proteins in cells are prenylated. Dysregulation of prenylation has been implicated in several diseases where it affects protein localization and function of these proteins in the cell. Ras proteins are members of a broad family of small GTPases that are prenylated and therefore able to localize to the cell membrane and turn on downstream signaling. Because of these roles, inhibiting the prenylation of oncogenic Ras proteins may serve as a method to control Ras mutation-related cancers. To understand the mechanism of Ras protein prenylation and subsequent interactions, chemically modified forms of Ras can be particularly useful. In this chapter, a platform to prepare modified Ras proteins using expressed protein ligation is described. The workflow involves the expression and purification of a truncated Ras thioester protein, the synthesis of a hypervariable region peptide, and the subsequent ligation of these two fragments to obtain the full-length protein.

1. Introduction

Protein prenylation is one type of lipidation that occurs in cells where cysteine residues positioned within a C-terminal CaaX sequence become modified with an isoprenoid. There are two groups of enzymes that catalyze prenylation: farnesyltransferase (FTase), which attaches a 15-carbon isoprenoid lipid from farnesyl diphosphate (FPP), and geranylgeranyl transferases (GGTase type I, GGTase type II, GGTase type III), which attach one or two 20-carbon isoprenoid lipids derived from geranylgeranyl diphosphate (GGPP) (Casey et al., 1989, 1991; Park et al., 1997). FTase prefers sequences when X is Ser, Met, or Gln and modifies cysteine with FPP, whereas GGTase type I prefers Leu and Phe and modifies with GGPP. GGTase type II, also known as RabGGTase, is commonly found to modify proteins in the Rab family, recognizing two cystines located in CC, CCXX, or CXC motifs at the C-termini with GGPP (Kinsella & Maltese, 1992). GGTase type III, a more recently identified enzyme, transfers a geranylgeranyl group to a prefarnesylated protein (Kuchay et al., 2019). Approximately 2 % of proteins in the cell are prenylated and that modification directs them to cell membrane and allows them to transduce signals from receptors to downstream proteins (Marshall, 1993; Palsuledesai & Distefano, 2015; Venkatachalapathy et al., 2025).

Ras proteins are small GTP-binding proteins that switch between binding GTP- and GDP-bound forms. There are three Ras protein isoforms related to cancer: H-Ras, N-Ras, and K-Ras. K-Ras includes two splice variants denoted as K-Ras4A and K-Ras4B, respectively. In the sequence of these Ras proteins, the first 165 amino acids are highly conserved. The last 24 amino acids belong to the hypervariable region, which is unique to each one (Pai et al., 1989; Valencia et al., 1991). After expression in the cell, the Ras protein is prenylated and then translocates to the endoplasmic reticulum and Golgi, where the last three amino acids in the CaaX sequence are cleaved off and the resulting C-terminal prenylcysteine is methylated. After these post-translational modifications, the Ras proteins localize to the cell membrane (Choy et al., 1999; Hancock et al., 1990, 1991). Growth factor binding to receptors on the apical cell surface trigger Ras proteins to bind GTP causing conformational changes resulting in downstream signaling. The most widely known mechanism of Ras signal transduction is the MAP kinase (MAPK) pathway. There, growth factors bind with receptor tyrosine kinases (RTKs) and cause tyrosine kinases to be phosphorylated. SOS binds with the phosphorylated tyrosine kinase and causes Ras to exchange GDP for GTP. The GTP-bound species activates Raf kinases and causes the phosphorylation of MEK which then phosphorylates ERK. ERK then translocates to the nucleus and regulates the transcription of genes related to the growth, proliferation, and cellular differentiation. Under normal circumstances, signaling ends when GTP is hydrolyzed to GDP by Ras. Previous research has shown that inhibiting the prenylation of Ras proteins prevents them from anchoring to the plasma membrane and hence arrests downstream signaling (Downward, 2003; Soriano et al., 2021).

Beyond membrane localization, prenylation also modulates protein-protein interactions. One protein, PDEδ, works as a cytosolic shuttle protein for prenylated Ras proteins, showing no interaction with unprenylated Ras (Chandra et al., 2012; Dharmaiah et al., 2016). Also, two splice variants of SmgGDS show different affinities between the prenylated and unprenylated forms of Ras, which indicates a mechanism for how chaperone proteins may facilitate and regulate the process of lipidation (Berg et al., 2010; Brandt et al., 2020; Schuld et al., 2014). These examples highlight that Ras proteins must be correctly prenylated and localized for effective cell signaling. Oncogenic mutations trap Ras proteins in the "Ras On" mode, leading to uncontrolled signaling, cell division and tumor formation. Because of this, numerous inhibitors have been designed to prevent Ras farnesylation (Simanshu et al., 2017).

Tipifarnib, a farnesyltransferase inhibitor (FTIs), is an anti-tumor drug currently in phase II clinical trials, showing good efficacy in H-Ras related head and neck cancers (Ho et al., 2021). However, in pancreatic adenocarcinoma, a disease driven primarily by K-Ras mutations, FTIs typically yield a poor response (Gilardi et al., 2020). This problem occurs because K-Ras4B can be recognized by both FTase and GGTase-I. Hence, when FTIs are used to inhibit farnesylation, K-Ras4B can be alternatively prenylated by GGTase-I. This situation also indicates that prenylation and membrane association of the K-Ras protein are not straightforward (Baranyi et al., 2020; Ho et al., 2021). The critical role of K-Ras4B mutants in driving cancer underscores the need for new methods that can be used to improve understanding or K-Ras4B prenylation and subsequent downstream interactions.

A number of methodologies have been used to generate chemically modified forms of K-Ras4B incorporating various reporter groups including simple chemical modification and non-canonical amino acid incorporation. Though powerful, these methods both have limitations. Recent developments in peptide/protein chemistry have provided a useful alternative. In native chemical ligation (NCL), a peptide bearing a C-terminal thioester can be ligated with a second peptide bearing an N-terminal cysteine to produce a longer peptide. In that case, transthioesterification followed by an S-to-N acyl shift results in the formation of a native amide bond (Fig. 1). Whereas this can be performed in an iterative manner to generate longer proteins, assembly of large proteins such as K-Ras4B is laborious. To address that limitation, Muir and colleagues developed a modification of that method denoted as expressed protein ligation (EPL) (Muir et al., 1998).

In EPL, the construction of a truncated protein thioester is facilitated by intein-mediated purification with an affinity chitin-binding tag (IMPACT

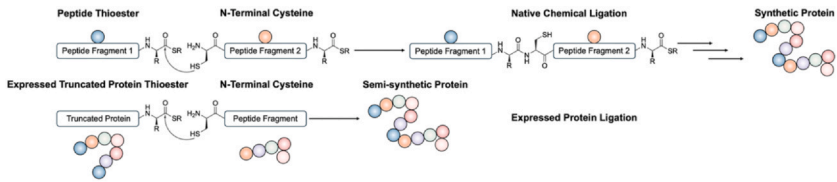

Fig. 1 Method to construct a synthetic protein. The method on top is native chemical ligation (NCL). Protein constructed by NCL requires a large number of peptide fragments. Based on NCL and recombinant protein expression, expressed protein ligation (EPL, the bottom method) streamlines the synthesis.

system). The gene of the target protein is introduced into a plasmid (pTWIN1/pTWIN2) that already encodes an intein-chitin binding domain (intein-CBD) (Evans et al., 1999). The truncated protein fused with the intein-CBD is then captured on a chitin column and can be released via transthioesterification with an external thiol reagent to produce a truncated fragment (containing the intact N-terminal portion of the protein) terminating in a C-terminal thioester. The desired ligated protein is obtained by the same rearrangement mechanism employed for native chemical ligation after reaction with a synthetic peptide (containing the C-terminal portion of the target protein) including an N-terminal cysteine (Fig. 2).

In 2020, Chen and coworkers first introduced the gene for K-Ras4B$^{1-174}$ into a pTWIN2 vector, which is designed for use in the IMPACT system, and transfected the resulting construct into BL21(DE3) cells. The target protein, K-Ras4B$^{1-174}$-MESNA thioester (K-Ras4BΔ15, Table 1), was purified via chitin column chromatography and semisynthetic K-Ras4B protein was successfully constructed and established to be correctly folded (Chen et al., 2010). Those investigators followed up on this by preparing a form of K-Ras4B containing a phosphorylated serine residue at position 181. That protein was prepared by ligating a pentapeptide incorporating the desired phosphoserine with K-Ras4BΔ15 (Zhang et al., 2017). The biological data obtained with that construct clearly established the utility of using EPL to prepare variants of K-Ras4B. In this chapter, a method to construct a semisynthetic K-Ras4B protein containing a dansylated residue near the C-terminus at position 184 (in the wild type sequence) is described

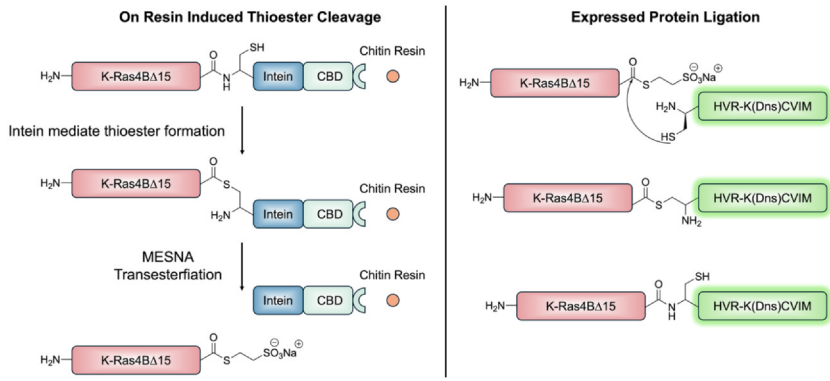

Fig. 2 The construction of semi-synthetic K-Ras4B protein. A K-Ras4BΔ15 will be purified on a chitin column. And a K(Dns)HVR peptide which has a cysteine at N-terminal will be synthesized for EPL.

Table 1 Abbreviations for K-Ras4B species described here.

K-Ras4BΔ15	K-Ras4B$^{1-174}$-MESNA thioester, a truncated form of K-Ras4B protein lacking the last 15 residues, but containing a C-terminal MESNA thioester. Note: wild-type K-Ras4B is 188 residues in length. However, the semisynthetic form generated here has an extra residue due to the addition of a cysteine at the N-terminus of the peptide fragment introduced to permit ligation. The truncated form described here lacks the 14C-terminal residues in wild-type K-Ras4B so it could be named as K-Ras4BΔ14. However, since this method deals with the preparation of the semisynthetic form with an extra cysteine, the species is denoted as K-Ras4BΔ15.
K(Dns)HVR	A dansyl-modified peptide from the hypervariable region of K-Ras4B (residues 175-189). Note: This peptide contains an additional N-terminal cysteine as noted above, relative to the sequence of wild-type K-Ras4B. Peptide sequence: CKKKKKKSKTK(Dns)CVIM
K(Dns)K-Ras4B	A semisynthetic form of K-Ras4B containing a dansylated lysine residue in the hypervariable region at position 185. This protein was generated by ligating K-Ras4BΔ15 (prepared by *E. coli* expression) with the synthetic K(Dns) HVR peptide. Note: This protein contains one additional cysteine as noted above, relative to the sequence of wild-type K-Ras4B making the protein 189 residues in length.

(K(Dns)K-Ras4B, Table 1). This selectively modified form of K-Ras4B protein can be used in a spectrofluorimetric enzyme activity assay, to determine the rate of prenylation of K-Ras4B protein in vitro.

2. *Escherichia Coli* transformation

In this section, the method for transforming competent cells with a plasmid encoding a K-Ras4B$^{1-174}$-Intein-Chitin Binding Domain (CBD) fusion. That fusion protein contains 10 arginine and 10 isoleucine residues; however, the majority of *E. coli* strains produce limited levels of tRNAs for arginine and isoleucine, thereby limiting translation. Here, BL21-CodonPlus (DE3)-RIPL competent cells, a strain containing extra copies of genes that encode the tRNAs for arginine, isoleucine, leucine, and proline was used to ultimately give higher levels of protein product.

2.1 Reagents and materials

- BL21-CodonPlus(DE3)-RIPL competent cells (Agilent Technologies #230280)
- Tris-EDTA buffer (TE buffer, pH 7.5), molecular biology grade, ultrapure (Thermo Fisher #J75893. AE) consists of 10 mM Tris and 1 mM EDTA in high-purity RO water
- β-mercaptoethanol (Sigma-Aldrich #M6250, make a 12.5 M stock solution in TE buffer)
- Super Optimal broth with catabolite repression medium (S.O.C medium, Thermo Scientific #10084318)
- Plasmid DNA encoding K-Ras4B$^{1-174}$-intein-chitin binding domain (pTWIN1-K-Ras4BΔ15) (Zhang et al., 2017)
- Ampicillin sodium salt (Fisher Bioreagents #BP1760-25). Make a 100 mg/mL stock solution in H_2O.
- LB agar with ampicillin (50 μg/mL) plates for culturing *E. coli*

2.2 Equipment

- 15 mL Falcon® conical centrifuge tubes
- Water bath set to 42 °C.
- Culture tubes (5 mL Polypropylene round bottom with 2-position screw caps, Fisher scientific, #14-959-11A)
- Incubation shaker
- Oven incubator set to 37 °C.

2.3 Procedure

1. Thaw 1 tube (100 μL) BL21-CodonPlus(DE3)-RIPL competent cells on ice.
2. Dilute β-mercaptoethanol (12.5 M stock) 1:10 with TE buffer.
3. Transfer the contents of one tube of competent cells (100 μL) to a 14 mL Falcon tube. Mix the competent cells by flicking the tube. *Notice: The size of the tube will affect the heat shock efficiency in step 8.*
4. Add 2 μL of the 10-fold diluted β-mercaptoethanol (Final concentration 25 mM) into the tube of competent cells and gently flick the tube to mix.
5. Incubate the cells on ice for 10 min and flick the tube every 2−3 min
6. Add 10 ng of plasmid DNA (pTWIN1-K-Ras4BΔ15) to the cells and flick the tube to mix. Incubate the tube for 30 min on ice.
7. While the DNA is incubating with the competent cells, prepare a 42 °C water bath and preheat the SOC media in the 42 °C water bath.

8. Heat-shock the *E. coli* in the 42 °C water bath for 30 s
9. Incubate the mixture on ice for 2 min
10. Add 900 μL preheated SOC media to the tube and transfer the mixture into a 5 mL culture tube.
11. Incubate the mixture at 37 °C for 2 h with shaking at 225 rpm.
12. After incubation, spread 20 μL, 50 μL, 100 μL, and 200 μL of the *E. coli* mixture using a sterile spreader or glass beads on LB agar plates that contain ampicillin (50 μg/mL) as an antibiotic.
13. Incubate the plates in an oven incubator at 37 °C for at least 16–20 h and observe the growth of the *E. coli* colonies.

3. Expression and purification of K-Ras4BΔ15 (MESNA thioester)

In this section, the method to express and purify the K-Ras4B-Intein-CBD fusion protein in *E. coli* is described. The purification is performed under non-denaturing conditions and the whole process takes approximately 2 days. Generally, following this procedure yields 5 mg of the protein thioester from 1 L of *E. coli* culture. It is recommended that the purified protein thioester be used immediately for expressed protein ligation. Background hydrolysis of the thioester in buffer over time results in the formation of a C-terminal free acid that cannot undergo ligation.

3.1 Reagent and materials

- Luria Broth (LB), molecular biology grade (Research Products International #L24040-2000.0)
- Ampicillin sodium salt (Fisher Bioreagents #BP1760-25; prepare a 100 mg/mL stock solution in H_2O, sterile filtered through a sterile PES membrane filter (Nalgene Syringe Filter, #725-2520, 25 mm diameter, 0.2 μm)
- Chloramphenicol (Thermo Scientific #AC227920250); prepare a 25 mg/mL stock solution in 75 % ethanol
- Isopropyl-β-D-1-thiogalactoside (IPTG, Goldbio #I2481C50); make a 1 M stock solution in ultrapure water)
- Protease inhibitor cocktail tablets (Roche, cOmplete Tablets, Mini EDTA-free, EASYpack, #04693159001)
- Chitin resin (New England BioLabs, #S6651S)
- Sodium-2-mercaptoethanesulfonate (MESNA, Asta Tech #46862)

3.2 Equipment

- One 500 mL bacterial culture flask and one 5 L bacterial culture flask
- High temperature sterilizer autoclave machine
- Incubation shaker
- UV-Vis spectrophotometer
- 50 mL Falcon® conical centrifuge tubes
- Sonicator
- Amicon® Ultra Centrifugal Filters (10 kDa MWCO, 50 mL, Millipore # UFC901024)
- 15 % SDS-PAGE gels, buffers and apparatus for running them
- LC/ESI-MS (Orbitrap Elite Hybrid Mass Spectrometer, LC column: Agilent, ZORBAX 300 SB-C3, 2.1 × 100 mm, 1.8 μm, Cat: 858750-909)

3.3 Procedure

3.3.1 LB media preparation

1. Prepare 100 mL of LB medium consisting of 2.5 g of LB in ultrapure water in a 500 mL culture flask and 1 L of LB using 25 g of LB in ultrapure water in a 5 L culture flask. Cover these flasks with aluminum foil and autoclave.
2. Cool down the LB media to 50-60 °C. Add 100 μL ampicillin (Final concentration 100 μg/mL) and 200 μL chloramphenicol (Final concentration 50 μg/mL) the flask containing 100 mL of LB media.

3.3.2 Growth of E. coli

1. Pick one single colony from the LB agar plate containing BL21-CodonPlus(DE3)-RIPL competent cells transformants and use it to inoculate the flask containing 100 mL of LB media.
2. Grow the 100 mL LB culture at 37 °C overnight with shaking at 225 rpm.
3. Add 1 mL of ampicillin stock (Final concentration 100 μg/mL) and 2 mL chloramphenicol stock (Final concentration 50 μg/mL) to the 1 L of LB media.
4. Add 10 mL of the overnight culture to the 1 L of LB media.
5. Incubate 1 L LB culture at 37 °C with shaking at 225 rpm.
6. Check the OD_{600} value every 1 h. When the OD_{600} value reaches 0.3, check it every 15-30 min until the OD_{600} value reaches 0.8.

3.3.3 Induce the expression of K-Ras4B$^{1-174}$-Intein-CBD

1. Add 500 μL IPTG stock (Final concentration 0.5 mM) to the 1 L culture to induce protein expression.

2. Reduce the temperature to 16 °C and grow for 20 additional h with shaking at 220 rpm.
3. Recover the cells by centrifugation at 5400 g for 30 min and collect the cell pellet.
4. Transfer the cell pellet to a 50 mL Falcon tube and store a −80 °C prior to lysis.

3.3.4 Purification of K-Ras4BΔ15 (MESNA thioester)

1. Prepare the following buffers:
   - Lysis buffer: 50 mM Sodium HEPES, 500 mM NaCl, 1 mM $MgCl_2$, 0.1 % (v/v) Triton-X100, pH 7.5
   - Column equilibration buffer: 50 mM Sodium HEPES, 500 mM NaCl, 1 mM $MgCl_2$, pH 7.5
   - Column wash buffer: 50 mM Sodium HEPES, 500 mM NaCl, 1 mM $MgCl_2$, pH 7.5
   - Intein splicing buffer: 50 mM Sodium HEPES, 500 mM NaCl, 1 mM $MgCl_2$, 250 mM MESNA, pH 7.5
   - Column elution buffer: 50 mM Sodium HEPES, 500 mM NaCl, 1 mM $MgCl_2$, pH 7.5
   - Stock buffer: 50 mM Sodium HEPES, 100 mM NaCl, 5 mM $MgCl_2$, pH 7.3
2. Thaw the cell pellet in cold lysis buffer (4 °C) on ice. A cell pellet from a 1 L culture requires at least 50 mL of lysis buffer. Add 1 tablet of protease inhibitor cocktail to 50 mL of lysis buffer.
3. Vortex the cell pellet in the lysis buffer to dissolve the protease inhibitor cocktail and resuspend the cells.
4. Separate the resuspended cells into two 25 mL Falcon tubes (labeled as tube 1 and tube 2), and lyse the cell by sonication on ice. Sonication set up: 50 W, 10 s on/10 s off for 10 min for tube 1, exchange the tube and sonicate tube 2 for 10 min. Repeat this 2 for the two tubes. Thus, the total sonication for each tube is 20 min
5. Centrifuge the lysate at 13,000 x g for 30 min at 4 °C and discard the supernatant. Retain a 10 μL sample from the supernatant for SDS-PAGE analysis.
6. Equilibrate the chitin column (2.0 ×6.0 cm, column volume: 10 mL) using 20 column volumes (CV, 200 mL) of equilibrium buffer.
7. Load the supernatant onto the Chitin column (Flow rate: max. 1 mL/min). Retain 10 μL of the eluate from this step for SDS-PAGE analysis.

8. Wash the column with 15 CV (150 mL) wash buffer (Flow rate: 1 mL/min). Retain 10 μL of the eluate from this step every 5 CV (50 mL) for SDS-PAGE analysis.
9. Quickly wash (2−3 mL/min) the column with 5 CV (50 mL) intein splicing buffer. Retain 10 μL of the eluate for SDS-PAGE analysis.
10. Stop the flow and incubate the column with intein splicing buffer for 16 h at 4 °C.
11. Elute the protein with 2 CV (20 mL) elution buffer. Retain 10 μL of the eluate for SDS-PAGE analysis.
12. Analyze the purification using SDS-PAGE with the samples taken (15 % SDS-PAGE, run at 120 V, 90 min).
13. Analyze the purified protein using LC/ESI-MS. Chromatography was performed at a flow rate of 300 μL/min. The buffer system used included solvent A: H_2O/0.1 %TFA and solvent B: CH_3CN/0.1 % TFA. The gradient was as follows: 1 min at 20 % solvent B, 2 min linear gradient to 100 % B, 2 min hold at 100 % B and then 1 min linear gradient down to 20 % B. The retention time for K-Ras4BΔ15 (MESNA thioester) was 3.23 min. The calculated mass of K-Ras4BΔ15 was 19888 Da.
14. Concentrate and exchange the buffer of the eluted solution with stock buffer, using a 50 mL Amicon Ultra Centrifugal Filter (10 kDa MWCO, 5000 × g, 15 min × 6 times at 4 °C). *Note: If the ligation reaction or labeling reaction is not performed immediately after the protein is purified, the addition of 10 mM MESNA is necessary. This helps to suppress the hydrolysis of the thioester.*
15. Estimate the concentration of the purified Ras4BΔ15 with a BCA protein assay using BSA as a standard.
16. Freeze the protein thioester with 10 % glycerol and store at −80 °C.

4. Synthesis of the hypervariable region (HVR) peptide

For expressed protein ligation, an HVR peptide has containing an N-terminal cysteine is required. A variety of modifications can be incorporated into the HVR peptide design using the solid phase peptide synthesis (SPPS). In this section, a peptide incorporating a dansyl lysine (K(Dns)HVR) is described as an example. This modification can be useful for measuring the rate of protein prenylation since lipidation alters the hydrophobicity in proximity to the dansyl group resulting in a substantial (up to an 8-fold increase). The process includes solid peptide synthesis, peptide cleavage, peptide characterization using LC-MS, and peptide purification using HPLC.

4.1 Reagents and materials

- Fmoc-Met-Wang resin (p3bio Systems #51020)
- Amino acids (Select depending on type of modification and make a 333 mM stock solution in DMF)
- Piperidine (Sigma-Aldrich # 104094, prepare a 20 % piperidine solution in DMF)
- HCTU (p3bio Systems #31003, make a 333 mM stock solution in DMF)
- N,N-diisopropylethylamine (DIPEA, Sigma Aldrich #387649, make a 1.3 M stock solution in DMF)
- Acetic anhydride (Ac_2O, Fisher chemical #A10−500)
- Reagent K (5 mL scale, consists of 5 mL Trifluoroacetic acid (TFA, Sigma Aldrich #T6508, Reagent plus, 99 %), 250 mg phenol, 250 μL thioanisole, 125 μL 1,2-ethanedithiol, 250 μLH_2O)
- Diethyl ether, anhydrous (Et_2O, Fisher Chemical # E138500)
- Ninhydrin test reagent:

Reagent A: Dissolve 16.5 mg of KCN in 25 mL of distilled water and dilute 1 mL of this solution with 49 mL of pyridine.

Reagent B: Dissolve 1 g of ninhydrin in 20 mL of n-butanol.

Regent C: Dissolve 40 g of phenol in 20 mL of n-butanol.

4.2 Equipment

- Gyros Chorus automated peptide synthesizer
- 40 mL reaction vessel for Gyros Chorus
- 10 mL polypropylene syringe with bottom filter and cap (Torviq #SF-1000)
- 50 mL Falcon conical centrifuge tube
- Hydrophobic PTFE syringe filter (Millipore Millex-FG, d=25 mm, 0.2 μm)
- Analytical column for LC-MS (Agilent ZORBAX 300-SB-C18, 5 μm, 4.6 ×250 mm)
- Semi-preparative column for HPLC purification (Agilent ZORBAX 300SB-C18, 5 μm, 9.4 ×250 mm)

4.3 Procedure

4.3.1 Synthesis of CVIM tetrapeptide (0.2 mmol scale)

1. Place Fmoc-Met-Wang resin (0.43 mmol/g, use 465 mg) into the instrument's 40 mL reaction vessel.
2. Swell the resin use 10 mL DMF for 10 min and drain away the DMF. Repeat 3 times.

3. Remove the Fmoc group from the resin bound Met residue using 10 mL of 20 % piperidine for 5 min. Repeat 2 times. Next, wash with 10 mL DMF for 30 s. Repeat 2 times.
4. Activate the subsequent amino acids using 3 mL HCTU (stock concentration 333 mM) and 3 mL DIPEA (stock concentration 1.3 M) and couple with the resin for 20 min
5. Drain away the solution containing the activated amino acid and wash the resin with 10 mL DMF for 30 s. Repeat 3 times.
6. Cap any unreacted amine groups after coupling using 3 mL Ac_2O in 3 mL DIPEA (stock concentration 1.3 M) for 15 min
7. Wash the resin with 10 mL DMF.
8. Repeat steps 3 to step 7 including the addition of Fmoc-Cys(Trt)-OH (the fourth residue from the C-terminus).
9. Wash the resin with CH_2Cl_2 and dry the resin in vacuo.
10. Remove the resin from the synthesizer and couple the Fmoc-Lys (Dansyl)-OH manually as described below.

4.3.2 Manual coupling of Fmoc-Lys(Dansyl)-OH

1. Swell the resin using 5 mL DMF for 5 min. Repeat 3 times.
2. Remove the Fmoc group using 5 mL 20 % piperidine in DMF (v/v) for 10 min. Repeat 2 times. *Note: A ninhydrin test is recommended to be performed before and after deprotection. The free amine formed after deprotection is directly related to the yield of the coupling reaction.*
3. Dissolve 2 equivalents (equiv) Fmoc-Lys(Dansyl)-OH (0.2 mmol), 4 equiv HCTU (0.4 mmol), 4 equiv HOAt (0.4 mmol) and 8 equiv DIPEA (0.8 mmol) in 2 mL DMF. Transfer the solution into the syringe (containing a filter) and rotate the syringe at room temperature. Monitor the reaction using the ninhydrin test. Stop the reaction when the ninhydrin test is colorless. Usually, the manual coupling takes 3–6 h.
4. Wash the resin using 5 mL DMF for 5 min. Repeat 3 times.
5. Wash the resin with CH_2Cl_2 and dry the resin in vacuo.
6. Transfer a few resin beads to a 3 mL polypropylene syringe and cleave the peptide with 1–2 mL reagent K.
7. Confirm the presence of the desired peptide using LC-MS. *Note: Steps 6–7 are not required when the ninhydrin test reveals a clear difference before and after coupling. However, the ninhydrin test cannot confirm high conversion. A second coupling reaction is needed when the yield of coupling is low. Swell the resin using 5 mL DMF for 5 min. Repeat 3 times.*

4.3.3 Elongate the remainder of the HVR peptide on peptide synthesizer

1. Put the resin after manual coupling back in the synthesizer and restart the instrument.
2. Swell the resin with 10 mL DMF for 10 min and drain away the DMF. Repeat 3 times.
3. Repeat steps 3–7 in 4.3.1 until the last amino acid in the HVR sequence is coupled to the resin.
4. Dry the resin and store it in a 10 mL polypropylene syringe with bottom filter.

4.3.4 Cleavage of K(Dns)HVR peptide

1. Place 0.1 mmol peptide on resin (half of the resin from the preceding resin) in a polypropylene filter syringe with a cap.
2. Prepare reagent K (~5 mL, consisting of 5 mL TFA, 250 mg phenol, 250 μL thioanisole, 125 μL 1,2-ethanedithiol, 250μLH_2O).
3. Add the Reagent K to the resin and allow to react for 2 h with rotation at room temperature.
4. Cool 50 mL of Et_2O in a dry ice/*iso*-propanol bath.
5. Precipitate the peptide by adding the mixture of reagent K and peptide into the cold Et_2O prepared in step 4.
6. Recover the peptide by centrifugation at 3000 x g for 8 min. Discard the supernatant and dry the pellet in a fume hood at room temperature.
7. Dissolve the peptide in a solvent mixture suitable for LC-MS analysis (2−5 mL, 50 % CH_3CN and 50 % H_2O without TFA).

4.3.5 General procedure of identification of HVR peptide using LC-MS

1. Filter the sample through a 0.2 μm hydrophobic PTFE filter.
2. Perform identification using an analytical column (Agilent ZORBAX 300-SB-C18, 5 μm, 4.6 × 250 mm, solvent system: Solvent A: H_2O/0.1 %TFA; Solvent B: CH_3CN/0.1 %TFA).
3. The gradient for the peptide synthesized here was as follows: 1-5 min hold at 1 % B, 5−30 min linear gradient to 100 % B, 30−35 min hold at 100 % B, 35-46 min linear gradient to 1 % B. The mass for K(Dns)HVR is 2013.1 Da.

4.3.6 General procedure of purification of peptide using HPLC

1. Filter the sample through a 0.2 μm hydrophobic PTFE filter.
2. Perform identification using a semi-preparative scale column (2−10 mg) peptide per injection, Agilent ZORBAX 300SB-C18, 5 μm, 9.4 × 250 mm, solvent system: Solvent A: H_2O/0.1 %TFA; Solvent B: CH_3CN/0.1 %TFA.

3. The gradient for the peptide synthesized here was as follows: 1−5 min, hold at 1 % B; 5−15 min, linear gradient to 20 % B; 15−45 min linear gradient to 40 % B; 45−50 min linear gradient to 100 % B, 50−60 min hold at 100 % B, 60-70 min linear gradient to 1 % B. The target peak has absorbance under 325 nm and 280 nm detector. Flow rate: 2.5 mL/min.
4. Set collection time on fraction collector to collect peaks (44–47 min). Set a volume to collect of no more than 151 drops (about 5 mL) per tube.
5. Collect the fraction(s) that contain the dansyl-modified HVR peptide.
6. Evaporate the CH_3CN using a stream of N_2.
7. Flash-freeze the sample using liquid N_2 and lyophilize it to dryness.

5. Expressed protein ligation

In this section, the general procedure for the preparation of semi-synthetic K-Ras4B containing a chemically modified peptide via expressed protein ligation is delineated. Expressed protein ligation for K-Ras4B can reach close to 100 % conversion by preforming the reaction either for 3 h at room temperature or overnight at 4 °C. These conditions prevent the hydrolysis of thioester, which limits the ligation yield and also slows the speed of the oxidation of cysteine on the peptide. A high concentration of MPAA also accelerates the ligation.

5.1 Reagents and materials

- Ellman's reagent (5,5′-Dithio-*bis*-(2-nitrobenzoic acid), DTNB, ThermoFisher Scientific #22582)
- 4-Mercaptophenylacetic acid (MPAA, Sigma Aldrich #653152)
- K-Ras4BΔ15 (MESNA thioester, stock concentration: 663 μM, buffer in 50 mM Sodium-HEPES, 100 mM NaCl, 5 mM $MgCl_2$, pH 7.3)
- K(Dns)HVR peptide (Stock concentration: 8.9 mM, buffer in 50 mM Sodium-HEPES, 100 mM NaCl, 5 mM $MgCl_2$, pH 7.3)
- Freshly made Ligation buffer (pH 7.3): 50 mM Sodium-HEPES, 100 mM NaCl, 5 mM $MgCl_2$, 100 mM MPAA. Note: it is necessary to adjust the pH after the addition of MPAA by adding NaOH. To prepare 5 mL of this buffer, it typically requires ∼50 μL of 10 M NaOH. It is necessary to vortex this solution when adding the base to dissolve the MPAA.

- TCEP (0.5 M, pH 7.0, Millipore Sigma #646547, Stock concentration: 50 mM, buffer in 50 mM Sodium-HEPES, 100 mM NaCl, 5 mM $MgCl_2$, pH 7.3) Note: It is important to use the neutral TCEP solution to prepare this buffer since use of the hydrochloride salt alters the pH.

5.2 Equipment

- Eppendorf tube (1.5 mL, Thermo Fisher Scientific # 3451)

5.3 Procedure

1. Dissolve the lyophilized peptide in ultrapure water and estimate the concentration of the peptide using Ellman's assay following the manufacturer's protocol.
2. Prepare the ligation buffer before the reaction and purge with Argon (g). Check the pH before using.
3. For 100 μL reaction: pre-mix HVR peptide (11 μL, final concentration 1 mM) with TCEP stock (10 μL, final concentration 5 mM) and incubate for 15 min at room temperature.
4. Begin reaction by adding K-Ras4BΔ15 (15 μL, final concentration 100 μM) and 64 μL ligation buffer (make up to 100 μL). *Note: The concentration of MPAA should be at least 30 mM, which is enough to efficiently catalyze the reaction. Also, if the peptide amount is lower than 3 equivalents of the protein thioester, this reaction needs to be protected by argon gas to prevent oxidation of cysteine.*
5. Maintain the mixture at room temperature and react for at least 3 h. *Note: This condition can also be set to 4 °C and reacted overnight.*
6. Take small aliquots from the ligation reaction mixture every hour and monitor the reaction progress by analyzing via SDS-PAGE. Usually under these conditions, 1−3 μL (2 μg) aliquots of the sample are sufficient for this purpose. The conversion of EPL is determined by densitometry of the Coomassie stained gel.

6. Purification of the full-length ligated protein product

In this section, the purification of the full-length ligated protein is described. For this, a HiTrap desalting column is used to remove small molecules including MPAA and the majority of unreacted peptide. If a cation exchange chromatography step is also needed, the desalting column can also be used to exchange the buffer prior to the next step. A high-affinity cation

exchange column, HiTrap SP FF, is used to separate the full-length protein from the K-Ras4BΔ15 reactant. When the conversion of the ligation is low, this chromatographic step is necessary. However, this results in low overall yield. Hence, to streamline the purification process and obtain maximal product, a high extent of conversion rate for the ligation is preferable.

6.1 Reagents and materials

- Desalting buffer: 10 mM Sodium-HEPES, 150 mM NaCl, 5 mM $MgCl_2$, pH 7.4
- Buffer B: Cation exchange loading buffer: 25 mM NaOAc, 1 mM $MgCl_2$, pH 6.3
- Buffer C: Cation exchange elution buffer: 25 mM NaOAc, 1 mM $MgCl_2$, 1 M NaCl, pH 6.3
- Stock buffer for the full-length product: 10 mM Sodium-HEPES, 150 mM NaCl, 5 mM $MgCl_2$, pH 7.4

6.2 Equipment

- Fast Protein Liquid Chromatography System (FPLC, KNAUER 6.1 L)
- HiTrap™ desalting column (5 mL, Cytiva #17140801)
- HiTrap™ SP FF cation exchange column (5 mL, Cytiva # 17515701)
- Amicon® Ultra Centrifugal Filter (10 kDa MWCO, Millipore # UFC901024)
- SDS-PAGE gels and apparatus
- LC/ESI-MS

6.3 Procedure

1. Buffer preparation:
   - Prepare desalting buffer
   - Prepare cation loading buffer
   - Prepare cation exchange elution buffer NaCl, pH 6.3
   - Prepare stock buffer for full-length protein: 10 mM Sodium-HEPES, 150 mM NaCl, 5 mM $MgCl_2$, pH 7.4

2. *When the conversion in the ligation reaction reaches near 100 %, purify K(Dns) K-Ras4B using a HiTrap Desalting column:*

a) Equilibrate the HiTrap Desalting column with 20 column volumes (100 mL, 1 mL/min) of desalting buffer.

b) Load the ligation reaction mixture (100 μL) onto the column.

c) Wash the column using desalting buffer (1 mL/min, 30 min). The elution is monitored at 280 nm and collect the sample which has A_{280} absorbance (4−9 min, Fractions 4−9).

When the extent of ligation does not reach 100 %, purify K(Dns)K-Ras4B using both a cation exchange column and a desalting column:

a) Equilibrate Hi-Trap SP-XL column using 20 CV (100 mL) cation exchange loading buffer (1 mL/min).

b) Load the fraction(s) from the HiTrap Desalting column mentioned above (500 μL sample per injection) onto the HiTrap SP-FF column. The gradient for each injection: 1−5 min 100 % Buffer B, 5−10 min linear gradient to 100 % Buffer C, 10−40 min maintain at 100 % Buffer C, 40−45 min back to 100 % Buffer B. The flow rate is 1 mL/min. Monitor the purification at 280 nm and collect the product (6−12 min. Fraction 6−12).

c) Exchange the buffer and concentrate the fraction that contains K(Dns)K-Ras4B into a stock solution using ultrafiltration with a 50 mL Amicon centrifugal filter. Typically, 1 mL of protein is diluted into 15 mL and centrifuged at 5000 × g for 30 min until 250 μL remains. Repeat 3 times.

3. Analyze the purified protein (2 μg) and the protein after desalting (2 μg) via SDS-PAGE. Compared to the protein after desalting, the purified protein should have only one band near the 20 kDa marker when stained with Coomassie brilliant blue. That band should be fluorescent under UV light due to the presence of the dansyl group.

4. Verify the correct mass of the full-length protein using LC/ESI-MS. In each run, the column was washed with 20 % solvent B and for the first 1 min followed by elution with a linear gradient from 20 % solvent B to 100 % solvent B over 3 min. The column was then washed with 100 % solvent B for 2 min. The retention time for K(Dns)K-Ras4B was 3.20 min. The calculated mass of K(Dns)K-Ras4B product is 21759 Da.

5. Estimate the concentration of the K(Dns)K-Ras4B using a BCA Assay kit, following the manufacture protocol with BSA as a standard.

6. Add glycerol to the stock protein solution to a final concentration of 10 % (v/v) and flash-freeze the protein at −80 °C.

7. Enzymatic activity assay based on the fluorescence of K(Dns)K-Ras4B

The dansyl group is an environmentally sensitive fluorophore. Because of that, the dansyl group fluorescence is enhanced when prenylation occurs at the adjacent Cys residue. This has been widely used in

enzymatic activity assays to monitor prenylation (Cassidy et al., 1995; Dolence et al., 1995; Pompliano et al., 1992). In most cases, the fluorescent substrate is a pentapeptide containing an N-terminal dansyl-glycine and CaaX sequence. Dansyl-GCVLS and dansyl-GCVIA have been used extensively for such experiments and hence serve as a good point of comparison. However, the ability to prepare proteins incorporating fluorophores near the C-terminus by expressed protein ligation opens up the possibility of measuring the rate of prenylation using full-length protein substrates. Such measurements are potentially more biologically relevant. In this section, the procedure for enzymatic activity measurement using the K(Dns)K-Ras4B protein is described.

7.1 Reagents and materials

- Enzymatic activity assay stock buffer: 0.5 M Tris-HCl pH 7.5, 20 mM $ZnCl_2$, 1 M $MgCl_2$, 0.5 M dithiothreitol (DTT), 0.4 % n-dodecyl-β-maltoside (DDM)
- Enzyme dilution buffer: 50 mM Tris-HCl pH 7.5, 10 μM $ZnCl_2$, 10 mM $MgCl_2$, 5 mM DTT, 1 mg/mL BSA
- Blank sample: 50 mM Tris-HCl pH 7.5, 10 μM $ZnCl_2$, 10 mM $MgCl_2$, 5 mM DTT, 0.04 % DDM
- Farnesyl diphosphate (FPP, stock concentration: 25 mM in $[NH_4][HCO_3]$, pH 8)
- K(Dns)HVR (stock concentration: 178 μM, buffer in 50 mM Sodium-HEPES, 100 mM NaCl, 5 mM $MgCl_2$, pH 7.3)
- K(Dns)K-Ras4B (stock concentration: 77.9 μM, buffer in 50 mM Sodium-HEPES, 100 mM NaCl, 5 mM $MgCl_2$, pH 7.3)
- Yeast farnesyltransferase (yFTase, stock concentration: 54.5 μM) Note: the purification of this enzyme has been previously published (Khatwani et al., 2012). Alternatively, rat farnesyltransferase is commercially available (Sigma-Aldrich, #344145)

7.2 Equipment

- Cary Eclipse Fluorescence Spectrophotometer with multicell holder
- Four quartz cuvettes (JingRui Optical Company, four quartz surfaces, z = 20 mm, sample volume: 100 μL)

7.3 Procedure

1. Sample preparation (for 1 mL), Solution concentrations are list in Table 2:

Table 2 The buffer system of enzymatice activity assay.

	Stock concentration	Volume	Final concentration
Tris HCl pH 7.5	0.5 M	100 μL	50 mM
$ZnCl_2$	20 mM	10-fold dilution 5 μL	10 μM
$MgCl_2$	1 M	10 μL	10 mM
DTT	0.5 M	10 μL	5 mM
DDM	0.4 %	100 μL	0.04 %

2. Add K(Dns)K-Ras4B (13 μL, final concentration 1 μM) or K(Dns) HVR (5.6 μL, final concentration 1 μM) in the buffer prepared above and incubate on ice for 15−30 min. This serves to reduce any disulfide bonds formation that may have formed during protein storage.
3. After incubation, add FPP (4 μL of a 10-fold dilution from stock, final concentration 10 μM) into the reaction mixture.
4. Add ultrapure water (765.4 μL in K(Dns)HVR mixture or 758 μL in K(Dns)K-Ras4B mixture, to make volume up to 1 mL).
5. Dilute the yFTase using enzyme dilution buffer. (Concentration after dilution: 1 μM).
6. Transfer 100 μL of the above reaction mixtures which contains K(Dns) K-Ras4B or K(Dns)HVR to a quartz cuvette and put into the Spectrophotometer.
7. Set the spectrophotometer excitation wavelength to 340 nm and the emission wavelength to 505 nm (Slit widths of 10 nm for both excitation and emission), and the stop time to 180 min
8. Zero the spectrofluorometer using the blank sample.
9. To perform the assay, monitor and record the fluorescence for 2 min to determine the fluorescence of the unmodified peptide or protein substrate. Then remove the cuvette and add yFTase (2 μL, final concentration 20 nM).
10. Mix yFTase briefly using a micropipette and then return the cuvette back into the instrument. Record the reaction progress for 180 min
11. Determine the initial rate of the reaction by determining the slope of the progress curve for the first few minutes after enzyme addition when the rate is linear.

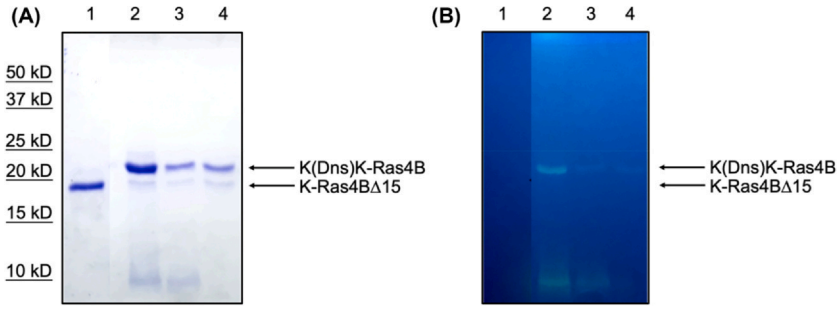

Fig. 3 SDS-PAGE analysis of expressed protein ligation and purification of K(Dns)K-Ras4B. (A) Coomassie blue stained SDS-PAGE for EPL. Lane 1: K-Ras4BΔ15 (2 μg). Lane 2: EPL reaction mixture (1 μL ligation mixture, around 2 μg protein in total. Conversion: 93 % based on densitometry). Lane 3: EPL reaction mixture after centrifugation at 2000 × g (1 μL supernatant). The difference between lane 2 and lane 3 indicates that some precipitation of the K(Dns)K-Ras4B protein after EPL had occurred. However, the protein remaining in solution is enough for purification and the rate measurements. Lane 4: Sample after desalting (1 μg). (B) SDS-PAGE (3A) under UV illumination. Due to the addition of the dansyl group, the protein after EPL is fluorescent, whereas the unreacted/hydrolyzed K-Ras4BΔ15 is not. Excess peptide can be seen in Lanes 2 and 3 but not 4, showing successful removal.

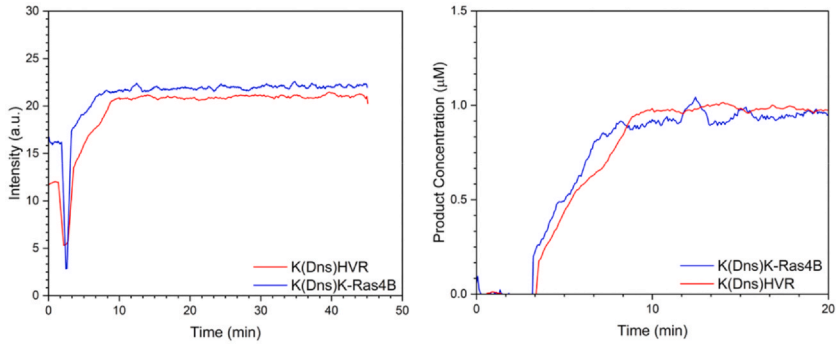

Fig. 4 Progress curves for enzymatic activity assay. Left: Fluorescence intensity versus time plot. Right: Product concentration versus time plot. This was determined by using the equation: [Product] = IP_0*(F-F_0)/(F_f-F_0) where IP_0 is the initial peptide or protein concentration in the reaction, F is the observed fluorescence, F_0 is the initial fluorescence of the unprenylated species and F_f is the fluorescence of the prenylated product upon reaction completion. Both the K(Dns)HVR peptide and the K(Dns) K-Ras4B are effectively farnesylated by the enzyme.

8. Summary and conclusion

This chapter outlines a detailed procedure for the construction of a semi-synthetic K-Ras4B protein, K(Dns)K-Ras4B, using expressed protein ligation. A key feature of this methodology is that it includes a C-terminal peptide incorporating chemical modification that allows it to be used to monitor the rate of enzymatic farnesylation. Since there are numerous chaperones that regulate the prenylation of the K-Ras4B protein in the cell and other proteins that modulate its membrane localization, the strategy described here should be particularly useful for investigating those processes in more detail. An SDS gel used to monitor the expressed protein ligation reaction in shown in Fig. 3. In that gel, the starting K-Ras4BΔ15 migrating near 18 kDa (Fig. 3A, Lane 1) is almost completely consumed after ligation as a new band near 20 kDa is formed (Fig. 3A, Lane 2 and 3). The new, higher molecular weight band is fluorescent, due to the addition of the dansyl group (Fig. 3B, Lanes 2 and 3).

Introduction of the dansyl group allows the prenylation of the full-length K-Ras4B protein to be monitored due to the increase in hydrophobicity of the fluorophore environment. Progress curves showing the increase in dansyl group fluorescence over time using three different substrates are shown in Fig. 4. When that raw data is converted to concentration versus time progress curves, it can be seen that the rates using K(Dns)HVR (HVR peptide containing dansyl lysine) and K(Dns)K-Ras4B (full length protein with dansyl lysine-containing HVR peptide) are similar. These results highlight the utility of this assay to study the prenylation of full-length proteins.

Acknowledgements

The authors acknowledge Dr. Yingchun Zhao and Dr. Peter Villalta in the Analytical Biochemistry Shared Resource of the Masonic Cancer Center, designated by the National Cancer Institute and supported by P30 CA077598 for their assistance with ESI-MS data collection. We would also like to thank Sneha Venkatachalapathy for helpful discussions.

Funding

This work was supported by the National Institute of Health grant R35GM141853.

References

Baranyi, M., Buday, L., & Hegedűs, B. (2020). K-Ras prenylation as a potential anticancer target. *Cancer and Metastasis Reviews, 39*(4), 1127–1141. https://doi.org/10.1007/s10555-020-09902-w.

Berg, T. J., Gastonguay, A. J., Lorimer, E. L., Kuhnmuench, J. R., Li, R., Fields, A. P., et al. (2010). Splice variants of SmgGDS control small GTPase prenylation and membrane localization. *Journal of Biological Chemistry, 285*(46), 35255–35266. https://doi.org/10.1074/jbc.M110.129916.

Brandt, A. C., McNally, L., Lorimer, E. L., Unger, B., Koehn, O. J., Suazo, K. F., et al. (2020). Splice switching an oncogenic ratio of SmgGDS isoforms as a strategy to diminish malignancy. *Proceedings of the National Academy of Sciences, 117*(7), 3627–3636. https://doi.org/10.1073/pnas.1914153117.

Casey, P. J., Solski, P. A., Der, C. J., & Buss, J. E. (1989). P21ras is modified by a farnesyl isoprenoid. *Proceedings of the National Academy of Sciences, 86*(21), 8323–8327. https://doi.org/10.1073/pnas.86.21.8323.

Casey, P. J., Thissen, J. A., & Moomaw, J. F. (1991). Enzymatic modification of proteins with a geranylgeranyl isoprenoid. *Proceedings of the National Academy of Sciences, 88*(19), 8631–8635. https://doi.org/10.1073/pnas.88.19.8631.

Cassidy, P. B., Dolence, J. M., & Dale Poulter, C. (1995). [4] Continuous fluorescence assay for protein prenyltransferases. *Methods in Enzymology, 250*, 30–43. https://doi.org/10.1016/0076-6879(95)50060-X.

Chandra, A., Grecco, H. E., Pisupati, V., Perera, D., Cassidy, L., Skoulidis, F., et al. (2012). The GDI-like solubilizing factor PDEδ sustains the spatial organization and signalling of Ras family proteins. *Nature Cell Biology, 14*(2), 148–158. https://doi.org/10.1038/ncb2394.

Chen, Y.-X., Koch, S., Uhlenbrock, K., Weise, K., Das, D., Gremer, L., et al. (2010). Synthesis of the Rheb and K-Ras4B GTPases. *Angewandte Chemie, 122*(35), 6226–6231. https://doi.org/10.1002/ange.201001884.

Choy, E., Chiu, V. K., Silletti, J., Feoktistov, M., Morimoto, T., Michaelson, D., et al. (1999). Endomembrane trafficking of ras. *Cell, 98*(1), 69–80. https://doi.org/10.1016/S0092-8674(00)80607-8.

Dharmaiah, S., Bindu, L., Tran, T. H., Gillette, W. K., Frank, P. H., Ghirlando, R., et al. (2016). Structural basis of recognition of farnesylated and methylated KRAS4b by PDEδ. *Proceedings of the National Academy of Sciences, 113*(44), https://doi.org/10.1073/pnas.1615316113.

Dolence, J. M., Cassidy, P. B., Mathis, J. R., & Poulter, C. D. (1995). Yeast protein farnesyltransferase: Steady-state kinetic studies of substrate binding. *Biochemistry, 34*(51), 16687–16694. https://doi.org/10.1021/bi00051a017.

Downward, J. (2003). Targeting RAS signalling pathways in cancer therapy. *Nature Reviews. Cancer, 3*(1), 11–22. https://doi.org/10.1038/nrc969.

Evans, T. C., Benner, J., & Xu, M.-Q. (1999). The cyclization and polymerization of bacterially expressed proteins using modified self-splicing inteins. *Journal of Biological Chemistry, 274*(26), 18359–18363. https://doi.org/10.1074/jbc.274.26.18359.

Gilardi, M., Wang, Z., Proietto, M., Chillà, A., Calleja-Valera, J. L., Goto, Y., et al. (2020). Tipifarnib as a precision therapy for *HRAS* -mutant head and neck squamous cell carcinomas. *Molecular Cancer Therapeutics, 19*(9), 1784–1796. https://doi.org/10.1158/1535-7163.MCT-19-0958.

Hancock, J. F., Cadwallader, K., & Marshall, C. J. (1991). Methylation and proteolysis are essential for efficient membrane binding of prenylated p21K-ras(B). *The EMBO Journal, 10*(3), 641–646. https://doi.org/10.1002/j.1460-2075.1991.tb07992.x.

Hancock, J. F., Paterson, H., & Marshall, C. J. (1990). A polybasic domain or palmitoylation is required in addition to the CAAX motif to localize p21ras to the plasma membrane. *Cell, 63*(1), 133–139. https://doi.org/10.1016/0092-8674(90)90294-O.

Ho, A. L., Brana, I., Haddad, R., Bauman, J., Bible, K., Oosting, S., ... Gualberto, A. (2021). Tipifarnib in head and neck squamous cell carcinoma with *HRAS* mutations. *Journal of Clinical Oncology, 39*(17), 1856–1864. https://doi.org/10.1200/JCO.20.02903.

Khatwani, S. L., Kang, J. S., Mullen, D. G., Hast, M. A., Beese, L. S., Distefano, M. D., et al. (2012). Covalent protein–oligonucleotide conjugates by copper-free click reaction. *Bioorganic & Medicinal Chemistry, 20*(14), 4532–4539. https://doi.org/10.1016/j.bmc.2012.05.017.

Kinsella, B. T., & Maltese, W. A. (1992). Rab GTP-binding proteins with three different carboxyl-terminal cysteine motifs are modified in vivo by 20-carbon isoprenoids. *Journal of Biological Chemistry, 267*(6), 3940–3945. https://doi.org/10.1016/S0021-9258(19)50616-0.

Kuchay, S., Wang, H., Marzio, A., Jain, K., Homer, H., Fehrenbacher, N., et al. (2019). GGTase3 is a newly identified geranylgeranyltransferase targeting a ubiquitin ligase. *Nature Structural & Molecular Biology, 26*(7), 628–636. https://doi.org/10.1038/s41594-019-0249-3.

Marshall, C. J. (1993). Protein prenylation: A mediator of protein-protein interactions. *Science (New York, N. Y.), 259*(5103), 1865–1866. https://doi.org/10.1126/science.8456312.

Muir, T. W., Sondhi, D., & Cole, P. A. (1998). Expressed protein ligation: A general method for protein engineering. *Proceedings of the National Academy of Sciences, 95*(12), 6705–6710. https://doi.org/10.1073/pnas.95.12.6705.

Pai, E. F., Kabsch, W., Krengel, U., Holmes, K. C., John, J., & Wittinghofer, A. (1989). Structure of the guanine-nucleotide-binding domain of the Ha-ras oncogene product p21 in the triphosphate conformation. *Nature, 341*(6239), 209–214. https://doi.org/10.1038/341209a0.

Palsuledesai, C. C., & Distefano, M. D. (2015). Protein prenylation: Enzymes, therapeutics, and biotechnology applications. *ACS Chemical Biology, 10*(1), 51–62. https://doi.org/10.1021/cb500791f.

Park, H.-W., Boduluri, S. R., Moomaw, J. F., Casey, P. J., & Beese, L. S. (1997). Crystal structure of protein farnesyltransferase at 2.25 angstrom resolution. *Science (New York, N. Y.), 275*(5307), 1800–1804 (JSTOR).

Pompliano, D. L., Gomez, R. P., & Anthony, N. J. (1992). Intramolecular fluorescence enhancement: A continuous assay of Ras farnesyl:protein transferase. *Journal of the American Chemical Society, 114*(20), 7945–7946. https://doi.org/10.1021/ja00046a070.

Schuld, N., Hauser, A., Gastonguay, A., Wilson, J., Lorimer, E., & Williams, C. (2014). SmgGDS-558 regulates the cell cycle in pancreatic, non-small cell lung, and breast cancers. *Cell Cycle (Georgetown, Tex.), 13*(6), 941–952. https://doi.org/10.4161/cc.27804.

Simanshu, D. K., Nissley, D. V., & McCormick, F. (2017). RAS proteins and their regulators in human disease. *Cell, 170*(1), 17–33. https://doi.org/10.1016/j.cell.2017.06.009.

Soriano, O., Alcón-Pérez, M., Vicente-Manzanares, M., & Castellano, E. (2021). The crossroads between RAS and RHO signaling pathways in cellular transformation, motility and contraction. *Genes, 12*(6), 819. https://doi.org/10.3390/genes12060819.

Valencia, A., Chardin, P., Wittinghofer, A., & Sander, C. (1991). The ras protein family: Evolutionary tree and role of conserved amino acids. *Biochemistry, 30*(19), 4637–4648. https://doi.org/10.1021/bi00233a001.

Venkatachalapathy, S., Lichtenfels, C., Wagner, C. R., & Distefano, M. D. (2025). Engineering protein prenylation: An emerging tool for selective protein modification. *Biochemical Society Transactions, 53*(04), 1129–1149. https://doi.org/10.1042/BST20253076.

Zhang, S.-Y., Sperlich, B., Li, F.-Y., Al-Ayoubi, S., Chen, H.-X., Zhao, Y.-F., et al. (2017). Phosphorylation weakens but does not inhibit membrane binding and clustering of K-Ras4B. *ACS Chemical Biology, 12*(6), 1703–1710. https://doi.org/10.1021/acschembio.7b00165.

CHAPTER ELEVEN

A fluorescence and HPLC-based activity assay system for lipid-modifying enzymes: Lipin/Pah phosphatidic acid phosphatase as an optimized example

Franceine S. Welcome, Lingshuang Wu, Tereza Vitkovska, Jiyao Chai, Shujuan Gao, and Michael V. Airola*
Department of Biochemistry and Cell Biology, Stony Brook University, Stony Brook, NY, United States
*Corresponding author. e-mail address: michael.airola@stonybrook.edu

Contents

1. Introduction 236
2. Purification 239
   2.1 Equipment 239
   2.2 Buffers and reagents 240
   2.3 Transformation 240
   2.4 Expression 241
   2.5 Purification 241
3. Activity assay 243
   3.1 Equipment 244
   3.2 Buffers and reagents 244
   3.3 Micelle preparation 245
   3.4 Liposome preparation 245
   3.5 Assay protocol 245
4. Quantification of DAG production 246
   4.1 Diacylglycerol standard curve 246
   4.2 Sample data and quantification 247
Acknowledgements 248
References 248

Abstract

Quantitating the enzymatic activity of lipid-modifying enzymes is a critical aspect of their study. Here, we describe a general approach to measure the activity of lipid-modifying enzymes using fluorescently labeled lipid substrates. This approach uses high-performance liquid chromatography (HPLC) to separate the resulting fluorescent lipid product(s) of enzymatic catalysis from the fluorescent lipid substrates, and to

Methods in Enzymology, Volume 728
ISSN 0076-6879, https://doi.org/10.1016/bs.mie.2026.01.003
Copyright © 2026 Elsevier Inc. All rights are reserved, including those for text and data mining, AI training, and similar technologies.

concurrently quantify the products using a fluorescence detector. Here, we focus on a version of this assay that has been optimized for lipin/Pah phosphatidic acid phosphatases, a class of enzymes that catalyze the magnesium-dependent hydrolysis of phosphatidic acid into diacylglycerol. Details for delivery of a fluorescent lipid substrate to an enzyme in detergent mixed-micelles and liposomes are provided. We also describe methods to purify recombinant lipin/Pah phosphatidic acid phosphatases using *E. coli* as an overexpression system, which can present challenges given the role of phosphatidic acid as a central precursor in bacterial phospholipid synthesis. Overall, the fluorescence and HPLC-based activity assay described here is generally applicable to any lipid modifying enzyme and additionally allows for the detection of unsuspected products that would remain undetected by conventional methods.

1. Introduction

Lipins/Pahs are magnesium-dependent phosphatidic acid phosphatases (PAPs) that catalyze the hydrolysis of phosphatidic acid (PA) to generate diacylglycerol (DAG) and inorganic phosphate (Han, Wu, & Carman, 2006). Lipins catalyze the penultimate step of triglyceride synthesis (Takeuchi & Reue, 2009), thus playing a major role in *de novo* phospholipid biosynthesis (Khalil, Blais, Figeys, & Yao, 2010; Reue & Wang, 2019), lipid metabolism (Coleman & Mashek, 2011; Siniossoglou, 2013), and energy storage (Reue & Donkor, 2006) (Fig. 1). Lipins are evolutionarily conserved

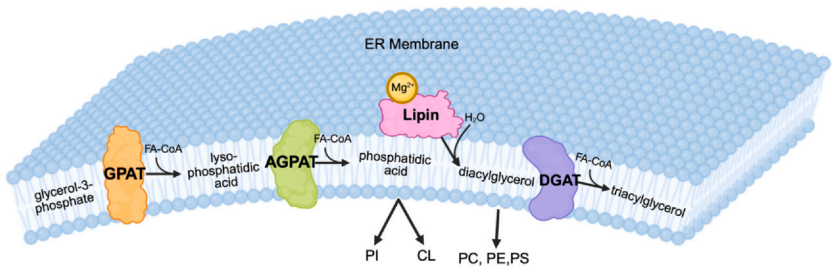

Fig. 1 The glycerol-3-phosphate pathway. Lipin catalyzes a key branch point in the glycerol-3-phosphate pathway. Lipin is the only peripheral membrane protein in this pathway. The other members, glycerol phosphate acyltransferase (GPAT), acylglycerol phosphate acyltransferase (AGPAT), and diacylglycerol acyltransferase (DGAT) are integral membrane proteins and use one molecule of fatty acyl coenzyme A (FA-CoA) to generate their product. Lipin is a magnesium-dependent enzyme that generates diacylglycerol (DAG) from the hydrolysis of phosphatidic acid (PA). DAG is a starting material for the *de novo* biosynthesis of major membrane phospholipids phosphatidylcholine (PC), phosphatidylethanolamine (PE), and phosphatidylserine (PS). PA is a precursor for other lipids such as phosphatidylinositol (PI) and cardiolipin (CL).

from mammals (Péterfy, Phan, Xu, & Reue, 2001; Reue & Wang, 2019) to plants (Chapman, Aziz, Dyer, & Mullen, 2019; Eastmond et al., 2010; Nakamura et al., 2009; Xu & Shanklin, 2016) and yeast (Pascual & Carman, 2013; Pillai, Shukla, Gautam, & Rahaman, 2017), with the number of orthologs varying (Harris & Finck, 2011).

One of the first enzymatic assays to be developed that allowed the characterization of PAP activity involved monitoring the release of ^{32}P-labeled inorganic phosphate from phosphatidic acid (Carman & Lin, 1991; Martin, Gomez-Muñoz, Jamal, & Brindley, 1991; Walsh & Bell, 1986). This assay represented a critical breakthrough in the field and allowed several seminal discoveries and studies to be conducted (Donkor, Sariahmetoglu, Dewald, Brindley, & Reue, 2007; Donkor et al., 2009; Eaton, Mullins, Brindley, & Harris, 2013; Eaton et al., 2014; Granade & Harris, 2018; Han & Carman, 2010; Han et al., 2006; Han, Siniossoglou, & Carman, 2007; Schweitzer et al., 2019; Stukey, Han, & Carman, 2023). This radioactive assay remains a common method to assess lipin/Pah PAP activity. In these assays, the PA substrate for PAP assays is prepared by reacting γ^{32}P-labeled adenosine triphosphate and unlabeled DAG using bacterial DAG kinase to generate ^{32}P-labelled PA that can be isolated using preparative TLC (Walsh & Bell, 1986). This ^{32}P-PA can be used as a substrate for lipin, which generates ^{32}P-inorganic phosphate that can be separated from the ^{32}P-labeled PA substrate and newly generated DAG using an organic extraction. The radioactive ^{32}P-inorganic phosphate generated from the reaction is present in the aqueous phase, while unreacted ^{32}P-labelled PA and the DAG generated remain in the organic phase. The radioactive ^{32}P-inorganic phosphate can then be quantified. This approach has many advantages including using a natural PA substrate that only differs from native PA by the isotope of phosphorus but has the disadvantage that the generation of ^{32}P-labeled PA requires certain expertise and equipment and must be used within the relatively short half-life limits of ^{32}P (Dey, Han, & Carman, 2020).

Alternative approaches have more recently been described. One report used NBD-PA (1-hexanoyl-2-[6-[(7-nitro-2–1,3-benzoxadiazol-4-yl)amino] hexanoyl]-*sn*-glycero-3-phosphate) as a substrate and separated the enzymatic product, NBD-DAG, using TLC (Sasser et al., 2012). Another group utilized HPLC to quantify lipin activity from mammalian tissues using solubilized fluorescently labeled PA as a substrate (Burgdorf, Prey, Richardt, & Kurz, 2008; Burgdorf et al., 2009). Our group later modified these approaches to use HPLC with a fluorescence detector to both separate NBD-PA from the

NBD-DAG generated and quantitate lipin/Pah PAP activity from purified recombinant protein.

This approach can be applied to homogenized tissues (Burgdorf et al., 2008; Burgdorf et al., 2009; Csaki et al., 2014; Nadra et al., 2012), cell lysates (Han et al., 2006), and purified recombinant protein (Gao, Carrasquillo Rodríguez, Bahmanyar, & Airola, 2024; Khayyo et al., 2020; Vitkovska et al., 2025). However, production of recombinant protein in *E. coli* requires careful preparation, because PA is the precursor for all phospholipid synthesis in *E. coli*. Thus, overexpression of active lipin/Pah PAPs in our hands has often resulted in several observations including difficultly in pelleting of the *E. coli* cells upon centrifugation due to accumulated DAG in cells. These artifacts can be avoided by expressing inactive lipin/Pah PAPs, which suggests overexpression of lipin/Pah PAPs can be somewhat toxic. Thus, as part of this chapter, we first describe approaches to produce active recombinant lipin/Pah PAP proteins using *E. coli* as an overexpression system. We then describe the incorporation of NBD-PA into Triton X-100 mixed micelles and liposomes as a method to deliver the substrate to the enzyme. Finally, we described the activity assay

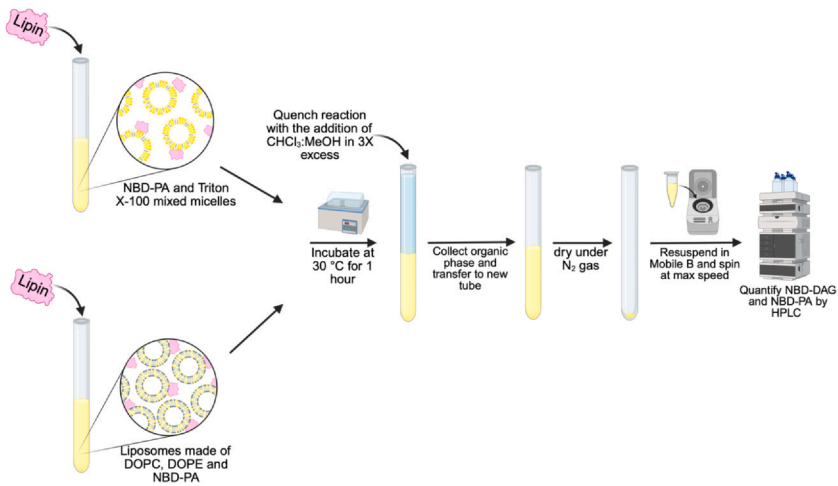
Lipin
NBD-PA and Triton X-100 mixed micelles
Quench reaction with the addition of CHCl3:MeOH in 3X excess
Incubate at 30 °C for 1 hour
Collect organic phase and transfer to new tube
dry under N2 gas
Resuspend in Mobile B and spin at max speed
Quantify NBD-DAG and NBD-PA by HPLC
Lipin
Liposomes made of DOPC, DOPE and NBD-PA

Fig. 2 Fluorescence-based phosphatidic acid phosphatase activity assay. Either mixed micelles (top) or liposomes (bottom) are combined with protein in 1:1 ratio, then incubated at 30 °C for one hour. The reaction is quenched with the addition of chloroform ($CHCl_3$) and methanol (MeOH) in a 1:1 ratio, in three times excess of the reaction volume. The lower organic phase is collected and transferred to a new tube, where it is dried under nitrogen gas. The lipids are then resuspended in Mobile phase B, then spun at max speed. This mixture is then applied to HPLC to quantify and separate peaks corresponding to NBD-DAG and NBD-PA.

used in our lab which is broadly applicable to many other lipid modifying enzymes (Fig. 2) and was recently used by our lab to detect unanticipated products generated by the lipid modifying enzyme DDHD2, which possesses dual enzymatic functionality (Wu et al., 2025).

2. Purification

The protein preparation method described here has been successful for minimal lipin constructs that do not possess the long linker between the N-Lip and C-Lip regions, such as *Tt* Pah2 (Khayyo et al., 2020), mouse lipin-2 (Khayyo et al., 2020), and other minimal lipin/Pah PAPs from yeast and mammals (unpublished data). This method has also shown some success with full length lipins from yeast. Typically, these constructs are expressed in the ppSUMO vector with a SUMO tag, in addition to 6X-His tag, to increase protein solubility. This SUMO tag is cleaved with ULP1 protease after the nickel purification step. Expression of these active proteins in *E. coli* often results in the accumulation of DAG within cells, making the cells harder to pellet due to the accumulation of neutral lipids, even with prolonged and high force centrifugation. In fact, when overexpressing active lipin/Pah PAPs, it is normal for the pellets to have a slimy consistency. In this case, it is sufficient to pour off as much media as possible after centrifugation and flash freeze the cell pellet.

The purification buffers described below have been optimized by a thermal shift assay that demonstrated phosphate buffer at pH 7, specifically containing monobasic potassium phosphate and dibasic sodium phosphate, best stabilized a series of lipin/Pah PAP proteins. Additionally, the addition of the detergent Triton X-100 in the lysis buffer aids in solubilizing the protein from the membrane but is no longer necessary for the soluble protein after lysis, and it can be excluded from any subsequent buffers involved in washing and eluting the recombinant proteins from Ni-NTA (Nickel nitrilotriacetic acid) affinity columns.

2.1 Equipment

- Incubator
- Incubated Shaker
- 2.5 L Ultra Yield Flasks (Thompson Instrument Company #931136-B)
- Refrigerated Centrifuge
- Sonicator

- Fast Protein Liquid Chromatography (FPLC) Instrument
- HiLoad 26/600 Superdex 75 pg Gel Filtration Column (GE Healthcare)
- Ni-NTA Resin
- Gravity Filter Column
- Spectrophotometer
- Protein Concentration Spin Columns

2.2 Buffers and reagents

- Luria Broth (LB) Media
- *E. coli* BL21 (DE3) RIPL cells
- Glycerol
- Terrific Broth (TB) Media
- Kanamycin sulfate
- Isopropyl β-D-1-thiogalactopyranoside (IPTG)
- β-Mercaptoethanol (βME)
- Phenylmethanesulfonyl fluoride (PMSF)
- SDS-PAGE tank setup
- Ubiquitin-like protease 1 (ULP1)
- Dithiothreitol (DTT)
- Precision Plus Protein Dual Color Standards (Bio-Rad Cat#: 1610374)
- Lysis Buffer: [100 mM KH_2PO_4+ Na_2HPO_4 buffer pH 7, 500 mM NaCl, 60 mM imidazole, 5 % (v/v) glycerol, 1 % Triton X-100, 2 mM βME, 0.5 mM PMSF]
- Wash Buffer: [100 mM KH_2PO_4 + Na_2HPO_4 buffer pH 7, 500 mM NaCl, 60 mM imidazole, 5 % (v/v) glycerol, 2 mM βME]
- Elution Buffer: [100 mM KH_2PO_4 + Na_2HPO_4 buffer pH 7, 500 mM NaCl, 300 mM imidazole, 5 % (v/v) glycerol, 2 mM βME]
- Gel Filtration Buffer: [20 mM Tris pH 8, 150 mM NaCl, 10 mM βME, 1 mM DTT]

2.3 Transformation

1. Thaw 50 μL of *E. coli* BL21 (DE3) RIPL cells on ice and add to 14 mL round bottom tube on ice.
2. Add 100 ng of lipin/Pah plasmid to round bottom tube with competent cells.
3. Incubate tube on ice for 15 min.
4. Heat shock tube at 42 °C for 45 s
5. Return tube to ice for 2 min.
6. Add 200 μL of LB media to tube and transfer tube to incubator to shake at 37 °C for one hour at 250 rpm.

7. Plate 150 µL of transformation reaction on LB agar plate with appropriate antibiotic.
8. Allow plate to dry then incubate overnight at 37 °C to allow for colony growth.

2.4 Expression

Day 1 – *Starter Culture*.

1. Pick a single colony and use to inoculate 20 mL of LB supplemented with appropriate antibiotic in a 250 mL Erlenmeyer flask.
2. Grow this starter culture overnight with shaking at 37 °C and 250 rpm.
3. Prepare 1 L of TB media supplemented with 4 mL glycerol in 2.5 L Ultra Yield flask, seal top of flask with foil, and autoclave. Allow to cool overnight.

Day 2 – *Expression*.

1. Pre-warm TB by placing in incubator shaker at 37 °C for 30 min.
2. Add appropriate antibiotic, then inoculate each liter with 15 mL of the overnight starter culture.
3. Shake at 250 rpm until an OD_{600} of ~1.2 is reached.
4. Cool cultures at 10 °C with shaking for two hours.
5. Induce cultures with the addition of a final concentration of 30 µg/mL IPTG.

   Note: Increased concentrations of IPTG can be used to increase protein expression.
6. Increase incubator shaker temperature to 15 °C and allow expression for ~18 h.

Day 3 – *Harvesting Culture*.

1. Transfer cultures to centrifuge tubes and spin down in pre-cooled centrifuge for 15 min at 4000 rpm (3320 × g) and 4 °C to pellet cells.
2. Pour off media, then transfer cell pellet to 50 mL falcon tube. Store cell pellets at −80 °C.

   Note: Very active proteins will not form firm cell pellet due to accumulation of diacylglycerol. In this case, pour off as much media as possible and flash freeze 'slimy' pellet.

2.5 Purification

Nickel Affinity Chromatography.

1. Remove cell pellet from −80 °C and allow to thaw at room temperature for one hour.
2. Resuspend the pellet in the least amount of lysis buffer possible to obtain a homogenous mixture. To mix, invert tube and vortex,

ensuring as little bubbles as possible. Once resuspended, decant mixture into ice cold metal beaker.

Note: Add PMSF and βME to lysis buffer directly before using. PMSF has a short half-life in water.

3. Sonicate this mixture at 85 % power for 5 min total, in 1 min intervals with bursts of 2 s on/ 2 s off on ice. Make sure mixture stays cold. Replace ice under metal beaker as necessary. Take an SDS-PAGE sample after sonication as 'total lysate'.

   Note: At this step it is crucial to avoid foaming and heating of the cell lysate, as this can denature proteins. Lysing of cells can be monitored by visual cues, such as the clarification of cell lysate during sonication, although this does not always occur.

4. Transfer cell lysate into precooled centrifuge tubes. Spin down at 26,000 rpm (81,770 × g) at 4 °C for 30 min to pellet cell debris. During this time, equilibrate 4 mL Ni-NTA resin with wash buffer.

   Note: The volume of Ni-NTA resin described here is a starting point and can be adjusted in subsequent purifications by monitoring the amount of protein lost during the wash step.

5. Incubate soluble fraction with equilibrated Ni-NTA beads and gently agitate this mixture at 4 °C for one hour to bind protein with beads. Take an SDS-PAGE sample at this time as 'soluble fraction'.

6. Pour this mixture into gravity column with filter. Take first few drops from the gravity column as SDS-PAGE sample as 'flow-through' fraction.

7. Wash the nickel column with 5–15 column volumes of wash buffer. Take first few drops from the gravity column as SDS-PAGE sample as 'wash' fraction.

   Note: The wash volume described here is just a starting point and can be adjusted as necessary in subsequent purifications by monitoring the purity of the protein eluted from the nickel column. If there is a lot of contamination from proteins that are nonspecifically bound to the column, increase the wash volume. Add βME to buffers right before using.

8. Elute protein in 10 × 1 mL fractions with elution buffer. Keep fractions on ice and take a gel sample of each.

   Note: Gravity column can be kept at room temperature as long as buffers are kept ice cold.

9. Run each SDS-PAGE sample on a gel and visualize protein with Coomassie Blue staining. Pool fractions containing protein for size exclusion chromatography.

10. Add ULP-1 protease to cleave SUMO tag (if needed). Store at 4 °C overnight.

Gel Filtration.

1. Filter gel filtration buffer with 0.22 μm filter. Add βME and DTT directly before use and keep buffer cold.
2. Prepare Superdex 75 column by washing with 1 column volume of gel filtration buffer on FPLC.
3. Load pooled nickel elution fractions onto the column, follow with isocratic elution using gel filtration buffer. Collect fractions after the void volume.
4. Concentrate protein fractions using spin filters and refrigerated centrifuge. Use spectrophotometer to determine protein absorbance at 280 nm and calculate protein concentration. Aliquot protein and flash freeze in PCR tubes in liquid nitrogen. Store at −80 °C.

3. Activity assay

When generating Triton X-100 mixed micelles and liposomes with fluorescently labeled lipids, it is essential to keep them protected from light as much as possible, typically by using amber vials for storage and covering preparatory glass tubes with foil. Incorporating PA into liposomes and mixed micelles can require more time than other lipids, due to the small, negatively charged headgroup of PA. During the setup of a series of enzymatic reactions, it is imperative to keep all samples ice cold until they are placed in a water bath to prevent starting the reaction prematurely.

It is absolutely critical to ensure the reaction rate is linear with respect to both time and amount of enzyme added to the reaction. Typically, an ideal amount of enzyme for the linear range will turn over about 10–20 % of substrate, but this amount may vary.

Quenching of the reaction involves the purification of lipids using the addition of a 1:1 ratio of chloroform and methanol, first described by Folch (Folch, Lees, & Stanley, 1957) and Bligh and Dyer (Bligh & Dyer, 1959). In this assay, the organic phase is collected, as we monitor the amount of NBD-DAG generated. The aqueous phase contains the inorganic phosphate released as well as protein. Due to this, it is essential to collect as much of the organic layer as possible without collecting the protein at the interface between the organic and aqueous phases because large amounts of protein can clog the HPLC column. As an additional

method to prevent this, there is also a high-speed spin at the final step of this assay that should pellet any remaining denatured protein. When removing the sample to be directly applied to HPLC, one should avoid disturbing any potential pellet at the bottom of the tube.

Extensive controls have been done to ensure the method detailed below generates unilamellar vesicles. Dynamic light scattering was performed to confirm the size of the vesicles (Choi et al., 2023), as well as other characterization methods like dithionite quenching to determine unilamellarity.

3.1 Equipment

- High-Performance Liquid Chromatography (HPLC) instrument (Agilent)
- Spectra C8SR column (Peeke Scientific, 3 μm particle, 3.0 × 150 mm)
- Tip sonicator
- Centrifuge
- Heated water bath
- Vortexer
- Water bath sonicator
- Nitrogen gas blowdown system
- Hamilton syringe
- Amber HPLC vials

3.2 Buffers and reagents

- Triton X-100 detergent
- 14:12 NBD-PA (1-myristoyl-2-[12-[(7-nitro-2-1,3-benzoxadiazol-4-yl) amino]dodecanoyl]-sn-glycero-3-phosphate, Avanti)
- NBD-DAG (1-NBD-1,2-*bis*[O-decanoyl-*sn*-glycerol], Cayman)
- 2X Micelle Assay Buffer: [40 mM Tris pH 7.5, 20 mM $MgCl_2$, 300 mM NaCl, 4 mM βME]
- Liposome Buffer: [50 mM HEPES pH 8, 50 mM NaCl]
- HPLC grade Chloroform
- HPLC grade Methanol
- Mass spectrometry grade ammonium formate
- LC/MS grade Formic acid
- HPLC Mobile Phase A: [1 mM ammonium formate, 0.2 % formic acid in HPLC grade H_2O]
- HPLC Mobile Phase B: [1 mM ammonium formate, 0.2 % formic acid in HPLC grade MeOH]

3.3 Micelle preparation

1. Dry the appropriate amount of NBD-PA under nitrogen gas to have the bulk PA concentration at 200 μM when resuspended in the volume of Triton X-100 that will allow 50 μL of micelles per reaction.

   Note: Using 100 μM NBD-PA = 3 mol% gives a good signal without maxing out the detector on HPLC. Lower concentrations down to 20 μM may be sufficient.
2. Resuspend dried NBD-PA in the appropriate concentration of Triton X-100 to generate micelles with desired mol% of NBD PA in your final volume. Pipet up and down to mix.
3. Solubilize NBD-PA by placing tube in water bath sonicator in 15 min bursts, pipetting up and down between, for up to an hour.

   Note: NBD-PA is properly solubilized when the solution is homogeneous and clear. Keep micelles protected from light.

3.4 Liposome preparation

1. Dry appropriate amounts of DOPC, DOPE, and NBD-PA in 80:20:2 ratio under nitrogen gas to give final concentrations of 1 mM DOPC, 0.25 mM DOPE and 25 μM NBD-PA when resuspended.
2. Resuspend lipids in the appropriate volume of liposome buffer and pipet up and down.
3. To generate large unilamellar vesicles, freeze liposome solution in liquid nitrogen, then thaw in water. Repeat 6 times for a total of 7 freeze/thaw cycles.
4. Sonicate in water bath sonicator for five minutes. Keep protected from light.

3.5 Assay protocol

1. Dilute protein to desired concentrations in 2X activity assay buffer with βME added fresh prior to use. Keep on ice.
2. Mix protein and micelles/liposomes in 1:1 ratio, typically 50 μL of each is suitable. Keep tubes protected from light.
3. Incubate at 30 °C in water bath for one hour.

   Note: This temperature is just a suggestion and can be varied. However, 37 °C can sometimes denature PAP enzymes.
4. Quench reactions with the addition of 1:1 HPLC grade chloroform:methanol in 3 times excess of reaction volume.
5. Vortex each reaction for 10 s to mix. Then spin down for 2 min at 2000 rpm (771 × g) at room temperature to separate aqueous and organic phases.

6. Use Hamilton syringe to transfer organic phase (bottom) to fresh tube without collecting any of the aqueous phase. Dry organic phase under nitrogen gas.

   Note: Aqueous phase contains denatured protein, and collecting it and applying to HPLC can clog column.
7. Resuspend organic phase in 100 μL of Mobile Phase B. Spin at max speed in tabletop centrifuge for five minutes.
8. Transfer 60 μL of reaction to amber HPLC vial without collecting from or disturbing the bottom of the tube.
9. Inject 10 μL of reaction onto HPLC column and run the following method with these parameters:

   Parameters and acquisition settings:
   Flow rate: 0.5 mL/min
   Method Length: 16 min
   PMT Gain: 10
   Excitation wavelength: 470 nm
   Emission wavelength: 530 nm

Method settings.

Time (min)	% Mobile A	% Mobile B
1-8	20	80
8-12.5	2	98
12.5-16	20	80

4. Quantification of DAG production

4.1 Diacylglycerol standard curve

To best quantify the amount of DAG produced from reactions, a standard curve correlating the area of peaks generated by known quantities of NBD-DAG should be used (Fig. 3). A standard curve can be generated by drying down NBD-DAG under nitrogen gas, then resuspending in Mobile Phase B at varying concentrations and applying samples to the HPLC. The HPLC automatically integrates the area under each curve, then the area under each curve can be plotted against the pmol of DAG in each sample and fit to a simple linear regression to determine the equation for the line. The equation for this line can be used to quantitate how much NBD-DAG is produced by this assay.

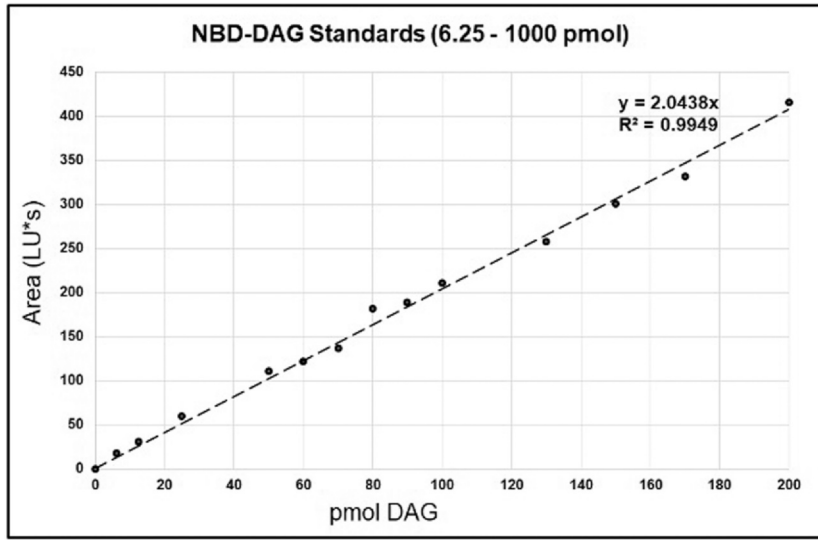

Fig. 3 Graph of NBD-DAG standards. This standard curve was generated by drying down NBD-DAG under nitrogen gas, then resuspending in Mobile Phase B at varying concentrations and applying samples to HPLC. The area under each curve was plotted against the pmol of DAG in each sample and fit to a simple linear regression to determine the equation for the line.

4.2 Sample data and quantification

When the samples from this activity assay are run on the HPLC, there should be two distinct peaks for product and substrate (Fig. 4). Running a blank sample of the substrate only with no protein added (Fig. 4A) is necessary to be able to distinguish the product peak (NBD-DAG) from the substrate peak (NBD-PA) (Fig. 4B). The HPLC mobile phase A and mobile phase B buffers described here are optimized for our specific HPLC column with hydrophobic resin (Spectra C8SR column, Peeke scientific). On our column, NBD-DAG has a shorter retention time, eluting first. The area corresponding to the peak for NBD-DAG can be correlated to the pmol of DAG produced using the equation derived from a standard curve. This pmol value is then multiplied by factor of 10 to quantitate the pmol of DAG in the entire 100 μL sample from the activity assay, since because 10 μL of this sample was injected into the HPLC. In cases where multiple, unsuspected peaks are present, these samples may be suitable for mass spectrometry to determine the identity of the unknown peak.

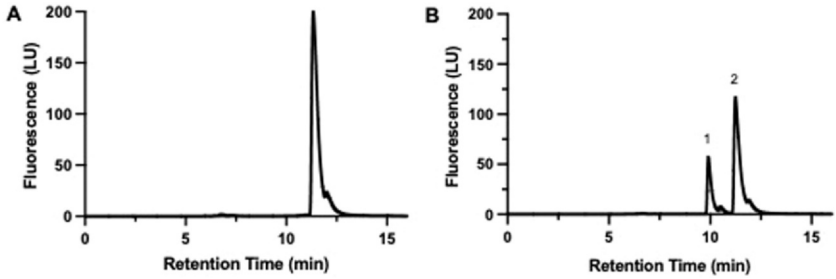

Fig. 4 HPLC chromatograms of NBD-PA and NBD-DAG. (A) Chromatogram from blank sample containing 3 mol% NBD-PA Triton X-100 mixed micelles without protein added. Single peak with right shoulder has retention time of 11.34 min. Shoulder peak is present because the commercially available substrate contains slight impurity. (B) Chromatogram from 3 mol% NBD-PA Triton X-100 mixed micelle reacted with *Tt* Pah2. Peak 1 corresponds to NBD-DAG with a retention time of 9.91 min and peak 2 corresponds to NBD-PA with a retention time of 11.24 min. The described method gives good separation of substrate and product.

Acknowledgements

This work was supported by the National Institutes of Health grant R35GM128666 (to MVA), a Howard Hughes Medical Institute (HHMI) Gilliam Fellowship GT15815 (to FSW), an American Heart Association predoctoral fellowship 23PRE1019634 (to LW) and a Sloan Research Fellowship (to MVA).

References

Bligh, E. G., & Dyer, W. J. (1959). A rapid method of total lipid extraction and purification. *Canadian Journal of Biochemistry and Physiology, 37*(8), 911–917. https://doi.org/10.1139/o59-099.

Burgdorf, C., Hänsel, L., Heidbreder, M., Jöhren, O., Schütte, F., Schunkert, H., & Kurz, T. (2009). Suppression of cardiac phosphatidate phosphohydrolase 1 activity and lipin mRNA expression in Zucker diabetic fatty rats and humans with type 2 diabetes mellitus. *Biochemical and Biophysical Research Communications, 390*(1), 165–170. https://doi.org/10.1016/j.bbrc.2009.09.108.

Burgdorf, C., Prey, A., Richardt, G., & Kurz, T. (2008). A HPLC-fluorescence detection method for determination of phosphatidic acid phosphohydrolase activity: Application in human myocardium. *Analytical Biochemistry, 374*(2), 291–297. https://doi.org/10.1016/j.ab.2007.10.039.

Carman, G. M., & Lin, Y.-P. (1991). *[54] Phosphatidate phosphatase from yeast. Methods in enzymologyvol. 197. Methods in enzymology.* Academic Press 548–553. https://doi.org/10.1016/0076-6879(91)97182-X.

Chapman, K. D., Aziz, M., Dyer, J. M., & Mullen, R. T. (2019). Mechanisms of lipid droplet biogenesis. *Biochemical Journal, 476*(13), 1929–1942. https://doi.org/10.1042/bcj20180021.

Choi, Y. M., Ajjaji, D., Fleming, K. D., Borbat, P. P., Jenkins, M. L., Moeller, B. E., ... Airola, M. V. (2023). Structural insights into perilipin 3 membrane association in response to diacylglycerol accumulation. *Nature Communications, 14*(1), 3204. https://doi.org/10.1038/s41467-023-38725-w.

Coleman, R. A., & Mashek, D. G. (2011). Mammalian triacylglycerol metabolism: Synthesis, lipolysis, and signaling. *Chemical Reviews, 111*(10), 6359–6386. https://doi.org/10.1021/cr100404w.

Csaki, L. S., Dwyer, J. R., Li, X., Nguyen, M. H. K., Dewald, J., Brindley, D. N., ... Reue, K. (2014). Lipin-1 and lipin-3 together determine adiposity in vivo. *Molecular Metabolism, 3*(2), 145–154. https://doi.org/10.1016/j.molmet.2013.11.008.

Dey, P., Han, G.-S., & Carman, G. M. (2020). A review of phosphatidate phosphatase assays. *Journal of Lipid Research, 61*(12), 1556–1564. https://doi.org/10.1194/jlr.R120001092.

Donkor, J., Sariahmetoglu, M., Dewald, J., Brindley, D. M., & Reue, K. (2007). Three mammalian lipins act as phosphatidate phosphatases with distinct tissue expression patterns. *Journal of Biological Chemistry, 282*(6), 3450–3457.

Donkor, J., Zhang, P., Wong, S., O'Loughlin, L., Dewald, J., Kok, B. P., ... Reue, K. (2009). A conserved serine residue is required for the phosphatidate phosphatase activity but not the transcriptional coactivator functions of lipin-1 and lipin-2. *The Journal of Biological Chemistry, 284*(43), 29968–29978. https://doi.org/10.1074/jbc.M109.023663.

Eastmond, P. J., Quettier, A.-L., Kroon, J. T. M., Craddock, C., Adams, N., & Slabas, A. R. (2010). Phosphatidic acid phosphohydrolase1 and 2 regulate phospholipid synthesis at the endoplasmic reticulum in arabidopsis. *The Plant Cell, 22*(8), 2796–2811. https://doi.org/10.1105/tpc.109.071423.

Eaton, J. M., Mullins, G. R., Brindley, D. N., & Harris, T. E. (2013). Phosphorylation of lipin 1 and charge on the phosphatidic acid head group control its phosphatidic acid phosphatase activity and membrane association. *The Journal of Biological Chemistry, 288*(14), 9933–9945. https://doi.org/10.1074/jbc.M112.441493.

Eaton, J. M., Takkellapati, S., Lawrence, R. T., McQueeney, K. E., Boroda, S., Mullins, G. R., ... Harris, T. E. (2014). Lipin 2 binds phosphatidic acid by the electrostatic hydrogen bond switch mechanism independent of phosphorylation. *Journal of Biological Chemistry, 289*(26), 18055–18066. https://doi.org/10.1074/jbc.M114.547604.

Folch, J., Lees, M., & Stanley, G. H. S. (1957). A simple method for the isolation and purification of total lipides from animal tissues. *Journal of Biological Chemistry, 226*(1), 497–509. https://doi.org/10.1016/S0021-9258(18)64849-5.

Gao, S., Carrasquillo Rodríguez, J. W., Bahmanyar, S., & Airola, M. V. (2024). Structure and mechanism of the human CTDNEP1-NEP1R1 membrane protein phosphatase complex necessary to maintain ER membrane morphology. *Proceedings of the National Academy of Sciences of the United States of America, 121*(22), e2321167121. https://doi.org/10.1073/pnas.2321167121.

Granade, M. E., & Harris, T. E. (2018). Chapter Thirteen - Purification of lipin and measurement of phosphatidic acid phosphatase activity from liposomes. In K. N. Allen (Vol. Ed.), *Methods in Enzymology: vol. 607*, (pp. 373–388). Academic Press. https://doi.org/10.1016/bs.mie.2018.04.028.

Han, G.-S., & Carman, G. M. (2010). Characterization of the human LPIN1-encoded phosphatidate phosphatase isoforms. *The Journal of Biological Chemistry, 285*, 14628–14638.

Han, G.-S., Siniossoglou, S., & Carman, G. M. (2007). The cellular functions of the yeast lipin homolog Pah1p are dependent on its phosphatidate phosphatase activity. *Journal of Biological Chemistry, 282*(51), 37026–37035. https://doi.org/10.1074/jbc.M705777200.

Han, G. S., Wu, W. I., & Carman, G. M. (2006). The Saccharomyces cerevisiae lipin homolog is a Mg2+-dependent phosphatidate phosphatase enzyme. *The Journal of Biological Chemistry, 281*(14), 9210–9218. https://doi.org/10.1074/jbc.M600425200.

Harris, T. E., & Finck, B. N. (2011). Dual function lipin proteins and glycerolipid metabolism. *Trends in Endocrinology & Metabolism, 22*(6), 226–233. https://doi.org/10.1016/j.tem.2011.02.006.

Khalil, M. B., Blais, A., Figeys, D., & Yao, Z. (2010). Lipin — The bridge between hepatic glycerolipid biosynthesis and lipoprotein metabolism. *Biochimica et Biophysica Acta (BBA) - Molecular and Cell Biology of Lipids, 1801*(12), 1249–1259. https://doi.org/10.1016/j.bbalip.2010.07.008.

Khayyo, V. I., Hoffmann, R. M., Wang, H., Bell, J. A., Burke, J. E., Reue, K., & Airola, M. V. (2020). Crystal structure of a lipin/Pah phosphatidic acid phosphatase. *Nature Communications, 11*(1), 1309. https://doi.org/10.1038/s41467-020-15124-z.

Martin, A., Gomez-Muñoz, A., Jamal, Z., & Brindley, D. N. (1991). *[55] Characterization and assay of phosphatidate phosphatase. Methods in enzymologyvol. 197. Methods in enzymology* .Academic Press 553–563. https://doi.org/10.1016/0076-6879(91)97183-Y.

Nadra, K., Médard, J.-J., Mul, J. D., Han, G.-S., Grès, S., Pende, M., ... Chrast, R. (2012). Cell autonomous lipin 1 function is essential for development and maintenance of white and brown adipose tissue. *Molecular and Cellular Biology, 32*(23), 4794–4810. https://doi.org/10.1128/MCB.00512-12.

Nakamura, Y., Koizumi, R., Shui, G., Shimojima, M., Wenk, M. R., Ito, T., & Ohta, H. (2009). *Arabidopsis* lipins mediate eukaryotic pathway of lipid metabolism and cope critically with phosphate starvation. *Proceedings of the National Academy of Sciences, 106*(49), 20978–20983. https://doi.org/10.1073/pnas.0907173106.

Pascual, F., & Carman, G. M. (2013). Phosphatidate phosphatase, a key regulator of lipid homeostasis. *Biochimica et Biophysica Acta (BBA) - Molecular and Cell Biology of Lipids, 1831*(3), 514–522. https://doi.org/10.1016/j.bbalip.2012.08.006.

Péterfy, M., Phan, J., Xu, P., & Reue, K. (2001). Lipodystrophy in the fld mouse results from mutation of a new gene encoding a nuclear protein, lipin. *Nature Genetics, 27*(1), 121–124. https://doi.org/10.1038/83685.

Pillai, A. N., Shukla, S., Gautam, S., & Rahaman, A. (2017). Small phosphatidate phosphatase (TtPAH2) of Tetrahymena complements respiratory function and not membrane biogenesis function of yeast PAH1. *Journal of Biosciences, 42*(4), 613–621. https://doi.org/10.1007/s12038-017-9712-7.

Reue, K., & Donkor, J. (2006). Lipin: A determinant of adiposity, insulin sensitivity and energy balance. *Future Lipidology, 1*(1), 91–101. https://doi.org/10.2217/17460875.1.1.91.

Reue, K., & Wang, H. (2019). Mammalian lipin phosphatidic acid phosphatases in lipid synthesis and beyond: Metabolic and inflammatory disorders. *Journal of Lipid Research, 60*(4), 728–733. https://doi.org/10.1194/jlr.S091769.

Sasser, T., Qiu, Q.-S., Karunakaran, S., Padolina, M., Reyes, A., Flood, B., ... Fratti, R. A. (2012). Yeast lipin 1 orthologue Pah1p regulates vacuole homeostasis and membrane fusion. *Journal of Biological Chemistry, 287*(3), 2221–2236. https://doi.org/10.1074/jbc.M111.317420.

Schweitzer, G. G., Collier, S. L., Chen, Z., McCommis, K. S., Pittman, S. K., Yoshino, J., ... Finck, B. N. (2019). Loss of lipin 1-mediated phosphatidic acid phosphohydrolase activity in muscle leads to skeletal myopathy in mice. *The FASEB Journal, 33*(1), 652–667. https://doi.org/10.1096/fj.201800361R.

Siniossoglou, S. (2013). Phospholipid metabolism and nuclear function: Roles of the lipin family of phosphatidic acid phosphatases. *Biochimica et Biophysica Acta, 1831*(3), 575–581. https://doi.org/10.1016/j.bbalip.2012.09.014.

Stukey, G. J., Han, G. S., & Carman, G. M. (2023). Phosphatidate phosphatase Pah1 contains a novel RP domain that regulates its phosphorylation and function in yeast lipid synthesis. *The Journal of Biological Chemistry, 299*(8), 105025. https://doi.org/10.1016/j.jbc.2023.105025.

Takeuchi, K., & Reue, K. (2009). Biochemistry, physiology, and genetics of GPAT, AGPAT, and lipin enzymes in triglyceride synthesis. *American Journal of Physiology-Endocrinology and Metabolism, 296*(6), E1195–E1209. https://doi.org/10.1152/ajpendo.90958.2008.

Vitkovska, T., Welcome, F. S., Khayyo, V. I., Gao, S., Wymore, T., & Airola, M. V. (2025). Structures of a lipin/Pah phosphatidic acid phosphatase in distinct catalytic states reveal a signature motif for substrate recognition. *Journal of Biological Chemistry*. https://doi.org/10.1016/j.jbc.2025.110830.

Walsh, J. P., & Bell, R. M. (1986). sn-1,2-Diacylglycerol kinase of Escherichia coli. Mixed micellar analysis of the phospholipid cofactor requirement and divalent cation dependence. *The Journal of Biological Chemistry, 261*(14), 6239–6247.

Wu, L., Choi, Y. M., Omrane, M., Chai, J., Gao, S., Thiam, A. R., ... Airola, M. V. (2025). DDHD2 possesses both lipase and transacylase capacities that remodel triglyceride acyl chains. *Proceedings of the National Academy of Sciences of the United States of America, Online ahead of print*. https://doi.org/10.1073/pnas.2500527122.

Xu, C., & Shanklin, J. (2016). Triacylglycerol metabolism, function, and accumulation in plant vegetative tissues*. *Annual Review of Plant Biology, 67*(2016), 179–206. https://doi.org/10.1146/annurev-arplant-043015-111641.

CHAPTER TWELVE

Use of novel synthetic analogs to decipher the interactome of phosphatidic acid species in neurosecretory cells

Alexander Wolf[a], Emeline Tanguy[a], Charles Decraene[a], Steven Vertueux[b], Jean-Marc Strub[c,d], Stéphane Ory[a], Sébastien Balieu[b], Pierre-Yves Renard[b], Stéphane Gasman[a,*], and Nicolas Vitale[a,*]

[a]Institut des Neurosciences Cellulaires et Intégratives, Centre National de la Recherche Scientifique, Université de Strasbourg, Strasbourg, France
[b]Université de Rouen Normandie, INSA Rouen Normandie, CNRS, Université de Caen Normandie, ENSICAEN, Normandie Université, CARMeN UMR 6064, INC3M FR, Rouen, France
[c]Laboratoire de Spectrométrie de Masse BioOrganique, IPHC UMR 7178, CNRS, Université de Strasbourg, Strasbourg, France
[d]Infrastructure Nationale de Protéomique ProFI - UAR2048, Strasbourg, France
*Corresponding authors. e-mail address: sgasman@unistra.fr; vitalen@unistra.fr

Contents

1. Introduction 254
2. Phosphatidic acid incorporation into cells 258
   2.1 PA preparation for cellular incorporation 258
   2.2 Validation of PA incorporation within cellular membranes 259
   2.3 Functional validation of synthetic PAs using ERK1/2 phosphorylation 260
3. Identification of PA interactors in live cells 263
   3.1 Photo-crosslinking of dedicated partners 263
   3.2 Click chemistry-based enrichment of PA-protein complexes 265
4. Conclusion 268
5. Reagents and materials 269
Acknowledgements 272
Author contribution 272
References 272

Abstract

Understanding how phospholipids orchestrate cellular signaling requires tools that preserve their native complexity to reveal their modular function. Here, we introduce a versatile chemical approach to map the phosphatidic acid (PA) interactome directly within membranes of living cells. Using synthetic PA analogues, modified on the glycerol backbone with a bioorthogonal azide group, we generated functional probes

Methods in Enzymology, Volume 728
ISSN 0076-6879, https://doi.org/10.1016/bs.mie.2026.01.010
Copyright © 2026 Elsevier Inc. All rights are reserved, including those for text and data mining, AI training, and similar technologies.

that retain natural headgroup and acyl-chain composition and properties. These analogues can be coupled to photoactivatable crosslinkers, allowing covalent capture of transient PA-protein partners upon UV illumination. We present here approaches to validate their integration and functionality through recruitment assays using PA-binding sensor and ERK1/2 phosphorylation readouts. Applying this framework in neurosecretory PC12 cells, we identified specific PA-binding partners across distinct secretory states, revealing both acyl chain-dependent and activity-specific interaction patterns. This methodology bridges lipid chemistry and cell biology by enabling dynamic, species-specific exploration of phospholipid signaling networks. Beyond neurosecretion, the approach provides a broadly applicable platform for dissecting lipid-mediated processes across diverse physiological and pathological contexts, from membrane trafficking to disease-associated lipid signaling.

1. Introduction

Phospholipids occupy a unique position in cell biology, functioning both as the structural foundation of membranes, establishing semi-permeable bilayers (Gorter & Grendel, 1925) and acting as dynamic signalling molecules regulating cellular processes in time and space (Yang et al., 2018). Among them, phosphoinositides (PIP) are the canonical example of signalling lipids. They define subcellular compartments membrane identity and, through complex metabolic networks, are able to coordinate trafficking events such as endocytosis (Posor et al., 2022). Despite being less studied the anionic phospholipid phosphatidic acid (PA) has recently emerged as another pleiotropic signalling lipid. Signalling PA is mainly produced through the action of PLDs, DGKs, and LPAATs (Tanguy et al., 2018), enabling it to regulate membrane trafficking and cell survival. Consequently, PA impacts diverse physiological functions, including neurosecretion (Humeau et al., 2001; Vitale et al., 2001; Schwarz et al., 2011), exosome biogenesis (Ghossoub et al., 2014), synaptic plasticity (Goldschmidt et al., 2016), and phagocytosis (Kassas et al., 2017). Accordingly, dysregulation of PA metabolism lies at the core of multiple pathologies, ranging from fragile X syndrome (Tabet et al., 2016), cancer metastasis (Ghoroghi et al., 2021), cardiometabolic diseases (Arimoto et al., 2006) and viral replication (Tabata et al., 2021), to mood disorders such as depression (Edwards et al., 2022) and neurodegenerative diseases (Oliveira et al., 2010). Elucidating the signalling functions of PA is therefore critical both for advancing our fundamental understanding of life at the cellular level and for deciphering mechanisms underlying diverse pathological conditions.

PA exerts its cellular function through at least two complementary mechanisms. On the one hand, its conical shape affects the biophysical properties of membranes, for instance by promoting negative membrane curvature (Kooijman et al., 2005) or by favoring insertion of proteins within the bilayer (Burger et al., 2000). On the other hand, the negative charge of its phosphate headgroup enables electrostatic interactions with proteins involved in processes such as membrane trafficking (Manifava et al., 2001) and cell survival (Fang et al., 2001). These dual roles often complicate mechanistic interpretation of experimental observations. Hence, key questions emerge: do proteins recruit PA to specific microdomains to exploit its membrane-shaping properties, or do PA microdomains themselves recruit target proteins at the right time?

Regardless of the modality of lipid-protein interactions, for them to happen, proteins typically harbour a conserved lipid-binding domain. These domains can be used to quickly predict potential partners. For example, more than 2000 PIP-binding domains have been identified to date and classified into 60 families (Overduin & Kervin, 2021). In contrast, despite several validated PA-binding proteins, including the mTOR complex (Fang et al., 2001), the SNARE protein syntaxin 1A (Lam et al., 2008), and chromogranin A (Carmon et al., 2020), no consensus PA-binding domain (PABD) has been identified to date (Tanguy et al., 2018). Nevertheless, the data currently available establish that curvature stress and local lipid composition within membranes, together with the biophysical properties of PA, are key determinants of the binding characteristics of PA with specific proteins. A minimalist theoretical model known as the electrostatic–hydrogen bond switch model is largely based on the unique ionization properties of the phosphomonoester of PA. This model proposes that the initial interaction between a cytosolic phosphatidic acid binding domain and the membrane is primarily electrostatic in nature. The local membrane environment is then thought to enable discrimination of PA from the other anionic lipids such as PS. Subsequently, PA-protein interactions involving hydrogen bonds between basic residues in the binding domain and the phosphate group of PA, and potentially hydrophobic interactions with the fatty acyl chains, promote a transition of the PABD from a loosely associated to a stably docked state on the membrane. During this progression, the ionization of PA can switch from −1 to −2, further anchoring the PABD to the membrane (Loew et al., 2013). Furthermore, molecular dynamics simulations of the interaction of the PA and the yeast Spo20p indicated that 6 PA molecules interact with a single polypeptide (Potocký et al., 2014). These

data suggest that a progressive increase in affinity is possible in membrane and thatphoto PA binding proteins could locally concentrate PA, thereby favouring changes in membrane topology.

This absence of a consensus motif for bioinformatic analysis significantly hinders systematic identification of PA interactors and complicates efforts to define PA's signalling functions. This challenge is compounded by the fact that the acyl chain composition of PA is also a factor shaping signalling functions. For example, only polyunsaturated PA species interact with L-lactate dehydrogenase (Hoshino & Sakane, 2020) or with the clathrin assembly protein AP180 to regulate endocytosis (Hoshino & Sakane, 2022). Conversely, saturated and mono-unsaturated PA produced by DGKα selectively target HSP27 and regulate its cancer-progressive function in melanoma cells (Yachida et al., 2023). Chemically engineered PA analogues with photolabile acyl chains further demonstrate that variation in chain orientation within the bilayer can impact downstream signalling pathways (Tei et al., 2021). Our own work also supports this concept. More than 40 distinct PA species were detected in neuroendocrine cells, with ~10 showing strongly increased levels at the plasma membrane upon stimulation for exocytosis. Among these, mostly were mono- and polyunsaturated PAs. These species were shown to regulate, respectively, vesicle docking and the dynamic of the fusion pore during exocytosis (Tanguy et al., 2020). Finally, other membrane lipids can also modulate PA interactions with proteins. For instance, this is the case for PS (Kassas et al., 2017) and for cholesterol, known to preferentially interact with saturated or monounsaturated phospholipids (Demel et al., 1972). Accordingly, cholesterol has recently been shown to tune PA-protein binding properties (Kwarteng et al., 2025).

The main strategy used to identify novel PA-binding proteins has been to incubate cellular extracts with PA-conjugated beads (Kattan et al., 2022; Manifava et al., 2001). However, such bead-based assays poorly recapitulate the complex behavior of PA within biological membranes. For instance, they account with difficulty for acyl chain variability and specificity, fail to mimic the native membrane environment, and lack temporal resolution. As a result, these approaches cannot link dynamic cellular states with specific binding partners. A more advanced approach has been developed using bifunctional phospholipids, which are chemically modified on their fatty acids or headgroups to identify novel potential lipid interactants *in cellulo*. This strategy is based on the addition of a diazirine group. Upon UV illumination, this moiety forms a covalent bond between

the labelled lipid and neighbouring protein under native condition. Following cell lysis, these lipid-protein complexes can be extracted using bioorthogonal click-chemistry and identified via mass spectrometry (Best et al., 2011). While powerful, such a strategy implies modification of either acyl chains or headgroups of phospholipids, which is not compatible with reproducing the subtle differences occurring within natural PA species. To overcome these limitations, we recently reported a new chemical strategy to synthesize PA analogues. In this design, an azide moiety is introduced on the glycerol backbone, enabling bioorthogonal conjugation of diverse functional groups such as photocrosslinkers (PCL) or chromophores via SPAAC (strain promoted azide alkyne cycloaddition). Importantly, in these new PA-N_3 analogues, both the acyl chains and headgroup remain unaltered, preserving natural dynamic and functional specificities of PA species (Fig. 1). When applied to primary chromaffin cells in photocrosslinking experiments, these probes enabled the identification of hundreds of potential PA-interacting proteins, many of which displayed clear species specificities and were sensitive to the stimulation status of the cells (Schlichter et al., 2025).

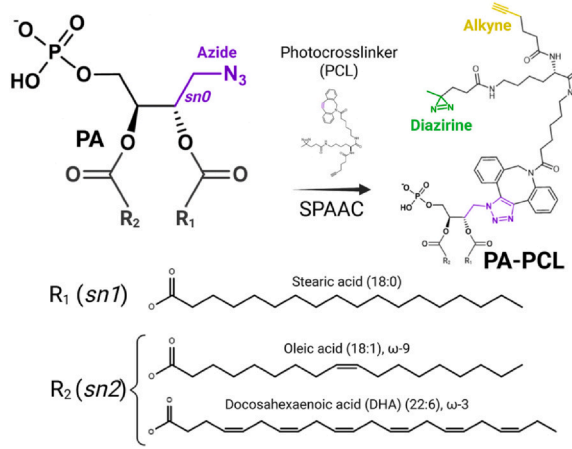

Fig. 1 Novel synthetic phosphatidic acids for interactomics studies. Schematic representation of the synthetic PA species described in this chapter. Each analogue contains a stearic acid (18:0) at the sn-1 position and either an oleic acid (18:1) or docosahexaenoic acid (22:6, DHA) at the sn-2 position, generating mono- or polyunsaturated PA variants. An azide moiety introduced at the sn-0 position on the glycerol backbone enables bioorthogonal "click" conjugation of diverse functional groups such as photo-crosslinkers, while preserving the native acyl-chain and headgroup composition of PA.

In this chapter, we present the overall strategy that enables identification of interactors using chemical probes and photo-crosslinking. The aim is to provide a reproducible framework that can be applied more broadly to the study of PA and other signalling phospholipids within cells. As a model system, we describe a series of photo-crosslinking experiments performed on PC12 cell, a rat pheochromocytoma-derived cell line. First, we will present the process of PA addition to cells and assays for validating incorporation into biological membranes and functionality of modified PAs. Then, we will present the photo-crosslinking procedure and purification of PA interacting proteins before mass spectrometry analysis.

2. Phosphatidic acid incorporation into cells

2.1 PA preparation for cellular incorporation

Lipid addition to cells presents specific challenges. Because phospholipids are largely hydrophobic, they are not soluble in standard aqueous media and require additional steps to ensure cellular incorporation. Complexation with fatty-acid-free bovine serum albumin (BSA) is the conventional approach to increase their apparent solubility. But such methods typically require long incubation times for cellular uptake. For PA, short incubation periods are essential, since it serves as a key metabolic intermediate for the synthesis of all other phospholipids. Prolonged exposure might induce experimental bias because of the rapid conversion of PA into downstream lipid species. To circumvent this issue, PA can be introduced directly into membranes by taking advantage of its intrinsic non-bilayer forming properties. Upon sonication, PA forms small lipid aggregates that transiently fuse with the plasma membrane, allowing rapid and efficient delivery into cells.

Before any experimental procedure, appropriate storage of PA and synthetic PA analogues is essential. Lipids should be resuspended in pure chloroform at 5 mg/mL (w/v) and stored in glass vials to prevent adsorption onto plastic surfaces and avoid degradation of plastic by the solvent. Moreover, because phospholipid acyl chains, especially when containing multiple unsaturations, are prone to peroxidation, it is highly recommended to flush each vial with nitrogen gas (N_2) before sealing tightly with parafilm for long-term storage at −20 °C. This inert gas flushing must be repeated each time the vial is open. Oxidation of unsaturated chains leads to formation of lipid hydroperoxides, compromising

experimental reproducibility. If possible, for extended preservation, dedicated argon-filled or inert-gas-purged storage systems can provide additional safeguard against peroxidation.

PA solutions are freshly prepared at a concentration of 1 mM immediately before usage. Because PA forms transient micellar or non-bilayer aggregates, such suspensions should not be stored for extended periods. For preparation, the required amount of PA stock in chloroform (5 mg/mL) is transferred into a glass vial (e.g., 10 μL, corresponding to 50 μg of PA, adjusted according to experimental requirements). The solvent is gently evaporated under a stream of nitrogen to form a thin lipid film on the vial wall. Air drying is avoided and, long term vacuum desiccation is not recommended, as exposure to ambient oxygen may cause peroxidation. After complete solvent removal, 37 °C ultrapure water is added to rehydrate the film (e.g., 70 μL for 50 μg of PA (18:0–18:1), the volume might need to be adjusted depending on the molecular weight of the PA subspecies and chemical modifications). The suspension is then sonicated twice for 10 min in a benchtop ultrasonic cleaner (B200 Bransonic), filled with 37 °C water. Maintaining the temperature above PA's phase-transition point (typically 30–35 °C, depending on acyl-chain composition) is essential to promote homogeneous micelle formation and reproducible incorporation into membranes.

2.2 Validation of PA incorporation within cellular membranes

Because both natural and synthetic PA-N_3 and PA-PCL are non-fluorescent and not directly detectable within cells, incorporation is routinely assessed using the Spo20p-GFP recruitment assay. This PA biosensor, derived from the yeast Spo20p protein, is typically localized in the nucleus of mammalian cells when overexpressed. Upon PA production, at the plasma membrane, or following exogenous PA addition, Spo20p-GFP rapidly redistributes to the cell periphery (Kassas et al., 2017; Tanguy et al., 2020). This relocalization provides a convenient and reliable readout to confirm whether natural or synthetic PAs are effectively incorporated into cellular membranes.

Spo20p-GFP expression in PC12 cells is achieved using a standard JetPEI transfection protocol. 50,000 cells are seeded one day prior to transfection on 12 mm poly-L-lysine (PLL) coated glass coverslips in 1 mL culture medium (DMEM high glucose, supplemented with 10 % horse serum, 5 % heat-inactivated foetal bovine serum, and penicillin/streptomycin at 5 μg/mL). We recommend preparing two coverslips per tested

PA species (one for natural PA and one for the chemically modified PA) and one additional coverslip for the control condition. On the day of transfection, per well, 1 μg of Spo20p-GFP encoding plasmid is mixed with 50 μL of 150 mM NaCl solution and vortexed. In a separate microtube, 2 μL of JetPEI reagent is mixed with 50 μL of the NaCl solution and gently mixed. The JetPEI-NaCl mixture is then added to the DNA solution, vortexed, and incubated for 20 min at room temperature. The resulting 100 μL complex is added dropwise into each well and cells are incubated for 24 h at 37 °C, 5 % CO_2 for appropriate expression of the PA sensor.

Cells are then washed twice with pre-warmed normal Locke's solution at 37 °C (140 mM NaCl, 4.7 mM KCl, 2.5 mM $CaCl_2$, 1.2 mM KH_2PO_4, 1.2 mM $MgSO_4$, 11 mM glucose, 560 μM ascorbic acid, 10 μM EDTA and 15 mM HEPES, pH adjusted to 7.5). The 1 mM PA suspension, prepared as described in Section 2.1, is then added to the cells to reach a final concentration of 100 μM (Prepared by adding 50 μL of PA solution into 450 μL Locke's solution already present on the cells). Control cells receive an equal volume of ultrapure water. Cells are incubated for 5, 10 or 15 min at 37 °C, then fixed with 4 % cold paraformaldehyde in PBS, followed by 5 PBS washes. Nuclei are stained for 10 min at room temperature with Hoechst 33342 in PBS. Coverslips are mounted on Mowiol 4–88 mounting medium and allowed to cure overnight at room temperature.

Samples are best imaged within 24 h of mounting, as partial diffusion of Spo20p-GFP can occur over time. Confocal microscopy is recommended to visualize single optical sections through the equatorial plane of cells, where the nucleus remains visible. When comparing conditions, cells with similar expression levels should be selected. In control conditions, Spo20p-GFP typically remains nuclear with minimal peripheral fluorescence. In contrast, incubation with natural PA species for 5–15 min consistently induces Spo20p-GFP recruitment to the plasma membrane of the sensor (Fig. 2A). Comparable relocalization is observed when using synthetic PA-N_3 analogues bearing an azide linker (Fig. 2A), confirming that these compounds are efficiently taken up by PC12 cells and can integrate biological membranes similarly to native PA.

2.3 Functional validation of synthetic PAs using ERK1/2 phosphorylation

PA membrane incorporation does not necessarily indicate biological activity. It is therefore essential to validate that synthetic PAs are able to recapitulate known functional effects of endogenous PA. A convenient

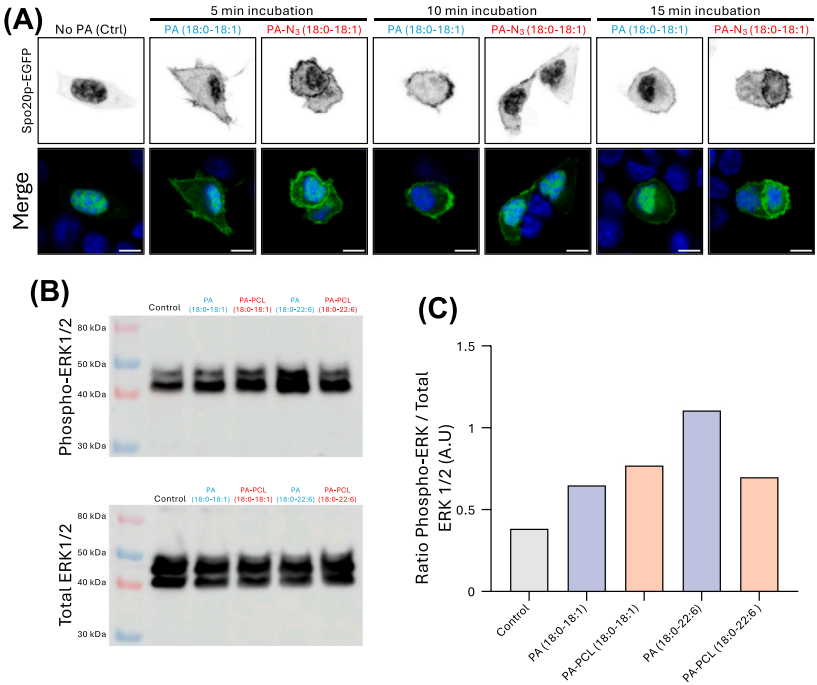

Fig. 2 Validation of synthetic PA analoguesv. (A) Representative confocal images of PC12 cells overexpressing the PA sensor Spo20p–GFP following incubation of the cells with 100 µM of the indicated PA species or analogue for 5, 10, or 15 min prior to fixation. Images are shown as inverted grayscale for Spo20p–GFP and as merged channels (blue, nuclei; green, Spo20p–GFP). Scale bar: 5 µm. (B) Representative Western blots of total and phosphorylated ERK1/2 from PC12 cells incubated for 15 min with the indicated PA species or analogue. (C) Quantification of the ratio of phospho-ERK1/2 to total ERK1/2 signal from (B).

approach is to measure phosphorylation of ERK1/2, a downstream effector frequently activated upon PA-mediated stimulation of mTORC1 and mitogenic signalling pathways (Winter et al., 2010). Comparing the capacity of natural versus synthetic PAs to induce ERK1/2 phosphorylation thus provides a functional validation of their ability to mimic signalling within cells.

800,000 PC12 cells are seeded into PLL-coated 12-well culture dishes one day prior to the experiment. For the experiments described here, two wells are used for each tested PA species(natural PA and PA-PCL) in addition to one control well with no PA incubation. After confirming proper cell adherence, the cells are washed once with serum-free medium

(DMEM high glucose, supplemented with penicillin/streptomycin at 5 μg/mL) and incubated for 6 h at 37 °C in 5 % CO_2 in serum-free medium. Serum starvation minimizes basal ERK1/2 activation otherwise caused by lipids contained in foetal bovine serum. After starvation, cells are washed twice with pre-warmed Locke's solution and incubated with PA to a final concentration of 100 μM (prepared 100 μL of 1 mM PA suspension added to 900 μL Locke's medium already present on the cells). Likewise, control cells receive equal volume of ultrapure water. Following 15 min incubation with PA at 37 °C, cells are lysed immediately in 300 μL prechilled lysis buffer supplemented with 1 % protease inhibitor cocktail (PIC) and 2 % phosphatase inhibitor cocktail (PHIC) for 3 min on ice. Cells are scraped, transferred to pre-chilled microtubes, and the wells rinsed with an additional 200 μL of lysis buffer to recover remaining material. Extracts are incubated on ice for 15 min with brief vortexing every 5 min, then centrifuged (12,000 g, 10 min, 4 °C). The clarified supernatants are transferred to new tubes and total protein concentration is determined by a Bradford assay.

Equal amounts of proteins (20 μg) are mixed with loading dye and resolved on 4–12 % Bis-Tris gels with MES-SDS buffer at 180 V for 45 min. Two gels need to be run in parallel, for phospho-ERK1/2 and for total ERK1/2. Proteins are transferred to nitrocellulose membranes using a semidry transfer system, and transfer efficiency is validated by Ponceau staining. Membranes are blocked for 1 h in Tris-buffered saline (TBS) containing 0.1 % Tween-20 and 3 % BSA (milk-based blocking is avoided to prevent interference with phospho-specific antibodies). Blots are incubated overnight at 4 °C with rabbit anti-ERK1/2 or rabbit anti-phospho-ERK1/2 antibodies (1:1000 dilution in TBS-Tween-BSA 3 %). After washing five times with TBS-Tween, membranes are incubated for 1 h at room temperature with HRP-conjugated goat anti-rabbit secondary antibodies (1:50,000 in TBS-Tween-BSA 3 %). After five additional washes, membranes are incubated for 10 min in PBS and visualized with SuperSignal West Dura Extended Duration substrate on an Amersham Imager 680.

Band intensities are quantified using FIJI software. The ratio of phosphorylated to total ERK1/2 (phospho-ERK/ERK) is calculated for each condition (Fig. 2B and C). An increase in this ratio following treatment with synthetic PAs comparable to that induced by natural PA was observed indicating that the chemical modifications preserve the lipid's ability to activate canonical PA-dependent signalling pathways.

3. Identification of PA interactors in live cells

3.1 Photo-crosslinking of dedicated partners

To covalently capture transient PA-protein interactions in living cells, photoactivatable PA analogues (PA-PCL) bearing a diazirine moiety are used. The diazirine group remains inert under normal conditions. However, upon UV illumination (365 nm), forms a highly reactive carbene intermediate that covalently binds with nearby molecules, thereby producing PA-proteins complexes for subsequent enrichment. This reaction typically occurs within nanoseconds (Das, 2011), reflecting to the short carbene live-time, making it ideally suited to capture transient PA-protein interactions such as those occurring during neurosecretion (Fig. 3A). If no protein is present in close vicinity, the carbene reacts with surrounding water molecules, and is unable to further react, thus limiting false-positive cross-linking.

5,000,000 PC12 cells are seeded one day prior to the experiment onto 60 mm culture dishes in 10 mL of standard growth medium (DMEM high glucose, supplemented with 10 % horse serum, 5 % heat-inactivated fetal bovine serum, and penicillin/streptomycin at 5 μg/mL). Four dishes are prepared for each tested PA species to cover resting, stimulation and post-stimulation interactants together with a non-illuminated control. On the day of photo-crosslinking, cells are washed twice with prewarmed Locke's solution and incubated 15 min with PA-PCL (18:0–18:1) or PA-PCL (18:0–22:6) at a final concentration of 100 μM (e.g. 500 μL of 1 mM PA solution in 4.5 mL of Locke's solution). Dishes are kept covered with aluminium foil to prevent premature activation of the diazirine group. Longer incubation times are possible, but they can increase the likelihood of PA being metabolized into other phospholipids.

To compare PA-protein interactions in different secretory states, photo-crosslinking is performed under three different conditions at 37 °C (Fig. 3B):

- Resting: Cells are incubated in Locke's solution for 3 min
- Stimulated: Cells are incubated for 3 min in 59 K^+ Locke's solution (85.7 mM NaCl, 59 mM KCl, 2.5 mM $CaCl_2$, 1.2 mM KH_2PO_4, 1.2 mM $MgSO_4$, 11 mM glucose, 560 μM ascorbic acid, 10 μM EDTA and 15 mM HEPES, pH adjusted to 7.2). This depolarizing medium activates voltage-gated calcium channels and triggers secretory granule exocytosis.
- Post-stimulation: Cells are returned to standard Locke's solution immediately after stimulation for 3 min

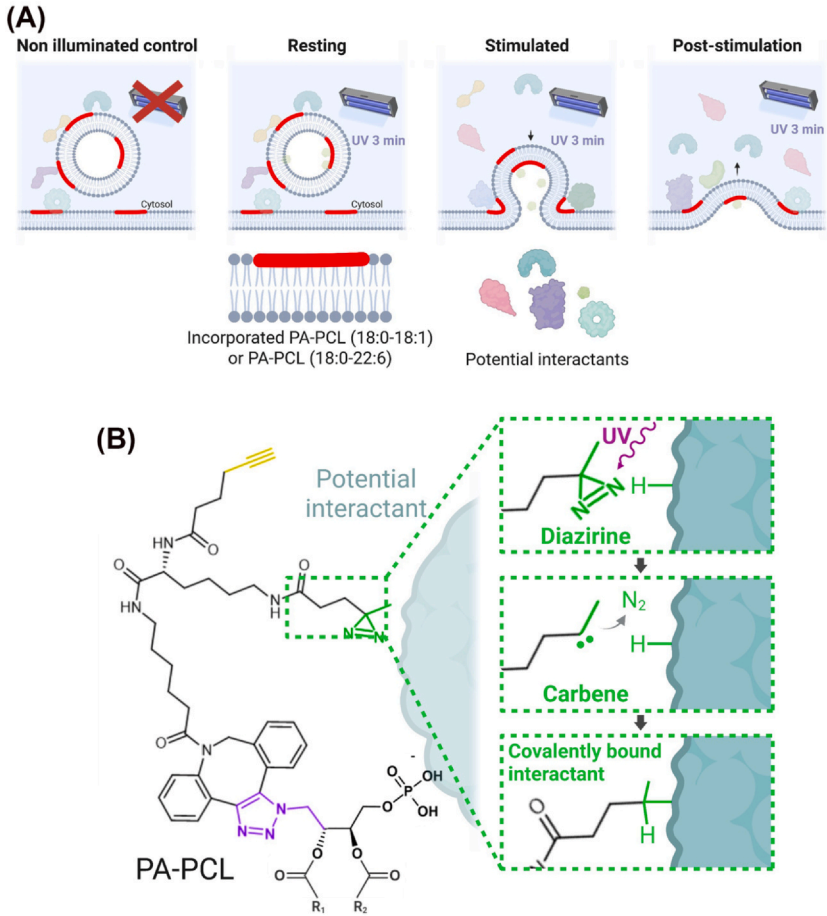

Fig. 3 Photo-crosslinking of PA interacting proteins under distinct physiological conditions. (A) Schematic representation of the experimental conditions used for photo-crosslinking: (1) non-illuminated control to assess background binding; (2) 3 min UV illumination in resting conditions (normal Locke's solution); (3) 3 min illumination in stimulated conditions (59 mM K^+ Locke's solution); and (4) 3 min stimulation followed by 3 min illumination in normal Locke's solution (post-stimulation). (B) Illustration of the photo-crosslinking reaction mechanism. Upon 365 nm UV illumination, the diazirine moiety on PA–PCL undergoes photolysis to generate a short-lived carbene intermediate, which rapidly forms covalent bonds with proteins located near synthetic PAs at the precise time of illumination.

During the 3 min incubation time for each condition, cells are exposed to UV light (365 nm, with a 36W Nailstar lamp) at approximately 3 cm above the dish. This inexpensive setup ensures a uniform UV exposure across the whole plate. At this stage, the generated singlet carbene reacts with neighbouring molecules, forming stable PA-PCL-interactant complexes. It is also essential to remove the lid of each dish during illumination as plastic absorbs most of the UVs. For each tested PA species, a parallel dish in resting condition is processed identically but kept under foil; these controls are essential for assessing background labelling during downstream enrichment.

Following illumination, cells are placed on ice and incubated for 10 min in prechilled cell lysis buffer containing 1 % protease inhibitor cocktail (PIC). Lysates are collected with a cell scraper and transferred to prechilled microtubes and incubated for 10 additional minutes on ice, with brief 1–2 s sonication bursts (MSE Soniprep 150). Over-sonication should be avoided to prevent sample heating and protein degradation. Following lysis, samples are spun (5 min, 4 °C, 10,000 g), to remove membrane debris, and 900 μL of the supernatant is transferred into new prechilled microtubes. Each sample is then subjected to click-chemistry based enrichment of PA-bound proteins as described in the next section.

3.2 Click chemistry-based enrichment of PA-protein complexes

After photo-crosslinking, the resulting PA-PCL-protein complexes are purified through a copper-catalyzed azide-alkyne cycloaddition (CuAAC) reaction with azide-tagged resin. For this purpose, the photoactivatable PCL group of the PA probe carries a terminal alkyne moiety, which reacts with azide-tagged agarose beads. This bioorthogonal click chemistry reaction covalently couples the crosslinked proteins to the resin, allowing stringent washing and subsequent digestion for identification of interactants (Fig. 4A).

Enrichment is performed by using the *Click-and-Go*^{TM} *proteins enrichment kit* (see Click Chemistry Tools/Vector Labs) according to the manufacturer's instructions, with minor optimizations. Picolyl-azide agarose resin is first washed with ultrapure water (200 μL resin and 1.3 mL water, vortex, centrifuge at 1000 g for 2 min and aspirate the supernatant). The CuAAC reaction is assembled by mixing 200 μL resin, 800 μL of photo-crosslinked cell lysate (from Section 3.1) and 1 mL of provided copper(I) catalyst solution. Samples are incubated for 20 h at room temperature on a

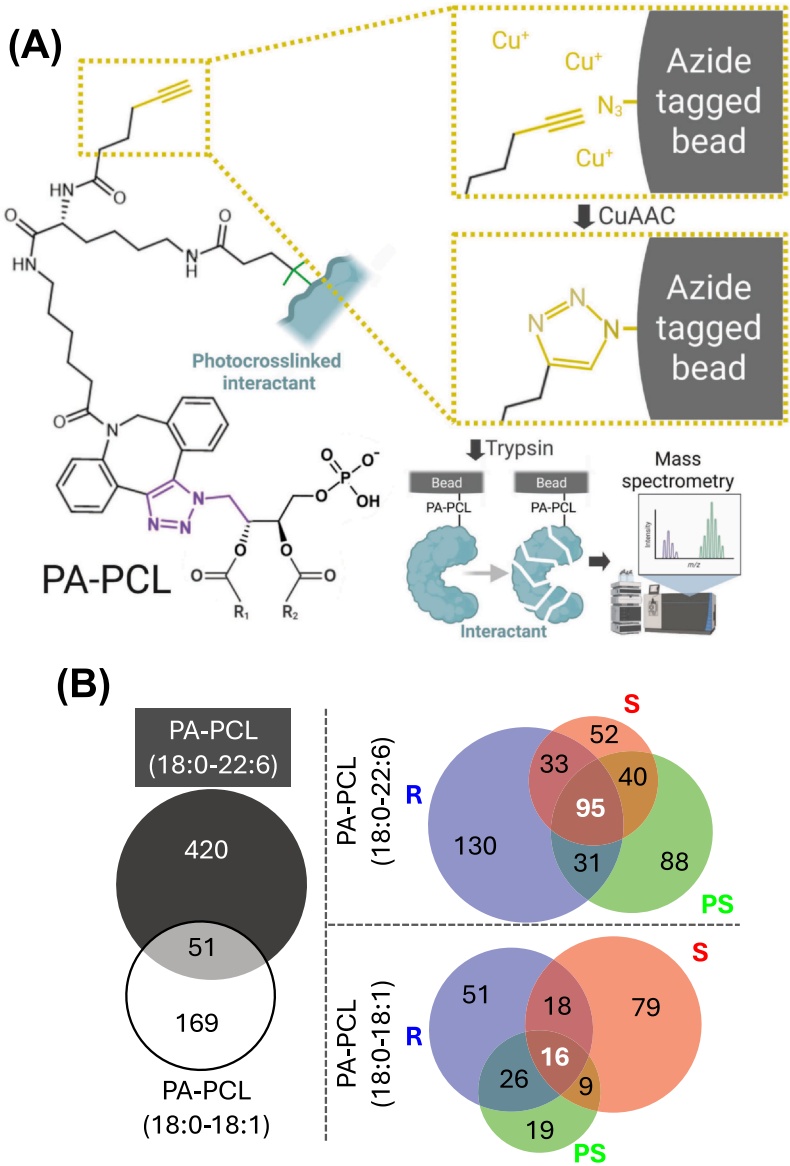

Fig. 4 Enrichment and identification of phosphatidic acid interacting proteins via click-chemistry. (A) Schematic representation of the CuAAC used to covalently link photo-crosslinked PA–PCL–protein complexes to azide-tagged agarose beads. Bound proteins are then digested with trypsin, and the resulting peptides are analyzed by mass spectrometry. (B) Left, quantification of the total number of proteins identified from the interactomes of two different PA–PCL species and right, under resting (R, blue), stimulated (S, red), and post-stimulation (PS, green) conditions.

rotating wheel and protected from light with aluminium foil to prevent any potential photo-crosslinking of remaining diazirine. After covalently bonding the synthetic PAs with the beads, samples are centrifuged (1000 g, 1 min), the supernatant removed and washed once with 1.8 mL ultrapure water (prevent resin clumping).

After removal of the supernatant, disulfide bonds between proteins are reduced by adding 1 mL of freshly prepared 10 mM DTT in SDS wash buffer, followed by incubation for 15 min at 70 °C. The sample is then cooled for 30 min at room temperature. After pelleting (1000 g, 5 min) and removal of the supernatant, the resin is treated with 1 mL of 40 mM iodoacetamide in SDS containing wash buffer for 30 min at room temperature in the dark to prevent re-oxidation of cysteine residues. After the reaction, the beads are transferred to the provided spin columns, plugged onto a vacuum manifold and sequentially washed under denaturating conditions by:

- Five washes with SDS containing agarose-wash buffer, to remove all proteins that are not bound to the resin.
- Ten washes with 8 M urea, 100 mM Tris-HCl, pH 8, to remove residual SDS.
- Ten washes with 20 % acetonitrile diluted in ultrapure water for final desalting.

Spin columns are sealed with the provided cap and the resin is resuspended in 1 mL of trypsin digestion buffer (100 mM Tris-HCl, 2 mM $CaCl_2$, 10 % acetonitrile) and transferred into a new microtube. Samples are pelleted (1000 g, 5 min) and 800 µL of supernatant is removed leaving ~200 µL of beads, and ~200 µL of buffer. 10 µL of mass spectrometry-grade trypsin (0.1 g/L in digestion buffer) is added to each microtube, and samples are incubated overnight at 37 °C with gentle agitation for protein digestion.

The following morning, beads are pelleted (1000 g, 5 min), and the peptide containing supernatant (~200 µL) is transferred into a clean microtube. The remaining resin is washed once with 500 µL ultrapure water, pelleted (1000 g, 5 min), and the wash is combined with the previous supernatant. The pooled eluate is brought to a final volume of 1 mL with ultrapure water (~300 µL) and acidified with 2 µL of trifluoroacetic acid to stop proteolysis. Samples can be stored at −20 °C until identification of PA interactants using mass spectrometry.

Following MS analysis (Bouyssié et al., 2020), a typical experiment yields ~1000 proteins in the background of PC12 cells. Many of these,

including actin, tubulin, heat shock proteins and histones are commonly detected in affinity-based proteomics and represent non-specific binders (Mellacheruvu et al., 2013). After subtracting this background from the photo-crosslinked conditions, we typically identify ~600 different candidate PA interactors (Fig. 4C). Among these are several well established PA-binding proteins, including several ones involved in neurosecretion such as syntaxin 1 A (Lam et al., 2008), or annexin A2 (Gabel et al., 2019), but also multiple mTORC1 subunits, consistent with the ERK1/2 phosphorylation assays (Section 2.3).

Notably, the interactome outcome strongly depends on the acyl chain composition of the tested PA species as only about 10 % of interactors are shared between PA-PCL (18:0–18:1) and PA-PCL (18:0–22:6). Furthermore, the set of proteins recovered is highly dependent of the stimulation state of the cells, with only ~10 % overlap across all conditions for monounsaturated PAs and ~20 % for polyunsaturated ones. Relevantly, even already known PA-binding proteins display such specificity. For example, syntaxin 1 A interacts predominantly with polyunsaturated PAs upon stimulation, underscoring the physiological relevance of acyl-chain and activity-dependent PA-protein interactions.

4. Conclusion

This chapter presents a novel strategy to study signalling phospholipids in their native, dynamic cellular context. The approach we present here relies in the design of modular, clickable PA analogues, in which an azidomethyl moiety is introduced onto the glycerol backbone. This modification preserves both the natural headgroup and the acyl chains of PA while enabling bioorthogonal conjugation to a wide range of strained alkyne-tagged functional groups. As a result, these synthetic PAs constitute a versatile chemical platform for probing lipid signalling with unprecedented specificity.

We describe a stepwise workflow to assess both the membrane incorporation and the functional validity of functionalized PA probes: first, by monitoring recruitment of the PA sensor Spo20p-GFP, and second by verifying their ability to reproduce canonical PA-dependent signalling, such as ERK1/2 phosphorylation. Together, these assays provide a robust and generalisable framework to validate newly functionalized PAs across different cellular models and applications.

Finally, we detail the use of PA-PCL analogues to covalently capture and enrich transient PA-protein complexes in living cells. This methodology enables the systematic mapping of the PA interactome under defined physiological states. Although illustrated here in PC12 neurosecretory cells, the same strategy can be readily adapted to other systems. For instance, to dissect the role of distinct PA species during viral infection (Tabata et al., 2021), cancer metastasis (Wolf et al., 2022) or other lipid-dependent pathologies. Beyond interactomics, the azide handle offers a potential broad range of applications, including conjugation with chromophores, as we have reported recently (Schlichter et al., 2025) or nanoscale localization of PA species by adapting already established lipid expansion microscopy techniques (White et al., 2022).

Altogether, this modular chemical-biological framework provides a powerful means to interrogate PA signalling with temporal and molecular precision, paving the way for a new way to study lipid-protein interaction in living cells.

5. Reagents and materials

The table below recapitulates all reagents and references required to perform the experiments described in this chapter.

Product	Supplier	References
Material		
36 W UV lamp	NailStar	NS-01
Amersham Imager 680	GE Healthcare/Cytiva	N/A
Benchtop ultrasonic cleaner	Branson	B200
Confocal microscope	Leica	SP5II
Sonicator	MSE	Soniprep 150
Trans-Blot Turbo System	Bio-Rad	N/A
Vacuum manifold for spin columns	Zymo Research	N/A
Phospholipids & probes		
PA (18:0-18:1)	Avanti Polar Lipids	840861C
PA (18:0-22:6)	Avanti Polar Lipids	840864C

PA-N_3 (18:0-18:1)	As reported by Schlichter et al., 2025	
PA-PCL (18:0-18:1)	As reported by Schlichter et al., 2025	
PA-PCL (18:0-22:6)	As reported by Schlichter et al., 2025	
Glass vials	Waters	186000327C
Chloroform	Sigma-Aldrich	C2432
Cell culture		
4 well culture plates	Thermo Scientific	176740
12 well culture plates	Falcon	353043
60 mm culture dishes	Falcon	353004
Cover slips	MGF-Slides	65.300.21
DMEM high glucose	Sigma-Aldrich	D5796
Foetal bovine serum (heat-inactivated)	Gibco	10270106
Horse serum	Gibco	26050070
Penicillin/Streptomycin	Sigma-Aldrich	P4458
Poly-L-Lysine	Sigma-Aldrich	P6282
Plasmid and transfection		
150 mM NaCl solution (for JetPEI)	Polyplus	FP9219
JetPEI	Polyplus	201000002
Spo20p-GFP plasmid	Reported in Zeniou-Meyer et al., 2007	
Reagents for Locke's buffer		
Ascorbic acid	Sigma-Aldrich	A4544
$CaCl_2$	Sigma-Aldrich	C7902
EDTA	Merck	1.08418
Glucose	Sigma-Aldrich	G7021
HEPES	Sigma-Aldrich	H3375
KCl	Sigma-Aldrich	P5405
KH_2PO_4	Sigma-Aldrich	P3786
NaCl	Sigma-Aldrich	S5886
$MgSO_4$	Merck	1.05886

Stains, buffers, mounting		
Hoechst 33342	Thermo Scientific	62249
Mowiol 4-88	Millipore Sigma	475904
PBS 10X	Euromedex	ET330
PFA (16% aqueous; diluted to 4%)	Electron Microscopy Sciences	15710
Electrophoresis and Western blot		
4-12%, Bis-Tris Gel	Thermo Scientific	NW04125
5x loading dye	Thermo Scientific	39000
Bradford reagent (Protein Assay Dye Reagent Concentrate)	BioRad	500-0006
BSA	Sigma-Aldrich	A7030
Cell lysis buffer	Invitrogen	FNN0011
Goat anti-rabbit-ECL antibody	Invitrogen	31460
MES SDS running buffer	Thermo Scientific	NP0002
Novex sharp prestained protein standard	Invitrogen	LC5800
Phosphatase inhibitor cocktail	MilliporeSigma	524629
Protease inhibitor cocktail	Sigma-Aldrich	P8340
Rabbit anti-ERK1/2 antibody	Cell Signalling Technology	9101
Rabbit anti-phospho-ERK1/2 antibody	Cell Signalling Technology	9102
SuperSignal West Dura Extended Duration Substrate	Thermo Scientific	34076
TBS 10X	Euromedex	ET220
Transblot turbo, transfer pack mini	BioRad	1704158
Tween-20	Sigma-Aldrich	P9416
Click-chemistry enrichment of PA interactants		
Click-&-Go protein enrichment kit	Click Chemistry Tools	1235
Copper(I) catalyst solution	Click Chemistry Tools	In kit
Lysis buffer (for fishing)	Click Chemistry Tools	In kit

Picolyl Azide Agarose resin	Click Chemistry Tools	In kit
SDS agarose wash buffer	Click Chemistry Tools	In kit
Spin columns	Click Chemistry Tools	In kit
Acetonitrile	Sigma-Aldrich	34851
$CaCl_2$	Sigma-Aldrich	C7902
DTT	Euromedex	3483-12-3
Iodoacetamide	Sigma-Aldrich	A3221
Mass spectrometry grade trypsin	Sigma-Aldrich	650277
Trifluoroacetic acid	Sigma-Aldrich	302031
Tris-HCl	Sigma-Aldrich	252859
Urea	Sigma-Aldrich	U6504

Acknowledgements

This work was supported by grants from "Agence Nationale pour la Recherche" (ANR-19-CE44–0019) to NV, French Proteomic Infrastructure (ProFI) project (grant ANR-10-INBS-08 & ANR-24-INBS-0015), and "Fondation pour la Recherche Médicale" (FDT 202304016618) granted to AW. We also acknowledge the In Vitro Imaging Platform - NeuroPôle - Strasbourg (UAR3156), member of the national infrastructure France-BioImaging supported by the French National Research Agency (ANR-10-INBS-04). INSERM is providing salary to SG and NV.

Author contribution

NV and AW wrote the original manuscript. AW prepared figures. All authors reviewed the manuscript.

References

Arimoto, T., Takeishi, Y., Takahashi, H., Shishido, T., Niizeki, T., Koyama, Y., ... Kubota, I. (2006). Cardiac-specific overexpression of diacylglycerol kinase ζ prevents Gq protein-coupled receptor agonist-induced cardiac hypertrophy in transgenic mice. *Circulation, 113*, 60–66. https://doi.org/10.1161/CIRCULATIONAHA.105.560771.

Best, M. D., Rowland, M. M., & Bostic, H. E. (2011). Exploiting bioorthogonal chemistry to elucidate Protein–Lipid binding interactions and other biological roles of phospholipids. *Accounts of Chemical Research, 44*, 686–698. https://doi.org/10.1021/ar200060y.

Bouyssié, D., Hesse, A.-M., Mouton-Barbosa, E., Rompais, M., Macron, C., Carapito, C., ... Bruley, C. (2020). Proline: An efficient and user-friendly software suite for large-scale proteomics. *Bioinformatics, Statistics and Computational Biology, 36*, 3148–3155. https://doi.org/10.1093/bioinformatics/btaa118.

Burger, K. N., Demel, R. A., Schmid, S. L., & de Kruijff, B. (2000). Dynamin is membrane-active: Lipid insertion is induced by phosphoinositides and phosphatidic acid. *Biochemistry, 39*, 12485–12493. https://doi.org/10.1021/bi000971r.

Carmon, O., Laguerre, F., Riachy, L., Delestre-Delacour, C., Wang, Q., Tanguy, E., ... Montero-Hadjadje, M. (2020). Chromogranin a preferential interaction with Golgi phosphatidic acid induces membrane deformation and contributes to secretory granule biogenesis. *FASEB Journal : Official Publication of the Federation of American Societies for Experimental Biology, 34*, 6769–6790. https://doi.org/10.1096/fj.202000074R.

Das, J. (2011). Aliphatic diazirines as photoaffinity probes for proteins: Recent developments. *Chemical Reviews, 111*, 4405–4417. https://doi.org/10.1021/cr1002722.

Demel, R. A., Geurts van Kessel, W. S. M., & van Deenen, L. L. M. (1972). The properties of polyunsaturated lecithins in monolayers and liposomes and the interactions of these lecithins with cholesterol. *Biochimica et Biophysica Acta (BBA) - Biomembranes, 266*, 26–40. https://doi.org/10.1016/0005-2736(72)90116-2.

Edwards, M. J., Wilson, G. C., Keitsch, S., Soddemann, M., Wilker, B., Müller, C. P., ... Gulbins, E. (2022). Molecular targets of endothelial phosphatidic acid regulating major depressive disorder. *Journal of Neurochemistry, 163*, 357–369. https://doi.org/10.1111/jnc.15708.

Fang, Y., Vilella-Bach, M., Bachmann, R., Flanigan, A., & Chen, J. (2001). Phosphatidic acid-mediated mitogenic activation of mTOR signaling. *Science, 294*, 1942–1945. https://doi.org/10.1126/science.1066015.

Gabel, M., Delavoie, F., Royer, C., Tahouly, T., Gasman, S., Bader, M.-F., ... Chasserot-Golaz, S. (2019). Phosphorylation cycling of Annexin A2 Tyr23 is critical for calcium-regulated exocytosis in neuroendocrine cells. *Biochimica et Biophysica Acta – Molecular Cell Research, 1866*, 1207–1217. https://doi.org/10.1016/j.bbamcr.2018.12.013.

Ghoroghi, S., Mary, B., Larnicol, A., Asokan, N., Klein, A., Osmani, N., ... Hyenne, V. (2021). Ral GTPases promote breast cancer metastasis by controlling biogenesis and organ targeting of exosomes. *eLife, 10*, e61539. https://doi.org/10.7554/eLife.61539.

Ghossoub, R., Lembo, F., Rubio, A., Gaillard, C. B., Bouchet, J., Vitale, N., ... Zimmermann, P. (2014). Syntenin-ALIX exosome biogenesis and budding into multivesicular bodies are controlled by ARF6 and PLD2. *Nature Communications, 5*, 3477. https://doi.org/10.1038/ncomms4477.

Goldschmidt, H. L., Tu-Sekine, B., Volk, L., Anggono, V., Huganir, R. L., & Raben, D. M. (2016). DGKθ catalytic activity is required for efficient recycling of presynaptic vesicles at excitatory synapses. *Cell Reports, 14*, 200–207. https://doi.org/10.1016/j.celrep.2015.12.022.

Gorter, E., & Grendel, F. (1925). On bimolecular layers of lipoids on the chromocytes of the blood. *The Journal of Experimental Medicine, 41*, 439–443.

Hoshino, F., & Sakane, F. (2022). Docosahexaenoic acid-containing phosphatidic acid interacts with clathrin coat assembly protein AP180 and regulates its interaction with clathrin. *Biochemical and Biophysical Research Communications, 587*, 69–77. https://doi.org/10.1016/j.bbrc.2021.11.097.

Hoshino, F., & Sakane, F. (2020). Polyunsaturated fatty acid-containing phosphatidic acids selectively interact with L-lactate dehydrogenase a and induce its secondary structural change and inactivation. *Biochimica Et Biophysica Acta-Molecular and Cell Biology of Lipids, 1865*, 158768. https://doi.org/10.1016/j.bbalip.2020.158768.

Humeau, Y., Vitale, N., Chasserot-Golaz, S., Dupont, J. L., Du, G., Frohman, M. A., ... Poulain, B. (2001). A role for phospholipase D1 in neurotransmitter release. *Proceedings of the National Academy of Sciences of the United States of America, 98*, 15300–15305. https://doi.org/10.1073/pnas.261358698.

Kassas, N., Tanguy, E., Thahouly, T., Fouillen, L., Heintz, D., Chasserot-Golaz, S., ... Vitale, N. (2017). Comparative characterization of phosphatidic acid sensors and their localization during frustrated phagocytosis. *Journal of Biological Chemistry, 292*, 4266–4279. https://doi.org/10.1074/jbc.M116.742346.

Kattan, R. E., Han, H., Seo, G., Yang, B., Lin, Y., Lin, M., ... Wang, W. (2022). Interactome analysis of human phospholipase D and phosphatidic acid-associated protein network. *Molecular & Cellular Proteomics*100195. https://doi.org/10.1016/j.mcpro.2022.100195.

Kooijman, E. E., Chupin, V., Fuller, N. L., Kozlov, M. M., de Kruijff, B., Burger, K. N. J., & Rand, P. R. (2005). Spontaneous curvature of phosphatidic acid and lysophosphatidic acid. *Biochemistry, 44*, 2097–2102. https://doi.org/10.1021/bi0478502.

Kwarteng, D. O., Wolf, A., Langdon, M., Kassas, N., Vitale, N., & Kooijman, E. E. (2025). Cholesterol affects the binding of proteins to phosphatidic acid without influencing its ionization properties. *Journal of Lipid Research, 66*, 100749. https://doi.org/10.1016/j.jlr.2025.100749.

Lam, A. D., Tryoen-Toth, P., Tsai, B., Vitale, N., & Stuenkel, E. L. (2008). SNARE-catalyzed fusion events are regulated by Syntaxin1A-lipid interactions. *Molecular Biology of the Cell, 19*, 485–497. https://doi.org/10.1091/mbc.e07-02-0148.

Loew, S., Kooijman, E. E., & May, S. (2013). Increased pH-sensitivity of protein binding to lipid membranes through the electrostatic-hydrogen bond switch. *Chemistry and Physics of Lipids, Computational Approaches to Understanding Lipid-Protein Interactions, 169*, 9–18. https://doi.org/10.1016/j.chemphyslip.2013.01.008.

Manifava, M., Thuring, J. W. J. F., Lim, Z.-Y., Packman, L., Holmes, A. B., & Ktistakis, N. T. (2001). Differential binding of traffic-related proteins to phosphatidic acid- or phosphatidylinositol (4,5)- bisphosphate-coupled affinity reagents. *Journal of Biological Chemistry, 276*, 8987–8994. https://doi.org/10.1074/jbc.M010308200.

Mellacheruvu, D., Wright, Z., Couzens, A. L., Lambert, J.-P., St-Denis, N., Li, T., ... Nesvizhskii, A. I. (2013). The CRAPome: A contaminant repository for affinity purification mass spectrometry data. *Nature Methods, 10*, 730–736. https://doi.org/10.1038/nmeth.2557.

Oliveira, T. G., Chan, R. B., Tian, H., Laredo, M., Shui, G., Staniszewski, A., ... Di Paolo, G. (2010). Phospholipase d2 ablation ameliorates Alzheimer's disease-linked synaptic dysfunction and cognitive deficits. *The Journal of Neuroscience : The Official Journal of the Society for Neuroscience, 30*, 16419–16428. https://doi.org/10.1523/JNEUROSCI.3317-10.2010.

Overduin, M., & Kervin, T. A. (2021). The phosphoinositide code is read by a plethora of protein domains. *Expert Review of Proteomics, 18*, 483–502. https://doi.org/10.1080/14789450.2021.1962302.

Posor, Y., Jang, W., & Haucke, V. (2022). Phosphoinositides as membrane organizers. *Nature Reviews. Molecular Cell Biology, 23*, 797–816. https://doi.org/10.1038/s41580-022-00490-x.

Potocký, M., Pleskot, R., Pejchar, P., Vitale, N., Kost, B., & Žárský, V. (2014). Live-cell imaging of phosphatidic acid dynamics in pollen tubes visualized by Spo20p-derived biosensor. *The New phytologist, 203*, 483–494. https://doi.org/10.1111/nph.12814.

Schlichter, A., Wolf, A., Ferrand, T., Cocq, A., Riachy, L., Vertueux, S., ... Balieu, S. (2025). Designing new natural-mimetic phosphatidic acid: A versatile and innovative synthetic strategy for glycerophospholipid research. *Angewandte Chemie (International ed. in English), 64*, e202510412. https://doi.org/10.1002/anie.202510412.

Schwarz, K., Natarajan, S., Kassas, N., Vitale, N., & Schmitz, F. (2011). The synaptic ribbon is a site of phosphatidic acid generation in ribbon synapses. *The Journal of Neuroscience, 31*, 15996–16011. https://doi.org/10.1523/jneurosci.2965-11.2011.

Tabata, K., Prasad, V., Paul, D., Lee, J.-Y., Pham, M.-T., Twu, W.-I., ... Bartenschlager, R. (2021). Convergent use of phosphatidic acid for hepatitis C virus and SARS-CoV-2 replication organelle formation. *Nature Communications, 12*, 7276. https://doi.org/10.1038/s41467-021-27511-1.

Tabet, R., Moutin, E., Becker, J. A. J., Heintz, D., Fouillen, L., Flatter, E., ... Moine, H. (2016). Fragile X mental retardation protein (FMRP) controls diacylglycerol kinase activity in neurons. *Proceedings of the National Academy of Sciences of the United States of America, 113*, E3619–E3628. https://doi.org/10.1073/pnas.1522631113.

Tanguy, E., Costé de Bagneaux, P., Kassas, N., Ammar, M.-R., Wang, Q., Haeberlé, A.-M., ... Vitale, N. (2020). Mono- and poly-unsaturated phosphatidic acid regulate distinct steps of regulated exocytosis in neuroendocrine cells. *Cell Reports, 32*, 108026. https://doi.org/10.1016/j.celrep.2020.108026.

Tanguy, E., Kassas, N., & Vitale, N. (2018). Protein-Phospholipid interaction motifs: A focus on phosphatidic acid. *Biomolecules, 8*. https://doi.org/10.3390/biom8020020.

Tei, R., Morstein, J., Shemet, A., Trauner, D., & Baskin, J. M. (2021). Optical control of phosphatidic acid signaling. *ACS Central Science, 7*, 1205–1215. https://doi.org/10.1021/acscentsci.1c00444.

Vitale, N., Caumont, A. S., Chasserot-Golaz, S., Du, G., Wu, S., Sciorra, V. A., ... Bader, M. F. (2001). Phospholipase D1: A key factor for the exocytotic machinery in neuroendocrine cells. *The EMBO Journal, 20*, 2424–2434. https://doi.org/10.1093/emboj/20.10.2424.

White, B. M., Kumar, P., Conwell, A. N., Wu, K., & Baskin, J. M. (2022). Lipid expansion microscopy. *Journal of the American Chemical Society, 144*, 18212–18217. https://doi.org/10.1021/jacs.2c03743.

Winter, J. N., Fox, T. E., Kester, M., Jefferson, L. S., & Kimball, S. R. (2010). Phosphatidic acid mediates activation of mTORC1 through the ERK signaling pathway. *The American Journal of Physiology-Cell Physiology, 299*, C335–C344. https://doi.org/10.1152/ajpcell.00039.2010.

Wolf, A., Tanguy, E., Wang, Q., Gasman, S., & Vitale, N. (2022). Phospholipase D and cancer metastasis: A focus on exosomes. *Advances in Biological Regulation*, 100924. https://doi.org/10.1016/j.jbior.2022.100924.

Yachida, N., Hoshino, F., Murakami, C., Ebina, M., Miura, Y., & Sakane, F. (2023). Saturated fatty acid- and/or monounsaturated fatty acid-containing phosphatidic acids selectively interact with heat shock protein 27. *Journal of Biological Chemistry, 299*, 103019. https://doi.org/10.1016/j.jbc.2023.103019.

Yang, Y., Lee, M., & Fairn, G. D. (2018). Phospholipid subcellular localization and dynamics. *Journal of Biological Chemistry, 293*, 6230–6240. https://doi.org/10.1074/jbc.R117.000582.

Zeniou-Meyer, M., Zabari, N., Ashery, U., Chasserot-Golaz, S., Haeberlé, A.-M., Demais, V., ... Vitale, N. (2007). Phospholipase D1 production of phosphatidic acid at the plasma membrane promotes exocytosis of large dense-core granules at a late stage. *Journal of Biological Chemistry, 282*, 21746–21757. https://doi.org/10.1074/jbc.M702968200.

CHAPTER THIRTEEN

Expression and purification of Steroidogenic Factor-1 (NR5A1) nuclear receptor ligand binding domain complexed with the signaling phosphoinositide lipid $PI(3,4,5)P_3$

Alexis N. Campbell[a], Alexander J. Cutright[b], Jessica Martin[b], Arwa Kheda[b], Mong Na Claire Loi[b], and Raymond D. Blind[a,b,*]

[a]Department of Biochemistry, Vanderbilt University School of Medicine, Nashville, TN, United States
[b]Division of Diabetes, Department of Medicine, Endocrinology & Metabolism, Vanderbilt University Medical Center, Nashville, TN, United States
*Corresponding author. e-mail address: ray.blind@vanderbilt.edu

Contents

1. Introduction 278
2. Plasmid construction, transformation into escherichia coli, and glycerol stock preparation 279
3. *Escherichia coli* encoded His_6-SF-1-LBD expression and purification 281
   - 3.1 Equipment 281
   - 3.2 Materials 281
   - 3.3 Growth procedure 282
   - 3.4 SF-1 LBD purification protocol 282
   - 3.5 Expected outcomes 283
   - 3.6 Advantages 284
   - 3.7 Cautions and troubleshooting 284
4. Bacterial phospholipid exchange with PIP_3 of SF-1 LBD 284
   - 4.1 Equipment 284
   - 4.2 Materials 284
   - 4.3 PIP_3 micelle preparation 285
   - 4.4 SF-1/bPL exchange with PIP_3 285
   - 4.5 Isolating SF-1/PIP3 by AIEX column 285
   - 4.6 Expected outcomes 286
   - 4.7 Advantages 286
   - 4.8 Cautions and troubleshooting 286
5. Conclusions 287

References 287

Methods in Enzymology, Volume 728
ISSN 0076-6879, https://doi.org/10.1016/bs.mie.2026.01.014
Copyright © 2026 Elsevier Inc. All rights are reserved, including those for text and data mining, AI training, and similar technologies.

Abstract

Steroidogenic Factor-1 (SF-1, NR5A1) is an orphan nuclear receptor that plays a critical role in proper development and adult function of the adrenals, gonads and the ventral medial hypothalamus in the brain. Structural studies have revealed that the SF-1 ligand-binding domain is capable of interaction with glycerophospholipids, such as phosphoinositides, in its binding pocket. Of these, the phosphoinositide PI(3,4,5)P_3 (PIP_3) has a high affinity for SF-1 and functions as a key regulatory ligand. This paper details the methods for the recombinant expression and purification of the SF-1 protein, as well as a novel protocol for isolating pure SF-1 bound to PIP3. These methods are a foundational step for future biophysical assays, crystallography studies, and the development of targeted therapeutics for SF-1-dependent adrenocortical carcinoma.

1. Introduction

Steroidogenic Factor-1 (SF-1, *NR5A1*) is an orphan nuclear receptor that functions as a transcription factor, playing a key role in the proper regulation of gene expression, steroidogenesis, sex determination and adrenal gland development and adult functions (Schimmer & White, 2010). Critical functions of SF-1 in development have been highlighted in mice studies showing developmental knockout of SF-1 causes death around postnatal day 8 due to a complete lack of corticosteroid production, as both males and females do not have adrenal glands (Luo et al., 1994; Campbell et al., 2024). These mice can be rescued by adrenal transplants and perinatal corticosteroid injections but typically develop an obese phenotype (Majdic et al., 2002). Conversely, overexpression of SF-1 has been linked to adrenocortical carcinoma, and the proliferation of these cells decreases when inhibiting SF-1 (Doghman et al., 2007).

The ligand binding domain (LBD) of SF-1 is crucial for its regulation, as this is classically where nuclear receptors interact with regulatory ligands (Campbell et al., 2024). Published crystal structures of the LBD reveal a largely hydrophobic core of the pocket with a hydrophilic area near its opening (Li et al., 2005; Sablin et al., 2009; Krylova et al., 2005; Wang et al., 2005; Cato et al., 2023; Mays et al., 2020; Weikum et al., 2018; Ortlund et al., 2005). This structure helps regulate which endogenous ligands are able to bind to SF-1, the most well-characterized being the signaling phosphoinositide lipids PI(4,5)P_2 and PI(3,4,5)P_3 (PIP_3) (Bryant et al., 2021a; Blind et al., 2012a; Chi et al., 2023; Blind et al., 2014a; Bryant et al., 2021b; Mullaney et al., 2010; Blind, 2014; Blind et al., 2012b). It is known that the

positioning of the acyl chains and headgroups of phosphoinositides repeats the same pattern in which the acyl chains follow the same path to reach deep within the hydrophobic core of SF-1, whereas the headgroup is exposed outside the pocket, in a highly solvent-exposed position (Bryant et al., 2021a; Blind et al., 2014b).

The phosphoinositide PI(3,4,5)P_3 (PIP_3) binds with high affinity to SF-1 and has been suggested as a regulatory ligand of SF-1, verified by several crystal structures. These structures and follow-up functional work all suggest both the headgroups of bound phospholipids (Sablin et al., 2009; Chi et al., 2023; Blind et al., 2014a, 2012b; Sablin et al., 2015; Campbell et al., 2023) as well as the composition of the acyl chains (Bryant et al., 2021b) can regulate SF-1, partly through distinct mechanisms (Bryant et al., 2021a; Blind et al., 2014b). Levels of PIP_3 in mammalian cells associate with activation of SF-1 function in gene regulation (Blind et al., 2012a; Lin et al., 2009), dependent on the ability of SF-1 to bind phospholipids (Blind et al., 2012a). Although many structures now exist of SF-1 bound to various phosphoinositides, the technical path to expression and purification of these complexes has been anything but straightforward. Here, we present a standardized approach to expression and purification of SF-1, and how to complex SF-1 with the phosphoinositides PIP_2 and PIP_3, for use in further characterizing the biophysical functions of these intriguing protein–lipid complexes.

2. Plasmid construction, transformation into escherichia coli, and glycerol stock preparation

The design of a high-yield human SF-1-encoding cDNA is dependent on numerous factors, including but not limited to expression system, codon optimization, and the optimization of the final product. Many constructs have been used to express human and mouse SF-1 LBD, and all expression and purification conditions are identical for human vs. mouse SF-1 LBD (Sablin et al., 2009; Krylova et al., 2005). A Cys-lite version (C247S, C412S) of human SF-1 LBD has been used successfully for crystallography spanning amino acids 218–461 of the human SF-1 sequence (RefSeq Transcript ID NM_004959.5, RefSeq Protein ID NP_004950.2) in a pET-based expression vector for production of His_6-containing proteins in standard BL21 DE3 bacterial expression systems (Fig. 1).

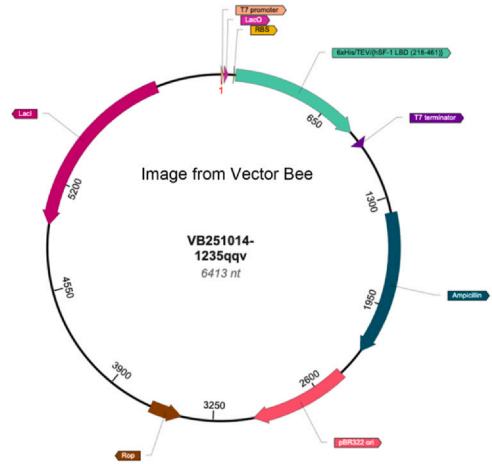

Plasmid Element	Plasmid Position	Size (bp)	Description	Notes
T7 promoter	1-17	17	T7 promoter	Promoter that drives expression of SF-1 gene in bacteria that also express T7 RNA polymerase.
LacO	20-44	25	Lac operator	IPTG induces Lac repressor to release from this Lac Operator element, allowing adjacent SF-1 gene to be transcribed.
RBS	76-80	5	Ribosome bind site	RBS recruits ribosome to transcript.
6xHis/TEV/SF-1 LBD (218-461)	88-864	777	6X-His/TEV/Human SF-1 LBD	Human SF-1 LBD used to crystallized with PIP2 and PIP3, 218-461 with 2 mutations of Cys residues (C247S, C412S).
T7 terminator	929-975	47	T7 terminator	Transcription termination by bacteriophage T7 RNA polymerase.
Ampicillin	1396-2256	861	Ampicillin resistance	Ampicillin resistance gene
pBR322 ori	2427-3015	589	pBR322 Origin	Origin of replication for plasmid.
Rop	3442-3633	192	Repressor of primer	Rop is a protein in combination with pBR322 origin of replication results in low copy number of the plasmid.
LacI	4945-6027	1083	Lac repressor	IPTG binds Lac repressor to release inhibition of transcription of genes downstream of the lac operator.

Fig. 1 Plasmid construction of human SF-1 LBD. SF-1 LBD (218–461) plasmid design uses a pET-based backbone with a standard T7 promoter for IPTG induction, with an N-terminal 6X-His tag and a TEV protease cleavage site. Table below explains the function of each element contained in the vector. *Image from Vector Bee; table adapted from information provided by VectorBuilder.*

1) BL21-GOLD (DE3) cells and SF-1 LBD encoding plasmids were set on ice to thaw gradually.
2) Add 1 μl (~10 ng) plasmid DNA to the cell mixture. Carefully flick the tube 4–5 times to mix cells and DNA.
3) Place the mixture on ice for 30 min and allow the mixture to equilibrate
4) Heat shock at exactly 42 °C for exactly 10 s on a heating block.
5) Place on ice for 5 min.
6) Pipette 950 μl of room temperature SOC into the mixture over a flame to avoid contamination.
7) Attach the tube to a shaker, set to 37 °C, 200 rpm, for 60 min.
8) Warm selection plates (LA/Ampicillin) to 37 °C.
9) Mix the cells thoroughly by repeatedly drawing in and expelling with a P200 micropipette.
10) Spread 100 μl onto a selection plate, allowing all liquid to dry before flipping the plate over, and incubate overnight at 37 °C.
11) Select a single colony, and add to a 250 mL Furnbach flask containing 100 mL TB/ampicillin (100 μg/mL) overnight culture, shaking at 200 rpm, 37 °C.
12) Mix 750 μl overnight culture with 750 μl 50 % glycerol (v/v). This stock should be stored at −80 °C.

3. *Escherichia coli* encoded His_6-SF-1-LBD expression and purification

3.1 Equipment

- Refrigerated shaker-incubator
- Low-speed centrifuge, rotors, and 1 L bottles
- Ultrasonic Cell Disruptor
- High-speed centrifuge and rotor for 30-50 mL bottles
- ÄKTA pure protein purification system (Cytiva)
- Nanodrop spectrophotometer (ThermoFisher)

3.2 Materials

- His_6-SF-1 LBD encoded BL21-GOLD (DE3) bacterial cells
- 250 mL Fernbach flask with 100 mL Terrific Broth (TB) and 100 μg/mL ampicillin
- 4 L Fernbach flasks with 1 L Terrific Broth (TB) and 100 μg/mL ampicillin

- 1 M solution Sterile-filtered Isopropyl-β-D-thiogalactopyranoside (IPTG) in water
- Complete protease inhibitor tablets, EDTA-free (Roche)
- 10,000 MWCO Slide-A-Lyzer G3 Dialysis Cassette (ThermoFisher)
- Amicon Ultra Centrifugal Filters, 15 mL, 10,000 NMWL (MilliporeSigma)
- His_6-TEV
- Lysis Buffer: 50 mM HEPES pH 7.5, 300 mM KCl, 20 mM imidazole, 2 mM chapes, 5 % (v/v) glycerol, 5 mM β-mercaptoethanol (β-ME)
- Elution Buffer: 50 mM HEPES pH 7.5, 150 mM KCl, 300 mM imidazole, 2 mM chapes, 5 % (v/v) glycerol, 5 mM β-mercaptoethanol (β-ME)
- Buffer A: 50 mM HEPES pH 7.5, 2 mM CHAPS, 5 mM β-mercaptoethanol (β-ME)
- Buffer B: 50 mM HEPES pH 7.5, 1 M NaCl, 2 mM CHAPS, 5 mM β-mercaptoethanol (β-ME)
- Gravity columns (100 mL and 20 mL volumes)
- HisPur cobalt resin (ThermoFisher)
- Two HiTrap Desaltin 5 mL columns with Sephadex G-25 resin (Cytiva)
- HiTrap Capto Q 1 mL anion exchange chromatography column (Cytiva)

3.3 Growth procedure

1) Using a sterile micropipette tip, a 250 mL Furnbach flask containing 100 mL TB/ampicillin (100 μg/mL) was inoculated with His_6-SF-1 LBD containing BL21-GOLD (DE3) cells from a previously made glycerol stock, and grown overnight at 37 °C.

2) A 10 mL aliquot of the overnight culture was added to each 4 L Furnbach flash containing 1 L TB/ampicillin (100 μg/mL). This is shaken at 37 °C, 200 rpm, until the OD_{600} reaches 0.6, at which point the cultures are cooled by refrigeration for 10−20 min, and 1 mL of 1 M IPTG is added. The culture is then allowed to grow overnight at 18 °C, 180 rpm.

3) The cells are then centrifuged at 5000 rpm at 4 °C for 30−40 min, collecting the pellet.

3.4 SF-1 LBD purification protocol

1) All steps are completed at 4 °C.

2) Each liter of cell pellet is homogenized in 40-50 mL of lysis buffer and one cOmplete tablet, EDTA-free.

3) The rehomogenized cells are then sonicated in an ultrasonic cell disruptor for 10 min at 70 % amplification, 30 % duty cycle (3 s on, 7 s off) on ice.

4) Lysed cells are then centrifuged at 15,000 rpm, 4 °C, for 30−40 min with the supernatant being collected.
5) The lysate is then nutated overnight with 0.5 mL HisPur Cobalt resin.
6) The lysate/HisPure cobalt resin is then added to a 100 mL gravity column, and the flowthrough is collected and removed.
7) The HisPure cobalt resin is then washed three times with 20-40 mL lysis buffer.
8) 25 mL of elution buffer is then added to the column and allowed to incubate for 30 min, at which point a slow elution is completed, collecting five 5 mL fractions.
9) His_6-TEV is added to the eluted SF-1 LBD at a ratio of 2 mg TEV: 50 mg His_6-SF-1 LBD and loaded into a rehydrated 10,000 MWCO Slide-A-Lyzer dialysis cassette and dialyzed overnight in 2 L lysis buffer.
10) An SDS-PAGE is run to ensure complete cleavage of the poly-His tag (cleaved SF-1 LBD should run slightly lower on the gel).
11) The cleaved SF-1 LBD and TEV are then nutated for 30 min with 0.1 mL HisPure cobalt resin.
12) The sample is then loaded in a 20 mL gravity column and the flow-through is collected.
13) The flowthrough is then desalted by two HiTrap Sephadex G-25 columns pre-equilibrated with buffer A, on an ÄKTA pure protein purification system by an isocratic flow of buffer A.
14) The eluted protein is then concentrated by centrifugation in a 10,000 NMWL filter unit at 3000 rpm, 4 °C, to 4-5 mL.
15) The concentrated sample is then loaded onto a buffer A pre-equilibrated 1 mL HiTrap CaptoQ column on an ÄKTA pure protein purification system.
16) The loaded column is then equilibrated with 30-50 mL buffer A. SF-1 LBD is then eluted by a 0–50 % gradient of buffer B (Fig. 2).
17) If desired, the sample can be concentrated as described in step 14. At this point the sample can also be dialyzed into a buffer without Chapes.
18) The concentration of SF-1 LBD is determined by molar absorptivity at 280 nm by nanodrop ($\varepsilon = 20{,}315\ M^{-1}\ cm^{-1}$, 1.422 g/L)

3.5 Expected outcomes

A typical yield of SF-1 LBD is at least 12.5 mg/L of culture, of properly folded SF-1 LBD is observed.

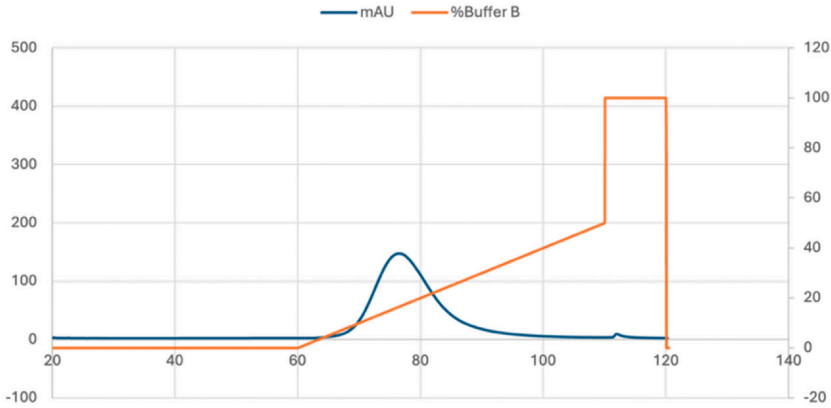

Fig. 2 Chromatography purification of SF-1 LBD. Anion exchange chromatography was used for initial purification of SF1-LBD by CaptoQ cytivia column. Featured in this figure is a chromatogram of percentage of Buffer B needed to elute off SF-1 LBD. Protein elution is identified by absorbance values (mAU).

3.6 Advantages

This purification utilizes readily available and procedurally defined poly-His tag affinity chromatographic methods, which makes the procedure easily accessible and easily completed by trainees.

3.7 Cautions and troubleshooting

- The TB must be cooled to < 25 °C before induction with IPTG
- CHAPS must be maintained at a minimum concentration of 2 mM to prior to ion exchange chromatography.

4. Bacterial phospholipid exchange with PIP_3 of SF-1 LBD

4.1 Equipment

- ÄKTA pure protein purification (Cytiva)
- Nanodrop spectrophotometer (ThermoFisher)
- Ultrasonic Bath 1.9 L (Fisher Scientific)

4.2 Materials

- Phosphatidylinositol-3,4,5-triphosphate (Cayman Chemical)
- HiTrap Capto Q 1 mL anion exchange chromatography column (Cytiva)
- Two HiTrap Desaltin 5 mL columns with Sephadex G-25 resin (Cytiva)

- Buffer A: 50 mM HEPES pH 7.5
- Buffer B: 50 mM HEPES pH 7.5, 1 M NaCl
- Thin borosilicate glass tube (Fisherbrand)

4.3 PIP_3 micelle preparation

1) Reconstitute the vacuum-sealed PIP_3 from Cayman Chemical to 1 mg/mL in Buffer A. Use a 1 mL syringe with at least a 22-gauge needle to pierce the septum and draw water into the glass vial. If lyophilized phosphoinositide is used as the starting material under vacuum, micelles result from this procedure. If a film of lipids at the bottom of the vial is used, multi-lamellar vesicles result, in which the vast majority of the lipids are inaccessible to SF-1 for binding, due to the multi-lamellar nature of the vesicles. This is why micelles are used, such that 100 % of the lipid is available for binding to SF-1.

2) Sonicate the vesicle in a room temperature or heated water bath glass ware sonicator for at least 5 min to generate micelles. This sonication procedure should be repeated after micelles have rested for an hour, so re-sonicate the micelles often.

4.4 SF-1/bPL exchange with PIP_3

1) Place the desired amount of SF-1/bPL previously desalted into Buffer, into a tall, thin borosilicate glass tube.

2) Add 1 μg/μl of the prepared PIP_3 solution dropwise to the surface of the SF-1 solution.

3) Mix the SF-1/PIP_3 solution thoroughly using a P1000 pipette.

4) Carefully layer nitrogen gas over the reaction mixture before sealing the glass tube to minimize air-water interface.

5) Incubate the mixture at room temperature for 16 h while gently nutating on a belly dancer or similar shaker.

4.5 Isolating SF-1/PIP3 by AIEX column

1) Following the overnight incubation, load the sample onto a MonoQ 5/50 column.

2) Elute the protein using a gradient of Buffer B against Buffer A.

3) The SF-1/PIP_3 complex is expected to elute later off the column than the unexchanged SF-1 bound to bPL (Fig. 3). *Pool the fractions corresponding to the SF-1/PIP_3 fraction peak.*

4) Add 2uL of freshly sonicated 1 g/L PIP_3 micelles to isolated SF-1/PIP_3 to maintain complex stability.

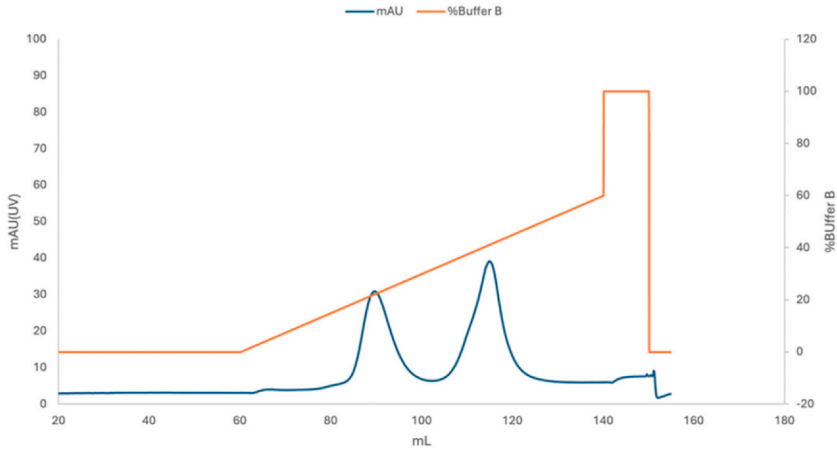

Fig. 3 Chromatography Isolation of SF-1: PIP_3. Anion exchange chromatography was used for collection of PIP_3 bound SF1-LBD by MonoQ 5/50 Cytiva Column. Featured in this figure is a chromatogram of percentage of Buffer B needed to elute off SF-1:PIP_3. Protein elution is identified by absorbance values (mAU).

4.6 Expected outcomes

When a 3-fold molar excess of PIP_3 to SF1 is incubated, a yield of 40–50 % of SF-1 bound to PIP_3 can be expected.

4.7 Advantages

This purification method allows for the isolation of pure SF-1 bound to PIP_3, which can readily be used for downstream applications such as biophysical assays and crystallography.

4.8 Cautions and troubleshooting

- It is ideal to minimize the air-water interface during the exchange, as PIP_3 can potentially arrange itself at this interface inhibiting the exchange
- The exact molar ratio of PIP_3 to SF-1 may need to be optimized to your specific protein batch as well as the acyl chain composition of PIP_3 ligand used to achieve the highest yield.
- Before running columns ensure that the SF-1 protein is completely desalted into Buffer A before loading on the column to ensure the protein is able to stay on the columns.

5. Conclusions

Though Steroidogenic Factor 1 (SF-1) is classified as an orphan nuclear receptor, in vitro analysis suggests that phosphoinositides such as $PI(3,4,5)P_3$ (PIP_3) may serve as key regulatory ligand. Understanding the mechanisms by which SF-1 is regulated biologically is imperative for the treatment of conditions like adrenocortical carcinoma. The protocol outline in this paper provides a simple, reliable way to generate pure SF-1/PIP_3 complexes for further study. These purified complexes can be used to conduct both biophysical and structural assays. The information acquired from this further analysis can be leveraged to clarify the regulatory mechanism of SF-1, ultimately providing a targetable mechanism for the treatment of SF-1-dependent cancers such as adrenocortical carcinoma.

References

Blind, R. D. (2014). Disentangling biological signaling networks bydynamic coupling of signaling lipids tomodifying enzymes. *Advances in Biological Regulation, 54*.

Blind, R. D., et al. (2014a). The signaling phospholipid PIP 3 creates a new interaction surface on the nuclear receptor SF-1. *Proceedings of the National Academy of Sciences, 111*, 15054–15059.

Blind, R. D., et al. (2014b). The signaling phospholipid PIP3 creates a new interaction surface on the nuclear receptor SF-1. *Proceedings of the National Academy of Sciences of the United States of America, 111*, 15054–15059.

Blind, R. D., Suzawa, M., & Ingraham, H. A. (2012a). Direct modification and regulation of a nuclear receptor-PIP2 complex by the nuclear inositol-lipid kinase IPMK. *Science Signaling, 5*, ra44.

Blind, R. D., Suzawa, M., & Ingraham, H. A. (2012b). Direct modification and activation of a nuclear receptor - PIP2 complex by the inositol lipid kinase IPMK. *Science Signaling, 5*.

Bryant, J. M., et al. (2021a). The acyl chains of phosphoinositide PIP3 alter the structure and function of nuclear receptor Steroidogenic Factor-1. *Journal of Lipid Research, 62*, 100081.

Bryant, J. M., et al. (2021b). The acyl chains of phosphoinositide PIP3 alter the structure and function of nuclear receptor Steroidogenic Factor-1 (NR5A1). *Journal of Lipid Research*, 100081. https://doi.org/10.1016/j.jlr.2021.100081.

Campbell, A. N., et al. (2023). Steroidogenic Factor-1 form and function: From phospholipids to physiology. *Advances in Biological Regulation*. https://doi.org/10.1016/J.JBIOR.2023.100991https://doi.org/10.1016/J.JBIOR.2023.100991.

Campbell, A. N., et al. (2024). Steroidogenic Factor-1 form and function: From phospholipids to physiology. *Advances in Biological Regulation, 91*, 100991.

Cato, M. L., et al. (2023). Comparison of activity, structure, and dynamics of SF-1 and LRH-1 complexed with small molecule modulators. *The Journal of Biological Chemistry, 299*.

Chi, E. S., Stivison, E. A., & Blind, R. D. (2023). SF-1 Induces Nuclear PIP2. *Biomolecules, 13*, 1509.

Doghman, M., et al. (2007). Increased Steroidogenic Factor-1 dosage triggers adrenocortical cell proliferation and cancer. *Molecular Endocrinology, 21*, 2968–2987.

Krylova, I. N., et al. (2005). Structural analyses reveal phosphatidyl inositols as ligands for the NR5A orphan receptors SF-1 and LRH-1. *Cell, 120*, 343–355.
Li, Y., et al. (2005). Crystallographic identification and functional characterization of phospholipids as ligands for the orphan nuclear receptor Steroidogenic Factor-1. *Molecular Cell, 17*, 491–502.
Lin, B. C., et al. (2009). Stimulating the GPR30 estrogen receptor with a novel tamoxifen analogue activates SF-1 and promotes endometrial cell proliferation. *Cancer Research, 69*, 5415–5423.
Luo, X., Ikeda, Y., & Parker, K. L. (1994). A cell-specific nuclear receptor is essential for adrenal and gonadal development and sexual differentiation. *Cell, 77*, 481–490.
Majdic, G., et al. (2002). Knockout mice lacking steroidogenic factor 1 are a novel genetic model of hypothalamic obesity. *Endocrinology, 143*, 607–614.
Mays, S. G., et al. (2020). Enantiomer-specific activities of an LRH-1 and SF-1 dual agonist. *Scientific Reports, 10*.
Mullaney, B. C. C., et al. (2010). Regulation of C. elegans fat uptake and storage by acyl-CoA synthase-3 is dependent on NR5A family nuclear hormone receptor nhr-25. *Cell Metabolism, 12*, 398–410.
Ortlund, E. A., et al. (2005). Modulation of human nuclear receptor LRH-1 activity by phospholipids and SHP. *Nature Structural & Molecular Biology, 12*, 357–363.
Sablin, E. P., et al. (2009). Structure of SF-1 bound by different phospholipids: Evidence for regulatory ligands. *Molecular Endocrinology, 23*.
Sablin, E. P., et al. (2015). Structure of NR5A2 (LRH-1) with PIP3 hormone bound in the ligand binding pocket. *Journal of Structural Biology, 192*, 342–348.
Schimmer, B. P., & White, P. C. (2010). Minireview: Steroidogenic factor 1: Its roles in differentiation, development, and disease. *Molecular Endocrinology, 24*, 1322–1337.
Wang, W., et al. (2005). The crystal structures of human steroidogenic factor-1 and liver receptor homologue-1. *Proceedings of the National Academy of Sciences of the United States of America, 102*, 7505–7510.
Weikum, E. R., Liu, X., & Ortlund, E. A. (2018). The nuclear receptor superfamily: A structural perspective. *Protein Science, 27*, 1876–1892.

CHAPTER FOURTEEN

Reconstitution strategies for exploring interactions of Ebola virus matrix protein with host membrane mimetics☆

Sreetama Pal[a,b], **Shalini T. Low-Nam**[a,c,d,*], **and Robert V. Stahelin**[b,d,*]
[a]Tarpo Department of Chemistry, Purdue University, West Lafayette, IN, United States
[b]Borch Department of Medicinal Chemistry and Molecular Pharmacology, Purdue University, West Lafayette, IN, United States
[c]Department of Physics, Purdue University, West Lafayette, IN, United States
[d]Purdue Institute of Inflammation, Immunology, and Infectious Disease, Purdue University, West Lafayette, IN, United States
*Corresponding authors. e-mail address: slownam@purdue.edu; rstaheli@purdue.edu

Contents

1. Introduction 290
2. Materials and equipment 291
   2.1 Materials 291
   2.2 Equipment 293
3. Protocols for reagent generation 294
   3.1 Endogenous EBOV VP40 294
   3.2 Supported lipid bilayers (SLBs) 297
4. SLB-based assays for quantitative assessment of EBOV VP40 interaction with host membrane mimetics 299
   4.1 Ensemble/single-molecule TIRF microscopy 299
   4.2 Data analysis 301
5. Expected outcomes and conclusions 301
Acknowledgments 301
References 301

Abstract

Ebola virus (EBOV), an enveloped virus of the *Filoviridae* family, is an excellent biophysical model for studying enveloped virus assembly, despite its status as a BSL-4 pathogen. The expression of the EBOV matrix protein VP40 (viral protein 40 kDa) is necessary and sufficient for virus assembly/budding in human cells. VP40, in its dimeric form, interacts with the host plasma membrane (PM) inner leaflet and forms higher-order hexamers critical for EBOV assembly. The dependence of viral maturation

☆ *Membrane Interactions of Viral Matrix Peripheral Proteins*

Methods in Enzymology, Volume 728
ISSN 0076-6879, https://doi.org/10.1016/bs.mie.2026.01.006
Copyright © 2026 Elsevier Inc. All rights are reserved, including those for text and data mining, AI training, and similar technologies.

on VP40 dynamics provides the opportunity to quantify biophysical requirements for the EBOV life cycle using a reductionist approach to measure VP40-membrane interactions. There are significant gaps in our understanding of the regulation underlying VP40 recruitment at the host cell PM, and how it culminates in the assembly/budding of mature, infectious virions. Here, we describe (i) reconstitution strategies for mimicking the VP40-host cell membrane interface in a controlled, biologically relevant manner and (ii) total internal reflection fluorescence microscopy-based detection of endogenous VP40 association with membranes under regulation of anionic lipid content. These methods are applicable for analyzing peripheral proteins and their interactions with lipid membranes.

1. Introduction

Ebola virus (EBOV), an enveloped virus of the *Filoviridae* family, is an excellent biophysical model for studying enveloped virus assembly, despite its status as a BSL-4 pathogen (Rojek et al., 2025). Presence of the EBOV matrix protein VP40 (viral protein 40 kDa) is necessary and sufficient for virus assembly/budding in human cells (Jasenosky et al., 2001; Licata et al., 2004; Noda et al., 2002). VP40, in its dimeric form, interacts with host plasma membrane (PM; yellow arrows in Fig. 1A) and eventually forms higher-order hexamers critical for EBOV assembly (Motsa & Stahelin, 2021). The presence of anionic lipids, such as PS (Adu-Gyamfi et al., 2015; Del Vecchio et al., 2018; Husby et al., 2022) and PIP2 (Johnson et al., 2016, 2024), has been shown to be critical in supporting VP40-host PM interactions. Many questions about VP40-membrane-interactions remain

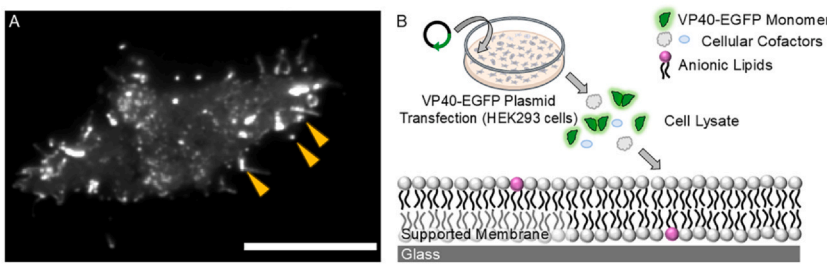

Fig. 1 Expression of VP40-EGFP for lysate collection. (A) Representative image of HEK expressing VP40-EGFP. Imaging in TIRF. Arrows indicate example sites of VP40-EGFP accumulation. Scale bar = 10 microns. (B) The VP40-host membrane interface critical for EBOV assembly can be recapitulated with reconstitution strategies employing endogenous VP40 from mammalian cell lysates and supported lipid bilayers with PS presentation.

unanswered, particularly in understanding how VP40 binding/accumulation at the host cell PM culminates into the formation of a VP40 scaffold, that, in turn, triggers virus assembly and egress. *In vitro* reconstitution offers a tunable strategy to measure these interactions under tight control of lipid composition and as a function of VP40 oligomerization state.

Here, we demonstrate a planar, glass-supported-lipid bilayer (SLB)-based approach for measuring VP40-anionic lipid interactions. Detection of individual VP40 complexes is achieved using a membrane-selective total internal reflection fluorescence (TIRF) configuration. Although this strategy has been extensively used to study protein-membrane interactions, these often rely on recombinant, purified proteins that do not recapitulate the *in vivo* landscape. To address this, several studies have extended this approach by capturing the protein-of-interest from whole cell lysates that permit post-translational modifications and other relevant interactions for the target protein function to be assessed (Jain et al., 2011; Lee et al., 2017). We introduce the cell lysate approach for the quantification of VP40 recruitment and assembly (Fig. 1B) as a platform to study viral assembly.

2. Materials and equipment

2.1 Materials

Key materials/chemicals required for this protocol are detailed in Table 1. All other chemicals used were of the highest purity available. Water purified with a Milli-Q system was used throughout.

Table 1 Key resources table.

Chemicals, Peptides, and Recombinant Proteins

1. Bovine serum albumin	Sigma	A6003
2. Albumin, Bovine Serum, Fraction V, Low Heavy Metals	Millipore Sigma	12659
3. Cell Culture Phosphate Buffered Saline (10X)	Fisher Scientific	MT-46013CM
4. 18:1 (delta9-Cis) PC (DOPC)	Avanti Research	850375
5. Dulbecco's Modified Eagles Medium	Gibco	11965-092
6. Fetal bovine serum	Biotechne	S11150

(continued)

Table 1 Key resources table. (*cont'd*)

Chemicals, Peptides, and Recombinant Proteins		
7. Beta-Glycerophosphate	Sigma	G9422
8. 100x Halt Protease Inhibitor Cocktail	Thermo Scientific	78430
9. Hellmanex III	Millipore Sigma	Z805939
10. Hydrogen peroxide, 30%	Fisher	H325
11. Opti-MEM™ I Reduced Serum Medium	Gibco	31985070
12. PEI MAX® - Transfection Grade Linear Polyethylenimine Hydrochloride (MW 40,000)	Kyfora Bio	24765-100
13. 18:1 PS (DOPS)	Avanti Research	840035
14. Sodium pyrophosphate tetrabasic	Millipore Sigma	P8010
15. Sulfuric acid GR ACS	Sigma	SX1244-5
16. 0.25% Trypsin-ETDA	Gibco	25200056
Commercial Assays		
1. Pierce™ BCA Protein Assay Kits	Thermo Fisher	23225
Experimental Models: Cell Lines		
1. HEK293T cells	ATCC	CRL-3216
Recombinant DNA		
1. Ebola VP40-EGFP	Generated in house	Adu-Gyamfi et al. (2012)
2. EGFP	Generated in house	Adu-Gyamfi et al. (2012)
Software and Algorithms		
1. NIS Elements version 5.42.03	Nikon Instruments	
1. MATLAB version 2022b	MathWorks	

Other

1. Attofluor Imaging Chamber	Thermo Fisher	A7816
2. Extruder Set Without Holder/ Heating Block	Avanti Research	610023
3. Filter support	Avanti Research	610014
4. Gastight Syringe (1000 uL)	Avanti Research/ Hamilton	610017
5. High tolerance round cover glass, (#1.5 thickness, 25 mm, round) CS-25R17	Warner Instruments	64-0735
6. 0.1 μm Membranes	Avanti Research	610005
7. BD PrecisionGlide™ Single-use Needles, 25G1	Fisher Scientific	14-821-13
8. Steriflip Vacuum Filtration System, 0.22 uM membrane PES	Millipore Sigma	SCGP00525

2.2 Equipment

2.2.1 Mammalian cell culture incubators and biosafety level 2 cabinets

Mammalian cells were cultured in a ThermoFisher 1300 Series A2 biosafety level 2 cabinet and grown in a humidified incubator (ThermoScientific HeraCell Vios 160i) maintained at 37 °C and 5% CO_2. A Sorvall Legend X1R refrigerated centrifuge (Thermo Scientific) was used for spinning down cells. HEK cells in culture were visualized using a Ts2R epifluorescence microscope (Nikon Instruments) to assess confluency and cell health.

2.2.2 Equipment for liposome preparation

Chloroform stocks of lipids were dried into a lipid film using a rotary evaporator coupled to a Scholar B-100 heating bath and a Buchi V-100 vacuum pump. Hydrated lipid films were extruded using the Avanti Mini-Extruder (Avanti Research) fitted with two 1-mL gastight syringes (Hamilton Co).

2.2.3 Total internal reflection fluorescence (TIRF) microscope

An inverted Nikon Ti2 TIRF microscope is recommended to measure recruitment of proteins (VP40, here) to membrane mimetics. A 100x TIRF objective, laser lines with 488 and 561 nm excitation, an interference reflection microscopy (IRM) cube, a LED lamp (X-Cite), and an EM-CCD camera (Andor iXon Life) were used here. The IRM cube is used for high contrast, label-free characterization of bilayers and substrate surfaces.

2.2.4 Confocal microscope

A A1Rsi confocal laser scanning microscope (Nikon Instruments) equipped with a 100x objective and a 488-nm laser line was used to assess levels of transfected protein in HEK cells.

2.2.5 Other small equipment

Branson 2800 and Lyitahome ultrasonic bath sonicators were used for cleaning Attofluor chamber components and glass coverslips. A LabNet Prism refrigerated tabletop microcentrifuge (LabNet International) was used for cell lysate preparation.

3. Protocols for reagent generation

3.1 Endogenous EBOV VP40

3.1.1 Harvest from mammalian cell lysates

(a) Plate HEK293T cells in complete DMEM (containing 10% FBS and 1% penicillin-streptomycin) in 6-well plates to target a ~65–70% confluency for transfection at 20–24 hours after plating.

(b) On the day of transfection, gently rinse cells with PBS and add fresh media, ensuring ample coverage (~1.5 mL/well). Cell debris in solution can diminish transfection efficiency.

(c) Transfect cells with 3 μg plasmids/well. Suggested constructs are (i) Ebola VP40 tagged with EGFP (VP40-EGFP) and (ii) cytosolic EGFP. A typical transfection solution, prepared in separate microcentrifuge tubes, contains 50–60 μL of Opti-MEM and each of plasmid DNA and PEI_{max} at a final ratio of 1:3 (mass/mass). Mix each tube with a few cycles of gentle pipetting before adding the DNA aliquot to the PEI_{max} aliquot. The order of addition (DNA to PEI_{max}) is crucial to minimize frothing and bubbles. Allow formation of DNA/PEI_{max} complexes by incubation for 10–15 minutes at room temperature. Ensure that the incubation

period does not exceed 15 min. Add DNA-PEI_{max} solution to cells dropwise and gently mix by swirling plate. Include control cells that are mock-transfected (Opti-MEM and PEI_{max}, no plasmid).

(d) Supplement with ~0.5 mL of warmed complete media at 8 hours post transfection. Mix by gentle side-to-side tilting of the 6-well plate.

(e) Immediately before cell lysate harvest, prepare detergent-free lysis buffer (calculations for 1 mL; 150 μL used per well of a 6-well plate – corresponds to ~1 million cells), as published before (Arauz et al., 2016)

- 100 μL of 400 mM HEPES, pH 8.0
- 100 μL of 1.5 M NaCl
- 100 μL of 100 mM β-glycerophosphate
- 100 μL of 100 mM Na pyrophosphate
- 40 μL of 0.5 M EDTA
- 1 μL of 100x Halt Protease Inhibitor Cocktail
- 559 μL fresh MilliQ Water (18 MΩ·cm)

Note: Keep lysis buffer on ice and use cold.

(f) At 48 hours post transfection, check that cells are expressing proteins of interest using an epifluorescence or confocal microscope (Fig. 2A). Remove media, wash cells in 1x PBS, and incubate cells at 37 °C for 5 min with 0.2 mL of 0.25% trypsin-EDTA/well. Neutralize remaining trypsin with 2 mL complete DMEM, pellet cells by gently centrifuging at 750 × g for 4 minutes at 4 °C, discard supernatant and keep cell pellets on ice.

(g) Add lysis buffer to pellets and incubate on ice for 60 minutes with intermittent mixing with a 1-mL pipette (suggested, ever 15–20 minutes). Minimize bubbles. If required, make wide-bore pipette tips by cutting off the bottom of 1-mL tips with clean, ethanol-sterilized scissors.

(h) Pass cell suspension through a 25G1 BD PrecisionGlide syringe at least 11 times. Keep cell suspension on ice for 30 minutes to ensure a well-packed pellet.

(i) Spin suspension at 14000 × g for 45 minutes at 4 °C and collect supernatant into fresh tubes. Aliquot supernatants into single-use fractions in microcentrifuge tubes.

(j) Store supernatants on ice if required immediately or at -20 °C for later use. Alternatively, a nominal amount of glycerol (~10% by final volume) could be added to the lysate for cryoprotection and the aliqouts drop-frozen in liquid nitrogen.

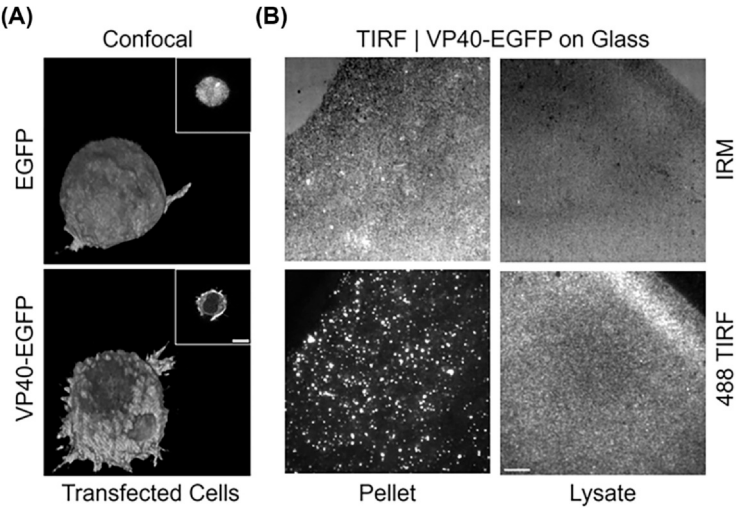

Fig. 2 Characterization of VP40-EGFP cell lysate. (A) 3D reconstruction of HEK cells expressing EGFP and VP40-EGFP at 48 hours post transfection from Z-stacks imaged on a confocal microscope. Images are reconstructed using the Alpha blending mode in NIS Elements. Expressed VP40 is preferentially localized at the plasma membrane, where EGFP is predominantly cytosolic. Inset shows a 2D image of the midplane of each cell. All images are at the same scale and scale bar = 10 microns. (B) Representative images of pellet and cell lysate fractions collected from VP40-EGFP expressing HEK cells in the IRM and 488 TIRF channel. Images for each channel are at the same scale and scale bar = 10 microns.

(k) Thaw frozen cell lysate aliquots gently on ice when needed. Check for any precipitation or cloudiness. Avoid subjecting cell lysate aliquots to more than one cycle of freeze-thaw.

3.1.1.1 Optimization and troubleshooting

(a) If a pellet is not observed after step (i) above, spin the suspension at higher speeds (up to 80000 × g, 75 minutes, 4 °C).

(b) For the first cell lysate preparation for a new DNA construct and/or cell line, check if the pellet reappears in the cell lysate aliquot after one or more cycles of freeze/thaw. If it does, characterize cell lysates again (see below; Section 3.1.2), and increase the amount of lysis buffer used (per 1 million cells) and freeze cell lysate in diluted aliquots.

3.1.1.2 Alternative methods

Detergent-free cell lysates can also be prepared using the Dounce homogenizer (Decaprio & Kohl, 2019).

3.1.2 Characterization of VP40 containing cell lysates

(a) Clean Attofluor imaging chambers and O-rings by sonicating for 30 minutes at 37 °C in a bath sonicator, first with 2% Hellmanex in Milli-Q water (MQW) and then with 1:1 isopropanol:MQW. Rinse 5x with fresh MQW after each step. After cleaning, store O-rings submerged in fresh MQW in a clean glass beaker. Dry imaging chambers in a hot air oven set to 110 °C.

(b) Clean No. 1.5 glass coverslips by sonicating for 30 minutes in with 1:1 isopropanol:MQW at room temperature and rinsing 5x with fresh MQW. Keep immersed in MQW in a clean beaker.

(c) On the day of imaging, remove chambers from hot air oven and let them cool completely.

(d) Assemble Attofluor chambers with an etched coverslip and check for leaks using 1 mL MQW or 1x PBS. Remove this solution and allow the coverslip to dry.

(e) Place ~5 μL of freshly thawed VP40 cell lysate or pellet dropwise in the middle of the coverslip. Allow to dry and then backfill with 1 mL of 1x PBS.

(f) Image samples on a TIRF microscope using a 488-nm excitation to check for VP40 levels in the cell lysate. As shown in Fig. 2B, the cell lysate sample should have diffuse intensity indicating the presence of VP40, whereas the pellet sample should have more punctate intensity reflecting the protein fraction retained on the membrane. Recommended settings for imaging are ~1% laser power and 100 ms exposure time.

3.1.2.1 Optimization and troubleshooting

Cell-like morphologies observed for the pellet fraction (in a diascopic or IRM channel) signifies incomplete lysis. Optimize the cell lysate preparation protocol (Section 3.1.1) accordingly.

3.2 Supported lipid bilayers (SLBs)

3.2.1 Assembling imaging chambers

(a) Clean Attofluor imaging chambers as detailed in Section 3.1.2.

(b) Clean No. 1.5 glass coverslips by sonicating for 30 minutes in with 1:1 isopropanol:MQW at room temperature, rinsing 5x with fresh MQW, and etching for 5–8 minutes with a piranha solution consisting of 3:1 (v/v) of sulfuric acid and hydrogen peroxide. After etching, dispose of used Piranha solution safely and rinse etched coverslips with MQW. Keep immersed in MQW in a clean beaker and use immediately.

(c) On the day of SLB deposition and imaging, remove imaging chambers from hot air oven and let them cool completely.

(d) Assemble Attofluor chambers with an etched coverslip and check for leaks using MQW or 1x PBS. Keep coverslip under water and chambers covered with lint-free paper until ready for SLB deposition.

3.2.1.1 Safety considerations

Piranha solution is extremely corrosive and should be handled only inside a chemical fume hood or acid hood. Use of a full suite of personal protective equipment including goggles, face shield, a long-sleeved lab coat with a rubber apron on top, covered shoes, and double gloving with chemical resistant gloves is mandatory. Disposal of used Piranha solution must be in accordance with regulations and protocols in place at specific workplaces. Any surfaces suspected to be contaminated with trace amounts of Piranha solution must be immediately neutralized with powdered sodium bicarbonate and rinsed with water.

3.2.2 Preparation of large unilamellar vesicles

(a) Transfer required lipid amounts to an etched, dried, and cooled round bottomed flask containing some amount of chloroform using positive displacement pipettes or gastight Hamilton syringes. A typical lipid composition is based on mole percentages of different lipids with the bulk made up of a neutral lipid such as DOPC. Here, compositions included 2 or 30 mole percent PS, with the remainder comprised of DOPC.

(b) Make lipid films by evaporating solvent from the round bottomed flask(s) on a rotary evaporator. Hydrate with required amounts of freshly dispensed MQW to make multilamellar vesicles. Recommended lipid concentration is 1 mg/mL. Keep on ice.

(c) Make liposomes by extruding suspension containing multilamellar vesicles through 100 nm polycarbonate membranes for 21 times or more (must be an odd number of passes). Keep on ice till deposition. Use within 12 hours.

3.2.3 Depositing SLBs

(a) Remove most of the water from coverslips. From this point on, ensure that the coverslip does not dry out completely during any of the steps.

(b) Add 80–100 μL of 1 mg/mL liposomes and 300 μL 10x PBS (final liposome concentration of 0.4 mg/mL) to the imaging chamber. Incubate for at least 10 minutes and rinse 5 times with 1x PBS (5 mL volume for each wash step). These volumes and ionic strength conditions

are known to support liposome rupture and SLB formation, as reviewed extensively elsewhere (Lin et al., 2010).

(c) During the incubation period, prepare a solution of 2% BSA (w/v) in 2x PBS. Minimize frothing by dissolving BSA with a rotating mixer and filter through 0.2 mm PES membrane filter units.

(d) Block with 1% BSA in 1x PBS by adding 500 μL of filtered 2% BSA in 2x PBS in each chamber and incubating for 20 minutes. Rinse 5 times with 1x PBS (5 mL volume for each wash step). Store bilayers at room temperature until imaging.

4. SLB-based assays for quantitative assessment of EBOV VP40 interaction with host membrane mimetics

4.1 Ensemble/single-molecule TIRF microscopy

4.1.1 Optical imaging of VP40 accumulation at SLBs

(a) Thaw cell lysates on ice immediately before imaging. Check that there is no pellet. Estimate total protein concentration by BCA assay.

(b) Pre-warm imaging chamber on a 37 °C heating block for at least 5 minutes. Load imaging chamber on the microscope stage and set the focal plane to the glass interface.

(c) Recommended for each lipid composition: label one SLB with DiI (or any other lipophilic fluorophore) for a diagnostic check on SLB quality. Make the labeling solution by 1:200 dilution of DiI (stock concentration of 1 mg/mL) with 1x PBS. Remove 200 μL of 1x PBS from the imaging chamber, add equivalent volume of the DiI labeling solution, and incubate for 2 min. Wash with 1x PBS (5 mL volume). Check that the SLBs are uniform and devoid of defects which may appear as dark holes in the image. In case a large amount of unruptured liposomes or tubules are noted, wash 5x with 1x PBS (5 mL volume for each step) to remove unruptured liposomes.

(d) Confirm that the labeled bilayer is mobile by running a fluorescence recovery after photobleaching (FRAP) experiment, as follows:
- Bleach the field of view with a high laser power (~15–20%)
- Track recovery of fluorescence at the bleach spot by imaging the field of view at lower laser power (~1%) every 5 seconds.
- Fluid phase SLBs should exhibit near-complete recovery of intensity in the bleach spot.

(e) Load a fresh pre-warmed bilayer on the microscope stage.

(f) Acquire several (~10 fields-of-view recommended) images of the bilayer in the 488 TIRF channel. Recommended imaging settings are 5–12% laser power and 100 ms exposure time. Optimum signal to noise ratios may also be achieved by changing the TIRF angle such that the collected signal is predominantly from the bilayer surface. Confirm minimal signal or non-specific signal in other channels, such as 561-nm.

(g) Add cell lysate on the bilayer (on the microscope stage) and incubate for 10 minutes to allow engagement with the lipids. The lysate concentration needs to be optimized so that recruited VP40 assemblies can be isolated for quantification. Acquire images at the 488-channel using same settings as (f) to track VP40 accumulation on the SLB (representative images in Fig. 3B-C).

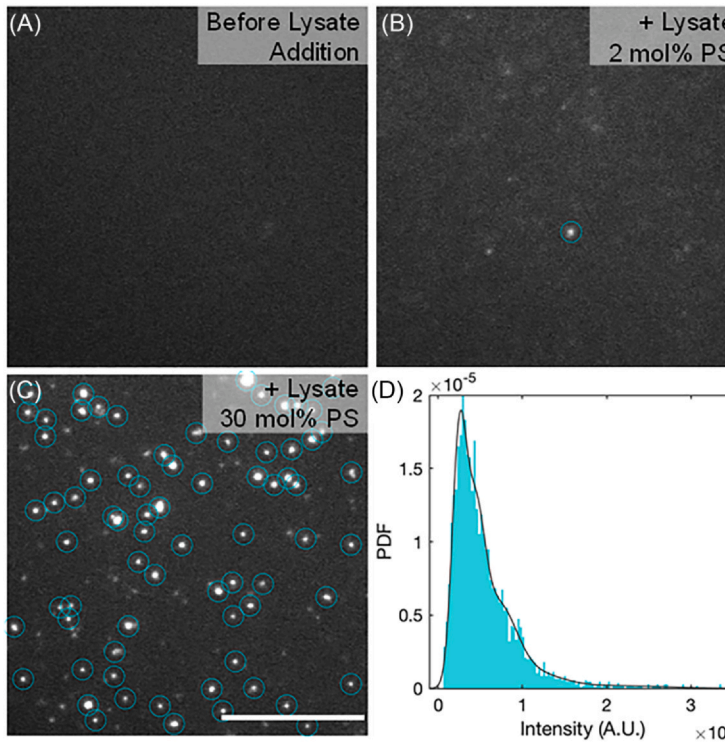

Fig. 3 Recruitment of VP40 captured from cell lysates to supported membranes with phosphatidylserine lipids. (A) Example image in 488 TIRF of SLB prior to lysate addition. Example images of SLB containing (B) 2 mol% PS lipids and (C) 30 mol% PS lipids after addition of VP40-EGFP-containing lysate. Localized objects are circled in cyan. All images (A-C) are at the same scale and scale bar = 10 microns. (D) Intensity distribution for thousands of objects localized on 30 mol% SLBs. Black line is plotted to guide the eye and show the shoulder and tail of intensities of high values.

4.2 Data analysis

4.2.1 VP40 accumulation

(a) TIRF 488 images are background corrected by subtracting the average pixel value for the images in the absence of lysate over regions that are at least 200 × 200 pixels from each raw data image.

(b) VP40-eGFP particles are assumed to have Gaussian fluorescence patterns. Fitting using custom algorithms in MATLAB are used to isolate each particle (Lidke et al., 2011; Low-Nam et al., 2011; Smith et al., 2010). Standard software such as TrackMate (FIJI) can be used. The center of the field of view is fit (256 × 256 pixels) to avoid the need for flatfield correction.

(c) In addition to object localization, the integrated intensity of each object is extracted.

5. Expected outcomes and conclusions

The protocols outlined here are expected to generate minimal systems that can recapitulate the membrane interaction behavior of a range of peripheral proteins. Combining these reconstituted interfaces with TIRF-based optical imaging would enable precise estimates of features of membrane accumulation exhibited by these proteins, both at the ensemble and single-molecule level. As an example, Fig. 3A-C recapitulates the dependence on PS lipids known to govern recruitment of VP40 to host PM. Further, the intensity distribution (shown in Fig. 3D) of localized VP40 spots on the SLB reflect intrinsic distributions in membrane-bound VP40 clusters and could be relevant in understanding how VP40-membrane interactions culminate into the large-scale membrane remodeling required for EBOV assembly and egress. These strategies, in combination with the cell lysate approach, will expand our capabilities of interrogating interactions of viral matrix peripheral proteins with host membrane mimetics in the context of different host environments.

Acknowledgments

This work was supported by a National Institutes of Health grant to R.V.S. (AI158220) and an Indiana CTSI PDT grant (S.L.N. and R.V.S.).

References

Adu-Gyamfi, E., Digman, M. A., Gratton, E., & Stahelin, R. V. (2012). Investigation of Ebola VP40 assembly and oligomerization in live cells using number and brightness analysis. *Biophysical Journal, 102*(11), 2517–2525. https://doi.org/10.1016/j.bpj.2012.04.022.

Adu-Gyamfi, E., Johnson, K. A., Fraser, M. E., Scott, J. L., Soni, S. P., Jones, K. R., ... Stahelin, R. V. (2015). Host cell plasma membrane phosphatidylserine regulates the assembly and budding of Ebola virus. *Journal of Virology, 89*(18), 9440–9453. https://doi.org/10.1128/jvi.01087-15.

Arauz, E., Aggarwal, V., Jain, A., Ha, T., & Chen, J. (2016). Single-molecule analysis of lipid-protein interactions in crude cell lysates. *Analytical Chemistry, 88*(8), 4269–4276. https://doi.org/10.1021/acs.analchem.5b04127.

Decaprio, J., & Kohl, T. O. (2019). Using dounce homogenization to Lyse cells for immunoprecipitation. *Cold Spring Harbor Protocols, 2019*(7), 551–554. https://doi.org/10.1101/pdb.prot098574.

Del Vecchio, K., Frick, C. T., Gc, J. B., Oda, S. I., Gerstman, B. S., Saphire, E. O., ... Stahelin, R. V. (2018). A cationic, C-terminal patch and structural rearrangements in Ebola virus matrix VP40 protein control its interactions with phosphatidylserine. *Journal of Biological Chemistry, 293*(9), 3335–3349. https://doi.org/10.1074/jbc.M117.816280.

Husby, M. L., Amiar, S., Prugar, L. I., David, E. A., Plescia, C. B., Huie, K. E., ... Stahelin, R. V. (2022). Phosphatidylserine clustering by the Ebola virus matrix protein is a critical step in viral budding. *EMBO Reports, 23*(11), https://doi.org/10.15252/embr.202051709.

Jain, A., Liu, R., Ramani, B., Arauz, E., Ishitsuka, Y., Ragunathan, K., ... Ha, T. (2011). Probing cellular protein complexes using single-molecule pull-down. *Nature, 473*(7348), 484–488. https://doi.org/10.1038/nature10016.

Jasenosky, L. D., Neumann, G., Lukashevich, I., & Kawaoka, Y. (2001). Ebola Virus VP40-Induced Particle Formation and Association with the Lipid Bilayer. *Journal of Virology, 75*(11), 5205–5214. https://doi.org/10.1128/jvi.75.11.5205-5214.2001.

Johnson, K. A., Budicini, M. R., Bhattarai, N., Sharma, T., Urata, S., Gerstman, B. S., ... Stahelin, R. V. (2024). PI(4,5)P2 binding sites in the Ebola virus matrix protein VP40 modulate assembly and budding. *Journal of Lipid Research, 65*(3), https://doi.org/10.1016/j.jlr.2024.100512.

Johnson, K. A., Taghon, G. J. F., Scott, J. L., & Stahelin, R. V. (2016). The Ebola Virus matrix protein, VP40, requires phosphatidylinositol 4,5-bisphosphate (PI(4,5)P 2) for extensive oligomerization at the plasma membrane and viral egress. *Scientific Reports, 6*. https://doi.org/10.1038/srep19125.

Lee, Y. K., Low-Nam, S. T., Chung, J. K., Hansen, S. D., Lam, H. Y. M., Alvarez, S., & Groves, J. T. (2017). Mechanism of SOS PR-domain autoinhibition revealed by single-molecule assays on native protein from lysate. *Nature Communications, 8*. https://doi.org/10.1038/ncomms15061.

Licata, J. M., Johnson, R. F., Han, Z., & Harty, R. N. (2004). Contribution of Ebola Virus glycoprotein, nucleoprotein, and VP24 to budding of VP40 virus-like particles. *Journal of Virology, 78*(14), 7344–7351. https://doi.org/10.1128/jvi.78.14.7344-7351.2004.

Lidke, D. S., Low-Nam, S. T., Cutler, P. J., & Lidke, K. A. (2011). Determining FcεRI diffusional dynamics via single quantum dot tracking. *Methods in Molecular Biology (Clifton, N.J.), 748*, 121–132. https://doi.org/10.1007/978-1-61779-139-0_8.

Lin, W., Yu, C., Triffo, S., & Groves, J. T. (2010). Supported membrane formation, characterization, functionalization, and patterning for application in biological science and technology. *Current Protocols in Chemical Biology, 2*(4), 235–269. https://doi.org/10.1002/9780470559277.ch100131.

Low-Nam, S. T., Lidke, K. A., Cutler, P. J., Roovers, R. C., Van Bergen En Henegouwen, P. M. P., Wilson, B. S., & Lidke, D. S. (2011). ErbB1 dimerization is promoted by domain co-confinement and stabilized by ligand binding. *Nature Structural and Molecular Biology, 18*(11), 1244–1249. https://doi.org/10.1038/nsmb.2135.

Motsa, B. B., & Stahelin, R. V. (2021). Lipid-protein interactions in virus assembly and budding from the host cell plasma membrane. *Biochemical Society Transactions, 49*(4), 1633–1641. https://doi.org/10.1042/BST20200854.

Noda, T., Sagara, H., Suzuki, E., Takada, A., Kida, H., & Kawaoka, Y. (2002). Ebola virus VP40 drives the formation of virus-like filamentous particles along with GP. *Journal of Virology, 76*(10), 4855–4865. https://doi.org/10.1128/jvi.76.10.4855-4865.2002.

Rojek, A., Fieggen, J., Apiyo, P., Caluwaerts, S., Fowler, R. A., Kaleebu, P., ... Horby, P. (2025). Ebola disease: Bridging scientific discoveries and clinical application. *The Lancet Infectious Diseases, 25*(3), e165–e176. https://doi.org/10.1016/S1473-3099(24)00673-X.

Smith, C. S., Joseph, N., Rieger, B., & Lidke, K. A. (2010). Fast, single-molecule localization that achieves theoretically minimum uncertainty. *Nature Methods, 7*(5), 373–375. https://doi.org/10.1038/nmeth.1449.

CHAPTER FIFTEEN

Palmitoylation-dependent probes for labeling the Golgi apparatus

Shunsuke Sawada[a], Keita Tsutsui[b], and Shinya Tsukiji[b,c,d,*]
[a]Department of Environment and Sustainability, Mukogawa Women's University, Nishinomiya, Japan
[b]Department of Nanopharmaceutical Sciences, Nagoya Institute of Technology, Nagoya, Japan
[c]Department of Life Science and Applied Chemistry, Nagoya Institute of Technology, Nagoya, Japan
[d]OptoBioTechnology Research Center, Nagoya Institute of Technology, Nagoya, Japan
*Corresponding author. e-mail address: stsukiji@nitech.ac.jp

Contents

1. Introduction 306
2. Method 1: Chemical synthesis of myrGC^{3Me}-conjugated fluorescent probes 308
   2.1 Before you begin 310
   2.2 Synthesis of myr-^{Me}Gly-^{Me}Cys(Trt)-^{Me}Adox-Lys-NH_2 311
   2.3 Synthesis of mgc^{3Me}FDA 315
   2.4 Synthesis of mgc^{3Me}DEAC 315
   2.5 Synthesis of mgc^{3Me}TMR 316
3. Method 2: Fluorescent staining of the Golgi apparatus in living cells 317
   3.1 Before you begin 318
   3.2 Staining and fluorescent imaging of live-cell Golgi 319
4. Method 3: Visualization of Golgi dynamics under drug treatment 320
   4.1 Before you begin 320
   4.2 Time-lapse fluorescence imaging of Golgi dynamics during BFA treatment 321
5. Method 4: Visualization of Golgi dynamics during cell division 322
   5.1 Before you begin 322
   5.2 Time-lapse fluorescence imaging of Golgi dynamics during cell division 323
Acknowledgments 323
References 324

Abstract

Small-molecule fluorescent probes that selectively stain the Golgi apparatus in living cells are valuable tools for investigating Golgi-associated biology and disease. Conventional ceramide-based stains have been widely used, but they require complex staining procedures and often exhibit low Golgi specificity. To address these limitations, we recently developed a series of fluorescent probes incorporating the tri-*N*-methylated myristoyl-Gly-Cys (myrGC^{3Me}) motif, which targets the Golgi membrane via *S*-palmitoylation. Modular conjugation of this motif with organic fluorescent dyes yielded blue, green, and red fluorescent probes. Here, we provide detailed procedures for the chemical synthesis and application of these probes to enable simple and rapid

Methods in Enzymology, Volume 728
ISSN 0076-6879, https://doi.org/10.1016/bs.mie.2026.01.005
Copyright © 2026 Elsevier Inc. All rights are reserved, including those for text and data mining, AI training, and similar technologies.

staining of the Golgi in living cells with high specificity and negligible cytotoxicity. We also describe procedures for visualizing dynamic changes in Golgi morphology during drug treatments and cell division.

1. Introduction

The Golgi apparatus plays essential roles in the regulation of cell physiology. The lumen of the Golgi serves as a hub for the glycosylation of proteins and lipids (Colley, 1997; Varki, 1998; Zhang & Wang, 2016), while various biological processes, including membrane trafficking (Brandizzi, & Barlowe, 2013; Glick, & Nakano, 2009), protein *S*-palmitoylation (Ernst et al., 2018; Fukata & Fukata, 2010; Salaun et al., 2010), signaling (Cancino & Luini, 2013; Crilly & Puthenveedu, 2021; Fehrenbacherb et al., 2009; Hannun & Obeid, 2008), and lipid transport (Hannun & Obeid, 2008) are regulated at the cytoplasmic face of the Golgi membrane. Importantly, the Golgi exhibits different morphologies depending on cell type, tissue, and cellular conditions (Ireland et al., 2020). Abnormal Golgi morphology is associated with various neurodegenerative diseases, such as Alzheimer's disease, amyotrophic lateral sclerosis (ALS), and Parkinson's disease, as well as many cancers (Bexiga & Simpson, 2013; Bui et al., 2021; Caracci et al., 2019; Malhoul et al., 2019; Sundaramoorthy et al., 2015). Therefore, methods to visualize Golgi structure and its dynamics in living cells are indispensable tools for studying Golgi-associated cell biology and disease.

Fluorescent protein-based Golgi markers have been established for visualizing the Golgi apparatus in living cells (Llopis et al., 1998; Storrie et al., 1998). These markers are genetically encoded and require exogenous plasmid transfection, a process that is time-consuming and applicable only to cells amenable to gene transfection. Furthermore, excessive expression of fluorescent protein-based markers frequently perturbs native Golgi morphology. In contrast, Golgi-targeted small-molecule fluorescent probes enable Golgi staining without genetic manipulation. To date, BODIPY FL and BODIPY TR ceramide probes, developed and commercialized by Molecular Probes, have long been used as Golgi stains (Lipsky & Pagano, 1985; Makiyama et al., 2015; Pagano et al., 1991). Ceramide probes accumulate in the Golgi through their trafficking from the endoplasmic reticulum (ER) via the ceramide transporter CERT (Perry & Ridgway, 2005). However, they have several serious limitations. Golgi staining with BODIPY FL/TR ceramide probes involves a cumbersome multistep

protocol, including bovine serum albumin (BSA) complexation, incubation at 4 °C, washing, and subsequent re-incubation at 37 °C (Lipsky & Pagano, 1985; Pagano et al., 1991). Most critically, ceramide-based fluorescent probes exhibit nonspecific localization to the ER, resulting in only low-to-moderate specificity for Golgi visualization. Consequently, the development of new small-molecule Golgi stains that are easy to use and offer higher Golgi specificity has long been awaited.

We recently developed a new class of Golgi-localizing small-molecule fluorescent probes. These probes are based on our recently identified synthetic palmitoylation motif consisting of a tri-*N*-methylated myristoyl-Gly-Cys (myrGC^{3Me}) lipopeptide (Sawada et al., 2020). The myrGC^{3Me} motif undergoes *S*-palmitoylation of the Cys residue by palmitoyl acyltransferases (PATs) at the Golgi surface and specifically localizes to Golgi membranes (Fig. 1A). By modularly conjugating this motif with different

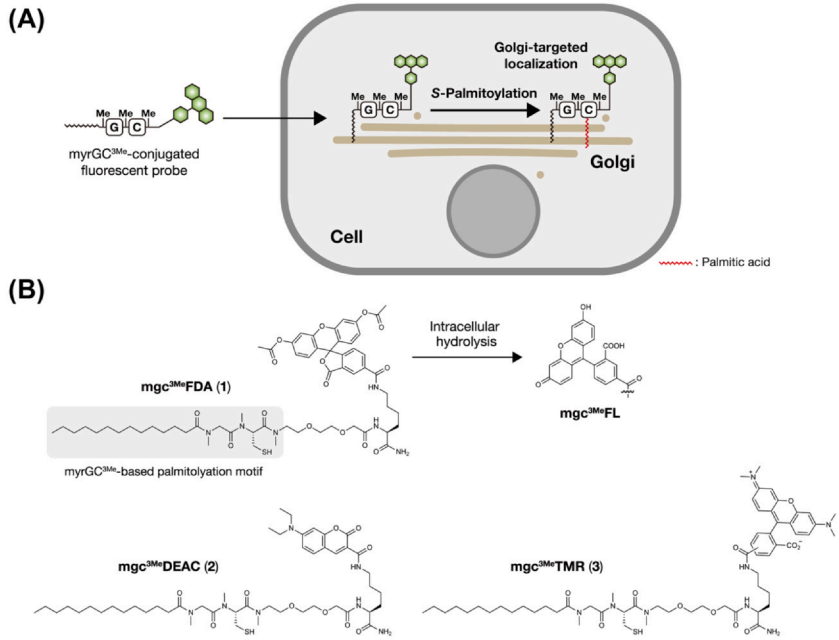

Fig. 1 Golgi-targeted fluorescent probes. (**A**) Schematic illustration of palmitoylation-dependent Golgi localization of myrGC^{3Me}-tethered fluorescent probes. (**B**) Chemical structures of the Golgi-targeted fluorescent probes described in this protocol: **mgc^{3Me}FDA** (**1**), **mgc^{3Me}DEAC** (**2**), and **mgc^{3Me}TMR** (**3**). Upon cell entry, the acetyl groups of the fluorescein diacetate moiety in **mgc^{3Me}FDA** (non-fluorescent) undergo hydrolysis by intracellular esterases, yielding fluorescein-based **mgc^{3Me}FL** (fluorescent) in cells.

organic fluorophores, we generated blue, green, and red fluorescent Golgi probes (Fig. 1B) (Sawada et al., 2020). These probes show negligible cytotoxicity and can rapidly stain the Golgi of various cell lines through a simple incubation and wash procedure. In this chapter, we describe detailed protocols for their chemical synthesis (**Method 1**) and for their application to fluorescent Golgi staining (**Method 2**), as well as visualization of live-cell Golgi dynamics during drug treatments (**Method 3**) and cell division (**Method 4**).

2. Method 1: Chemical synthesis of myrGC^{3Me}-conjugated fluorescent probes

The chemical synthesis of palmitoylation-dependent fluorescent Golgi probes combines solid-phase synthesis and solution-phase synthesis. The core Golgi-targeting structure—comprising the tri-*N*-methylated myrGC^{3Me} motif, a flexible linker, and a terminal lysine (Lys) residue—is prepared by a modified Fmoc-based solid-phase peptide synthesis protocol coupled with an on-resin *N*-methylation protocol (Fig. 2) (Biron et al., 2006). The resulting

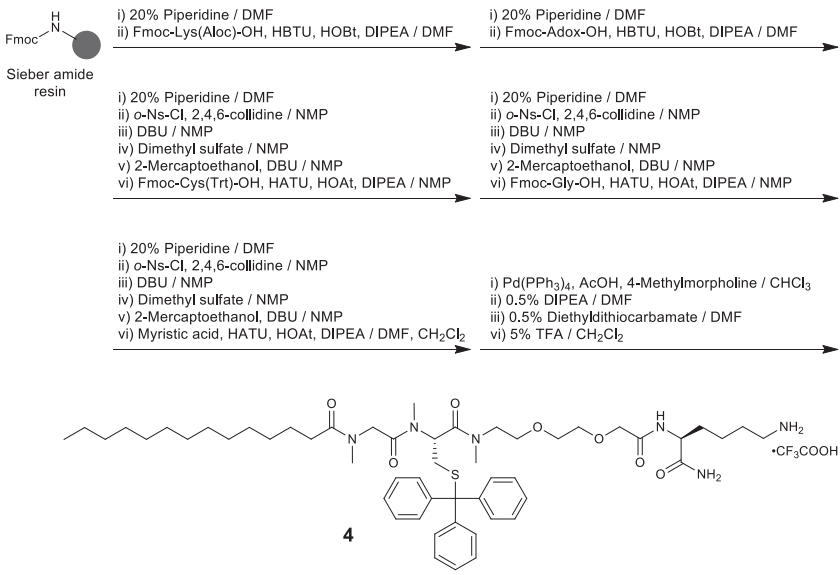
Fmoc
H
N
Sieber amide resin
i) 20% Piperidine / DMF
ii) Fmoc-Lys(Aloc)-OH, HBTU, HOBt, DIPEA / DMF
i) 20% Piperidine / DMF
ii) Fmoc-Adox-OH, HBTU, HOBt, DIPEA / DMF
i) 20% Piperidine / DMF
ii) o-Ns-Cl, 2,4,6-collidine / NMP
iii) DBU / NMP
iv) Dimethyl sulfate / NMP
v) 2-Mercaptoethanol, DBU / NMP
vi) Fmoc-Cys(Trt)-OH, HATU, HOAt, DIPEA / NMP
i) 20% Piperidine / DMF
ii) o-Ns-Cl, 2,4,6-collidine / NMP
iii) DBU / NMP
iv) Dimethyl sulfate / NMP
v) 2-Mercaptoethanol, DBU / NMP
vi) Fmoc-Gly-OH, HATU, HOAt, DIPEA / NMP
i) 20% Piperidine / DMF
ii) o-Ns-Cl, 2,4,6-collidine / NMP
iii) DBU / NMP
iv) Dimethyl sulfate / NMP
v) 2-Mercaptoethanol, DBU / NMP
vi) Myristic acid, HATU, HOAt, DIPEA / DMF, CH_2Cl_2
i) $Pd(PPh_3)_4$, AcOH, 4-Methylmorpholine / $CHCl_3$
ii) 0.5% DIPEA / DMF
iii) 0.5% Diethyldithiocarbamate / DMF
vi) 5% TFA / CH_2Cl_2
O
N
S
NH_2
$\cdot CF_3COOH$
4

Fig. 2 Synthetic route of compound 4.

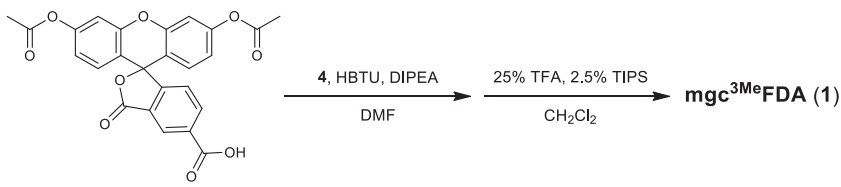

Fig. 3 Synthetic route of mgc^{3Me}FDA.

Fig. 4 Synthetic route of mgc^{3Me}DEAC.

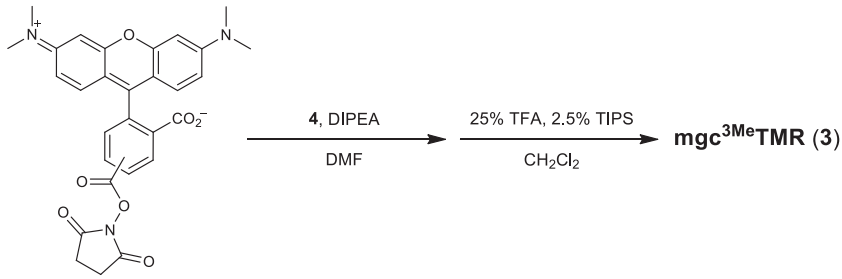

Fig. 5 Synthetic route of mgc^{3Me}TMR.

fragment contains a Cys thiol side chain protected by an acid-sensitive trityl (Trt) group, while the Lys side chain amine remains free. The amine-functionalized, thiol-protected myrGC^{3Me} fragment is then conjugated to carboxylic acid derivatives of organic fluorescent dyes via a solution-phase coupling reaction (Figs. 3–5). Subsequent acid treatment removes the Trt group to yield the target molecules. Here, we describe protocols for the synthesis of myrGC^{3Me}-conjugated fluorescein diacetate [**mgc^{3Me}FDA** (**1**)], diethylcoumarin [**mgc^{3Me}DEAC** (**2**)], and tetramethylrhodamine [**mgc^{3Me}TMR** (**3**)]. This synthetic strategy can readily be adapted to generate other Golgi-targeted molecules by changing the fluorophore conjugated to the myrGC^{3Me} motif. Note that myrGC^{3Me}FDA is also commercially available from Funakoshi Co., Ltd.

2.1 Before you begin

2.1.1 Reagents

Amino acids and building blocks

- Sieber amide Resin
- Fmoc-Lys(Aloc)-OH
- Fmoc-8-amino-3,6-dioxaoctanoic acid (Fmoc-8-Adox-OH)
- Fmoc-Cys(Trt)-OH
- Fmoc-Gly-OH
- Myristic acid
- 5-Carboxyfluorescein diacetate
- 7-(Diethylamino)coumarin-3-carboxylic acid
- 5,6-Carboxytetramethylrhodamine succinimidyl ester

Solvents and other reagents

- *N*,*N*-Dimethylformamide (DMF), peptide synthesis grade
- 20 % Piperidine in DMF for Fmoc deprotection
- Kaiser test solution
  - **(i)** Ninhydrin/ethanol (0.5 g/10 mL)
  - **(ii)** Phenol/ethanol (40 g/10 mL)
  - **(iii)** Potassium cyanide (KCN)/pyridine (0.2 mL of 1 mM KCN aqueous solution + 9.8 mL pyridine)
- Mix solutions (i)–(iii) at a 1:1:1 ratio before use.
- HBTU [2-(1H-benzotriazole-1-yl)−1,1,3,3-tetramethyluronium hexafluorophosphate]
- HOBt (1-hydroxybenzotriazole monohydrate)
- HATU [1-[bis(dimethylamino)methylene]−1*H*-1,2,3-triazolo[4,5-*b*] pyridinium 3-oxide hexafluorophosphate]
- HOAt (1-hydroxy-7-azabenzotriazole)
- *N*,*N*-Diisopropylethylamine (DIPEA)
- 1-Methyl-2-pyrrolidone (NMP), peptide synthesis grade
- 2-Nitrobenzenesulfonyl chloride (*o*-Ns-Cl)
- 2,4,6-Collidine
- 1,8-Diazabicyclo[5.4.0]undec-7-ene (DBU)
- Dimethyl sulfate
- Chloranil test solution
  - **(i)** Acetaldehyde/DMF (1 mL/49 mL)
  - **(ii)** Chloranil/DMF (1 g0/49 mL)

    Mix solutions (i) and (ii) at a 1:1 ratio before use.

- 2-Mercaptoethanol
- Dichloromethane (CH_2Cl_2)
- Chloroform ($CHCl_3$)
- Tetrakis(triphenylphosphine)palladium(0) [$Pd(PPh_3)_4$]
- Acetic acid
- 4-Methylmorpholine
- Diethyldithiocarbamate
- Methanol (MeOH)
- Trifluoroacetic acid (TFA)
- Triisopropylsilane (TIPS)
- Acetonitrile (MeCN), high-performance liquid chromatography (HPLC) grade
- Toluene
- Diethyl ether (Et_2O)

2.1.2 Equipment

- Empty polypropylene column with filter (e.g., empty PD-10 column; GE Healthcare)
- Rotary shaker (for solid-phase synthesis) (e.g., KMS-3; Kokusan Chemical)
- Evaporator equipped with a vacuum pump (e.g., EYELA N-1110)
- 1.5-mL glass tube (for Kaiser and chloranil tests)
- 50-mL eggplant flask
- 1.5-mL microcentrifuge tube (Eppendorf type)
- Micropipette (e.g., NICHIRYO Nichipet EX Plus II)
- Heating dry bath incubator settable at 100 °C (for Kaiser test) (e.g., Nisshin Thermo Block ND-M01)
- HPLC system equipped with a UV detector (e.g., Hitachi LaChrome system)
- C4 HPLC column [e.g., YMC-Pack C4 column (5 μm, 10 × 250 mm)]
- Lyophilizer (e.g., EYELA FDU-1200)

2.2 Synthesis of myr-^{Me}Gly-^{Me}Cys(Trt)-^{Me}Adox-Lys-NH_2

The synthetic scheme is shown in Fig. 2. The following protocol describes the synthesis on a 40 μmol scale.

1. Add Sieber amide resin (loading: 0.79 mmol/g, 50.6 mg, 40 μmol) into a polypropylene column and place it on a rotary shaker.
2. Swell the resin in DMF (ca. 3 mL) by agitation.
3. Remove DMF by vacuum filtration.
4. Add 20 % piperidine in DMF (3 mL) to the resin.
5. Agitate the resin at room temperature for 15 min

6. Wash the resin with DMF (ca. 4 mL) three times.
7. (Optional) Take a small portion of the resin beads and confirm Fmoc deprotection by the Kaiser test. Both the test solution and the resin beads should appear deep purple.
8. Add a solution of Fmoc-Lys(Aloc)-OH (56.1 mg, 124 μmol, 3.1 eq.), HBTU (45.5 mg, 120 μmol, 3.0 eq.), HOBt (18.4 mg, 120 μmol, 3.0 eq.), and DIPEA (40.8 μL, 240 μmol, 6.0 eq.) in DMF (0.6 mL) to the resin.
9. Agitate the resin at room temperature for 30 min
10. Take a small portion of the resin beads and check the completion of coupling by the Kaiser test. The resin beads should remain colorless. If a purplish color is observed, repeat steps 8–9.
11. Wash the resin with DMF (ca. 4 mL) three times.
12. Add 20 % piperidine in DMF (3 mL) to the resin.
13. Agitate the resin at room temperature for 15 min
14. Wash the resin with DMF (ca. 4 mL) three times.
15. (Optional) Take a small portion of the resin beads and confirm Fmoc deprotection by the Kaiser test, as in step 7.
16. Add a solution of Fmoc-Adox-OH (47.8 mg, 124 μmol, 3.1 eq.), HBTU (45.5 mg, 120 μmol, 3.0 eq.), HOBt (18.4 mg, 120 μmol, 3.0 eq.), and DIPEA (40.8 μL, 240 μmol, 6.0 eq.) in DMF (0.6 mL) to the resin.
17. Agitate the resin at room temperature for 30 min
18. Take a small portion of the resin beads and check the completion of coupling by the Kaiser test. The resin beads should remain colorless. If a purplish color is observed, repeat steps 16–17.
19. Wash the resin with DMF (ca. 4 mL) three times.
20. Add 20 % piperidine in DMF (3 mL) to the resin.
21. Agitate the resin at room temperature for 15 min
22. Wash the resin with DMF (ca. 4 mL) three times, followed by three washes with NMP (ca. 4 mL).
23. (Optional) Take a small portion of the resin beads and confirm Fmoc deprotection by the Kaiser test, as in step 7.
24. Add a solution of *o*-Ns-Cl (35.5 mg, 160 μmol, 4.0 eq.) and 2,4,6-collidine (52.7 μL, 400 μmol, 10.0 eq.) in NMP (0.8 mL) to the resin.
25. Agitate the resin at room temperature for 15 min
26. Wash the resin with NMP (ca. 4 mL) three times.
27. Take a small portion of the resin beads and check the completion of *N*-nosylation by the Kaiser test. The resin beads should remain colorless. If a purplish color is observed, repeat steps 24–26.

28. Add a solution of DBU (54.4 μL, 360 μmol, 9.0 eq.) in NMP (0.8 mL) to the resin.
29. Agitate the resin at room temperature for 3 min
30. Remove the DBU solution by vacuum filtration.
31. Add a solution of dimethyl sulfate (37.9 μL, 400 μmol, 10.0 eq.) in NMP (0.8 mL) to the resin.
32. Agitate the resin at room temperature for 2 min
33. Remove the solution and repeat steps 28–32.
34. Wash the resin with NMP (ca. 4 mL) three times.
35. Take a small portion of the resin beads and check the *N*-methylation by the chloranil test. The resin beads should remain colorless. If a bluish color is observed, repeat steps 28–34.
36. Add a solution of 2-mercaptoethanol (27.9 μL, 400 μmol, 10.0 eq.) and DBU (30.2 μL, 200 μmol, 5.0 eq.) in NMP (0.8 mL) to the resin.
37. Agitate the resin at room temperature for 5 min
38. Remove the solution and repeat steps 36–37.
39. Wash the resin with NMP (ca. 4 mL) three times.
40. Take a small portion of the resin beads and confirm nosyl group deprotection by the chloranil test. The resin beads should appear deep blue.
41. Add a solution of Fmoc-Cys(Trt)-OH (96.1 mg, 164 μmol, 4.1 eq.), HATU (60.8 mg, 160 μmol, 4.0 eq.), HOAt (21.8 mg, 160 μmol, 4.0 eq.), and DIPEA (54.4 μL, 320 μmol, 8.0 eq.) in NMP (0.6 mL) to the resin.
42. Agitate the resin at room temperature for 180 min
43. Wash the resin with NMP (ca. 4 mL) three times.
44. Take a small portion of the resin beads and check the completion of coupling by the chloranil test. The resin beads should remain colorless. If a bluish color is observed, repeat steps 41–43.
45. Repeat steps 20–40 to introduce *N*-methylation to the Cys residue.
46. Add a solution of Fmoc-Gly-OH (48.8 mg, 164 μmol, 4.1 eq.), HATU (60.8 mg, 160 μmol, 4.0 eq.), HOAt (21.8 mg, 160 μmol, 4.0 eq.), and DIPEA (54.4 μL, 320 μmol, 8.0 eq.) in NMP (0.6 mL) to the resin.
47. Repeat steps 42–44 to couple Fmoc-Gly-OH to the N-terminal cysteine.
48. Repeat steps 20–40 to introduce *N*-methylation to the Gly residue.
49. Add a solution of myristic acid (28.3 mg, 124 μmol, 3.1 eq.), HATU (45.6 mg, 120 μmol, 3.0 eq.), HOAt (16.3 mg, 120 μmol, 3.0 eq.), and DIPEA (40.8 μL, 240 μmol, 6.0 eq.) in DMF/CH_2Cl_2 (1:1) (0.6 mL) to the resin.
50. Repeat steps 42–44 to couple myristic acid to the N-terminal glycine.

51. Wash the resin with DMF (ca. 4 mL), MeOH (ca. 4 mL), and CH_2Cl_2 (ca. 4 mL).
52. Dry the resin in vacuo.
53. Swell the resin in $CHCl_3$ (ca. 3 mL) by agitation.
54. Remove $CHCl_3$ by vacuum filtration.
55. Add a solution of tetrakis(triphenylphosphine)palladium(0) [$Pd(PPh_3)_4$] (138.7 mg, 120 μmol, 3.0 eq.), 5.0 % acetic acid, and 2.5 % 4-methylmorpholine in $CHCl_3$ (2 mL) to the resin under an argon atmosphere.
56. Agitate the resin at room temperature for 180 min
57. Take a small portion of the resin beads and confirm Aloc deprotection by the Kaiser test. Both the test solution and the resin beads should appear deep purple. If the solution does not appear deep purple, remove the solution and repeat steps 55–56.
58. Wash the resin with DMF containing 0.5 % DIPEA (ca. 2 mL) five times, DMF containing 0.5 % sodium diethyldithiocarbamate (ca. 2 mL) five times, MeOH (ca. 4 mL) five times, and CH_2Cl_2 (ca. 4 mL) five times.
59. Dry the resin in vacuo.
60. Add 2 mL of CH_2Cl_2 containing 5 % TFA to the resin to cleave the product from the resin.
61. Agitate the resin at room temperature for 5 min
62. Collect the filtrate in a 50-mL eggplant flask and repeat steps 60–61 four times.
63. Add 10 mL of toluene to the flask.
64. Evaporate the solvent in vacuo to yield a crude residue.
65. Dissolve the residue in MeCN/H_2O (1:1) (1 mL).
66. Purify the residue by reversed-phase HPLC. Elute with a 30-min linear gradient from 55 % MeCN/0.1 % aqueous TFA to 100 % MeCN/0.1 % aqueous TFA (C4 column, 10 × 250 mm; flow rate = 3.0 mL/min). Monitor at 220 nm. Note that if the residue is sufficiently pure, it can be used for subsequent reactions without HPLC purification.
67. Collect the fraction eluting at ~24.5 min and lyophilize the combined fractions to afford **4** as a white powder [27.2 mg, 64 % (as a mono-TFA salt)].

^{1}H NMR (400 MHz, CD_3OD): mixture of rotamers, δ 7.42–7.36 (6H, m), 7.32–7.28 (6H, m), 7.25–7.21 (3H, m), 5.62–5.10 (1H, m), 4.44–4.40 (1H, m), 4.40–4.16 (1H, m), 4.00–3.94 (2H, m), 3.77–3.54 (8H, m), 3.52–3.46 (1H, m), 3.12–2.85 (10H, m), 2.73–2.68 (2H, m),

2.66–2.49 (1H, m), 2.47–2.38 (2H, m), 2.28–2.12 (1H, m), 1.93–1.83 (1H, m), 1.73–1.66 (2H, m), 1.64–1.55 (2H, m), 1.48–1.40 (2H, m), 1.34–1.23 (20H, m), 0.92–0.86 (3H, m).

HRMS (ESI): calculated for $[M+H]^+$, 945.5882; found, 945.5883.

2.3 Synthesis of mgc^{3Me}FDA

The synthetic scheme is shown in Fig. 3.

1. Add compound **4** (6.8 mg, 6.4 μmol) and 5-carboxyfluorescein diacetate (2.9 mg, 6.4 μmol, 1.0 eq.) into a 1.5 mL microcentrifuge tube.
2. Dissolve the compounds in DMF (0.2 mL).
3. Add HBTU (2.4 mg, 6.4 μmol, 1.0 eq.) and DIPEA (3.3 μL, 19.2 μmol, 3.0 eq.) to the solution.
4. Stir the solution at room temperature for 2 h.
5. Transfer the solution to a 50-mL eggplant flask.
6. Evaporate the solvent in vacuo.
7. Add 1 mL of CH_2Cl_2 containing 25 % TFA and 2.5 % TIPS to the flask to remove the Trt group.
8. Stir the solution at room temperature for 20 min
9. Add 5 mL of toluene to the flask and evaporate the solution in vacuo.
10. Add 5 mL of Et_2O to precipitate the crude product.
11. Collect the precipitate by centrifugation and dry it in vacuo.
12. Purify the crude product by reversed-phase HPLC. Elute with a 30-min linear gradient from 45 % MeCN/0.1 % aqueous TFA to 100 % MeCN/0.1 % aqueous TFA (C4 column, 10 × 250 mm; flow rate = 3.0 mL/min). Monitor at 220 nm.
13. Collect the fraction eluting at ~21.4 min, combine the fractions, and lyophilize to afford **mgc^{3Me}FDA** as a white solid [2.0 mg, 27 %].

^{1}H NMR (400 MHz, CD_3OD): mixture of rotamers, δ 8.47 (1H, s), 8.23 (1H, d, J = 8.0 Hz), 7.38 (1H, d, J = 8.0 Hz), 7.21 (2H, d, J = 1.7 Hz), 6.91 (4H, m), 4.47–4.44 (1H, m), 4.37–4.34 (1H, m), 4.02 (2H, s), 3.77–3.68 (8H, m), 3.44 (2H, m), 3.17–2.65 (13H, m), 2.43–2.40 (2H, m), 2.29 (6H, s), 1.77–1.74 (2H, m), 1.70 (2H, m), 1.58 (2H, m), 1.56 (2H, m), 1.27 (20H, m), 0.89 (3H, t, J = 6.0 Hz).

HRMS (ESI): calculated for $[M+H]^+$, 1145.5475; found, 1145.5472.

2.4 Synthesis of mgc^{3Me}DEAC

The synthetic scheme is shown in Fig. 4.

1. Add compound **4** (25.5 mg, 24.1 μmol) and 7-(diethylamino)coumarin-3-carboxylic acid (6.3 mg, 24.1 μmol, 1.0 eq.) into a 1.5 mL microcentrifuge tube.
2. Dissolve the compounds in DMF (0.2 mL).
3. Add HBTU (9.6 mg, 24.1 μmol, 1.0 eq.) and DIPEA (18.3 μL, 108 μmol, 4.5 eq.) to the solution.
4. Stir the solution at room temperature for 2 h.
5. Transfer the solution to a 50-mL eggplant flask.
6. Evaporate the solvent in vacuo.
7. Add 1 mL of CH_2Cl_2 containing 25 % TFA and 2.5 % TIPS to the flask to remove the Trt group.
8. Add 5 mL of toluene to the flask and evaporate the solution in vacuo.
9. Add 5 mL of Et_2O to precipitate the crude product.
10. Collect the precipitate by centrifugation and dry it in vacuo.
11. Purify the residue by reversed-phase HPLC. Elute with a 30-min linear gradient from 35 % MeCN/0.1 % aqueous TFA to 100 % MeCN/0.1 % aqueous TFA (C4 column, 10 × 250 mm; flow rate = 3.0 mL/min). Monitor at 220 nm.
12. Collect the fraction eluting at ~24.5 min, combine the fractions, and lyophilize to afford **mgc^{3Me}DEAC** as a yellow solid [11.2 mg, 50 %].

^{1}H NMR (400 MHz, CD_3OD): mixture of rotamers, δ 8.62 (1H, s), 7.55 (1H, d, J = 9.05 Hz), 6.82 (1H, dd, J = 9.05, 2.32 Hz), 6.58 (1H, d, J = 2.20 Hz), 5.67–5.32 (1H, m), 4.46–4.43 (1H, m), 4.41–4.11 (2H, m), 4.03–4.01 (2H, m), 3.81–3.57 (8H, m), 3.53 (4H, q, J = 7.09 Hz), 3.42 (2H, t, J = 6.79 Hz), 3.15–2.88 (10H, m), 2.85–2.55 (2H, m), 2.44–2.40 (1H, m), 2.30–2.19 (1H, m), 1.95–1.84 (1H, m), 1.81–1.73 (1H, m), 1.71–1.62 (2H, m), 1.62–1.55 (2H, m), 1.52–1.44 (2H, m), 1.38–1.25 (20H, m), 1.25–1.19 (6H, m), 0.89 (3H, t, J = 6.72).

HRMS (ESI): calculated for $[M+H]^+$, 946.5682; found, 946.5684.

2.5 Synthesis of mgc^{3Me}TMR

The synthetic scheme is shown in Fig. 5.

1. Add compound **4** (8.0 mg, 7.6 μmol) and 5,6-carboxytetramethylrhodamine succinimidyl ester (4.0 mg, 7.6 μmol, 1.0 eq.) into a 1.5 mL microcentrifuge tube.
2. Dissolve the compounds in DMF (0.2 mL).
3. Add DIPEA (3.9 μL, 22.7 μmol, 3.0 eq.) to the solution.

4. Stir the solution at room temperature for 2 h.
5. Transfer the solution to a 50-mL eggplant flask.
6. Evaporate the solvent in vacuo.
7. Add 1 mL of CH_2Cl_2 containing 25 % TFA and 2.5 % TIPS to the flask to remove the Trt group.
8. Add 5 mL of toluene to the flask and evaporate the solution in vacuo.
9. Add 5 mL of Et_2O to precipitate the crude product.
10. Collect the precipitate by centrifugation and dry it in vacuo.
11. Purify the residue by reversed-phase HPLC. Elute with a 30-min linear gradient from 50 % MeCN/0.1 % aqueous TFA to 100 % MeCN/0.1 % aqueous TFA (C4 column, 10 × 250 mm; flow rate = 3.0 mL/min). Monitor at 220 nm.
12. Collect the fractions eluting at ~14.7 min and at 15.1 min, combine the fractions, and lyophilize to afford **mgc^{3Me}TMR** as a red solid [2.7 mg, 32 %].

^{1}H NMR (400 MHz, CD_3OD): mixture of 5-/6-isomers and rotamers, δ 8.76 (1H, m), 8.26 (1H, dd, J = 7.95, 1.71 Hz), 7.53 (1H, d, J = 7.95 Hz), 7.24–7.14 (2H, m), 7.13–7.04 (2H, m), 7.03–6.94 (2H, m), 5.69–5.31 (1H, m), 4.55–4.45 (1H, m), 4.42–4.11 (2H, m), 4.09–3.95 (2H, m), 3.87–3.55 (8H, m), 3.52–3.49 (2H, m), 3.45–3.41 (1H, m), 3.16–2.90 (10H, m), 2.82–2.56 (1H, m), 2.50–2.38 (1H, m), 2.30–2.19 (1H, m), 2.00–1.90 (1H, m), 1.89–1.79 (1H, m), 1.79–1.68 (1H, m), 1.67–1.58 (2H, m), 1.57–1.47 (2H, m), 1.30–1.28 (20H, m), 0.96–0.86 (3H, m).

HRMS (ESI): calculated for $[M+H]^+$, 1115.6210; found, 1115.6198.

3. Method 2: Fluorescent staining of the Golgi apparatus in living cells

The myrGC^{3Me} lipopeptide–based fluorescent probes afford robust Golgi staining in a rapid and convenient manner, while exhibiting high specificity for the Golgi apparatus compared with conventional ceramide-based fluorescent probes. Moreover, these probes are non-toxic and easy to handle, making them highly suitable for live-cell imaging applications. In this section, we provide protocols for fluorescent staining of the Golgi apparatus in HeLa cells, which are widely employed as a standard model cell line in cell biology. The procedure can also be applied to other cell lines, including NIH/3T3 fibroblasts and COS-7 cells.

3.1 Before you begin

3.1.1 Reagents and media

- **mgc^{3Me}FDA**, synthesized as described in Section 2.3 or obtained commercially (Funakoshi, FDV-0053)
- **mgc^{3Me}DEAC**, synthesized as described in Section 2.4
- **mgc^{3Me}TMR**, synthesized as described in Section 2.5
- Dimethyl sulfoxide (DMSO)
- Bovine serum albumin (BSA), fatty acid-free, cell culture grade (e.g., Sigma-Aldrich A8806)
- HeLa cells (e.g., from the Cell Resource Center for Biomedical Research, Institute of Development, Aging and Cancer, Tohoku University)
- Dulbecco's Modified Eagle's Medium (DMEM) supplemented with 10 % heat-inactivated fetal bovine serum (FBS), penicillin (100 U/mL), and streptomycin (100 μg/mL) [$DMEM_{culture}$]
- Trypsin–EDTA solution [0.05 % (w/v) trypsin, 0.53 mM EDTA]. Aliquot and store at –20 °C.
- FBS- and phenol red-free DMEM supplemented with penicillin (100 U/mL) and streptomycin (100 μg/mL) [$DMEM_{imaging}$]. DMEM lacking FBS but containing phenol red is also suitable.
- FBS- and phenol red-free DMEM supplemented with 3 mg/mL BSA, penicillin (100 U/mL), and streptomycin (100 μg/mL) [$DMEM_{wash}$]. DMEM lacking FBS but with phenol red and BSA is also suitable.

3.1.2 Equipment

- 1.5-mL microcentrifuge tube (Eppendorf type)
- 35-mm glass-bottom dish (IWAKI)
- Confocal laser-scanning microscope equipped with lasers at 445 nm (**mgc^{3Me}DEAC**), 488 nm (**mgc^{3Me}FDA**), and 561 nm (**mgc^{3Me}TMR**) [e.g., EVIDENT IX83/FV3000 equipped with a 60 × oil objective, Z-drift compensator module (IX3-ZDC2), and a stage-top incubator (Tokai Hit)]. Standard epi-fluorescence microscopes are also suitable.

3.1.3 Preparation of stock solutions

The following molecular weights are used to calculate the concentrations of stock solutions: **mgc^{3Me}FDA**, 1145.38; **mgc^{3Me}DEAC**, 946.26; **mgc^{3Me}TMR,** 1115.44. Note that the powders are hygroscopic and may form gels or droplets. They also often adhere to the walls of the tubes.

1. Dissolve **mgc^{3Me}FDA** and **mgc^{3Me}DEAC** separately in DMSO to prepare 10 mM stock solutions, and **mgc^{3Me}TMR** in DMSO to prepare a 30 mM stock solution.
2. Aliquot the stock solutions into small volumes (e.g., 5 or 10 μL).
3. Store the aliquots at –20 °C. To avoid oxidation of the Cys side chain, avoid repeated freeze–thaw cycles.

3.1.4 Cell culture

Culture cells using standard protocols appropriate for each cell type.

3.2 Staining and fluorescent imaging of live-cell Golgi

1. Seed 2×10^5 HeLa cells in a 35 mm glass-bottom dish.

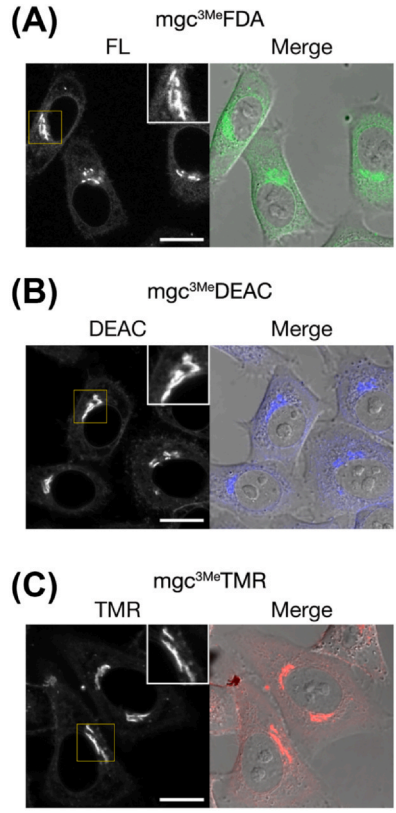

Fig. 6 Live-cell Golgi staining with myrGC^{3Me}-based probes. Representative confocal fluorescence images of HeLa cells stained with (**A**) **mgc^{3Me}FDA**, (**B**) **mgc^{3Me}DEAC**, and (**C**) **mgc^{3Me}TMR**. Left panels: fluorescence images; right panels: differential interference contrast (DIC) images merged with the fluorescence images. Each inset shows a high-magnification view of the region indicated by the yellow box. Scale bars, 15 μm.

2. Culture the cells in 2 mL of $DMEM_{culture}$ at 37 °C for 24–48 h in 5 % CO_2.
3. Remove the medium, wash the cells twice with 1 mL of $DMEM_{imaging}$, and add 1 mL of $DMEM_{imaging}$ to the dish.
4. Add 1 mL of $DMEM_{imaging}$ to a 1.5 mL microcentrifuge tube.
5. Add 2 μL of 10 mM **mgc^{3Me}FDA**, 10 mM **mgc^{3Me}DEAC**, or 30 mM **mgc^{3Me}TMR** into the tube and mix gently by pipetting to give concentrations of 20 μM **mgc^{3Me}FDA**, 20 μM **mgc^{3Me}DEAC**, or 60 μM **mgc^{3Me}TMR**. Proceed to step 6 immediately after mixing to avoid oxidation of the Cys residue and, in the case of **mgc^{3Me}FDA**, hydrolysis of the acetyl groups.
6. Add the entire probe solution to the cell culture dish prepared in step 3 and mix gently by pipetting, giving final concentrations of 10 μM **mgc^{3Me}FDA**, 10 μM **mgc^{3Me}DEAC**, or 30 μM **mgc^{3M}eTMR** in the dish.
7. Incubate the cells at room temperature for 10 min
8. Remove the medium and wash the cells twice with 1 mL of $DMEM_{wash}$ to eliminate excess probe.
9. Add 1–2 mL of fresh $DMEM_{imaging}$ to the dish.
10. Place the dish on the stage of a confocal laser-scanning microscope.
11. Acquire fluorescence images using standard protocols, adjusting laser intensity and detector gain to minimize photobleaching and phototoxicity. Representative imaging data are provided in Fig. 6.

4. Method 3: Visualization of Golgi dynamics under drug treatment

Brefeldin A (BFA) disrupts vesicular trafficking by inhibiting ARF1 activation, thereby causing rapid disassembly of the Golgi apparatus (Klausner et al., 1992; Ohashi et al., 2021). This pharmacological effect provides a robust model system for investigating Golgi dynamics and membrane trafficking in living cells. In this section, we describe protocols for visualizing BFA-induced Golgi disassembly using **mgc^{3Me}FDA** in combination with confocal time-lapse imaging.

4.1 Before you begin

4.1.1 Reagents and media

- **mgc^{3Me}FDA**, synthesized as described in Section 2.3 or obtained commercially (Funakoshi, FDV-0053)

- Brefeldin A (BFA) (e.g., Cayman Chemical, 11861)
- DMSO
- HeLa cells (see Section 3.1.1)
- $DMEM_{culture}$ (see Section 3.1.1)
- $DMEM_{imaging}$ (see Section 3.1.1)
- $DMEM_{wash}$ (see Section 3.1.1)

4.1.2 Equipment

See Section 3.1.2.

4.1.3 Preparation of stock solutions

The stock solution of **mgc^{3Me}FDA** is prepared as described in Section 3.1.3. BFA is dissolved in DMSO to prepare a 1 mM stock solution.

4.2 Time-lapse fluorescence imaging of Golgi dynamics during BFA treatment

1. Prepare and stain HeLa cells with **mgc^{3Me}FDA** as described in Section 3.2.
2. Ensure that the volume of $DMEM_{imaging}$ in the dish is 1 mL.
3. Place the dish on the stage of a confocal laser-scanning microscope.
4. Start acquiring time-lapse fluorescence images of the cells using standard protocols.

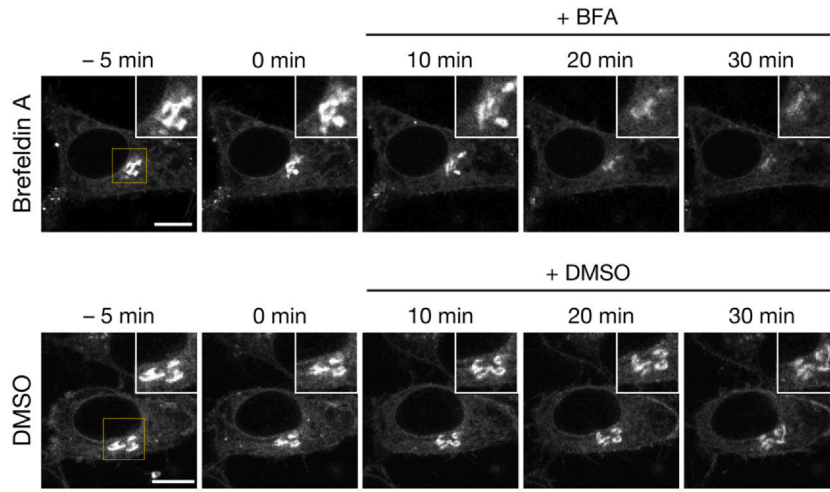

Fig. 7 Golgi disassembly induced by drug treatment. Representative time-lapse confocal fluorescence images of HeLa cells stained with mgc^{3Me}FDA before and after treatment with BFA (1 μM, top) or with 0.1 % DMSO as a control (bottom). Each inset shows a high-magnification view of the region indicated by the yellow box. Scale bars, 10 μm.

5. Prepare 1 mL of 2 μM BFA solution in $DMEM_{imaging}$ by adding 2 μL of 1 mM BFA stock solution to 1 mL of $DMEM_{imaging}$.
6. At the desired time point, add the entire BFA solution to the dish and mix gently by pipetting, giving a final concentration of 1 μM in the dish. Take care not to touch or move the dish while it is mounted on the microscope stage.
7. Continue time-lapse imaging to monitor the disappearance of the Golgi apparatus. Adjust laser intensity, detector gain, and time interval to minimize both photobleaching and phototoxicity. Representative time-lapse imaging data are provided in Fig. 7.

5. Method 4: Visualization of Golgi dynamics during cell division

The Golgi apparatus undergoes characteristic morphological changes during the cell cycle, including events such as fragmentation during mitosis and reassembly upon cytokinesis. Monitoring these dynamic transitions in living cells yields important insights into the regulation of membrane trafficking. This section describes protocols for time-lapse imaging of Golgi dynamics during cell division using **mgc^{3Me}FDA**. To enable long-term monitoring of Golgi dynamics, cells are incubated with a low concentration of **mgc^{3Me}FDA** while omitting the washing step.

5.1 Before you begin

5.1.1 Reagents and media

- **mgc^{3Me}FDA**, synthesized as described in Section 2.3 or obtained commercially (Funakoshi, FDV-0053)
- DMSO
- HeLa cells (see Section 3.1.1)
- $DMEM_{culture}$ (see Section 3.1.1)
- $DMEM_{imaging}$ (see Section 3.1.1)

5.1.2 Equipment

See Section 3.1.2.

5.1.3 Preparation of stock solutions

A 2.5 mM stock solution of **mgc^{3Me}FDA** is prepared as described in Section 3.1.3.

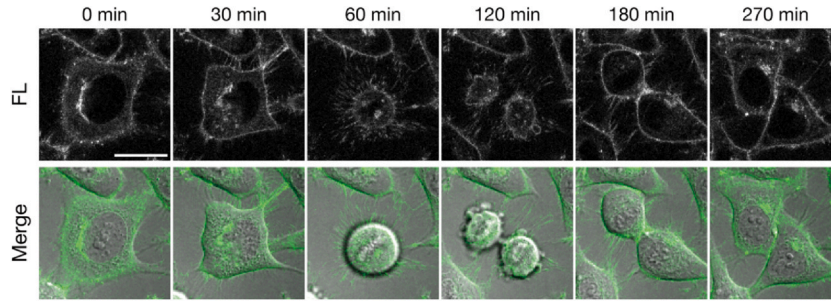

Fig. 8 Golgi dynamics during cell division. Representative time-lapse confocal fluorescence images of HeLa cells stained with mgc^{3Me}FDA (2.5 μM) during cell division. Fluorescence images (top) and merged DIC and fluorescence images (bottom) are shown. Scale bar, 15 μm.

5.2 Time-lapse fluorescence imaging of Golgi dynamics during cell division

1. Seed 5×10^4 HeLa cells in a 35 mm glass-bottom dish.
2. Culture the cells in 2 mL of $DMEM_{culture}$ at 37 °C for 24–48 h in 5 % CO_2.
3. Remove the medium, wash the cells twice with 1 mL of $DMEM_{imaging}$, and add 1 mL of $DMEM_{imaging}$ to the dish.
4. Prepare 1 mL of 5 μM **mgc^{3Me}FDA** solution in $DMEM_{imaging}$ by adding 2 μL of 2.5 mM **mgc^{3Me}FDA** stock solution to 1 mL of $DMEM_{imaging}$.
5. Add the entire probe solution to the cell culture dish prepared in step 3 and mix gently by pipetting, giving a final concentration of 2.5 μM **mgc^{3Me}FDA** in the dish.
6. Incubate the cells at room temperature for 30 min
7. Without washing, place the dish on the stage of a confocal laser-scanning microscope.
8. Acquire time-lapse fluorescence images of the cells using standard protocols to monitor the Golgi dynamics during cell division. Adjust laser intensity, detector gain, and time interval to minimize both photobleaching and phototoxicity. Representative time-lapse imaging data are provided in Fig. 8.

Acknowledgments

This work was supported by JSPS KAKENHI Grant Numbers JP24K01645 and JP21H05226 (S.T.) and by the Nakatani Foundation (S.T.). K.T. was supported by a JSPS Research Fellowship for Young Scientists (Grant Number JP23KJ1142). This work was also partially supported by JSPS KAKENHI Grant Number JP25K24454 (S.S.).

References

Bexiga, M. G., & Simpson, J. C. (2013). Human diseases associated with form and function of the Golgi complex. *International Journal of Molecular Sciences (IJMS), 14*, 18670–18681. https://doi.org/10.3390/ijms140918670.

Biron, E., Chatterjee, J., & Kessler, H. (2006). Optimized selective N-methylation of peptides on solid support. *Journal of Peptide Science: an Official Publication of the European Peptide Society, 12*, 213–219.

Brandizzi, F., & Barlowe, C. (2013). Organization of the ER–Golgi interface for membrane traffic control. *Nature Reviews. Molecular Cell Biology, 14*, 382–392.

Bui, S., Mejia, I., Díaz, B., & Wang, Y. (2021). Adaptation of the Golgi apparatus in cancer cell invasion and metastasis. *Frontiers in Cell and Developmental Biology, 9*, 806482. https://doi.org/10.3389/fcell.2021.806482.

Cancino, J., & Luini, A. (2013). Signaling circuits on the Golgi complex. *Traffic (Copenhagen, Denmark), 14*, 121–134.

Caracci, M. O., Fuentealba, L. M., & Marzolo, M.-P. (2019). Golgi complex dynamics and its implication in prevalent neurological disorders. *Frontiers in Cell and Developmental Biology, 7*, 75.

Colley, K. J. (1997). Golgi localization of glycosyltransferases: More questions than answers. *Glycobiology, 7*, 1–13.

Crilly, S. E., & Puthenveedu, M. A. (2021). Compartmentalized GPCR signaling from intracellular membranes. *The Journal of Membrane Biology, 254*, 259–271.

Ernst, A. M., Syed, S. A., Zaki, O., Bottanelli, F., Zheng, H., Hacke, M., et al. (2018). S-Palmitoylation sorts membrane cargo for anterograde transport in the Golgi. *Developmental Cell, 47*, 479–493.

Fehrenbacherb, N., Bar-Sagia, D., & Philips, M. (2009). Ras/MAPK signaling from endomembranes. *Molecular Oncology, 3*(4), 297–307.

Fukata, Y., & Fukata, M. (2010). Protein palmitoylation in neuronal development and synaptic plasticity. *Nature Reviews. Neuroscience, 11*, 161–175.

Glick, B. S., & Nakano, A. (2009). Membrane traffic within the Golgi apparatus. *Annual Review of Cell and Developmental Biology, 25*, 113–132.

Hannun, Y. A., & Obeid, L. M. (2008). Principles of bioactive lipid signalling: Lessons from sphingolipids. *Nature Reviews. Molecular Cell Biology, 9*, 139–150.

Ireland, S., Ramnarayanan, S., Fu, M., Zhang, X., Zhang, J., Li, J., et al. (2020). Cytosolic Ca^{2+} modulates Golgi structure through PKCα-mediated GRASP55 phosphorylation. *iScience, 23*, 100952.

Klausner, R. D., Donaldson, J. G., & Lippincott-Schwartz, J. (1992). Brefeldin A: insights into the control of membrane traffic and organelle structure. *The Journal of Biological Chemistry, 116*, 1071–1080.

Lipsky, N. G., & Pagano, R. E. (1985). A vital for the Golgi apparatus. *Science (New York, N. Y.), 228*, 745–747.

Llopis, J., Mccaffery, J. M., Miyawaki, A., Farquhar, M. G., & Tsien, R. Y. (1998). Measurement of cytosolic, mitochondrial, and Golgi pH in single living cells with green fluorescent proteins. *Proceedings of the National Academy of Sciences of the United States of America, 95*, 6803–6808.

Makiyama, T., Nakamura, H., Nagasaka, N., Yamashita, H., Honda, T., Yamaguchi, N., ... Murayama, T. (2015). Trafficking of acetyl-C16-ceramide-NBD with long-term stability and no cytotoxicity into the Golgi complex. *Traffic (Copenhagen, Denmark), 16*, 476–492.

Malhoul, C., Gosavi, P., & Gleeson, P. A. (2019). Golgi dynamics: the morphology of the mammalian Golgi apparatus in health and disease. *Frontiers in Cell and Developmental Biology, 7*, 112.

Ohashi, Y., Iijima, H., Yamaotsu, N., Yamazaki, K., Sato, S., Okamura, M., ... Yamori, T. (2021). AMF-26, a novel inhibitor of the Golgi system, targeting ADP-ribosylation factor 1 (Arf1) with potential for cancer therapy. *The Journal of Biological Chemistry, 287*, 3885–3897.

Pagano, R. E., Martin, O. C., Kang, H. C., & Haugland, R. P. (1991). A novel fluorescent ceramide analogue for studying membrane traffic in animal cells: accumulation at the Golgi apparatus results in altered spectral properties of the sphingolipid precursor. *The Journal of Cell Biology, 113*, 1267–1279.

Perry, R. J., & Ridgway, N. D. (2005). Molecular mechanisms and regulation of ceramide transport. *Biochimica et Biophysica Acta, 1734*, 200–234.

Salaun, C., Greaves, J., & Chamberlain, L. H. (2010). The intracellular dynamic of protein palmitoylation. *The Journal of Cell Biology, 191*, 1229–1238.

Sawada, S., Nakamura, A., Yoshii, T., Kuwata, K., Nakatsu, F., & Tsukiji, S. (2020). Protein-recruiting synthetic molecules targeting the Golgi surface. *Chemical Communications, 56*, 15422–15425.

Storrie, B., White, J., Rottger, S., Stelzer, E. H. K., Suganuma, T., & Nilsson, T. (1998). Recycling of Golgi-resident glycosyltransferases through the ER reveals a novel pathway and provides an explanation for nocodazole-induced Golgi scattering. *The Journal of Cell Biology, 143*, 1505–1521.

Sundaramoorthy, V., Sultana, J. M., & Atkin, J. D. (2015). Golgi fragmentation in amyotrophic lateral sclerosis, an overview of possible triggers and consequences. *Frontiers in Neuroscience, 9*, 400.

Varki, A. (1998). Factors controlling the glycosylation potential of the Golgi apparatus. *Trends in Cell Biology, 8*, 34–40.

Zhang, X., & Wang, Y. (2016). Glycosylation quality control by the Golgi structure. *Journal of Molecular Biology, 428*, 3183–3193.

CHAPTER SIXTEEN

Real-time measurement of the ATG8 lipidation reaction by fluorescence spectroscopy

Wenxin Zhang[a], Sharon A. Tooze[b], and Taki Nishimura[c,d,*]
[a]Mechanisms of Cellular Quality Control, Max Planck Institute of Biophysics, Frankfurt am Main, Hesse, Germany
[b]Molecular Cell Biology of Autophagy Laboratory, The Francis Crick Institute, London, United Kingdom
[c]Institute for Protein Research, The University of Osaka, Osaka, Japan
[d]Graduate School of Frontier Biosciences, The University of Osaka, Osaka, Japan
*Corresponding author. e-mail address: ntaki@protein.osaka-u.ac.jp

Contents

1. Before you begin 328
2. Key resources table 329
3. Materials and equipment 331
4. Step-by-step method details 332
   4.1 Expression and purification of ATG7 from insect Sf9 cells 332
   4.2 Expression and purification of ATG3 from bacteria BL21 (DE3) cells 334
   4.3 Expression and purification of ATG8 (LC3B S3C) from bacteria BL21 (DE3) cells 336
   4.4 NBD-labeling of LC3B S3C proteins with single cysteine mutation 337
   4.5 Liposome preparation 338
   4.6 Real-time ATG8 lipidation assay 340
5. Expected outcomes 341
6. Quantification and statistical analysis 342
7. Advantages 343
8. Limitations 343
9. Optimization and troubleshooting 343
Acknowledgments 344
References 344

Abstract

Autophagy is a highly conserved intracellular degradation pathway, in which damaged organelles and/or dysfunctional cytosolic components are enveloped via double-membraned autophagosomes and subsequently delivered to lysosomes for degradation. The ubiquitin-like ATG8 family proteins (LC3s and GABARAPs) are covalently conjugated to phosphatidylethanolamine (PE) on autophagic membranes via ubiquitin-like conjugation systems, a process known as ATG8 lipidation. Lipidated ATG8 is the

Methods in Enzymology, Volume 728
ISSN 0076-6879, https://doi.org/10.1016/bs.mie.2026.01.011
Copyright © 2026 Elsevier Inc. All rights are reserved, including those for text and data mining, AI training, and similar technologies.

most widely used membrane marker for autophagosomes, and its flux is commonly used as a readout for autophagy activity. *In vitro* reconstitution of the ATG8 lipidation reaction is well-established, and the end-point reaction is typically resolved by SDS-PAGE. This endpoint readout is not suitable to monitor the kinetics of this reaction, and tools to study this process have been lacking. Here, we describe a real-time assay to measure the ATG8 lipidation reaction. This approach not only reveals the subsequential formation of covalently bound intermediates of ATG8 with the E1 (ATG7) and E2 (ATG3) enzymes, as well as ATG8—PE itself, but also provides insights into the interaction interface of ATG8 with proteins and membranes during the conjugation reaction.

1. Before you begin

Autophagy constitutively occurs at a basal level in response to metabolic demands. Upon autophagy induction, a unique cup-shaped structure called the phagophore appears, sequesters cytosolic materials, forms double-membraned autophagosomes, and eventually fuses with lysosomes for degradation. It is a critical process to maintain cell homeostasis and cell survival.

Autophagy is highly regulated by autophagy-related (ATG) proteins (Nishimura & Tooze, 2020). ATG8 is the only ATG protein that covalently binds to the autophagic membrane, via a ubiquitin-like conjugation reaction, known as lipidation. ATG8 plays an important role in autophagosome biogenesis, cargo recognition, membrane closure and autophagosome-lysosome fusion, thus contributing to the entire autophagy process, reviewed in (Martens & Fracchiolla, 2020).

Before the conjugation, ATG8 is first processed by the cysteine protease ATG4 to expose its C-terminal glycine. Then, ATG8 is activated by ATG7 (the E1-activating enzyme), transferred to ATG3 (the E2-conjugating enzyme), and finally conjugated to the head group of phosphatidylethanolamine (PE) with assistance of the ATG12—ATG5-ATG16L1 complex (hereafter, the E3 complex) (Mizushima, 2020). The ATG8 lipidation reaction is one of the landmark discoveries in the autophagy field, and lipidated ATG8 flux has been widely used as a standard marker to assess autophagy activity (Mizushima et al., 2010).

ATG8 lipidation was the first autophagy process that has been successfully reconstituted in vitro (Ichimura et al., 2004). Using purified E1, E2, E3 complex, and ATG8 protein components with the synthetic model membranes, such as large unilamellar vesicles (LUVs), the end-point reaction can be resolved by SDS-PAGE, where the lipidated ATG8s show an increased mobility. It has been employed to examine the activity of ATG7 (Noda et al., 2011; Taherbhoy et al., 2011), ATG3 (Nath et al., 2014), the

E3 complex (Lystad et al., 2019), and the upstream regulators of the ATG8 conjugation machinery (Fracchiolla et al., 2020). However, the endpoint assay is not sufficient to read out the dynamic events during lipidation, and there is lack of tools to assess the reaction kinetics in real time, which would allow the detection not only of the final ATG8—PE formation, but also of the rates of intermediate formation.

Recently, we developed a real-time assay to monitor the ATG8 conjugation reaction using site-directed labeling and fluorescence spectroscopy (Zhang et al., 2023). In this protocol, we use the human ATG8 protein LC3B as an example, substituting its N-terminal serine 3 to cysteine (S3C), and labeling it with 7-nitrobenz-2-oxa-1,3-diazol-4-yl (NBD). NBD is an environmental-sensitive fluorescence probe and its fluorescence emission increases when it transfers from an aqueous to a hydrophobic environment (Raghuraman & Chatterjee and Das, 2019). We have shown that the ATG8 N-terminus is highly dynamic and encounters a hydrophobic environment provided by ATG7 or ATG3 (protein-protein interface), and finally by PE conjugation to membranes (protein-membrane interaction). Thus, this assay can be readily applied to investigate the ubiquitin-like enzymatic activity in the ATG8 conjugation reaction, the role of specific lipid compositions and other upstream regulators.

2. Key resources table

Note that not all areas will be used in every protocol.

Bacterial and virus strains		
BL21 (DE3) E. coli	New England BioLabs	C2527H
Biological Samples		
Sf9 cells	ATCC	CRL-1711
Chemicals, Peptides, and Recombinant Proteins		
Sf-900™ II SFM medium	Thermo Fisher Scientific	10902104
Fugene HD transfection reagent	Promega	E2311
flashBAC™ GOLD	Oxford Expression Technologies	100202
Gentamicin	Thermo Fisher Scientific	15710049
Amphotericin B	Thermo Fisher Scientific	15290018

Ampicillin	Sigma-Aldrich	A9518
Kanamycin	Sigma-Aldrich	K4000
Tris(2-carboxyethyl) phosphine hydrochloride solution	Sigma-Aldrich	646547
Benzamidine	Sigma-Aldrich	B6506-25G
Dimethyl sulfoxide (DMSO)	Sigma-Aldrich	D2650
L-cysteine	Sigma-Aldrich	168149
Isopropyl-β-D-thio-galactopyranoside (IPTG)	Melford	I56000
AEBSF Hydrochloride	AppliChem	A1421
cOmplete™, EDTA-free Protease Inhibitor Cocktail	Roche	11873580001
Glutathione Sepharose® 4B	Cytiva	17075605
IANBD (N,N'-Dimethyl-N-(Iodoacetyl)-N'-(7-Nitrobenz-2-Oxa-1,3-Diazol-4-yl) Ethylenediamine)	Invitrogen	D2004
16:0-18:1 PC (POPC)	Avanti Polar Lipids	850457 C
18:1 (Δ9-Cis) PE (DOPE)	Avanti Polar Lipids	850725 C
MgATP Solution	R&D Systems	B-20
ATG12—ATG5-ATG16L1 (E3 complex)	Zhang et al., 2023	None
GST-3C (PreScission protease) 5 mg/mL	The Francis Crick Institute, Structural Biology platform	None
Recombinant DNA		
pBacPAK-His_3-GST-ATG7	Zhang et al., 2023	None
pGEX6P1-GST-3C-ATG3	Zhang et al., 2023	None
pAL-GST-3C-LC3B $_{(1\text{-}120)}$ S3C	Zhang et al., 2023	None
Software and Algorithms		
Excel	Microsoft Office	https://www.office.com/
GraphPad Prism 9	GraphPad Prism Software	https://www.graphpad.com/

Other		
Centrifugal Filters (0.2 μm)	VWR	516-0233
Vivaspin 20 concentrator column (MWCO 10 K)	Cytiva	28932360
Vivaspin 6 concentrator column (MWCO 30 K)	Cytiva	28932317
ÄKTA pure™ chromatography system	Cytiva	N/A
Superdex 200 16/600 GL column	Cytiva	28989335
Superdex 200 10/300 GL column	Cytiva	28990944
PD Minitrap™ G-25	Sigma-Aldrich	GE28-9180-07
Extruder Set with Holder/Heating Block including mini-extruder, 2 syringes, Polycarbonate Membranes 0.1 μm 19 mm, 100 filter supports, and 1 holder/heating block	Avanti Polar Lipids	610000-1EA
Polycarbonate Membranes 0.2 μm 19 mm	Avanti Polar Lipids	610006-1EA
Eppendorf™ Concentrator Plus	Eppendorf™ Concentrator Plus	N/A
Zetasizer Nano ZS	Malvern Instruments	N/A
Disposable Solvent Resistant Micro Cuvette	Malvern Instruments	ZEN0040
Ultra-Micro-cuvette 10 mm path length, 100 μL	Hellma Analytics	105.201-QS
FP-8300 Spectrofluorometer	JASCO	N/A

3. Materials and equipment

In the key resources table, we have listed the materials, equipment and reagents used in our laboratory. These reagents can be sourced from alternative suppliers. All the buffers should be prepared in advance and pre-cooled at 4 °C.

Buffer for protein purification:

Lysis buffer 1:
50 mM Tris-HCl, pH 8.0
500 mM NaCl

0.5 mM TCEP
1x cOmplete™, EDTA-free Protease Inhibitor
Lysis buffer 2:
50 mM Tris-HCl, pH 8.0
500 mM NaCl
0.5 mM TCEP
0.4 mM AEBSF
15 μg/mL benzamidine
Wash buffer:
50 mM Tris-HCl, pH 8.0
500 mM NaCl
0.5 mM TCEP
Equilibration buffer:
25 mM Tris-HCl, pH 8.0
150 mM NaCl
0.5 mM TCEP

Buffer for NBD labeling:
Labeling buffer:
25 mM Tris-HCl, pH 7.5
150 mM NaCl

4. Step-by-step method details

4.1 Expression and purification of ATG7 from insect Sf9 cells

Timing: 3–4 weeks

1. Generation of P1 baculovirus harboring His_3-GST-ATG7 construct.
   - **a)** Filter sterilize the transfer plasmid pBacPAK-His_3-GST-ATG7 through a Centrifugal Filters (0.2 μm) before use.
   - **b)** Seed 0.5×10^6 Sf9 cells per well in a 6-well plate and incubate in a static incubator at 27 °C for at least 1 h to allow the cells to attach.
   - **c)** Mix 0.5 μg the transfer plasmid with 50 ng flashBAC GOLD DNA in 200 μL Sf-900™ II SFM medium. Then, add 2 μL FuGENE transfection reagent. Incubate the transfection mixture at room temperature for 20 min
   - **d)** Add 800 μL Sf-900™ II SFM medium into the transfection mixture.

e) Remove the medium from the cells in the 6-well plate and add ~1 mL of the mixture. Place the plate in a sandwich box filled with wet tissue at the bottom and incubate at 27 °C in a static incubator overnight.
f) Add another 1 mL of Sf-900™ II SFM medium containing Gentamycin (10 μg/mL) and Amphotericin B (0.25 μg/mL) onto the cells in the 6-well plate.
g) Incubate at 27 °C in a static incubator for another 4 days.
h) Harvest the cells and supernatant and transfer the mixture containing P1 virus (~2 mL) into a sterile 2 mL Cryogenic vial.

Note: Each step is carried out in a sterile tissue culture hood.

2. P1 to P2 virus amplification.
At this stage, the viral titer (P1) is low and needs to be further amplified.
a) Prepare 50 mL of healthy Sf9 cells (viability > 98 %) at a density of 1×10^6 cells/mL in a sterile 500 mL Erlenmeyer flask with a vent cap.
b) Add 1.5 mL of the mixture (cells + P1 virus) to the 50 mL of Sf9 cells.
c) Incubate the cell culture in a shaking incubator at 27 °C and 140 rpm for 3 days.
d) Pellet cells at 1000 rpm, at 4 °C for 10 min. Collect the supernatant and transfer it into a 50 mL black Falcon tube. Store at 4 °C. This is the P2 viral stock.

Note: Count the cells every day. After the P1 viral infection, cell growth should stop after 1–2 days.

3. P2 to P3 amplification
a) To further "boost" the viral titer, add 50 μL of the P2 virus to 50 mL of healthy Sf9 cells (viability > 98 %) at a density of 1×10^6 cells/mL in 500 mL Erlenmeyer flask with a vent cap.
b) Incubate the cell culture in a shaking incubator at 27 °C and 140 rpm for 3 days.
c) Harvest the supernatant by centrifugation at 1000 rpm and 4 °C for 10 min. Keep the supernatant in 50 mL black Falcon tube and store at 4 °C. This is the P3 viral stock for protein expression, as shown below.

Note: Count the cells every day. After the P2 viral infection, cell growth should stop after 1–2 days. Keep the cell pellets to analyze protein expression.

Pause Point: P2 and P3 virus can be stored at 4 °C for up to 6–12 months.

4. ATG7 expression with P3 baculovirus
   a) Prepare 400 mL of healthy Sf9 in a 2 L Roller bottle with vent cap at a density of 0.7-0.8 × 106 cells/mL and incubate overnight in a shaking incubator at 27 °C and 140 rpm.
   b) Next day, add 1 mL of the P3 virus to the cell culture.
   c) After 60 h of infection, harvest cell pellets by centrifugation at 1000 rpm and 4 °C for 10 min.

Pause Point: Cell pellets can be snap frozen in liquid nitrogen and stored at −80 °C for up to 6 months.

5. ATG7 protein purification
   a) Resuspend the cell pellet in 30 mL of Lysis buffer 1.
   b) Lyse the cells on ice by sonication under the following conditions: 50 % amplitude, 10 s on/60 s off, repeat 3-5 times.
   c) Remove cell debris by centrifugation at 30,000 x g for 30 min at 4 °C.
   d) Collect the cleared lysate and incubate it with 2 mL of Glutathione Sepharose® 4B slurry (1 mL of resin) rolling at 4 °C for 90 min
   e) Pellet the resin at 500 x g for 3 min at 4 °C. Wash the resin with Wash buffer five times.
   f) Resuspend the resin in 5 mL of Wash buffer and add 100 μL of GST-3C (5 mg/mL). Incubate at 4 °C overnight to cleave ATG7 from the resin.
   g) Collect the protein elute and concentrate it using a Vivaspin 6 concentrator column (MWCO 30 K) until the volume is reduced to 300–500 μL.
   h) Further purify the protein by size exclusion on ÄKTA pure system equipped with Superdex 200 10/300 GL column pre-equilibrated with Equilibration buffer.
   i) Determine peak, pool, and check purity by SDS-PAGE, and then concentrate the peak fractions using a Vivaspin 6 concentrator column (MWCO 30 K) to a final concentration of ~2 mg/mL.
   j) Aliquot and snap freeze in liquid nitrogen. Store at −80 °C until use.

4.2 Expression and purification of ATG3 from bacteria BL21 (DE3) cells

Timing: 1–2 weeks

6. ATG3 expression in BL21 (DE3) cells
   a) Transform pGEX6P1-GST-3C-ATG3 plasmid into BL21 (DE3) cells, spread the bacteria on an LB agar plate containing 100 μg/mL of ampicillin. Incubate the plate at 37 °C overnight.

b) Pick a single colony to inoculate 120 mL of LB medium containing 100 μg/mL ampicillin. Incubate at 37 °C shaking at 180 rpm overnight.

c) Transfer 25-30 mL of the culture into 1 L of LB medium containing 100 μg/mL ampicillin in a 2 L flask (initial OD_{600} around 0.1). Prepare a total of 4 L bacterial culture. Grow at 37 °C and 200 rpm for 3-5 hrs until OD_{600} reaches 0.8.

d) Add 500 μL 1 M IPTG to each 1 L culture (final IPTG concentration ~0.5 mM). Incubate at 18 °C and 200 rpm overnight.

e) Harvest the bacteria pellet by centrifugation at 4000 x g for 15 min and discard the supernatant.

f) Resuspend the bacterial pellet in 50 mL of Lysis buffer 2 and directly place it in −20 °C freezer for at least 1 day. The aim is to break bacteria by gradual ice formation. Alternatively, bacteria can be disrupted by French press.

Pause Point: After transformation, the bacteria plate can be stored at 4 °C for up to two weeks. The resuspended bacteria pellet in Lysis buffer 2 can be stored at −20 °C for up to one month.

7. ATG3 protein purification

a) Thaw bacteria pellet in Lysis buffer 2 in ice water and lyse cells by sonication under the following conditions: maximum amplitude, 40 s on/60 s off, repeat 5–10 times.

b) Pellet the cell debris by centrifugation at 25,000 x g for 30 min, at 4 °C.

c) Collect the cleared cell lysate and add 4 mL of Glutathione Sepharose® 4B slurry (2 mL of resin) rolling at 4 °C for 90 min.

d) Pellet the resin at 500 x g for 3 min at 4 °C. Wash the resin with Wash buffer five times.

e) Resuspend the resin in 10 mL of Wash buffer and add 200 μL of GST-3C (5 mg/mL). Incubate at 4 °C overnight to cleave the protein from the resin.

f) Collect the protein elute and concentrate it using a Vivaspin 20 concentrator column (MWCO 10 K) until the volume is reduced to 1-2 mL.

g) Further purify the protein by size exclusion on ÄKTA pure system equipped with Superdex 200 10/600 GL column pre-equilibrated with Equilibration buffer.

h) Determine peak, pool, and check purity by SDS-PAGE, and then concentrate the peak fractions using a Vivaspin 20 concentrator column (MWCO 10 K) to a final concentration of ~6 mg/mL.

i) Aliquot and snap freeze in liquid nitrogen. Store at −80 °C until use.

4.3 Expression and purification of ATG8 (LC3B S3C) from bacteria BL21 (DE3) cells

Timing: 1–2 weeks

8. LC3B S3C expression in BL21 (DE3) cells

a) Transform pAL-GST-3C-LC3B S3C plasmid into BL21 (DE3) cells, spread the bacteria on an LB agar plate containing 50 μg/mL of kanamycin. Incubate the plate at 37 °C overnight.

b) Pick a single colony to inoculate 120 mL of LB medium containing 50 μg/mL kanamycin. Incubate at 37 °C shaking at 180 rpm overnight.

c) Transfer 25-30 mL of the culture into 1 L of LB medium containing 50 μg/mL kanamycin in a 2 L flask (initial OD_{600} around 0.1). Prepare a total of 4 L bacterial culture. Grow at 37 °C and 200 rpm for 3-5 hrs until OD_{600} reaches 0.8.

d) Add 500 μL 1 M IPTG to each 1 L culture (final IPTG concentration ~0.5 mM) to induce protein expression. Incubate at 18 °C and 200 rpm overnight, or alternatively, incubate at 25 °C and 200 rpm for 5 hrs after the induction.

e) Harvest the bacteria pellet by centrifugation at 4000 x g for 15 min and discard the supernatant.

f) Resuspend the bacterial pellet in 50 mL of Lysis buffer 2 and directly place it in −20 °C freezer for at least 1 day. It aims to break bacteria by gradual ice formation. Alternatively, bacteria can be disrupted by French press.

9. LC3B S3C protein purification

Purification steps are performed as described above in Step 7. The protein is concentrated to a final concentration of ~7 mg/mL. Aliquot and snap freeze in liquid nitrogen. Store at −80 °C until use.

Note: Other ATG8 family proteins can be purified with this protocol. Protein purification steps of ATG7, ATG3 and LC3B S3C are resolved by SDS-PAGE gels (Fig. 1).

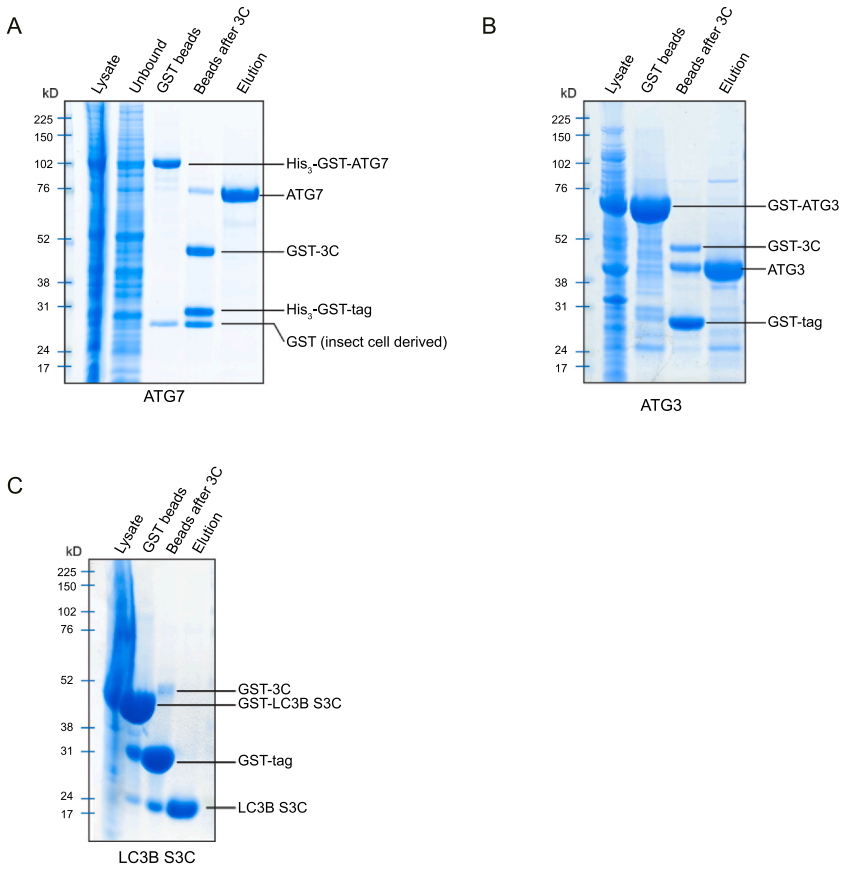

Fig. 1 SDS-PAGE gels showing **(A)** ATG7, **(B)** ATG3 and **(C)** LC3B S3C purification steps. Lysate: cell lysate after lysis and centrifugation to remove cell debris. Unbound: lysate sample collected after incubation with Glutathione Sepharose® 4B resin with cell lysate. GST beads: resin sample containing protein samples. Beads after 3 C: resin sample after GST-3C protease cleavage overnight. Elution: protein elute collected and further purified by size-exclusion chromatography.

4.4 NBD-labeling of LC3B S3C proteins with single cysteine mutation

Timing: 2 h

10. Protein buffer exchange

a) Equilibrate a PD Minitrap G-25 column with 8 mL of Labeling buffer without the reducing agent TCEP.

b) Add 250 µL 5 mg/mL LC3B S3C to the column and collect the protein elute.

c) Measure LC3B S3C protein concentration after the buffer exchange.

11. LC3B S3C fluorescent labeling

a) Prepare 10 mM IANBD-amide stock in DMSO and store at −20 °C until use.

b) Mix 400 μL of 100 μM LC3B S3C with 100 μL 10 mM IANBD-amide, and incubate the reaction mix at room temperature in the dark for 1 hr.

c) Add 20 μL of 100 mM L-cysteine to quench the reaction (final concentration ~3.8 mM).

d) Equilibrate a new PD Minitrap G-25 column with 8 mL of Equilibration buffer. Add ~500 μL of the reaction mix into the column and collect the elute. The unbound IANBD-amide is removed at this step.

e) Measure NBD-labeled LC3B S3C concentration by Bradford assay and check whether there is residual unbound IANBD-amide in the reaction by SDS-PAGE (residual dye migrates in dye front).

f) Add glycerol to NBD-labeled LC3B S3C to a final concentration of 20 %. Aliquot and snap freeze in liquid nitrogen. Store at −80 °C for up to 3 months.

Alternatives: Other buffer exchange approaches such as dialysis can be used as well.

NBD labelled LC3B S3C is resolved by SDS-PAGE (left panel) and fluorescent imaging (right panel) (Fig. 2A). It has similar activity as wild type LC3B in in vitro lipidation reaction (Fig. 2B).

4.5 Liposome preparation

Timing: 3–4 h

12. Liposome stock preparation (final concentration 2 mM, 1 mL) (Fig. 3A)

a) Mix POPC and DOPE lipid in chloroform at a molar ratio of 50 %: 50 %.

b) Dry the lipid mix under a stream of nitrogen gas for approximately 5 min, until lipid films form on the tube wall. Further dry the lipid films in Eppendorf™ Concentrator for 2 hrs to remove residual chloroform.

c) Rehydrate the lipid films with 1 mL of Equilibration buffer. Vortex rigorously until the lipid films is fully resuspended. The lipid suspension should appear turbid and mainly contain multilamellar vesicles (MLVs).

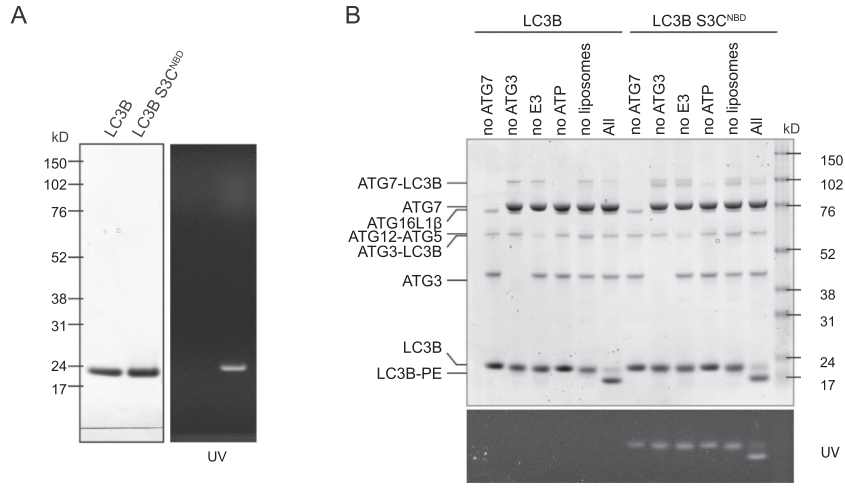

Fig. 2 NBD labelled LC3B S3C has the similar activity as wild type LC3B. (A) NBD labelling of LC3B S3C is analyzed by SDS-PAGE gel, imaged first under a UV irradiator, followed by Coomassie blue staining. **(B)** In vitro lipidation reaction of LC3B and LC3B S3C^{NBD}. Full reaction contains: 1 μM ATG7, 1 μM ATG3, 0.25 μM the E3 complex, 5 μM LC3B or LC3B S3C^{NBD}, 1 mM 100 nm liposomes composed of 50 % POPC/50 % DOPE and 5 mM MgATP. The reactions are incubated at 37 °C for 90 min, followed by SDS-PAGE analysis. The gel was illuminated under UV and stained with Coomassie blue.

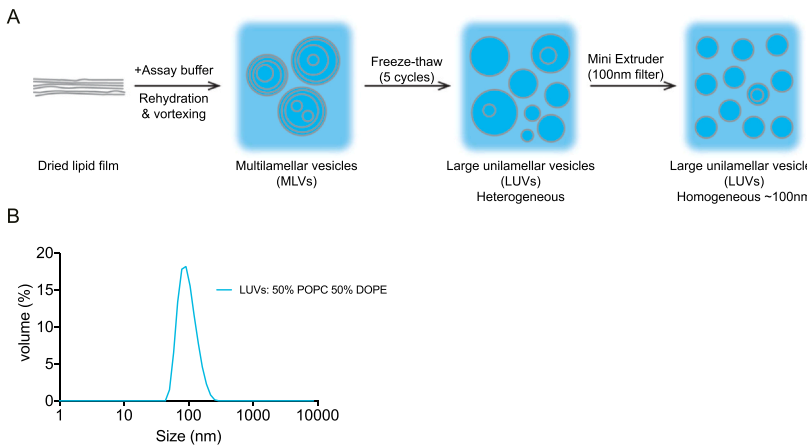

Fig. 3 Schematic overview of liposome preparation. (A) Lipid mix is dried under nitrogen gas and further vacuum-dried for at least 2 hrs to remove residual chloroform. The dried lipid film is resuspended in assay buffer by vortexing. Multilamellar vesicles (MLVs) are formed during this step and subsequently converted to large unilamellar vesicles (LUVs) by freeze-thaw cycles. Homogeneous LUVs are generated by extruding liposome solution through a 100 nm polycarbonate membrane. **(B)** An example result of liposome size distribution measured by dynamic light scattering. Average size 105.5 nm, polydispersity index (PDI) = 0.07.

d) Perform 5 times freeze-thaw cycles using liquid nitrogen and 42 °C water bath until the liposome solution is fully thawed.

e) Prepare the unilamellar vesicles by filter extrusion method. Equilibrate the Mini Extruder (Avanti Polar Lipids) with Equilibration buffer, and check for leakage before use.

f) Extrude the liposome solution first by passing it 10 times through 0.2 μm polycarbonate membrane. Then, extrude the liposomes by passing it at least 20 times through 0.1 μm polycarbonate membrane. One pass is the equivalent of pushing the solution through the membrane back and forth between two syringes (input and output syringes). Collect the liposome solution from the output syringe.

Pause Point: Lipid film can be stored at 4 °C for approximate one week after vacuum dry. The extruded liposomes can be stored at 4 °C for approximate 3 days. Measure the liposomes size before the experiments.

Note: To prepare homogenous liposomes around 100 nm, it is recommended to pass the liposome solution through 0.2 μm membrane before through 0.1 μm membrane. The liposome solution should be completely transparent after extrusion through 0.1 μm membrane.

13. Size of liposomes are determined by dynamic light scattering (DLS).

a) Mix 10 μL liposome solution with 90 μL Equilibration buffer (1: 10 dilution).

b) Add 100 μL diluted liposome solution in the micro cuvette and measure the liposome size using Zetasizer Nano ZS (Fig. 3B).

Note: Homogenous liposomes typically have a polydispersity index (PDI) below 0.2 (Soema et al., 2015).

4.6 Real-time ATG8 lipidation assay

Timing: 3–4 h

14. Reaction mixture preparation

a) The full lipidation reaction except ATP contains 0.2 μM ATG7, 0.2 μM ATG3, 0.05 μM the E3 complex, 1 μM NBD-labelled LC3B S3C, 1 mM liposomes (50 mol% POPC/50 mol% DOPE). Prepare 80 μL of the reaction mixture either containing all the components or having one component missing, such as conditions "No ATG7", "No ATG3" or "No E3".

15. Time course measurement by FP-8300

a) Record NBD fluorescence (ex/em 468 nm/535 nm) over time with the time course measurement program.

b) Set excitation at 468 nm (bandwidth 5 nm) and emission at 535 nm (bandwidth 10 nm).

c) Set cuvette holder temperature at 37 °C.

d) Set the total measurement time 20 min (1200 s) with two measurement ranges:

Time range 1	Interval: 20 s	End time: 80 s
Time range 2	Interval: 10 s	End time: 1200 s

e) Transfer the reaction mixture into a 10 mm path length quartz cuvette.

f) Start the measurement. Perform one measurement at a time. During Time range 1, between 60-80 s, add MgATP (final concentration: 1 mM) to initiate the reaction.

Note: The quartz cuvette is rinsed with excess water, followed by ethanol, and then dried under a stream of compressed air before the next measurement.

5. Expected outcomes

This protocol provides the detailed steps for the real-time ATG8 lipidation assay. A representative measurement is shown in Fig. 4A-C. With the full lipidation reaction ("All"), the NBD fluorescence signal increases significantly over time following the addition of ATP. In contrast, "No ATG7" and "No ATP" groups show no increase in the NBD fluorescence signal, suggesting the lipidation reaction cannot be initiated without the E1-activating enzyme or ATP, respectively. We also observed a modest increase in NBD signals in the absence of ATG3 ("No ATG3") and a further increase in the absence of liposomes ("No liposomes"), suggesting ATG7~LC3B and/or ATG3~LC3B intermediate formation. Furthermore, in the absence of the E3 complex ("No E3"), a slight increase in NBD signal compared with the "No liposomes" condition reflects a weak conjugation between LC3B to PE.

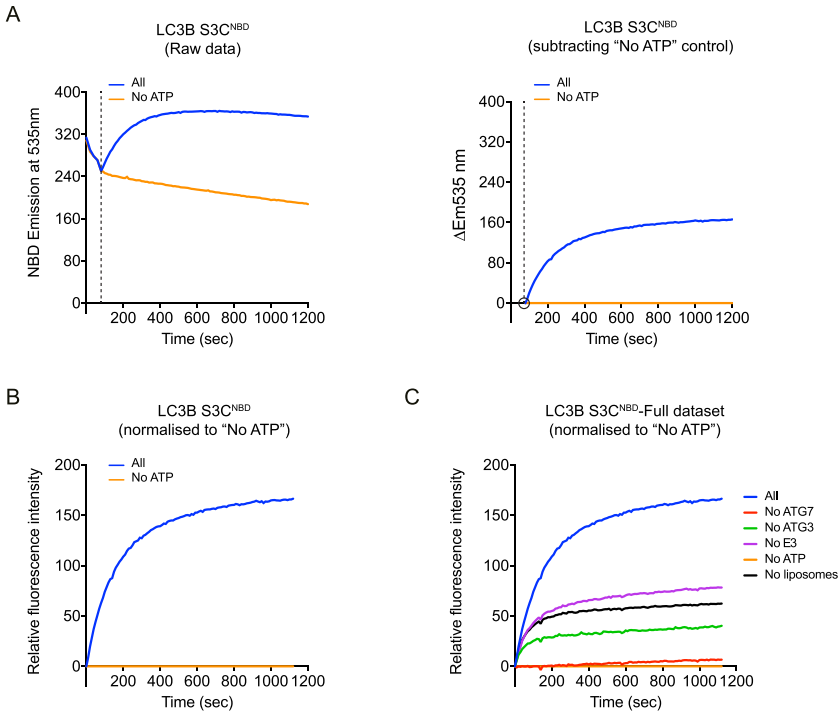

Fig. 4 Real-time ATG8 lipidation assay. (A) Left: raw data of NBD fluorescence intensity ("All" vs. "No ATP" conditions). NBD fluorescence increases after adding ATP between 60 and 80 s "No ATP" condition add the same volume of Equilibration buffer. Right: NBD fluorescence increase (ΔEm535 nm), calculated by subtracting the NBD signal from "No ATP" group (control) from each condition at the corresponding time point. The dashed line suggests time point at 80 s **(B)** Result plot shows the relative fluorescent intensity with full reaction ("All) normalized to no ATP condition at time point 80 s. Time range 1 (0–80 s) is not shown in the final plot. **(C)** Result plot shows the relative fluorescent intensity with full dataset. *Data represents a single experiment, derived from Zhang et al. (2023).*

6. Quantification and statistical analysis

1. The measurement files are exported and analyzed in Excel.
2. The NBD fluorescence increase (ΔEm535 nm) at each time point starting from 80 s in each reaction group is calculated by subtracting the fluorescence recorded in the control group ("No ATP") (Fig. 4A).

$$\Delta Em535\ nm\,(t) = F_{reaction}\,(t) - F''_{No\ ATP''}\,(t)$$

$$\Delta Em535\ nm\,(t = 80s) = F_{reaction}\,(t = 80s) - F''_{No\ ATP''}\,(t = 80s)$$

3. The relative fluorescence intensity (ΔF) at each time point was then normalized to the ΔEm535 nm at 80 s (Fig. 4B).

$$\Delta F\,(t) = \Delta Em535\ nm\,(t) - \Delta Em535\ nm\,(t = 80s)$$

4. The result figures are plotted using GraphPad Prism 9.0.

7. Advantages

This protocol provides a kinetic measurement of ATG8 lipidation reaction in real time. It is a useful tool to monitor not only the activity of the E1-E2-E3 enzymatic cascade, but also the upstream regulators that mediate the ATG8 lipidation reaction (Zhang et al., 2023, 2024).

8. Limitations

This protocol allows to track ATG8 lipidation reaction in a real-time manner. However, the increase in NBD fluorescence reflects not only the end-point ATG8 lipidation, but also the formation of intermediates. Therefore, it is important to design the appropriate control experiments to determine where the increased NBD signal results from. In addition, these control experiments should be performed every time, especially when comparing different lipid compositions or other regulatory proteins that mediate the lipidation reaction. However, due to the instrument model and setup in our laboratory, one measurement could be performed at a time. While the current setup may not be high-throughput, the fluorescence measurement is highly sensitive.

9. Optimization and troubleshooting

Problem 1. Sf9 cells keep growing after the viral infection.

Potential solution. If Sf9 cells continue to grow after P1 viral infection, it is likely that the initial transfection has failed. In this case, repeat Step 1. If Sf9 cells do not stop growing after P2 or P3 viral infection, add more medium to prevent the culture becoming too dense, and monitor the cell number and viability every day. Alternatively, add more virus to infect the cells.

Problem 2. Low efficiency of NBD labeling.

Potential solution. The presence of reducing agents in buffer may hinder cysteine labeling with NBD. If the labeling efficiency is low, consider the possibility that residual TCEP remains. In this case, repeat buffer exchange (Step 10) before NBD labeling, or try alternative buffer exchange approaches, such as dialysis or HiTrap™ Desalting columns.

Problem 3. NBD fluorescence signal photobleached over time.

Potential solution. In this protocol, measurements are recorded every 10 s (Time range 2) after adding ATP to initialize the reaction. To reduce photobleaching of NBD fluorescence over time, the measurement interval can be extended.

Acknowledgments

We thank Alicia Alonso for sharing human ATG7 and ATG3 plasmids, Svend Kjaer for pBacPAK-His3-GST plasmid and the technical assistance on insect cell culture, and Simone Kunzelmann for the technical assistance on fluorescence spectroscopy. We also thank Colin Davis and Anne Schreiber for providing the E3 complex. This work is supported by the Francis Crick Institute, which receives its core funding from Cancer Research UK (CC2134 to S.A.T.), the UK Medical Research Council (CC2134 to S.A.T.). This research was funded in whole, or in part, by the Wellcome Trust (CC2134 to S.A.T.). W.Z. and S.A.T received funding from the European Research Council under the European Union's Seventh Framework Programme (FP7/2007–2013)/ERC grant agreement n° 788708. This study was supported by PRESTO (JPMJPR20EC to T.N.) from Japan Science and Technology (JST), a Grant-in-Aid for Transformative Research Areas (B) (grant 21H05146 to T.N.) from the Japan Society for the Promotion of Science (JSPS), and a grant from the Japan Foundation for Applied Enzymology (to T.N.).

References

Fracchiolla, D., Chang, C., Hurley, J. H., & Martens, S. (2020). A PI3K-WIPI2 positive feedback loop allosterically activates LC3 lipidation in autophagy. *Journal of Cell Biology, 219*(7), e201912098. https://doi.org/10.1083/jcb.201912098.

Ichimura, Y., Imamura, Y., Emoto, K., Umeda, M., Noda, T., & Ohsumi, Y. (2004). *In* vivo and in vitro reconstitution of atg8 conjugation essential for autophagy. *Journal of Biological Chemistry, 279*(39), 40584–40592. https://doi.org/10.1074/jbc.M405860200.

Lystad, A. H., Carlsson, S. R., de la Ballina, L. R., Kauffman, K. J., Nag, S., Yoshimori, T., ... Simonsen, A. (2019). Distinct functions of ATG16L1 isoforms in membrane binding and LC3B lipidation in autophagy-related processes. *Nature Cell Biology, 21*(3), https://doi.org/10.1038/s41556-019-0274-9.

Martens, S., & Fracchiolla, D. (2020). Activation and targeting of ATG8 protein lipidation. *Cell Discovery, 6*(1), 23. https://doi.org/10.1038/s41421-020-0155-1.

Mizushima, N. (2020). The ATG conjugation systems in autophagy. *Current Opinion in Cell Biology, 63*, 1–10. https://doi.org/10.1016/j.ceb.2019.12.001.

Mizushima, N., Yoshimori, T., & Levine, B. (2010). Methods in mammalian autophagy research. *Cell, 140*(3), 313–326. https://doi.org/10.1016/j.cell.2010.01.028.

Nath, S., Dancourt, J., Shteyn, V., Puente, G., Fong, W. M., Nag, S., ... Melia, T. J. (2014). Lipidation of the LC3/GABARAP family of autophagy proteins relies on a membrane-curvature-sensing domain in Atg3. Article 5. *Nature Cell Biology, 16*(5), https://doi.org/10.1038/ncb2940.

Nishimura, T., & Tooze, S. A. (2020). Emerging roles of ATG proteins and membrane lipids in autophagosome formation. Article 1 *Cell Discovery, 6*(1), https://doi.org/10.1038/s41421-020-0161-3.

Noda, N. N., Satoo, K., Fujioka, Y., Kumeta, H., Ogura, K., Nakatogawa, H., ... Inagaki, F. (2011). Structural basis of Atg8 activation by a homodimeric E1, Atg7. *Molecular Cell, 44*(3), 462–475. https://doi.org/10.1016/j.molcel.2011.08.035.

Raghuraman, H., Chatterjee, S., & Das, A. (2019). Site-directed fluorescence approaches for dynamic structural biology of membrane peptides and proteins. *Frontiers in Molecular Biosciences, 6*. https://doi.org/10.3389/fmolb.2019.00096.

Soema, P. C., Willems, G.-J., Jiskoot, W., Amorij, J.-P., & Kersten, G. F. (2015). Predicting the influence of liposomal lipid composition on liposome size, zeta potential and liposome-induced dendritic cell maturation using a design of experiments approach. *European Journal of Pharmaceutics and Biopharmaceutics, 94*, 427–435. https://doi.org/10.1016/j.ejpb.2015.06.026.

Taherbhoy, A. M., Tait, S. W., Kaiser, S. E., Williams, A. H., Deng, A., Nourse, A., ... Schulman, B. A. (2011). Atg8 transfer from Atg7 to Atg3: A distinctive E1-E2 architecture and mechanism in the autophagy pathway. *Molecular Cell, 44*(3), 451–461. https://doi.org/10.1016/j.molcel.2011.08.034.

Zhang, W., Litschel, T., D'Antuono, R., Davis, C., Schreiber, A., & Tooze, S.A. (2024). Mechanistic studies of autophagic cargo recruitment and membrane expansion through in vitro reconstitution (p. 2024.12.24.630225). bioRxiv. https://doi.org/10.1101/2024.12.24.630225.

Zhang, W., Nishimura, T., Gahlot, D., Saito, C., Davis, C., Jefferies, H. B., ... Tooze, S. A. (2023). Autophagosome membrane expansion is mediated by the N-terminus and cis-membrane association of human ATG8s. *eLife, 12*, e89185. https://doi.org/10.7554/eLife.89185.

CHAPTER SEVENTEEN

Optogenetic phospholipase C for measuring phosphoinositide turnover and DAG generation

Yeon-Jeong Kim[a], Ayako M. Watabe[b], and Toshihisa Ohtsuka[a,*]
[a]Department of Biochemistry, Faculty of Medicine, Graduate School of Medicine, University of Yamanashi, Yamanashi, Japan
[b]Institute of Clinical Medicine and Research, Research Center for Medical Sciences, The Jikei University School of Medicine, Chiba, Japan
*Corresponding author. e-mail address: tohtsuka@yamanashi.ac.jp

Contents

1. Introduction 348
2. Structure and operating mechanism of the opto-PLCβ system 349
3. Materials and methods 351
4. Before you begin 351
5. Key resources table 352
6. Materials and equipment 354
7. Step-by-step method details 354
   7.1 Cell preparation and transfection 354
   7.2 Live-cell imaging on confocal microscope 355
   7.3 Image analysis using FIJI 357
8. Expected outcomes 358
9. Quantification and statistical analysis 360
10. Advantages 360
11. Limitations 361
12. Optimization and troubleshooting 361
   12.1 Problem (low transfection efficiency) 361
   12.2 Potential solution to optimize the procedure (low transfection efficiency) 362
   12.3 Problem (Weak or inconsistent fluorescence signals). 362
   12.4 Potential solution to optimize the procedure (weak or inconsistent fluorescence signals) 362
   12.5 Problem (High background fluorescence). 362
   12.6 Potential solution to optimize the procedure (high background fluorescence) 362
13. Safety considerations and standards 363
14. Alternative methods/procedures 363
15. Discussion: Implications of lipid restoration kinetics 364
16. Conclusion 365

Methods in Enzymology, Volume 728
ISSN 0076-6879, https://doi.org/10.1016/bs.mie.2026.01.008
Copyright © 2026 Elsevier Inc. All rights are reserved, including those for text and data mining, AI training, and similar technologies.

17. Future directions 365
Declaration of generative AI and AI-assisted technologies in the writing process 366
References 366

Abstract

Phospholipase C plays a pivotal role in cellular signaling by hydrolyzing phosphatidylinositol 4,5-bisphosphate (PIP_2) into diacylglycerol (DAG) and inositol 1,4,5-trisphosphate (IP_3), thereby initiating lipid- and calcium-mediated signaling cascades. Conventional approaches to studying PLC activity often rely on receptor activation or pharmacological stimulation, which can introduce variability and unintended signaling crosstalk. To improve these limitations, this chapter presents a dual-imaging strategy using opto-PLCβ, a light-activated PLC variant, enabling precise temporal control of phosphoinositide turnover in live cells. By integrating optogenetic stimulation with DAG- and PIP_2-specific fluorescent biosensors and confocal microscopy, this method allows real-time, quantitative analysis of lipid turnover kinetics and spatial dynamics, offering enhanced resolution and reliability compared to conventional techniques.

1. Introduction

Cell membranes serve as dynamic hubs for signal transduction, where lipid composition and turnover critically influence cellular physiology (Wen et al., 2021). Among the key lipid signaling molecules, phosphatidylinositol 4,5-bisphosphate (PIP_2), long with its metabolic products inositol 1,4,5-trisphosphate (IP_3) and diacylglycerol (DAG), play central roles in regulating calcium mobilization, cytoskeletal remodeling, and membrane trafficking (Sun et al., 2013). The hydrolysis of PIP_2 by phospholipase C (PLC) generates DAG and IP_3, initiating distinct signaling branches: DAG remains membrane-associated and activates protein kinase C (PKC), while IP_3 diffuses into the cytosol to trigger calcium release from intracellular stores (Brown et al., 2008; Sun et al., 2013; Wen et al., 2021).

Accurate measurement of DAG and PIP_2 turnover is essential for dissecting lipid-mediated signaling pathways (Luan et al., 2025; Schultz, 2023). Conventional approaches, including receptor-mediated activation via G protein-coupled receptors (GPCRs) or receptor tyrosine kinases, have been widely used (Luan et al., 2025; Schultz, 2023). However, these methods suffer from limited temporal resolution, receptor desensitization, and unintended signaling crosstalk, complicating the interpretation of lipid dynamics and reducing experimental precision (Luan et al., 2025). To address these limitations, optogenetic tools have been developed to enable

spatially and temporally controlled manipulation of lipid metabolism. Light-activated enzymes such as optoPLDs (Tei & Baskin, 2020) and opto-PLCβ (Kim et al., 2024) variants offer temporally precise and spatially confined control of lipid turnover, minimizing off-target effects and enabling localized activation of signaling pathways (Luan et al., 2025; Schultz, 2023; Tei & Baskin, 2021).

In this chapter, we describe the implementation of an optogenetic PLCβ3 system in HEK293T cells, coupled with dual fluorescent biosensors for PIP_2 and DAG. Lipid changes are visualized using two biosensors: a PIP_2 probe based on the PH domain of PLCδ tagged with miRFP670nano3, and a DAG probe comprising the C1A domain of PKCγ fused to mCherry (Kim et al., 2024). This dual-imaging strategy enables real-time quantification of lipid turnover with subcellular resolution, offering a robust platform for investigating the biological significance of phosphoinositide signaling.

2. Structure and operating mechanism of the opto-PLCβ system

The opto-PLCβ system is a modular optogenetic platform engineered to enable precise and reversible control of phospholipase C (PLC) activity in living cells. It comprises two engineered components: a membrane-anchored light-sensing module, the light-induced dimer (iLID) (Guntas et al., 2015), and a cytosolic effector enzyme, PLCβ3, which is modified for light-dependent membrane recruitment and activation. The domain architecture and predicted structure of the system, modeled using AlphaFold3, are shown in Fig. 1.

At the core of the system is the improved light-induced dimer (iLID) module, which contains a light-oxygen-voltage (LOV2) domain. In response to blue light (473 nm), the LOV2 domain undergoes a conformational change that exposes the SsrA sequence, enabling interaction with its binding partner, SspB, fused to a truncated form of PLCβ3 (Fig. 1A). The iLID domain is anchored to the plasma membrane via a CAAX motif derived from KRas4B (Fig. 1B), ensuring spatially restricted activation.

The effector component, PLCβ3(ΔX–Y)-SspB, is engineered by removing the C-terminal domain (CTD) of PLCβ3 to eliminate Gq-dependent activation (Fig. 1C). The SspB domain is inserted in place of the X–Y linker, an intrinsically disordered region known to mediate autoinhibition (Fig. 1C). This design maintains the enzyme in an inactive state under dark conditions,

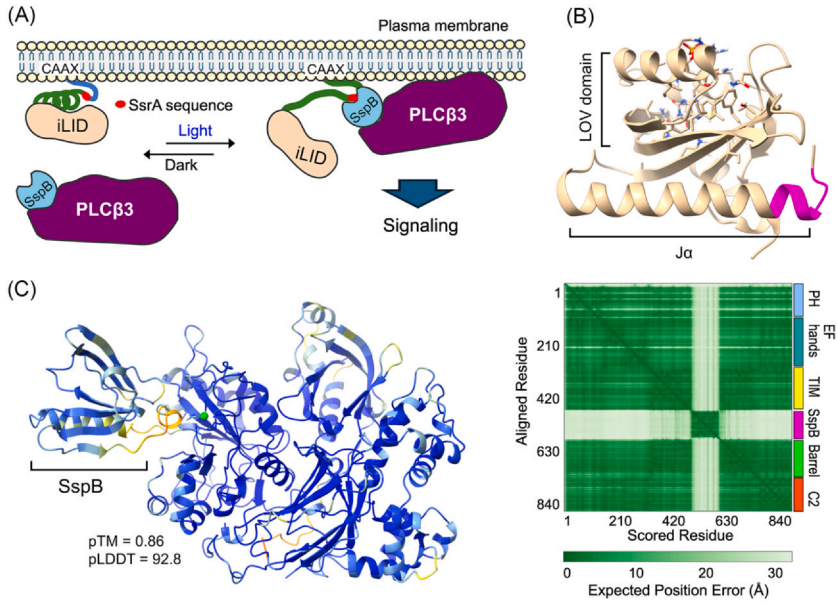

Fig. 1 Structural and functional design of the opto-PLCβ system. (A) Illustration of light-dependent recruitment of PLCβ3(ΔX–Y)-SspB to the plasma membrane via the iLID system. In the absence of light, the LOV2 domain remains in a closed conformation, concealing the SsrA tag and preventing interaction with SspB. Exposure to blue light (473 nm) induces a conformational change in LOV2 that reveals the SsrA tag, allowing binding to SspB and membrane translocation of PLCβ3, where it hydrolyzes PIP_2 into DAG and IP_3. (B) Structural model of the iLID module based on PDB ID: 4WF0, showing the LOV2 domain and Jα helix. The module is anchored to the plasma membrane via a KRas4B-derived CAAX motif, enabling spatially confined activation of PLCβ3. (C) Predicted structure of the engineered PLCβ3(ΔX–Y)-SspB effector generated by AlphaFold3. The SspB domain is inserted into the X–Y linker region to maintain autoinhibition in the dark. The plot shows the predicted alignment error across residues, with domain annotations including PH, EF hands, TM, and C2, indicating high-confidence structural predictions (pTM = 0.86, pLDDT = 92.8).

minimizing basal activity. Blue light irradiation triggers rapid translocation of the SspB-tagged PLCβ3 to the membrane through iLID–SspB interaction, initiating hydrolysis of PIP_2 and production of DAG and IP_3 (Fig. 1A).

Functionally, the system exhibits robust light-dependent activation of downstream signaling pathways, including PKC and ERK phosphorylation, intracellular calcium mobilization, and inositol phosphate accumulation. Importantly, the autoinhibitory capacity of the SspB-inserted X–Y linker is preserved, enabling reversible and tightly regulated activation.

3. Materials and methods

HEK293T cells were cultured and transfected with plasmids encoding a light-controlled PLC system composed of iLID-CAAX and an engineered PLCβ3 variant. To monitor lipid dynamics, plasmids encoding fluorescent biosensors for PIP_2 and DAG were co-transfected. Four hours after transfection, cells were recovered and seeded onto collagen-coated glass-bottom dishes for imaging. Live-cell imaging was performed using a confocal microscope equipped with a stage top incubator. After brief photostimulation with a 473 nm laser line, fluorescence changes in the lipid biosensors were recorded in real time. Image analysis was conducted using FIJI software to quantify changes in cytoplasmic fluorescence intensity. Detailed procedures are provided in the sections below.

4. Before you begin

Timing: 1 day

This protocol outlines the preparation and imaging of HEK293T cells expressing optogenetically controlled PLCβ and fluorescent lipid probes. It enables real-time visualization of DAG and PIP_2 dynamics. Consider the following before starting:

- Cell line selection: HEK293T cells are recommended due to high transfection efficiency. COS7 cells are also compatible.
- Reagent and medium preparation: Prepare PEI MAX transfection reagent, culture medium (DMEM + 10 % FBS + NEAA), and imaging medium (HBSS + 0.1 % FBS).
- Glass-bottom dish coating: Use collagen I to enhance cell adhesion for imaging.

1. Preparation of Buffers and Media

a) PEI MAX serves as the primary transfection reagent and requires careful preparation to ensure optimal performance. Begin with 100 mg of polyethylenimine MAX powder and add it to a clean beaker containing approximately 70 ml of deionized water along with a magnetic stir bar. Stir the mixture using a magnetic stirrer until the powder is fully dissolved. Adjust the pH to 7.0 by adding sodium hydroxide solution dropwise while monitoring with a

calibrated pH meter. Transfer the solution to a measuring cylinder and bring the final volume to 100 ml with additional deionized water. Filter-sterilize the solution using a 0.22 μm pore size membrane filter and aliquot into sterile containers for storage. The prepared solution remains stable for up to 6 months at 4 °C, or can be stored at −70 °C for long-term use.

b) HEK293T cells are maintained in Dulbecco's Modified Eagle Medium (DMEM) supplemented with 10 % fetal bovine serum (FBS) and 1 × MEM non-essential amino acids (NEAA). Before use, pre-warm the required volume to 37 °C in a water bath for at least 10 min. Do not add antibiotics, as penicillin and streptomycin significantly reduce transfection efficiency.

c) The imaging medium consists of Hank's Balanced Salt Solution (HBSS) without phenol red, supplemented with 0.1 % FBS (optional).

2 Collagen Coating of Glass-bottom Dish

a) Diute collagen I to 10 μg/ml in sterile phosphate-buffered saline (PBS).

b) Add solution to glass-bottom and incubate at room temperature for at least 1 h.

c) Remove solution, wash the dish three times with PBS and air dry.

5. Key resources table

Reagent or Resource	Source	Identifier
Chemicals, Peptides, and Recombinant Proteins		
PEI MAX Transfection Grade Linear Polyethylenimine Hydrochloride (MW 40000)	Polysciences	Cat# 24765-1
Opti-MEM	Gibco	Cat# 31985062
Dulbecco's Modified Eagle Medium	Nacalai tesque	Cat# 08458-45
MEM non-essential amino acids solution	Gibco	Cat# 11140050
Fetal bovine serum	Biowest	
HBSS (+) without phenol red	Fujifilm	Cat# 084-08965
Collagen I stock solution	Corning	Cat# 354236

Trypsin-EDTA solution	Nacalai tesque	Cat# 35554-64
Dulbecco's phosphate-buffered saline (D-PBS)	Fujifilm	Cat# 043-29791
Experimental Models: Cell Lines		
HEK293T	ATCC	#CRL-3216; RRID:CVCL_0063
Recombinant DNA		
pUY-muGFP-iLID-CAAX	Kim et al.	N/A
pUY-PLCb3(ΔX-Y)-SspB-ALFA	Kim et al.	N/A
pUY-PLCb3Δ847-ALFA	Kim et al.	N/A
pUY-PLCδ (PH)-mCherry-NES	This study	N/A
pUY-Flag-prkcg (C1A)-miRFPnano3-NES	This study	N/A
pcDNA5-PLCb3(ΔX-Y)-SspB-Flag	Kim et al.	N/A
pcDNA5-PLCb3(ΔX-Y)-Flag	Kim et al.	N/A
Software and Algorithms		
FIJI	https://fiji.sc/	RRID: SCR_002285 https://fiji.sc/
Microsoft Excel	Microsoft	RRID: SCR016137 https://www.microsoft.com/
Olympus Fluoview FV10-ASW	Olympus	RRID: SCR_014215 https://www.olympus-lifescience.com/en/
Prism 5	GraphPad	RRID: SCR_002798 https://www.graphpad.com/
Other		
Olympus FV1200 confocal system Inverted microscope (IX83)	EVIDENT	https://www.olympus-lifescience.com/en/laser-scanning/fv1200/
Stage Top Incubator (Model: INUBTF-WSKM-A141)	TOKAI HIT	https://www.tokaihit.com/about-stage-top-incubator/
Glass bottom dish	Matsunami	Cat# D11130H
6-well plate	Corning	Cat# 353046

6. Materials and equipment

The experimental setup requires a cell culture incubator capable of maintaining 5 % CO_2 atmosphere at 37 °C with humidity control. A Class II biosafety cabinet provides the sterile working environment necessary for cell culture manipulations. An inverted microscope equipped with phase contrast optics allows for cell monitoring and quality assessment throughout the procedure.

Additional instrumentation includes a benchtop centrifuge capable of reaching 3000 rpm for pelleting cells and debris. pH measurement requires a calibrated pH meter accurate to at least 0.1 pH units. An analytical balance with 0.1 mg precision ensures accurate weighing of reagents.

Consumable materials encompass cell culture plates and flasks appropriate for the specific cell lines being used. Sterile pipettes and tips in various sizes accommodate different volume requirements throughout the protocol. Sterile 0.22 μm filter units enable solution sterilization, while 15 ml and 50 ml centrifuge tubes provide containers for solution preparation and storage.

- PEI MAX transfection reagent
- Opti-MEM
- Cell culture medium
- HBSS (without phenol red)
- Collagen I-coated glass-bottom dish
- Confocal microscope (Olympus FV1200)
- Stage top incubator
- FIJI software

Alternatives: Other transfection reagents, such as Lipofectamine, may be used if PEI MAX is unavailable.

7. Step-by-step method details

7.1 Cell preparation and transfection

Timing: 2 days

This step prepares HEK293T cells for transfection with plasmids encoding the required probes and proteins for visualizing PLC-mediated lipid dynamics.

1. The day before transfection, seed 1×10^6 HEK293T cells in 2 ml of culture medium in a single well of a 6-well plate.
2. Incubate cells at 37 °C, 5 % CO_2 for 16 h.
3. Prepare the PEI MAX: DNA complex (see Table 1) in Opti-MEM medium and incubate for 20 min at room temperature. The final volume of the transfection mixture should be 0.2 ml.
4. Add the transfection mixture to the culture and mix thoroughly.
5. Incubate the cells for 4 h in a humidified incubator with 5 % CO2 at 37 °C.
6. Add 1 ml of trypsin-EDTA solution and immediately aspirate the solution.
7. Add 2 ml of the culture medium to detach the cells.
8. Centrifuge the cell suspension at 300g for 5 min
9. Aspirate the medium and resuspend the cells in 2 ml of fresh culture medium.
10. Seed 120 μl of the cell suspension onto a collagen-coated glass-bottom dish, and incubate the cells for 1 h.
11. After 1 h of incubation, confirm that the cells have attach to the bottom, and then refill the dish with 2 ml of culture medium.
12. Incubate the cells overnight.

Note: Avoid antibiotics in culture medium to maintain transfection efficiency.

7.2 Live-cell imaging on confocal microscope

Timing: 1–4 h

This step prepares the microscope for live-cell time-lapse imaging by setting the temperature conditions, configuring imaging parameters, optimizing settings to prevent saturation, acquiring the image sequence, and saving the data for further analysis.

Table 1 Preparation of PEI MAX–plasmid DNA complex.

Plasmids	DNA (μg)	PEI max (μl)	Opti-MEM (μl)	Total (μl)
pUY-muGFP-iLID-CAAX	0.5	10	180	200
pUY-plcb3(ΔX-Y)-SspB-Flag	1			
pUY-PLCδ (PH)-mCherry-NES	0.25			
pUY-Flag-prkcg (C1A)-miRFPnano3-NES	0.25			

1. Set the temperature of the stage top incubator (for the top heater, stage heater, bath heater, and lens heater) to 25 °C.
2. Position the culture dish within the stage top incubator, and let the temperature equilibrate between the culture and the environment for 10 min
3. Set the image acquisition mode to SIM (SIMultaneous) scanning mode. Configure the following parameters for image acquisition (see Table 2) and photo-stimulation (see Table 3).
4. Adjust the focus, the detector HV, and the power of the scanning laser. To prevent the saturation of fluorescent intensity, change the lookup table (LUT) to the Hi-Lo setting.
5. Keep the cells for 5 min in the dark to maintain their resting state.
6. Acquire the time-lapse image sequence.
7. Save the image file in.oib format with your chosen file name.

Table 2 Parameters for confocal microscope image acquisition.

Image acquisition	Parameter
Primary dimensions	X × Y
Image size	512 × 512 pixels
Objective lens	UPLSAPO60XO NA:1.35
Scan mode	XYT
Scan speed	2 ms/pixel
Confocal aperture	400 mm

Table 3 Stimulation parameters.

Stimulation	Parameter
Power of 473 nm Laser	5 %
Scan speed	2 ms/pixel
Pre-activation	3 frames
Activation	2 frames

Critical: Insufficient temperature equilibration in the stage top incubator can lead to inconsistent focusing during time-lapse imaging.

7.3 Image analysis using FIJI

Timing: Variable

This step outlines how to analyze fluorescence microscopy image data using the FIJI software. It involves opening the image file(s), splitting channels if needed, setting measurement parameters, defining regions of interest (ROIs) within cell cytoplasmic areas, recording multiple ROIs, measuring fluorescence intensities across the specified ROIs, and exporting the data. The final step normalizes the fluorescence intensity values over time using a provided equation.

1. Launch FIJI and open the desired image file(s)
   Note: If working with dual-channel images, such as probes fused to miRFP670nano3 and mScarlet, split the channels into separate windows during file opening.
2. Go to the toolbar and select "Analyze" followed by "Set Measurement."
3. In the "Set Measurements" window, check only the "Mean gray value" option, then close the window.
4. Select the elliptical or oval selection tool and define the region of interest (ROI).
   Note: Restrict the ROI to the cytoplasmic region.
5. Press the 'T' key to open the ROI Manager.
6. Define ROIs for additional cells by repeating step 22, pressing 'T' after each ROI selection to record them in the ROI Manager.
7. In the ROI Manager window, click "More" and choose "Multi Measure".
   Note: This will display fluorescence intensity data for all specified ROIs.
8. Save the intensity data as a.csv file, or alternatively, directly copy and paste the data into a Microsoft Excel spreadsheet.
9. Process the data to normalize the relative fluorescence intensity using the following equation:
   $\frac{\Delta F}{F} = \frac{F(t) - F0}{F0}$ where F0 is the initial resting fluorescence value, and F (t) is the fluorescence value at a given time point.

8. Expected outcomes

The experiment should result in successfully co-transfected HEK293T cells that express both the PIP_2 and DAG probes. Under the confocal microscope, clear fluorescence signals from both probes should be visible. In the resting state, the PIP_2 probe is expected to be concentrated at the plasma membrane, while the DAG probe remains diffused in the cytoplasm (Fig. 2, dark). Once photo-stimulation is applied, the PIP_2 probe moves from the membrane into the cytoplasm, while the DAG probe relocates from the cytoplasm to the membrane (Fig. 2, light). After the initial redistribution, the probes gradually return to their original localization: the PIP_2 probe reaccumulates at the plasma membrane, and the DAG probe redistributes back into the cytoplasm (Fig. 2, restoration). This recovery phase marks the resynthesis of PIP_2 and the clearance of DAG, signaling a return to the basal lipid state.

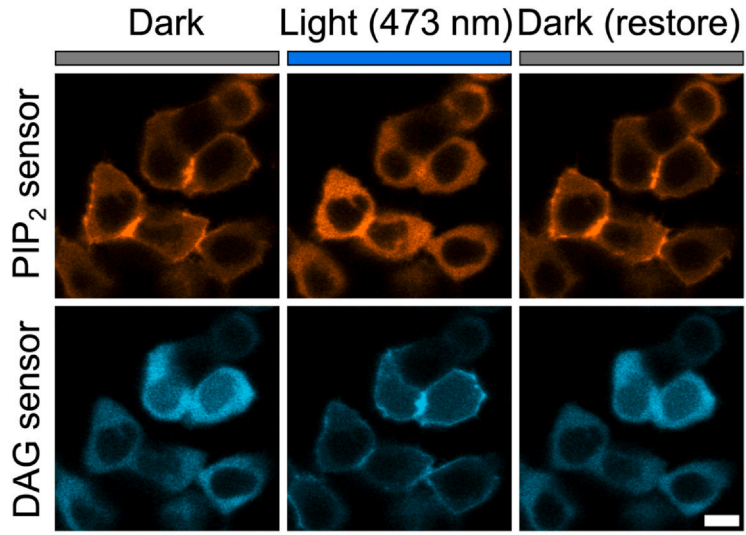

Fig. 2 Light-controlled redistribution of PIP_2 and DAG biosensors in HEK293T cells. Fluorescence confocal microscopy images show the localization of PIP_2 and DAG biosensors under three conditions: dark (resting), light stimulation at 473 nm, and recovery after light cessation (dark restore). In the dark, the PIP_2 probe (PH domain of PLCδ fused to miRFP670nano3) is concentrated at the plasma membrane. Light stimulation causes the probe to translocate to the cytoplasm, indicating hydrolysis of PIP_2. After the light is turned off, the probe gradually returns to the membrane, reflecting resynthesis of PIP_2. The DAG probe (C1A domain of PKCγ fused to mCherry) is initially distributed in the cytoplasm. Light stimulation induces its recruitment to the plasma membrane, consistent with DAG production. During recovery, the probe redistributes back to the cytoplasm, indicating DAG clearance. Scale bar = 10 μm.

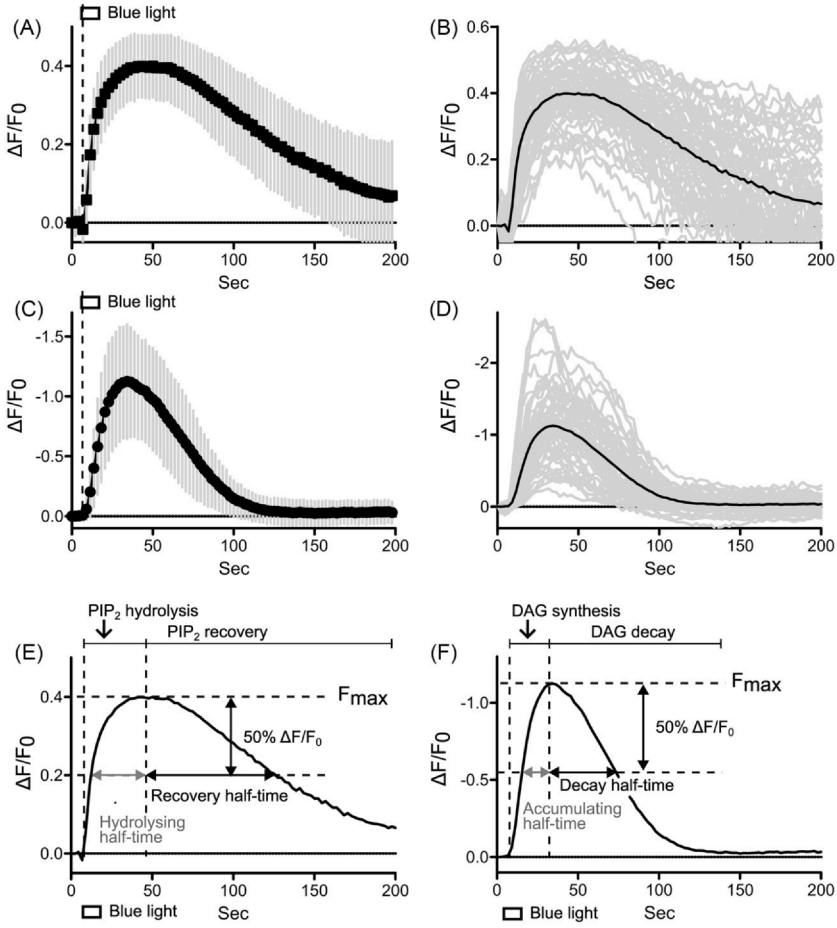

Fig. 3 Quantitative analysis of PIP_2 and DAG turnover kinetics following activation of opto-PLCβ. (A and B) Time-course plots of normalized fluorescence intensity ($\Delta F/F_0$) for the PIP_2 biosensor. Panel A shows the averaged response with standard deviation, while Panel B displays individual cell traces with the mean overlaid (n = 83 cells). Blue light stimulation induces a rapid increase in cytoplasmic fluorescence, indicating hydrolysis of PIP_2 at the plasma membrane, followed by gradual recovery. (C and D) Time-course plots of normalized fluorescence intensity ($\Delta F/F_0$) for the DAG biosensor. Panel C shows the averaged response, and Panel D presents individual traces (n = 83 cells). Light stimulation leads to an increase in membrane fluorescence, reflecting DAG production, followed by a decay phase. (E) Summary of PIP_2 turnover kinetics. The plot illustrates the hydrolysis and recovery phases, with annotations for peak amplitude (Fmax), hydrolyzing half-time, and recovery half-time. (F) Summary of DAG turnover kinetics. The plot shows the accumulation and decay phases, with annotations for peak amplitude (Fmax), accumulating half-time, and decay half-time.

9. Quantification and statistical analysis

Fluorescence intensity data are extracted from time-lapse images using FIJI. After opening the image files, channels corresponding to the PIP_2 and DAG probes are separated. Regions of interest (ROIs) are manually defined within the cytoplasm of individual cells, avoiding nuclear regions and areas with high background. The mean gray value for each ROI is measured across all time points and normalized relative to baseline intensity before stimulation.

Quantitative analysis of fluorescence intensity changes over time reveals the kinetics of PIP_2 hydrolysis (Fig. 3A and B) and DAG production (Fig. 3C and D). Restoration kinetics for both probes are further characterized by measuring parameters such as Fmax, half-times for hydrolysis and recovery (Fig. 3E), and accumulation and decay (Fig. 3F). These measurements provide insight into the temporal regulation of lipid signaling following photo-stimulation.

This approach enables detailed examination of the spatiotemporal characteristics of PLC-mediated lipid dynamics in live cells and can be used to compare signaling dynamics across different cell types or experimental conditions. To ensure reliable interpretation, multiple cells should be analyzed across independent experiments. Statistical comparisons between conditions can be performed using Student's *t*-test or one-way ANOVA, depending on the experimental design.

10. Advantages

This protocol enables precise and real-time visualization of lipid signaling events in live cells. Optogenetic control of PLCβ activity allows temporally defined stimulation without the need for chemical ligands, helping to avoid receptor desensitization and unintended signaling crosstalk. Confocal microscopy provides high spatial resolution, and the dual-probe system allows simultaneous monitoring of both PIP_2 depletion and DAG production.

The modular design of the plasmids and probes makes the system adaptable to various cell types and experimental contexts. This approach is well suited for dissecting lipid-mediated signaling pathways with minimal off-target effects.

11. Limitations

This protocol for dual imaging of phospholipase C (PLC) activity using a confocal microscope, while powerful, has several potential limitations. Overexpression of fluorescent probes such as the pleckstrin homology (PH) domain of PLCδ and the C1A domain of PKCγ may alter endogenous lipid dynamics or cellular physiology, potentially introducing artifacts or non-physiological responses.

Spatial resolution is constrained by the diffraction limit of light microscopy, which may obscure fine details of lipid localization and dynamics. Temporal resolution is limited by the speed of image acquisition and the need to balance signal quality with imaging frequency, potentially missing rapid events. The use of a single focal plane may also limit the ability to capture three-dimensional lipid dynamics.

Variability in transfection efficiency between cells and experiments can complicate quantitative comparisons. Additionally, the reliance on indirect measurements through fluorescent probes may not fully reflect native lipid behavior. Environmental factors such as temperature fluctuations and mechanical instability during imaging can affect focus and signal consistency.

Phototoxicity and photobleaching from prolonged or intense light exposure may damage cells and degrade fluorescent signals, limiting imaging duration. The protocol's effectiveness may vary across different cell types, requiring optimization for each. Finally, the need for specialized equipment and expertise in confocal microscopy and image analysis may limit accessibility and reproducibility across research settings.

12. Optimization and troubleshooting

12.1 Problem (low transfection efficiency)

Low transfection efficiency can result in insufficient probe expression, reduced signal quality, and inconsistent imaging outcomes. This issue may arise from suboptimal cell conditions, incorrect DNA-to-reagent ratios, or compromised plasmid quality. Cell density and the presence of antibiotics in the culture medium can also negatively affect transfection.

12.2 Potential solution to optimize the procedure (low transfection efficiency)

Begin with healthy, actively proliferating cells free from contamination. Use fresh culture medium and confirm cell morphology and viability under a microscope. Optimize the DNA-to-PEI ratio, typically starting with a 1:5 ratio (μg:μl), and use high-quality, endotoxin-free plasmid DNA. Seed cells at 70–80 % confluency to maximize uptake. If efficiency exceeds 30 %, the experiment can proceed. For difficult-to-transfect cell types, consider lipid-based reagents or electroporation.

12.3 Problem (Weak or inconsistent fluorescence signals).

Weak or inconsistent signals can hinder detection of lipid dynamics and compromise quantitative analysis. Causes include low probe expression, suboptimal imaging settings, or insufficient time for protein folding and maturation.

12.4 Potential solution to optimize the procedure (weak or inconsistent fluorescence signals)

Verify probe expression levels and allow 24–48 h after transfection for sufficient protein maturation and localization. Adjust imaging parameters such as laser power, detector gain, and exposure time to avoid under-exposure or saturation. Use Hi-Lo LUT settings to visualize signal intensity effectively. Confirm proper folding and localization of fluorescent proteins using control markers if needed.

12.5 Problem (High background fluorescence).

High background fluorescence can obscure probe signals and reduce the accuracy of intensity measurements. This issue may be caused by auto-fluorescence from the medium or dish, excessive probe expression, or inappropriate imaging settings.

12.6 Potential solution to optimize the procedure (high background fluorescence)

To reduce background fluorescence, imaging medium should be prepared without phenol red, which is known to interfere with fluorescence detection. Autofluorescence can also be minimized by using high-quality glass-bottom dishes and selecting appropriate filter sets for the microscope. Probe expression levels should be optimized to avoid over-saturation, and confocal settings such as aperture size and scan speed

should be adjusted to improve signal-to-noise ratio. Ensuring consistent and moderate expression of the probes will help maintain clarity and reproducibility in the imaging data.

13. Safety considerations and standards

All procedures should be conducted under biosafety level 1 conditions. Cell culture work must be performed in a certified biosafety cabinet using sterile technique. PEI MAX is a cationic polymer and should be handled with gloves and eye protection.

Biological waste, including transfected cells and media, must be disposed of in accordance with institutional and national regulations. Laser safety protocols must be followed during confocal imaging. This includes the use of protective eyewear and proper training for all personnel involved.

Electrical equipment such as incubators and microscopes should be regularly inspected and maintained to prevent hazards. Operators should be familiar with the manuals and safety procedures associated with each instrument. Routine checks and documentation of equipment status are recommended to ensure compliance and minimize risk.

14. Alternative methods/procedures

If optogenetic stimulation is not feasible due to equipment limitations or experimental constraints, chemical activation of PLC can be considered as an alternative approach. This method involves the use of receptor agonists such as carbachol or histamine to stimulate endogenous G protein-coupled receptors or receptor tyrosine kinases, which in turn activate PLC signaling pathways.

To ensure consistent and reproducible stimulation, a perfusion system is required. Continuous or pulse perfusion allows precise timing and concentration control of the agonist, minimizes variability in ligand exposure, and prevents desensitization effects that may occur with static application.

However, this approach introduces additional complexity, including potential signaling crosstalk and the need for careful calibration of flow rates and agonist concentrations. Despite these challenges, chemical stimulation combined with perfusion remains a viable alternative for studies where optogenetic tools are not available or applicable.

15. Discussion: Implications of lipid restoration kinetics

The kinetic profiles of PIP_2 recovery and DAG decay following optogenetic activation of PLCβ reveal temporally distinct yet mechanistically coupled lipid turnover events at the plasma membrane (PM). Quantitative parameters, including peak amplitude (F_{max}), hydrolysis and recovery half-times for PIP_2, and accumulation and decay half-times for DAG, demonstrate that lipid restoration is a tightly regulated process involving multiple coordinated pathways (Fig. 3). The rapid hydrolysis of PIP_2 and concurrent accumulation of DAG reflect the canonical PLCβ-mediated cleavage of phosphatidylinositol 4,5-bisphosphate, initiating a cascade of lipid remodeling and second messenger signaling.

DAG clearance proceeds through at least two major routes: enzymatic conversion to phosphatidic acid (PA) via diacylglycerol kinase (DGK) (Cai et al., 2009; Carrasco & Mérida, 2007), and translocation into the endoplasmic reticulum (ER) membrane by extended synaptotagmins (E-Syts) (Bian et al., 2018; Giordano et al., 2013; Saheki et al., 2016) for further metabolism. In contrast, PIP_2 resynthesis requires the transport of phosphatidylinositol (PI) from the ER to the plasma membrane, followed by sequential phosphorylation. These directional lipid fluxes between membrane compartments are facilitated by lipid transfer proteins such as Nir2 and Nir3 (Chang & Liou, 2015; Kim et al., 2015), as well as E-Syts, which tether ER–PM contact sites and enable efficient exchange.

The entire restoration process is modulated by second messengers generated during PLC activation, including calcium ions, DAG, and inositol trisphosphate (IP_3) (Dennis et al., 1991). Calcium influx and IP_3-mediated ER calcium release may enhance lipid transport and enzyme activity (Hilgemann et al., 2018). DAG itself serves both as a substrate and a signaling molecule that recruits effector proteins to the membrane (Hilgemann et al., 2018). The interplay between these messengers ensures that lipid composition is dynamically adjusted in response to signaling demands (Dennis et al., 1991; Hilgemann et al., 2018).

Our data underscore the utility of the opto-PLCβ system for resolving lipid signaling events with high temporal precision. They also reveal how cells orchestrate membrane remodeling through spatially and temporally integrated biochemical networks. The restoration kinetics captured in these fluorescence traces provide mechanistic insight into how lipid homeostasis is maintained during and after PLC activation.

16. Conclusion

The optogenetic activation of PLCβ3 combined with dual biosensor imaging provides a powerful tool for dissecting phosphoinositide signaling in live cells (Kim et al., 2024). This method offers precise temporal control on the millisecond scale, subcellular spatial resolution, and quantitative measurement of lipid turnover. It avoids variability from receptor-based activation and enables detailed study of dynamic membrane signaling events.

Compared to rhodopsin-based opto-GPCRs (Airan et al., 2009; Masseck et al., 2014; Morri et al., 2018; Tichy et al., 2019; Tichy et al., 2022), opto-PLCβ does not require retinal supplementation, has fast off kinetics, and features narrow spectral specificity that allows multiplexed imaging. This protocol can be applied to a variety of cell types such as COS7, HeLa, and primary neurons, and it can be combined with pharmacological treatments, calcium imaging, or super-resolution microscopy to explore complex signaling networks (Zhang & Cui, 2015). The modular design also supports swapping in other PLC isoforms or biosensors for tailored investigations of lipid signaling.

17. Future directions

Future work will expand the use of opto-PLCβ in organotypic cultures and in vivo preparations to investigate PLC-driven lipid dynamics and plasticity across different neural circuits. In our recent study, we demonstrated that photoactivation of opto-PLCβ in the basolateral amygdala enhances long-term potentiation at thalamic synapses and significantly improves associative fear learning in behaving mice (Kim et al., 2024). This finding establishes a causal link between precise PLC activation and neural plasticity in vivo and suggests that similar approaches could be applied to other brain regions involved in memory, decision making, or sensory processing.

Building on these in vivo results, integration of opto-PLCβ with simultaneous calcium or voltage imaging in animals will enable real-time correlation between lipid turnover and neural activity during behavior. Enhancing light delivery techniques for deep brain regions, optimizing spectral properties for multiplexed imaging, and engineering photoswitch variants with tailored kinetics will further expand the versatility of this

system. These developments will support rigorous investigation of membrane editing systems, including PLC-mediated lipid signaling, and facilitate precise dissection of membrane-associated processes, contributing to a deeper understanding of cellular regulation across biological systems.

Declaration of generative AI and AI-assisted technologies in the writing process

During the preparation of this work the authors used Microsoft Copilot in order to assist with the editing of scientific English. After using this tool, the authors reviewed and edited the content as needed and take full responsibility for the content of the publication.

References

Airan, R. D., Thompson, K. R., Fenno, L. E., Bernstein, H., & Deisseroth, K. (2009). Temporally precise in vivo control of intracellular signalling. *Nature, 458*(7241), 1025–1029. https://doi.org/10.1038/nature07926.

Bian, X., Saheki, Y., & De Camilli, P. (2018). Ca(2+) releases E-Syt1 autoinhibition to couple ER-plasma membrane tethering with lipid transport. *The EMBO Journal, 37*(2), 219–234. https://doi.org/10.15252/embj.201797359.

Brown, S. A., Morgan, F., Watras, J., & Loew, L. M. (2008). Analysis of phosphatidylinositol-4,5-bisphosphate signaling in cerebellar Purkinje spines. *Biophysical Journal, 95*(4), 1795–1812. https://doi.org/10.1529/biophysj.108.130195.

Cai, J. J., Abramovici, H., Gee, S. H., & Topham, M. K. (2009). Diacylglycerol kinases as sources of phosphatidic acid. *Biochimica Et Biophysica Acta-Molecular and Cell Biology of Lipids, 1791*(9), 942–948. https://doi.org/10.1016/j.bbalip.2009.02.010.

Carrasco, S., & Mérida, I. (2007). Diacylglycerol, when simplicity becomes complex. *Trends in Biochemical Sciences, 32*(1), 27–36. https://doi.org/10.1016/j.tibs.2006.11.004.

Chang, C. L., & Liou, J. (2015). Phosphatidylinositol 4,5-bisphosphate homeostasis regulated by Nir2 and Nir3 proteins at endoplasmic reticulum-plasma membrane junctions. *The Journal of Biological Chemistry, 290*(23), 14289–14301. https://doi.org/10.1074/jbc.M114.621375.

Dennis, E. A., Rhee, S. G., Billah, M. M., & Hannun, Y. A. (1991). Role of phospholipase in generating lipid second messengers in signal transduction. *The FASEB Journal, 5*(7), 2068–2077. https://doi.org/10.1096/fasebj.5.7.1901288.

Giordano, F., Saheki, Y., Idevall-Hagren, O., Colombo, S. F., Pirruccello, M., Milosevic, I., ... De Camilli, P. (2013). PI(4,5)P(2)-dependent and Ca(2+)-regulated ER-PM interactions mediated by the extended synaptotagmins. *Cell, 153*(7), 1494–1509. https://doi.org/10.1016/j.cell.2013.05.026.

Guntas, G., Hallett, R. A., Zimmerman, S. P., Williams, T., Yumerefendi, H., Bear, J. E., & Kuhlman, B. (2015). Engineering an improved light-induced dimer (iLID) for controlling the localization and activity of signaling proteins. *Proceedings of the National Academy of Sciences of the United States of America, 112*(1), 112–117. https://doi.org/10.1073/pnas.1417910112.

Hilgemann, D. W., Dai, G., Collins, A., Lariccia, V., Magi, S., Deisl, C., & Fine, M. (2018). Lipid signaling to membrane proteins: From second messengers to membrane domains and adapter-free endocytosis. *The Journal of General Physiology, 150*(2), 211–224. https://doi.org/10.1085/jgp.201711875.

Kim, Y. J., Guzman-Hernandez, M. L., Wisniewski, E., & Balla, T. (2015). Phosphatidylinositol-phosphatidic acid exchange by Nir2 at ER-PM contact sites maintains phosphoinositide signaling competence. *Developmental Cell, 33*(5), 549–561. https://doi.org/10.1016/j.devcel.2015.04.028.

Kim, Y. J., Tohyama, S., Nagashima, T., Nagase, M., Hida, Y., Hamada, S., ... Ohtsuka, T. (2024). A light-controlled phospholipase C for imaging of lipid dynamics and controlling neural plasticity. *Cell Chemical Biology, 31*(7), 1336–1348.e7. https://doi.org/10.1016/j.chembiol.2024.03.001.

Luan, L., Frederick, N. P., & Baskin, J. M. (2025). Emerging approaches for studying lipid dynamics, metabolism, and interactions in cells. *Annual Review of Biochemistry, 94*(1), 417–446. https://doi.org/10.1146/annurev-biochem-083024-110827.

Masseck, O. A., Spoida, K., Dalkara, D., Maejima, T., Rubelowski, J. M., Wallhorn, L., & Herlitze, S. (2014). Vertebrate cone opsins enable sustained and highly sensitive rapid control of Gi/o signaling in anxiety circuitry. *Neuron, 81*(6), 1263–1273. https://doi.org/10.1016/j.neuron.2014.01.041.

Morri, M., Sanchez-Romero, I., Tichy, A. M., Kainrath, S., Gerrard, E. J., Hirschfeld, P. P., & Janovjak, H. (2018). Optical functionalization of human Class A orphan G-protein-coupled receptors. *Nature Communications, 9*(1), 1950. https://doi.org/10.1038/s41467-018-04342-1.

Saheki, Y., Bian, X., Schauder, C. M., Sawaki, Y., Surma, M. A., Klose, C., & De Camilli, P. (2016). Control of plasma membrane lipid homeostasis by the extended synaptotagmins. *Nature Cell Biology, 18*(5), 504–515. https://doi.org/10.1038/ncb3339.

Schultz, C. (2023). Chemical tools for lipid cell biology. *Accounts of Chemical Research, 56*(10), 1168–1177. https://doi.org/10.1021/acs.accounts.2c00851.

Sun, Y., Thapa, N., Hedman, A. C., & Anderson, R. A. (2013). Phosphatidylinositol 4,5-bisphosphate: Targeted production and signaling. *Bioessays: News and Reviews in Molecular, Cellular and Developmental Biology, 35*(6), 513–522. https://doi.org/10.1002/bies.201200171.

Tei, R., & Baskin, J. M. (2020). Spatiotemporal control of phosphatidic acid signaling with optogenetic, engineered phospholipase Ds. *Journal of Cell Biology, 219*(3), https://doi.org/10.1083/jcb.201907013.

Tei, R., & Baskin, J. M. (2021). Induced proximity tools for precise manipulation of lipid signaling. *Current Opinion in Chemical Biology, 65*, 93–100. https://doi.org/10.1016/j.cbpa.2021.06.005.

Tichy, A. M., Gerrard, E. J., Sexton, P. M., & Janovjak, H. (2019). Light-activated chimeric GPCRs: Limitations and opportunities. *Current Opinion in Structural Biology, 57*, 196–203. https://doi.org/10.1016/j.sbi.2019.05.006.

Tichy, A. M., So, W. L., Gerrard, E. J., & Janovjak, H. (2022). Structure-guided optimization of light-activated chimeric G-protein-coupled receptors. *Structure (London, England: 1993), 30*(8), 1075–1087.e4. https://doi.org/10.1016/j.str.2022.04.012.

Wen, Y., Vogt, V. M., & Feigenson, G. W. (2021). PI(4,5)P(2) clustering and its impact on biological functions. *Annual Review of Biochemistry, 90*, 681–707. https://doi.org/10.1146/annurev-biochem-070920-094827.

Zhang, K., & Cui, B. (2015). Optogenetic control of intracellular signaling pathways. *Trends in Biotechnology, 33*(2), 92–100. https://doi.org/10.1016/j.tibtech.2014.11.007.

CHAPTER EIGHTEEN

Pharmacological modulation of lipid signaling

Ashutosh Sharma and Wonhwa Cho*
Department of Chemistry, University of Illinois Chicago, Chicago, IL, United States
*Corresponding author. e-mail address: wcho@uic.edu

Contents

1. Introduction 370
2. Development of lipid-protein interaction inhibitors 372
   2.1 A high-throughput inhibitor screening protocol 372
   2.2 Determination of inhibition constant 378
   2.3 Target validation 381
   2.4 Determination of in vivo inhibitory activity 384
3. Concluding Remarks 386
Acknowledgements 386
References 386

Abstract

Lipids regulate a broad spectrum of cellular functions through spatiotemporally controlled lipid–protein interactions. Dysregulation of lipid metabolism and lipid-mediated signaling is associated with diverse human diseases, including cancer, metabolic disorders, and neurodegenerative conditions. Consequently, selective inhibition of site-specific lipid–protein interactions has emerged as a promising therapeutic strategy to modulate aberrant cell signaling at the membrane interface. Here, we present a streamlined, quantitative workflow for the discovery, characterization, and evaluation of small-molecule inhibitors that disrupt lipid-dependent membrane association and activation of cytosolic signaling proteins. The protocol integrates a high-throughput fluorescence-quenching assay for inhibitor screening, detailed biochemical and cellular target-validation methods, and standardized procedures for in vitro and in vivo assessment of inhibitor potency, specificity, and safety. These general protocols provide a versatile and reproducible platform for developing potent, specific, and mechanistically defined inhibitors targeting a wide range of lipid-binding proteins implicated in disease.

Methods in Enzymology, Volume 728
ISSN 0076-6879, https://doi.org/10.1016/bs.mie.2026.01.025
Copyright © 2026 Elsevier Inc. All rights are reserved, including those for text and data mining, AI training, and similar technologies.

1. Introduction

Lipids play complex and essential regulatory roles in cell physiology beyond their basic function as membrane building blocks and energy sources (Cho & Stahelin, 2005; Saliba et al., 2015). They dynamically orchestrate cell signaling, intracellular trafficking, cell metabolism, and membrane organization by engaging in spatiotemporally regulated lipid-lipid and lipid–protein interactions (LPIs) (Cho & Stahelin, 2005; Saliba et al., 2015). Many signaling proteins reversibly associate with membranes via an expanding group of lipid-binding domains and motifs, including canonical PH, C1, C2, PX, FYVE, ENTH, FERM domains (Cho & Stahelin, 2006; Lemmon, 2008; Hammond & Balla, 2015) and non-canonical SH2 (Park et al., 2016), and PDZ (Chen et al., 2012) domains, enabling localized activation of signaling networks. The reversible nature of these interactions allows cells to achieve exquisite spatiotemporal control of signaling pathways.

Dysregulation of lipid metabolism and LPI-mediated signaling is an emerging hallmark of numerous pathological conditions (Di Paolo & De Camilli, 2006; Kihara, 2020). Aberrant cellular lipid composition or distribution can lead to mislocalization and hyperactivation of key signaling proteins, leading to cancer, metabolic disorders, cardiovascular diseases, inflammatory diseases and neurodegenerative diseases (Di Paolo & De Camilli, 2006; Kihara, 2020). Given the pivotal role of LPIs in disease, selective disruption of LPI has emerged as a viable therapeutic strategy complementary to conventional enzyme inhibition or receptor antagonism (Singaram et al., 2023; Sharma et al., 2025). Since aberrant LPI drives hyperactivation of signaling proteins primarily in diseased cells, LPI inhibitors typically do not interfere with physiological function of the signaling protein, thereby causing much less on-target toxicity than conventional inhibitors. However, rational discovery of LPI inhibitors is inherently challenging due to the complex and dynamic nature of LPI (Cho & Stahelin, 2006; Lemmon, 2008) and the lack of high-resolution structural information about the membrane-bound cytosolic proteins. Many canonical lipid binding domains, such as PH domains, interact with both a specific target lipid and bulk lipids surrounding the target lipid, making it difficult to quantify LPI and develop rapid quantitative assays for LPI (Cho & Stahelin, 2006). Due to this limitation in conjunction with the dearth of chemical libraries targeting the LPI space, few small molecules have been developed that selectively modulate lipid–protein contacts (Singaram et al., 2023; Sharma et al., 2025).

To address these challenges, we developed a fluorescence-quenching–based membrane-binding assay that quantitatively monitors protein–membrane association in real time (Kim et al., 2013; Cho et al., 2016). The method utilizes fluorescent protein (FP)-tagged lipid-binding proteins and lipid vesicles containing a nonfluorescent quenching lipid, such that membrane binding results in fluorescence quenching proportional to

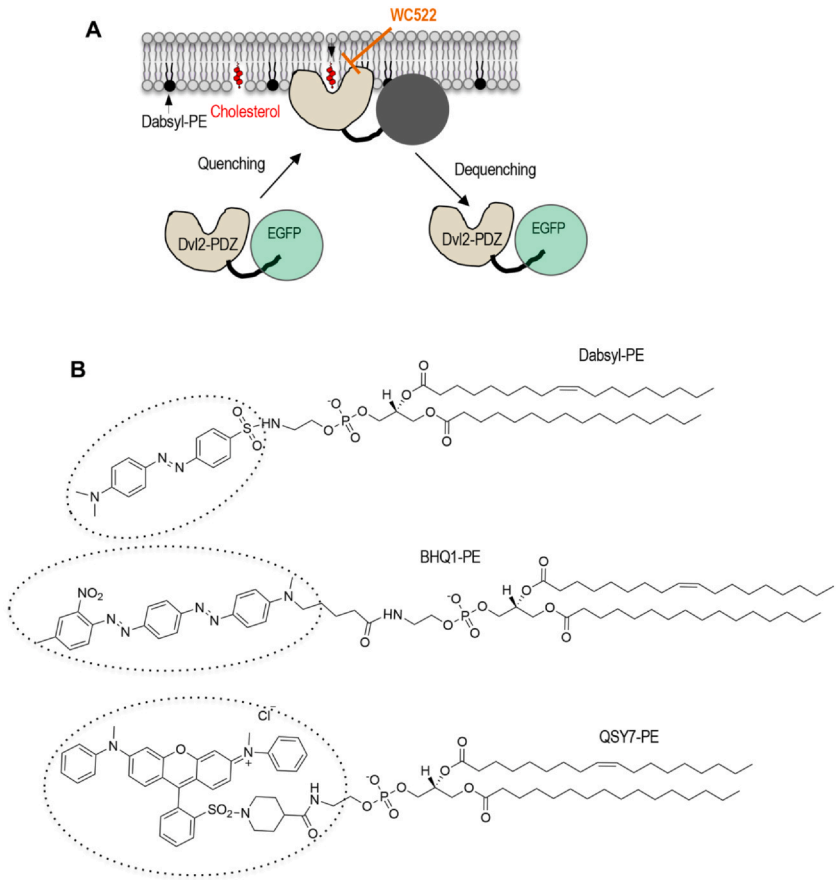

Fig. 1 Principles and components of the fluorescence quenching-based LPI assay. (A) The general strategy of the assay. To the solution of an FP-fusion protein (e.g., Dvl2-PDZ-EGFP) is added vesicles containing a target lipid (e.g., cholesterol) and a dark quencher, such as dabsyl-PE. Membrane binding of the protein leads to quenching of FP fluorescence by dabsyl-PE while LPI inhibition de-quenches the fluorescence signal by inducing membrane unbinding of the protein, allowing quantitative analysis of LPI and LPI inhibition. (B) The chemical structures of dabsyl-PE, BHQ1-PE, and QSY7-PE. Quenching moieties are shown in broken ovals.

binding extent (Kim et al., 2013; Cho et al., 2016). This design allows high-throughput screening of small molecules that inhibit or enhance protein–membrane interactions by monitoring de-quenching of FP fluorescence (Fig. 1). Compared to intrinsic tryptophan or chemical-labeling methods, this approach provides higher sensitivity, reproducibility, and versatility, and has been successfully applied to develop LPI inhibitors for diverse lipid-binding domains (Singaram et al., 2023; Sharma et al., 2025). For example, we developed WC522, a small-molecule inhibitor that selectively blocks cholesterol binding of the Dishevelled2 (Dvl2) PDZ domain by screening chemical libraries by this assay and optimizing the lead compound through the structure-activity relationship approach and the advanced computational analysis of LPI and LPI inhibition (Sharma et al., 2025). WC522 potently and specifically inhibits plasma membrane recruitment of Dvl2 in colorectal cancer cells, and suppresses hyper-activated canonical Wnt/β-catenin signaling and tumor growth without causing adverse effects to normal cells both in vitro and in vivo (Sharma et al., 2025). These results not only validated LPI interfaces as druggable sites but also demonstrated the feasibility and advantages of targeting LPI in cancer drug development. The overall workflow described in this chapter builds upon these discoveries to provide a streamlined and quantitative process for identifying, validating, and evaluating small-molecule LPI inhibitors using WC522 as an example. This integrated, universally applicable approach should serve as a platform for developing a wide range of positive and negative modulators of lipid-mediated signaling.

2. Development of lipid-protein interaction inhibitors

2.1 A high-throughput inhibitor screening protocol

2.1.1 Assay design

The lack of a fast, quantitative and convenient assay for LPI, which is essential for high-throughput screening of small-molecule LPI inhibitors, has been a major obstacle in LPI inhibitor-based drug discovery (Kim et al., 2013; Cho et al., 2016). Assays based on the intrinsic tryptophan fluorescence of proteins lack sufficient sensitivity and general applicability, while those based on chemical labeling of proteins suffer from complex, labor-intensive, and often incomplete processes. To overcome these limitations, we employed a fluorescence-quenching assay in which all candidate proteins are homogeneously expressed as fluorescent-protein (FP) fusion

constructs. Binding of the FP-tagged protein to lipid vesicles containing a non-fluorescent quenching lipid (dark quencher) result in reduced FP emission intensity proportional to the extent of membrane binding (Fig. 1). The approach is robust, quantitative, and compatible with automated multi-well plate formats for screening libraries of small molecules that either block or enhance lipid-dependent membrane association.

Enhanced green fluorescence protein (EGFP) is commonly used owing to its stability and ability to stabilize the fusion protein (Park et al., 2016; Kim et al., 2013; Cho et al., 2016), but alternative fluorophores such as mNeonGreen (Shaner et al., 2013) or mStayGold (Ando et al., 2024) can be substituted when higher brightness and sensitivity is required. Dark quenchers are typically incorporated into the headgroup of phosphatidylethanolamine (PE), resulting in quenching phospholipids, such as dabsyl-PE, BHQ1-PE, or QSY7-PE with tunable spectral properties (Fig. 1); BHQ1-PE offers ≈ 30 % higher quenching efficiency than dabsyl-PE for EGFP, whereas QSY7-PE is optimal for YFP-based constructs due to its longer absorption maximum (~570 nm) (Cho et al., 2016). The overall quenching efficiency depends on the spatial proximity of the FP tag to the membrane-binding interface and can be optimized by adjusting the molecular location of the FP tag or the length of the linker connecting the FP to the host protein. This fluorescence-quenching assay has been successfully applied for screening LPI inhibitors for signaling proteins containing diverse lipid-binding domains, including PH, PDZ, and SH2 modules.

2.1.2 Preparation of quencher lipid vesicles

Robust and reproducible preparation of quencher-containing lipid vesicles is essential for reliable fluorescence-based analysis of LPI. The composition of lipids, including that of the quencher lipid, in the vesicles is tailored according to the target protein's lipid specificity and the assay's sensitivity requirements.

2.1.2.1 Selection of the lipid composition

All PE-based quenching lipids, such as dabsyl-PE, BHQ1-PE, or QSY7-PE, carry a net negative charge and can nonspecifically enhance membrane binding of cationic proteins. To maintain physiological relevance and minimize electrostatic artifacts, the proportion of a quenching lipid should be kept as low as possible while allowing robust fluorescence quenching. Typically, a quenching efficiency of ~40 % is sufficient to yield a strong and

reproducible signal. For initial high-throughput screens or low-affinity LPI systems, the quenching lipid concentration may be increased slightly to enhance sensitivity. Background correction is critical to account for non-specific membrane absorption. For each test vesicle composition, a control vesicle lacking the target lipid is used for background subtraction. For instance, if 1-palmitoyl-2-oleoyl-*sn*-glycero-3-phosphocholine (POPC)/1-palmitoyl-2-oleoyl-*sn*-glycero-3-phosphoserine (POPS)/cholesterol/dabsyl-PE (60:20:10:10 in mol%) vesicles are used to assess cholesterol binding of a protein, POPC/POPS/dabsyl-PE (70:20:10) vesicles are employed for correction. POPC serves as a bulk lipid due to its zwitterionic nature and relatively low affinity for most cellular proteins.

2.1.2.2 Choice of vesicle size

Large unilamellar vesicles (~100 nm diameter) produced by extrusion exhibit excellent uniformity and are well-suited for robust determination of membrane-binding affinities. Small unilamellar vesicles (<20 nm diameter) are preferred for high-throughput applications since they are easier to prepare and offer a higher surface-to-volume ratio for tighter protein binding. They are, however, less stable and homogeneous, and should be used within a few hours of preparation. Uniform distribution of the quencher among vesicles is essential, as nonuniform populations can reduce overall quenching efficiency by sequestering fluorescent proteins away from quencher-containing membranes.

Preparation of lipid stock solutions.

1. **Neutral and anionic lipids:** POPC (Cat. No. 850457), POPE (Cat. No. 850757), POPS (Cat. No. 840034), and soy phosphatidylinositol (Cat. No. 840044) are obtained from Avanti Polar Lipids and dissolved in oxygen-free chloroform to 10 mg/mL. Stock solutions are stored in Teflon-sealed vials under nitrogen at −20 °C. All solvents, including chloroform (C607-4), methanol (53816), triethylamine (O4885-1), and dichloromethane (D37-1), are of analytical grade (ThermoFisher).
2. **Phosphoinositides:** 1,2-Dipalmitoyl derivatives of phosphoinositides such as PtdIns(3,4,5)P_3 (Cayman Chemical, Cat. No. 64920) are dissolved in chloroform/methanol/water (3:3:1, v/v/v) to 0.5 mg/mL and stored at −20 °C under nitrogen.

Synthesis of quencher lipids

3. **Dabsyl-PE synthesis:** POPE (50 mg) is dissolved in 2 mL chloroform and combined with dabsyl chloride (22.6 mg; Tokyo Chemical Industry,

Cat. No. D1382) and triethylamine (0.2 mL) in 5 mL chloroform. The reaction is stirred for 6 h at room temperature in the dark. Solvent is evaporated under reduced pressure, and the crude product is purified by silica column chromatography (CH_2Cl_2/MeOH = 9:1). The orange dabsyl-PE solid is dissolved in chloroform (10 mg/mL) and stored in Teflon-sealed vials at −20 °C.

4. **BHQ1-PE and QSY7-PE synthesis:** POPE (8 mg) and BHQ1 or QSY7 succinimidyl ester (5 mg; LGC Biosearch Technologies Cat. No. BHQ-1000S-5; ThermoFisher Cat. No. Q10193) are dissolved in 800 μL chloroform with 200 μL triethylamine. The reaction proceeds for 6 h at room temperature, followed by purification as above. 10 mg/mL chloroform stocks are prepared and stored under nitrogen at −20 °C.

Vesicle formation

5. **Large unilamellar vesicles:** Lipid mixtures are combined in chloroform according to the desired molar composition (e.g., 87:10:3; POPC/dabsyl-PE/PtdIns(3,4,5)P_3). The solvent is evaporated gently under nitrogen to form a thin film, which is then hydrated with 20 mM Tris-HCl buffer (pH 7.4) containing 0.16 M NaCl. The suspension is vortexed and sonicated briefly to disperse multilamellar aggregates, followed by extrusion through a 100-nm polycarbonate filter (Avanti Cat. No. 610005) using a mini-extruder (Avanti Cat. No. 610000) until clarity is achieved.
6. **Small unilamellar vesicles:** Lipid films of identical composition are hydrated with the same buffer and sonicated using a Branson Sonifier until the solution becomes clear, indicating formation of SUVs (<15 nm diameter). SUVs should be used within 3–4 h of preparation to ensure consistent quenching performance.

Practical notes:

Uniform vesicle quality and stable incorporation of the quencher lipid are critical for reproducibility. When extending this assay to new LPI systems, initial optimization of quencher mole% and vesicle size should always precede large-scale screening. The same vesicle preparation strategy has been used successfully to identify and characterize several LPI inhibitors, including the Dvl–cholesterol interaction inhibitor WC522 (Sharma et al., 2025).

2.1.3 Preparation of fluorescence protein-tagged proteins

Expression of target proteins as FP fusion constructs eliminates the need for chemical labeling, enhances protein stability and solubility, and allows

direct and sensitive real-time quantification of binding via fluorescence quenching. Both N-terminal and C-terminal fusions can be employed, and the optimal tag position should be determined empirically to preserve the intrinsic lipid-binding properties of the target protein while maximizing quenching efficiency. In general FP-tagged proteins with a proper linker show the same membrane binding properties as non-tagged proteins, when assayed by a label-free method, such as surface plasmon resonance analysis.

2.1.3.1 Tag design and optimization

The choice of fusion site (N- or C-terminus) and the linker length can significantly influence the fluorescence signal and membrane-binding geometry. FP tags are typically attached through a flexible linker of 5–15 residues (e.g., GGGGS repeats) to minimize steric hindrance. Each FP fusion is co-expressed with a His_6 affinity tag to facilitate purification by Ni^{2+}-NTA chromatography. For certain electrostatically neutral proteins, the His_6 tag may enhance nonspecific binding to negatively charged vesicles. In such cases, the tag should be enzymatically removed after purification (e.g., via TEV protease cleavage) or assays performed at slightly alkaline pH (≈7.8) to minimize protonation of histidine residues and reduce non-specific membrane affinity. Alternative protein-based affinity tags such as glutathione-S-transferase are not generally recommended because they tend to make the final constructs too large to be efficiently expressed in bacteria.

2.1.3.2 Bacterial expression and purification

A representative workflow for producing EGFP- and His_6-tagged lipid-binding proteins is outlined below.

1. **Culture initiation:** Inoculate 500 mL Luria broth (BD Cat. No. 244610) containing 50 μg/mL kanamycin or 100 μg/mL ampicillin with E. coli BL21 (DE3) or RIL cells transformed with the FP-tagged construct.
2. **Growth and induction**: Grow cells at 37 °C until the optical density at 600 nm reaches 0.6. Induce protein expression by adding 100 μM isopropyl β-D-thiogalactopyranoside (IPTG; Gold Biotechnology Cat. No. 12481C5) and continue incubation at 25 °C for 14 h with shaking to promote soluble expression.
3. **Cell lysis**: Harvest cells by centrifugation (2,500g, 10 min, 4 °C) and resuspend the pellet in 20 mL lysis buffer: 50 mM Tris-HCl (pH 7.9),

300 mM NaCl, 10 mM imidazole, and 10 % (v/v) glycerol. Lyse cells by sonication (5 min total, 30 s on/off intervals) on ice.

4. **Cell Extract preparation**: Centrifuge the lysate (39,000g, 30 min, 4 °C) and collect the supernatant for affinity purification.
5. **Affinity purification**: Incubate the cleared lysate with 1 mL Ni–NTA agarose resin (Qiagen Cat. No. 151032765) for 30 min at 4 °C with gentle agitation. Wash the resin sequentially with 50 mL wash buffer containing 20 mM imidazole, followed by another 50 mL containing 40 mM imidazole in 50 mM Tris-HCl (pH 7.4). Elute the protein using buffer containing 300 mM imidazole.
6. **Protein purity and concentration**: Analyze the eluted fractions by SDS–PAGE (18 % acrylamide) to confirm purity. Determine concentration using Bradford or BCA assay (Bio-Rad Cat. No. 5000006). Aliquots are flash-frozen in liquid nitrogen and stored at −20 °C (short term) or −80 °C (long term) in 10 % glycerol.

2.1.3.3 Practical notes

An optimal concentration of a FP-tagged protein for the assay is typically ~100 nM in a 200 μL reaction volume, but this may be adjusted based on the quenching efficiency and brightness of the fluorophore. Care should be taken to avoid prolonged exposure to light or repeated freeze–thaw cycles of protein solutions, as both can decrease the stability and activity of the protein and the quantum yield of the fluorophore. This approach has been applied to a wide range of lipid-binding domains, enabling reproducible high-throughput screening of LPI inhibitors.

2.1.4 High-throughput screening of membrane binding inhibitors

The fluorescence-quenching assay described above can be readily adapted for high-throughput identification of small molecules that modulate LPI through orthosteric or allosteric regulation. The assay quantitatively monitors changes in fluorescence of FP-tagged proteins upon membrane association or dissociation in the presence of test compounds. Inhibitors of membrane binding cause a de-quenching (i.e., an increase) of fluorescence intensity, whereas molecules that promote membrane binding enhance quenching (i.e., a decrease) of the FP signal (Fig. 1). Because the fluorescence change occurs in real time and is directly proportional to membrane occupancy of the protein, this approach offers high sensitivity and is compatible with microplate-based automation. Rigorous controls and background correction are required, as some small molecules may serve as a

direct quencher due to their intrinsic fluorescence properties. Each plate therefore includes "no-lipid" and "no-compound" reference wells for baseline correction. The assay is typically executed in two stages; (1) an initial single-point screen at a fixed vesicle concentration providing ~50–80 % quenching of EGFP; and (2) a secondary quantitative analysis using serial compound dilutions and multiple vesicle concentrations to confirm potency and specificity.

2.1.4.1 General procedure

1. **Reaction setup:** In a 96-well or 384-well plate, combine fixed concentrations of FP-tagged protein and quencher-containing vesicles in 200 μL assay buffer (20 mM Tris-HCl, pH 7.4, 0.16 M NaCl). Typical working concentrations are 100 nM protein and vesicles adjusted to produce ≈ 80 % of maximal quenching under control conditions.
2. **Compound addition:** Add inhibitors from DMSO stocks to a final DMSO content ≤2 % (v/v) to avoid protein destabilization. For primary screening, a single 20 μM concentration is sufficient; secondary screening employs serial dilutions (e.g., 0.5–50 μM) for IC_{50} estimation.
3. **Background and reference wells:** Include matched wells lacking vesicles for background fluorescence subtraction and wells containing vesicles without inhibitor as the maximal-binding reference.
4. **Incubation**: Mix gently and incubate at 25 °C for 10 min to allow equilibration between the protein, vesicles, and the inhibitor.
5. **Fluorescence measurement:** Measure fluorescence intensity at 509 nm with excitation at 488 nm using a plate reader equipped with appropriate optics for EGFP (or alternate excitation/emission settings for other FPs).
6. **Data analysis:** Express fluorescence changes as relative de-quenching (% of control). Compounds showing reproducible fluorescence recovery (>3 SD above mean of controls) are considered primary hits.

2.2 Determination of inhibition constant

2.2.1 Assays in the cell-free system

The inhibition constant (K_i) of LPI inhibitors can be directly determined by either the fluorescence quenching assay described herein or the surface plasmon resonance analysis. In the former, the FP-tagged lipid-binding protein and quencher-lipid vesicles are maintained at fixed concentrations, while the inhibitor concentration is varied. The inhibitor interferes with membrane binding of the protein and thus drives membrane unbinding of

the protein, resulting in a restoration of fluorescence intensity (de-quenching) proportional to the extent of displacement. Because the signal change directly reflects binding equilibrium, the fluorescence-quenching assay allows precise determination of true equilibrium K_i values under defined conditions.

2.2.1.1 General procedure

1. **Reaction mixture**: In a 96-well plate, combine the FP-tagged protein (typically 100 nM) with quencher-lipid vesicles adjusted to yield approximately 80 % quenching in the absence of inhibitor. Use 200 μL assay buffer per well (20 mM Tris-HCl pH 7.4, 0.16 M NaCl).
2. **Inhibitor titration**: Add increasing concentrations of inhibitor from DMSO stocks to maintain a constant final DMSO concentration (≤2 % v/v) across all wells. A 10-point serial dilution spanning 0–50 μM is generally sufficient for accurate curve fitting.
3. **Equilibration**: Incubate the plate for 10 min at 25 °C with gentle shaking to allow binding equilibrium between the protein, vesicles, and inhibitor.
4. **Measurement**: Record fluorescence emission at 509 nm (excitation 488 nm) using a multimode microplate reader. For background correction, include corresponding wells lacking vesicles (protein + inhibitor only) to subtract baseline FP fluorescence.
5. **Data analysis**: Calculate the relative fluorescence change (ΔF) as the difference between the fluorescence intensity with and without vesicles. Normalize values to the fully bound (no inhibitor) condition (ΔF_0). Calculate the inhibition constant (K_i) by nonlinear least-squares analysis using the equation: $\Delta F = \Delta F_0/(1 + [I]/K_i)$ where [I] is the free inhibitor concentration. Curve fitting is performed using software such as GraphPad Prism, Origin, or SigmaPlot. Data are typically expressed as mean ± SD from at least three independent experiments.

2.2.1.2 Practical notes

For direct comparison of inhibitory activity, the same vesicle and protein concentrations should be employed across all compounds. Deviations in quenching efficiency or background fluorescence must be corrected by including corresponding controls on each plate. Some inhibitors may possess intrinsic fluorescence overlapping with EGFP or the quencher dye; such compounds should be cross-checked using control wells lacking protein or quencher. Temperature and the ionic strength of the

solution can influence membrane affinity and inhibitor potency. Assays should therefore be conducted in the standardized buffer and the same temperature.

2.2.2 Assays in the cell-based system

Many cytosolic proteins that orchestrate cell signaling networks, including kinases and adaptor/scaffolding proteins, rely on lipid-dependent membrane recruitment for activation, protein-protein interaction, and signaling functions. Thus, inhibitors that block their membrane binding often alter cell signaling activities, which are typically detected as changes in post-translational modification of proteins, most notably phosphorylation. Quantifying these changes using phospho-specific antibodies serves as a sensitive, pathway-specific readout of the potency and specificity of LPI inhibitors.

2.2.2.1 General procedure

1. **Cell preparation:** Seed cells (disease-relevant lines) in 6-well plates ($\approx 1 \times 10^5$ cells per well) and culture overnight in DMEM (or appropriate medium) supplemented with 10 % FBS and 1 % penicillin–streptomycin until 60-70 % confluent.
2. **Compound treatment:** Prepare serial dilutions of the test inhibitor in complete medium, maintaining final DMSO ≤ 0.2 % (v/v). Replace the growth medium with 2 mL inhibitor-containing medium and incubate for 1–2 h at 37 °C to allow compound uptake and equilibrium binding.
3. **Pathway stimulation:** Add the appropriate agonist or ligand to activate the signaling cascade if necessary. For canonical Wnt signaling, use recombinant Wnt3a (100 ng/mL) and incubate for 30–60 min. Include negative (no ligand) and vehicle (DMSO + ligand) controls for normalization.
4. **Cell lysis:** Quickly place plates on ice, wash once with cold PBS, and lyse cells in 150–200 μL ice-cold RIPA buffer (50 mM Tris–HCl pH 7.5, 150 mM NaCl, 1 % NP-40, 0.1 % SDS, 0.5 % sodium deoxycholate) supplemented with phosphatase (10 mM NaF, 1 mM Na_3VO_4) and protease inhibitors. Collect lysates, incubate 10 min on ice, and centrifuge 15,000g for 10 min at 4 °C to remove debris.
5. **Protein quantification and immunoblotting:** Determine protein concentration by BCA assay and normalize samples to equal loading (30–50 μg per lane). Mix with 4 × Laemmli buffer, heat 95 °C for 5 min, and resolve by SDS-PAGE followed by transfer to PVDF membrane.

Block with 5 % BSA/TBST and probe overnight (4 °C) with phospho-specific antibodies against pathway markers along with total protein and loading controls. Detect with HRP-conjugated secondary antibodies and ECL reagents within the linear dynamic range. Perform all treatments in triplicate ($n \geq 3$) to ensure reproducibility

6. **Data analysis:** Quantify band intensities using ImageJ or similar software. Calculate phosphoprotein/total protein ratios (pX/X) and normalize to vehicle + ligand controls. Plot normalized values against inhibitor concentration and fit using a four-parameter logistic equation to determine IC_{50} using the equation, $pX/X = 1/(1 + IC_{50} / [I])$ (I:% inhibition, [I]: inhibitor concentration). Evaluate statistical significance by an appropriate test, e.g., one-way ANOVA.

2.2.2.2 Practical notes

Some LPI inhibitors may be cytotoxic to the cells especially at high concentrations. Thus, inhibitor concentrations used for the phosphorylation assay should be kept below cytotoxic levels to ensure robust and reproducible inhibition studies. Because LPI inhibition alters membrane association of the target proteins, the cellular activity of inhibitors should be independently confirmed by measuring the subcellular localization of target proteins by confocal or TIRF microscopy.

2.3 Target validation

Following identification of active compounds through fluorescence-based screening and optimization, subsequent validation is required to confirm that the observed inhibition arises from direct binding to the target protein rather than from nonspecific effects. Target validation is typically carried out in both cell-free and cell-based systems to establish direct molecular interaction, biochemical inhibition, and cellular engagement.

2.3.1 Target validation in the cell-free system

The direct binding of an LPI inhibitor to the purified target protein can be validated by biophysical analyses, such as surface plasmon resonance (SPR), isothermal titration calorimetry, and the thermal shift assay, or by the structural determination of a protein-inhibitor complex. Although structural determination provides the ultimate evidence for the protein-inhibitor binding, it may not be feasible for many LPI inhibitors as their effective protein binding may require the presence of the membrane. Here we describe the protocols for the SPR analysis using WC522 as an example.

1. **Instrument and the sensor ship:** Any commercial SPR equipment and sensor chip can be used for the measurements. This protocol is described for the streptavidin-coated SA chip (Cytiva) in the Biacore 1 K+ system (Cytiva).
2. **Synthesis of a biotinylated derivative of WC522 (WC522B):** Functionalize WC522 with biotin at a position distal to its pharmacophore to retain cholesterol-competitive activity as described previously (Sharma et al., 2025). Validate that the biotinylated analogue (i.e., WC522B) retains full inhibitory activity by the fluorescence-quenching assay.
3. **Inhibitor coating:** Coat the SA chip equilibrated in 20 mM Tris, pH 7.4, containing 0.16 M NaCl at 23 °C with WC522B for 60 s at 10 μL/min prior to each sample injection.
4. **Protein injection:** Inject the protein solution (typically 100-500 nM) in the equilibration buffer for 120 s at 30 μL/min
5. **Regeneration:** Inject the regeneration solution (10 mM Glycine-HCl, pH 2.5) for 60 s at a flow rate of 30 μL/min.
6. **Data Analysis:** Determine K_d values for the protein-inhibitor binding by global kinetic analysis of association and dissociation curves using the heterogenous analyte curve fitting of single cycle kinetic graphs with the Biacore (Cytiva) curve fitting software.

2.3.1.1 Additional notes

To demonstrate the specificity of inhibitor-target protein binding, it is often necessary to include negative controls employing non-target proteins or a mutant of the target protein and completive displacement of the target protein from the chip surface by the non-biotinylated inhibitor.

2.3.2 Target validation in the cell-based system

Two orthogonal assays are widely used for demonstrating direct target engagement of LPI inhibitors in intact cells: the Cellular Thermal Shift Assay (CETSA) (Martinez Molina & Nordlund, 2016), which detects compound-induced thermal stabilization of the target, and the biotin–pull-down assay, which verifies physical binding of the inhibitor to its target protein or complex components within cellular lysates (Sharma et al., 2025). Together, these complementary approaches provide evidence for selective cellular target engagement.

2.3.2.1 Cellular thermal shift assay (CETSA)

1. **Treatment:** Treat cells with graded concentrations of inhibitors (e.g., 0, 2, 5, 10 μM) for 1 h at 37 °C.
2. **Harvesting and aliquoting:** Wash cells with PBS and resuspend ~1×10^6 cells per 200 μL PBS + protease inhibitors. Dispense 20–30 μL aliquots into PCR tubes.
3. **Thermal challenge:** Heat samples for 3 min at different temperatures (45–70 °C), then cool 3 min on ice.
4. **Lysis and clarification:** Lyse by three freeze–thaw cycles or brief sonication, centrifuge 15 000g, 10 min, 4 °C, and collect supernatants.
5. **Data Analysis:** Analyze soluble fractions by SDS-PAGE and immunoblot for the target protein. Normalize (I_{norm}) the gel intensity (I) using the equation: $I_{norm} = (I - I_{min})/(I_{max} - I_{min})$ where I_{max} and I_{min} are maximal and minimal I values, respectively, for each measurement. Plot I_{norm} versus temperature (T in °C) and analyze the plot by the non-linear least-squares analysis using the equation: $I_{norm} = 1 - 1/(1 + e^{(Tm - T)/slope})$ where T_m and slope indicate melting temperature and the slope of curve, respectively. A positive shift (ΔT_m) indicates target protein stabilization by inhibitor binding.

2.3.2.2 Biotin pull-down assay

To directly confirm binding of a LPI inhibitor to its target under physiological conditions, a biotin-conjugated analogue of the inhibitor with intact inhibitory activity is synthesized and used for cellular pull-down assay. Here we describe the protocol using WC522B (see above) as an example.

1. Preparation of WC522B: See above.
2. Binding reaction: Treat the cells with the mild non-ionic lysis buffer (50 mM Tris-HCl pH 7.4, 150 mM NaCl, 0.5 % NP-40, protease inhibitors) and collect the supernatant after centrifugation of the cell lysates (≈1 mg/mL total protein). Incubate the supernatant with 2 μM WC522B for 1 h at 4 °C with gentle rotation to allow complex formation.
3. Affinity capture: Add 50 μL streptavidin magnetic beads (Thermo Fisher Pierce #88817) to each lysate and continue incubation for 1 h at 4 °C. Control samples include lysates treated with free biotin or with WC522B + 200 μM unlabeled WC522 for competition analysis.
4. Washing and elution: Wash the beads 4 × with lysis buffer + 300 mM NaCl to remove nonspecific proteins and once with PBS. Release

bound proteins from the beads by boiling in 2 × SDS sample buffer or by incubation with 2 mM biotin solution.

5. Detection: Analyze the eluates by SDS–PAGE and by immunoblotting for the target protein and known interactors. Enrichment of the target in WC522B pulldowns, with signal loss upon competition by excess free WC522, confirms specific binding.

2.4 Determination of in vivo inhibitory activity

In vivo evaluation of an LPI inhibitor using a preclinical animal model is a critical step in the translational research. The process integrates pharmacokinetic (PK) studies, efficacy testing, and toxicity evaluation to establish whether the LPI inhibitor possesses suitable bioavailability, stability, and therapeutic potential in an animal model. The following procedures outline general approaches for evaluating small-molecule LPI inhibitors in murine models, using WC522 as an example.

2.4.1 Pharmacokinetic (PK) analysis

PK profiling defines the absorption, distribution, metabolism, and excretion (ADME) characteristics of the inhibitor. Quantifying plasma concentrations over time provides parameters such as half-life ($t_{1/2}$), clearance (CL), area under the curve (AUC), and maximum concentration (Cmax), which are critical for dose and schedule optimization.

1. **Formulation:** Dissolve the compound in a biocompatible vehicle such as 10 % DMSO/40 % PEG-400/50 % saline (v/v/v). Filter-sterilize the solution through a 0.22 μm syringe filter before administration.
2. **Dosing:** Administer to male C57BL/6 or athymic nude mice (8 weeks old) by intraperitoneal injection at 10-100 mg/kg (10 mL kg^{-1} volume). Record body weight and health status throughout.
3. **Sample collection:** Collect ~30–50 μL blood via submandibular vein or tail nick at 0.1, 0.25, 0.5, 1, 2, 4, 8, 12, and 24 h post-dose. Centrifuge to obtain plasma and store at −80 °C.
4. **Sample preparation and LC–MS/MS analysis:** Mix 20 μL plasma with 60 μL acetonitrile containing internal standard, vortex, centrifuge 15 000g (10 min), and inject supernatant for LC–MS/MS quantification.
5. **Data analysis:** Construct concentration–time profiles and calculate PK parameters using non-compartmental analysis (Phoenix WinNonlin). Following a single 100 mg/kg intraperitoneal dose, WC522 exhibited a Cmax within 0.5 h and a plasma $t_{1/2}$ of ≈4-5 h, with detectable levels up to 12 h. This data supported once-daily dosing for efficacy studies.

2.4.2 In vivo efficacy testing

This protocol is established to determine whether biochemical inhibition of lipid-dependent signaling translates into measurable suppression of tumor growth or other disease phenotypes in immunocompromised animals for xenograft studies.

1. **Xenograft establishment:** Inject 1×10^6 disease-relevant cells (e.g., colorectal cancer cells) subcutaneously into the flank of athymic nude mice in 100 μL 1:1 PBS: Matrigel. Monitor tumor formation until mean volume reaches ≈100 mm^3 .
2. **Group allocation and treatment:** Randomize mice (n = 8–10 per group) into vehicle and two dose groups (e.g., 5–100 mg/kg). Treat once daily for 21 days. Record tumor dimensions and body weight three times per week.
3. **Endpoint collection:** At study termination, excise tumors, record weights, and either snap-freeze for Western analysis or fix in 10 % formalin for immunohistochemistry.
4. **Molecular analysis:** Analyze tumor lysates or sections for target protein engagement and specific signaling perturbation.
5. **Data evaluation**: Calculate tumor growth inhibition (%TGI): %TGI = 100 x [1−(ΔT/ΔC)], where ΔT and ΔC are mean tumor volume changes in treated and control groups, respectively. Analyze growth curves using two-way ANOVA with repeated measures. For WC522, daily administration of 10 $mg\,kg^{-1}$ WC522 significantly suppressed human colorectal cancer cell (HCT15) xenograft growth (~60 % TGI) without weight loss or behavioral changes. Tumor biopsies showed marked reductions in phospho-Dvl2, active β-catenin, and cyclin D1, confirming target pathway inhibition in vivo (Sharma et al., 2025).

2.4.3 Toxicity testing

Toxicity studies ensure that pharmacological effects are not accompanied by systemic or organ-specific adverse events.

1. **Acute and repeat-dose design**: Conduct single-dose tolerability (5, 15, 50 $mg\,kg^{-1}$ i.p.) with 7-day observation, followed by 14-day repeat-dose (q.d.) studies at escalating doses.
2. **Clinical monitoring**: Record body weight, activity, and appearance daily. Note any signs of distress or toxicity.
3. **Serum chemistry and hematology**: Collect blood on day 14 for ALT, AST, ALP, bilirubin, BUN, and creatinine measurements. Evaluate CBC to detect hematological changes.

4. **Necropsy and histopathology:** Weigh major organs (liver, kidney, heart, spleen, lung) and examine H&E-stained sections for pathological lesions.
5. **Determination of NOAEL**: Define the No-Observed-Adverse-Effect Level (NOAE L) as the highest dose with no significant clinical, biochemical, or histological abnormalities.
6. **For WC522:** Mice tolerated daily WC522 doses up to 200 mg/kg i.p. for 14 days without weight loss or organ abnormalities. Serum ALT, AST, BUN, and creatinine remained within normal limits, and no histopathological lesions were observed, indicating a favorable safety profile and a wide therapeutic margin (Sharma et al., 2025).

3. Concluding Remarks

The systematic framework described in this chapter provides a comprehensive workflow for the discovery and validation of small-molecule LPI inhibitors. The streamlined process integrating fluorescence-quenching–based high-throughput screening, quantitative determination of inhibition constants, cell-based in vitro evaluation, and in vivo pharmacological evaluation, should enable thorough and rigorous evaluation of the potency, specificity, and mechanism of action of any LPI inhibitor. The combination of biochemical, biophysical, and cellular validation tools ensures robust identification of bona fide lipid-binding modulators. The successful identification and characterization of WC522, a cholesterol-competitive inhibitor of the Dvl2 PDZ domain, exemplify the utility of this workflow in uncovering novel therapeutics that selectively target lipid-mediated signaling. This generally applicable strategy can be adapted to a wide range of lipid-binding proteins, providing a foundation for developing next-generation modulators of membrane-associated signal transduction and lipid-driven pathologies.

Acknowledgements

The work is supported by National Institutes of Health grant GM-R35–122530.

References

Ando, R., Shimozono, S., Ago, H., Takagi, M., Sugiyama, M., Kurokawa, H., Hirano, M., ... Miyawaki, A. (2024). StayGold variants for molecular fusion and membrane-targeting applications. *Nature Methods, 21*(4), 648–656.

Chen, Y., Sheng, R., Kallberg, M., Silkov, A., Tun, M. P., Bhardwaj, N., Kurilova, S., ... Cho, W. (2012). Genome-wide Functional Annotation of Dual-Specificity Protein- and Lipid-Binding Modules that Regulate Protein Interactions. *Molecular Cell, 46*(2), 226–237.

Cho, W., Kim, H., & Hu, Y. (2016). High-throughput fluorometric assay for membrane-protein interaction. *Methods in Molecular Biology, 1376*, 163–174.

Cho, W., & Stahelin, R. V. (2005). Membrane-protein interactions in cell signaling and membrane trafficking. *Annual Review of Biophysics and Biomolecular Structure, 34*, 119–151.

Cho, W., & Stahelin, R. V. (2006). Membrane binding and subcellular targeting of C2 domains. *Biochimica et Biophysica Acta, 1761*(8), 838–849.

Hammond, G. R., & Balla, T. (2015). Polyphosphoinositide binding domains: Key to inositol lipid biology. *Biochimica et Biophysica Acta, 1851*(6), 746–758.

Kihara, Y. (2020). Introduction: Druggable lipid signaling pathways. *Advances in Experimental Medicine and Biology, 1274*, 1–4.

Kim, H., Afsari, H. S., & Cho, W. (2013). High-throughput fluorescence assay for membrane-protein interaction. *Journal of Lipid Research, 54*(12), 3531–3538.

Lemmon, M. A. (2008). Membrane recognition by phospholipid-binding domains. *Nature Reviews. Molecular Cell Biology, 9*(2), 99–111.

Martinez Molina, D., & Nordlund, P. (2016). The cellular thermal shift assay: A novel biophysical assay for in situ drug target engagement and mechanistic biomarker studies. *Annual Review of Pharmacology and Toxicology, 56*, 141–161.

Di Paolo, G., & De Camilli, P. (2006). Phosphoinositides in cell regulation and membrane dynamics. *Nature, 443*(7112), 651–657.

Park, M. J., Sheng, R., Silkov, A., Jung, D. J., Wang, Z. G., Xin, Y., Kim, H., ... Cho, W. (2016). SH2 domains serve as lipid-binding modules for pTyr-signaling proteins. *Molecular Cell, 62*, 7–20.

Saliba, A. E., Vonkova, I., & Gavin, A. C. (2015). The systematic analysis of protein-lipid interactions comes of age. *Nature Reviews. Molecular Cell Biology, 16*(12), 753–761.

Shaner, N. C., Lambert, G. G., Chammas, A., Ni, Y., Cranfill, P. J., Baird, M. A., Sell, B. R., ... Wang, J. (2013). A bright monomeric green fluorescent protein derived from Branchiostoma lanceolatum. *Nature Methods, 10*(5), 407–409.

Sharma, A., Zalejski, J., Bendre, S. V., Kavrokova, S., Hasdemir, H. S., Ozgulbas, D. G., Sun, J., ... Cho, W. (2025). Cholesterol-targeting Wnt-beta-catenin signaling inhibitors for colorectal cancer. *Nature Chemical Biology, 21*(9), 1376–1386.

Singaram, I., Sharma, A., Pant, S., Lihan, M., Park, M. J., Pergande, M., Buwaneka, P., ... Cho, W. (2023). Targeting lipid-protein interaction to treat Syk-mediated acute myeloid leukemia. *Nature Chemical Biology, 19*(2), 239–250.